frontiers | Research Topics

Schistosomiasis: Host-parasite interactions - volume II

Edited by
Thiago Almeida Pereira and Michael Harrison Hsieh

Published in
Frontiers in Immunology

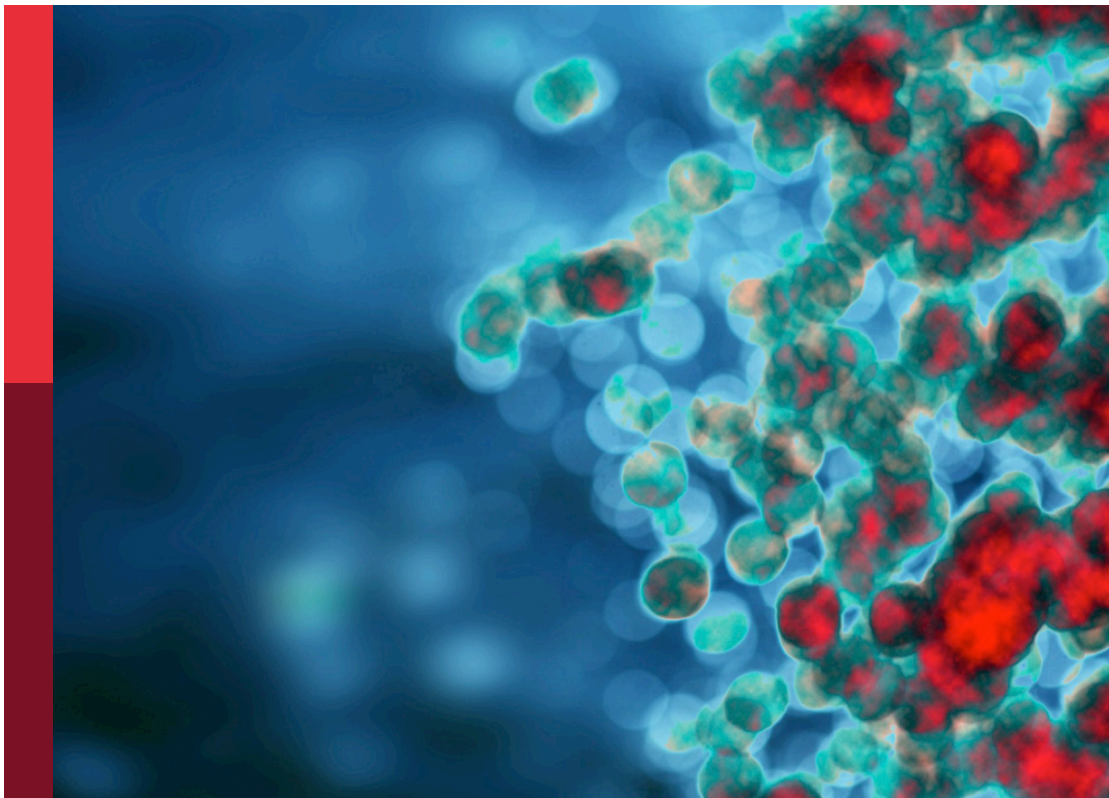

ISSN 1664-8714
ISBN 978-2-83251-213-5
DOI 10.3389/978-2-83251-213-5

About Frontiers

Frontiers is more than just an open access publisher of scholarly articles: it is a pioneering approach to the world of academia, radically improving the way scholarly research is managed. The grand vision of Frontiers is a world where all people have an equal opportunity to seek, share and generate knowledge. Frontiers provides immediate and permanent online open access to all its publications, but this alone is not enough to realize our grand goals.

Frontiers journal series

The Frontiers journal series is a multi-tier and interdisciplinary set of open-access, online journals, promising a paradigm shift from the current review, selection and dissemination processes in academic publishing. All Frontiers journals are driven by researchers for researchers; therefore, they constitute a service to the scholarly community. At the same time, the *Frontiers journal series* operates on a revolutionary invention, the tiered publishing system, initially addressing specific communities of scholars, and gradually climbing up to broader public understanding, thus serving the interests of the lay society, too.

Dedication to quality

Each Frontiers article is a landmark of the highest quality, thanks to genuinely collaborative interactions between authors and review editors, who include some of the world's best academicians. Research must be certified by peers before entering a stream of knowledge that may eventually reach the public - and shape society; therefore, Frontiers only applies the most rigorous and unbiased reviews. Frontiers revolutionizes research publishing by freely delivering the most outstanding research, evaluated with no bias from both the academic and social point of view. By applying the most advanced information technologies, Frontiers is catapulting scholarly publishing into a new generation.

What are Frontiers Research Topics?

Frontiers Research Topics are very popular trademarks of the *Frontiers journals series*: they are collections of at least ten articles, all centered on a particular subject. With their unique mix of varied contributions from Original Research to Review Articles, Frontiers Research Topics unify the most influential researchers, the latest key findings and historical advances in a hot research area.

Find out more on how to host your own Frontiers Research Topic or contribute to one as an author by contacting the Frontiers editorial office: frontiersin.org/about/contact

Schistosomiasis: Host-parasite interactions - volume II

Topic editors

Thiago Almeida Pereira — Stanford University, United States

Michael Harrison Hsieh — Children's National Hospital, United States

Citation

Pereira, T. A., Hsieh, M. H., eds. (2023). *Schistosomiasis: Host-parasite interactions - volume II*. Lausanne: Frontiers Media SA.

doi: 10.3389/978-2-83251-213-5

Table of contents

frontiers | Frontiers in Immunology

ORIGINAL RESEARCH
published: 06 May 2022
doi: 10.3389/fimmu.2022.887213

Potential Utility of Systemic Plasma Biomarkers for Evaluation of Pediatric Schistosomiasis in Western Kenya

Bartholomew N. Ondigo[1], Rachael E. Hamilton[2,3], Edwin O. Magomere[1], Isaac O. Onkanga[4], Pauline N. Mwinzi[5], Maurice R. Odiere[4] and Lisa Ganley-Leal[3]*

[1] Department of Biochemistry and Molecular Biology, Faculty of Science, Egerton University, Egerton, Kenya, [2] School of Public Health, Boston University, Boston, MA, United States, [3] Global Development, Elegance Biotechnologies, Wayne, PA, United States, [4] Centre for Global Health Research, Kenya Medical Research Institute (KEMRI), Kisumu, Kenya, [5] Regional Office for Africa, World Health Organization, Brazzaville, Democratic Republic of Congo

OPEN ACCESS

Edited by:
Thiago Almeida Pereira, Stanford University, United States

Reviewed by:
Lisa M. Shollenberger, Old Dominion University, United States
Elisângela Santos, São Paulo State University, Brazil

***Correspondence:**
Bartholomew N. Ondigo
ondigo2002@gmail.com

Specialty section:
This article was submitted to Parasite Immunology, a section of the journal Frontiers in Immunology

Received: *01 March 2022*
Accepted: *08 April 2022*
Published: *06 May 2022*

Citation:
Ondigo BN, Hamilton RE, Magomere EO, Onkanga IO, Mwinzi PN, Odiere MR and Ganley-Leal L (2022) Potential Utility of Systemic Plasma Biomarkers for Evaluation of Pediatric Schistosomiasis in Western Kenya. Front. Immunol. 13:887213. doi: 10.3389/fimmu.2022.887213

Introduction: Current diagnostic tools for schistosomiasis are limited, and new tests are necessary to enhance disease diagnosis and surveillance. Identification of novel disease-specific biomarkers may facilitate the development of such tests. We evaluated a panel of biomarkers used in sepsis and parasitic diseases for their potential suitability in the diagnosis of schistosomiasis.

Objective: The study evaluated the levels of systemic plasma biomarkers in relation to *Schistosoma mansoni* infection and parasite burden.

Methods: Six biomarkers were measured in the plasma of children from schistosomiasis-endemic regions using ELISA. The concentration of soluble CD23 (sCD23) and lipopolysaccharide (LPS) was tested in 199 and 124 plasma samples, respectively, while interleukin-6 (IL-6), soluble triggering receptor expressed on myeloid (sTREM) cells, eotaxin-1, and fatty acid-binding protein (FABP) concentrations were tested in 30 plasma samples.

Results: The concentration of IL-6, eotaxin-1, FABP, and LPS was similar between schistosome-infected and uninfected children. The schistosome-infected children had higher median levels of sTREM and sCD23 as compared to uninfected children, 119.0 (29.9–208.9) versus 10.7 (0.0–73.4) (p = 0.046) and 2,549.0 (1,899.0–3,356.0) vs. 2,035.0 (1,448.0–2,939.0) (p = 0.05), respectively. In addition, sTREM was positively correlated with egg density (p = 0.017).

Conclusion: Our data show that active schistosomiasis *per se* is associated with elevated levels of sTREM and sCD23. sTREM has potential diagnostic and prognostic values. However, these biomarkers did not distinguish between children with low egg burden and uninfected children.

Keywords: biomarkers, schistosomiasis, infection, intensity, diagnosis

INTRODUCTION

Schistosomiasis is a tropical disease affecting communities with limited access to safe water and with inadequate sanitation (1, 2). The disease affects over 200 million people worldwide, about 90% of whom reside in Sub-Saharan Africa. A significant number (123.6 million) of those affected are children (3). Children from endemic areas are infected at the age of 2 years and may remain chronically infected throughout their school-going age (4). The disease results in 3.3 million disability-adjusted life years (DALYs) lost annually due to overt and sub-clinical morbidities (5). In Kenya, about 17.4 million people are at risk of schistosomiasis (6, 7). The main parasite species causing infections in Kenya are *Schistosoma haematobium* and *Schistosoma mansoni* (6, 8, 9).

Immune molecules such as interleukin-6 (IL-6), soluble triggering receptor expressed on myeloid (sTREM), eotaxin-1, fatty acid-binding protein (FABP), soluble CD23 (sCD23), and lipopolysaccharide (LPS) have been evaluated in previous studies as potential diagnostic markers for parasitic infections and sepsis (10–13). Triggering receptor expressed on myeloid cells-1 (TREM-1) is a transmembrane receptor expressed by innate immune cells, including endothelial cells, mature monocytes, and macrophages and platelets (14). In addition to its expression in a cell membrane-bound form, TREM-1 is released as a soluble factor (sTREM-1). sTREM-1 has been investigated and is a reliable biomarker of disease severity and outcome in septic shock (15). TREM-1 is increased in the skin, biological fluids, and tissues with bacterial and fungal infections (16, 17). sTREM-1 released into the blood and other bodily fluids interacts with a 12-kDa DNAX-activating protein (DAP12) amplifying pathogen-induced signals (18). This interaction triggers the release of pro-inflammatory cytokines including IL-1b and IL-8 and monocyte chemotactic protein (19). A gradual increase in levels of sTREM has been observed in *S. mansoni* over the course of infection (20), which appeared to upregulate *DAP12* and *IL-8* gene expression, suggesting the important role of sTREM in parasitic infections (21).

IL-6 and eotaxin-1 levels are altered among individuals with parasitic infection (22), suggesting their potential utility in diagnosis (22). FABP induces protective immunity against *S. mansoni* infection by triggering a Th1-like immune response during infection (23); as such, its plasma concentration can be monitored to assess disease progression. CD23 is a surface membrane receptor for IgE on B cells. The receptor is initially expressed as a 45-kDa type II membrane protein and subsequently released as sCD23 fragments by the action of an endogenous metalloprotease (24). sCD23 levels were increased with schistosome infection intensity but declined significantly with schistosome-specific IgE levels (12). Elevated levels of serum sCD23 prior to diagnosis were associated with an increased risk of non-Hodgkin lymphoma (25). Increased synthesis of CD23 signals a corresponding increase in the synthesis of its ligand (IgE) (24, 26). CD23 expressed on the B-cell surface may bind IgE and regulate production and concentration in plasma (19). A previous study demonstrated the role of sCD23 in developing resistance to reinfection in schistosomiasis (27). Nonetheless, elevated levels of LPS in plasma of hepatosplenic schistosomiasis caused by *S. mansoni* have been demonstrated to be potential biomarkers for diagnosis of schistosomiasis (28).

The Kato–Katz technique is the gold standard method for the diagnosis of schistosomiasis. This tool relies on the detection of eggs in stool for most species apart from *S. haematobium*, whose eggs are detected in urine (29). A major setback of using the microscopy method is that it has a low sensitivity among individuals with low parasite burden and its dependence on the appearance of eggs in the stool, which may occur 6–8 weeks after infection (30). To improve the sensitivity and accuracy of diagnosis, an opportunity exists for developing biomarker-based diagnostic tools that can complement microscopy and help to monitor disease progression. We sought to investigate whether systemic plasma biomarkers can be used to distinguish between children infected with schistosomiasis and healthy controls (uninfected children). We also assessed the correlation between the biomarkers and their ability to distinguish infection intensities (light, moderate, and heavy) and changes in hemoglobin levels. The study hypothesized that children infected with *S. mansoni* would have unique biomarker profiles that could ultimately be exploited to aid in diagnosis.

The diagnosis of schistosomiasis currently relies on microscopic detection of schistosome eggs in stool or urine samples and serological assays. Identification of schistosomiasis-specific biomarkers will complement existing diagnostic methods with the added advantage of early diagnosis before schistosome eggs appear in stool and the ability to track disease progression. The optimization of novel diagnostic approaches may be accomplished by the selection of specific biomarkers of infection. In this study, we assessed the potential utility of systemic plasma biomarkers for the evaluation of pediatric schistosomiasis in western Kenya.

MATERIALS AND METHODS

Study Population

Samples analyzed in this study were collected from children aged between 10 and 12 years from Lwanda Kotieno in Uyoma, Rarieda District, a schistosomiasis-endemic region in western Kenya. Eligible children provided stool samples for three consecutive days. The stool samples were used to diagnose the presence of *S. mansoni* eggs based on the Kato–Katz technique. At the enrolment visit, the study nurse conducted a clinical examination consisting of an assessment of nutritional status, body temperature, determination of liver or spleen sizes (by measuring extensions below the rib cage), and palpation of liver and spleen [for determination of the firmness of the organ(s)]. Height and weight were also measured and used to calculate a body mass index (BMI). Mid-upper arm circumference (MUAC) was measured to assess nutritional status. All plasma samples were from archived specimens collected as part of an ongoing study. Thus, all samples were collected from well-characterized participants. A total of 199 and 124 samples were analyzed for

sCD23 and LPS, respectively. A subset of samples was assayed for IL-6, sTREM, eotaxin-1, and FABP. The uninfected control children were those attending the same schools but with stools samples negative for *S. mansoni* eggs at three continuous time points. The sample sizes tested were chosen based solely on the sufficiency of plasma volume to allow for the testing of multiple analytes.

Ethical Approval

This study was approved by the Scientific and Ethics Review Unit (SERU) of Kenya Medical Research Institute (KEMRI) (protocol # SERU/KEMRI/CGHR/009/3025). Written parental informed consent and child assent were obtained for all participants.

Sample Collection and Storage

Blood samples were collected in heparinized tubes and transported on ice to KEMRI-CGHR, Neglected Tropical Diseases (NTD) laboratory in Kisumu within 6 h of collection. In the laboratory, a blood sample was fractioned by centrifuging for 10 min at approximately 2,000 × *g*. Plasma was then aspirated and stored in a 0.5-ml Sarstedt tube at −20°C until further analysis. All the samples had never been thawed prior to the assays in this study. Stool samples for the detection of eggs were collected in sterile aluminum bags. The bags were issued to each participant labeled with a unique identifier number. An oral description of the use and proper handling of the stool bag and samples was given, and each participant was instructed to collect a fresh stool sample. Upon reception, samples were assessed for possible contamination and volume adequacy. The samples were transported in a cooler box within 6 h of collection to KEMRI-CGHR, NTD Laboratory, in Kisumu for analyses.

Stool Sample Microscopy

Stool samples were processed using the Kato–Katz technique for the detection of *S. mansoni* eggs based on duplicate slides using the 41.7-mg template (31). Slides were viewed under a light microscope by two independent microscopists under ×40 magnification. The eggs counted for each sample were recorded as eggs per gram (EPG), while samples with zero eggs were recorded as negative. The number of *S. mansoni* eggs was counted, recorded, and multiplied by 24 to determine the number of eggs per gram of feces. Infection intensity was classified as light (1–99 EPG), medium (100–399 EPG), or heavy (≥400 EPG) according to the WHO guidelines.

Assessment of Interleukin-6, Soluble Triggering Receptor Expressed On Myeloid, Eotaxin-1, and Fatty Acid Binding Protein

Plasma levels of IL-6, sTREM, eotaxin-1, and FABP were measured by commercially available quantikine ELISAs (R&D Systems, Minneapolis, MN, USA) according to the manufacturer's protocol. Briefly, 100 µl in duplicate of standards, controls, or plasma samples was transferred to appropriate wells; the plate was then covered with an adhesive seal and incubated for 1 h at room temperature (RT) to allow for the target proteins to bind plate-coated antibodies. The unbound proteins were washed four times using the wash buffer in a plate washer. One hundred microliters of diluted biotinylated antibodies was added to each well and allowed to bind to captured biomarkers for 1 h at RT. At the end of the incubation period, six rounds of wash were performed, and 100 µl of the diluted streptavidin–peroxidase conjugate was added and incubated for 1 h at RT. Detection was performed by adding tetramethylbenzidine (TMB) substrate to the washed plate, and the reaction was allowed to take place for 20 min. The reaction was stopped by adding 100 µl of stop solution, and the plates were immediately read at 450 nm on a Spectramax Emax plate reader (Molecular Devices, San Jose, CA, USA). Absorbance was recorded for each biomarker and converted to concentration using the standard curve.

Assessment of sCD23

The sCD23 ELISA (catalog # BMS 227-2) was performed according to the manufacturer's recommendation (Bender MedSystems, Vienna, Austria).

Assessment of Plasma Lipopolysaccharide

Plasma levels were evaluated using the chromogenic endpoint LPS amoebocyte lysate detection assay (catalog # A39553, ThermoFisher Scientific, Waltham, MA, USA) according to the manufacturer's instructions. Samples were measured on a microplate absorbance reader at 405 nm on a Spectramax Emax plate reader (Molecular Devices, San Jose, CA, USA). The kit had a minimum detection limit of 0.01 EU/ml.

Statistical Analysis

Medians were used as measures of central tendency. Comparisons between two groups were performed using the Mann–Whitney U test for non-normally distributed variables. The comparison between three groups was evaluated using the Kruskal–Wallis test, and the strength of association between variables was analyzed using a Spearman's rank-order correlation (r_s). Data were considered statistically significant at $p \leq 0.05$. All statistical analyses were performed using GraphPad Prism version 6.0 for Windows (GraphPad Software, Inc., San Diego, CA, USA).

RESULTS

A total of 199 children comprised the final dataset for analysis. The children's ages, other general characteristics, and the status of their parasitological infections are presented in **Table 1**.

Concentration of Biomarkers by Infection Status: Soluble Triggering Receptor Expressed On Myeloid Is Elevated in Children With Schistosomiasis

We compared the levels of biomarkers (IL-6, sTREM, eotaxin-1, FABP, sCD23, and LPS) between children with schistosomiasis (detectable eggs) and uninfected children (undetectable eggs).

TABLE 1 | Demographic characteristics of the study participants and the status of infection.

Demographic characteristic	Infected participants (n = 177)	Healthy uninfected controls (n = 22)
Median (IQR) years	11 (10–11)	11 (10–12)
Sex (no. M/no. F)	97/80	8/14
Median (IQR) BMI	15.36 (14–16.59)	15.89 (14.61–17.40)
Median (IQR) MUAC	18.45 (17.4–19.5)	18.86 (18.15–19.96)

n, count; m, male; f, female; IQR, interquartile range; BMI, body mass index; MUAC, mid-upper arm circumference.

There was a significant difference in concentration of sTREM and sCD23 between the infected and uninfected children (p = 0.046 and p = 0.05, respectively). The median levels of plasma IL-6, eotaxin-1, FABP, and LPS were marginally higher in the infected group but not different from the uninfected group (**Table 2**).

Concentration of Biomarkers by Infection Intensity: Soluble Triggering Receptor Expressed on Myeloid Discriminates Between Light, Moderate, and Heavy Infection

Plasma concentration of sTREM showed a difference between the three infection groups: light, moderate, and heavy; $p < 0.0001$. Between-group comparisons of other biomarkers (IL-6, eotaxin-1, FABP, sCD23, and LPS) did not show significant differences (**Figure 1**).

Biomarker Correlation: Soluble Triggering Receptor Expressed on Myeloid Correlates With Eotaxin-1 and Interleukin-6 But Not With Eggs per Gram

We next evaluated the correlation of sTREM with other biomarkers. There was a strong correlation between sTREM and eotaxin-1 ($p < 0.0001$, r = 0.7628), sTREM and IL-6 (p = 0.0191, r = 0.3898), and sTREM and sCD23 (p = 0.008, r = 0.4370). LPS and FABP did not correlate significantly with sTREM (**Figure 2**). Evaluation of the association of various biomarkers with EPG revealed no significant correlations (**Figure 3**), suggesting that presence of eggs in stool did not affect biomarker concentration.

Correlation of Biomarkers With Hemoglobin Levels: Biomarker Concentration Is Not Associated With Hemoglobin Levels

Analysis of the correlation between biomarker (sTREM, IL-6, eotaxin-1, FABP, sCD23, and LPS) concentration and hemoglobin levels revealed no significant correlation. Moreover, Hb levels in egg positive and egg negative children were not different (**Figure 4**).

DISCUSSION

Human schistosome parasites can be eliminated from the body, and the disease can be cured before progressing to complications if early-stage and sensitive diagnostic approaches are available. Additionally, prompt treatment can reverse morbidity (32). However, the currently used gold standard method is not sensitive and can only detect *Schistosoma* eggs in stool 6–8 weeks after infection (33). Therefore, there is a need to develop robust tools for the diagnosis of human schistosomiasis. In this study, the utility of systemic biomarkers (IL-6, sTREM, eotaxin-1, FABP, sCD23, and LPS) was assessed to determine their potential use as diagnostic markers.

This study reported significantly higher levels of sTREM in infected compared to uninfected children. The level of sTREM also increased with egg burden, discriminating between light, moderate, and heavy infections, $p < 0.001$. A subtle increase in levels of IL-6, eotaxin-1, FABP, sCD23, and LPS among schistosomiasis-infected children signaled a change in the

TABLE 2 | Comparison of median serum level of biomarkers between infected and uninfected children.

	Median level (25th–75th percentile)		
Biomarkers	**Infected individuals n = 177**	**Healthy controls n = 22**	***p***
IL-6	0.87 (0.2–3.9)	0.39 (0.0–4.8)	0.594
sTREM	119.00 (29.9–208.9)	10.65 (0.0–73.4)	0.046*
Eotaxin-1	30.15 (11.0–49.0)	15.59 (10.8–23.3)	0.144
FABP	315.01 (174.7–507.2)	419.06 (382.3–559.2)	0.201
sCD23	2,548.60 (1,899.0–3,356.0)	2,035.09 (1,448.0–2,939.0)	0.050*
LPS	0.26 (0.1–0.5)	0.18 (0.0–0.5)	0.773

The analysis was performed with Mann–Whitney U.

IL-6, interleukin-6; sTREM, soluble triggering receptor expressed on myeloid; FABP, fatty acid-binding protein; sCD23, soluble CD23; LPS, lipopolysaccharide.

**Significant difference at $p \leq 0.05$.*

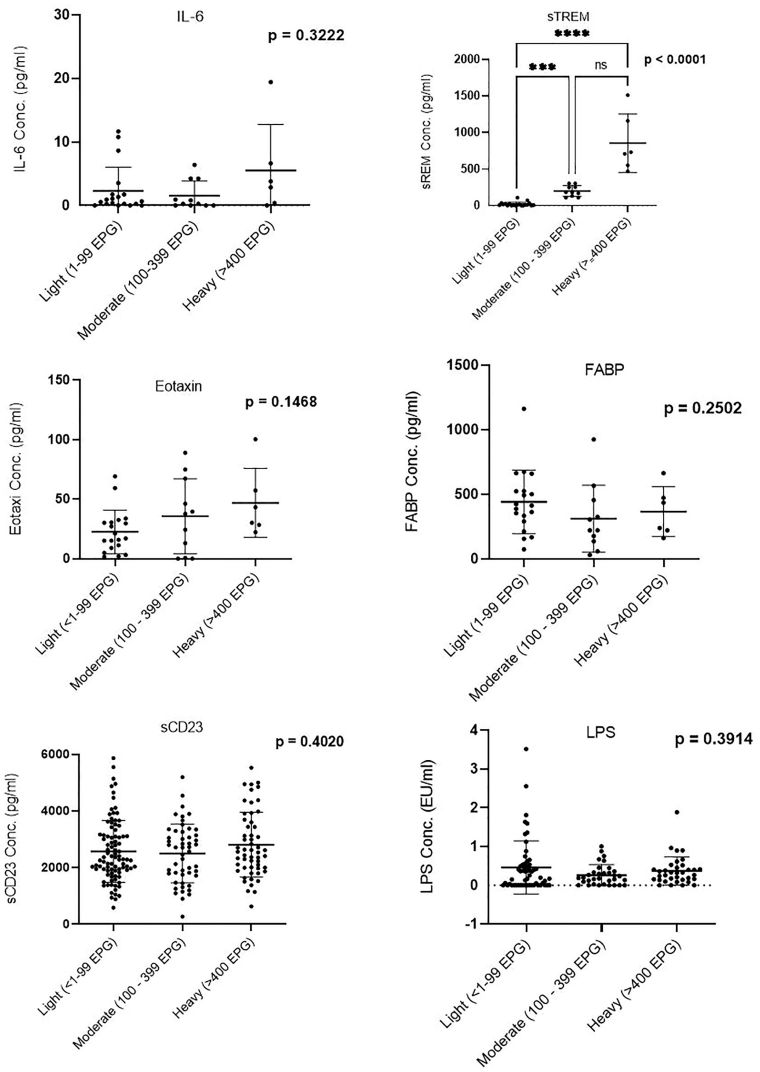

FIGURE 1 | Comparison of biomarker plasma concentration in infection groups. Groups were categorized based on the egg counts into low (1–99 EPG), moderate (100–399 EPG), and heavy (≥400 EPG). EPG, eggs per gram. *** (Moderatly significant, p < 0.0008); **** (Highly significant level p<00001). ns, not significant.

concentration of these systemic biomarkers during schistosomiasis triggered by an immune response. Increased secretion of cytokines and chemokines such as IL-6 and eotaxin-1 (CCL11) during schistosomiasis infection has been reported (34). IL-6 has both pro-inflammatory and anti-inflammatory activities (35), while chemokine eotaxin-1 plays a role in parasite-induced inflammation by mediating mobilization, recruitment, and proliferation of primary eosinophils to the site of infection (22). Their participation in immune response warrants observed increased concentration among *S. mansoni* egg-positive children, suggestive of an increase in synthesis and secretion of these systemic biomarkers. The increased secretion of sTREM among schistosomiasis-infected children is noteworthy considering the primary role in amplifying the inflammatory response to parasite infection through the adaptor protein DAP12 (18, 36). Moreover, sTREM mediates macrophage activation in response to microbial infection, and increased levels have been demonstrated in schistosome infections (20).

FABP constitutes a family of transport proteins that have been shown to induce protective immunity against *S. mansoni* (23). However, despite its role in schistosomiasis, its correlation with EPG was not significant. CD23, a 45-kDa transmembrane low-affinity IgE receptor expressed on the surface of naïve IgM+ IgD+ B cells (24), was found to be associated with the development of resistance to schistosomes (12). This phenomenon is mediated by its ability to elicit the synthesis and production of IgE (27). The CD23 receptors are also expressed on the surface of macrophages, platelets, monocytes, and eosinophils in response to schistosomiasis infection (37).

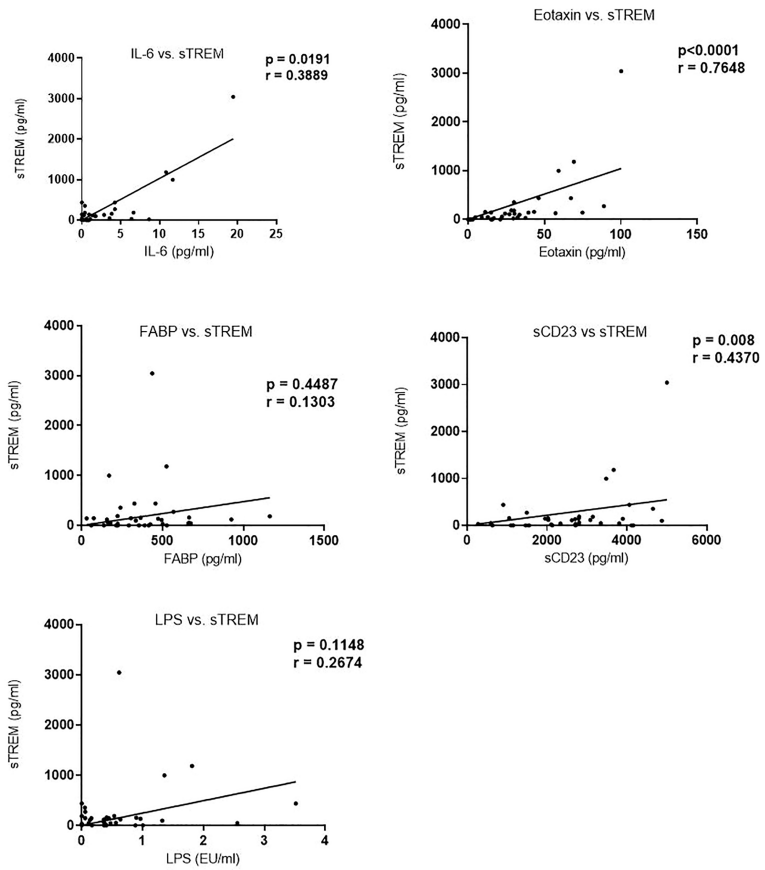

FIGURE 2 | Correlation between sTREM and other biomarkers in children in western Kenya. Data plotted are those with corresponding values (n = 36) for each of the biomarkers. sTREM, soluble triggering receptor expressed on myeloid.

Although not significant, sCD23 was higher among children with heavy infection. These findings corroborated the finding from a previous study in western Kenya, where CD23 was found to be elevated among schistosomiasis but did not correlate with egg burden (38).

The role of the assessed plasma biomarkers in immunity underpins the observed changes in their concentration during schistosomiasis. Particularly, the significant changes in sTREM levels suggest its potential use as a diagnostic marker of schistosome infection. Previous studies have demonstrated increased sTREM levels in sepsis and pneumonia patients (10, 39), albeit in non-schistosome conditions. Furthermore, our study showed consistency of sTREM concentration with egg burden ($p < 0.0001$). A strong positive correlation was also reported between sTREM and both eotaxin-1 and IL-6. These changes were consistent with the role of sTREM in triggering immunological response against infections by stimulating the secretion of IL-6 and eotaxin-1 (40). The increased secretion of sTREM in schistosome-infected children reaffirmed the applicability of sTREM in the diagnosis of schistosomiasis.

Changes in the concentration of FABP and LPS among schistosome-infected children were not significant, and their concentration did not correlate with infection intensity. Contrary to our findings, Aly et al. (41) reported a significant increase in FABP among *S. mansoni*-infected children. Nonetheless, mixed results have previously been reported on the association between LPS levels and schistosomal infection status. Onguru et al. (13) reported an increase in LPS among schistosome-infected individuals, while Klemperer et al. (28) showed that the level of LPS in schistosome-infected women did not change. We observed a subtle increase in the mean level of LPS among schistosome-infected children. There was no association between the biomarkers and hemoglobin levels, suggesting that they are not good indicators for anemia in schistosomiasis. However, Nakagawa et al. (42) reported a positive correlation between IL-6 and hemoglobin levels in individuals infected with schistosomiasis.

This study has provided evidence to suggest an increased concentration of sTREM in children infected with *S. mansoni* as well as its association with both eotaxin-1 and IL-6. These findings support the use of sTREM as a potential marker for

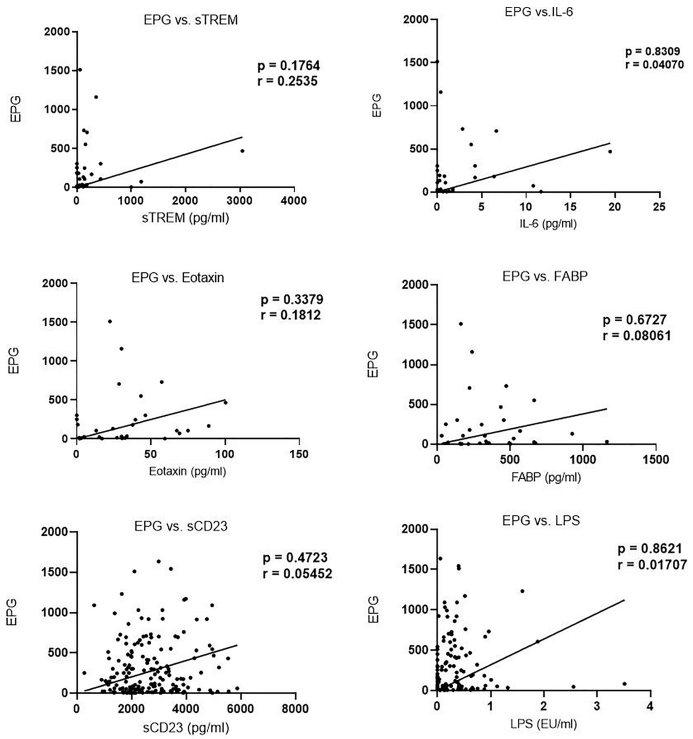

FIGURE 3 | Correlation between biomarker concentration and eggs per gram (EPG) among infected children.

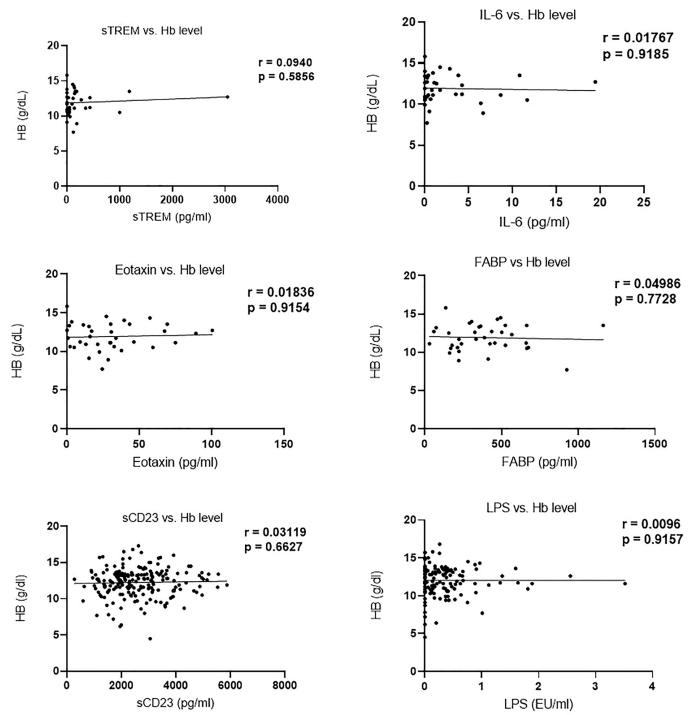

FIGURE 4 | Correlation of biomarker concentration and hemoglobin (g/dl) levels among study participants.

the diagnosis of schistosomiasis. However, large-scale studies are required to validate the specificity of this candidate marker for the diagnosis of schistosomiasis infection. Future serological investigations of schistosomiasis could focus on comparing the concentration of these biomarkers in different *Schistosoma* species to establish possible cross-species variation.

CONCLUSION

sTREM is a potential biomarker for diagnosis of schistosomiasis. A combination of biomarkers (sTREM and eotaxin-1) has the potential to complement the existing diagnostic methods.

DATA AVAILABILITY STATEMENT

The original contributions presented in the study are included in the article/**Supplementary Material**. Further inquiries can be directed to the corresponding author.

ETHICS STATEMENT

The studies involving human participants were reviewed and approved by the Scientific and Ethics Review Unit (SERU) of the Kenya Medical Research Institute (KEMRI). Written informed consent to participate in this study was provided by the participants' legal guardian/next of kin.

AUTHOR CONTRIBUTIONS

PM, MO, and LG-L participated in the study design. IO led the enrolment of subjects and the collection of specimens. BO, RH, and IO performed the laboratory assays of the specimens. BO and EM analyzed the data. BO, EM, IO, MO, PM, and LG-L wrote the manuscript. All authors participated in reviewing and editing the manuscript and concurred with the final manuscript.

FUNDING

This study was supported by the National Institutes of Allergy and Infectious Diseases (R01AI116593) awarded to LG-L.

ACKNOWLEDGMENTS

We thank the parents and children for participation in this study and appreciate the support of staff members at Kenya Medical Research Institute, Centre for Global Health Research, Kisumu, Kenya. This work is published with the permission of the Office of the Director of the Kenya Medical Research Institute.

SUPPLEMENTARY MATERIAL

The Supplementary Material for this article can be found online at: https://www.frontiersin.org/articles/10.3389/fimmu.2022.887213/full#supplementary-material

REFERENCES

1. Hailu T, Mulu W, Abera B. Effects of Water Source, Sanitation and Hygiene on the Prevalence of *Schistosoma Mansoni* Among School Age Children in Jawe District, Northwest Ethiopia. *Iranian J Parasitology* (2020) 15(1):124. doi: 10.18502/ijpa.v15i1.2535
2. Mulopo C, Chimbari MJ. Water, Sanitation, and Hygiene for Schistosomiasis Prevention: a Qualitative Analysis of Experiences of Stakeholders in Rural KwaZulu-Natal. *J Water Sanitation Hygiene Dev* (2021) 11(2):255–70. doi: 10.2166/WASHDEV.2021.182
3. WHO. Global Update on Implementation of Preventive Chemotherapy Against Neglected Tropical Diseases in 2018. *Weekly epidemiological record No 38* (2019) 94:425–40.
4. Ezeamama AE, Bustinduy AL, Nkwata AK, Martinez L, Pabalan N, Boivin MJ, et al. Cognitive Deficits and Educational Loss in Children With Schistosome Infection—a Systematic Review and Meta-Analysis. *PloS Neglected Trop Dis* (2018) 12(1):1–23. doi: 10.1371/journal.pntd.0005524
5. French MD, Evans D, Fleming FM, Secor WE, Biritwum NK, Brooker SJ, et al. Schistosomiasis in Africa: Improving Strategies for Long-Term and Sustainable Morbidity Control. *PloS Neglected Trop Dis* (2018) 12(6):1–6. doi: 10.1371/JOURNAL.PNTD.0006484
6. Chadeka EA, Nagi S, Sunahara T, Cheruiyot NB, Bahati F, Ozeki Y, et al. Spatial Distribution and Risk Factors of *Schistosoma Haematobium* and Hookworm Infections Among Schoolchildren in Kwale, Kenya. *PloS Neglected Trop Dis* (2017) 11(9):e0005872. doi: 10.1371/journal.pntd.0005872
7. Onkanga IO, Mwinzi PNM, Muchiri G, Andiego K, Omedo M, Karanja DMS, et al. Impact of Two Rounds of Praziquantel Mass Drug Administration on *Schistosoma Mansoni* Infection Prevalence and Intensity: a Comparison Between Community Wide Treatment and School Based Treatment in Western Kenya. *Int J Parasitology* (2016) 46(7):439–45. doi: 10.1016/j.ijpara.2016.01.006
8. Sang HC, Muchiri G, Ombok M, Odiere MR, Mwinzi PN. *Schistosoma Haematobium* Hotspots in South Nyanza, Western Kenya: Prevalence, Distribution and Co-Endemicity With *Schistosoma Mansoni* and Soil-Transmitted Helminths. *Parasites Vectors* (2014) 7(1):1–12. doi: 10.1186/1756-3305-7-125
9. Odiere MR, Rawago FO, Ombok M, Secor WE, Karanja DMS, Mwinzi PNM, et al. High Prevalence of Schistosomiasis in Mbita and its Adjacent Islands of Lake Victoria, Western Kenya. *Parasites Vectors* (2012) 5(1):278. doi: 10.1186/1756-3305-5-278
10. Song X, Song Y, Zhang X, Xue H. Soluble Triggering Receptor Expressed on Myeloid Cells-1 as a Novel Marker for Abdominal Sepsis. *J Surg Inf* (2017) 18 (5):577–81. doi: 10.1089/sur.2016.174
11. Coufal S, Kokesova A, Tlaskalova-Hogenova H, Snajdauf J, Rygl M, Kverka M. Urinary Intestinal Fatty Acid-Binding Protein Can Distinguish Necrotizing Enterocolitis From Sepsis in Early Stage of the Disease. *J Immunol Res* (2016) 2016: 5727312. doi: 10.1155/2016/5727312
12. Rujeni N, Nausch N, Midzi N, Gwisai R, Mduluza T, Taylor DW, et al. Soluble CD23 Levels are Inversely Associated With Atopy and Parasite Specific IgE Levels But Not With Polyclonal IgE Levels in People Exposed to Helminth Infection. *Int Arch Allergy Immunol* (2013) 161(4):333–41. doi: 10.1159/000346545
13. Onguru D, Liang Y, Griffith Q, Nikolajczyk B, Mwinzi P, Ganley-Leal L. Human Schistosomiasis is Associated With Endotoxemia and Toll-Like Receptor 2 and 4-Bearing B Cells. *Am J Trop Med Hygiene* (2011) 84 (2):321–4. doi: 10.4269/ajtmh.2011.10-0397
14. Lemarié J, Gibot S. Soluble Triggering Receptor Expressed on Myeloid Cells-1: Diagnosis or Prognosis? *Crit Care Clinics* (2020) 36(1):41–54. doi: 10.1016/j.ccc.2019.08.004

15. François B, Wittebole X, Ferrer R, Mira JP, Dugernier T, Gibot S, et al. Nangibotide in Patients With Septic Shock: a Phase 2a Randomized Controlled Clinical Trial. *Intensive Care Med* (2020) 46(7):1425–37. doi: 10.1007/s00134-020-06109-z
16. Bouchon A, Facchetti F, Weigand MA, Colonna M. TREM-1 Amplifies Inflammation and is a Crucial Mediator of Septic Shock. *nature* (2001) 410 (6832):1103–7. doi: 10.1038/35074114
17. Colonna M, Facchetti F. TREM-1 (Triggering Receptor Expressed on Myeloid Cells): a New Player in Acute Inflammatory Responses. *J Infect Dis* (2003) 187 (Supplement_2):S397–401. doi: 10.1086/374754
18. Duramaz BB, Ankay N, Yesilbas O, Kihtir HS, Yozgat CY, Petmezci MT, et al. Role of Soluble Triggering Receptor Expressed in Myeloid Cells-1 in Distinguishing SIRS, Sepsis, and Septic Shock in the Pediatric Intensive Care Unit. *Arch Pédiatrie* (2021) 28(7):567–72. doi: 10.1016/J.ARCPED.2021.06.001
19. Tessarz AS, Cerwenka A. The TREM-1/DAP12 Pathway. *Immunol Lett* (2008) 116(2):111–6. doi: 10.1016/J.IMLET.2007.11.021
20. Cheng PC, Lin CN, Chen YJ, Chang FS, Tsaihong JC, Lee KM. Triggering Receptor Expressed on Myeloid Cells (TREM)-1 Participates in *Schistosoma Mansoni* Inflammatory Responses. *Parasite Immunol* (2011) 33(5):276–86. doi: 10.1111/J.1365-3024.2011.01284.X
21. Bomfim LGS, Magalhães LS, Santos-Filho MAA, Peres NTA, Corrêa CB, Tanajura DM, et al. *Leishmania Infantum* Induces the Release of sTREM-1 in Visceral Leishmaniasis. *Front Microbiol* (2017) 8:2017.02265/BIBTEX(NOV). doi: 10.3389/FMICB.2017.02265/BIBTEX
22. Geiger SM, Jardim-Botelho A, Williams W, Alexander N, Diemert DJ, Bethony JM. Serum CCL 11 (Eotaxin-1-1) and CCL 17 (TARC) are Serological Indicators of Multiple Helminth Infections and are Driven by *Schistosoma Mansoni* Infection in Humans. *Trop Med Int Health* (2013) 18 (6):750–60. doi: 10.1111/tmi.12095
23. Vicente B, López-Abán J, Rojas-Caraballo J, Del Olmo E, Fernández-Soto P, Muro A. Protection Against *Schistosoma Mansoni* Infection Using a Fasciola Hepatica-Derived Fatty Acid Binding Protein From Different Delivery Systems. *Parasites Vectors* (2016) 9(1):216. doi: 10.1186/s13071-016-1500-y
24. Cooper AM, Hobson PS, Jutton MR, Kao MW, Drung B, Schmidt B, et al. Soluble CD23 Controls IgE Synthesis and Homeostasis in Human B Cells. *J Immunol* (2012) 188(7):3199–207. doi: 10.4049/JIMMUNOL.1102689
25. Purdue MP, Lan Q, Kemp TJ, Hildesheim A, Weinstein SJ, Hofmann JN, et al. Elevated Serum Scd23 and Scd30 Up to Two Decades Prior to Diagnosis Associated With Increased Risk of non-Hodgkin Lymphoma. *Leukemia* (2015) 29(6):1429–31. doi: 10.1038/leu.2015.2
26. Engeroff P, Vogel M. The Role of CD23 in the Regulation of Allergic Responses. *Allergy* (2021) 76(7):1981–9. doi: 10.1111/ALL.14724
27. Mwinzi PNM, Ganley-Leal L, Black CL, Secor WE, Karanja DMS, Colley DG. Circulating CD23+ B Cell Subset Correlates With the Development of Resistance to *Schistosoma Mansoni* Reinfection in Occupationally Exposed Adults Who Have Undergone Multiple Treatments. *J Inf Dis* (2009) 199 (2):272–9. doi: 10.1086/595792
28. Klemperer KM, Reust MJ, Lee MH, Corstjens PLAM, van Dam GJ, Mazigo HD, et al. Plasma Endotoxin Levels Are Not Increased in *Schistosoma Mansoni*–Infected Women Without Signs or Symptoms of Hepatosplenic Disease. *Am J Trop Med Hygiene* (2020) 102(6):1382–5. doi: 10.4269/ajtmh.19-0875
29. Dood CJ, Hoekstra PT, Mngara J, Kalluvya SE, van Dam GJ, Downs JA, et al. Refining Diagnosis of *Schistosoma Haematobium* Infections: Antigen and Antibody Detection in Urine. *Front Immunol* (2018) 9(18):2635. doi: 10.3389/fimmu.2018.02635
30. Wami W, Nausch N, Bauer K, Midzi N, Gwisai R, Simmonds P, et al. Comparing Parasitological vs Serological Determination of Schistosoma haematobium Infection Prevalence in Preschool and Primary School-Aged Children: Implications for Control Programmes. *Parasitology* (2014) 141 (14):1962–70. doi: 10.1017/S0031182014000213
31. Katz N, Chaves A, Pellegrino J. A Simple Device for Quantitative Stool Thick Smear Technique in *Schistosomiasis Mansoni*. *Rev Inst Med Trop Sao Paulo* (1972) 14(6):397–400.
32. Gunda DW, Kilonzo SB, Manyiri PM, Peck RN, Mazigo HD. Morbidity and Mortality Due to *Schistosoma Mansoni* Related Periportal Fibrosis: Could Early Diagnosis of Varices Improve the Outcome Following Available Treatment Modalities in Sub Saharan Africa? A Scoping Review. *Trop Med Infect Dis 2020* (2020) 5(1):20. doi: 10.3390/TROPICALMED5010020
33. Weerakoon KG, Gobert GN, Cai P, McManus DP. Advances in the Diagnosis of Human Schistosomiasis. *Clin Microbiol Rev* (2015) 28(4):939–67. doi: 10.1128/CMR.00137-14
34. Castro VN, Rodrigues JL, Cardoso DT, Resende SD, Magalhães FC, Souza DC, et al. Systemic Cytokine and Chemokine Profiles in Individuals With *Schistosoma Mansoni* Infection and Low Parasite Burden. *In Front Immunol* (2018) Vol. 9:2975. doi: 10.3389/fimmu.2018.02975
35. Borsini A, Di Benedetto MG, Giacobbe J, Pariante CM. Pro- and Anti-Inflammatory Properties of Interleukin *in Vitro*: Relevance for Major Depression and Human Hippocampal Neurogenesis. *Int J Neuropsychopharmacol* (2020) 23(11):738–50. doi: 10.1093/IJNP/PYAA055
36. Kardoush MI, Ward BJ, Ndao M. Identification of Candidate Serum Biomarkers for *Schistosoma Mansoni* Infected Mice Using Multiple Proteomic Platforms. *PloS One* (2016) 11(5):e0154465. doi: 10.1371/journal.pone.0154465
37. Stone KD, Prussin C, Metcalfe DD. IgE, Mast Cells, Basophils, and Eosinophils. *J Allergy Clin Immunol* (2010) 125(2 Suppl 2):S73. doi: 10.1016/J.JACI.2009.11.017
38. Onguru DO. Expression of CD23 by Schistosoma Mansoni Antigen-Activated B Cells of Highly Exposed Adult Males on the Shores of Lake Victoria, Western Kenya. Maseno University. (2016).
39. Bouchon A, Dietrich J, Colonna M. Cutting Edge: Inflammatory Responses Can Be Triggered by TREM-1, a Novel Receptor Expressed on Neutrophils and Monocytes. *J Immunol* (2019) 16410):4991–5. doi: 10.4049/jimmunol.164.10.4991
40. Jolly L, Carrasco K, Salcedo-Magguilli M, Garaud JJ, Lambden S, van der Poll T, et al. sTREM-1 is a Specific Biomarker of TREM-1 Pathway Activation. *Cell Mol Immunol* (2021) 18(8):2054–6. doi: 10.1038/s41423-021-00733-5
41. Aly IR, Diab M, El-Amir AM, Hendawy M, Kadry S. Fasciola Gigantica Fatty Acid Binding Protein (FABP) as a Prophylactic Agent Against *Schistosoma Mansoni* Infection in CD1 Mice. *Korean J Parasitology* (2012) 50(1):37. doi: 10.3347/kjp.2012.50.1.37
42. Nakagawa H, Tamura T, Mitsuda Y, Goto Y, Kamiya Y, Kondo T, et al. Inverse Correlation Between Serum Interleukin-6 and Iron Levels Among Japanese Adults: A Cross-Sectional Study. *BMC Hematol* (2014) 14(1):6. doi: 10.1186/2052-1839-14-6

Author Disclaimer: The findings and conclusions in this report are those of the authors and do not represent the views of the funding agency.

Conflict of Interest: Authors RH and LG-L was employed by company Elegance Biotechnologies.

The remaining authors declare that the research was conducted in the absence of any commercial or financial relationships that could be construed as a potential conflict of interest.

Publisher's Note: All claims expressed in this article are solely those of the authors and do not necessarily represent those of their affiliated organizations, or those of the publisher, the editors and the reviewers. Any product that may be evaluated in this article, or claim that may be made by its manufacturer, is not guaranteed or endorsed by the publisher.

frontiers | Frontiers in Immunology

ORIGINAL RESEARCH
published: 14 June 2022
doi: 10.3389/fimmu.2022.899311

Diagnostic Performance of Parasitological, Immunological, Molecular, and Ultrasonographic Tests in Diagnosing Intestinal Schistosomiasis in Fieldworkers From Endemic Municipalities in the Philippines

Ian Kim B. Tabios[1,2,3], Marcello Otake Sato[3]*, Ourlad Alzeus G. Tantengco[2], Raffy Jay C. Fornillos[1], Masashi Kirinoki[3], Megumi Sato[4], Raniv D. Rojo[2], Ian Kendrich C. Fontanilla[1], Yuichi Chigusa[5], Paul Mark B. Medina[6], Mihoko Kikuchi[7] and Lydia R. Leonardo[1,8,9,10]*

[1] Institute of Biology, College of Science, University of the Philippines Diliman, Quezon City, Philippines, [2] College of Medicine, University of the Philippines Manila, Manila, Philippines, [3] Laboratory of Tropical Medicine and Parasitology, Dokkyo Medical University, Tochigi, Japan, [4] Graduate School of Health Sciences, Niigata University, Niigata City, Japan, [5] Center for International Cooperation, Dokkyo Medical University, Tochigi, Japan, [6] Department of Biochemistry and Molecular Biology, College of Medicine, University of the Philippines Manila, Manila, Philippines, [7] Institute of Tropical Medicine, Nagasaki University, Nagasaki, Japan, [8] Office of Research Coordination, University of the East, Manila, Philippines, [9] College of Arts and Sciences, University of the Philippines Manila, Manila, Philippines, [10] University of the East Ramon Magsaysay Graduate School, Quezon City, Philippines

Schistosomiasis remains to ha/ve a significant public health impact in the Philippines. The Kato-Katz (K-K) technique is the reference standard and most used technique for definitive diagnosis of intestinal schistosomiasis for control programs in endemic regions. However, this has a very low sensitivity when applied in areas of low endemicity and patients with light infection. Hence, this study determined the diagnostic performance of immunological, molecular, parasitological, and ultrasonographic tests in diagnosing intestinal schistosomiasis in endemic municipalities in the Philippines. We performed a community-based cross-sectional study to determine the positivity of schistosomiasis in Leyte, Philippines. The diagnostic performance of five different detection techniques: (1) three stool K-K with duplicate smears; (2) soluble egg antigen IgG ELISA; (3) urine point-of-care circulating cathodic antigen (POC-CCA) test; (4) detection of *Schistosoma japonicum* circulating DNA (SjcDNA) in serum and urine samples; (5) focused abdominal ultrasound (US), were also obtained in this study. Multiple stool examinations enhanced the sensitivity of K-K from 26.2% (95% CI [16.4, 38.8]) with single stool to 53.8% (95% CI [41.1, 66.1]) and 69.2% (95% CI [56.4, 80.0]) with two and three stools from consecutive days, respectively. Among the SjcDNA nucleic acid amplification test (NAAT)-based detection assays, loop-mediated isothermal amplification (LAMP) PCR using sera had the highest sensitivity at 92.3% (95% CI

OPEN ACCESS

Edited by:
Thiago Almeida Pereira, Stanford University, United States

Reviewed by:
Edward Oliveira, Oswaldo Cruz Foundation (Fiocruz), Brazil
Fausto Edmundo Lima Pereira, Vila Velha University, Brazil

***Correspondence:**
Marcello Otake Sato
marcello@dokkyomed.ac.jp
Ian Kim B. Tabios
ibtabios2@up.edu.ph

Specialty section:
This article was submitted to Parasite Immunology, a section of the journal Frontiers in Immunology

Received: *18 March 2022*
Accepted: *09 May 2022*
Published: *14 June 2022*

Citation:
Tabios IKB, Sato MO, Tantengco OAG, Fornillos RJC, Kirinoki M, Sato M, Rojo RD, Fontanilla IKC, Chigusa Y, Medina PMB, Kikuchi M and Leonardo LR (2022) Diagnostic Performance of Parasitological, Immunological, Molecular, and Ultrasonographic Tests in Diagnosing Intestinal Schistosomiasis in Fieldworkers From Endemic Municipalities in the Philippines. Front. Immunol. 13:899311. doi: 10.3389/fimmu.2022.899311

[82.2, 97.1]) with LAMP consistently identifying more positive cases in both serum and urine samples. This study showed that single stool K-K, which remains the only diagnostic test available in most endemic areas in the Philippines, had low sensitivity and failed to identify most patients with light infection. SjcDNA detection assay and POC-CCA urine test were more sensitive than stool microscopy in detecting schistosomiasis. On the other hand, US was less sensitive than the widely utilized K-K technique in diagnosing schistosomiasis. This study emphasizes the need to revisit the use of single stool K-K in the surveillance and case detection of schistosomiasis in endemic areas of the Philippines. The availability of advanced and more sensitive diagnostic tests will help better control, prevent, and eliminate schistosomiasis in the country.

Keywords: *Schistosoma japonicum*, immunodiagnosis, LAMP, PCR, ultrasound, positivity

INTRODUCTION

Intestinal schistosomiasis caused by *Schistosoma japonicum* is a zoonotic disease with a significant public health impact in the Philippines. This neglected tropical disease is endemic in 28 of 81 provinces distributed in 12 of 18 regions (1). Approximately 12 million in 1,593 barangays are at risk of infection, with 2.5 million directly exposed to 3,012 snail-infested bodies of water, making *S. japonicum* a serious national public health problem (2). Most transmission foci are in Mindanao, particularly in the CARAGA region (3). There are 3,012 identified snail-infested bodies of water as of 2015, and 80% of these are in Mindanao, 18% in the Visayas, and only 2% in Luzon.

The reference standard and most used technique for definitive diagnosis of intestinal schistosomiasis for control programs in endemic regions is still the Kato-Katz (K-K) technique due to its simplicity and high specificity when performed by trained personnel (4, 5). However, microscopy-based techniques that detect parasite eggs in stools, like the K-K technique, have very low sensitivity when applied in regions of low endemicity and in patients with light infection (6, 7). In areas where yearly mass drug administration has been implemented, such as in endemic barangays in the Philippines, infection intensity is decreasing, with light infections (egg per gram [EPG] < 99) being more common (8). These patients with low egg count can be misdiagnosed. Hence no appropriate curative treatment is given (6, 7). Due to the low sensitivity of one stool thick smear K-K for light infections, three consecutive day stool K-K has been recommended but with limited acceptance due to the burden of collecting multiple fecal samples.

Accurate, cost-effective, and easy-to-use diagnostic tests are crucial in controlling and eliminating schistosomiasis (9). Several diagnostic techniques have been developed to improve the detection of schistosomiasis, especially in endemic areas (10). These diagnostic tests include soluble egg antigen (SEA) IgG ELISA, urine point-of-care circulating cathodic antigen (POC-CCA) test, and detection of *Schistosoma japonicum* circulating DNA (SjcDNA) in serum and urine samples using (NAAT)-based detection assays and loop-mediated isothermal amplification (LAMP) (5, 9–12). The utilization of most of these newer tests can give better results, but large-scale antigen production is still difficult (13, 14). PCR-based tests gained popularity due to their high degree of sensitivity and specificity. Previous studies have shown the utility of this test in detecting cell-free DNA in serum, urine, or saliva for *S. mansoni, S. haematobium*, and *S. japonicum* (9, 12). POC-CCA urine test has been validated in multiple African countries to diagnose *S. mansoni*, and the assay's diagnostic performance greatly varies with sensitivities ranging from 37% to 98% (15–17).

Aside from molecular and immunologic tests, focused abdominal ultrasound (US) was also helpful in diagnosing patients with sub-clinical hepatosplenic disease due to chronic schistosomiasis. This complication of schistosomiasis remains prevalent in endemic areas of the Philippines despite decreasing reports of schistosomiasis-related morbidity and mortality (18). The low sensitivity of the diagnostic test for schistosomiasis being used in endemic regions of the Philippines hinders the progress of the control and elimination program (19). It results in the persistence of sub-clinical hepatosplenic manifestations and low-intensity infections. With the national target of interrupting transmission by 2025, there is a need for more current and accurate diagnostic tests for diagnosing schistosomiasis in the Philippines. This study determined the positivity rate of intestinal schistosomiasis caused by S. japonicum in endemic places in Leyte, Philippines using orthogonal tests, including parasitological, immunological, molecular, and ultrasonographic tests.

MATERIALS AND METHODS

Ethical Considerations

This study was approved by the University of the Philippines Manila Research Ethics Board UPMREB Code 2017-369-01. Written informed consent was obtained from all participants at the beginning of the study.

Study Location

The study sites comprised eight schistosomiasis endemic barangays (the smallest administrative division in the Philippines) in the municipalities of Julita, Alang-alang, Palo, and Sta Fe in the province of Leyte (**Figure 1**). Schistosomiasis

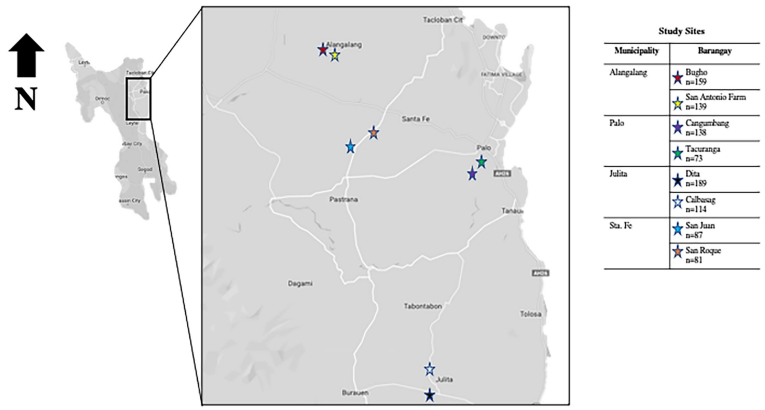

FIGURE 1 | Map showing the study sites in the schistosomiasis endemic island of Leyte, Philippines.

classification of the selected barangays in these municipalities was based on the 2013-2015 single stool sentinel survey performed by the Department of Health Region VIII. The estimated prevalence of schistosomiasis using single stool duplicate Kato-Katz thick smear based on a focal survey in 2015 was 6.01% for Alangalang (8). These municipalities have had active schistosomiasis control programs with annual mass drug administration (MDA) with praziquantel for consenting individuals aged 5-65 years old since 2008 (20, 21).

Study Design and Sampling Technique

Community-based cross-sectional study design and convenience sampling techniques were employed. Residents who were conveniently available during the fieldwork were invited to the study. All consenting individuals who submitted the required specimens were included in the study.

Eligibility Criteria

The inclusion criteria for the initial cross-sectional survey were the following: (1) age 18 to 49 years old; (2) resides in the study area for more than five years based on the interview; (3) presence of significant exposure to potentially contaminated water based on the interview; and (4) agrees to participate in the study with signed informed consent forms. Individuals with these characteristics were excluded: (1) history of hepatitis virus types B and C based on the interview; (2) severely underweight (BMI < 16.00) or extremely obese (BMI > 40.0); (3) diagnosed with other hepatic disease based on the interview; (4) known case of malignancy based on the interview; (5) pregnant and/or currently lactating based on the interview; and (6) ≥ 60 grams per day of ethanol consumption for at least ten years based on interview.

Participant Selection

One thousand ninety-five (1095) residents showed interest to participate, of which 980 completed the three-stool submission. Individuals who tested positive in at least one of the three stool K-K were given treatment (PZQ 60 mg/kg in two divided doses at least 4 hours apart) under the supervision of the MHO or other attending physician. All 980 patients who completed the three-stool submission were included in the positivity survey. For the diagnostic performance study, 230 of the 980 patients were conveniently selected from three barangays with different endemicity levels. Of the 45 stool-positive cases in the 230 patients, 25 were conveniently selected for a post-PZQ follow-up study (**Figure 2**).

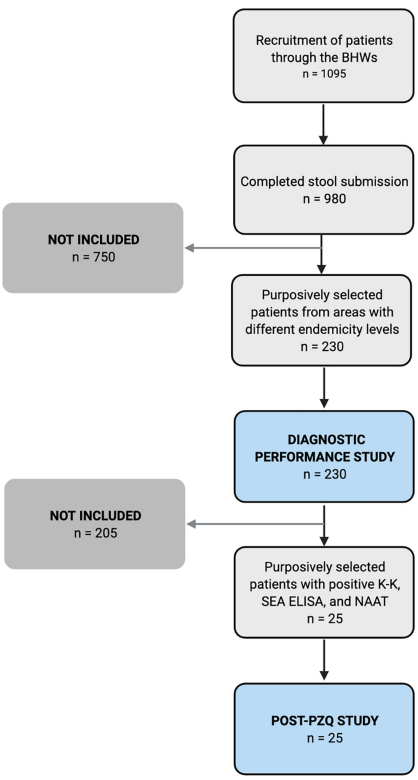

FIGURE 2 | Recruitment of participants for the diagnostic performance (n = 230) and post-treatment studies (n = 25).

Collection and Transport of Samples

Clean stool and urine containers were provided to participants. Three stool samples from three consecutive days were collected. Duplicate K-K thick smears per stool sample were immediately prepared following standard protocol and stored in sealed containers. A licensed medical technologist or trained phlebotomist performed venipuncture of the superficial veins of the upper limb. A strict aseptic technique was followed during blood extraction. At least 8-10 mL of blood were collected and transferred in 10 mL BD Vacutainer® Blood Collection Tubes with a red stopper. Blood samples were left at room temperature for 1 hour and were then centrifuged at 4,000 rpm for 10 minutes at 4°C. This was followed by another centrifugation for 10 min at 10,000 rpm at 4°C. Hemolyzed samples were excluded, and blood extraction was repeated to obtain a new specimen. Equal amounts of serum were carefully transferred into three RNase-free 2 mL tubes and stored in 4°C. Urine (3 mL) was concentrated to 140 µL using an Amicon® Ultra-15 Centrifugal Filter Device, 100K (Merck Millipore Ltd., Ireland). The urine concentrates were stored in 4°C inside sealed containers. Serum and urine samples were transported on ice. The universal precaution was done in handling the specimens. Materials like tubes and pipette tips used to evaluate the collected blood, serum, or urine were disinfected first with 0.5% hypochlorite solution, autoclaved, and disposed of as infectious waste material. Transfer of materials strictly followed regulations in the areas of origin and destination.

Schistosomiasis Diagnostic Tests

In this study, the composite reference standard or the true positives (TP) were defined as being positive in at least one of the following tests: three stool K-K (3 K-K) or detecting *S. japonicum* in at least one smear from the three stools submitted, serum LAMP (sLAMP), urine LAMP (uLAMP), serum PCR (sPCR), and urine PCR (uPCR). A true negative (TN) was designated negative in all the specified tests. Blood extraction and clinical and ultrasonographic evaluation of the liver and spleen were performed during day 1 of stool submission.

Stool Examination

Three consecutive day stool K-K with duplicate thick smears were prepared. Trained microscopists performed the duplicate examination of three stool specimens by K-K technique. Schistosomiasis infection intensity was estimated based on WHO criteria, namely low, moderate, and high-intensity infections defined as egg per gram of stool (EPG) of 1-99, 100-399, and ≥ 400, respectively (22). EPG was obtained by multiplying by 24 the number of egg found in the fecal smear. Eggs of other helminths were noted. As part of quality control, 10% of all slides were re-examined in a separate laboratory at the University of the Philippines Manila.

SEA IgG ELISA

Standard procedure for SEA ELISA was performed with slight modifications (23, 24). Anti-Human IgG-peroxidase antibody produced in rabbit and 3,3′,5,5′-tetramethylbenzidine (KPL, Gaithersburg, MD) served as the secondary antibody and substrate, respectively. Polystyrene 96-well ELISA plates (Greiner Bio-One, Co., Ltd., Germany) was sensitized separately with SEA (1µg/well). Antigen was diluted with 0.05M carbonate bicarbonate buffer (pH 9.6). After blocking with 1% bovine serum albumin (BSA) in phosphate-buffered saline with 0.05% Tween 20 (T-PBS) (T-PBS-1%BSA), serum samples were distributed on the antigen-coated wells. Human sera (0.1 mL) and secondary antibody (0.1 mL) was diluted 200-fold and 10,000-fold, respectively. Optical density (OD) at 450 nm was measured using a microplate reader. Each ELISA reaction utilized positive (8-weeks post-infected rabbit serum) and negative (diluting buffer) controls. Triplicates were performed. Mean absorbance of sera of healthy controls plus 3 standard deviations was used as cut-off value. Samples with mean absorbance higher than the cut-off value were considered positive.

Urine POC-CCA

The WHO NTD Department provided POC-CCA kit. Urine was subjected to POC-CCA following the manufacturer's instructions (Rapid Medical Diagnostics; Pretoria, South Africa). Briefly, a drop of urine was applied to the circular well in the test cassette, followed by a drop of the buffer. Two blinded observers read the test 20 minutes after adding the buffer. The presence of pink bands in both the test and control areas indicated a positive result. A faint band in the test area of the urine kit was noted and considered positive.

SjcDNA Detection in Serum and Urine Samples

Total DNA from urine was extracted using DNeasy Tissue Kit (QIAGEN Inc., Valencia, CA) according to the manufacturer's protocol. DNA extracts were stored at -20°C until use. The primer pair CF (5'-GATCGTAAATTTGGA/TACTGC-3') and CR (5'-CCAACCATAAACATATGATG-3') specific for *S. japonicum* mitochondrial cytochrome oxidase subunit 1 gene was used. The final PCR mixture composed of 1.0 µL DNA template, 13.8 µL distilled water, 2.0 µL of buffer, 1.6 µL of dNTP, 0.6 µL of 1.5 mM $MgCl_2$, 0.2 µL of 5 U/mL Taq DNA Polymerase (Takara, Otsu, Japan), and 0.5 µM each of forward and reverse primers. Standard PCR was done in an automated thermal cycler. PCR tubes were incubated for 40 cycles with the following programmed profile: initial denaturation for 10 min at 95°C and 40 cycles of amplification (denaturation for 15 sec at 95°C, annealing for 1 min at 60°C, and extension for 1 min at 72°C). The final extension segment at 72°C was prolonged to 10 min. PCR products were separated using 2.0% agarose gel in Tris-Acetic acid-EDTA buffer (TAE 40.0 mM Tris-base, 20.0 mM Acetic acid, 1.0 mM EDTA, pH 8.0) stained with 10 ng/mL ethidium bromide and left for 45 min in a TAE-filled electrophoresis chamber supplied with 100 V (Agarose gel electrophoresis; AGE). Amplicon size was estimated using the molecular weight ladders. Urine supplemented with adult *S. japonicum* DNA and urine of patients from non-endemic areas were used as positive and negative controls, respectively. A positive sample would show the presence of a single band with the expected molecular weight (254 base pairs) (24).

The closed-tube LAMP assay targeting the 28s rDNA gene was prepared in 25 µL total volume consisting of 1x Isothermal Amplification Buffer (New England Biolabs), 6 mM $MgSO_4$ (New England Biolabs), 1 mM each dNTPs (New England Biolabs), 0.8 M Betaine (Sigma-Aldrich), 0.2 µM each of Sj28F3 (5′-GCTTTGTCCTTCGGGCATTA-3′) and Sj28B3 (5′-GGTTTCGTAACGCCCAATGA-3′) primers, 1.6 µM each of Sj28FIP (5′-ACGCAACTGCCAACGTGACATACTG GTCGGCT TGTTACTAGC-3′) and Sj28BIP (5′-TG GTAGACGATCCACCTGACCCCTCGCGCACA TGTTA AACTC-3′) primers, 8 U *Bst* 2.0 WarmStart DNA Polymerase (New England Biolabs), 1x GelGreen (Sigma-Aldrich), and 1 µL gDNA sample. The reaction mixtures were incubated at 64°C for 60 min and followed by an inactivation step at 95°C for 5 min in an ABI thermal cycler. After incubation, the closed reaction tubes were visually assessed with the naked eye by two observers under a 254 nm UV transilluminator. LAMP products showing fluorescence were considered positives (25). To prevent cross contamination between samples, DNA extraction, reagent preparation, PCR and LAMP reactions, and product visualization were performed in separate rooms. Aseptic techniques and protocols to reduce DNA contamination in the laboratory were strictly adhered during processing. A closed-tube LAMP assay was used, which lessened risk of carry-over contamination of amplicons (26).

Ultrasound and Clinical Evaluation

A portable Vscan Pocket Ultrasound (GE Healthcare, United Kingdom) equipment was used in the study. US procedure followed the protocol of Ohmae etal. (27) with few modifications based on WHO recommendations (27, 28). All US examinations and interpretation at all time points were performed by two trained personnel to lessen inter-reader variability. Liver images were obtained by substernal, subcostal, intracostal, and sagittal scans, with the patients lying on their backs. Spleen images were taken by intracostal scans with the patients lying on their left sides. The following measurements were taken left liver lobe length in a longitudinal section left parasternal border; right liver lobe length based on the maximum oblique diameter using the right anterior axillary view; portal vein diameter in a right oblique view along the axis of the vessel with the internal diameter of the portal vein at its entry point into the liver; and spleen length in a left oblique view with the maximum length in a section measured through splenic hilus. Height-specific normal values for liver and spleen organometries were based on reference measurements among the healthy Chinese population due to the unavailability of data among healthy Filipinos. This reference measurement was chosen as the source study followed US protocol used in research involving schistosomiasis-induced liver pathology. Hepatosplenic enlargement and atrophy were defined as 2 standard deviations (SD) above and below the mean, respectively. Portal vein wall thickness was expressed as external diameter minus the lumen diameter. Portal vein dilatation and portal vein wall thickening were defined as 2 SD above the mean (29). US images of the liver were classified into three types based on the observed echogenic pattern and the thickness of the portal vein wall: 1.) within normal limits (WNL) or type 0 shows no echogenic patterns and absence of portal vein wall thickening; 2.) mild fibrosis or types 1 and 2 shows linear or tubular echogenic bands with mild, moderate, or severe echogenic thickening (6mm) of the portal vein wall; and 3.) network pattern or type 3 shows septal formation into regular geometric blocks, with more than three blocks surrounded by high echogenic bands (20). Analyses of images were performed in the Philippines.

Statistical Analyses

Disease positivity in each village was determined based on the results of the various examinations. The intensity of infection was calculated using the arithmetic mean of EPG in the six fecal smears. Results were presented as mean ± standard deviation (SD) for quantitative data and as percentages for qualitative data. Comparisons between groups for quantitative data were performed using the Chi-square test. One-way ANOVA was used for within-group comparisons for continuous variables. Sensitivity, specificity, positive predictive value, and negative predictive value were computed to assess diagnostic performances using a composite reference standard as recommended by WHO/TDR (30). The degree of agreement of the individual tests to the composite standard was assessed using Kappa statistics and classified according to the published guidelines (31). Double-entered data stored in EpiData 3.1 were analyzed using GraphPad Prism version 9 for Mac. A p-value of < 0.05 was considered statistically significant.

RESULTS

Supplementary Table 1 summarizes the pertinent socio-demographic and clinical characteristics of participants in the cross-sectional study. Among the dependent variables, being female ($p < 0.0438$), having no formal education (Chi-square test, $\chi^2 = 21.50$, df = 3, $p < 0.0001$), having a farming-related occupation ($p < 0.0001$), and inconsistent participation (missing at least one dose of praziquantel) in MDA in the last 2 years ($p < 0.0002$) were significantly associated with stool positivity. Other variables such as living or working near snail colonies ($p = 0.8799$), ownership of latrine ($p = 0.8535$), presence of symptoms suggestive of schistosomiasis ($p = 0.2810$), history of schistosomiasis based on stool examination ($p = 0.1351$), previous abdominal US ($p = 0.6705$), and reactivity to HBsAg ($p = 0.7172$) were not significantly correlated with stool positivity.

Table 1 presents the estimated positivity rate of schistosomiasis at 95% CI based on 3 K-K, SEA ELISA, and the hepatosplenic US. SEA ELISA reported the highest proportion of cases (41.6%) followed by 3 K-K (27.4%), with the US detecting the least cases (23.7%). The number of cases detected by SEA ELISA was higher than the other tests in all endemic barangays. Among the study sites, the highest proportion of stool positives was recorded in Dita at 35.5% (95% CI [29.2, 43.0]), while San Roque had the lowest proportion of stool positive individuals at 18.5% (95% CI [11.7, 29.2]).

Among the 980 participants, parenchymal fibrosis of the liver was the most common US pathology, observed in 232 patients

TABLE 1 | Positivity of schistosomiasis at baseline based on conventional diagnostic tests.

Study Sites		Schistosomiasis Positivity (%)					
Municipality	**Barangay**	**3 K-K**		**SEA ELISA**		**US**	
		N	**%(95% CI)**	**N**	**%(95% CI)**	**N**	**%(95% CI)**
Alangalang	Bugho n = 159	45	28.3 (22.0-36.2)	85	53.5 (46.2 – 61.8)	46	28.9 (22.7 – 36.9)
	SAF n = 139	37	26.6 (20.2-35.1)	69	49.6 (42.0 – 58.7)	23	16.5 (11.4 – 24.0)
Palo	Cangumbang n = 138	28	20.3 (14.6-28.2)	42	30.4 (23.6 – 39.2)	38	27.5 (21.0 – 36.1)
	Tacurangan n = 73	24	32.9 (23.7-45.6)	42	57.5 (47.2 – 70.1)	9	12.3 (6.7 – 22.7)
Julita	Dita n = 189	67	35.5 (29.2-43.0)	79	41.8 (35.3 – 49.5)	52	27.5 (21.8 – 34.7)
	Calbasag n = 114	29	25.4 (18.6-34.8)	31	27.2 (20.1 – 36.7)	31	27.2 (20.1 – 36.7)
Sta Fe	San Juan n = 87	24	27.6 (19.6-38.8)	37	42.5 (33.3 – 54.3)	23	26.4 (18.6 – 37.5)
	San Roque n = 81	15	18.5 (11.7-29.2)	23	28.4 (20.0 – 40.1)	10	12.3 (6.9 – 22.1)
TOTAL (n = 980)		269	27.4 (24.8-30.4)	408	41.6 (38.7 – 44.8)	232	23.7 (21.2 – 26.5)

3 K-K, Three stool Kato-Katz; (SEA) ELISA, Soluble Egg Antigen; US, Ultrasound.

(23.7%). Other US findings consistent with schistosomiasis were splenomegaly in 81 patients (8.3%), hepatomegaly in 69 patients (7.0%), and portal vein wall fibrosis in 55 patients (5.6%). Using the Ohmae etal. (27) classification, there were 748 (76.3%), 101 (10.3%), and 131 (13.4%) with type 0 (no fibrosis), types 1-2 (mild fibrosis), and type 3 (severe fibrosis) US findings, respectively (27). Most had no clinical manifestations of hepatic disease. Six had signs and symptoms suggestive of decompensated liver disease.

All examinations except for the US were more sensitive than the widely utilized K-K technique, even with repeated fecal sampling. **Table 2** summarizes the diagnostic performance parameters and agreement values with the composite reference standard (CRS) of the various examinations performed on samples from 230 patients (**Supplementary Table 2**). Multiple stool examinations enhanced the sensitivity of K-K from 26.2% (95% CI [16.4, 38.8]) with single stool to 53.8% (95% CI [41.1, 66.1]) and 69.2% (95% CI [56.4, 80.0]) with two and three stools from consecutive days, respectively. Among the SjcDNA nucleic acid amplification test (NAAT)-based detection assays, loop-mediated isothermal amplification (LAMP) PCR using sera had the highest sensitivity at 92.3% (95% CI [82.2, 97.1]) with LAMP consistently identifying more positive cases in both serum and urine samples. Regarding sample type, SjcDNA was detected more in sera than in urine samples. Although POC-CCA had the same sensitivity with three stool K-K, the former had low specificity (69.7%). US (K 0.15, 95% CI [0, 0.31]) had slight agreement while POC-CCA (K 0.34, 95% CI [0.21, 0.47]) and 1 K-K (K 0.33, 95% CI [0.17, 0.50]) had fair agreement. SEA ELISA (K 0.6, 95% CI [0.49, 0.71]), 2 K-K (K 0.62, 95% CI [0.50, 0.75]), and 3 K-K (K 0.76, 95% CI [0.66, 0.86]) had substantial agreement. All the SjcDNA detection assays had an excellent agreement.

Figure 3 depicts the correlation of EPG based on three stool K-K, an indirect measure of infection intensity, with results of single stool K-K (Spearman's rho = 0.48, $p < 0.001$), POC-CCA (Spearman's rho = 0.44, $p < 0.001$), and serum PCR (Spearman's rho = 0.268, $p = 0.075$). POC-CCA and single stool K-K were more likely to miss diagnosing light infections than the SjcDNA detection assays.

Among the 45 stool positive cases in the diagnostic study, 25 patients positive in SEA ELISA, urine LAMP (uLAMP), serum LAMP (sLAMP), POC-CCA, and 3 K-K at baseline were selected to participate in the post-chemotherapy study done at 5 and 7 months after PZQ treatment (**Table 3**). All 25 cases had negative 3 K-K at 5 and 7 months post-PZQ. The number of positive patients in sLAMP, uLAMP, and POC-CCA decreased at 5 and 7 months from 11 to 8, 15 to 6, and 10 to 4, respectively (**Figure 4**). SEA ELISA had a low rate of conversion to negativity of the results, with only five patients (16.1%) being non-reactive even at seven months post-PZQ.

TABLE 2 | Diagnostic performances of the different schistosomiasis examinations of samples collected from 230 participants using a composite reference standard (CRS).

Examination	Diagnostic Performance				
	Sensitivity (95% CI)	**Specificity (95% CI)**	**PPV (95% CI)**	**NPV (95% CI)**	**K**
sLAMP	92.3 (82.2-97.1)	100.0 (97.2-100.0)	100.0 (92.5-100.0)	97.1 (92.9-98.9)	0.95
uLAMP	83.1 (71.3-90.9)	100.0 (97.2-100.0)	100.0 (91.7-100.0)	93.8 (88.8-96.7)	0.88
POC-CCA	69.2 (56.4-79.8)	69.7 (62.0-76.5)	47.4 (37.1-57.8)	85.2 (77.8-90.5)	0.34
sPCR	87.7 (76.6-94.2)	100.0 (97.2-100.0)	100.0 (92.1-100.0)	95.4 (90.8-97.8)	0.91
uPCR	80.0 (67.9-88.5)	100.0 (97.2-100.0)	100.0 (91.4-100.0)	92.7 (87.6-95.9)	0.85
3 K-K	69.2 (56.4-80.0)	100.0 (97.2-100.0)	100.0 (90.2-100.0)	89.2 (83.6-93.1)	0.76
2 K-K	53.8 (41.1-66.1)	100.0 (97.2-100.0)	100.0 (87.7-100.0)	84.6 (78.6-89.2)	0.63
1 K-K	26.2 (16.4-38.8)	100.0 (97.2-100.0)	100.0 (77.1-100.0)	77.5 (71.1-82.8)	0.34
SEA ELISA	84.6 (73.1-92.0)	81.8 (74.9-87.2)	64.7 (53.5-74.6)	93.1 (87.3-96.5)	0.61
US	30.8 (20.2-43.6)	83.6 (76.9-88.8)	42.6 (28.6-57.7)	75.4 (68.4-81.3)	0.16

Sn, Sensitivity; Sp, Specificity; PPV, Positive Predictive Value; NPV, Negative Predictive Value; K, Kappa Coefficient; sLAMP, Serum LAMP; uLAMP, Urine LAMP; POC-CCA, Point-of-care circulating cathodic antigen urine test; sPCR, Serum PCR; uPCR, Urine PCR; 3 K-K, Three stool Kato-Katz; 2 K-K, Two stool Kato-Katz; 1 K-K, Single stool Kato-Katz; (SEA) ELISA, Soluble Egg Antigen; US, Ultrasound.

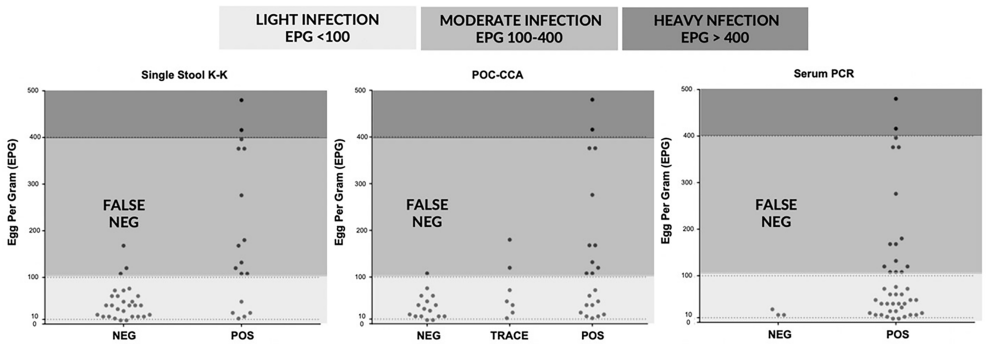

FIGURE 3 | Correlations of egg per gram (EPG) determined by three stool Kato-Katz with results of single stool Kato-Katz, point of care circulating cathodic antigen (POC-CCA) urine test, and serum PCR (n = 45).

DISCUSSION

Despite the multiple studies showing its poor sensitivity in areas of low prevalence and among patients with light infection, K-K stool examination remains the primary technique used in endemic regions for different diagnostic purposes (32–34). The low sensitivity of K-K examination using single stool has erroneously resulted in reports of the apparent absence of cases in some endemic villages in the Philippines, with some regional schistosomiasis coordinators requesting to stop mass drug administration (MDA) in their localities (8). Single stool K-K detected *S. japonicum* eggs in most patients with moderate to heavy infection but missed the diagnosis of most individuals with light infection (**Figure 3**). Although repeated fecal collection and examination improved diagnostic sensitivity, this procedure might compromise the inherent simplicity and low cost of K-K (35).

SjcDNA was detected in more sera than urine samples despite using an additional DNA concentration technique for urine, possibly due to unequal distribution of SjcDNA in the two body fluids. The mature adult schistosomes lodged in the portal or mesenteric veins and the migrating schistosomula are in direct contact with the venous blood, resulting in higher levels of SjcDNA in serum than in urine (36). Compared with tests using serum, urine-based diagnostics are generally easier, less invasive, and result in better community compliance. Using bigger volumes of urine might increase the yield of urine SjcDNA detection (9).

LAMP assay detected more individuals with SjcDNA in their sera and urine samples than conventional PCR. This is consistent with previous reports showing LAMP to be more sensitive than endpoint PCR in detecting schistosome circulating DNA in body fluids (37). Aside from better diagnostic performance, LAMP is more field applicable than PCR as the former does not require a thermal cycler and electrophoresis set-up. Although the currently applied LAMP system is not yet field-deployable due to the need for DNA extraction, modifications can be done to enable on-site LAMP analyses, such as using simpler DNA extraction protocols with shorter incubation time and lesser need for expensive equipment.

Similar to previous studies, the different diagnostic tests were compared to a composite reference standard, which is used in the absence of a single suitable "gold standard" (38–41). Despite using duplicate smears from multiple stools collected from different days, Kato-Katz is still an imperfect test to diagnose intestinal schistosomiasis. POC-CCA showed a sensitivity of 69.2%, which is superior to single and two stool K-K, comparable to three stool K-K, and inferior to the SjcDNA detection assays. Similar diagnostic sensitivity of POC-CCA against multiple stool K-K was reported in studies done in Asia (15), Africa (42), and South America (43, 44). An important limitation of POC-CCA shown in this study is its high number of false positives, resulting in low specificity (69.7%) and only fair agreement ($\kappa = 0.34$) with the CRS (**Table 2**). Previous studies have recognized that the false positives of POC-CCA might be due to its cross-reactivity with pregnancy, conditions associated with proteinuria and hematuria, and other helminthic diseases such as opisthorchiasis and hookworm infection (45, 46). Additional information is necessary to elucidate the diagnostic implications of trace results and co-infection when applying POC-CCA for Intestinal schistosomiasis.

TABLE 3 | Negative conversion of the different diagnostic examinations in 25 patients 5 and 7 months after completion of praziquantel treatment.

Periods after treatment	N of examined cases	Negative conversion, N (%)				
		3 K-K	sLAMP	uLAMP	POC-CCA	SEA ELISA
5 months	25	25 (100)	14 (56.0)	10 (40.0)	15 (60.0)	3 (9.7)
7 months	25	25 (100)	17 (68.0)	19 (76.0)	21 (84.0)	5 (16.1)

3 K-K, Three stool Kato-Katz; sLAMP, Serum LAMP; uLAMP, Urine LAMP; POC-CCA, Point-of-care circulating cathodic antigen urine test; (SEA) ELISA, Soluble Egg Antigen.

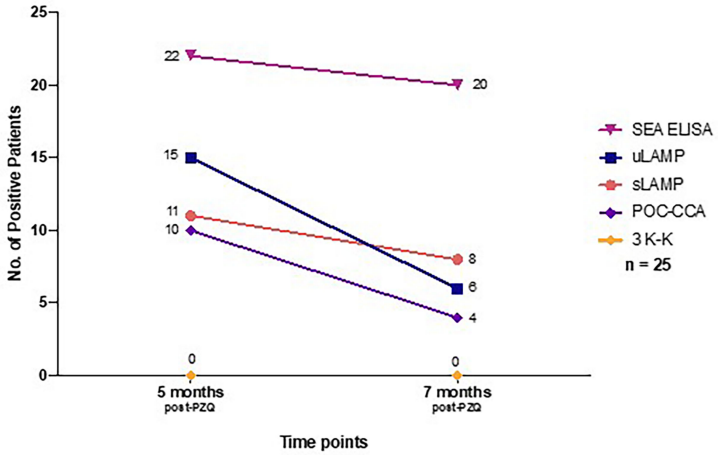

FIGURE 4 | Number of positive patients at 5 months and 7 months post-PZQ treatment based on different diagnostic tests (n = 25). PZQ, Praziquantel; SEA IgG ELISA, Soluble Egg Antigen; uLAMP, Urine LAMP; sLAMP, Serum LAMP; POC-CCA, Point-of-care circulating cathodic antigen urine test; 3 K-K, Three consecutive days stool Kato-Katz.

The other diagnostic test available, albeit not widely used in selected endemic areas of the Philippines are antibody testing using the COPT and US. US is a reliable and field applicable tool for evaluating the severity of schistosome egg-induced hepatosplenic abnormalities. US is more useful in establishing the presence of chronic disease with the presence of liver and spleen morbidities (33, 47). In this study, 20.4% were positive based on US findings. The presence of liver abnormalities based on US was higher than stool positivity, which was similarly reported in other areas of the Philippines (20). US abnormality usually manifests as hepatic fibrosis without overt clinical signs of liver disease. Even in the absence of active schistosomiasis infection, patients with this residual chronic liver pathology are at risk of developing more serious forms of liver disease from other communicable and non-communicable causes (48).

This study also assessed the ability of the different examinations to record treatment effectiveness. After completion of the PZQ regimen, all 25 cases enrolled in the treatment effectiveness study had negative stool examination at 5 and 7 months. The negative seroconversion rate of SEA ELISA remained low, while for the serum and urine LAMP assays and POC-CCA, their conversion rates to negativity of the results increased at 5 and 7 months. The remaining LAMP and POC-CCA positive cases might represent one of the following scenarios: (1) delayed clearance of the SjcDNA and CCA after successful treatment, (2) incomplete elimination of schistosomes, or (3) re-infection. Post-treatment studies using animal models have shown that SjcDNA was undetectable 6-8 weeks after PZQ exposure (37, 49, 50). Since patients in this study are constantly exposed to contaminated water bodies and might be chronically infected, delayed clearance of the SjcDNA might be due to the slower release of DNA from dead eggs deposited in the patient's tissues (12).

A significant limitation of our study is that the CRS used to estimate the diagnostic performance of the different tests consists of in-house or non-commercial assays. Although the conventional PCR and LAMP assays were based on previous publications and the current study strictly adhered to their written protocols, there are still critical procedural variations that can affect the performance of these tests. Since there are no widely available commercial tests for intestinal schistosomiasis in the Philippines, the study still opted to include the in-house molecular tests in the CRS. The purposive sampling of high-risk individuals enrolled in the cohort is another limitation. The positivity using the different tests cannot be the basis for estimating schistosomiasis prevalence and should be cautiously interpreted.

CONCLUSION

In conclusion, this study provides further evidence that single stool K-K remains the only diagnostic test available in most endemic areas in the Philippines. It had low sensitivity and failed to identify most patients with light infection. Newer diagnostic tests such as SjcDNA detection assay and POC-CCA urine test were more sensitive than stool microscopy in detecting schistosomiasis. On the other hand, US was less sensitive than the widely utilized K-K technique in diagnosing schistosomiasis. However, it is more helpful in establishing the presence of chronic disease with the presence of liver and spleen morbidities. This study emphasizes the need to revisit the use of single stool K-K in the surveillance and case detection of schistosomiasis in endemic areas of the Philippines. The availability of advanced and more sensitive diagnostic tests will help better control, prevent, and eliminate schistosomiasis in the country.

DATA AVAILABILITY STATEMENT

The original contributions presented in the study are included in the article/**Supplementary Material**. Further inquiries can be directed to the corresponding authors.

ETHICS STATEMENT

The studies involving human participants were reviewed and approved by University of the Philippines Manila Research Ethics Board UPMREB Code 2017-369-01. The patients/participants provided their written informed consent to participate in this study.

AUTHOR CONTRIBUTIONS

IT, LL, PM, and MiK formulated the research objectives and prepared the study protocol. IT, RF, RR, YC, and MK performed participant examination, data acquisition, and sample collection in the field. IT, RF, MOS, MS, MaK, YC, and MiK performed the different diagnostic tests in the field and in the laboratory. IT and OT performed data analysis and prepared the draft manuscript. LL and IF reviewed and edited the manuscript. All authors contributed to the article and approved the submitted version.

FUNDING

This study was supported by the Department of Science and Technology Philippine Council for Health Research and Development (DOST PCHRD) and Japan Society for the Promotion of Science (JSPS) Grant-in-Aid for Research (KAKENHI) Project Number: 15K08445 awarded to MK.

ACKNOWLEDGMENTS

We would like to thank DOST-PCHRD, JSPS, the University of the Philippines in Diliman and Manila, Dokkyo Medical University, and Nagasaki University for supporting the study. We would also like to express our utmost gratitude to the staff of the local government units, Department of Health Eastern Visayas CHD, and Schistosomiasis Research and Training Center led by Ms. Agnes Cuayzon who helped us in the field collection.

SUPPLEMENTARY MATERIAL

The Supplementary Material for this article can be found online at: https://www.frontiersin.org/articles/10.3389/fimmu.2022.899311/full#supplementary-material

REFERENCES

1. Leonardo L, Rivera P, Saniel O, Villacorte E, Lebanan MA, Crisostomo B, et al. A National Baseline Prevalence Survey of Schistosomiasis in the Philippines Using Stratified Two-Step Systematic Cluster Sampling Design. *J Trop Med* (2012) 2012:936128. doi: 10.1155/2012/936128
2. Leonardo L, Acosta LP, Olveda RM, Aligui GDL. Difficulties and Strategies in the Control of Schistosomiasis in the Philippines. *Acta Trop* (2002) 82:295–9. doi: 10.1016/S0001-706X(02)00022-0
3. Leonardo L, Rivera P, Saniel O, Villacorte E, Crisostomo B, Hernandez L, et al. Prevalence Survey of Schistosomiasis in Mindanao and the Visayas, The Philippines. *Parasitol Int* (2008) 57:246–51. doi: 10.1016/j.parint.2008.04.006
4. Katz N, Chaves A, Pellegrino J. A Simple Device for Quantitative Stool Thick-Smear Technique in Schistosomiasis Mansoni. *Rev Inst Med Trop Sao Paulo* (1972) 14:397–400.
5. Ajibola O, Gulumbe BH, Eze AA, Obishakin E. Tools for Detection of Schistosomiasis in Resource Limited Settings. *Med Sci (Basel Switzerland)* (2018) 6:39. doi: 10.3390/medsci6020039
6. Bärenbold O, Raso G, Coulibaly JT, N'Goran EK, Utzinger J, Vounatsou P. Estimating Sensitivity of the Kato-Katz Technique for the Diagnosis of Schistosoma Mansoni and Hookworm in Relation to Infection Intensity. *PLoS Negl Trop Dis* (2017) 11:e0005953. doi: 10.1371/journal.pntd.0005953
7. Bärenbold O, Garba A, Colley DG, Fleming FM, Assaré RK, Tukahebwa EM, et al. Estimating True Prevalence of Schistosoma Mansoni From Population Summary Measures Based on the Kato-Katz Diagnostic Technique. *PLoS Negl Trop Dis* (2021) 15:e0009310. doi: 10.1371/journal.pntd.0009310
8. Leonardo L, Chigusa Y, Kikuchi M, Kato-Hayashi N, Kawazu S-I, Angeles JM, et al. Schistosomiasis in the Philippines: Challenges and Some Successes in Control. *Southeast Asian J Trop Med Publich Heal* (2016) 47:651–66.
9. Weerakoon K, Mcmanus DP. Cell-Free DNA as a Diagnostic Tool for Human Parasitic Infections. *Trends Parasitol* (2016) 32:378–91. doi: 10.1016/j.pt.2016.01.006
10. Weerakoon K, Gobert G, Cai P, McManus DP. Advances in the Diagnosis of Human Schistosomiasis. *Clin Microbiol Rev* (2015) 28:939–67. doi: 10.1128/CMR.00137-14
11. Utzinger J, Becker SL, van Lieshout L, van Dam GJ, Knopp S. New Diagnostic Tools in Schistosomiasis. *Clin Microbiol Infect* (2015) 21:529–42. doi: 10.1016/j.cmi.2015.03.014
12. Weerakoon K, Gordon CA, McManus DP. DNA Diagnostics for Schistosomiasis Control. *Trop Med Infect Dis* (2018) 3:81. doi: 10.3390/tropicalmed3030081
13. Alarcón de Noya B, Ruiz R, Losada S, Colmenares C, Contreras R, Cesari IM, et al. Detection of Schistosomiasis Cases in Low-Transmission Areas Based on Coprologic and Serologic Criteria: The Venezuelan Experience. *Acta Trop* (2007) 103:41–9. doi: 10.1016/j.actatropica.2007.04.018
14. Rahman MO, Sassa M, Parvin N, Islam MR, Yajima A, Ota E. Diagnostic Test Accuracy for Detecting Schistosoma Japonicum and S. Mekongi in Humans: A Systematic Review and Meta-Analysis. *PLoS Negl Trop Dis* (2021) 15:e0009244. doi: 10.1371/journal.pntd.0009244
15. Dam GJ, Odermatt P, Acosta L, Bergquist R, De CJ, Kornelis D, et al. Evaluation of Banked Urine Samples for the Detection of Circulating Anodic and Cathodic Antigens in Schistosoma Mekongi and S . Japonicum Infections: A Proof-of-Concept Study. *Acta Trop* (2015) 141:198–203. doi: 10.1016/j.actatropica.2014.09.003
16. Mwinzi PNM, Kittur N, Ochola E, Cooper PJ, Campbell jr CH, King CH, et al. Additional Evaluation of the Point-of-Contact Circulating Cathodic Antigen Assay for Schistosoma Mansoni Infection. *Front Public Heal* (2015) 3:48. doi: 10.3389/fpubh.2015.00048
17. Kildemoes AO, Vennervald BJ, Tukahebwa EM, Kabatereine NB, Magnussen P, de Dood CJ, et al. Rapid Clearance of Schistosoma Mansoni Circulating Cathodic Antigen After Treatment Shown by Urine Strip Tests in a Ugandan Fishing Community – Relevance for Monitoring Treatment Efficacy and Re-Infection. *PLoS Negl Trop Dis* (2017) 11:1–16. doi: 10.1371/journal.pntd.0006054

18. Olveda RM, Gray DJ. Schistosomiasis in the Philippines: Innovative Control Approach Is Needed If Elimination is the Goal. *Trop Med Infect Dis* (2019) 4:66. doi: 10.3390/tropicalmed4020066
19. Belizario V, Destura R, Gabunada RR, Petronio-Santos JA, de la Tonga A, Amarillo ML, et al. Evaluation of Fecal and Serological Tests for the Diagnosis of Schistosomiasis in Selected Near-Elimination and Endemic Areas in the Philippines. *Southeast Asian J Trop Med Public Health* (2018) 49:198–207.
20. Olveda D, Inobaya M, Olveda R, Vinluan M, Ng S, Weerakoon K, et al. Diagnosing Schistosomiasis-Induced Liver Morbidity: Implications for Global Control. *Int J Infect Dis* (2017) 54:138–44. doi: 10.1016/j.ijid.2016.10.024
21. Department of Health Republic of the Philippines. *Schistosomiasis Control and Elimination Program* (2018). Available at: https://doh.gov.ph/node/211/pdf.pdf?page=21 (Accessed March 17, 2022).
22. Lin D-D, Liu J-X, Liu Y-M, Hu F, Zhang Y-Y, Xu J-M, et al. Routine Kato–Katz Technique Underestimates the Prevalence of Schistosoma Japonicum: A Case Study in an Endemic Area of the People's Republic of China. *Parasitol Int* (2008) 57:281–6. doi: 10.1016/j.parint.2008.04.005
23. Angeles JM, Goto Y, Kirinoki M, Leonardo L, Tongol-Rivera P, Villacorte E, et al. Human Antibody Response to Thioredoxin Peroxidase-1 and Tandem Repeat Proteins as Immunodiagnostic Antigen Candidates for Schistosoma Japonicum Infection. *Am J Trop Med Hyg* (2011) 85:674–9. doi: 10.4269/ajtmh.2011.11-0245
24. Kato-Hayashi N, Leonardo LR, Arevalo NL, Tagum MNB, Aspin J, Agsolid LM, et al. Detection of Active Schistosome Infection by Cell-Free Circulating DNA of Schistosoma Japonicum in Highly Endemic Areas in Sorsogon Province, in the Philippines. *Acta Trop* (2015) 141:178–83. doi: 10.1016/j.actatropica.2014.05.003
25. Kumagai T, Furushima-shimogawara R, Ohmae H, Wang T, Lu S, Chen R, et al. Detection of Early and Single Infections of Schistosoma Japonicum in the Intermediate Host Snail, Oncomelania Hupensis, by PCR and Loop-Mediated Isothermal Amplification (LAMP) Assay. *Am J Trop Med Hyg* (2010) 83:542–8. doi: 10.4269/ajtmh.2010.10-0016
26. Aslanzadeh J. Preventing PCR Amplification Carryover Contamination in a Clinical Laboratory. *Ann Clin Lab Sci* (2004) 34:389–96.
27. Ohmae H, Tanaka M, Hayashi M, Matsuzaki Y, Kurosaki Y, Blas B, et al. Ultrasonographic and Serologic Abnormalities in Schistosoma Japonicum Infection in Leyte, the Philippines. *Am J Trop Med Hyg* (1992) 46:89–98. doi: 10.4269/ajtmh.1992.46.89
28. Richter J, Campange G, Hatz G, Berquist NR, Jenkins JM. *Ultrasound in Schistosomiasis: A Practical Guide to the Standardized Use of Ultrasonography for the Assessment of Schistosomiasis-Related Morbidity. Second International Workshop, October 22-26 1996, Niamey, Niger: World Health Organization; 2000*. (1996).
29. Li Y, Kardorff R, Richter J, Sun KY, Zhou H, McManus DP, et al. Ultrasound Organometry: The Importance of Body Height Adjusted Normal Ranges in Assessing Liver and Spleen Parameters Among Chinese Subjects With Schistosoma Japonicum Infection. *Acta Trop* (2004) 92:133–8. doi: 10.1016/j.actatropica.2004.06.009
30. Banoo S, Bell D, Bossuyt P, Herring A, Mabey D, Poole F, et al. Evaluation of Diagnostic Tests for Infectious Diseases: General Principles. *Nat Rev Microbiol* (2006) 4:S21–31. doi: 10.1038/nrmicro1523
31. Landis JR, Koch GG. The Measurement of Observer Agreement for Categorical Data. *Biometrics* (1977) 33:159–74. doi: 10.2307/2529310
32. Zhou Y-B, Yang M-X, Wang Q-Z, Zhao G-M, Wei J-G, Peng W-X, et al. Field Comparison of Immunodiagnostic and Parasitological Techniques for the Detection of Schistosomiasis Japonica in the People's Republic of China. *Am J Trop Med Hyg* (2007) 76:1138–43. doi: 10.4269/ajtmh.2007.76.1138
33. Olveda D, Olveda R, Lam A, Chau T, Li Y, Gisparil A, et al. Utility of Diagnostic Imaging in the Diagnosis and Management of Schistosomiasis. *Clin Microbiol* (2014) 3(2). doi: 10.1016/j.drugalcdep.2008.02.002.A
34. Inobaya MT, Olveda RM, Tallo V, Mcmanus DP, Williams GM, Harn DA, et al. Schistosomiasis Mass Drug Administration in the Philippines: Lessons Learnt and the Global Implication. *Microbes Infect* (2015) 17:6–15. doi: 10.1016/j.micinf.2014.10.006
35. Liu C, Lu L, Zhang L, Bai Y, Medina A, Rozelle S, et al. More Poop, More Precision: Improving Epidemiologic Surveillance of Soil-Transmitted Helminths With Multiple Fecal Sampling Using the Kato – Katz Technique. *Am J Trop Med Hyg* (2017) 97:870–5. doi: 10.4269/ajtmh.16-0728
36. Colley DG, Secor WEA. Immunology of Human Schistosomiasis. *Parasite Immunol* (2014) 36:347–57. doi: 10.1111/pim.12087
37. Xu J, Guan ZX, Zhao B, Wang YY, Cao Y, Zhang HQ, et al. DNA Detection of Schistosoma Japonicum: Diagnostic Validity of a LAMP Assay for Low-Intensity Infection and Effects of Chemotherapy in Humans. *PLoS Negl Trop Dis* (2015) 9:e0003668. doi: 10.1371/journal.pntd.0003668
38. Knopp S, Corstjens PLAM, Koukounari A, Cercamondi CI, Ame SM, Ali SM, et al. Sensitivity and Specificity of a Urine Circulating Anodic Antigen Test for the Diagnosis of Schistosoma Haematobium in Low Endemic Settings. *PLoS Negl Trop Dis* (2015) 9:e0003752. doi: 10.1371/journal.pntd.0003752
39. Sousa MS, van Dam GJ, Pinheiro MCC, de Dood CJ, Peralta JM, Peralta RHS, et al. Performance of an Ultra-Sensitive Assay Targeting the Circulating Anodic Antigen (CAA) for Detection of Schistosoma Mansoni Infection in a Low Endemic Area in Brazil. *Front Immunol* (2019) 10:682. doi: 10.3389/fimmu.2019.00682
40. World Health Organization. *Diagnostic Target Product Profiles for Monitoring, Evaluation and Surveillance of Schistosomiasis Control Programmes*. Geneva PP - Geneva: World Health Organization (2021). Available at: https://apps.who.int/iris/handle/10665/344813.
41. Hoekstra PT, Chernet A, de Dood CJ, Brienen EAT, Corstjens PLAM, Labhardt ND, et al. Sensitive Diagnosis and Post-Treatment Follow-Up of Schistosoma Mansoni Infections in Asymptomatic Eritrean Refugees by Circulating Anodic Antigen Detection and Polymerase Chain Reaction. *Am J Trop Med Hyg* (2022) 106:1240–6. doi: 10.4269/ajtmh.21-0803
42. Colley DG, Binder S, Campbell C, King CH, Tchuem Tchuenté L-A, N'Goran EK, et al. A Five-Country Evaluation of a Point-of-Care Circulating Cathodic Antigen Urine Assay for the Prevalence of Schistosoma Mansoni. *Am J Trop Med Hyg* (2013) 88:426–32. doi: 10.4269/ajtmh.12-0639
43. Bezerra FSM, Leal JKF, Sousa MS, Pinheiro MCC, Ramos AN, Silva-Moraes V, et al. Evaluating a Point-of-Care Circulating Cathodic Antigen Test (POC-CCA) to Detect Schistosoma Mansoni Infections in a Low Endemic Area in North-Eastern Brazil. *Acta Trop* (2018) 182:264–70. doi: 10.1016/j.actatropica.2018.03.002
44. Graeff-Teixeira C, Favero V, Pascoal VF, de Souza RP, Rigo F, de V, et al. Low Specificity of Point-of-Care Circulating Cathodic Antigen (POCCCA) Diagnostic Test in a Non-Endemic Area for Schistosomiasis Mansoni in Brazil. *Acta Trop* (2021) 217:105863. doi: 10.1016/j.actatropica.2021.105863
45. Greter H, Krauth SJ, Ngandolo BNR, Alfaroukh IO, Zinsstag J, Utzinger J. Validation of a Point-of-Care Circulating Cathodic Antigen Urine Cassette Test for Schistosoma Mansoni Diagnosis in the Sahel, and Potential Cross-Reaction in Pregnancy. *Am J Trop Med Hyg* (2016) 94:361–4. doi: 10.4269/ajtmh.15-0577
46. Homsana A, Odermatt P, Southisavath P, Yajima A, Sayasone S. Cross-Reaction of POC-CCA Urine Test for Detection of Schistosoma Mekongi in Lao PDR: A Cross-Sectional Study. *Infect Dis Poverty* (2020) 9:1–9. doi: 10.1186/s40249-020-00733-z
47. Carlton EJ, Hsiang M, Zhang Y, Johnson S, Hubbard A, Spear RC. The Impact of Schistosoma Japonicum Infection and Treatment on Ultrasound-Detectable Morbidity: A Five- Year Cohort Study in Southwest China. *PLoS Negl Trop Dis* (2010) 4:e685. doi: 10.1371/journal.pntd.0000685
48. Andrade Z. Schistosomiasis and Liver Fibrosis. *Parasite Immunol* (2009) 31:656–63. doi: 10.1111/j.1365-3024.2009.01157.x
49. Xia CM, Rong R, Lu ZX, Shi CJ, Xu J, Zhang HQ, et al. Schistosoma Japonicum: A PCR Assay for the Early Detection and Evaluation of Treatment in a Rabbit Model. *Exp Parasitol* (2009) 121:175–9. doi: 10.1016/j.exppara.2008.10.017
50. Ullah H, Qadeer A, Giri BR. Detection of Circulating Cell-Free DNA to Diagnose Schistosoma Japonicum Infection. *Acta Trop* (2020) 211:105604. doi: 10.1016/j.actatropica.2020.105604

Conflict of Interest: The authors declare that the research was conducted in the absence of any commercial or financial relationships that could be construed as a potential conflict of interest.

this article, or claim that may be made by its manufacturer, is not guaranteed or endorsed by the publisher.

frontiers | Frontiers in Immunology

ORIGINAL RESEARCH
published: 22 June 2022
doi: 10.3389/fimmu.2022.868077

Schistosoma mansoni Fibroblast Growth Factor Receptor A Orchestrates Multiple Functions in Schistosome Biology and in the Host-Parasite Interplay

Xiaofeng Du[1,2], *Donald P. McManus*[1,2], *Conor E. Fogarty*[3], *Malcolm K. Jones*[4] *and Hong You*[1*]

[1] Infection and Inflammation Program, QIMR Berghofer Medical Research Institute, Brisbane, QLD, Australia, [2] Faculty of Medicine, The University of Queensland, Brisbane, QLD, Australia, [3] Genecology Research Centre, University of the Sunshine Coast, Brisbane, QLD, Australia, [4] School of Veterinary Science, The University of Queensland, Gatton, QLD, Australia

OPEN ACCESS

Edited by:
Thiago Almeida Pereira, Stanford University, United States

Reviewed by:
Benyamin Rosental, Ben-Gurion University of the Negev, Israel
Matthew Berriman, Wellcome Sanger Institute (WT), United Kingdom

***Correspondence:**
Hong You
Hong.You@qimrberghofer.edu.au

Specialty section:
This article was submitted to Parasite Immunology, a section of the journal Frontiers in Immunology

Received: *02 February 2022*
Accepted: *26 May 2022*
Published: *22 June 2022*

Citation:
Du X, McManus DP, Fogarty CE, Jones MK and You H (2022) Schistosoma mansoni Fibroblast Growth Factor Receptor A Orchestrates Multiple Functions in Schistosome Biology and in the Host-Parasite Interplay. Front. Immunol. 13:868077. doi: 10.3389/fimmu.2022.868077

Stem cells play significant roles in driving the complex life cycle of *Schistosoma mansoni*. Fibroblast growth factor (FGF) receptor A (SmFGFRA) is essential for maintaining the integrity of schistosome stem cells. Using immunolocalization, we demonstrated that SmFGFRA was distributed abundantly in germinal/stem cells of different *S. mansoni* life stages including eggs, miracidia, cercariae, schistosomula and adult worms. Indeed, SmFGFRA was also localized amply in embryonic cells and in the perinuclear region of immature eggs; von Lichtenberg's layer and the neural mass of mature eggs; the ciliated surface and neural mass of miracidia; the tegument cytosol of cercariae, schistosomula and adult worms; and was present in abundance in the testis and vitellaria of adult worms of *S. mansoni*. The distribution pattern of SmFGFRA illustrates the importance of this molecule in maintaining stem cells, development of the nervous and reproductive system of schistosomes, and in the host-parasite interplay. We showed SmFGFRA can bind human FGFs, activating the mitogen activated protein kinase (MAPK) pathway of adult worms *in vitro*. Inhibition of FGF signaling by the specific tyrosine kinase inhibitor BIBF 1120 significantly reduced egg hatching ability and affected the behavior of miracidia hatched from the treated eggs, emphasizing the importance of FGF signaling in driving the life cycle of *S. mansoni*. Our findings provide increased understanding of the complex schistosome life cycle and host-parasite interactions, indicating components of the FGF signaling pathway may represent promising targets for developing new interventions against schistosomiasis.

Keywords: *Schistosoma mansoni*, fibroblast growth factor receptor A, stem cell marker, immunolocalization, host-parasite interplay

INTRODUCTION

Schistosomiasis is first on the scale of devastating parasitic helminth diseases, causing more than 250 million human infections in 74 countries and leading to considerable morbidity and an estimated loss of 1.9 million disability-adjusted life years (1–3). There are three main schistosome species (*Schistosoma mansoni, S. japonicum* and *S. haematobium*) causing human schistosomiasis. Currently no human vaccines are available and, as clinical treatment relies entirely on the single drug praziquantel, the potential emergence of drug resistance is an ever-present concern (1). Recent studies have demonstrated that stem cells play vital roles in driving and maintaining the complex schistosome life cycle (4–8). Adult schistosomes parasitize mammals and lay eggs many of which eventually escape these definitive hosts in feces or urine. An egg gives rise to a ciliated larva, the miracidium, which infects a specific freshwater snail host and then undergoes a dramatic body conversion to produce an obligate asexually-reproducing parasitic stage, the mother sporocyst. Endogenous proliferation of stem cells in mother sporocysts leads to a new asexual stage - the daughter sporocyst. These 'daughters', in turn, can generate by stem cell proliferation either more daughters, or the next stage, the migratory cercaria (-ae), that escapes from the snail into the aquatic environment. The cercariae then penetrate the skin of a mammalian host to transform into a schistosomulum (-a), before entering the host vascular system. These juvenile schistosomes develop a functional digestive system and sexual reproductive organs through *de novo* processes that commence by differentiation of pluripotent stem cells (6), early in the development of schistosomula. The larvae then mature into sexual dimorphic adults and the female worms lay eggs into the mesenteric venules of the host (9). Given the critical roles that stem cells play in schistosome biology (10), targeting genes vital for controlling the integrity of these cells may, by impeding parasite development at critical phases of the life cycle, provide a novel strategy for drug and/or vaccine development against schistosomiasis.

The fibroblast growth factor (FGF) signaling pathway in mammals is critically involved in a variety of processes during embryonic development and adult homeostasis through promoting cell proliferation, cell differentiation, cell survival, tissue repair/regeneration, drug resistance, and apoptosis (7, 11–15). Significantly, FGF signaling is crucial in stem cell control in various model systems including both vertebrates (5, 16–18) and invertebrates (14, 19–22). The mammalian FGF pathway is activated by binding FGF ligands to FGFRs, thereby phosphorylating mitogen-activated protein kinase (MAPK), phosphoinositide 3-kinase (PI3K)/AKT (protein kinase B, also called PKB), phospholipase C gamma (PLCγ), and signal transducers and activators of transcription (STAT) (23–25). The FGF signalling pathway has been shown present in various multicellular organisms ranging from vertebrates, such as humans and mice (13, 26–31), to invertebrates including *Drosophila* (32, 33) and the free-living nematode, *Caenorhabditis elegans* (34, 35). The FGF signaling pathway has also been demonstrated in members of the animal clade Lophotrochozoa (6, 7, 14, 20, 36, 37). For the Platyhelminthes, flatworms capable of exquisite regenerative or generative capacity, the FGF pathway has been described in free-living triclad planarians, with expression of FGF receptors found in stem cells of Dugesia japonica (19, 20) and Schmidtea mediterranea (21, 22). *Similarly, three* genes encoding FGFRs (*emfr1*, *emfr2*, *emfr3*) have been identified in the cestode *Echinococcus multilocularis*, a parasite capable of invasive growth in host livers as it undergoes internal asexual generation of abundant infectious tapeworm scoleces for infection of a new host (14). Expression patterns of the *E. multilocularis* FGFs suggested that only *emfr2* and *emfr3* could be expressed in the parasite's stem cells or their immediate progeny, while *emfr1* did not have a typical stem cell-specific expression pattern (14). Whereas no endogenous FGF ligands were identified in *E. multilocularis*, human FGF ligands were shown able to activate all three *Echinococcus* FGFRs and stimulate parasite development *in vitro* (14), thereby highlighting the importance of the interaction between host-derived hormones and the corresponding receptors of evolutionarily conserved parasite signaling pathways (14).

To date, two FGFR-encoding genes (*SmfgfrA* and *SmfgfrB*) have been described in *S. mansoni* (6, 36). *SmfgfrA* is expressed in the germinal cells of larvae (4, 6) and the stem cells of adult *S. mansoni* (7, 38, 39), emphasizing the vital roles SmFGFRA plays in the maintenance and proliferation of *S. mansoni* stem cells (6, 7, 27, 40). Hahnel *et al.* found the transcriptional levels of both SmFGRFs were upregulated following adult worm pairing, indicative of their importance in schistosome reproduction (36).

The role played by FGF signaling in different schistosome life cycle stages is unclear. To address this issue, we examined the expression of SmFGFRA in different developmental stages of *S. mansoni* by real-time PCR and immunolocalization and explored the co-localization of SmFGFRA and stem cells in adult worms. Furthermore, by employing protein binding and phosphorylation assays, we determined the binding affinity between SmFGFRA and host FGF ligands and showed this binding can activate the MAPK pathway in *S. mansoni*. In addition, we assessed the effects of the inhibitor BIBF 1120 on the development of eggs and the behavior of hatched miracidia of *S. mansoni*. BIBF 1120 is a highly selective adenosine triphosphate (ATP)-competitive tyrosine kinase (TK) inhibitor that has been shown to significantly reduce the numbers of somatic stem cells in adult worms of *S. mansoni* (36).

MATERIALS AND METHODS

Ethics

All experiments were approved by the Animal Ethics Committee (ethics number P242) of the QIMR Berghofer Medical Research Institute. The study was conducted according to the guidelines of the National Health and Medical Research Council of Australia, as published in the Australian Code of Practice for the Care and Use of Animals for Scientific Purposes, 7th edition, 2004 (www.nhmrc.gov.au). All work involving live *S. mansoni* life cycle

stages was performed in quarantine-accredited laboratories as required by Australian Biosecurity law.

Parasites

Swiss mice (female, 6 weeks old) were infected subcutaneously with 100 *S. mansoni* cercariae. Seven weeks post-infection the mice were euthanised and adult worms were obtained by portal perfusion with 37°C pre-warmed RPMI Medium 1640 (Gibco, Sydney, Australia). Mouse livers were removed at necropsy and liver eggs were isolated (41, 42), with immature and mature liver eggs separated as described (43). Miracidia were harvested by hatching mature eggs in deionized water under light (41). *S. mansoni* cercariae were obtained by shedding infected *Biomphalaria glabrata* snails under bright light. Schistosomula were obtained by mechanical transformation of cercariae *in vitro* as described (2), and cultured in Basch's medium (2) for five days to produce 5-day old schistosomula.

Sequence Analysis of SmFGFRs

Searches for SmFGFRs sequences were conducted using genome version Smansoni_v7, GCA_000237925.3 (44, 45) on the WormBase ParaSite website (https://parasite.wormbase.org/Schistosoma_mansoni_prjea36577/Info/Index). Searches for homologous FGFR protein sequences were performed using the Basic Local Alignment Search Tool (BLAST) on the NCBI website (http://blast.ncbi.nlm.nih.gov/Blast.cgi) and the WormBase ParaSite website (http://parasite.wormbase.org/Multi/Tools/Blast). Protein sequence identity was analyzed using EMBOSS Needle (https://www.ebi.ac.uk/Tools/psa/emboss_needle/) (46, 47). Signal peptides were predicted by the SignalP-5.0 Server (http://www.cbs.dtu.dk/services/SignalP/). Protein molecular weight and isoelectric point were calculated using the ExPASy-Compute pI/Mw tool (http://web.expasy.org/compute_pi/). Domain predictions were conducted using the Simple Modular Architecture Research Tool (SMART) (http://smart.embl-heidelberg.de/). Prediction of SmFGFRA 3D structures was performed using I-TASSER (https://zhanglab.dcmb.med.umich.edu/I-TASSER/) (48–50). Searching the *S. mansoni* single-cell atlas was carried out using the SchistoCyte resource (http://www.collinslab.org/schistocyte/) (39, 51).

SmfgfrA Transcription Levels in Different Life Cycle Stages Determined by Real-Time PCR

Total RNAs were extracted from *S. mansoni* eggs, miracidia, cercariae, schistosomula and adult male and female worms using RNeasy Mini Kits (Qiagen, Melbourne, Australia), followed by cDNA synthesis using QuantiTect Reverse Transcription Kits (Qiagen). Quantitative real-time PCR (qPCR) was performed with QuantiNova SYBR® Green PCR Kits (Qiagen) using a Corbett Rotor Gene 6000 Real-Time PCR system. Forward primer (5'-ATGGGACTCAATTACGCATT-3') and reverse primer (5'-CACCACTGTCTTCCGACCTG-3') for *SmfgfrA* were designed using the Primer 3 software (http://frodo.wi.mit.edu/), and the specificity of the primer sequences was confirmed by BLAST. The *S. mansoni* Glyceraldehyde-3-Phosphate Dehydrogenase (GAPDH) housekeeping gene was used as reference gene (52). The qPCR reactions comprised 10 µl 2xSYBR Green PCR Master Mix, 100 ng cDNA, and 0.7 µM of each primer. The cycling parameters were as follows: 95°C for 2 min, 40 cycles of 95°C for 5 s and 58°C for 10 s. Relative gene transcriptional levels were normalized to the GAPDH gene and determined using the $2^{-\Delta\Delta Ct}$ calculation.

Protein Expression, Purification and Antibody Generation

The SmFGFRA extracellular ligand binding domain (from T^{39} to L^{386}, SmFGFRA-L) coding sequence (excluding signal peptide) was amplified from *S. mansoni* cDNA using a forward primer (5'-TACTTCCAATCCAATGCAACTTTACACTGTGCGTGTGACGC-3') and a reverse primer (5'-TTATCCACTTCCAATGTTATTATCACAATCCACTATCCCCTATAGGACAAATTTTC-3'). The full length SmFGFRA (from L^{27} to H^{918}) coding gene, without signal peptide, was amplified from *S. mansoni* cDNA using a forward primer (5'-TACTTCCAATCCAATGCACTTGAGTGTAAATCACAATCAATGTACGAA-3') and a reverse primer (5'-TTATCCACTTCCAATGTTATTATCACTAGTGTAAATACTGTCGCGGTTCCAAGT-3'). Both fragments were expressed in *Escherichia coli* after cloning into the pET His6 TEV LIC cloning vector (1B) (a gift from Scott Gradia, Addgene, Watertown, Massachusetts, USA); a Ligation Independent Cloning (LIC) fusion tag was added at the 5' end of each primer (underlined in each primer sequence). The vector was linearized using the SspI-HF restriction enzyme (New England Biolabs, Melbourne, Australia) and then purified using a QIAquick Gel Extraction Kit (Qiagen). The linearized vector and insert were treated with T4 polymerase and then annealed at a molecular ratio of 1:3 at room temperature for 5 min followed by the addition of 1 µl 25 mM EDTA to stop the reaction. After sequence confirmation, the reconstructed vectors were transformed into *E. coli* (Rosseta strain) for expression induced with 1 mM IPTG (isopropyl-β-D-thiogalactopyranoside) (Sigma-Aldrich, Sydney, Australia) at 37°C for 3 h. Recombinant protein was purified using a Ni-NTA His-tag affinity kit (Qiagen). HALT protease inhibitor cocktail (Thermo Fisher Scientific) was added during protein purification. The His-tag on the purified protein was then removed by ProTEV Plus (Promega, Sydney, Australia) according to the manufacturer's instructions.

A polyclonal antibody against the recombinant SmFGFRA-L (rSmFGFRA-L) was generated in SWISS mice (8 weeks old, female). Briefly, five mice were injected intraperitoneally with rSmFGFRA-L protein (25 µg/each mouse) adjuvanted with Montanide ISA 720 VG (SEPPIC, Courbevoie, France) three times at 2-weekly intervals (3). Blood was collected 2 weeks after the third injection. The titre of the antibody was determined using an enzyme-linked immunosorbent assay (ELISA) as described (53–55). In brief, an ELISA plate (Thermo Fisher Scientific, Brisbane, Australia) was coated with rSmFGFRA-L protein (1 µg/ml, 100 µl/well) in 0.05 M Carbonate-Bicarbonate coating buffer (pH 9.6) overnight at 4°C, followed by blocking at

37°C for 1 h with blocking buffer [1% (w/v) bovine serum albumin (BSA) (Sigma-Aldrich) in PBS containing 0.05% (v/v) Tween-20 (PBST)]. Serially diluted serum in blocking buffer (100 µl/well) was added and the plate incubated at 37°C for 1 h. As negative controls, naïve mouse serum was used. Following 3 x washes with 0.05% PBST, a secondary antibody, Novex™ Goat anti-Mouse IgG (H+L) - cross-adsorbed, horseradish peroxidase (HRP) conjugate (Thermo Fisher Scientific), was added (1:2,000, 100 µl/well) and the plate was incubated at 37°C for 1 h. After 3 x washes with 0.05% PBST, 1-Step™ Ultra TMB-ELISA Substrate Solution (Thermo Fisher Scientific) was added (50 µl/well) followed by 10 min incubation at room temperature prior to stopping the reaction with 2 M sulphuric acid (50 µl/well). The absorbance of each well was measured at 450 nm using a POLARstar OPTIMA multi-detection microplate reader (BMG LABTECH, Victoria, Australia). A positive antibody response was defined as an OD450 higher than 2.1 times the mean of the OD450 of serum samples from control mice.

Western Blot Analysis

S. mansoni, *S. japonicum*, and *S. haematobium* soluble worm antigen preparation (SWAP) (53) and *S. mansoni* soluble egg antigen (SEA) (56) were prepared as described. The mouse anti-rSmFGFRA-L serum was utilized in western blots to probe electrophoresed schistosome SWAP and *S. mansoni* SEA. Protein samples were separated on 12% SDS-PAGE gels and transferred to an Immun-Blot low fluorescence-PVDF membrane (Bio-rad, Sydney, Australia). The membrane was first blocked with Odyssey Blocking Buffer (PBS) (LI-COR Biosciences, Lincoln, Nebraska, USA) for 1 h at room temperature. Then, the membrane was incubated with the mouse anti-rSmFGFRA-L serum (1:100 diluted in Odyssey buffer with 0.1% Tween-20) for 1 h followed by four washes in phosphate-buffered saline (PBS) plus 0.1% Tween-20 (0.1% PBST). Subsequently, the membrane was incubated with IRDye-labeled 680LT goat anti-mouse IgG antibody (Li-COR Biosciences) (1:15,000 diluted in Odyssey buffer with 0.1% Tween-20 and 0.01% SDS) for 1 h with shaking in a dark chamber. After washing (4X) with 0.1% PBST, the membrane was dried in the dark and visualized using the Odyssey CLx Infrared Imaging System (53).

Immunolocalization of SmFGFRA in Different Life Cycle Stages of *S. mansoni* and Co-Localization of SmFGFRA and Stem Cells

S. mansoni adult worms, immature eggs, mature eggs, miracidia, cercariae, and 5-day old schistosomula were fixed in 10% (w/v) formalin in PBS prior to paraffin embedding. Sections (3-4 µm) prepared from the paraffin blocks were affixed to positively charged adhesive slides, air-dried overnight at 37°C and then dewaxed and rehydrated through xylol and descending graded alcohols to water. Subsequently, the sections were transferred to Dako Target Retrieval Buffer (pH 9.0) (Dako, Carpinteria, California, USA) and subjected to 30 min heat antigen retrieval at 95°C. This was followed by washing three times in 0.1% PBST. Sections were blocked in Biocare Medical Background Sniper with 2% (w/v) BSA (Sigma-Aldrich) for 15 min to stop non-specific binding and then incubated at room temperature overnight with mouse anti-rSmFGFRA-L antibody (1:50 dilution). After washing three times with 0.1% PBST, the sections were incubated with Alexa Fluor® 555 donkey anti-mouse IgG (Invitrogen, Melbourne, Australia) (1:300 dilution) for 2 h at room temperature.

To determine the co-localization of SmFGFRA and stem cells in adult *S. mansoni*, freshly perfused worms were cultured overnight in RPMI complete medium [RPMI Medium 1640 (Gibco, Sydney, Australia) supplemented with 10% (v/v) heat-inactivated fetal bovine serum (FBS, Gibco) and 100 IU/ml penicillin and 100 µg/ml streptomycin (Gibco)] at 37°C in 5% CO_2. Then the worms were incubated for 24 h with 10 µM EdU (thymidine analog 5-ethynyl-2'-deoxyuridine) (Thermo Fisher Scientific), which only stains stem cells in schistosomes (7). The stained worms were fixed in 10% formalin, paraffin embedded and sectioned. Sections (4 µm) of EdU-labeled adult worms were subjected to EdU detection using a Click-iT™ EdU Cell Proliferation Kit (Alexa Fluor™ 488 dye) (Thermo Fisher Scientific) according to the manufacturers' instructions. Then the same sections were subjected to SmFGFRA immunolocalization as described above. Nuclei in all tissue sections were also stained with diamidino-2-phenylindole (DAPI) gold (Invitrogen) and visualized using a Zeiss 780 NLO confocal microscope (Zeiss, Oberkochen, Germany).

Protein Binding Assay

The binding affinity between rSmFGFRA-L/human FGFR1 and human acidic FGF (aFGF)/basic FGF (bFGF) was determined using the Octet RED 96 System (FortéBio, Menlo Park, California, USA) in standard Greiner black 96-well microplates (Sigma-Aldrich) as described (53). Briefly, to investigate the binding between rSmFGFRA-L and human aFGF/bFGF, the rSmFGFRA-L protein was biotinylated using a NHS-PEO4-biotin kit (Thermo Fisher Scientific), desalted with a Zeba Spin Desalting Column (Thermo Fisher Scientific), and then the protein was immobilized to a Streptavidin Biosensor (FortéBio). Prior to the assay, the Biosensors were hydrated in kinetic buffer (PBS with 15 mM NaCl, 0.1 mg/ml BSA, 0.002% Tween-20) for 60 min. Subsequently, a duplicate set of Biosensors were first incubated in kinetic buffer for 300 s as baseline and followed by immobilization for 600 s in 200 µl of 150 ng/µl biotinylated rSmFGFRA-L protein. Next, the Biosensors were washed in kinetic buffer for another 300 s. Finally, the sensors were exposed to a series (200 µl volume) of diluted concentrations of human aFGF/bFGF (Thermo Fisher Scientific). To further explore whether the binding affinity between human bFGF and rSmFGFRA-L is comparable to that between human bFGF and human FGFR1, human bFGF (8 ng/µl) was biotinylated and immobilized to Biosensors and then exposed to different concentrations (30 ng/µl and 23 ng/µl) of rSmFGFR-L and recombinant extracellular ligand binding domain of human FGFR1 (R^{22}-I^{376}) (FGFR1-L) (Sigma-Aldrich). PBS was used as a negative control. The association

of the two proteins was detected for 1000 s followed by dissociation in the kinetic buffer for 1000 s. Experiments were run at 30°C with the orbital agitation of the microplate set to 1000 rpm. Data were analyzed using the FortéBio Data Analysis 7.1 program and included a double reference subtraction. The sample subtraction was conducted using PBS as a reference control, and sensor subtraction was performed on all samples automatically (53).

Detection of MAPK Using an Anti-Phospho-P44/42 MAPK (Erk1/2) Antibody

An anti-phospho-P44/42 MAPK (Erk1/2) (Thr202/Tyr204) antibody (Cell Signaling Technology, New England Biolabs, Ipswich, USA) was used to detect activated (phosphorylated) extracellular signal regulated kinases 1 and 2 (Erk1/2) in *S. mansoni* adult worms (53) following stimulation with human aFGF or bFGF. Briefly, freshly perfused *S. mansoni* adult worms were cultured overnight in RPMI complete medium at 37°C in 5% CO_2. The parasites were then cultivated for 30 min in RPMI complete medium containing 10 nM human aFGF, or 10 nM bFGF, or 10 nM aFGF and bFGF (the same concentration used in a previous study (14)). For the inhibitor treatment group, adult *S. mansoni* were cultured in RPMI complete medium with 10 μM BIBF 1120 (dissolved in dimethyl sulfoxide (DMSO) and then diluted to different concentrations) (Sigma-Aldrich), or 0.1% DMSO (negative control) for 30 min as described (14). After each treatment, worms were harvested for SWAP extraction as described (53) in the presence of HALT protease inhibitor cocktail. Isolated SWAP was then separated on a 10% SDS-PAGE gel and analyzed by western blotting as described above.

Tyrosine Kinase Activity Assay

A Universal Tyrosine Kinase Assay Kit (Takara, Melbourne, Australia) was used to determine the enzymatic activity of rSmFGFRA at different concentrations (100 ng/μl - 0.78 ng/μl) in the presence or absence of 5 μM and 10 μM BIBF 1120 as described (14, 36), following the manufacturer's instructions. DMSO (0.1%) was served as negative control. The activity of rSmFGFRA was determined by comparing its absorbance with that of control protein tyrosine kinase (PTK), supplied with the kit, according to the manufacturer's instructions. Technical duplicates were performed and the experiment was repeated twice.

BIBF 1120 Treatment of *S. mansoni* Eggs *In Vitro* and Measurement of the Behavior of Miracidia Hatched From the Treated Eggs

S. mansoni eggs were cultured overnight at 37°C in RPMI complete medium under an atmosphere of 5% CO_2. The eggs were then treated with different concentrations of BIBF 1120 (2.5 μM, 5 μM, 10 μM, 20 μM) or 0.1% DMSO (negative control). After seven days, the eggs were collected and miracidia were hatched in deionized water under light as described above. The egg hatching efficiency (%) in each group was calculated by dividing the number of hatched eggs with the total number of examined eggs X 100. The behavior of miracidia hatched from treated and control eggs was also monitored using a published bioassay (57, 58). Briefly, around 30 *S. mansoni* miracidia in 100 μl deionized water were, using a pipette, evenly distributed to the centre of a microscope slide. Miracidial movement (swimming) was monitored using an Olympus-CKX41 microscope equipped with an Olympus DPI Digital Microscope Camera DP22 (25 frames per second at 2.8-megapixel image quality). Miracidial movement in the field of view (FOV) was recorded for 1 minute by video. Then the videoed miracidial tracks were analyzed using FIJI software to calculate three individual behavioral measurements including velocity of miracidial movement, duration (time) of miracidia staying within the FOV, and tortuosity (the ratio of track length to maximum displacement) of miracidial movement (57). The miracidial movement velocity was calculated in pixel/s using the rolling mean subtraction method (57, 58). Miracidial location was tracked in each frame along an x-y axis and the trajectories were interpolated using the plugin for FIJI software, known as TrackMate (58, 59). Employing the MTrackJ plugin, the average velocity, duration, and tortuosity of miracidia in the FOV were determined. Heatmaps, representing the movement pattern of individual miracidia, were generated as described (58, 60).

Statistical Analysis

All data are displayed as the mean ± SE. Differences between groups were analyzed for statistical significance by One-way ANOVA. GraphPad Prism software (Version 8.2.1, La Jolla, CA, USA) was used for all statistical analyses. A statistically significant difference for a particular comparison was defined as a p value ≤ 0.05. * p value≤ 0.05, ** p value≤ 0.01, *** p value ≤ 0.001, **** p value ≤ 0.0001, not significant (ns).

RESULTS

SmFGFRA Sequence and Structural Analysis

SmfgfrA (Smp_175590) encodes SmFGFRA and *SmfgfrB* (Smp_157300) has two transcripts encoding SmFGFRB1 and SmFGFRB2, respectively. SmFGFRA shares 78.4% amino acid sequence identity with *S. haematobium* FGFR2 (ShFGFR2, MS3_0015372) and 59.9% identity with *S. japonicum* FGFR2 isoform 2 (SjFGFR2-2, EWB00_002899). In contrast, SmFGFRA shares only 17.4% and 17.9% amino acid sequence identity with SmFGFRB1 and SmFGFRB2, respectively, and their common amino acids are mainly distributed in the conserved TK domain. SmFGFRA shares 21.7% sequence identity with human FGFR1.

The tertiary structures of the SmFGFRs were predicted by the I-TASSER server (**Figure 1**). The ligand binding residues (L^{588}, G^{589}, G^{591}, V^{596}, A^{617}, K^{619}, I^{650}, R^{651}, F^{652}, I^{664}, L^{666} - A^{669}, G^{672}, V^{754}, C^{764}, D^{765}, F^{766}) and the enzyme active site residue (R^{751}) of SmFGFRA were predicted as shown in **Figure 1**. The ligand binding residues (I^{292} - A^{295}, G^{297}, I^{298}, Y^{300}, A^{321}, K^{323}, I^{353}, M^{369}, E^{370} -A^{372}, N^{376}, R^{425}, L^{428}, A^{438}, D^{439}) and enzyme active site residue (R^{425}) of SmFGFRB1, and the ligand binding residues (L^{312}, V^{320}, A^{341},

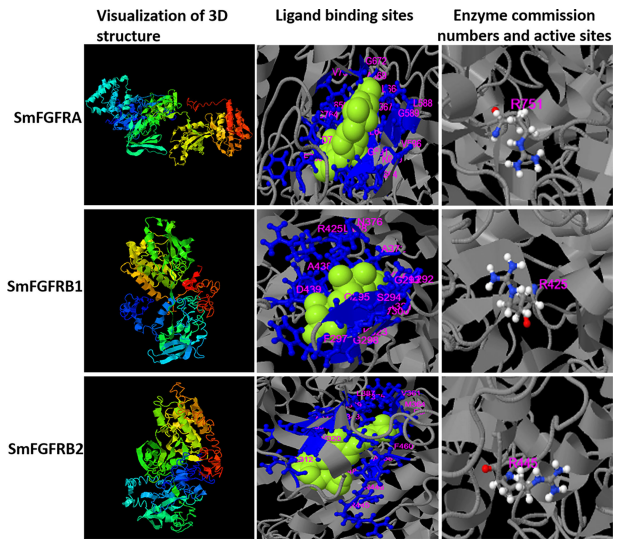

FIGURE 1 | Three-dimensional (3D) structure (column 1), the predicted binding ligands (green spheres) and binding residues (blue balls and sticks) (column 2), and enzyme active sites (colored balls and sticks) (column 3) for *S. mansoni* FGFRA (Confidence score=-2.22), FGFRB1 (Confidence score=-2.7) and FGFRB2 (Confidence score=-3.74) predicted by the I-TASSER server. The residue numbers are shown in pink.

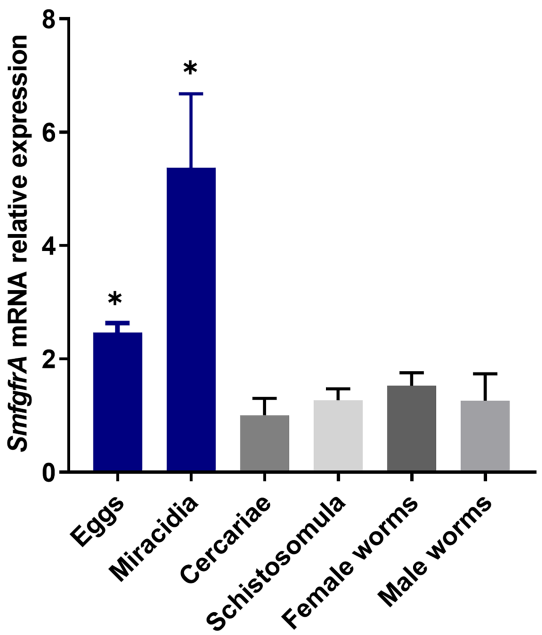

FIGURE 2 | Quantification of *SmfgfrA* gene transcripts in different life cycle stages of *S. mansoni*. The relative expression of *SmfgfrA* in eggs, miracidia, cercariae, schistosomula, and adult female and male worms were normalized to its expression in cercariae. Data are representative of the mean ± SE of three independent experiments. *P* values were calculated using cercariae as a comparison group. (*p value≤ 0.05, One-way ANOVA).

K^{343}, E^{360}, V^{361}, M^{364}, I^{373}, F^{375}, L^{387}, M^{389}, E^{390}-A^{392}, R^{445}, N^{446}, L^{448}, A^{458}, F^{460}) and the enzyme active site residue (R^{445}) of SmFGFRB2 are shown in **Figure 1** (14). The predicted domain structures of SmFGFRA and SmFGFRB1/2 are shown in Supplementary **Figure 1**. Neither signal peptides nor immunoglobulin (IG)-like domains that are responsible for protein-protein and protein-ligand interactions (61, 62) were found in either SmFGFRB1 or SmFGFRB2 (**Supplementary Figure 1**).

The predicted binding ability of SmFGFRA with its ligand indicated its potential in inducing dimerization of the extracellular domains of FGFRs [as demonstrated in mammalian cells (11, 12, 63)], and subsequent transautophosphorylation of the cytoplasmic TK domain, thereby activating downstream signal transduction in *S. mansoni*. However, no endogenous genes encoding FGF ligands have been identified in the genomes of *S. mansoni* (45, 64), suggesting that the parasite might explore host FGF ligands to stimulate its own signaling pathway.

Quantification of *SmfgfrA* Transcripts in Different *S. mansoni* Life Stages

Using real-time PCR assays, transcriptional levels of the *SmfgfrA* gene were quantified in eggs, miracidia, cercariae, schistosomula, and adult female and male worms of *S. mansoni*. We found *SmfgfrA* was transcribed in all the life cycle stages examined with eggs and miracidia having the highest expression levels (**Figure 2**).

Purification of Recombinant SmFGFRA and Antibody Generation

Purified rSmFGFRA-L and rSmFGFRA, expressed in *E. coli*, were shown by SDS-PAGE to migrate as bands at the predicted sizes of approximately 40 KDa (**Figure 3A**, Lane 1) and 105 KDa (**Figure 3A**, Lane 2), respectively. The smeared bands observed in the SDS-PAGE with purified full-length protein rSmFGFRA (**Figure 3A**, Lane 2) may indicate protein degradation during protein expression and/or purification, although cocktail protease inhibitors were added during the purification procedure.

Specific antibody against rSmFGFRA-L was generated in mice and the titer of the antibody (1:25,600) determined by ELISA. The anti-rSmFGFRA-L serum was used for western blot analysis and immunolocalization.

Reactivity of the Anti-rSmFGFRA-L Serum

To determine whether the anti-serum raised against SmFGFRA cross reacted with homologous components in SWAP extracts prepared from adult *S. japonicum* and *S. haematobium*, western blot analysis was performed using the generated mouse anti-rSmFGFRA-L serum. Western blots demonstrated that the anti-rSmFGFRA-L antibody (1:80) recognized a band at the expected molecular size of approximately 130 kDa in the SWAPs (50 μg/well) of *S. mansoni*, *S. japonicum* and *S. haematobium*, whereas no bands were evident when the SWAPs were probed with naïve mouse serum (**Figure 3B**). Similarly, native SmFGFRA (approximately 130 kDa) was also recognized by the anti-rSmFGFRA-L antibody in *S. mansoni* SEA while no band was recognized by the naïve mouse serum (**Figure 3B**).

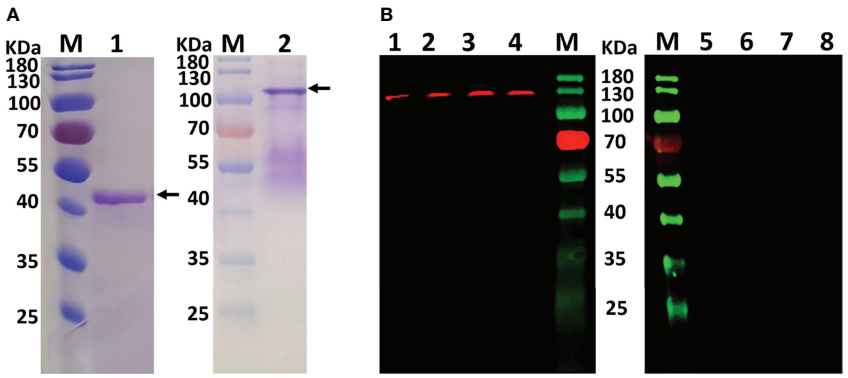

FIGURE 3 | **(A)** Purified rSmFGFRA-L (lane1) and rSmFGFRA (lane 2) observed in SDS-PAGE gels. **(B)** Western blot analysis using an anti-rSmFGFRA-L polyclonal antibody to probe *S. mansoni* SWAP (lane1), *S. japonicum* SWAP (lane 2), *S. haematobium* SWAP (lane 3), and *S. mansoni* SEA (lane 4). The naïve mouse serum served as a negative control to probe *S. mansoni* SWAP (lane 5), *S. japonicum* SWAP (lane 6), *S. haematobium* SWAP (lane 7), and *S. mansoni* SEA (lane 8).

Localization of SmFGFRA in Different Life Cycle Stages of *S. mansoni* and Co-Localization of SmFGFRA and Stem Cells

Immunolocalization was performed on sections of immature and mature eggs collected from *S. mansoni* infected mouse livers, miracidia, cercariae, 5-day old schistosomula, and adult male and female worms to determine the distribution of SmFGFRA in the different developmental stages. Immunofluorescence showed that native SmFGFRA was localized in the embryonic cells (**Figure 4B**) of immature eggs (egg embryogenesis stages 2-3) (65, 66). In positive cells, the SmFGFRA signal was detected in a perinuclear distribution. In mature eggs, SmFGFRA was detected in the inner envelope (von Lichtenburg's Layer), the peripheral cellular neural mass, the lateral and apical glands, and germinal cells (**Figure 4D**). SmFGFRA localization was not detected on the egg shell or in the central neuropile of the neural mass where no neuronal cells are present (67). The distribution of SmFGFRA was similar in miracidia to that observed in mature eggs being localized within the ciliated epithelium, neural mass, lateral glands, apical gland, and germinal cells (**Figure 4F**). SmFGFRA was also detectable in the tegument, oral sucker, preacetabular glands, germinal cells, and flame cells of cercariae (6, 68) (**Figure 4H**), and in the tegument and the internal cell masses, including germinal cells (4), of 5-day old schistosomula (**Figure 4J**). Significantly, SmFGFRA fluorescence labelling was detected in almost all tissues of the adult male worms including the tubercles (**Figure 5F**), tegument, parenchyma (**Figure 4L**), oral sucker, ventral sucker, and testes (69) (**Figure 5J**). Similarly, SmFGFRA was amply distributed in the tegument and inner cell masses of female worms including the vitellaria, but not the gastrodermis (**Figure 4N**). Naïve mouse serum served as negative control to probe fixed immature eggs (**Figure 4A**), mature eggs (**Figure 4C**), miracidia (**Figure 4E**), cercariae (**Figure 4G**), schistosomula (**Figure 4I**), adult male worms (**Figure 4K**) and female worms (**Figure 4M**).

EdU is known for its ability to incorporate into newly synthesized cellular DNA, and stains only proliferating stem cells in *S. mansoni* adults (7). To determine the relationship

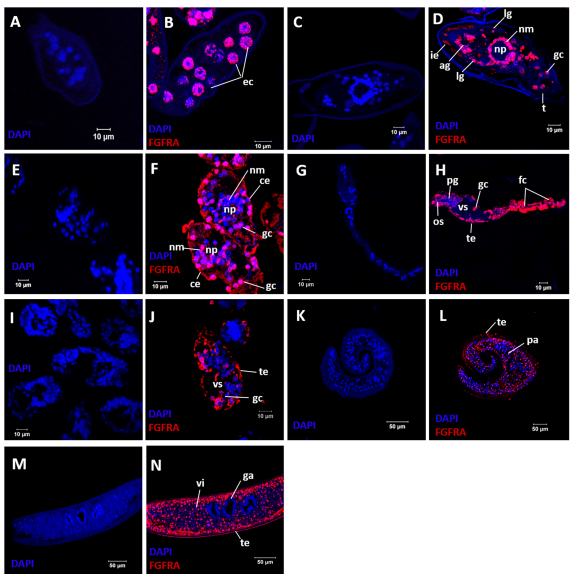

FIGURE 4 | Immunolocalization of SmFGFRA in different life cycle stages of *S. mansoni*. Sections of different *S. mansoni* stages were exposed to a mouse anti-rSmFGFRA-L antibody to examine the distribution of SmFGFRA (shown in red). Naïve mouse serum was employed as negative control. All samples were DAPI stained (in blue). Fixed immature eggs were incubated with naïve control mouse serum **(A)** and mouse anti-rSmFGFRA-L antibody **(B)**; mature eggs were exposed to naïve control mouse serum **(C)** and mouse anti-rSmFGFRA-L antibody **(D)**; miracidia were probed with naïve control mouse serum **(E)** and mouse anti-rSmFGFRA-L antibody **(F)**; cercariae were incubated with naïve control mouse serum **(G)** and mouse anti-rSmFGFRA-L antibody **(H)**; schistosomula were exposed to naïve control mouse serum **(I)** and mouse anti-rSmFGFRA-L antibody **(J)**; adult male worms were probed with naïve control mouse serum **(K)** and mouse anti-rSmFGFRA-L antibody **(L)**; adult female worms were exposed to naïve control mouse serum **(M)** and mouse anti-rSmFGFRA-L antibody **(N)**. ec, embryonic cells; ie, inner envelop; ig, lateral glands; ag, apical gland; nm, neural mass primordium; np, neuropile; gc, germinal cells; ce, ciliated epithelium; os, oral sucker; pg, preacetabular glands; fc, flame cells; te, tegument; vs, ventral sucker; pa, parenchyma; vi, vitellarium; ga, gastrodermis.

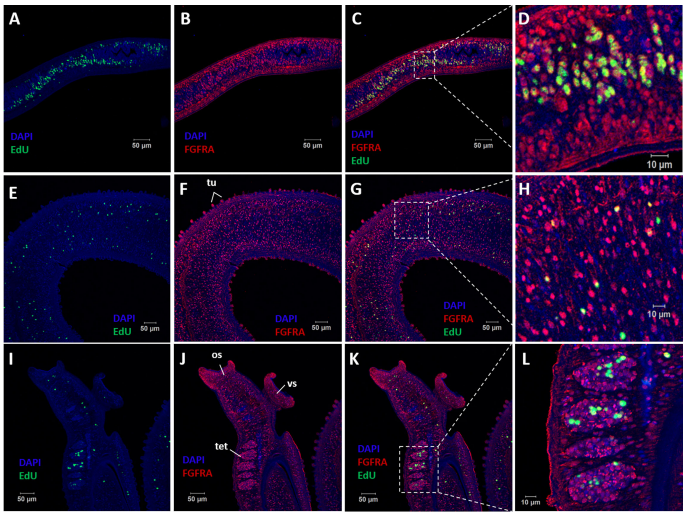

FIGURE 5 | Co-localization of SmFGFRA and EdU$^+$ cells in *S. mansoni* adult worms. Sequential staining of **(A)** EdU (green) and **(B)** anti-rSmFGFRA-L antibody (red) to sections of adult female worms. **(C)** Merging of **(A, B)**. **(D)** Magnified squared-areas in **(C)**. Sections of adult male worms were stained with **(E, I)** EdU and probed with **(F, J)** anti-rSmFGFRA-L antibody. **(G)** Merging of **(E, F)**. **(H)** Magnified squared-areas in **(G)**. **(K)** Merging of **(I, J)**. **(L)** Magnified squared-areas in **(K)**. All samples were DAPI-stained (blue). os, oral sucker; vs, ventral sucker; tet, testes; tu, tubercles.

between EdU$^+$ cells (stem cells) and cells that express SmFGFRA (SmFGFRA$^+$), we undertook immunolocalization of SmFGFRA using an anti-rSmFGFRA-L polyclonal antibody to probe sections of adult worms stained with EdU. All EdU$^+$ cells present in both adult female worms and male worms were SmFGFRA$^+$ (**Figure 5**), emphasizing the critical roles of SmFGFRA in maintaining stem cells at the translational level. However, not all SmFGFRA$^+$ cells were EdU$^+$, suggesting SmFGFRA is multi-functional in *S. mansoni*, being not only important in stem cell maintenance but also being involved in other critical biological processes.

SmFGFRA Has Strong Binding Affinity With Human bFGF

We performed real-time binding assays using the Octet RED system with 'biolayer interferometry' technology to investigate the binding affinity between rSmFGFRA-L and human bFGF/aFGF (**Figure 6**). A strong *in vitro* interaction between rSmFGFRA-L and human bFGF (protein concentration ranging from 5 ng/μl to 29.6 ng/μl) was detected (**Figure 6A**) (KD = 3.6E-10, coefficient of determination (r^2) = 0.98). Binding affinity was also evident, albeit less strongly, between rSmFGFRA-L and human aFGF (protein concentration

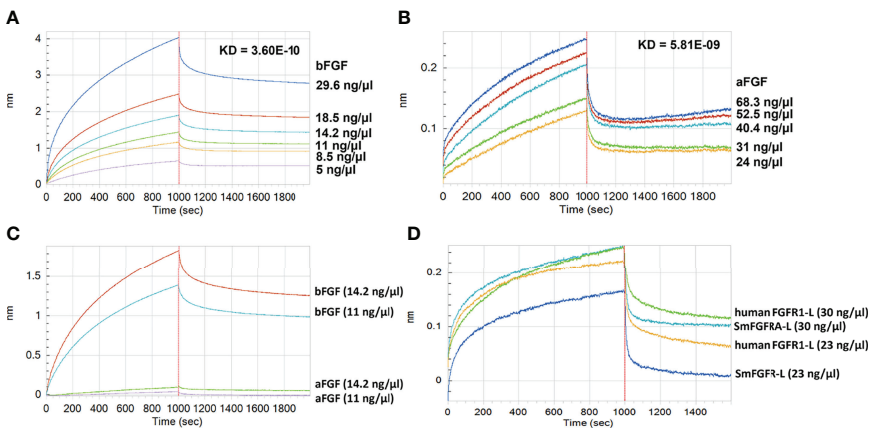

FIGURE 6 | Assays showing Binding between rSmFGFRA-L and human bFGF/aFGF using the Octet RED system. The real-time binding response between rSmFGFRA-L and **(A)** human bFGF and **(B)** human aFGF at different concentrations (ng/μl) was monitored in seconds. The parameters of the binding affinity (nm) and the KD value (M) of the binding affinity between rSmFGFRA-L and human bFGF/aFGF are shown. **(C)** Comparison of the rSmFGFRA-L binding affinity to human bFGF and aFGF at concentrations of 14.2 ng/μl and 11 ng/μl, respectively. **(D)** Comparison of the human bFGF binding affinity to human FGFR1-L and rSmFGFRA-L at concentrations of 30 ng/μl and 24 ng/μl, respectively.

ranging from 24 ng/µl to 68.3 ng/µl) (KD = 5.81E-09, $r^2 = 0.92$) (**Figure 6B**). Increasing the concentration of bFGF/aFGF resulted in an increased binding response with the dissociation phase slowly decreasing, demonstrating the specific binding ability presented between rSmFGFRA-L and bFGF/aFGF. To compare the binding affinity of rSmFGFRA-L to human bFGF and aFGF *in vitro*, rSmFGFRA-L immobilized sensors were exposed to bFGF or aFGF at 14.2 ng/µl and 11 ng/µl, respectively. At the same protein concentration, bFGF exhibited 19-33.7 times stronger binding affinity than aFGF to rSmFGFRA-L (**Figure 6C**). Notably, at the same concentration, human FGFR1-L demonstrated higher binding affinity than rSmFGFRA-L to human bFGF (**Figure 6D**).

Human FGFs Activate the *S. mansoni* MAPK Signaling Pathway

To explore whether human FGFs could activate the *S. mansoni* MAPK pathway by phosphorylating Erk1/2, we incubated adult worms for 30 minutes with either 10 nM aFGF or bFGF individually or in combination. Then, SWAP extracted from the treated parasites was subjected to western blot analysis using an anti-phospho-P44/42 MAPK (Erk1/2) (Thr202/Tyr204) antibody. Phosphorylation of Erk1/2 was readily detected at the expected band size (approximately 44 kDa) (53) in SWAP of adult *S. mansoni* stimulated with either aFGF or bFGF, or co-stimulated with both aFGF and bFGF; stronger band intensity was observed in worms treated with bFGF (**Figures 7A**, **S2**). The Erk band was detectable in an extract of control parasites (wild type, i.e. untreated worms; and worms incubated with 0.1% DMSO). By using an anti-actin (control) antibody, no significant differences were evident in band intensity detected in any of the tested or control groups (**Figure 7A**, **S2**). Furthermore, 30 minute treatment of adult worms with the TK inhibitor BIBF 1120 (10 µM), an agent considered to selectively inhibit *S. mansoni* FGF receptors (36), resulted in markedly depleted phosphorylation of Erk (**Figure 7A**, **s2**).

Tyrosine Kinase Activity of rSmFGFRA

SmFGFRA is a receptor tyrosine kinase (RTK) and the RTKs are important enzymes involved in the signal transduction pathway (12). A universal Tyrosine Assay Kit, used to measure the TK activity of rSmFGFRA, indicated, as might be expected, increased activity with increasing concentrations (0-100 ng/µl) of rSmFGFRA (**Figure 7B**). However, the TK activity of rSmFGFRA was considerably inhibited following incubation with the TK inhibitor, BIBF 1120; indeed, when the rSmFGFRA concentration was less than 6.25 ng/µl, TK activity was completely inhibited in the presence of 5 µM or 10 µM BIBF 1120 (**Figure 7B**).

BIBF 1120 Inhibits the Hatching of *S. mansoni* Liver Eggs

To further understand the effects of inhibiting the FGFRs by BIBF 1120 in *S. mansoni*, eggs isolated from the livers of infected mice were treated *in vitro* with different concentrations (2.5 - 20 µM) of the inhibitor, and then the egg hatching efficiency was examined. BIBF 1120 had clear concentration-dependent effects on egg hatching ability. In the presence of 2.5 µM BIBF 1120, egg hatching efficiency was moderately but not significantly reduced. However, egg hatching was markedly decreased by 21.3% (p=0.0077), 54.4% ($p \leq 0.0001$), and 65% ($p \leq 0.0001$) in the presence of 5 µM, 10 µM, and 20 µM BIBF 1120, respectively, compared with control eggs treated with 0.1% DMSO (**Figure 8**).

Behavioral Changes of *S. mansoni* Miracidia Hatched From Liver Eggs Treated With BIBF 1120

Behavioral changes of miracidia hatched from eggs treated with BIBF 1120 were investigated by analyzing recordings of miracidial movement tracks. Heatmaps of the miracidia movement patterns were created to illustrate the behavior of individual miracidia within the 1 min recording. The heatmaps of the control miracidia [wild type miracidia (WT) and miracidia hatched from eggs treated with 0.1% DMSO] depicted linear soft blue lines suggesting these miracidia had less circular but faster movement (**Figures 9A, B**). In contrast, there were more circular lines and more abundant red and yellow regions in heatmaps of miracidia hatched from the BIBF 1120-treated eggs (**Figures 9C–F**), indicating more turning and circling and relatively slower movement of these miracidia in the FOV. As shown in

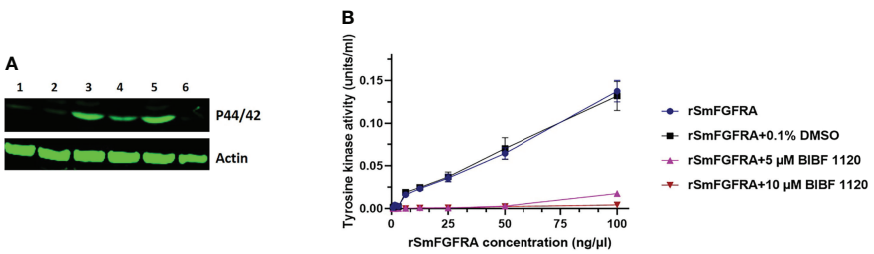

FIGURE 7 | **(A)** Effect of human aFGF or bFGF on the stimulation of extracellular signal regulated kinases 1 and 2 (Erk1/2) in adult *S. mansoni* worms. An anti-phospho p44/42 MAPK (Erk) antibody (upper panel) and an anti-actin antibody (lower panel) were used to probe a protein extract of wild type, untreated adult worms (Lane 1) and worms which were incubated with 0.1% DMSO (Lane 2), human bFGF (Lane 3), human aFGF (Lane 4), both human bFGF and aFGF (Lane 5), and 10 µM BIBF 1120 (Lane 6), respectively. **(B)** Tyrosine kinase activity of rSmFGFRA at different concentrations (0-100 ng/µl) in the presence or absence of 0.1% DMSO or BIBF 1120 (5 µM and 10 µM).

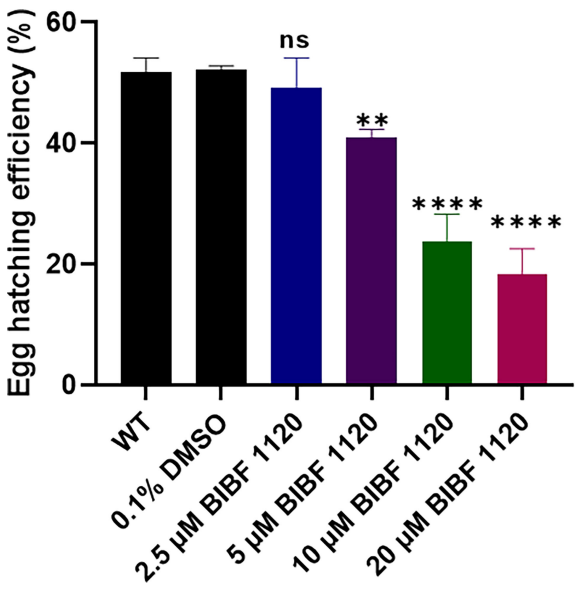

FIGURE 8 | Effects of BIBF 1120 on the hatching of *S. mansoni* eggs. The egg hatching efficiency (%) of untreated wild type (WT) *S. mansoni* eggs and eggs treated with 0.1% DMSO, or 2.5 μM, 5 μM, 10 μM, and 20 μM BIBF 1120 was calculated by dividing the number of hatched eggs by the total number of eggs (hatched and unhatched eggs) X 100. (ns, not significant; ***p* value≤ 0.01, *****p* value ≤ 0.0001 by One-way ANOVA).

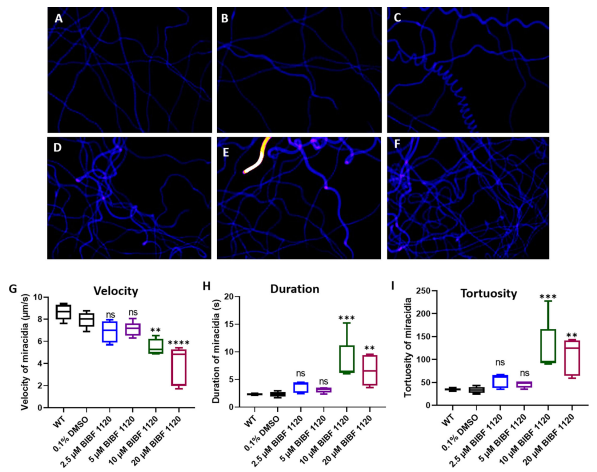

FIGURE 9 | Behavioral changes in *S. mansoni* miracidia hatched from liver eggs treated with BIBF 1120. The behavior of miracidia hatched from WT eggs and eggs treated with 0.1% DMSO or BIBF 1120 at concentrations of 2.5 μM, 5 μM, 10 μM, and 20 μM was determined. Heatmaps **(A–F)** represent the movement patterns of individual miracidia within a 1 min recording. Colors in the heatmaps **(A–F)** show the time miracidia spent at a specific position. Black: absence; Blue: shorter time presence; Yellow and Red: longer time presence. Boxplots showing **(G)** velocity **(H)** duration, and **(I)** tortuosity of miracidial movement. (ns, not significant; ***p* value≤ 0.01; ****p* value ≤ 0.001; *****p* value ≤ 0.0001; One-way ANOVA).

Figure 9G, the swimming velocity of miracidia hatched from eggs treated with 10 μM and 20 μM BIBF 1120 was significantly decreased by 30.7% (p=0.0023) and 51.3% ($p \leq 0.0001$), respectively, compared with that measured in the 0.1% DMSO-treated group. Markedly, the average time duration of miracidia hatched from eggs treated with 10 μM and 20 μM BIBF 1120 in the FOV was elevated by 72.1% (p=0.0006) and 72.7% (p=0.0088), respectively (**Figure 9H**). Similarly, the movement tortuosity of miracidia hatched from 10 μM and 20 μM BIBF 1120 treated eggs was dramatically increased by 61.7% (p=0.0003) and 68.8% (p=0.0024), respectively, compared with that observed in the 0.1% DMSO-treated group (**Figure 9I**). No significant behavioral modifications were evident in miracidia hatched from eggs treated with BIBF 1120 at concentrations of 2.5 μM and 5 μM.

DISCUSSION

The somatic stem cell marker SmFGFRA has stimulated increased attention due to the essential roles it plays in maintaining schistosome stem cells (4–7, 36, 38). Transcription of *SmfgfrA* has been identified in the germinal cells (also defined as totipotent stem cells (5)) of miracidia, sporocysts and schistosomula (4, 6) and in the stem cells of adult *S. mansoni* (7, 39) [neoblasts or adult pluripotent stem cells (5)]. Recently, using single-cell RNA sequencing (scRNA-seq) analysis, Wendt *et al.* (39) characterized 68 distinct cell populations from adult *S. mansoni*, including three cell clusters expressing somatic stem cells markers (including *SmfgfrA*). They found the majority of *SmfgfrA* mRNA was detected in neoblasts and the tegument cells of adult schistosomes (39, 51). However, the precise functional roles of SmFGFRA in driving the development and differentiation of each developmental stage allowing them to thrive in diverse and challenging environments remains unclear. Herein, by immunolocalization and functional studies, we demonstrated abundant protein expression of SmFGFRA in various tissues of all examined *S. mansoni* life cycle stages and extended the range of prospective host-parasite cross-communication systems to the FGF family, reinforcing its likely multiple and critical functions in the survival and development of this flatworm parasite (6, 7, 27, 39).

In immature eggs, SmFGFRA was localized to all embryonic cells which possess large round nuclei. Specifically, the location was in the perinuclear region which is heavily involved in maintaining genome integrity and the regulation of gene expression (70), indicating this molecule is of critical importance in the differentiation and development of schistosome eggs. During development, the eggs develop extraembryonic envelopes beneath the shell and the embryonic cells differentiate into different schistosome tissues and organs (65). We showed that in mature eggs, the distribution of SmFGFRA extended to various tissues including the extra-embryonic von Lichtenberg's layer, as well as the neural mass, lateral glands, the apical gland, and germinal cells of the miracidium. Of these, von Lichtenberg's layer, which is present only in mature eggs, is highly active metabolically and is

suggested to be the main source of immunogenic secretions that are released through eggshell pores into the host circulatory system to induce the host immune response (43, 71). This information supports the concept that SmFGFRA plays important roles in egg development and the host-parasite interplay.

The abundant expression of SmFGFRA in the neural mass of schistosome eggs and miracidia observed in our study and the transcription of *SmfgfrA* detected in almost all neuron cells of adult worms (39) suggest that expression of SmFGFRA in neurons occurs through all developmental stages of the parasite. SmFGFRA, as with its homologues in humans and mice (72–74), appears to promote neuronal cell development in schistosomes, but also plays a role in the continued activity of adult neurons. The inhibition of *S. mansoni* FGF signaling in schistosomes may affect neuronal development and function in schistosomes, and can provide the basis for developing an adjunct treatment to complement the currently widely used anti-schistosome drug, praziquantel, which induces severe but reversible contractions in worm muscles (75). Furthermore, clues to the potential importance of SmFGFA in neuronal function were evident by the remarkably changed behavior of miracidia hatched from BIBF 1120-treated eggs. The affected miracidia, which swim in freshwater by coordinated activity of cilia on their surface epithelial plates (76–78), displayed increased turning and circling motions in water. While the capacity of these affected miracidia to infect snails was not examined here, it seems improbable that they could navigate towards a *Biomphalaria* snail intermediate host in the natural aquatic environment after treatment with BIBF 1120 or a compound with comparable effects. Furthermore, treatment of *S. mansoni* eggs with BIBF 1120 resulted in a considerable reduction in egg hatching efficiency. These inhibitor-induced phenotype changes can be explained by the outcomes of a previous study showing the potential effects of BIBF1120 on mitotically active cells (such as proliferating cells or stem cells) in organs of adult *S. mansoni* (36), indicating the potential effect of BIBF 1120 in targeting SmFGFRA. BIBF 1120 is a selective inhibitor of mammalian FGFRs, vascular endothelial growth factor receptors (VEGFRs), platelet-derived growth factor receptors (PDGFRs) (79, 80), and Src-family kinases (81). Given the absence of VEGFR and PDGFR homologs in the genome of schistosomes, the SmFGFRs have been considered as the main targets of BIBF 1120 in these worms (36), a characteristic supported here by the capacity of BIBF 1120 to block the TK activity of SmFGFRA. However, a member of the Src family of cytoplasmic protein tyrosine kinases has been identified in *S. mansoni* (82) and further study is needed to investigate the effect of BIBF 1120 in regulating the functional activity of this and other Srcs in the blood fluke.

The presentation of SmFGFRA on the ciliated surface of newly released miracidia and internal cell masses (including the germinal cells), both of which are essential in the transformation of miracidia into primary sporocysts (6), implies a key role for SmFGFRA in promoting sporocyst growth and development. Miracidia penetrate the intermediate snail host resulting in the rapid shedding of ciliary epidermal plates from the larval surface during the development of the new tegumental syncytium of the developing sporocysts (83). Proteins (including SmFGFRA) in the epithelial cytoplasm, which are involved in the miracidium-to-sporocyst transformation (84), might also be important in modulating the immune response in the intermediate snail host, where cercariae are produced asexually and are released into fresh water as the next free-living stage of the life cycle (84). As expected, expression of SmFGFRA was detected in various tissues of cercariae including the tegument cytosol and oral sucker. Notably, a SmFGFRA-specific signal was also observed in the cercarial preacetabular glands which secrete enzymes for the penetration of mammalian host skin, in flame cells which are important for excretion processes (68, 85, 86), and in germinal cells. This pattern of localization suggests SmFGFRA is also associated with penetration of the mammalian host and in the transformation of cercariae to schistosomula. Importantly, the abundance of SmFGFRA in the germinal cells and tegument of cercariae would suggest that the molecule is produced in areas of rapid growth and differentiation in the development of schistosomula and further emphasize its critical role in the maturation of these juvenile worms into adults.

Given the pivotal role of stem cells in the renewal or repair of the tegument in adults (10, 87), the tegumental location of SmFGFRA in miracidia, cercariae, schistosomula and adult *S. mansoni* suggests the involvement of this protein in the process of stem cell - mediated tegumental regeneration. This is supported by scRNAseq data of cells isolated from adult worms showing *SmfgfrA* is transcribed in clusters of tegument 1 cells and tegument progenitor cells (39, 88). The tegumental location of SmFGFRA in adult schistosomes implies that SmFGFRA has potential as a vaccine and/or drug target, given the critical roles of tegumental proteins of schistosomes in the interplay with their mammalian hosts including hormone or nutrient uptake and immune evasion (89, 90). In addition, the pronounced expression of SmFGFRA in the testis of males and in the vitellaria of females, a stem cell-dependent tissue producing the yolk cells of eggs (39), suggests SmFGFRA is also heavily involved in egg production, reproductive system development and in the sexual maturation of adult schistosomes. These findings are also underpinned by the scRNAseq data which showed the presence of *SmfgfrA* transcripts in germline stem cells (GSC) and in vitellaria including vitellarium-specific stem cells (S1 cells) of both adult male and female worms, with higher levels in the S1 cells of females (39). To further determine the relationship between SmFGFRA and adult *S. mansoni* stem cells at the post-transcriptional level, we employed sequential labelling of EdU and using an anti-rSmFGFRA-L antibody in both males and female worms. We found all EdU^+ stem cells expressed SmFGFRA, but not all cells expressing SmFGFRA were EdU^+. This confirms the critical role of this protein in the functioning of schistosome stem cells and also highlights potentially multiple roles for SmFGFRA in *S. mansoni.*

To further explore the mammalian host and parasite interplay, we examined the conservation of FGF RTKs in *S. mansoni*, using 3D structure and domain structural analysis of

SmFGFRA, SmFGFRB1 and SmFGFRB2. The similarity in structure between SmFGFRA and human mammalian FGFRs (27, 91) predicted a potential interaction between SmFGFRA and host FGFs. Since no *S. mansoni* endogenous FGF ligands have so far been identified, it is likely that activation of the SmFGFRA/FGF pathway in schistosomes is triggered by host FGFs, a scenario that is strongly supported by the protein interaction assay results we presented here showing SmFGFRA can bind the most active members of the human FGF family (26, 92, 93) - aFGF and bFGF, with much stronger binding affinity to the latter. Human bFGF is an essential exogenous growth factor required for maintaining the self-renewal of human embryonic stem cells (ESC) and induced pluripotent stem cells in culture (94–97). The strong binding affinity of human bFGF with SmFGFRA implies a crucial role for human bFGF in maintaining and promoting *S. mansoni* stem cell growth. We also demonstrated that the binding between human aFGF/bFGF and SmFGFRA could significantly induce the phosphorylation of Erk1/2 in adult worms of *S. mansoni*. The Erk signaling pathway regulates cell proliferation, differentiation and survival, and is one of the main MAPK pathways pivotal for sexual maturation of the female schistosome and egg production (98–100). The role of SmFGFRA in activation of the Erk pathway emphasizes again the importance of SmFGFRA in parasite development and maturation. Furthermore, given the plentiful presence of SmFGFRA in neurons of miracidia and germinal cells of miracidia and cercariae (two free-living stages), it remains to be determined whether there are other endogenous molecules that stimulate FGFR activity in these larval schistosomes.

Collectively, the results presented here emphasize the fundamental importance of SmFGFRA in driving the life cycle of *S. mansoni* and reveal its potential multiple functions in the proliferation of schistosome stem cells, in promoting cellular differentiation into tissues and organs, in the development of the nervous and reproductive systems, and in the host-parasite interplay. Our findings provide important clues for exploiting components of the FGF signaling pathway as promising targets for developing new interventions against schistosomiasis.

DATA AVAILABILITY STATEMENT

The original contributions presented in the study are included in the article/**Supplementary Material**. Further inquiries can be directed to the corresponding author.

ETHICS STATEMENT

The animal study was reviewed and approved by Animal Ethics Committee (ethics number P242) of the QIMR Berghofer Medical Research Institute.

AUTHOR CONTRIBUTIONS

Conceived and designed the experiments: HY, XD and DM. Performed the experiments: XD and HY. Analyzed the data: XD, HY, CF, MJ, and DM. Contributed reagents/materials/analysis tools: XD and HY. Wrote the paper: XD, HY, DM and MJ. All authors contributed to the article and approved the submitted version.

FUNDING

XD holds a Research Training Program (RTP) Scholarship and Graduate School Scholarship from the University of Queensland, Australia. DPM is a National Health and Medical Research Council (NHMRC) of Australia Leadership Fellow and receives Program (APP1132975), Project (APP1098244) and Investigator Grant (APP1194462) support from the NHMRC for his research on schistosomes and schistosomiasis. HY holds a QIMR Berghofer Medical Research Institute Seed Funding Grant (SF-210005).

ACKNOWLEDGMENTS

We thank Mary Duke from QIMR Berghofer Medical Research Institute for the maintenance of the *S. mansoni* life cycle and the provision of parasite materials for this research. *B. glabrata* snails were provided by the NIAID Schistosomiasis Resource Center of the Biomedical Research Institute (Rockville, MD) through NIH-NIAID Contract HHSN272201700014I for distribution through BEI Resources.

SUPPLEMENTARY MATERIAL

The Supplementary Material for this article can be found online at: https://www.frontiersin.org/articles/10.3389/fimmu.2022.868077/full#supplementary-material

REFERENCES

1. McManus DP, Dunne DW, Sacko M, Utzinger J, Vennervald BJ, Zhou X-N. Schistosomiasis. *Nat Rev Dis Primers* (2018) 4:13. doi: 10.1038/s41572-018-0013-8
2. McManus DP, Bergquist R, Cai P, Ranasinghe S, Tebeje BM, You H. Schistosomiasis—from Immunopathology to Vaccines. *Semin Immunopathol* (2020) 42:355–71. doi: 10.1007/s00281-020-00789-x
3. Deol AK, Fleming FM, Calvo-Urbano B, Walker M, Bucumi V, Gnandou I, et al. Schistosomiasis—Assessing Progress Toward the 2020 and 2025 Global Goals. *N Engl J Med* (2019) 381:2519–28. doi: 10.1056/NEJMoa1812165
4. Wang B, Lee J, Li P, Saberi A, Yang H, Liu C, et al. Stem Cell Heterogeneity Drives the Parasitic Life Cycle of *Schistosoma Mansoni*. *Elife* (2018) 7:e35449. doi: 10.7554/eLife.35449
5. You H, Jones MK, Whitworth DJ, McManus DP. Innovations and Advances in Schistosome Stem Cell Research. *Front Immunol* (2021) 12:599014. doi: 10.3389/fimmu.2021.599014
6. Wang B, Collins JJIII, Newmark PA. Functional Genomic Characterization of Neoblast-Like Stem Cells in Larval *Schistosoma Mansoni*. *Elife* (2013) 2:e00768. doi: 10.7554/eLife.00768
7. Collins JJIII, Wang B, Lambrus BG, Tharp ME, Iyer H, Newmark PA. Adult Somatic Stem Cells in the Human Parasite *Schistosoma Mansoni*. *Nature* (2013) 494:476–9. doi: 10.1038/nature11924

8. Lu Z, Sessler F, Holroyd N, Hahnel S, Quack T, Berriman M, et al. Schistosome Sex Matters: A Deep View Into Gonad-Specific and Pairing-Dependent Transcriptomes Reveals a Complex Gender Interplay. *Sci Rep* (2016) 6:1–14. doi: 10.1038/srep31150
9. Gryseels B, Polman K, Clerinx J, Kestens L. Human Schistosomiasis. *Lancet* (2006) 368:1106–18. doi: 10.1016/S0140-6736(06)69440-3
10. Collins JJIII, Wendt GR, Iyer H, Newmark PA. Stem Cell Progeny Contribute to the Schistosome Host-Parasite Interface. *Elife* (2016) 5:e12473. doi: 10.7554/eLife.12473
11. Stauber DJ, DiGabriele AD, Hendrickson WA. Structural Interactions of Fibroblast Growth Factor Receptor With its Ligands. *Proc Natl Acad Sci* (2000) 97:49–54. doi: 10.1073/pnas.97.1.49
12. Lemmon MA, Schlessinger J. Cell Signaling by Receptor Tyrosine Kinases. *Cell* (2010) 141:1117–34. doi: 10.1016/s0092-8674(00)00114-8
13. Katoh M, Nakagama H. FGF Receptors: Cancer Biology and Therapeutics. *Med Res Rev* (2014) 34:280–300. doi: 10.1002/med.21288
14. Förster S, Koziol U, Schäfer T, Duvoisin R, Cailliau K, Vanderstraete M, et al. The Role of Fibroblast Growth Factor Signalling in *Echinococcus Multilocularis* Development and Host-Parasite Interaction. *PloS Negl Trop Dis* (2019) 13:e0006959. doi: 10.1371/journal.pntd.0006959
15. Xie Y, Su N, Yang J, Tan Q, Huang S, Jin M, et al. FGF/FGFR Signaling in Health and Disease. *Signal Transduct Target Ther* (2020) 5:1–38. doi: 10.1038/s41392-020-00222-7
16. Dvorak P, Dvorakova D, Hampl A. Fibroblast Growth Factor Signaling in Embryonic and Cancer Stem Cells. *FEBS Lett* (2006) 580:2869–74. doi: 10.1016/j.febslet.2006.01.095
17. Gotoh N. Control of Stemness by Fibroblast Growth Factor Signaling in Stem Cells and Cancer Stem Cells. *Curr Stem Cell Res* (2009) 4:9–15. doi: 10.2174/157488809787169048
18. Li Y-P, Duan F-F, Zhao Y-T, Gu K-L, Liao L-Q, Su H-B, et al. A TRIM71 Binding Long Noncoding RNA Trincr1 Represses FGF/ERK Signaling in Embryonic Stem Cells. *Nat Commun* (2019) 10:1–13. doi: 10.1038/s41467-019-08911-w
19. Auwal MA, Kashima M, Nishimura O, Hosoda K, Motoishi M, Kamimura A, et al. Identification and Characterization of a Fibroblast Growth Factor Gene in the Planarian *Dugesia Japonica*. *Dev Growth Differ* (2020) 62:527–39. doi: 10.1111/dgd.12696
20. Ogawa K, Kobayashi C, Hayashi T, Orii H, Watanabe K, Agata K. Planarian Fibroblast Growth Factor Receptor Homologs Expressed in Stem Cells and Cephalic Ganglions. *Dev Growth Differ* (2002) 44:191–204. doi: 10.1046/j.1440-169x.2002.00634.x
21. Alvarado AS. Planarian Regeneration: Its End Is Its Beginning. *Cell* (2006) 124:241–5. doi: 10.1016/j.cell.2006.01.012
22. Wagner DE, Ho JJ, Reddien PW. Genetic Regulators of a Pluripotent Adult Stem Cell System in Planarians Identified by RNAi and Clonal Analysis. *Cell Stem Cell* (2012) 10:299–311. doi: 10.1016/j.stem.2012.01.016
23. Mossahebi-Mohammadi M, Quan M, Zhang J-S, Li X. FGF Signaling Pathway: A Key Regulator of Stem Cell Pluripotency. *Front Cell Dev Biol* (2020) 8:79. doi: 10.3389/fcell.2020.00079
24. Choi S-C, Kim S-J, Choi J-H, Park C-Y, Shim W-J, Lim D-S. Fibroblast Growth Factor-2 and-4 Promote the Proliferation of Bone Marrow Mesenchymal Stem Cells by the Activation of the PI3K-Akt and ERK1/2 Signaling Pathways. *Stem Cells Dev* (2008) 17:725–36. doi: 10.1089/scd.2007.0230
25. Li J, Wang G, Wang C, Zhao Y, Zhang H, Tan Z, et al. MEK/ERK Signaling Contributes to the Maintenance of Human Embryonic Stem Cell Self-Renewal. *Differentiation* (2007) 75:299–307. doi: 10.1111/j.1432-0436.2006.00143.x
26. Ornitz DM, Itoh N. The Fibroblast Growth Factor Signaling Pathway. *Wiley Interdiscip Rev Dev Biol* (2015) 4:215–66. doi: 10.1002/wdev.176
27. Itoh N, Ornitz DM. Evolution of the Fgf and Fgfr Gene Families. *Trends Genet* (2004) 20:563–9. doi: 10.1016/j.tig.2004.08.007
28. Brady NJ, Chuntova P, Bade LK, Schwertfeger KL. The FGF/FGF Receptor Axis as a Therapeutic Target in Breast Cancer. *Expert Rev Endocrinol Metab* (2013) 8:391–402. doi: 10.1586/17446651.2013.811910
29. Beenken A, Mohammadi M. The FGF Family: Biology, Pathophysiology and Therapy. *Nat Rev Drug Discovery* (2009) 8:235–53. doi: 10.1038/nrd2792
30. Ghedini GC, Ronca R, Presta M, Giacomini A. Future Applications of FGF/FGFR Inhibitors in Cancer. *Expert Rev Anticancer Ther* (2018) 18:861–72. doi: 10.1080/14737140.2018.1491795
31. Hosaka K, Yang Y, Seki T, Du Q, Jing X, He X, et al. Therapeutic Paradigm of Dual Targeting VEGF and PDGF for Effectively Treating FGF-2 Off-Target Tumors. *Nat Commun* (2020) 11:1–15. doi: 10.1038/s41467-020-17525-6
32. Ahmad SM, Baker BS. Sex-Specific Deployment of FGF Signaling in *Drosophila* Recruits Mesodermal Cells Into the Male Genital Imaginal Disc. *Cell* (2002) 109:651–61. doi: 10.1016/s0092-8674(02)00744-4
33. Destalminil-Letourneau M, Morin-Poulard I, Tian Y, Vanzo N, Crozatier M. The Vascular Niche Controls *Drosophila* Hematopoiesis *via* Fibroblast Growth Factor Signaling. *Elife* (2021) 10:e64672. doi: 10.7554/eLife.64672
34. Borland CZ, Schutzman JL, Stern MJ. Fibroblast Growth Factor Signaling in *Caenorhabditis Elegans*. *Bioessays* (2001) 23:1120–30. doi: 10.1002/bies.10007
35. Lo T-W, Bennett DC, Goodman SJ, Stern MJ. *Caenorhabditis Elegans* Fibroblast Growth Factor Receptor Signaling can Occur Independently of the Multi-Substrate Adaptor FRS2. *Genetics* (2010) 185:537–47. doi: 10.1534/genetics.109.113373
36. Hahnel S, Quack T, Parker-Manuel SJ, Lu Z, Vanderstraete M, Morel M, et al. Gonad RNA-Specific qRT-PCR Analyses Identify Genes With Potential Functions in Schistosome Reproduction Such as SmFz1 and SmFGFRs. *Front Genet* (2014) 5:170. doi: 10.3389/fgene.2014.00170
37. Andrikou C, Hejnol A. FGF Signaling Acts on Different Levels of Mesoderm Development Within Spiralia. *Development* (2021) 148(10):dev196089. doi: 10.1242/dev.196089
38. Sarfati DN, Li P, Tarashansky AJ, Wang B. Single-Cell Deconstruction of Stem-Cell-Driven Schistosome Development. *Trends Parasitol* (2021) 37(9):790-802. doi: 10.1016/j.pt.2021.03.005
39. Wendt G, Zhao L, Chen R, Liu C, O'Donoghue AJ, Caffrey CR, et al. A Single-Cell RNA-Seq Atlas of *Schistosoma Mansoni* Identifies a Key Regulator of Blood Feeding. *Science* (2020) 369:1644–9. doi: 10.1126/science.abb7709
40. Wendt GR, Collins III JJ. Schistosomiasis as a Disease of Stem Cells. *Curr Opin Genet Dev* (2016) 40:95–102. doi: 10.1016/j.gde.2016.06.010
41. Du X, Jones MK, Nawaratna SS, Ranasinghe S, Xiong C, Cai P, et al. Gene Expression in Developmental Stages of *Schistosoma Japonicum* Provides Further Insight Into the Importance of the Schistosome Insulin-Like Peptide. *Int J Mol Sci* (2019) 20:1565. doi: 10.3390/ijms20071565
42. Dalton J, Day S, Drew A, Brindley P. A Method for the Isolation of Schistosome Eggs and Miracidia Free of Contaminating Host Tissues. *Parasitology* (1997) 115:29–32. doi: 10.1017/s0031182097001091
43. Ashton P, Harrop R, Shah B, Wilson R. The Schistosome Egg: Development and Secretions. *Parasitology* (2001) 122:329–38. doi: 10.1017/s0031182001007351
44. Berriman M, Haas BJ, LoVerde PT, Wilson RA, Dillon GP, Cerqueira GC, et al. The Genome of the Blood Fluke *Schistosoma Mansoni*. *Nature* (2009) 460:352–8. doi: 10.1038/nature08160
45. Protasio AV, Tsai IJ, Babbage A, Nichol S, Hunt M, Aslett MA, et al. A Systematically Improved High Quality Genome and Transcriptome of the Human Blood Fluke *Schistosoma Mansoni*. *PloS Negl Trop Dis* (2012) 6:e1455. doi: 10.1371/journal.pntd.0001455
46. Chojnacki S, Cowley A, Lee J, Foix A, Lopez R. Programmatic Access to Bioinformatics Tools From EMBL-EBI Update: 2017. *Nucleic Acids Res* (2017) 45:W550–3. doi: 10.1093/nar/gkx273
47. Rice P, Longden I, Bleasby A. EMBOSS: The European Molecular Biology Open Software Suite. *Trends Genet* (2000) 16:276–7. doi: 10.1016/S0168-9525(00)02024-2
48. Zhang Y. I-TASSER Server for Protein 3D Structure Prediction. *BMC Bioinform* (2008) 9:1–8. doi: 10.1186/1471-2105-9-40
49. Yang J, Zhang Y. I-TASSER Server: New Development for Protein Structure and Function Predictions. *Nucleic Acids Res* (2015) 43:W174–81. doi: 10.1093/nar/gkv342
50. Yang J, Yan R, Roy A, Xu D, Poisson J, Zhang Y. The I-TASSER Suite: Protein Structure and Function Prediction. *Nat Methods* (2015) 12:7–8. doi: 10.1038/nmeth.3213

51. Wendt GR, Reese ML, Collins III JJ. SchistoCyte Atlas: A Single-Cell Transcriptome Resource for Adult Schistosomes. *Trends Parasitol* (2021) 37 (7):585–7. doi: 10.1016/j.pt.2021.04.010
52. Barber RD, Harmer DW, Coleman RA, Clark BJ. GAPDH as a Housekeeping Gene: Analysis of GAPDH mRNA Expression in a Panel of 72 Human Tissues. *Physiol Genomics* (2005) 21:389–95. doi: 10.1152/physiolgenomics.00025.2005
53. Du X, McManus DP, Cai P, Hu W, You H. Identification and Functional Characterisation of a Schistosoma Japonicum Insulin-Like Peptide. *Parasit Vectors.* (2017) 10:1–12. doi: 10.1186/s13071-017-2095-7
54. Waritani T, Chang J, McKinney B, Terato K. An ELISA Protocol to Improve the Accuracy and Reliability of Serological Antibody Assays. *MethodsX* (2017) 4:153–65. doi: 10.1016/j.mex.2017.03.002
55. Klumpp-Thomas C, Kalish H, Drew M, Hunsberger S, Snead K, Fay MP, et al. Standardization of ELISA Protocols for Serosurveys of the SARS-CoV-2 Pandemic Using Clinical and at-Home Blood Sampling. *Nat Commun* (2021) 12:1–13. doi: 10.1038/s41467-020-20383-x
56. Zheng X, Hu X, Zhou G, Lu Z, Qiu W, Bao J, et al. Soluble Egg Antigen From *Schistosoma Japonicum* Modulates the Progression of Chronic Progressive Experimental Autoimmune Encephalomyelitis *via* Th2-Shift Response. *J Neuroimmunol* (2008) 194:107–14. doi: 10.1016/j.jneuroim.2007.12.001
57. Wang T, Wyeth RC, Liang D, Bose U, Ni G, McManus DP, et al. A *Biomphalaria Glabrata* Peptide That Stimulates Significant Behaviour Modifications in Aquatic Free-Living *Schistosoma Mansoni* Miracidia. *PloS Negl Trop Dis* (2019) 13:e0006948. doi: 10.1371/journal.pntd.0006948
58. Fogarty CE, Zhao M, McManus DP, Duke MG, Cummins SF, Wang T. Comparative Study of Excretory–Secretory Proteins Released by *Schistosoma Mansoni*-Resistant, Susceptible and Naïve Biomphalaria Glabrata. *Parasit Vectors.* (2019) 12:1–17. doi: 10.1186/s13071-019-3708-0
59. Tinevez J-Y, Perry N, Schindelin J, Hoopes GM, Reynolds GD, Laplantine E, et al. TrackMate: An Open and Extensible Platform for Single-Particle Tracking. *Methods* (2017) 115:80–90. doi: 10.1016/j.ymeth.2016.09.016
60. Wyeth RC, Braubach OR, Fine A, Croll RP. Videograms: A Method for Repeatable Unbiased Quantitative Behavioral Analysis Without Scoring or Tracking. In: *Zebrafish Neurobehavioral Protocols*. Totowa, New Jersey, United States: Humana Press (2011). p. 15–33.
61. Williams AF, Barclay AN. The Immunoglobulin Superfamily—Domains for Cell Surface Recognition. *Annu Rev Immunol* (1988) 6:381–405. doi: 10.1146/annurev.iy.06.040188.002121
62. Ahn J, Lee J, Jeong S, Kang S-m, Park B-J, Ha N-C. Beta-Strand-Mediated Dimeric Formation of the Ig-Like Domains of Human Lamin a/C and B1. *Biochem Biophys Res Commun* (2021) 550:191–6. doi: 10.1016/j.bbrc.2021.02.102
63. Plotnikov AN, Schlessinger J, Hubbard SR, Mohammadi M. Structural Basis for FGF Receptor Dimerization and Activation. *Cell* (1999) 98:641–50. doi: 10.1016/s0092-8674(00)80051-3
64. Berriman M, Haas BJ, LoVerde PT, Wilson RA, Dillon GP, Cerqueira GC, et al. The Genome of the Blood Fluke *Schistosoma Mansoni*. *Nature* (2009) 460:352. doi: 10.1038/nature08160
65. Jurberg AD, Gonçalves T, Costa TA, de Mattos ACA, Pascarelli BM, de Manso PPA, et al. The Embryonic Development of *Schistosoma Mansoni* Eggs: Proposal for a New Staging System. *Dev Genes Evol* (2009) 219:219. doi: 10.1007/s00427-009-0285-9
66. Jamieson BG. *Schistosoma: Biology, Pathology and Control*. Boca Raton, Florida, United States: CRC Press (2017).
67. Spocter MA, Hopkins WD, Barks SK, Bianchi S, Hehmeyer AE, Anderson SM, et al. Neuropil Distribution in the Cerebral Cortex Differs Between Humans and Chimpanzees. *J Comp Neurol* (2012) 520:2917–29. doi: 10.1002/cne.23074
68. Dorsey CH, Cousin CE, Lewis FA, Stirewalt MA. Ultrastructure of the *Schistosoma Mansoni* Cercaria. *Micron* (2002) 33:279–323. doi: 10.1016/s0968-4328(01)00019-1
69. de Oliveira CNF, de Oliveira RN, Frezza TF, Rehder VLG, Allegretti SM. Tegument of Schistosoma Mansoni as a Therapeutic Target. In: R El Ridi, editor. *Parasitic Diseases–Schistosomiasis*. Rijeka: InTech (2013). p. 151–77. doi: 10.5772/53653
70. Shaiken TE, Opekun AR. Dissecting the Cell to Nucleus, Perinucleus and Cytosol. *Sci Rep* (2014) 4:1–11. doi: 10.1038/srep04923
71. Takaki KK, Rinaldi G, Berriman M, Pagán AJ, Ramakrishnan L. *Schistosoma Mansoni* Eggs Modulate the Timing of Granuloma Formation to Promote Transmission. *Cell Host Microbe* (2021) 29:58–67. e55. doi: 10.1016/j.chom.2020.10.002
72. Ardizzone A, Scuderi SA, Giuffrida D, Colarossi C, Puglisi C, Campolo M, et al. Role of Fibroblast Growth Factors Receptors (FGFRs) in Brain Tumors, Focus on Astrocytoma and Glioblastoma. *Cancers (Basel)* (2020) 12:3825. doi: 10.3390/cancers12123825
73. Mudo G, Bonomo A, Di Liberto V, Frinchi M, Fuxe K, Belluardo N. The FGF-2/FGFRs Neurotrophic System Promotes Neurogenesis in the Adult Brain. *J Neural Transm* (2009) 116:995–1005. doi: 10.1007/s00702-009-0207-z
74. Gonzalez AM, Berry M, Maher PA, Logan A, Baird A. A Comprehensive Analysis of the Distribution of FGF-2 and FGFR1 in the Rat Brain. *Brain Res* (1995) 701:201–26. doi: 10.1016/0006-8993(95)01002-x
75. Cupit PM, Cunningham C. What is the Mechanism of Action of Praziquantel and How Might Resistance Strike? *Future Med Chem* (2015) 7:701–5. doi: 10.4155/fmc.15.11
76. Jones MK, Bong SH, Green KM, Holmes P, Duke M, Loukas A, et al. Correlative and Dynamic Imaging of the Hatching Biology of *Schistosoma Japonicum* From Eggs Prepared by High Pressure Freezing. *PloS Negl Trop Dis* (2008) 2:e334. doi: 10.1371/journal.pntd.0000334
77. Pan S-t. The Fine Structure of the Miracidium of *Schistosoma Mansoni*. *J Invertebr Pathol* (1980) 36:307–72. doi: 10.1016/0022-2011(80)90040-3
78. Ressurreição M, Rollinson D, Emery AM, Walker AJ. A Role for P38 MAPK in the Regulation of Ciliary Motion in a Eukaryote. *BMC Cell Biol* (2011) 12:1–11. doi: 10.1186/1471-2121-12-6
79. Rolfo C, Raez LE, Bronte G, Santos ES, Papadimitriou K, Buffoni L, et al. BIBF 1120/Nintedanib: A New Triple Angiokinase Inhibitor-Directed Therapy in Patients With non-Small Cell Lung Cancer. *Expert Opin Investig Drugs* (2013) 22:1081–8. doi: 10.1517/13543784.2013.812630
80. Ellis PM, Kaiser R, Zhao Y, Stopfer P, Gyorffy S, Hanna N. Phase I Open-Label Study of Continuous Treatment With BIBF 1120, a Triple Angiokinase Inhibitor, and Pemetrexed in Pretreated non–Small Cell Lung Cancer Patients. *Clin Cancer Res* (2010) 16:2881–9. doi: 10.1158/1078-0432.CCR-09-2944
81. Hilberg F, Roth GJ, Krssak M, Kautschitsch S, Sommergruber W, Tontsch-Grunt U, et al. BIBF 1120: Triple Angiokinase Inhibitor With Sustained Receptor Blockade and Good Antitumor Efficacy. *Cancer Res* (2008) 68:4774–82. doi: 10.1158/0008-5472.CAN-07-6307
82. Kapp K, Knobloch J, Schüßler P, Sroka S, Lammers R, Kunz W, et al. The *Schistosoma Mansoni* Src Kinase TK3 is Expressed in the Gonads and Likely Involved in Cytoskeletal Organization. *Mol Biochem Parasitol* (2004) 138:171–82. doi: 10.1016/j.molbiopara.2004.07.010
83. PAN SC-T. *Schistosoma Mansoni*: The Ultrastructure of Larval Morphogenesis in *Biomphalaria Glabrata* and of Associated Host-Parasite Interactions. *Jpn J Med Sci Biol* (1996) 49:129–49. doi: 10.7883/yoken1952.49.129
84. Wu X-J, Sabat G, Brown JF, Zhang M, Taft A, Peterson N, et al. Proteomic Analysis of *Schistosoma Mansoni* Proteins Released During *In Vitro* Miracidium-to-Sporocyst Transformation. *Mol Biochem Parasitol* (2009) 164:32–44. doi: 10.1016/j.molbiopara.2008.11.005
85. Senft AW, Philpott DE, Pelofsky AH. Electron Microscope Observations of the Integument, Flame Cells, and Gut of *Schistosoma Mansoni*. *J Parasitol* (1961) 47:217–29. doi: 10.2307/3275292
86. Collins JJIII, King RS, Cogswell A, Williams DL, Newmark PA. An Atlas for *Schistosoma Mansoni* Organs and Life-Cycle Stages Using Cell Type-Specific Markers and Confocal Microscopy. *PloS Negl Trop Dis* (2011) 5:e1009. doi: 10.1371/journal.pntd.0001009
87. Wendt GR, Collins JN, Pei J, Pearson MS, Bennett HM, Loukas A, et al. Flatworm-Specific Transcriptional Regulators Promote the Specification of Tegumental Progenitors in *Schistosoma Mansoni*. *Elife* (2018) 7:e33221. doi: 10.7554/eLife.33221
88. Soria CLD, Lee J, Chong T, Coghlan A, Tracey A, Young MD, et al. Single-Cell Atlas of the First Intra-Mammalian Developmental Stage of the Human Parasite. *Schistosoma mansoni Nat Commun* (2020) 11:1–16. doi: 10.1038/s41467-020-20092-5
89. Van Hellemond JJ, Retra K, Brouwers JF, van Balkom BW, Yazdanbakhsh M, Shoemaker CB, et al. Functions of the Tegument of Schistosomes: Clues From

the Proteome and Lipidome. *Int J Parasitol* (2006) 36:691–9. doi: 10.1016/j.ijpara.2006.01.007
90. Fonseca CT, Braz Figueiredo Carvalho G, Carvalho Alves C, de Melo TT. Schistosoma Tegument Proteins in Vaccine and Diagnosis Development: An Update. *J Parasitol Res* (2012) 2012:541268. doi: 10.1155/2012/541268
91. Santolla MF, Maggiolini M. The FGF/FGFR System in Breast Cancer: Oncogenic Features and Therapeutic Perspectives. *Cancers* (2020) 12:3029. doi: 10.3390/cancers12103029
92. Steiling H, Wüstefeld T, Bugnon P, Brauchle M, Fässler R, Teupser D, et al. Fibroblast Growth Factor Receptor Signalling Is Crucial for Liver Homeostasis and Regeneration. *Oncogene* (2003) 22:4380–8. doi: 10.1038/sj.onc.1206499
93. Seitz T, Hellerbrand C. Role of Fibroblast Growth Factor Signalling in Hepatic Fibrosis. *Liver Int* (2021) 41:1201–15. doi: 10.1111/liv.14863
94. Xu C, Rosler E, Jiang J, Lebkowski JS, Gold JD, O'Sullivan C, et al. Basic Fibroblast Growth Factor Supports Undifferentiated Human Embryonic Stem Cell Growth Without Conditioned Medium. *Stem Cells* (2005) 23:315–23. doi: 10.1634/stemcells.2004-0211
95. Dvorak P, Hampl A. Basic Fibroblast Growth Factor and Its Receptors in Human Embryonic Stem Cells. *Folia Histochem Cytobiol* (2005) 43:203–8. doi: 10.5603/4597
96. Avery S, Inniss K, Moore H. The Regulation of Self-Renewal in Human Embryonic Stem Cells. *Stem Cells Dev* (2006) 15:729–40. doi: 10.1089/scd.2006.15.729
97. Chen G, Gulbranson DR, Hou Z, Bolin JM, Ruotti V, Probasco MD, et al. Chemically Defined Conditions for Human iPSC Derivation and Culture. *Nat Methods* (2011) 8:424–9. doi: 10.1038/nmeth.1593
98. Wang L, Yang Z, Li Y, Yu F, Brindley PJ, McManus DP, et al. Reconstruction and *In Silico* Analysis of the MAPK Signaling Pathways in the Human Blood Fluke, *Schistosoma Japonicum*. *FEBS Lett* (2006) 580:3677–86. doi: 10.1016/j.febslet.2006.05.055
99. You H, Zhang W, Moertel L, McManus DP, Gobert GN. Transcriptional Profiles of Adult Male and Female Schistosoma Japonicum in Response to Insulin Reveal Increased Expression of Genes Involved in Growth and Development. *I Int J Parasitol* (2009) 39:1551–9. doi: 10.1016/j.ijpara.2009.06.006
100. Andrade L, Mourao M, Geraldo JA, Coelho FS, Silva LL, Neves RH, et al. Regulation of Schistosoma Mansoni Development and Reproduction by the Mitogen-Activated Protein Kinase Signaling Pathway. *PloS Negl Trop Dis* (2014) 8:e2949. doi: 10.1371/journal.pntd.0002949

Conflict of Interest: The authors declare that the research was conducted in the absence of any commercial or financial relationships that could be construed as a potential conflict of interest.

Publisher's Note: All claims expressed in this article are solely those of the authors and do not necessarily represent those of their affiliated organizations, or those of the publisher, the editors and the reviewers. Any product that may be evaluated in this article, or claim that may be made by its manufacturer, is not guaranteed or endorsed by the publisher.

frontiers | Frontiers in Immunology

ORIGINAL RESEARCH
published: 27 June 2022
doi: 10.3389/fimmu.2022.878029

Praziquantel Reduces Maternal Mortality and Offspring Morbidity by Enhancing Anti-Helminthic Immune Responses

Matthew Lacorcia[1], *Réka Kugyelka*[1], *Lorenz Spechtenhauser*[1,2], *Ulrich Fabien Prodjinotho*[1], *Youssef Hamway*[1], *Thomas Spangenberg*[3] *and Clarissa Prazeres da Costa*[1*]

[1] Technical University of Munich (TUM), School of Medicine, Institute for Med. Microbiology, Immunology and Hygiene, Munich, Germany, [2] Department of Biosciences, University of Salzburg, Salzburg, Austria, [3] Global Health Institute of Merck, Ares Trading S.A. (a subsidiary of Merck KGaA Darmstadt Germany), Eysins, Switzerland

OPEN ACCESS

Edited by:
Thiago Almeida Pereira, Stanford University, United States

Reviewed by:
Hermelijn Helene Smits, Leiden University Medical Center, Netherlands
Franco Harald Falcone, University of Giessen, Germany

***Correspondence:**
Clarissa Prazeres da Costa
clarissa.dacosta@tum.de

Specialty section:
This article was submitted to Parasite Immunology, a section of the journal Frontiers in Immunology

Received: *17 February 2022*
Accepted: *30 May 2022*
Published: *27 June 2022*

Citation:
Lacorcia M, Kugyelka R, Spechtenhauser L, Prodjinotho UF, Hamway Y, Spangenberg T and da Costa CP (2022) Praziquantel Reduces Maternal Mortality and Offspring Morbidity by Enhancing Anti-Helminthic Immune Responses. Front. Immunol. 13:878029. doi: 10.3389/fimmu.2022.878029

Alongside the wide distribution throughout sub Saharan Africa of schistosomiasis, the morbidity associated with this chronic parasitic disease in endemic regions is often coupled with infection-driven immunomodulatory processes which modify inflammatory responses. Early life parasite exposure is theorized to drive immune tolerance towards cognate infection as well as bystander immune responses, beginning with *in utero* exposure to maternal infection. Considering that 40 million women of childbearing-age are at risk of infection worldwide, treatment with Praziquantel during pregnancy as currently recommended by WHO could have significant impact on disease outcomes in these populations. Here, we describe the effects of anthelminthic treatment on parasite-induced changes to fetomaternal cross talk in a murine model of maternal schistosomiasis. Praziquantel administration immediately prior to mating lead to clear re-awakening of maternal anti-parasite immune responses, with persistent maternal immune activation that included enhanced anti-schistosome cytokine responses. Clearance of parasites also improved capacity of dams to endure the additional pressure of pregnancy during infection. Maternal treatment also drove lasting functional alterations to immune system development of exposed offspring. Prenatal anthelminthic treatment skewed offspring immune responses towards parasite clearance and reduced morbidity during cognate infection. Maternal treatment also restored offspring protective IgE antibody responses directed against schistosome antigens, which were otherwise suppressed following exposure to untreated maternal infection. This was further associated with enhanced anti-schistosome cytokine responses from treatment-exposed offspring during infection. In the absence of cognate infection, exposed offspring further demonstrated imprinting across cellular populations. We provide

further evidence that maternal treatment can restore a more normalized immune profile to such offspring exposed *in utero* to parasite infection, particularly in B cell populations, which may underlie improved responsiveness to cognate infection, and support the WHO recommendation of anthelminthic treatment during pregnancy.

Keywords: Schistosomiasis, transgenerational immune priming, Praziquantel (PZQ), anthelminthic, fetomaternal cross talk

INTRODUCTION

Alongside the wide distribution throughout sub Saharan Africa of schistosomiasis, a chronic parasitic disease caused mainly by *Schistosoma mansoni* and *Schistosoma haeamatobium*, the morbidity associated with chronic infection remains characterized by immunomodulation and a hyporesponsiveness dependent on parasite burden (1). One potential driver of this phenomenon is *in utero* exposure to circulating schistosome antigens during maternal infection, which could influence the developing immune system of children, and modify anti-schistosome immunity. Immunomodulatory effects of schistosome infection are well-described in the context of bystander immune responses (1, 2), as are modulated immune responses following exposure to maternal infection (3–5), increased levels of schistosome adult-worm specific IgE and IgG in newborns cord blood whose mothers were infected during pregnancy (and not treated) (6). Schistosome antigens can drive immunomodulatory changes *via* presence in breastmilk (7), and have been detected as persisting in human children and murine offspring following exposure to maternal infection (8, 9). Murine models demonstrate that exposure to maternal infection with schistosomes consistently modifies immune development, with recent findings included impact upon B cell priming and DC-T cell interactions (5), as well as NKT cells (3).

Further infant outcomes of maternal parasite infection include earlier immune maturation (B cells), spontaneous (polyclonal) IgE, decreased infantile eczema episodes, anti-parasite IgG, lower vaccine-induced Ig-titres, suppressed T cell responses (anti-parasite and against vaccine antigens), altered T helper cell responses, increased regulatory responses (IL-10), and modified APC status (as reviewed in (10) and (11)). Considering that 40 million women of reproductive age are at risk of infection worldwide, treatment with Praziquantel (PZQ) during pregnancy could have significant impact on disease outcomes in these populations. PZQ has been effectively used for decades against adult schistosomes, *via* a recently described mode of action targeting a transient receptor potential melastatin ion channel (12). However, there is hesitancy to follow the WHO recommendation for treatment during pregnancy, as PZQ, marketed as Biltricide®, and donated for use within WHO-agreement as Cesol 600, is classed as a Category B drug for pregnancy, with animal studies not indicating a risk to the fetus, but with insufficient controlled studies in humans at this point (13). In existing studies, Praziquantel treatment has not been associated with adverse events regarding birth weight, fetal mortality, or congenital abnormalities (14). Anthelminthic strategies have been described to drive further changes associated with the re-awaking of the anti-parasite immune response, through disturbance of the regulatory states maintained by live parasites to ensure their survival within hosts (1). However, altered inflammatory outcomes have been associated with maternal treatment during pregnancy, including modified allergic parameters (15), and boosted immune responses to schistosome antigens after pregnancy (16). Enhanced immune priming during treatment is thought to occur due to death and degradation of worms, leading to increased load of worm antigens in the system, contributing to a natural partial-resistance hypothesized to develop of slowly as exposures to dead worms accumulate (17).

Treatment-induced shifts in schistosome-directed immune responses, particularly to antigens found in adult worms, can re-focus the tolerogenic modulations accumulated through chronic infection. Accordingly, treatment of *S. haematobium* infected children increased their IgG4 and IgE to adult worm antigen (AWA) as well as IgE to soluble egg antigen (SEA) (18), and a similar boost was seen following PZQ treatment of pregnant women infected with *S. mansoni*, where treatment caused a boost in IgG1, IgG2, IgG4 specific against worm antigens and enhanced IgE levels against SEA in the mothers (16), and enhanced cytokine levels (19). The well-established mouse model of *S. mansoni* [summarized in (20)], benefits from using a human pathogen in its preferred niche of the hepatoportal vasculature, and previously revealed materno-fetal effects including transcriptional changes in the placenta (21), later validated in human cohorts (6). Similarly, previous studies in murine systems of employing direct infection of previously schistosome-exposed offspring demonstrated transfer of schistosome antigens and anti-schistosome antibodies *in utero* and through breast milk, further associated with modified infections and reduced immune responsiveness (22), with detectable antibodies in neonatal mice arising from acute maternal infection further associated with reduced liver pathology and lower worm burden (9).

The shifting character of the anti-schistosome immune response across phases of infection is well described (23), with maternal infection phase, and likely associated cytokine profiles, further reflected in later offspring immune responses, able to differentially modify reactivity to allergens (21). Differences of priming effects also occur when comparing routes of maternal exposure, such as *via* breastmilk or *in utero* exposure (7). Parasite

load presents another further variable, as-yet underexplored in maternal infection settings, yet determinants of worm burden are shown to impact host bystander immune responses (2). As such, the shared mechanisms behind transgenerational effects on cognate infection remain unclear, and with suggestions that these may involve processes linked to trained immunity (24) in innate cells, or specific priming in adaptive cells, such as in B cells, as has also been shown for other infections (25).

In line with these human cohort studies and murine models, here we focused on the interaction between immune imprinting effects of maternal helminth infection during pregnancy, and anthelminthic treatment with PZQ. Using this murine model, we explored the added implications of maternal treatment in transgenerational priming, and more specifically the hypothesis that the immune reactivation events triggered by PZQ-induced worm death during maternal treatment can imprint offspring immunity, with particular regard to cognate schistosome-direct immune responses. We link this to a profile of how prenatal treatment can disrupt the steady state immune priming imprinted *via* maternal parasite infection, changes that may not only underlie responses to schistosome infection, but also whether treatment of maternal infection can restore a more normalized immune profile to such offspring exposed *in utero* to parasite infection. These data provide supporting information regarding the WHO recommendation of anthelminthic treatment during pregnancy.

RESULTS

Beneficial Impact of Anthelminthic (PZQ) on Maternal Schistosomiasis Is Accompanied by Persistent Maternal Immune Activation

In order to compare the transmaternal priming effects induced by prenatal anthelminthic treatment, maternal mice were divided into groups at week 10 of infection, following the type-2 dominant immune phase that peaks between weeks 7-9, at which time half of these were given a single dose of 400mg/kg PZQ, the other half only the vehicle (as per scheme in **Figure 1A**), and paired with naïve males. By the end usual 21-day gestation period, there was a clear difference in the successful survival of treated dams, compared to untreated dams, some of which needed to be removed from the experiment, unable to successfully bear the additional burdens of birth and the nursing period alongside a heavy parasite burden, as indicated by the drop in the blue line (**Figure 1B**). Although treatment clearly enhanced the ability of infected dams to effectively manage the requirements of pregnancy and birth, those dams who were infected had significantly smaller litter sizes compared to uninfected, naïve dams, regardless of subsequent treatment (**Figure 1C**). This was further reflected in the more regular gestation period of naïve mothers, in general giving birth in

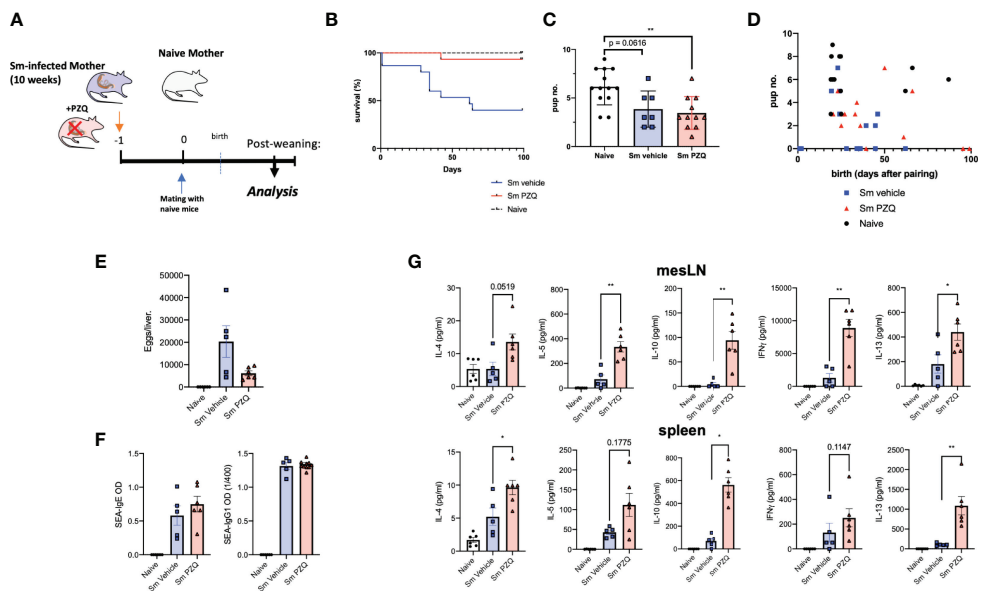

FIGURE 1 | Impact of Anthelminthic (PZQ) on Maternal Schistosomiasis. **(A)** Model of exposure to maternal schistosomiasis, with ("Sm PZQ") or without ("Sm vehicle") additional anthelminthic treatment with PZQ in female mice, with subsequent maternal immune analysis post-weaning, with pairing occurring at day 0. **(B)** Survival curve of infected, treated, and naïve dams over the 100-day mating period post-anthelminthic treatment. **(C)** Number of pups per litter for dams with successful mating outcomes. **(D)** Comparison of pup number per litter with time (days) until birth. **(E)** Numbers of schistosome eggs per liver of infected dams. **(F)** SEA-specific IgE and IgG1 antibody titres in serum of dams. **(G)** Levels of secreted IL-4, IL-5, IFNγ, IL-10, and IL-13 as determined by ELISA in splenocyte and mesenteric lymph node cell culture supernatants after *ex vivo* re-stimulation with schistosome egg antigens (SEA). **(B)** through **(D)** is pooled from 2 independent maternal cohorts, with an initial total of 15 dams per condition. **(E)** through **(G)** show data from a representative maternal cohort, with an initial 7 dams per condition. Statistical differences induced by treatment between infected dam cohorts obtained *via* two-tailed *via* student's T-test, or two-tailed Mann-Whitney U-test where data did not fit a normal distribution, *$p < 0.05$, **$p < 0.01$, shown as mean ± SEM.

relative unison at the 3-week time point, compared to the more variable infection groups (**Figure 1D**). Upon end-point analysis, all PZQ-treated dams showed typical liver pathology of schistosomiasis upon visual inspection of successful patent infection, with the presence of eggs, although with visible trend of lower average egg number per liver compared to untreated infected dams (**Figure 1E**). Perfusion of livers yielded no surviving worms from treated mice, nor could these be identified in the intestines, as further confirmation of successful infection followed by successful treatment-based killing of the parasites. PZQ treatment did not appear to have a detectable effect on schistosome (egg)-specific antibody titers (**Figure 1F**).

Alongside these expected beneficial modified outcomes to infection, treatment of infection led to a lasting (re-)activation of immune responses in infected dams. Across mesenteric lymph nodes (mesLN) and spleens, *ex vivo* responses to schistosome egg antigens (SEA) demonstrated a clear immune enhancing effect of maternal treatment. This included enhanced levels of IL-4, IL-5, IFN-gamma, and IL-13 in supernatants of SEA-stimulated cell suspensions from either or both of spleen and mesLNs (**Figure 1G**), and indicates not only a degree of maternal immune activation (MIA) previously described for maternal cytokine alterations following viral infection (or its mimicry) during pregnancy (26), but a persistence of altered cellular functionality many weeks after treatment. TCR-based stimulation yielded similar enhanced responses from cells of treated mothers, with clearly increased IL-4, IL-10, and IL-13 responses from mesLN cells and splenocytes (**Supplement 1A**). Serum cytokine levels revealed long-term maintenance of altered profiles even in the case of treatment, with infection increasing IL-2, IL-13, GM-CSF, IL-5, among other cytokines, but these were not markedly altered following treatment (**Supplement 1B**).

Prenatal Anthelminthic Treatment Skews Offspring Immune Responses Towards Parasite Clearance

Whether enhanced maternal anti-schistosomal immune responses induced by prenatal PZQ administration impacted subsequent offspring immunity to cognate infection was examined by *S. mansoni* infection of offspring either exposed to treated or untreated maternal schistosomiasis, as described earlier. These offspring themselves were examined after the 8th week of infection (depicted in **Figure 2A**). A typical loss of bodyweight during infection was observed in naïve offspring as part of the disease progression during infection compared to uninfected controls. Comparing the effects of maternal anthelminthic treatment, those offspring of PZQ-treated infected mothers exhibited closer to normal bodyweight after patent infection, compared to the lowered weights of those exposed to untreated schistosomiasis (**Figure 2B**). This was further associated with a reduced worm burden in these PZQ-treatment exposed offspring compared to those born to infected, untreated mothers, showing on average 31% less worms (P = 0.0278), as retrieved from liver perfusion and further inspection of intestines (**Figure 2C**). Average

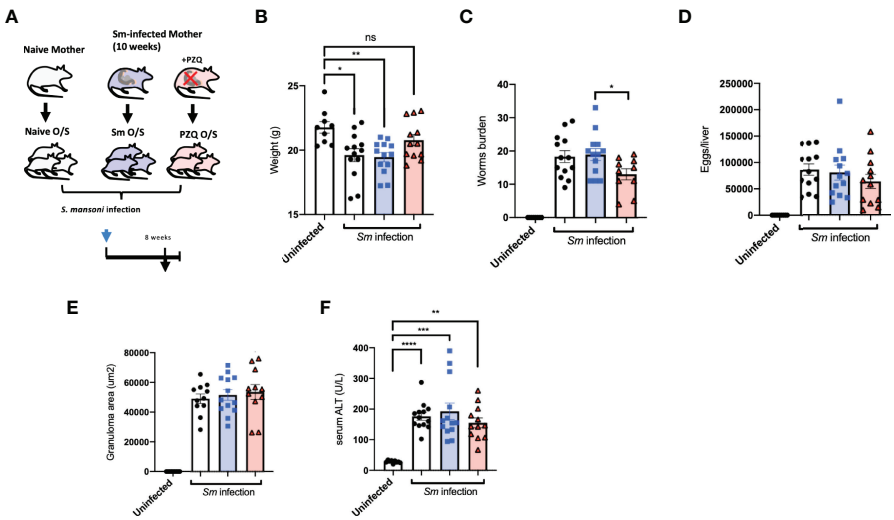

FIGURE 2 | Prenatal anthelminthic treatment modifies infection outcomes during cognate schistosomiasis. **(A)** Generation of offspring exposed to maternal schistosomiasis, with ("PZQ O/S") or without ("Sm O/S") additional anthelminthic treatment other mothers, or from naïve dams ("Naïve O/S"), and subsequent cognate infection of all 3 groups with schistosomiasis. **(B)** Weight of adult offspring following 8-weeks of schistosomiasis. **(C)** Number of worms retrieved from infected offspring mice. **(D)** Extrapolated schistosome egg count per liver of infected offspring mice. **E)** Average size (area) of granulomas observable within livers of infected offspring mice after Masson's trichrome stain of liver sections. **(F)** Alanine aminotransferase (ALT) levels in serum after cognate infection. Data from 2 independent infection experiments, each consisting of offspring from all 3 maternal exposures, with total n = 13-18 per infected group, with mothers: n = 3-6 per group. Statistical differences directly attributable to maternal treatment (i.e.: between offspring of infected dams) obtained *via* two-tailed *via* student's T-test, or two-tailed Mann-Whitney U-test where data did not fit a normal distribution, or Kruskal-Wallis test plus subsequent individual comparisons from among all groups, *p < 0.05, **p < 0.01, ***p < 0.001, ****p < 0.0001, ns = not significant, shown as mean ± SEM.

eggs per liver showed similar trends, which although were not significantly different between offspring cohorts (**Figure 2D**), were significantly correlated to number of retrieved worms (**Supplement 2A**). Examination of liver sections from infection offspring cohorts did not reveal major differences in terms of granuloma formation in association with pre-exposure to maternal schistosomiasis (**Figure 2E**). Levels of alanine aminotransferase (ALT) in serum, as indicative of hepatic disease, weakly followed the pattern seen in worm burden, but did not reveal major differences between infected offspring cohorts (**Figure 2F**). Offspring serum cytokine levels during cognate infection further reflected the milder disease progression in offspring of PZQ-treated mothers compared to other groups, showing lower levels of infection-induced CCL5 (RANTES), and indications of lower amounts of IL-13, IL-5, IL-1b, IL-10, and IL-12p40 compared to standard infection of unexposed offspring (**Supplement 2B**).

Prenatal Anthelminthic Treatment Enhances Schistosome-Specific Immune Responses

Ex vivo re-stimulation with SEA of offspring-derived splenic and mesLN cell suspensions after infection revealed distinct priming effects resulting from maternal exposure in terms of subsequent cytokine levels in culture supernatants. Specifically, T_H2-associated cytokines IL-4, IL-5, IL-10, and IL-13 from splenic cell preparations appeared elevated in offspring exposed to treated maternal schistosomiasis (**Figure 3A**). Further TCR-based stimulation induced increased levels of IL-13 production from PZQ-treatment exposed offspring during cognate infection (**Supplement 3**). In terms of site-specific effects, interestingly both treated and untreated pre-exposed offspring groups showed induction of IFN-gamma compared to uninfected mice in their mesLN suspensions, (**Figure 3B**) not observed in infected offspring from naïve mothers, indicating further disturbance of usual cytokine dynamics through prior transmaternal exposure to infection. This was not reflected in spleens, and more generally mesenteric cytokine responses (potentially due to proximity to the parasite niche) appeared to be a greater site of variation than spleens.

Antibody responses are induced strongly through schistosome infection, and as already described both schistosome-specific and polyclonal antibody titers have been suggested as induced through maternal helminth exposures. Overall, maternal schistosome infection drove lower SEA-IgG1 schistosome responses during infection (**Figure 3C**, upper), compared to infection of previously unexposed mice. Interestingly, however, was the apparent effect of maternal exposure on schistosome-specific IgE levels, known to be a specific part of the protective clearance response. Here, prior exposure to live maternal infection drove clearly lower levels of IgE (**Figure 3C**, lower), indicating a potential suppressive role on the ability to mount protective antibody responses (from live maternal infection), potentially indicating some degree of tolerance or ineffective response. This appeared instead restored with maternal PZQ-treatment, with those offspring instead displaying SEA-IgE titers closer to those of unexposed offspring.

Prenatal Anthelminthic Treatment Redirects Transgenerational Priming of DC and B cell Compartments

We then performed a further profiling of changes induced by maternal schistosomiasis, and in particularly how these are further impacted by the special case of PZQ treatment, within the steady-state (as in the overview **Figure 4A**). There were no clear alterations in serum cytokine concentrations, although

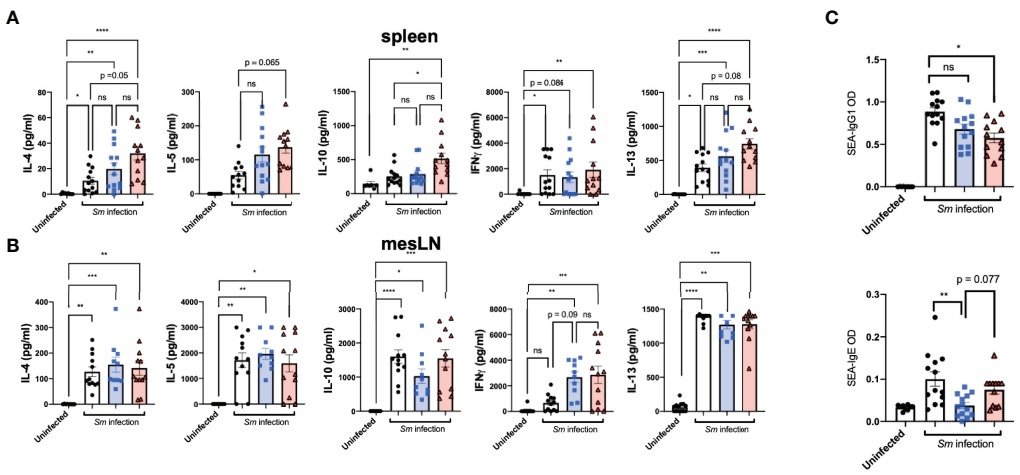

FIGURE 3 | Prenatal anthelminthic treatment modifies schistosome-directed cellular and humoral immune responses following cognate schistosome infection of offspring. Levels of secreted IL-4, IL-5, IFNγ, IL-10, and IL-13 as determined by ELISA in splenocyte **(A)** and mesenteric lymph node **(B)** cell culture supernatants after *ex vivo* re-stimulation with schistosome egg antigens (SEA). **(C)** SEA-specific IgE and IgG1 antibody titres in serum of dams. Data from 2 independent infection experiments, each consisting of offspring from all 3 maternal exposures, with total n = 13-18 per infected group, with mothers: n = 3-6 per group. Statistical differences analysed *via* Kruskal-Wallis test plus subsequent individual comparisons from among all groups, *p < 0.05, **p < 0.01, ***p < 0.001, ****p < 0.0001, ns = not significant, shown as mean ± SEM.

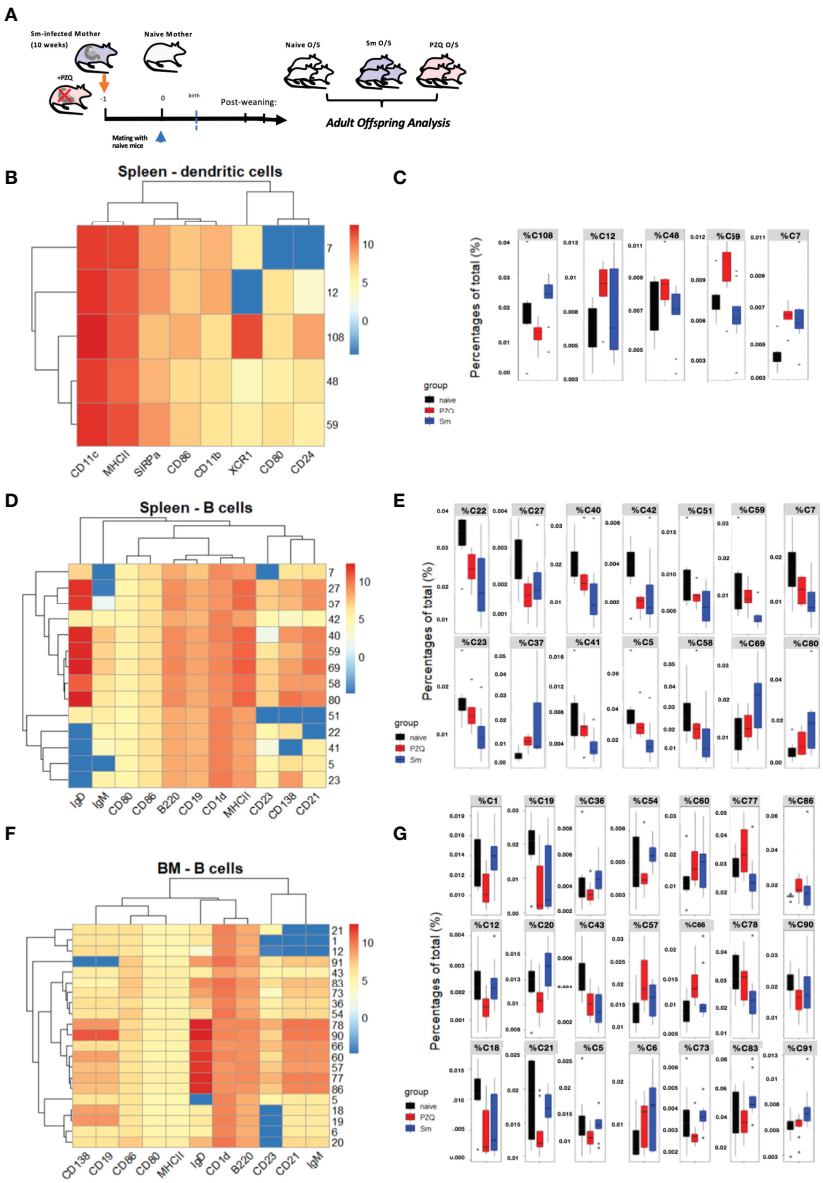

FIGURE 4 | Prenatal anthelminthic treatment redirects transgenerational priming via maternal schistosomiasis. **(A)** Generation of adult steady-state offspring exposed to maternal schistosomiasis, with ("PZQ O/S") or without ("Sm O/S") additional anthelminthic treatment other mothers, or from naïve dams ("Naïve O/S"). FlowSOM-based splenic DC analysis, with **(B)** as corresponding heatmap of cluster identities and **(C)** showing differential enrichment of clusters (cluster % of total cells) quantified according to offspring groups. Differential clusters profiled in heatmap **(D)** of splenic B cell populations, and quantified per group in **(E)**. Differential clusters from bone marrow B cell populations profiled in heatmap **(F)** and relative cluster enrichment quantified per group in **(G)**. Data from 2 independent experiments, each consisting of offspring from all 3 maternal exposures, with total n = 6-10 per group, with mothers: n = 3-6 per group.

some indications of mild increases in T_H2-type cytokines (including IL-4 and IL-5) after exposure to maternal schistosomiasis (**Supplement 4A**), with only limited signs of impact from maternal PZQ-treatment, which also appeared not to discernably alter transmaternally-induced SEA-specific antibody levels nor shifts in total IgE or IgG1 antibody titers at steady state during this infection phase (**Supplement 4B**). We further conducted multiparametric cytometric analysis, and generation of relatively high-dimensional data, sampling spleens and bone marrow and multicolour antibody panels with a focus on dendritic cells and B cells, which we recently identified as site of maternal priming after schistosome infection (5). We applied the FlowSom algorithm (27, 28) to the generated flow cytometry-based data sets, generating self-organizing maps through unsupervised clustering of the acquired events, and developing those into minimal spanning trees (MSTs) that visualize and distinguish the cell populations within samples as based on identified clusters and metaclusters. The MST

generated using manually pre-gated $CD11c^+MHCII^+$ conventional DCs (**Supplement 4D**), where group-wise comparisons identified 5 clusters where maternal schistosomiasis and/or its treatment with PZQ modified the relative enrichment of cells, the expression profile of these displayed in the heatmap (**Figure 4B**). Based on the proportion of cells within these clusters, as a percentage of total events (**Figure 4C**), both clusters C7 and C12 appear enriched in splenic DCs after exposure to maternal schistosomiasis, regardless of treatment, and are SIRP-α^+XCR1^{low}, indicative of cDC2-like subsets. C59, however, appears specifically enriched after exposure to PZQ-treated schistosomiasis, although its cluster-profile remains relatively indistinct. C108 has clear splenic cDC1 phenotype, high CD24 and XCR1, and relatively high CD86, and has clearly distinct group-wise effects: enriched after exposure to maternal schistosomiasis, but relatively reduced after exposure to treatment. Whether these cells represent the modified DC phenotype that we recently identified after chronic maternal schistosomiasis (5), particularly by bearing the CD86 signature of activation in both cDC1 and cDC2 populations *via* schistosomiasis and schistosome antigens (29), may warrant further mechanistic investigation in the switch that occurs following treatment.

When applied to pre-gated B cells, based on their B220 and/or CD19 expression, the FlowSOM output identifies many points of difference induced *via* maternal schistosomiasis (the expression profile of differentially enriched splenic B cell clusters shown in heatmap **Figure 4D**, with organization of all clusters instead visualized in the MST, **Supplement 4E**). In the spleen, untreated maternal schistosomiasis led to the largest effect in differential enrichment of the many clusters identified, with cells from offspring of PZQ-treated mothers instead showing an intermediate phenotype between naïve and schistosome-exposed (quantified in **Figure 4E**) with C59 representing a potentially interesting exception, with PZQ-primed offspring showing similar levels to naïve mice, and the underrepresentation of these MZ-like, $CD1d^{hi}$ cells potentially indicating a tolerogenic immunomodulation imprinted by the live-infection alone. Additionally, both Sm-primed offspring groups shown underrepresentation of C27, which forms its own metacluster (MC8), and exhibits a $CD21^{lo}$, IgM^{hi}. IgD^{lo} transitional B-cell-like phenotype. In the bone marrow, however, numerous clusters were identified to be differentially enriched in schistosome-exposed compared PZQ-treatment exposed offspring (expression profiles of these shown in heatmap **Figure 4F**, cluster proportions quantified in **Figure 4G**, and full MST visualization of cluster organization shown in Suppment 4F). This includes a set of clusters that exhibited marginal zone-like or IgM^+ innate-like memory phenotype (clusters 20, and 21, 1, and 12, respectively), which are all lowered in offspring by maternal PZQ-treated infection, with some instead showing enrichment after live schistosomiasis (such as cluster 20), which, considering the noted roles of these cells in maintenance of homeostasis and production of regulatory cytokines (and similarity to phenotypes displayed by SEA-induced regulatory B cells (29)), could be involved in the switch from tolerance to active protection observed in during cognate infection of offspring from these groups. Similarly, the clusters C91, C83, C73, C54, C20 show the highest amounts of CD1d, and further appear specifically enriched only after untreated Sm-only. These could further indicate cells with activation-induced regulatory functions as observed in schistosome infection, as an additional hallmark of such cells in previous studies was CD1d expression (30), which has also previously been linked to IL-10 production and therefore a pro-regulatory immune predisposition. Further, those B cell clusters significantly and specifically enriched in bone marrow of the PZQ-primed offspring (clusters C57, C66, C77 and C86), however, all fall within the central grouping of the heatmap, and are notable for high levels of IgD expression, as well as increased CD138, indicative together of an increased maturation profile, and therefore could be involved in the preparedness towards infection evidenced during cognate infection.

DISCUSSION

Environmental changes during early life are increasingly understood to impact proper development and education of the immune system. Of the many potential changes to the gestational environmental, maternal infection during pregnancy has been identified as a key factor driving heterologous immune responses (31). Maternal viral infection during pregnancy has been linked to numerous developmental changes, and has become explored experimentally through maternal immune activation models (26). Prenatal elimination of schistosomiasis through anthelminthic treatment has been shown to modify transgenerational effects of maternal schistosomiasis on atopy (15), and may poise the immune system for responsiveness to cognate infection. Indeed, recent discussions have highlighted the complexity of factors present during schistosome infection (11). Here, by means of a chronic schistosome infection mouse model, we uncover that the modified systemic immunological signature imparted by treating schistosomiasis is transferable from mothers to their offspring, distinguishable from active chronic infection by increased cytokine reactivity to schistosome antigens. Alongside improving pregnancy outcomes, prenatal treatment of schistosomiasis induced a form of maternal immune activation (otherwise described from maternal viral infection or models of this (26)) as signified by strongly increased antigen-specific T_H1 as well as T_H2 cytokines. We find that PZQ treatment boosted maternal cellular cytokine responses, in line with responses from treatment during pregnancy in human cohorts (19), and that this persists well beyond the point of weaning and therefore may impact the entire period of maternal contact for pups. The resultant improvements in offspring immunity to cognate schistosome infection indicate imprinting of this activation upon the developing immune system through transmaternal

exposure. This altered offspring immune response by such treatment-exposed offspring to cognate schistosome infection, characterized by enhanced T_H2-type cytokine responses to schistosome antigens, with a notably boost in SEA-induced IL-10 levels, and modified SEA-specific antibody levels. It is interesting to note that one of the clearest differences induced by exposure to treated maternal schistosomiasis was SEA-induced IL-10 levels, which reflects previous human studies where responses to schistosome antigens involving this cytokine was notable as elevated in children of PZQ-treated women (32). That maternal treatment was associated with normalized anti-schistosome IgE levels during cognate infection, otherwise suppressed by exposure to live maternal infection, reflects previous findings of detrimental effects of maternal schistosomiasis on effective induction of specific antibody titers (3). Treatment of helminth infection in humans was previously associated with increased IgG4 and IgE antibody responses (18), although pregnancy itself has been suggested to have a dampening effect of such boosting of antibodies (16). Recent data from our group demonstrated altered antibody transfer to children of schistosome-infected (yet untreated) mothers), in association with placental inflammatory parameters (6). Other infection parameters appeared largely unaltered by exposure to maternal infection in the absence of treatment, indicating only relatively faint specific immune effects in this setting, but the activating effect of maternal anthelminthic treatment was further associated with a modified appearance of infection-associated pathology, namely with reduced weight loss, lower worm burden, and associated signs of lower egg burden. Alongside the more general immune activation that follows treatment, the differential effect of exposure to PZQ treated versus non-treated maternal schistosomiasis may derive from specific induction on anti-worm versus anti-schistosome egg immune responses, the former not developing in the absence of worm death (17) and therefore may be enriched in the PZQ-treated groups. As with treatment leading to development of some resistance for infected hosts (33), this may similarly contribute to the transmaternally-primed partial resistance indicated in this study. This positions PZQ-treated maternal infection as a particular priming stimulus, that may differ in effect from untreated parasite infection, generally thought to downmodulate offspring anti-parasite responses to optimize the cross talk with the next generation of potential hosts, as observed in maternal malarial infection, where active (but not treated) maternal infection enhanced IL-10+ regulatory CD4+ T cells in cord blood that inhibited parasite-specific IFN-gamma responses (34). Additional dynamics of treatment (e.g.: PZQ given later during pregnancy) therefore represents a further avenue for research into this effect, as the timing of antigen release from dying worms, and the accompanying cytokine activation following treatment, could modify the amplitude of the priming effect on the next generation.

Despite the observance of reduced weight-loss during cognate infection following exposure to treated maternal schistosomiasis, the absence of a clear impact on schistosomiasis-induced liver pathology (in contrast to reports of total absence of egg-induced granulomas in some settings (9) suggests limits to protective effect of maternal treatment, at least in the context of a experimentally induced, high-burden infection. The reduced induction of serum cytokine levels, however, further supports an overall profile of reduced inflammatory pathology during infection. That these treatment-exposed offspring showed modified infection responses may further be linked to altered cellular priming, particularly within B cell activation state and B cell subset proportion, which we have observed after exposure to maternal schistosomiasis. Our cluster-based analysis allowed us to identify differences across subpopulations not immediately identified by manual gating, and further to assess these differences in an unsupervised way, and revealed the influence of maternal PZQ treatment. This includes a modification to the transgenerational priming driven by the parasites, which in the steady state did leave a signature of increased activation markers and modified enrichment of B cell subsets, evident in the bone marrow, which may further indicate priming alterations to hematopoiesis and trained immunity that remain to be elucidated, and deepens our profiling of the activation-induced enhanced regulatory phenotype described using manual gating-based analysis of DCs in our previous work (5). One such important change may be the underrepresentation of $CD1d^{hi}$ B cells in offspring primed by live infection, with SEA-loaded cells previously shown to activate NKT cells in a CD1d-dependent manner (35) and NKT functionality recently shown to be affected by maternal schistosomiasis and associated with dampened responsiveness to immunization in a cascade involving instead lower IL-4 and reduced B cell priming, when evaluated early at the onset egg-deposition in patent infection in mothers (3). This indicates a potential pathway for transgenerational immune interference by maternal infection, with possible links to the modified regulatory network postulated to alter offspring bystander immune responses. Late into chronic infection these suppressed offspring bystander responses are instead associated with an IL-4-skewed, modified type 2 phenotype (5), typical of the regulatory network present during chronic infection itself (36). Further, detailed analysis of differences in antigen-specific immunity and repertoire changes may further illuminate the transmaternal priming effect driven by PZQ-treatment, including potential differences that may exist in effector T cell and antibody-responses against worm-derived antigens compared to those direct against egg antigens. Findings from human studies of treatment during pregnancy have found that although treatment during pregnancy augmented cytokine responses to SEA, that overall schistosome-directed cytokine responses were dampened during pregnancy (19), indicating further cross talk between infection and the tolerogenic immune processes characteristic of pregnancy. The timepoint at which maternal immune responses were measured during our current study was well after when such potential dampening effects of pregnancy would be likely to be observed. As such, a further opportunity

offered by this murine model would be to explore in detail the direct effects on fetal development that occur during the *in utero* period (that is, earlier end-analysis of maternal immune responses), and deeper profiling of how infection and treatment alter the dynamic of cytokine environment to induce transgenerational priming following the maternal immune activation.

In humans, the currently running, prospective freeBILy study (registration number NCT03779437) gathers information on PZQ usage in pregnant women, a vulnerable population not usually included in mass drug administration programs, assessing the impact of diagnostics and PZQ-based treatment upon health-related quality of life in children, as well as incidence of schistosome infection in these individuals. The planned assessment of infant infection in association with maternal PZQ treatment (37) may add information about the priming effects of maternal infection and immune activation in human children. Through improved application of diagnostics, the results of such studies will facilitate integration of pregnant women into schistosomiasis treatment programs, as well as providing additional important safety information that will further inform guidelines (38). Our current murine-based study shows that maternal PZQ treatment can lead to non-specific priming effects, as well as partial resistance to cognate infection in mice, and would thus support the current WHO recommendation of anthelminthic treatment during pregnancy which is still met with hesitancy in the field. Further studies in human cohorts, such as FreeBILy, may provide additional valuable information on whether the observed effects translate to clinical settings.

MATERIALS AND METHODS

Animal experiments were performed under national and European Union guidelines 2010/63, and in accordance with specific approval by regional governmental authorities of Upper Bavaria (license AZ ROB-55.2-2532.Vet_02-17-145). C57BL/6J mice were purchased from Envigo (Germany). All mice were fed standard chow and housed under specific pathogen-free conditions at the Technical Univerity of Munich (TUM), Institute of Med. Microbiology, Immunology, and Hygiene, Munich, Germany.

C57BL/6 female mice were infected with 100 *S. mansoni* cercariae (using the in-house maintained Brazilian strain, with life cycle kept in mice), *via* subcutaneous injection into the flank (as demonstrated in **Figure 2C**, leading to on average 15-20 adult worms by week 8). These reached the 10^{th} week of infection (end of the peak T_H2 immune response) when half of the infected mice (8 out of 16) were then treated with a single oral dose of PZQ at 400mg/kg in 10% Cremaphor (in H_2O). This was given as a single treated at one-time point. Infected mice not receiving praziquantel received instead on the vehicle (10% Cremaphor), as did the control uninfected mice (all also *via* oral gavage). The following day, mice were mated with naïve male C57BL/6 mice. Offspring mice were weaned at 21-days of age. Upon end-analysis, dams were sacrificed, and successful infection plus treatment was confirmed by visual inspection of livers, in combination with absence of worms either retrieved *via* liver perfusion or inspection of intestines. For cognate infection experiments investigating offspring responses following maternal exposure, adult offspring cohorts (minimum of 6 weeks old) were infected *via* the same method, but were instead analyzed at week 8 after infection to assess peak responses. Infected mice were euthanized with sodium-pentobarbital (Narcoren, Boeringer Ingelheim) at a dose of 5ml/kg (800mg/kg) bodyweight.

For assessment of secreted cytokines in supernatant, cell suspensions were treated with SEA (produced in-house from hamster-derived schistosome eggs, at 20μg/ml), or anti-T cell receptor (TCR) stimulation *via* anti-CD3/CD28 (1μg/ml each). Unstimulated controls standardized to similar volumes using medium alone. Measurement of SEA-IgG1 and SEA-IgE in serum was performed with in-house ELISA as adapted from (39). Briefly, 1μg of SEA in 50μl PBS was used to coat each well of a 96-well microtiter plate overnight (NUNC). After washing 3x with PBST, these were blocked for 2h at RT with 3% (w/v) in PBS. After a further 3x washing, 100μl of serum diluted in BSA blocking buffer was probed for 2h at RT, washed again, then probed with 100μl detection antibody (biotinylated anti-mouse IgE or IgG1, Biolegend) diluted at 1:400 for 2h at RT. After washing, detection antibody was conjugated to 50μl Avidin-HRP peroxidase diluted 1:1000 for 30min at RT (in the dark), washed, then 50μl undiluted TMB substrate (eBioscience) was added per well and allowed to develop in the dark, before stopping with 50μl of 2 N H_2SO_4.

Granuloma area was calculated from formalin fixed (4%) paraffin-embedded cut sections (4μM) of liver and intestine samples after standard Masson's trichrome staining and microscopic analysis as previously described (40) using up to 40 granuloma per mouse to calculate an average area μm^2 per mouse. Determination of *S. mansoni* egg numbers per liver performed described previously (21) using 5% (w/v) KOH digestion of liver samples. Multiplexed analysis of serum cytokine levels was performed using Bio-Plex Pro Mouse Cytokine 23-plex Assay #M60009RDPD (Bio-Rad), according to manufacturer's instructions with an initial 1:4 dilution of sample, and run on a Bio-Plex 200 System (Bio-Rad). Culture supernatants were instead analyzed using Mouse Ready-Set-Go ELISA kits (IL-4, IL-5, IFNγ) (eBioscience) or Mouse Duo-Set ELISA kit (IL-10)(R&D), according to manufacturer's instructions. Alanine aminotransferase (ALT) levels in serum, indicative of hepatic disease, and were measured using a 1:4 dilution in PBS, and Reflotron GPT/ALT tests (Roche Diagnostics, Mannheim, Germany).

Flow-cytometry was performed as previously described (5), with cells were acquired using the flow cytometer Cytoflex S (Beckman Coulter) and initially analyzed in FlowJo 10 (v10 TreeStar). For B-cell analysis of spleen and bone marrow, live cells were gated on by excluding cells that were positive for propidium iodide (PI) (Biolegend), and pre-gated on cells positive for B220-APCH7 and CD19-BV510 (Biolegend). Further staining for B-cell subsets included IgM-BV605, IgD-PE-Cy7, CD23-AF700, CD21-PE-Dazzle594, CD138-PE, CD1d-BB700, CD80-FITC, and CD86-APC (all Biolegend), and MHCII-ef450 (eBioscience). For DC analysis, live cells were gated on by excluding cells that were positive for PI (double positive for PE

and ECD), monocytes and monocyte-derived macrophages were excluded by expression of CD64 PerCP5.5 (Biolegend), Tissue resident Macrophages were excluded by the expression of F4/80 PE (eBioscience). cDC were identified by the high expression of CD11c-PE-Cy7 (Biolegend) and MHCII-ef450 (eBioscience). Further staining for DC subsets included XCR1-BV650, CD11b-BV510, CD172a (Sirp-α)-APC/Fire 750, CD24-AF700, CD80-FITC, and CD86-APC (all Biolegend).

For the FlowSOM analysis, fcs files were pre-gated in FlowJo for $CD11c^{+}MHCII^{+}$ conventional DCs or B cells based on B220 and/or CD19 expression. The exported samples were quality controlled (removal of low-quality events) using the PeacoQC algorithm (41) then processed with the FlowSOM workflow (28) and concatenated from individual samples. The SOMs were visualized using minimal spanning trees (MST). For dendritic cells, 145 922 cells were used for producing a self-organizing map (SOM) with a 11x11 grid, producing 121 clusters and 10 metaclusters (**Supplement 4D**). For splenic B cells, 1 559 562 cells were clustered in a 9x9 grid, resulting in 81 clusters and 12 metaclusters (**Supplement 4E**). From the bone marrow, 335 603 B cells were used in a 10x10 grid, producing 100 clusters and 12 metaclusters (**Supplement 4F**). To find clusters that were differentially represented in the experimental groups, median percentages of clusters of total number of cells and fold changes per cluster were compared using a Wilcoxon test. Significant clusters where characterized by the mean fluorescence intensities (MFI) of the markers used for clustering, heatmaps show scaled MFI values (pheatmap package https://github.com/raivokolde/pheatmap).

Statistical tests were performed using GraphPad Prism 8.0.2 for Windows (GraphPad Software, San Diego California USA). Data was subjected to D'agostino and Pearson omnibus normality test. Where specified, normalization was calculated using standard or z-values, where $Z = (x - \text{mean of original experiment cohort})/\text{standard deviation of original sample cohort}$, which allowed re-scaling of data between repeat experiments, with normalized value calculated as: $Z^{*}(\text{repeat experiment standard deviation}) + \text{mean of repeat experiment cohort}$, to minimize artefacts when pooling repeat experiments. Differences between sample sets with a normal distribution were analyzed using an unpaired, two-tailed Student's t-test, while non-parametric data was assessed using an unpaired, two-tailed Mann-Whitney U-test, where p-values ≤ 0.05 were considered statistically significant. Analysis between multiple groups was performed using ANOVA or Kruskall-Wallis test for non-parametric data, with Dunn's *post-hoc* test for comparison between individual groups. Pearson and Spearman correlations calculated using Rstudio Version 1.4.1106 (© 2009-2021 RStudio, PBC).

DATA AVAILABILITY STATEMENT

The original contributions presented in the study are included in the article/**Supplementary Material**. Further inquiries can be directed to the corresponding author.

ETHICS STATEMENT

The animal study was reviewed and approved by Animal experiments were performed under national and European Union guidelines 2010/63, and in accordance with specific approval by regional governmental authorities of Upper Bavaria (Regierung von Oberbayern, license AZ ROB-55.2-2532.Vet_02-17-145).

AUTHOR CONTRIBUTIONS

ML conceptualized the project, carried out the experiments, analyzed the data, produced the figures and wrote the manuscript. RK performed the experiments and contributed to experimental design, and conceptualized data pipelines, performed analysis, interpreted data and contributed figures and writing of the manuscript. LS performed experiments. UP performed an experiment and contributed to data processing. YH contributed to figure development and visualization, as well as the editing of the manuscript. TS conceptualized the study, supervised its execution and contributed to the discussion and editing of the manuscript. CdC conceptualized the study, supervised its execution including development of the manuscript and figures, and edited the manuscript. All authors contributed to the article and approved the submitted version.

FUNDING

Financial support was provided by the Deutsche Forschungsgemeinschaft DFG CO 1469/16-1.

ACKNOWLEDGMENTS

The authors would like to thank Ulla Henn and Stephanie Fetzer for technical support and *S. mansoni* lifecycle maintenance, as well as Sabine Paul, Julian Eifler for technical assistance, and Maria Bui for additional technical assistance.

SUPPLEMENTARY MATERIAL

The Supplementary Material for this article can be found online at: https://www.frontiersin.org/articles/10.3389/fimmu.2022.878029/full#supplementary-material

Supplement 1 | (A) Levels of secreted IL-4, IL-5, IFNγ, IL-10, and IL-13 as determined by ELISA in splenocyte and mesenteric lymph node cell culture supernatants after TCR-based re-stimulation.

Supplement 2 | (A) Correlation (spearman) between number of eggs per liver and worms retrieved *via* liver perfusion of infected offspring and inspection of intestines. **(B)** Selected readouts from Bioplex-based analysis of serum cytokines during cognate infection.

Supplement 3 | (A) Levels of secreted IL-4, IL-5, IFNγ, IL-10, and IL-13 as determined by ELISA in splenocyte and mesenteric lymph node cell culture supernatants after TCR-based re-stimulation.

Supplement 4 | (A) Bioplex-based analysis of serum cytokine levels in steady-state offspring groups, as analyzed *via* FlowSOM in. **(B)** SEA-specific IgE and IgG1 titers from the same offspring groups at steady-state, with **(C)** displaying total IgE and IgG1 antibody titers. Statistical differences analyzed *via* Kruskal-Wallis test plus subsequent individual comparisons from among all groups, *p < 0.05, **p < 0.01, shown as mean ± SEM. MST from Splenic DC analysis **(D)**, splenic B cell populations **(E)**, and bone marrow B cell populations **(F)**.

REFERENCES

1. Wammes LJ, Mpairwe H, Elliott AM, Yazdanbakhsh M. Helminth Therapy or Elimination: Epidemiological, Immunological, and Clinical Considerations. *Lancet Infect Dis* (2014) 14(11):1150–62. doi: 10.1016/S1473-3099(14)70771-6
2. Resende SD, Magalhaes FC, Rodrigues-Oliveira JL, Castro VN, Souza CSA, Oliveira EJ, et al. Modulation of Allergic Reactivity in Humans Is Dependent on Schistosoma Mansoni Parasite Burden, Low Levels of IL-33 or TNF-Alpha and High Levels of IL-10 in Serum. *Front Immunol* (2018) 9:3158. doi: 10.3389/fimmu.2018.03158
3. Cortes-Selva D, Gibbs L, Ready A, Ekiz HA, O'Connell R, Rajwa B, et al. Maternal Schistosomiasis Impairs Offspring Interleukin-4 Production and B Cell Expansion. *PLoS Pathog* (2021) 17(2):e1009260. doi: 10.1371/journal.ppat.1009260
4. Santos P, Sales IR, Schirato GV, Costa VM, Albuquerque MC, Souza VM, et al. Influence of Maternal Schistosomiasis on the Immunity of Adult Offspring Mice. *Parasitol Res* (2010) 107(1):95–102. doi: 10.1007/s00436-010-1839-5
5. Lacorcia M, Bhattacharjee S, Laubhahn K, Alhamdan F, Ram M, Muschaweckh A, et al. Fetomaternal Immune Cross Talk Modifies T-Cell Priming Through Sustained Changes to DC Function. *J Allergy Clin Immunol* (2021) 148(3):843–57.e6. doi: 10.1016/j.jaci.2021.02.031
6. Ludwig E, Harder J, Lacorcia M, Honkpehedji YJ, Nouatin OP, van Dam GJ, et al. Placental Gene Expression and Antibody Levels of Mother-Neonate Pairs Reveal an Enhanced Risk for Inflammation in a Helminth Endemic Country. *Sci Rep* (2019) 9(1):15776. doi: 10.1038/s41598-019-52074-z
7. Santos P, Lorena VM, Fernandes Ede S, Sales IR, Nascimento WR, Gomes Yde M, et al. Gestation and Breastfeeding in Schistosomotic Mothers Differently Modulate the Immune Response of Adult Offspring to Postnatal Schistosoma Mansoni Infection. *Memorias Do Instituto Oswaldo Cruz* (2016) 111(2):83–92. doi: 10.1590/0074-02760150293
8. Attallah AM, Ghanem GE, Ismail H, El Waseef AM. Placental and Oral Delivery of Schistosoma Mansoni Antigen From Infected Mothers to Their Newborns and Children. *Am J Trop Med Hygiene* (2003) 68(6):647–51. doi: 10.4269/ajtmh.2003.68.647
9. Attallah AM, Abbas AT, Dessouky MI, El-emshaty HM, Elsheikha HM. Susceptibility of Neonate Mice Born to Schistosoma Mansoni-Infected and Noninfected Mothers to Subsequent S. Mansoni Infection. *Parasitol Res* (2006) 99(2):137–45. doi: 10.1007/s00436-006-0127-x
10. Lacorcia M, Prazeres da Costa CU. Maternal Schistosomiasis: Immunomodulatory Effects With Lasting Impact on Allergy and Vaccine Responses. *Front Immunol* (2018) 9:2960. doi: 10.3389/fimmu.2018.02960
11. Nono JK, Kamdem SD, Musaigwa F, Nnaji CA, Brombacher F. Influence of Schistosomiasis on Host Vaccine Responses. *Trends Parasitol* (2022) 38(1):67–79. doi: 10.1016/j.pt.2021.07.009
12. Park SK, Friedrich L, Yahya NA, Rohr CM, Chulkov EG, Maillard D, et al. Mechanism of Praziquantel Action at a Parasitic Flatworm Ion Channel. *Sci Transl Med* (2021) 13(625):eabj5832. doi: 10.1126/scitranslmed.abj5832
13. Bayer Healthcare Pharmaceuticals Inc. *Biltricide*. Wayne. p. NJ2010.
14. Olveda RM, Acosta LP, Tallo V, Baltazar PI, Lesiguez JL, Estanislao GG, et al. Efficacy and Safety of Praziquantel for the Treatment of Human Schistosomiasis During Pregnancy: A Phase 2, Randomised, Double-Blind, Placebo-Controlled Trial. *Lancet Infect Dis* (2016) 16(2):199–208. doi: 10.1016/S1473-3099(15)00345-X
15. Mpairwe H, Webb EL, Muhangi L, Ndibazza J, Akishule D, Nampijja M, et al. Anthelminthic Treatment During Pregnancy is Associated With Increased Risk of Infantile Eczema: Randomised-Controlled Trial Results. *Pediatr Allergy Immunol Off Publ Eur Soc Pediatr Allergy Immunol* (2011) 22(3):305–12. doi: 10.1111/j.1399-3038.2010.01122.x
16. Tweyongyere R, Mawa PA, Emojong NO, Mpairwe H, Jones FM, Duong T, et al. Effect of Praziquantel Treatment of Schistosoma Mansoni During Pregnancy on Intensity of Infection and Antibody Responses to Schistosome Antigens: Results of a Randomised, Placebo-Controlled Trial. *BMC Infect Dis* (2009) 9:32. doi: 10.1186/1471-2334-9-32
17. McManus DP, Dunne DW, Sacko M, Utzinger J, Vennervald BJ, Zhou XN. Schistosomiasis. *Nat Rev Dis Primers* (2018) 4(1):13. doi: 10.1038/s41572-018-0013-8
18. Grogan JL, Kremsner PG, van Dam GJ, Metzger W, Mordmuller B, Deelder AM, et al. Antischistosome IgG4 and IgE Responses are Affected Differentially by Chemotherapy in Children Versus Adults. *J Infect Dis* (1996) 173(5):1242–7. doi: 10.1093/infdis/173.5.1242
19. Tweyongyere R, Mawa PA, Ngom-Wegi S, Ndibazza J, Duong T, Vennervald BJ, et al. Effect of Praziquantel Treatment During Pregnancy on Cytokine Responses to Schistosome Antigens: Results of a Randomized, Placebo-Controlled Trial. *J Infect Dis* (2008) 198(12):1870–9. doi: 10.1086/593215
20. Cheever AW, Lenzi JA, Lenzi HL, Andrade ZA. Experimental Models of Schistosoma Mansoni Infection. *Memorias Do Instituto Oswaldo Cruz* (2002) 97(7):917–40. doi: 10.1590/S0074-02762002000700002
21. Straubinger K, Paul S, Prazeres da Costa O, Ritter M, Buch T, Busch DH, et al. Maternal Immune Response to Helminth Infection During Pregnancy Determines Offspring Susceptibility to Allergic Airway Inflammation. *J Allergy Clin Immunol* (2014) 134(6):1271–9.e10. doi: 10.1016/j.jaci.2014.05.034
22. Lenzi JA, Sobral AC, Araripe JR, Grimaldi Filho G, Lenzi HL. Congenital and Nursing Effects on the Evolution of Schistosoma Mansoni Infection in Mice. *Memorias Do Instituto Oswaldo Cruz* (1987) 82(Suppl 4):257–67. doi: 10.1590/S0074-02761987000800049
23. Lundy SK, Lukacs NW. Chronic Schistosome Infection Leads to Modulation of Granuloma Formation and Systemic Immune Suppression. *Front Immunol* (2013) 4:39. doi: 10.3389/fimmu.2013.00039
24. Crisan TO, Netea MG, Joosten LA. Innate Immune Memory: Implications for Host Responses to Damage-Associated Molecular Patterns. *Eur J Immunol* (2016) 46(4):817–28. doi: 10.1002/eji.201545497
25. Lutckii A, Strunz B, Zhirkov A, Filipovich O, Rukoiatkina E, Gusev D, et al. Evidence for B Cell Maturation But Not Trained Immunity in Uninfected Infants Exposed to Hepatitis C Virus. *Gut* (2020) 69(12):2203–13. doi: 10.1136/gutjnl-2019-320269
26. Choi GB, Yim YS, Wong H, Kim S, Kim H, Kim SV, et al. The Maternal Interleukin-17a Pathway in Mice Promotes Autism-Like Phenotypes in Offspring. *Science* (2016) 351(6276):933–9. doi: 10.1126/science.aad0314
27. Van Gassen S, Callebaut B, Van Helden MJ, Lambrecht BN, Demeester P, Dhaene T, et al. FlowSOM: Using Self-Organizing Maps for Visualization and Interpretation of Cytometry Data. *Cytometry A* (2015) 87(7):636–45. doi: 10.1002/cyto.a.22625
28. Quintelier K, Couckuyt A, Emmaneel A, Aerts J, Saeys Y, Van Gassen S. Analyzing High-Dimensional Cytometry Data Using FlowSOM. *Nat Protoc* (2021) 16(8):3775–801. doi: 10.1038/s41596-021-00550-0
29. Haeberlein S, Obieglo K, Ozir-Fazalalikhan A, Chaye MAM, Veninga H, van der Vlugt L, et al. Schistosome Egg Antigens, Including the Glycoprotein IPSE/alpha-1, Trigger the Development of Regulatory B Cells. *PLoS Pathog* (2017) 13(7):e1006539. doi: 10.1371/journal.ppat.1006539
30. van der Vlugt LE, Labuda LA, Ozir-Fazalalikhan A, Lievers E, Gloudemans AK, Liu KY, et al. Schistosomes Induce Regulatory Features in Human and Mouse CD1d(hi) B Cells: Inhibition of Allergic Inflammation by IL-10 and Regulatory T Cells. *PLoS One* (2012) 7(2):e30883. doi: 10.1371/journal.pone.0030883
31. Apostol AC, Jensen KDC, Beaudin AE. Training the Fetal Immune System Through Maternal Inflammation-A Layered Hygiene Hypothesis. *Front Immunol* (2020) 11:123. doi: 10.3389/fimmu.2020.00123

32. Tweyongyere R, Naniima P, Mawa PA, Jones FM, Webb EL, Cose S, et al. Effect of Maternal Schistosoma Mansoni Infection and Praziquantel Treatment During Pregnancy on Schistosoma Mansoni Infection and Immune Responsiveness Among Offspring at Age Five Years. *PloS Negl Trop Dis* (2013) 7(10):e2501. doi: 10.1371/journal.pntd.0002501
33. Nono JK, Mpotje T, Mosala P, Aziz NA, Musaigwa F, Hlaka L, et al. Praziquantel Treatment of Schistosoma Mansoni Infected Mice Renders Them Less Susceptible to Reinfection. *Front Immunol* (2021) 12:748387. doi: 10.3389/fimmu.2021.748387
34. Brustoski K, Moller U, Kramer M, Hartgers FC, Kremsner PG, Krzych U, et al. Reduced Cord Blood Immune Effector-Cell Responsiveness Mediated by CD4 + Cells Induced *In Utero* as a Consequence of Placental Plasmodium Falciparum Infection. *J Infect Dis* (2006) 193(1):146–54. doi: 10.1086/498578
35. Faveeuw C, Angeli V, Fontaine J, Maliszewski C, Capron A, Van Kaer L, et al. Antigen Presentation by CD1d Contributes to the Amplification of Th2 Responses to Schistosoma Mansoni Glycoconjugates in Mice. *J Immunol* (2002) 169(2):906–12. doi: 10.4049/jimmunol.169.2.906
36. Smits HH, Yazdanbakhsh M. Chronic Helminth Infections Modulate Allergen-Specific Immune Responses: Protection Against Development of Allergic Disorders? *Ann Med* (2007) 39(6):428–39. doi: 10.1080/07853890701436765
37. Honkpehedji YJ, Adegnika AA, Dejon-Agobe JC, Zinsou JF, Mba RB, Gerstenberg J, et al. Prospective, Observational Study to Assess the Performance of CAA Measurement as a Diagnostic Tool for the Detection of Schistosoma Haematobium Infections in Pregnant Women and Their Child in Lambarene, Gabon: Study Protocol of the freeBILy Clinical Trial in Gabon. *BMC Infect Dis* (2020) 20(1):718. doi: 10.1186/s12879-020-05445-1
38. Fusco D, Rakotozandrindrainy R, Rakotoarivelo RA, Andrianarivelo MR, Rakotozandrindrainy N, Rasamoelina T, et al. A Cluster Randomized Controlled Trial for Assessing POC-CCA Test Based Praziquantel Treatment for Schistosomiasis Control in Pregnant Women and Their Young Children: Study Protocol of the freeBILy Clinical Trial in Madagascar. *Trials* (2021) 22(1):822. doi: 10.1186/s13063-021-05769-6
39. Hoffmann KF, Cheever AW, Wynn TA. IL-10 and the Dangers of Immune Polarization: Excessive Type 1 and Type 2 Cytokine Responses Induce Distinct Forms of Lethal Immunopathology in Murine Schistosomiasis. *J Immunol* (2000) 164(12):6406–16. doi: 10.4049/jimmunol.164.12.6406
40. Layland LE, Wagner H, da Costa CU. Lack of Antigen-Specific Th1 Response Alters Granuloma Formation and Composition in Schistosoma Mansoni-Infected MyD88-/- Mice. *Eur J Immunol* (2005) 35(11):3248–57. doi: 10.1002/eji.200526273
41. Emmaneel A, Quintelier K, Sichien D, Rybakowska P, Maranon C, Alarcon-Riquelme ME, et al. PeacoQC: Peak-Based Selection of High Quality Cytometry Data. *Cytometry A* (2021) 101(4):325–38. doi: 10.1002/cyto.a.24501

Conflict of Interest: TS is an employee of Ares Trading SA, an affiliate of Merck KGaA, Darmstadt, Germany.

The remaining authors declare that the research was conducted in the absence of any commercial or financial relationships that could be construed as a potential conflict of interest.

The authors declare that this study received funding from Merck KGaA, Darmstadt, Germany. The funder was involved in the design of the study, data interpretation and preparation of the manuscript.

Publisher's Note: All claims expressed in this article are solely those of the authors and do not necessarily represent those of their affiliated organizations, or those of the publisher, the editors and the reviewers. Any product that may be evaluated in this article, or claim that may be made by its manufacturer, is not guaranteed or endorsed by the publisher.

frontiers | Frontiers in Immunology

ORIGINAL RESEARCH
published: 08 July 2022
doi: 10.3389/fimmu.2022.906338

Dynamics of Host Immune Response Development During *Schistosoma mansoni* Infection

Alice H. Costain[1,2†], Alexander T. Phythian-Adams[1†], Stefano A. P. Colombo[1†], Angela K. Marley[1], Christian Owusu[3], Peter C. Cook[1,4], Sheila L. Brown[1], Lauren M. Webb[1,5], Rachel J. Lundie[6], Hermelijn H. Smits[2], Matthew Berriman[3,7] and Andrew S. MacDonald[1]*

[1] Lydia Becker Institute of Immunology and Inflammation, University of Manchester, Manchester, United Kingdom, [2] Department of Parasitology, Leiden University Medical Center, Leiden, Netherlands, [3] Wellcome Sanger Institute, Wellcome Genome Campus, Hinxton, United Kingdom, [4] Medical Research Council Centre for Medical Mycology, University of Exeter, Exeter, United Kingdom, [5] Department of Immunology, University of Washington, Seattle, WA, United States, [6] 360biolabs, Melbourne, VIC, Australia, [7] Wellcome Centre for Integrative Parasitology, University of Glasgow, Glasgow, United Kingdom

OPEN ACCESS

Edited by:
Thiago Almeida Pereira, Stanford University, United States

Reviewed by:
Bartholomew N. Ondigo, Egerton University, Kenya
Sandra Grossi Gava, René Rachou Institute (Fiocruz), Brazil

***Correspondence:**
Andrew S. MacDonald
andrew.macdonald@manchester.ac.uk

[†]These authors have contributed equally to this work

Specialty section:
This article was submitted to Parasite Immunology, a section of the journal Frontiers in Immunology

Received: 28 March 2022
Accepted: 23 May 2022
Published: 08 July 2022

Citation:
Costain AH, Phythian-Adams AT, Colombo SAP, Marley AK, Owusu C, Cook PC, Brown SL, Webb LM, Lundie RJ, Smits HH, Berriman M and MacDonald AS (2022) Dynamics of Host Immune Response Development During Schistosoma mansoni Infection. Front. Immunol. 13:906338. doi: 10.3389/fimmu.2022.906338

Schistosomiasis is a disease of global significance, with severity and pathology directly related to how the host responds to infection. The immunological narrative of schistosomiasis has been constructed through decades of study, with researchers often focussing on isolated time points, cell types and tissue sites of interest. However, the field currently lacks a comprehensive and up-to-date understanding of the immune trajectory of schistosomiasis over infection and across multiple tissue sites. We have defined schistosome-elicited immune responses at several distinct stages of the parasite lifecycle, in three tissue sites affected by infection: the liver, spleen, and mesenteric lymph nodes. Additionally, by performing RNA-seq on the livers of schistosome infected mice, we have generated novel transcriptomic insight into the development of schistosome-associated liver pathology and fibrosis across the breadth of infection. Through depletion of $CD11c^+$ cells during peak stages of schistosome-driven inflammation, we have revealed a critical role for $CD11c^+$ cells in the co-ordination and regulation of Th2 inflammation during infection. Our data provide an updated and high-resolution account of how host immune responses evolve over the course of murine schistosomiasis, underscoring the significance of $CD11c^+$ cells in dictating host immunopathology against this important helminth infection.

Keywords: schistosomiasis, dendritic cells, pathology, chronic infection, transcriptomic (RNA-seq)

Abbreviations: Ag, Antigen; APCs, Antigen presenting cells; DCs, Dendritic cells; IL, Interleukin; MT, Masson's Trichrome; MLN, Mesenteric lymph nodes; Bregs, Regulatory B cells; Tregs, Regulatory T cells; SEA, Schistosome soluble egg Ag; Th, T helper; WPI, Wks post infection.

INTRODUCTION

Schistosomiasis is a complex and potentially life-threatening parasitic disease, caused by infection with blood flukes of the genus *Schistosoma. S. mansoni*, S. *haematobium* and S. *japonicum* are responsible for most human cases, with approximately 240 million individuals infected globally, predominantly clustering in specific regions of Africa, Asia, the Middle East, and South America (1).

Schistosomiasis has a distinctive triphasic immune profile that reflects transformative events within the parasite lifecycle (2). In brief, the host first progresses through a (pre-patent) acute phase (0-5 WPI; wks post infection), where it responds to immature, lung migrating schistosomula and developing worm pairs (3). In the second (post-patent) acute phase (5-12 WPI), the host is confronted daily with hundreds of highly immunogenic eggs, and must contend with accompanying inflammation and associated tissue damage (4). In the final chronic phase (12 WPI+), the host enters a more regulated or 'exhausted' state that follows prolonged exposure to parasite antigens (Ags) (5, 6). At each lifecycle stage schistosomes employ a wide range of immune evasion and manipulation strategies that enable mitigation against collateral tissue damage and promotion of long-term survival within the host (7). For example, as an appropriately regulated T Helper (Th) 2 response is essential for host and parasite survival (8–10), schistosomes produce an array of molecules that guide host immunity towards a Type 2 phenotype (11–17), whilst concurrently encouraging the expansion of regulatory networks that downregulate and resolve chronic inflammation (14, 15, 18–20).

The immune response triggered at each lifecycle stage has been thoroughly dissected in experimental murine infections and, to a lesser extent, human and primate work. Together, the following immune narrative has been established: during the initial 4-5 wks of pre-patency, migrating schistosomula and juvenile worms evoke a low-level mixed T helper 1 (Th1)/Th2 immune response (21–23). This profile takes a dramatic shift at around 5-6 WPI, with egg production skewing host immunity towards a Th2-dominated profile, including dramatic upregulation of interleukin (IL-) 4, IL-5, IL-13, IgE and eosinophilia. This Type 2 environment dwarfs and counteracts the early Type 1 component (21), peaks approximately 8-10 WPI, and is critical for coordinated granulomatous inflammation (8, 10, 24). Moreover, although Th17 responses are acknowledged during schistosomiasis, they are generally considered low level in relation to Th2 or Th1 responses, and typically only emerge in specific mouse strains (i.e. CBA mice but not C57BL/6 or BALB/C) (25, 26). The majority of data suggests Th17 responses act to promote immune pathology rather than benefit the host (27, 28). As infections progress into chronicity, Type 2 responses decline and regulatory responses prevail (5, 29–31). Down-modulation of Type 2 responses and suppression of severe disease is thought to be primarily mediated by IL-10 (32), with its secretion attributed to Regulatory B cells (Bregs) (33, 34) and T cells (Tregs) (30, 35–37). Tissue fibrosis (scarring) is central to schistosomiasis associated pathology, particularly in the liver, with IL-13 proposed as the main pro-fibrotic mediator in mice (38). This immunological picture has been established over decades of research, often focusing on a single tissue site, timepoint or event within the schistosome lifecycle. While time-course studies exist, very few have simultaneously evaluated the Th1/Th2/regulatory balance over the course of infection, in a range of tissue sites. Pioneering work in the early 1990s provided two splenic time-course studies, which form the basis of our understanding of the Th1-Th2 switch from the point of egg production (21, 22). However, these studies reflect the technical limitations of the time, and have received minimal follow-up with the resolution that is possible today.

Dendritic cells (DCs) are central players in the host immune system, poised to recognize and respond to invading threats and inflammation, and translate these danger signals into the activation and differentiation of T cells (39). DCs have proven key to orchestration of Th1 and Th2 inflammation, as well as the promotion of regulatory responses. In the context of schistosomiasis, we have previously shown that they play a fundamental role in the priming of $CD4^+$ T cell responses, with depletion of $CD11c^+$ DCs early in murine *S. mansoni* infection (wks 4 – 6) leading to a stark reduction in splenic and hepatic Th2 cells (IL-4, IL-5, and IL-13) and Tregs (24). However, the involvement of DCs in maintenance and/or regulation of schistosome infection beyond wk 6 remains unclear. Similarly, it is currently unknown whether DCs in later stages of infection remain vital for coordinating $CD4^+$ T cell function and cytokine secretion, or if other antigen presenting cells (APCs) adopt more dominant roles in this context.

We now provide a comprehensive account of schistosome-elicited immune responses over the course of infection and across multiple tissue sites (liver, spleen, and mesenteric lymph nodes [MLNs]). In addition to refined characterization of cell populations and cytokine dynamics across these compartments, we have interrogated how the host responds to infection and attempts to resolve egg-driven damage by RNA-seq analysis of liver samples isolated over the course of infection. Finally, we have revealed a critical role for $CD11c^+$ cells in the maintenance of hepatic Type 2 inflammation, with CD11c depletion from 6 WPI leading to compromised cytokine production and altered granulomatous pathology. These novel data elevate and update our fundamental understanding of immune response development over the course of murine schistosomiasis, and the significance of $CD11c^+$ cells in coordinating immunopathology against this important and relevant helminth infection.

MATERIALS AND METHODS

Mice

Experiments were performed using female C57BL/6 mice, CD11c.DOG (40) x C57BL/6 or CD11c.DOG x 4get IL-4-eGFP F1 mice (41), housed under specific pathogen free conditions at the University of Manchester or the University of Edinburgh, and used at 8-12 wks of age. Experiments were performed under a project license granted by the Home Office UK following ethical review by the University of Manchester or University of Edinburgh, and performed in accordance with the United Kingdom Animals (Scientific Procedures) Act of 1986.

Schistosoma mansoni Infections and Cell Depletions

Biomphalaria glabrata snails infected with *S. mansoni* parasites were obtained from Biomedical Research Institute, Rockville, MD. Mice were percutaneously infected (42) with 40-80 *S. mansoni* cercariae, with infections lasting 4, 6, 8, 12 or 15 wks in duration. To quantify parasite burden, *S. mansoni* eggs were isolated and counted from pieces of liver (approx. 1g in weight) or intestine, and digested overnight in 5% KOH (42). For CD11c depletion experiments, mice received daily intraperitoneal injections with 8 ng/g diphtheria toxin (Sigma-Aldrich) in PBS or with PBS alone (24, 40), from wk 6 of infection (days 42-51), and culled on day 52.

Cell Isolation

Single-cell suspensions of liver, MLN and spleen were prepared using the following methods, and as described previously (24). Spleens and MLNs were diced and digested at 37°C with 0.8 U/ml Liberase TL and 80 U/ml DNase I type IV in HBSS (all Sigma), supplemented with 50 U/ml penicillin and 50 µg/ml streptomycin (Invitrogen). After 30 min the digestion reaction was halted by the addition of 100 µl/ml 0.1 M, pH 7.3, EDTA (Ambion) stop solution, followed by addition of DMEM containing 50 U/ml penicillin and 50 µg/ml streptomycin. This was then passed through a 70 µm cell strainer to generate a cellular suspension, with splenocytes undergoing an additional RBC lysis incubation to remove contaminating erythrocytes. Livers were perfused, minced with sterile scalpel blades, and incubated at 37°C for 45 min using the digestion media detailed above. After addition of EDTA stop solution and DMEM, digested livers were passed through a 100 µm cell strainer. To separate leukocytes, liver cells were resuspended in 33% isotonic Percoll (GE healthcare) and centrifuged at 700 g. Pelleted cells were passed through a 40 µm cell strainer (for removal of *S. mansoni* eggs), followed by RBC lysis, counting and resuspension in PBS supplemented with 2% FBS, 2 mM EDTA, for flow cytometry or culture/stimulation.

Quantification of Cytokines

Cytokine assays were performed as previously described (43, 44). Single-cell suspensions of livers, MLNs and spleens were stimulated *ex vivo* with plate bound anti-CD3 (0.5 µg/well) or SEA (0.25 µg/well) in X-vivo 15 media (Lonza) supplemented with 2 mM L-Glutamine and 50 µM 2-ME (Sigma). Stimulation was carried out in 96 well U bottom plates, with 1 x 10^6 cells seeded per well in 200µl volumes. Cell supernatants were harvested 72 h later and stored at -20°C until further analysis. Paired capture and detection Abs were used for analysis of murine IL-4, IL-10, IL-17A (Biolegend) IL-5, IFNγ (produced from hybridomas in-house) and IL-13 (eBioscience).

Serum Antibody and IgE Levels

SEA-directed antibodies and IgE levels were measured as described previously (24). In brief, to quantify serum levels of SEA-specific IgG, IgG1, IgG2a, IgG2c and IgG3, 96 well plates (NUNC Maxisorp) were coated with 5 µg/mL SEA overnight, then blocked with 1% bovine serum albumin (BSA, Sigma) in PBS for 1 h at room temperature. Plates were then incubated with sera at doubling dilutions (1:50-1:6400). Alkaline phosphatase conjugated goat anti mouse IgG, IgG1, IgG2a, IgG2c and IgG3 (SouthernBiotech) were added to plates, followed by liquid PNPP substrate i.e. 'liquid PNPP substrate (Thermo Scientific), with absorbances read at 405 nm. Serum levels of IgE (BD) were measured using paired capture and biotinylated detection antibodies, with quantity assessed *via* standard curve and absorbances read at 450 nm. For all ELISAs, between individual incubation steps, plates were washed 3 times with PBS containing 0.05% Tween (Sigma). Data presented as endpoint dilutions.

Flow Cytometry

Single cell suspensions were washed with PBS and stained for viability with ZombieUV (1:2000; Biolegend) or LIVE/DEAD™ Fixable Aqua (1:500; Invitrogen). Cells were then incubated with 5 µg/ml FC block (αCD16/CD32; 2.4G2; Biolegend) in FACS buffer (PBS containing 2% FBS and 2 mM EDTA), before staining for surface markers for 30 min. After surface staining, cells were washed twice with FACS buffer before fixation in 1% PFA for 10 min. For intracellular staining, cells were permeabilized with eBio Fixation/Permeabilisation buffer for 1 h, before staining with relevant intracellular antibodies for 30 min. Samples were analyzed by flow cytometry (LSR Fortessa, BD) and data analyzed using FlowJo v10 software. A list of antibodies used is provided in **Table 1**.

Imaging

For histological analysis by light microscopy, median liver lobes were fixed in 10% NBF for 24 h, dehydrated through a series of graded alcohols and embedded in paraffin blocks. Tissues were cut into 5 µm thick sections using a microtome and stained with Masson's Trichrome (MT; granulomatous inflammation). For quantification of granulomatous pathology and fibrosis, MT stained liver sections were scanned with a dotslide digital slide scanner (Olympus BX51, VS-ASW FL Software), creating differential Interference Contrast (DIC) images of the whole slide (see **Figure 5A**). Using FIJI imaging analysis software (ImageJ 1.48r) (45) individual liver sections were cropped to obtain solely liver sections. Colour thresholds were set using hue, saturation and brightness (HSB) settings to select either granulomas alone (blue staining) or liver parenchyma (purple staining). HSB thresholds were set using an algorithm developed by Dr. Tim Kendall (Western General Hospital, Edinburgh), enabling the quantification of the number of pixels for the region of interest.

For immunohistochemistry (IHC) analysis by confocal microscopy, pieces of the left liver lobe were placed in optimum cutting temperature formulation (OCT) and stored at -80°C until further processing. Tissues were cut into 20 µm cyrosections, dried overnight at RT, then fixed in ice-cold acetone for 5 min before storage at -20°C. For confocal Immunohistochemistry, cryosections were thawed and rehydrated with 1X PBS before incubation for 1 h at RT with 10% blocking solution: 1% BSA, 10% FCS and 0.005 µg/µl FcR-Block (2.4G2) in PBS-T (Tween-20; 1:1000 in PBS). Samples were incubated overnight at 4°C with fluorescently labelled monoclonal antibodies (all eBioscience) for CD11c (N418; 1:250), Siglec-F (E50-2440; 1:100) TCRβ (H57-597; 1:50), in 2% blocking

TABLE 1 | List of flow cytometry antibodies and their clones.

Company	Target	Clone
BD	Siglec-F	E50-2440
Biolegend	CD11b	M1/70
Biolegend	CD11c	N418
Biolegend	CD169	3D6.112
Biolegend	CD172a	P84
Biolegend	CD26	DPP-4
Biolegend	CD4	RM4-5
Biolegend	CD45	30-f11
Biolegend	CD64	x54-5/7.1
Biolegend	CD8	53-6.7
Biolegend	F4/80	BM8
Biolegend	IFNy	XMG1.2
Biolegend	IL-10	JES5-16E3
Biolegend	IL-17	TC11-1810.1
Biolegend	IL-4	11B11
Biolegend	Ly6C	HK1.4
Biolegend	Ly6G	1A8
Biolegend	PDCA-1	927
Biolegend	XCR1	ZET
Ebioscience	B220	RA-6B2
Ebioscience	IL-13	ebio13A
Ebioscience	IL-5	TRFK.5
Ebioscience	MHCII	MS/114.15.2
Ebioscience	Ter119	TER-119
Invitrogen	CD19	Ebio(ID3)
Invitrogen	CD3	17A2
Invitrogen	FoxP3 (IN)	FJK-16s
Invitrogen	NK1.1	PK136
Invitrogen	TCRβ	H57-597
Biolegend	CD25	PC61-
Biolegend	CD49b	HMα2

solution (0.2% BSA, 2% FCS and 0.005 µg/ul FcR-Block in PBS-T). Stained cryosections were washed once with PBS-T followed by 2 washes with PBS, then stained with 1 µg/ml DAPI dissolved in PBS for 15 min at RT. Cryosections were subsequently mounted with coverslips using ProLong Gold antifade reagent (LifeTechnologies) and blinded before analysis. Analysis of confocal photographs was carried out using Volocity imaging software (PerkinElmer). For each photograph, the contrast was enhanced to remove background staining and schistosome eggs were cropped out of individual images to exclude possible autofluorescence during subsequent quantification steps. Snapshots of cropped images were captured separately for each fluorochrome used, and for each snapshot the surface area of positive staining above a fixed intensity was measured. Intensity was set using isotype controls for each fluorochrome labelled.

RNA Extraction and Sequencing

RNA extraction was performed in line with Peña-Llopis & Brugarolas (46). In brief, liver tissue samples weighing between 15 mg and 40 mg were homogenized in lysis buffer, followed by an acid-phenol chloroform extraction of total RNA. Polyadenylated mRNA was purified from liver total RNA using oligo(dT) Dynabead selection, followed by metal ion hydrolysis fragmentation with the Ambion RNA fragmentation kit. First strand cDNA was synthesized using randomly primed oligos followed by second strand synthesis using DNA polymerase I to produce double-stranded cDNA. This was followed by end repair with T4 and Klenow DNA polymerases and T4 polynucleotide kinase to blunt-end the DNA fragments. A single 3' adenosine nucleotide was added to the repaired ends using a Klenow fragment (3'→5' exo-) and dATP to deter concatemerization of templates, limit adapter dimers and increase the efficiency of adapter ligation. Adapters were then ligated (containing primer sites for sequencing). Ligated fragments were run on an agarose gel, size selected for 100-200 bp inserts and the DNA extracted according to the Qiagen gel extraction kit protocol, except for the dissolution of gel slices, which was done at room temperature rather than 50°C. Libraries were then amplified by PCR to add primers for flow cell surface annealing and to increase yield; sample cleanup was performed with AMPure SPRI beads. The libraries were quantified on an Agilent Bioanalyzer and Kapa Illumina SYBR Fast qPCR kit, and sequenced on the Illumina HiSeq 2500 platform as 75 bp paired end reads.

RNAseq Analysis

mRNA reads were aligned to the mouse reference transcriptome (GRCm38) using Bowtie2 v2.2.1 (47) and quantified using eXpress v1.3.0 (48). Briefly, the mouse cDNA reference was downloaded from the Ensembl Genomes FTP server and indexed prior to mapping using the Bowtie2-build command. Reads were aligned with Bowtie2 using default parameters apart from -X 800, which sets the maximum fragment length for concordant pairs at 800 bp, thus ensuring that reads from all valid fragments are considered; and -a, which reports all alignments. The Bowtie2 alignments were passed directly to eXpress for transcript quantification. As eXpress reports transcript-level counts, a custom perl script was used to aggregate and collapse the reported counts into their corresponding gene-level counts. The results were organized into a tab-delimited matrix with each row representing a gene and each column representing a sample.

Read counts were normalized and differential expression analysis performed using the DESeq2 package (49). Genes with low expression were removed prior to downstream analysis by removing those where the sum of the total read counts in all samples was fewer than 50. Gene names were assigned to ensembl IDs using the biomaRt package (50). Principle component analysis was performed using the DESeq2 package. For the production of volcano plots and heatmaps genes were considered significantly differentially expressed between conditions if they had an adjusted p value (padj) < 0.01 and a log2FoldChange in expression >1. Gene set enrichment analysis for GO terms associated with biological process was performed using the clusterProfiler package (51). Genes with padj < 0.01 (both up- and down-regulated) were selected for gene set enrichment analysis. The statistical significance of enriched terms was adjusted using the Holm method. GO terms with a padj > 0.01 were considered statistically significant. Redundant GO terms were removed using the 'simplify' function in clusterProfiler using a cutoff value of 0.5 when selecting by padj.

Statistical Analysis

Statistical analyses were performed using GraphPad Prism 9 or JMP software. As described in corresponding figure legends,

experimental groups were compared using an unpaired t-test, one-way or two-way ANOVA, followed by appropriate *post-hoc* tests. Significance for all statistical tests was shown in figures as $P < 0.05$ (*), $P < 0.01$ (**), $P < 0.001$ (***).

RESULTS

Dynamics and Development of Hepatic Pathology

Experimental schistosome infections of mice are commonly employed to model the pathological and immunological features of human infections (52, 53). To assess host responses at several distinct stages of schistosomiasis, mice were percutaneously infected with 40 cercariae, and animals taken for analysis after 4, 6, 8, 12 or 15 wks (**Figure 1A**). In brief, these wks correspond to pre-egg production/adult pairing and maturation (wk 4), the initial phase of egg production (wk 6), the peak of post-patent active disease (wk 8), progression into chronic disease (wk 12) and established chronicity (wk 15) (2-4). Egg-driven granulomatous responses generally peak at 8 wks post infection before declining in magnitude, with calcified and fibrotic granulomas accumulating during chronic infection stages, coincident with the immune response against freshly laid eggs being down-regulated (36, 54, 55). Importantly, as egg production is an ongoing, asynchronous process, infected tissues simultaneously present with newly formed, mature and resolving granulomas. To visualise the extent of granulomatous inflammation in the liver, sections from the median lobes of infected mice were stained with Masson's Trichrome (MT) (**Figure 1B**). Before the start of egg-laying (wk 4), there were no visible signs of damage or eggs in the livers of infected mice, whilst at later infection stages, eggs continued to accumulate within hepatic tissue (**Figure 1A** and **Supplementary Figure 1A**). Granulomatous inflammation became more pronounced at each ensuing stage, with infected livers showing extensive MT staining from wk 8, which accounted for approximately 50% of the total tissue section by wks 12 and 15 (**Figures 1B, C**). Closer assessment of wks 6-8 revealed that granulomatous inflammation in this transition phase started at approximately 45 days post infection, with significantly greater inflammation visualized by day 51 (**Supplementary Figures 1B, C**) and with evidence of enhanced DC, T cell and eosinophil infiltration to hepatic tissue, as assessed by confocal microscopy paired with quantification of $CD11c^+$, $TCR\beta^+$ and Siglec-F^+ staining (**Supplementary Figure 1D**). Furthermore, mirroring the exaggeration of hepatic pathology during later stages of infection (**Figures 1B, C**), infected mice displayed significantly higher serum levels of SEA-specific antibodies and IgE by wks 12 and 15 (**Supplementary Figures 1E, F**), as well as hepatosplenomegaly from wk 8, as defined by increased spleen and liver weight as a proportion of total body weight (**Supplementary Figure 1G**).

Tissue-Specific Cytokine Responses During Infection

Next, to define how parasite-specific cytokine responses develop across infection, we focused on three tissue sites that are differentially affected by schistosomiasis: the liver, spleen, and MLNs. More specifically, while the liver represents a principal effector site in which eggs deposit and granulomas form, the spleen and MLNs represent important immune priming sites against parasite Ags from systemic circulation and intestinal sites, respectively.

To evaluate Ag-specific cytokine secretion, isolated liver, spleen and MLN cells were cultured in the presence of SEA (**Figure 1D**). Irrespective of the tissue site in question, immune cells from infection produced very low levels of SEA-specific Th2 associated cytokines (IL-4, IL-5 and IL-13) at wk 4 post infection, with no statistically significant differences relative to naïve mice. In contrast, the Th1 associated cytokine IFNγ peaked at this time-point in infected animals. As infections progressed beyond wk 6 and splenic, MLN and hepatic IFNγ dramatically reduced. All tissues showed increased production of IL-4, IL-5 and IL-13 from wk 6, which either peaked at 8-12 wks post infection or remained elevated into chronic stages. IL-10 responses tended towards an increase during later stages of infection, which was particularly evident in the MLNs and liver. Similar cytokine profiles were seen upon stimulation of isolated cells with anti-CD3 (**Supplementary Figure 2**). This included peak Th2 cytokine potential at approximately 8 wks post infection, and increased IL-10 during chronicity, particularly in the liver and MLNs (**Supplementary Figure 2**). Moreover, while SEA-specific IL-17A production was minimal in all three sites, anti-CD3 stimulated liver cells from infected mice produced significantly increased levels of IL-17A than their naïve counterparts.

Cellular Responses to Schistosome Infection Vary Across Tissues

We next looked to identify the cell types responding at different sites over the course of infection. From as early as 4 wks post infection, despite the lack of egg production, cellular infiltration to the liver was significantly increased in infected animals compared with naïve (**Figure 2A**). Closer inspection of immune cell numbers (**Figures 2A, C**) and frequencies (**Figures 2B, D**) revealed a dramatic increase in hepatic eosinophils, macrophages, DCs, plasmacytoid DCs (pDCs), B cells, $CD4^+$ T cells and NK cells in comparison to naïve mice, but without any significant increase in their frequency. Similarly, while wk 6 saw an increase in overall cell numbers in the liver (aside from pDCs), cellular frequencies remained comparable to naïve controls. However, cell proportions altered significantly by wk 8 of infection, with an increased frequency of hepatic eosinophils, neutrophils, and monocytes, coinciding with a decline in B cell, T cell, NK cell, DC and macrophage proportions. These differences in percentages persisted into later wks of infection. Akin to the earlier observed peak in Th2 cytokine production (**Figure 1D**), liver cell counts peaked at 8 wks post infection before a gradual decline (**Figure 2A**). By 15 wks post infection, eosinophils and monocytes were the only cell types found to be significantly more numerous in infected livers than naïve.

Although there were clear differences in basal immune cell composition between priming (MLN and spleen) and effector (liver) sites (**Figure 2B**), changes in cellularity evoked by schistosome infection were largely comparable in all three tissues. MLN and spleen cell counts remained unchanged at

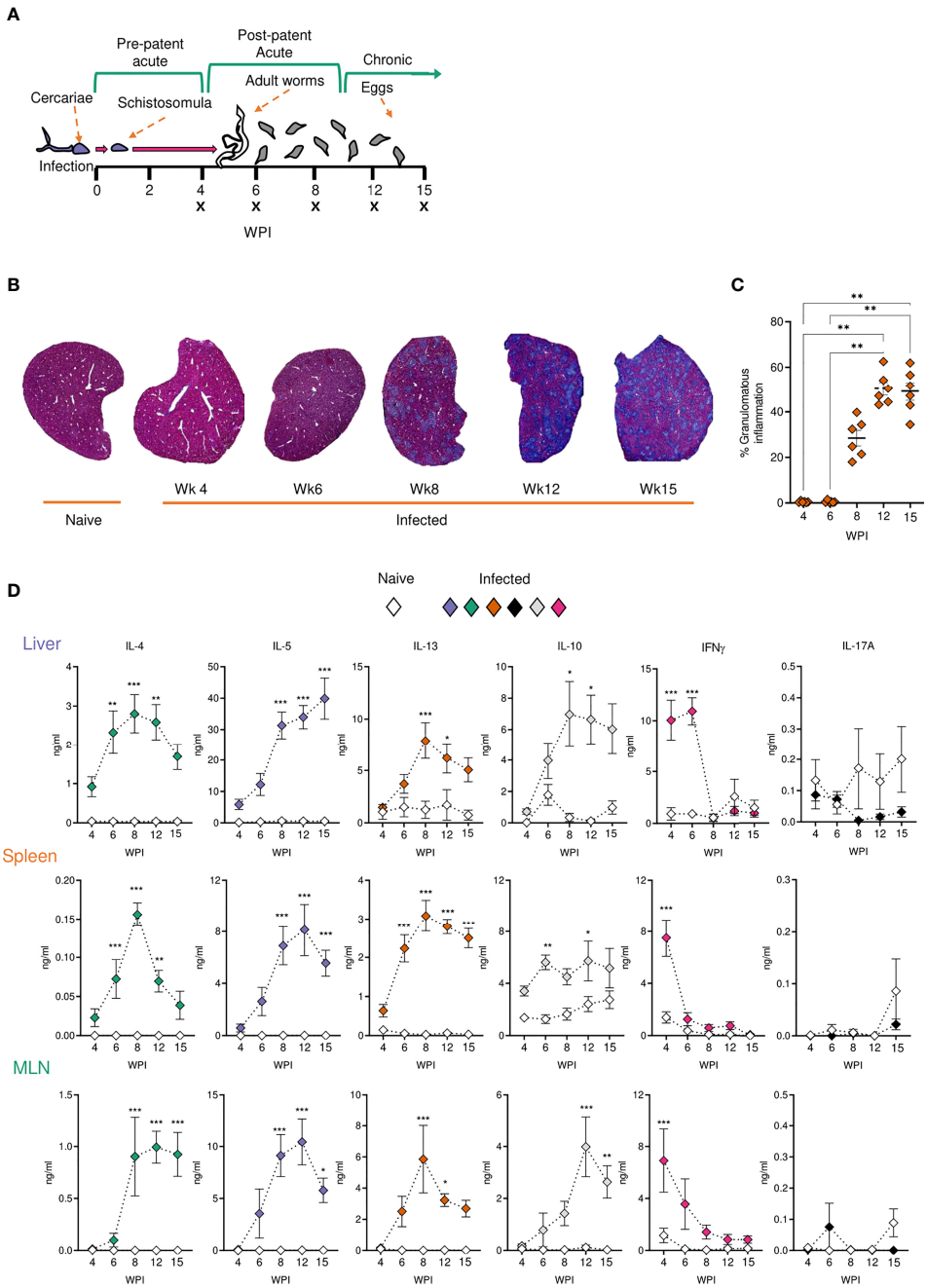

FIGURE 1 | Development of granulomatous pathology and a dominant Type 2 response during *S. mansoni* infection. **(A)** Schematic of infection setup. C57BL/6 mice were infected with 40 *S. mansoni* cercariae with infections lasting, 4, 6, 8, 12 or 15 wks in duration (indicated by X). **(B)** Representative images of liver sections stained with Masson's Trichrome (MT) at indicated wks, allowing for visualisation of inflammatory cell infiltration and type I collagen deposition. **(C)** The proportion of granulomatous inflammation per tissue section, using an objective algorithm to quantify the number of pixels of granulomatous inflammation in a defined region of interest. **(D)** At specified wks, liver, spleen and MLN cells from naïve and schistosome infected mice were cultured for 72 h with 0.25 µg of schistosome egg antigen (SEA; antigen-specific stimulation). Supernatants were collected and cytokine production (medium alone values subtracted) was assessed by ELISA. Data are from a single experiment **(B, C)** or pooled from 2 **(D)** separate experiments (n=36-10 animals per time point). Significance calculated by one-way **(C)** or two-way ANOVA **(D)**. Data presented as mean +/- SEM. *p < 0.05, **p < 0.01, ***p < 0.001.

wks 4 and 6 when compared to naïve mice but, similarly to the liver, a significant infiltration in immune cells was observed from wk 8 onwards in these sites that persisted into chronic stages of disease. Eosinophilia was a prominent feature of both MLNs and spleens from the 8 wk time-point onwards, but less dramatically than in the liver. Neutrophilia was also evident within MLN and splenic responses by wks 8 and 12 that, akin to the liver, was no longer significant by 15 wks post infection. Notably, the liver

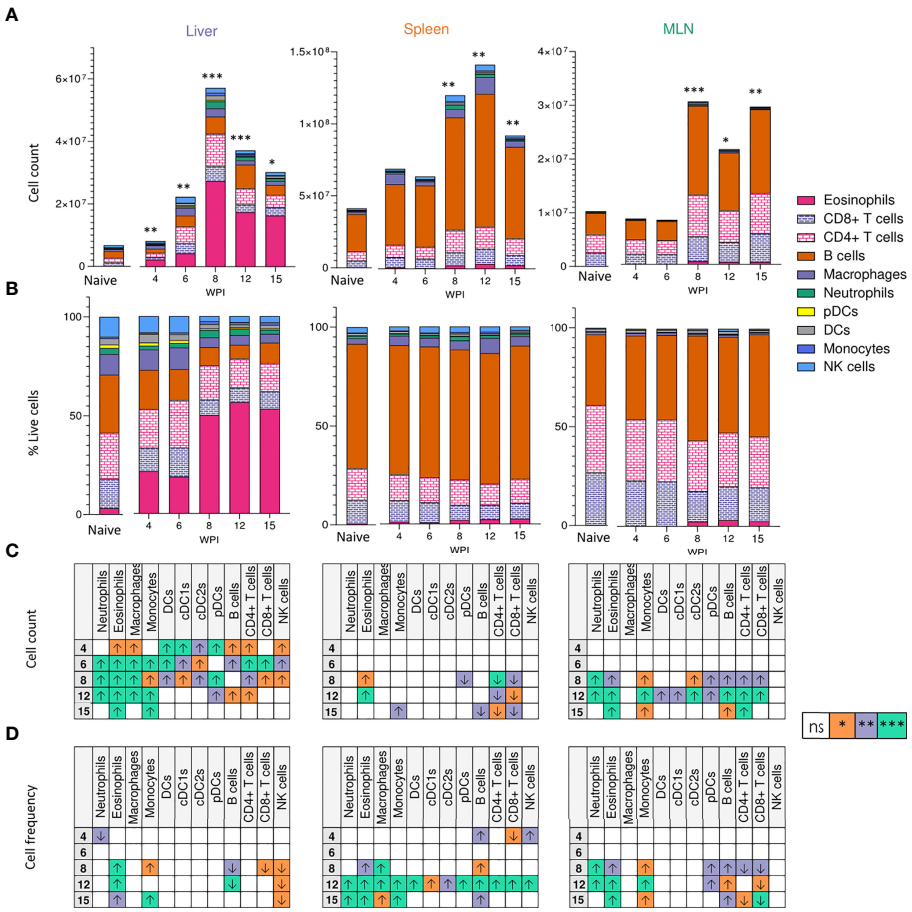

FIGURE 2 | Tissue-specific cellular responses during schistosomiasis. Stacked bar charts showing hepatic splenic and mesenteric **(A)** cell counts and **(B)** cell frequencies (as a proportion of total live cells) at indicated wks of infection when infected with 40 cercariae. For infected mice, data is presented as mean values for each given time point, with averages calculated from two pooled experiments per time point. n=6-8 per timepoint from two pooled experiments. Naïve data is presented as mean values for the entire infection, with averages calculated from two pooled time course experiments. n=30. Significance in **(A)** reflects comparison of total cell counts between naïve and infected mice. Statistics tables showing differences in **(C)** cell counts and **(D)** cell frequencies between naïve and infected mice, for the liver spleen and MLN. Arrows in table **(C, D)** represent the direction of cell frequency change in infected animals in comparison to naïve. Significance calculated by Kruskal-Wallis followed by Dunn's multiple comparisons test, with comparison between naïve and infected groups. *p < 0.05, **p < 0.01, ***p < 0.001, ns = non-significant (P > 0.05) .

showed a significant decrease in B cell frequency from wk 8-15 of infection, while increased B cell proportions were observed in the spleen and MLNs.

Tregs are key immunosuppressive cells that aid in control of immunopathology during *S. mansoni* infection (30, 36, 37, 56), commonly defined by their expression of the transcription factor FoxP3 (57) and/or the activation marker CD25 (IL-2 receptor α) (58) (**Figure 3A**). When looking at relative Treg proportions, we observed significant expansion of $CD25^+Foxp3^+$ Tregs within the liver of infected mice from 8 wk onwards (**Figure 3B**), whilst in the spleen and MLNs, an increase in $CD25^+Foxp3^+$ Treg frequency was observed at wk 12 in the MLNs only (**Figure 3B**). However, reflecting the infection-induced increase in liver, spleen, and MLN cellularity (**Figure 2A**), we observed significant numerical expansion of $CD25^+Foxp3^+$ Tregs by wks 8, 12 and 15 in the liver, spleen and MLNs (**Figure 3B**). Assessment of $CD25^+Foxp3^-$ $CD4^+$ T cells, representing activated effector $CD4^+$ T cells populations (59), revealed their numerical and proportional expansion in the liver from wk 8 of infection (**Figure 3C**). These $Foxp3^-$ populations showed numerical expansion in the MLNs at wks 8, 12 and 15, with significant proportional increases met at wk 15, while the least striking expansion of these effector cells was evident in the spleen (**Figure 3C**).

Transcriptional Signature of Schistosomiasis Associated Liver Pathology

Given the dramatic changes in liver pathology and granulomatous inflammation observed over the course of *S. mansoni* infection, we next sought to obtain a broader, deeper and less biased understanding of the changes occurring in the liver tissue over

the course of *S. mansoni* infection. RNA was isolated from the livers of infected mice and matched naïve controls at wks 3, 4, 6, 8, 12, and 15, with transcriptional profiling performed by RNAseq (**Supplementary Excel File 1**). As early as wk 3 post infection we were able to observe distinct transcriptional profiles in infected mice compared to naïve controls (**Figures 4A, B**) including increased expression of chemokines (Cxcl9 and Cxcl10) and genes associated with MHCII expression (*H2-Aa*, *H2-Ab1* and *H2-Eb1*) (**Figure 4B**). From wk 4-6 onward, significant upregulation of transcripts associated with maturation of myeloid cells and B cells (*Irf8*, *Cd74*, *Ly6d* and *Ear2*) was observed. Starting at wk 8 and continuing through wks 12 and 15 we observed collagens (*Col6a1* and *Col6a2*) and other genes associated with the extracellular matrix (ECM) (*Lpl*, *Lum*, *Anxa2*) among the most significantly upregulated differentially expressed genes (DEGs; **Figure 4B**).

To obtain an overview of the processes influenced by infection we performed gene set enrichment analysis (GSE) of gene ontology (GO) terms associated with biological processes using genes differentially expressed at each timepoint (**Figure 4C** and **Supplementary Excel File 2**). Whilst there were too few differentially expressed genes at wk 3 and wk 4 post infection to identify statistically meaningful enrichment of GO terms, we identified a range of terms to be enriched (both positively and negatively) from wk 6 onwards. As expected, we observed strong positive enrichment of terms associated with the immune response, including those related to antigen presentation, immune cell migration and cytokine production. Notably, our GSE analysis identified an number of terms associated with the synthesis of collagen and restructuring of the extracellular matrix at wk 12 and wk 15. Interestingly, we identified strong negative enrichment of a number of GO terms associated with metabolic processes, particularly those associated with the metabolism of nucleotides.

As we had observed substantial hepatic changes by MT staining (**Figure 1B**) we examined genes associated with extracellular matrix remodelling. Selecting the 15 most significant DEGs associated with GO terms relating to tissue remodelling revealed strong upregulation of matrix metalloproteases (MMPs) (*Mmp2* and *Mmp14*); a collagen (*Col1a2*) and ER-resident chaperon associated with collagen biosynthesis (*Serpinh1*); other secreted components of the extracellular matrix (*Dpt*, *Postn*, *Efemp2*, *Smoc2* and *Elna*); a catalytic enzyme required for matrix component crosslinking (*Loxl1*), a matrix binding protein (*Ccdc80*); and receptors associated with the regulation of matrix deposition (*Anxa2* and *Pdgfra*) (**Figure 4D**). In total we identified 76 DEGs associated matrix, including 13 encoding collagens, 5 Adamts (A Disintegrin and Metalloproteinase with Thrombospondin motifs) family members, 8 MMPs, and the transcription factor *Sox9* (**Supplementary Excel File 1**).

Interrogation of the most significantly differentially expressed genes associated with the immune response revealed a diverse array of genes linked to different aspects of immune function. We identified genes associated with immune cell chemotaxis (*Cd34*, *Cxcl14, Ear2* and *Pf4* (encoding CXCL4)); TLR4/RAGE binding S100 family members associated with triggering migration *via* NF-κB signalling (*S100a8* and *S100a9*); an actin regulator associated with macrophage function (*Gsn*); genes associated with interaction with and remodelling of the extracellular matrix (*Col3a1, Mmp2, Spp1*); genes related to B cell function including an alarmin receptor involved in B cell development (*Crlf2*) and components of immunoglobulins (*Iglc2* and *Jchain*); a signal transduction enzyme (*Smpd3*); and an antimicrobial peptide (*Slpi*) (**Figure 4E**).

These data demonstrated a dramatic change in the transcriptional profile of the liver during *S. mansoni* infection with strong enrichment of genes linked to the attraction and activation of leukocytes, and the restructuring of ECM. Additionally, we found significant downregulation of GO terms associated with various metabolic and catabolic processes. Although some of these changes were evident as early as 3 wks post infection, the major changes in gene expression occurred between wk 6 and wk 8, indicating that transcriptional reprogramming of the liver environment is associated with the start of egg production.

Hepatic Granuloma Composition Over the Course of Infection

We next sought to investigate some of the transcriptional changes we had observed at a location level, in hepatic granulomas (**Figure 5**). Schistosome granulomas consist of ECM, fibroblasts and a range of immune cells (predominantly Th2 cells), whose frequency and spatial distribution varies across the course of infection and the site in question (55, 60). To examine the spatial dynamics of granuloma formation and resolution and assess the localisation of key cell types, confocal microscopy was performed on liver sections at each stage of infection (**Figure 5A**).

While no eggs were found in livers from infected mice at wk 4, we observed disorganised clustering of immune cells with sporadic Siglec-F staining throughout that was not present in naïve mice (**Figure 5A**). By wk 6, immune cells began to assemble into more organised, compact, areas that enveloped tissue-trapped eggs and harboured $CD11c^+$ and Siglec-F^+ cells, and a small number of $TCR\beta^+$ cells, at their core. By wks 8 and 12, $CD11c^+$ and Siglec-F^+ cells now appeared distributed across granulomas, with new infiltration and co-localisation of $TCR\beta^+$ cells with $CD11c^+$ cells. By wk 15, $CD11c^+$ and $TCR\beta^+$ cells reduced in frequency but remained dispersed and colocalised across granulomas, while Siglec-F^+ cells were again evident within the innermost layer, along with some staining across granulomas. By quantifying the surface area for positive staining around individual eggs, we were able to assess the kinetics of these cell types within granulomas (**Figure 5B**). From wks 6-8, the staining for each marker increased markedly, but was only significant for CD11c and Siglec-F. After wk 8, Siglec-F decreased while CD11c remained consistently elevated until wk 15. TCRβ patterns were somewhat comparable to CD11c, but with a more dramatic reduction by wk 15. These histological data were generally consistent with the hepatic flow cytometry readouts for DCs, eosinophils and T cells (**Figure 2**).

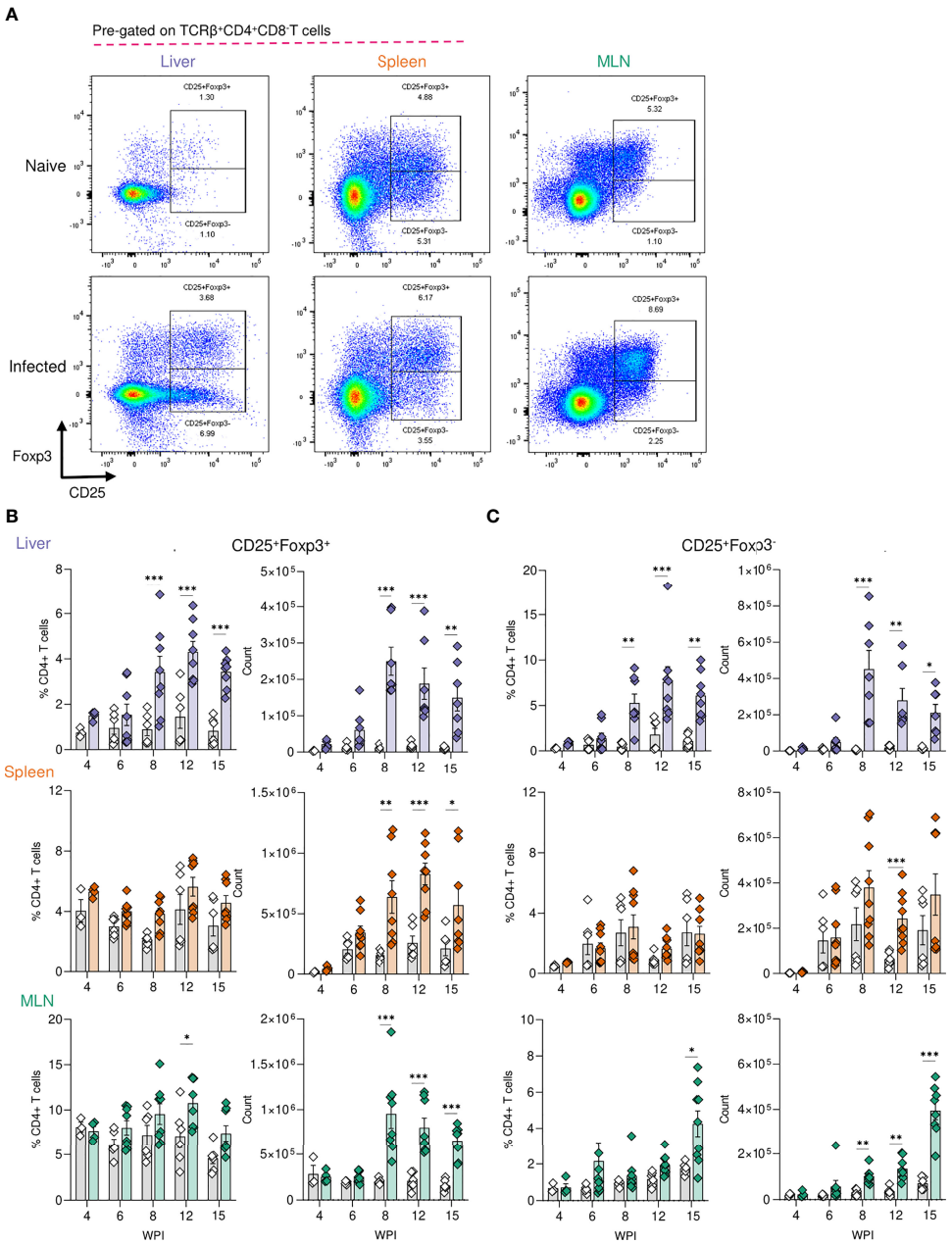

FIGURE 3 | Regulatory T cell dynamics across *S. mansoni* infected tissues. **(A)** Representative flow plots for $CD25^+Foxp3^+$ and $CD25^+Foxp3^-$ gating, pre-gating on live $CD45^+TCR\beta^+CD4^+CD8^-$ cells. The frequency and total numbers of **(B)** $CD25^+Foxp3^+$ T cells and **(C)** $CD25^+Foxp3^-$ cells in the liver, spleen and MLN of naïve and 40 cercariae infected mice, at indicated timepoints, and with frequency presented as % of total CD4+ T cells. **(B, C)**. Results are mean +/- SEM from two experiments pooled (wks 6-15) or a single experiment (wk4) (n=3-8 mice per group per time-point). Significance calculated by two-way ANOVA. *p < 0.05, **p < 0.01, ***p < 0.001.

CD11c Depletion Dramatically Impairs Hepatic Immune Cell Polarisation, Provoking Neutrophilia

In previous work, we used targeted $CD11c^+$ cell depletion to reveal a crucial role for $CD11c^+$ cells in Th2 induction during initial egg producing stages of *S. mansoni* infection (wk 4-6) (24), prior to the dramatic pathological and immunological changes that occur from 6–8-wks post infection (**Figures 1**–**5**). We next sought to explore how CD11c depletion would affect immunopathology and the maintenance of immune responses at later stages of infection using CD11c.DOG mice, in which the CD11c promotor controls expression of the human diphtheria toxin (DTx) receptor (DTR)

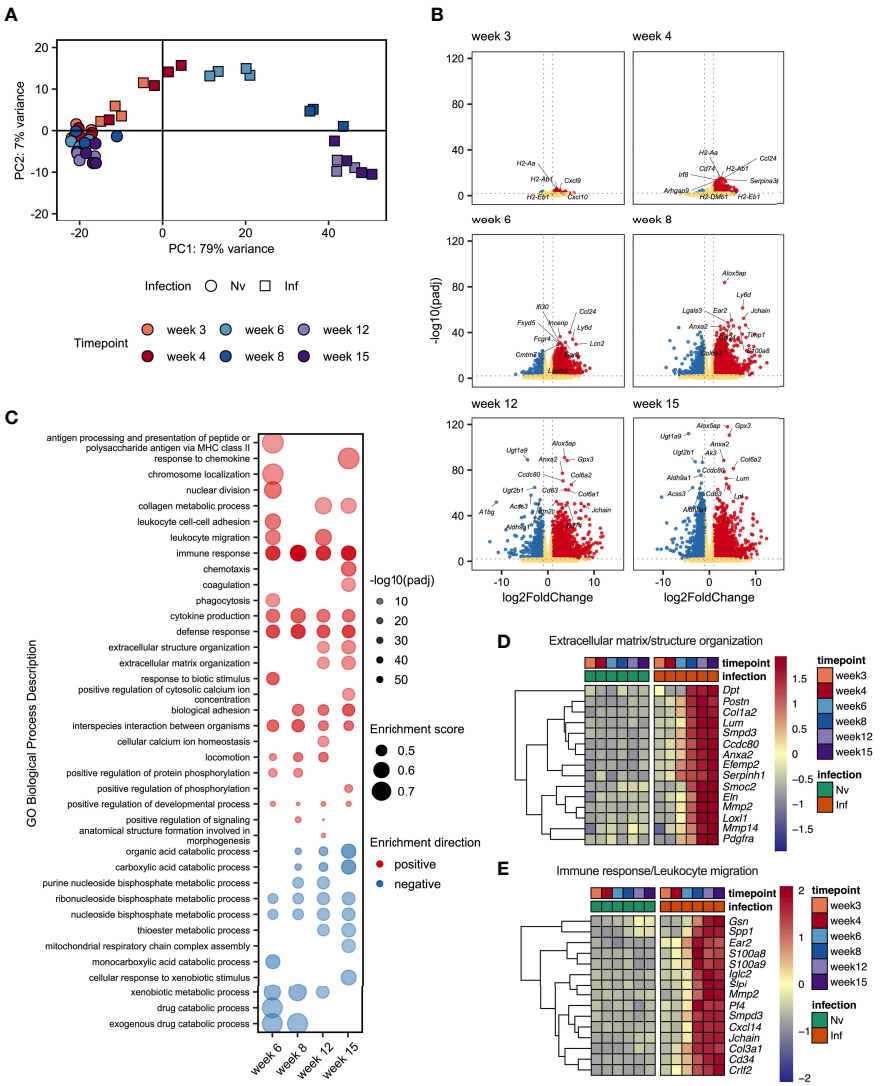

FIGURE 4 | Schistosome egg deposition dramatically alters the liver transcriptome. Livers from schistosome infected mice (Inf) or matched naïve controls (Nv) were harvested at 3, 4, 6, 8, 12 and 15 wks post infection (40 cercariae infection, n=3-4 per timepoint). RNA was isolated from the liver tissue and transcriptionally profiled by RNAseq. **(A)** Principal components analysis of total read counts. Points represent individual replicates. Point shape indicates group, Nv (○) Inf (□), and colour indicates timepoint. **(B)** Volcano plots of differentially expressed protein-coding genes in Inf vs Nv mice at each time point. Genes were considered significantly differentially expressed in Inf mice when the adjusted p value (padj) was < 0.01 and the log2FoldChange was > 1. Red dots indicate genes significantly up-regulated in Inf mice, blue dots indicate genes significantly down-regulated in Inf mice, yellow dots represent genes not significantly differentially expressed between Inf and Nv mice. **(C)** Gene set enrichment (GSE) analysis for Inf mice from wk 6 to wk 12 using GO Biological Process terms based on genes with a padj < 0.01 vs Nv mice. Points represent the enrichment score for a given GO term at each time point. Size of point indicates the enrichment score. Opacity of point indicates the significance value for that enrichment score expressed as -log10(padj). Point colour indicates whether a given GO term was positively (red) or negatively (blue) enriched. Blank spaces indicate that GO term was not significantly enriched at that timepoint. GO terms were considered significantly enriched if padj < 0.01. Heatmaps representing the mean expression of top 15 most significantly differentially expressed genes identified in specific GO terms: **(D)** "extracellular matrix structure" and "extracellular matrix organisation" and **(E)** "Immune response", and "Leukocyte migration". All genes presented by heatmap had a p value < 0.01. Differential expression analysis was performed using DESeq2, GSE analysis was performed using clusterProfiler.

(40). CD11c$^+$ cells were depleted from day 42 to 51 of infection, and host responses evaluated at day 52 (**Figure 6A**). CD11c depletion had no discernible impact on hepatosplenomegaly (**Figure 6B**), egg burden (**Figure 6C**) or the extent of hepatic granulomatous inflammation, as measured by quantification of MT staining (**Figure 6D**). However, closer inspection of hepatic granuloma composition revealed more inflammatory pathology following CD11c depletion (**Figure 6E**). As expected, CD11c$^+$ staining was significantly reduced in granulomas from DTx treated mice, indicating effective depletion (**Figures 6F, G**), coincident with a significant decrease in the proportion of TCRβ$^+$ and Siglec-F$^+$ cells (**Figures 6F, G**).

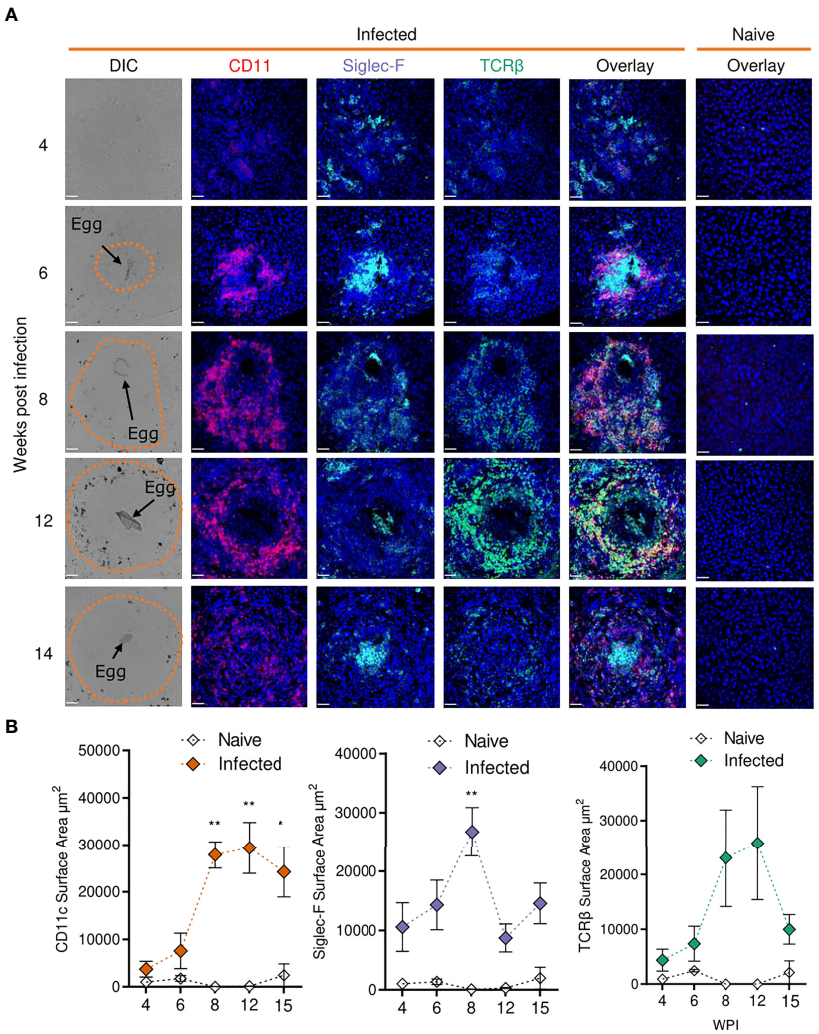

FIGURE 5 | Confocal microscopy analysis reveals distinct alterations in hepatic granuloma composition across infection timeline. At indicated stages of 40 cercarial dose infection, the infiltration and localization of CD11c$^+$, Siglec-F$^+$ and TCRβ$^+$ cells in hepatic granulomas was assessed by IHC. **(A)** Representative confocal microscopy images taken from livers of 5 *S. mansoni* infected mice at each timepoint. Top row showing differential Interference Contrast (DIC) images, with eggs indicated by arrows and dotted lines outlining granuloma periphery. **(B)** Quantification by Image J of positive Siglec-F, CD11c and TCRβ staining. 1 experiment. Significance calculated by Two-way ANOVA. Data presented as mean +/- SEM. *p < 0.05, **p < 0.01. Bars indicate SEM of from 3 sections of naïve hepatic tissue vs 10 granulomas from infected mice.

In support of our histological data (**Figures 6F, G**), assessment of liver cell populations by flow cytometry showed that DTx administration significantly depleted CD11c$^+$MHC-II$^+$ DCs (approximately 50% depletion across experiments), while hepatic macrophage proportions remained intact (**Figure 7A**). These changes were accompanied by a significant reduction in hepatic CD4$^+$ T cells, CD8$^+$ T cells and eosinophils, alongside a stark increase in hepatic neutrophilia (**Figure 7A**). Next, to explore the impact of CD11c depletion on cytokine dynamics, we evaluated hepatic responses following culture of isolated liver cells with SEA (**Figure 7B**) or anti-CD3 (**Figure 7C**). While CD11c depletion did not significantly alter Ag-specific cytokine production by isolated liver cells in culture, their potential to produce IL-4 and IL-10 in response to anti-CD3 was significantly diminished (**Figure 7C**). Together, these data showed that CD11c depletion significantly influenced the hepatic granulomatous response during schistosome infection, reducing eosinophilia and T cells, while increasing neutrophilia and impairing IL-4 and IL-10 potential, without dramatically affecting Ag-specific cytokine production.

DISCUSSION

In addition to elevating our basic understanding of immune response development over the course of murine *S. mansoni* infection, in both effector and priming sites, we have revealed a crucial role for CD11c$^+$ cells in hepatic granuloma coordination and maintenance in the post-patent phase of schistosome

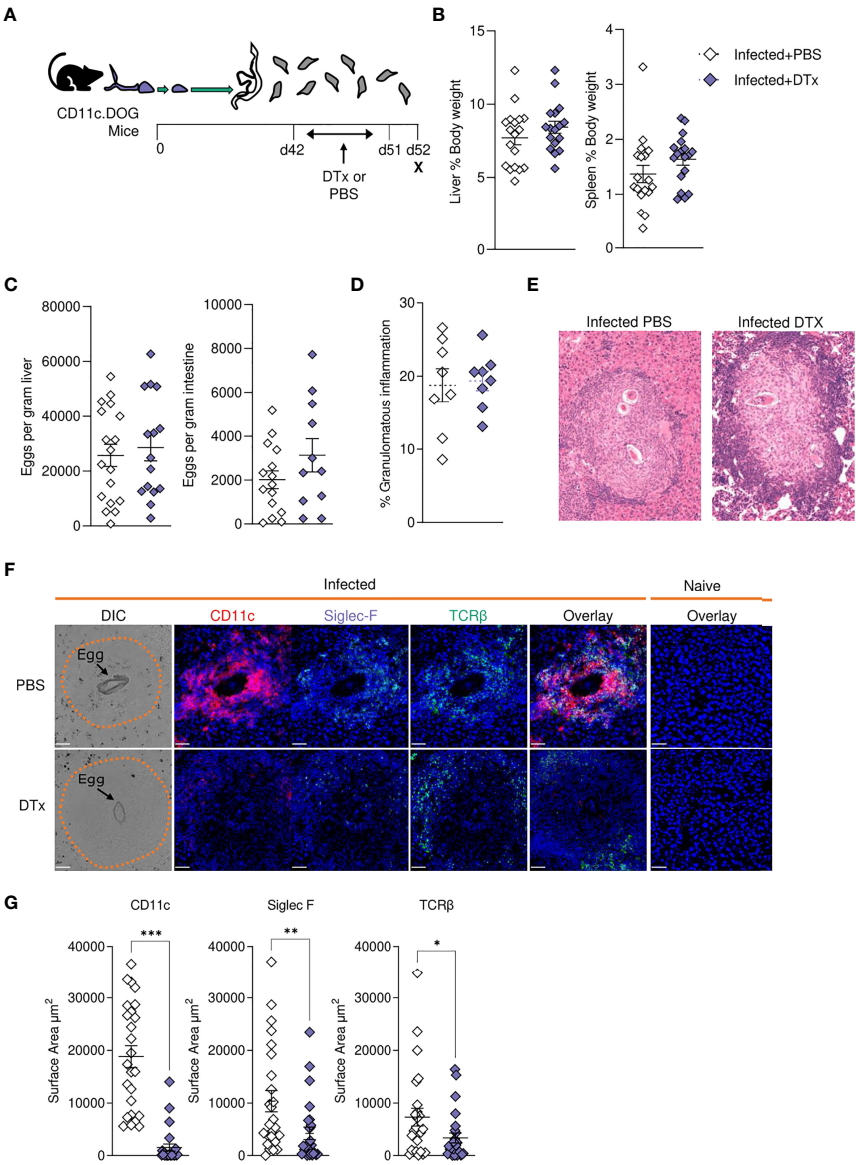

FIGURE 6 | CD11c depletion disrupts granulomatous pathology during *S. mansoni* infection. **(A)** Schematic of infection setup. CD11c.DOG mice were infected with 40 *S. mansoni* cercariae with CD11c$^+$ cells depleted *via* Dtx administration on days 42-51, and mice culled at d52. **(B)** Liver and spleen weights for infected mice with data represented as a proportion of total body weight. **(C)** The total number of schistosome eggs per gram of liver or intestinal tissue. **(D)** Quantification of granulomatous inflammation. **(E)** Representative images of hepatic granulomas stained with H&E. **(F)** Representative confocal microscopy granuloma images, with staining for CD11c, Siglec-F and TCRβ. First column showing differential Interference Contrast (DIC) images, with eggs indicated by arrows and dotted lines outlining granuloma periphery. **(G)** Quantification of positive Siglec-F, CD11C and TCRβ staining. Data are from a single experiment (D, E, F&G) or pooled from 3 **(A–C)** 3 separate experiments. Significance calculated by unpaired T-test. Data presented as mean +/- SEM. *p < 0.05, **p < 0.01, ***p < 0.001.

infection. The onset of egg production evoked pronounced pathological (**Figure 1** and **Supplementary Figure 1**), immunological (**Figures 1–3** and **Supplementary Figure 2**) and transcriptional host responses (**Figure 4**), with clear immunopathology by the eighth wk of infection (**Figures 1**, **4**, **5** and **Supplementary Figures 1**, **2**). As demonstrated through cytokine analysis of cultured liver, spleen or MLN cells *ex vivo* (**Figure 1** and **Supplementary Figure 2**), infection elicited a distinctive triphasic kinetic, including a Th1-skewed phase prior to egg production, a Th2-dominated response from egg deposition, and a more regulated profile in the chronic stage (**Figure 1** and **Supplementary Figure 2**). Egg deposition drastically remodelled the liver transcriptome, including dramatic enrichment of genes associated with granulocyte recruitment, tissue remodelling and leukocyte activation, and with the most pronounced transcriptional changes starting between wk 6 and 8 of infection (**Figure 4**). Histologically, distinctive hepatic granulomatous inflammation was evident by

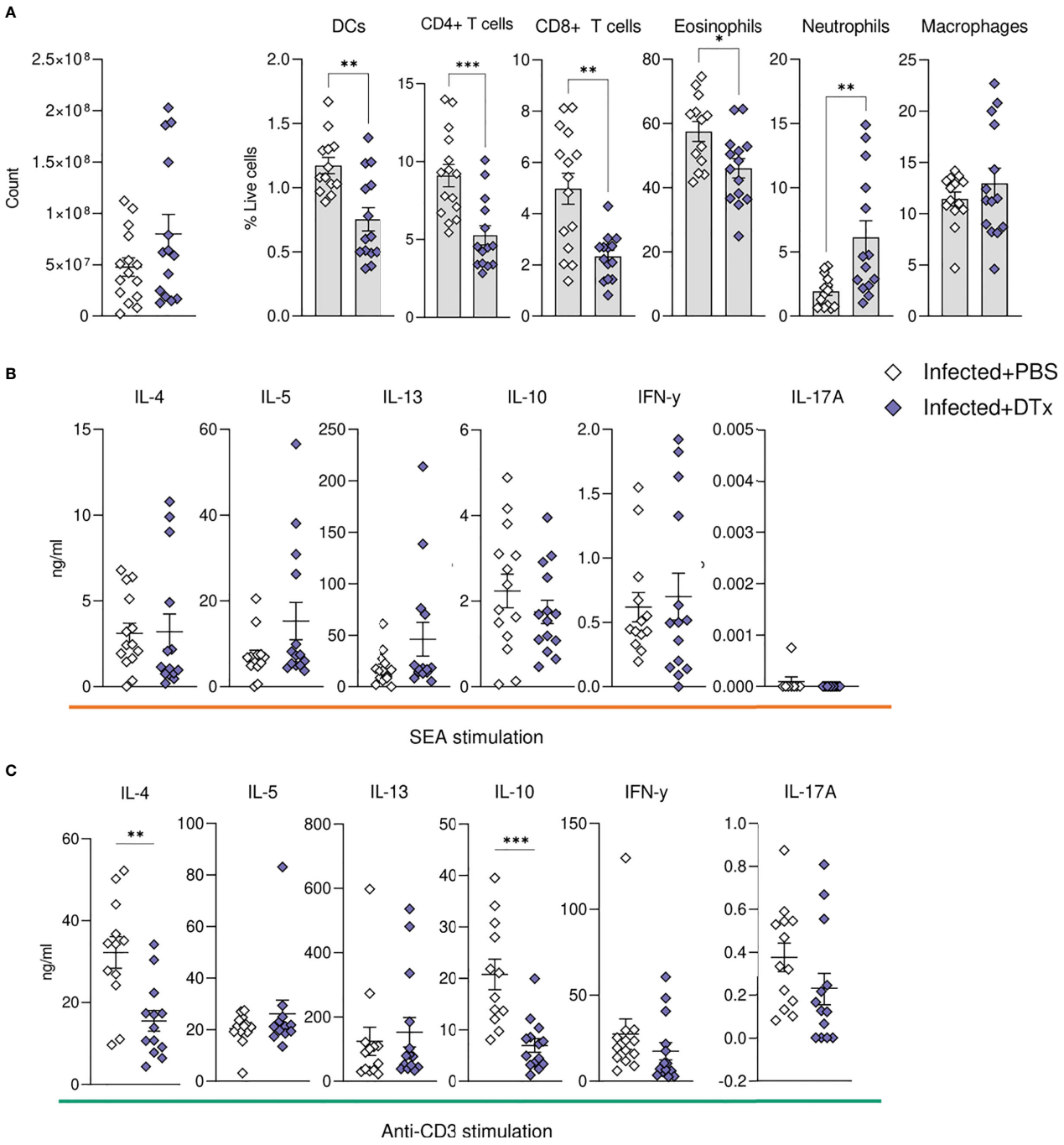

FIGURE 7 | CD11c depletion compromises hepatic cellular dynamics during *S. mansoni* infection. CD11c.DOG mice were infected with 40 S. mansoni cercariae, with CD11c+ cells depleted on d42-51 via Dtx administration, and mice culled on d52. The total number of liver cells **(A)** and the frequency of various immune cells in the liver of Dtx of PBS treated infected mice. Liver cells were cultured for 72 h with **(B)** 0.25 μg of SEA or **(C)** 0.5μg of anti-CD3. Supernatants were collected and cytokine production (medium alone values subtracted) was assessed by ELISA. Data are pooled from 3 separate experiments (n=12-18 animals per time point). Significance calculated by unpaired T-test. Data presented as mean +/- SEM. *p < 0.05, **p < 0.01, ***p < 0.001.

wk 6 of infection, which subsided by more chronic stages (**Figures 1**, **5**). Importantly, depletion of $CD11c^+$ cells between wks 6-8 of infection had a dramatic impact on the hepatic response, including disrupted granuloma formation and cellularity, increased neutrophilia, and impaired cytokine production (**Figures 6**, **7**).

Time Course Kinetics

We found that the dramatic granulomatous inflammation that develops in the liver from wk 6 of infection (**Figure 1**) became evident over the course of a matter of days, with day 45 representing a distinct tipping point between 'homeostasis' and stark pathology (**Supplementary Figure 1**). However, it is important to note that, although we selected representative images for each timepoint, granuloma development is asynchronous, due to differences in timing and location of egg deposition, egg maturity and secretions, and previous exposure to cross-reactive worm Ags (52, 61). To investigate granuloma development in a more synchronous manner, investigations could be made using intravenous injections into the portal vein or lung (52).

Schistosome infection actively modifies T cell responses in order to promote the Th1-Th2 switch, trigger regulatory cell networks, and induce a state of T cell hyperresponsiveness (8, 62, 63). We observed a reduced propensity for isolated cells from livers, spleens or MLNs of more chronically infected mice to produce cytokines in response to Ag-specific (SEA) stimulation (**Figure 1**), in support of previous studies suggesting $CD4^+$ T cell exhaustion during later stages of active disease (64, 65). In contrast, upon polyclonal (anti-CD3) stimulation, many cytokines continued to increase in the liver and MLNs beyond wk 12 of infection (**Supplementary Figure 2**). This might suggest that down-modulation of T cell activation during chronic infection is restricted to Ag-specific responses. Alternatively, it is possible that while Ag-specific T cells enter an exhausted state following repeat Ag stimulation (5), a pool of T cells undergo Ag-independent bystander activation towards circulating cytokines and TLR ligands, thus sustaining cytokine secretion across infection (66). Finally, the reduction in T cell activity may reflect the direct activity of schistosome products on T cells or modulation of APC activity (19, 65, 67, 68), which could include promoting the emergence of more tolerogenic APCs (65, 68) or those with a reduced capacity to elicit effector Th2 cell proliferation (69).

In keeping with regulatory responses being more apparent during chronicity (5, 29), we observed evidence for enhanced immunoregulation in later stages of infection (**Figures 1**, **2** and **Supplementary Figure 2**). $CD25^+Foxp3^+$ Tregs were expanded across all tissues at later infection phases, but with the most statistically robust expansion (both proportional and numerical) within the liver (**Figure 3**). These observations support previous studies showing enhanced Treg frequencies in the liver, MLN, spleen and colonic granulomas during infection (30, 36, 37) and suggest the hepatic inflammatory environment to most effectively support Treg activation and recruitment. This may result from the costimulatory environment (63), TGFβ (38), RELMα (70, 71) egg antigens (35, 37), or the higher levels of IL-4 and IL-13 (**Figure 1**), all of which have shown capable of inducing $CD25^+$ Tregs from peripheral naïve $CD25^-CD4^+$ T cells (72, 73). Although previous work has assessed Treg development in the spleen, MLN and liver during murine schistosomiasis (30, 36, 37), we are the first to show side by side comparison of tissue specific Treg kinetics over the course of infection. It remains to be addressed whether Breg and $CD8^+$ Treg (74) generation mirrors these $CD4^+$ Treg dynamics, and whether *S. mansoni* elicited Tregs harbour tissue-specific functions.

We also observed increased IL-10 levels as infection progressed, from isolated and cultured spleen, MLN and liver cells, with this profile being most evident with anti-CD3 stimulation (**Figure 1** and **Supplementary Figure 2**). This may reflect our choice of SEA for Ag-specific *ex vivo* restimulation, given that adult worm-derived molecules may preferentially expand regulatory responses (19, 68). Splenic IL-10 levels were low in comparison to the liver and MLN, which again could reflect the choice of stimulation or the relative abundance of cultured cell types. Furthermore, B cells can be meaningful sources of IL-10 during schistosomiasis (29, 34), quantification of which would require alternative approaches, such as stimulation *via* TLRs and CD40 (75), or the use of IL-10 reporter mice, which constitute an improved tool for visualisation of which cell types contribute to the IL-10 pool (76).

In terms of other cellular responses, $CD8^+$ T cells comprised a third of all T cells in the liver (**Figure 2**), with previous literature accrediting them with 'suppressor' functions in the downmodulation of egg-driven pathology (77, 78). Eosinophils showed increases across tissues during infection, a likely reflection of elevated levels of IL-5 (**Figure 1** and **Supplementary Figure 2**) or chemokines such as CCL24 (79) (**Figure 4**) or CXCL12 (80). Despite their dominating presence within schistosome infected tissues, the true function of eosinophils in schistosomiasis is not yet known, with eosinophil ablation (81) or IL-5 removal (82) failing to impede granuloma formation or fibrosis, influence hepatocellular damage, or impact Th2 development (83). Analysis of Siglec-F staining of liver sections showed eosinophilia during early stages of granuloma formation within the inner perimeter of circumoval inflammation (**Figure 5**). In previous reports, this localisation has only been shown through morphometric inspection of Giemsa or H&E-stained granulomas (55, 60, 81), and this pattern suggests that eosinophils may play an important role in granuloma formation and protection of parenchymal tissue, and/or in the destruction of the entrapped eggs (84). Indeed, an interesting feature of the hepatic response was that liver cells from infected mice had a greater potential to produce IL-5 as early as wk 4 of infection (**Figure 1** and **Supplementary Figure 2**), which could support the rapid recruitment of eosinophils during granuloma initiation and development from around wk 6. Moreover, we suggest that the hepatic immune infiltration observed at wk 4 (**Figure 2**) may be encouraged by the deposition of worm-derived antigens or regurgitation products within the liver. Indeed, schistosome-derived hemozoin has shown to deposit in large quantities the liver and influence components of host immunity, including alternative activation of macrophages (85). Further interrogation of this pre-patent inflammation would ideally entail comparison between naïve, mixed-sex and single-sex infections.

Transcriptomics is a powerful investigative tool, that offers a high-resolution and unbiased description of host processes at an RNA level. The transcriptional profile of the mammalian host

during schistosomiasis has been explored in a range of primate and rodent models (86–88), with more recent work exploring the human transcriptome during active infection (89, 90). However, only a few of these studies have interrogated the dynamics of host gene expression at multiple time points of schistosome infection (88), and no comprehensive overview of how the hepatic transcriptional environment changes across the course of infection yet exists. By defining hepatic transcriptional signatures during pre-patency, our data offers insight into first cellular responders and the mechanisms underlying their recruitment (**Figure 4**). Notably, the IFNγ-inducible chemokines *Cxcl9* and *Cxcl10 (*91) were among the most upregulated genes at wks 3 and 4 post infection, which is consistent with reports from murine *S. japonicum* infection (86) and suggests Th1-associated chemokines (91) may be associated with initial inflammatory cell recruitment and instigation of granulomatous inflammation. Similarly, expression of IFNγ-driven *Tgtp1* (T cell-specific GTPAse-; **Supplementary Excel File 1**), which is associated with M1 effector functions (92) links with literature showing enhanced frequency of M1-like macrophages during acute schistosomiasis (93, 94) and provides further clarity into the timing of their arrival and/or proliferation.

The transcriptome of the post-patent liver (**Figure 4**) clearly reflected the diverse populations of immune cells populating the tissue (**Figures 2**, **3**), as well as the structural and fibrotic changes the liver undergoes to counteract and/or compensate for egg-induced inflammation (**Figures 1**, **5**). From wk 6, infected livers transitioned into an inflammatory state, as evidenced by enhanced transcripts of acute-phase serum amyloid proteins, SAA1 and SAA2 (**Supplementary Excel File 1**), and moderate upregulation (relative to later wks of infection) of chemokines *Ccl8* and *Ccl24* (**Supplementary Excel File 1**). Interestingly, and in line with our histological analysis for Siglec-F$^+$ cells (**Figure 5**), the chemotactic ligand for eosinophils, *Ccl24* [encoding eotaxin-2 (95)], reached peak expression at wk 8 of infection before declining at more chronic phases (**Supplementary Excel File 1**). The list of upregulated genes from wk 8 onwards was dominated by genes associated with tissue restructuring and fibrosis, as well as the recruitment, activation and function of key immune cells, including mast cell proteases, eosinophilic elastases and a marker of macrophage alternative activation, chitinase-like 3 (*Chil3*, encoding Ym1; **Supplementary Excel File 1**), whose function during schistosomiasis has yet to be resolved. Our transcriptomic analysis may assist in the identification of novel cellular and molecular targets for the therapeutic control of schistosomiasis, or treatment of schistosomiasis associated hepatic fibrosis. Notably, the ratio of MMPs to tissue inhibitors of matrix metalloproteinases (TIMPs) **Figure 4**), is a suggested determining factor in the severity of schistosomiasis and may provide clarity on the differences in wound healing response and outcome between *S. japonicum* and *S. mansoni* infections (86, 96). Moreover, in terms of individual genes of interest, *Timp-1, Ccl24*, and *Sox9* all demonstrate sustained upregulation from the point of egg production and are all implicated in the exaggeration of fibrosis (97–99). Finally, the transcriptome of the chronically infected liver showed very interesting metabolic changes, including the downregulation of the cytochrome P450 family (CYPs), amongst other drug metabolising enzymes. Importantly, the downregulation of Cyp2b and Cyp3a (**Supplementary Excel File 1**) may have significant implications for the metabolism and clearance of the anti-schistosome drug praziquantel (100) and thus this could represent a therapeutically fruitful area of follow-up.

CD11c Depletion

Having generated a high-resolution picture of hepatic schistosomiasis at a transcriptional (**Figure 4**) and cellular (**Figures 2**, **3**, **5**) level, we next sought to identify the importance of CD11c$^+$ cells in coordinating the liver response to infection. The development of Th2 immunity is crucial for the control of excessive schistosome associated pathology (8, 10, 32, 38). Notably, mice in Th1 polarised settings (including IL-4 deficient or IL-10/IL-4 double-deficient mice) exhibit rapid weight loss at the onset of egg production, elevated expression of proinflammatory Th1 cytokines and mediators, and high levels of mortality between wks 8-10 of infection (10, 32, 101). The mechanisms underlying the dramatic transition from a mixed, low level Th1/Th2 to a Th2 dominated immune response have been thoroughly dissected, with central involvement of STAT-6 (102), IL-4 (10, 32) and IL-4Rα (9, 103) signalling, and DCs (24). However, there is less understanding of how granulomas and hepatic Th2 responses are maintained and regulated over the course of infection. Herein, we show CD11c depletion during peak development of schistosome-elicited Type 2 inflammation (wks 6-8) compromised hepatic granuloma composition (**Figure 6**). Although CD11c depletion at this stage of infection resulted in impaired liver cell potential to produce IL-4 and IL-10 (**Figure 7C**), it did not significantly impact Ag-specific cytokine responses (**Figure 7B**). This contrasts CD11c depletion at wks 4-6, which we have previously shown significantly reduces hepatic cell Ag-specific IL-4, IL-5 and IL-13 production (24). These data indicate that, while CD11c$^+$ DCs may be crucial for the induction and expansion of CD4$^+$ T cells in priming stages of infection (24) at later stages effector T cells can competently produce cytokines without their assistance, with other APCs such as B cells or macrophages potentially playing larger roles in effector T cell activation at later phases of infection (104). Alternatively, as hepatic CD11c depletion was incomplete in our experiments (**Figures 6**, **7**), it is possible that residual CD11c$^+$ DCs were sufficient to maintain hepatic Th2 effector responses. While Ag-specific liver cell cytokine responses were not significantly affected following CD11c depletion at this timepoint, production of both IL-4 and IL-10 was impaired following stimulation with anti-CD3, implicating CD11c$^+$ cells in dictating hepatic CD4$^+$ T cell potential to produce these cytokines during schistosomiasis. Taken together, these results suggest that CD11c$^+$ APCs play a supportive role in stimulation of T cell cytokine production in the liver effector site. In contrast, CD11c depletion dramatically altered granuloma and hepatic cellularity (**Figures 6**, **7**), in particular significantly reducing eosinophilia and T cells, without reducing overall granulomatous inflammation (**Figure 6D**). Deficits in hepatic recruitment and/or retention of eosinophils

and T cells following CD11c depletion may fit with the known ability of DCs to produce a range of chemokines (105–107). In line with this, in a model of schistosome egg induced pulmonary granulomatous inflammation, depletion of known eosinophil (105) and Th2 cell (108) chemokines CCL17 and CCL22, which can be produced by DCs (105–107), led to altered granuloma structure, including a dramatic reduction in eosinophilia (109).

In our experiments, neutrophils, which are normally minor constituents of *S. mansoni* granulomas due to the release of egg-derived chemokine-binding proteins and proteases that inhibit neutrophil function or recruitment (16, 110), significantly increased in the liver following CD11c depletion (**Figure 7**). The fact that schistosome eggs actively secrete neutrophil inhibiting molecules suggests that their presence is undesirable during infection, and their expansion may give rise to more damaging hepatic inflammation, as seen in murine *S. japonicum* infection (111). The cause of neutrophilic expansion is unclear, but this has been reported in other studies using CD11c DTR transgenic mice (112). We predict that the dysregulated granulomas observed in CD11c-depleted mice could have severe pathological consequences in later disease stages, with the absence of intact granuloma barrier leading to increased perfusion of hepatotoxic egg molecules into the tissues.

Together, these data indicate that $CD11c^+$ cells play a critical role in recruitment or retention of eosinophils and T cells in the liver from wk 6 of schistosome infection, while other $CD11c^-$ cells are generally sufficient for reactivation of cytokine production by hepatic effector T cells. Our results provide a platform for future interrogation of the role of $CD11c^+$ cells in more chronic stages of infection, alongside employment of more targeted CD11c depletion approaches (113), to enable a more holistic understanding of the role and importance of $CD11c^+$ APC subsets in governing immunopathology in effector sites such as the liver over the course of schistosome infection

In conclusion, this study provides a detailed and comprehensive analysis of immune response development over the course of schistosome infection at a resolution not previously achieved, providing a valuable resource to inform future work aiming to better understand the mechanisms that govern immunity, inflammation and pathology in this important neglected tropical disease.

DATA AVAILABILITY STATEMENT

The unprocessed fastq files relating to the RNA sequencing data presented in the manuscript are deposited in the European Nucleotide Archive, accession numbers SAMEA2668137 - SAMEA2668182. Processed read counts, and the results from the differential expression and gene set enrichment analyses are available in **Supplementary Material**.

ETHICS STATEMENT

All animal experiments were conducted under licenses granted by the Home Office UK, in accordance with local guidelines and following ethical review by the University of Manchester or the University of Edinburgh, and performed in accordance with the United Kingdom Animals (Scientific Procedures) Act of 1986.

AUTHOR CONTRIBUTIONS

ASM and AP-A conceived the study. AP-A, AKM, CO, PC, and SB performed the experiments. AC, SC, AP-A, CO, and ASM analyzed the data. AC and SC wrote the manuscript. AP-A, PC, MB, HS, and ASM read the manuscript and provided critical comments. All authors contributed to the manuscript and approved the submitted version.

FUNDING

This work was supported by the MRC (G0701437 and MR/W018748/1) and MCCIR core funding (to ASM), and The Wellcome Trust (098051 to MB). PCC is supported by a Wellcome Trust Sir Henry Dale Fellowship (218550/Z/19/Z) and the MRC Centre for Medical Mycology at the University of Exeter (MR/N006364/2).

ACKNOWLEDGMENTS

We thank Gareth Howell for assistance as part of the University of Manchester Flow Cytometry Core Facility. For advice and assistance with histological analysis, we thank Dr. Tim Kendall and Prof. Mark Arends at the Western General Hospital in Edinburgh.

SUPPLEMENTARY MATERIAL

The Supplementary Material for this article can be found online at: https://www.frontiersin.org/articles/10.3389/fimmu.2022.906338/full#supplementary-material

Supplementary Excel File 1 | Differential expression analysis from RNAseq on the liver during S. mansoni infection **(A)** Read counts for each identified transcript in individual samples **(B)** Sample meta data **(C)** Results from differential expression analysis comparing naive and infected mice irrespective of timepoint **(D)** Results from differential expression analysis comparing naive and infected mice at week 3 post infection **(E)** Results from differential expression analysis comparing naive and infected mice at week 4 post infection **(F)** Results from differential expression analysis comparing naive and infected mice at week 6 post infection **(G)** Results from differential expression analysis comparing naive and infected mice at week 8 post infection **(H)** Results from differentia expression analysis comparing naive and infected mice at week 12 post infection **(I)** Results from differential expression analysis comparing naive and infected mice at week 15 post infection.

Supplementary Excel File 2 | Results from gene set enrichment analysis, using Gene Ontology (gseGO) terms associated with biological processes, for genes identified as differentially expressed in the livers of mice infected with S. mansoni compared to naive mice. **(A)** gseGO results at week 4 post infection **(B)** gseGO results at week 6 post infection **(C)** gseGO results at week 8 post infection **(D)** gseGO results at week 12 post infection **(E)** gseGO results at week 15 post infection

Supplementary Figure 1 | Development of hepatic pathology and antibody responses during *S. mansoni* infection. **(A)** The total number of schistosome eggs per gram of liver or intestinal tissue. **(B)** Visualisation of hepatic granulomas at 36, 39, 42, 45, 48 and 51 days post infection (DPI). Representative images of liver sections stained with Masson's Trichrome (MT) **(C)** Quantification of granulomatous inflammation. **(D)** Quantification of positive CD11C, TCRβ and Siglec-F staining in liver sections. **(E)** SEA-specific IgG, IgG1, IgG2c and IgG3 titres in the serum of naïve and infected mice, presented as endpoint serum dilutions. **(F)** Serum IgE titres, presented as concentration. **(G)** Liver and spleen weights for infected mice with data represented as a proportion of total body weight. Data are from a single experiment **(B–F)** or pooled from 2 **(G)** or 3 separate experiments **(A)**, with 3-18 mice per timepoint, per infection group. Significance calculated by one-way or two-way ANOVA. Data presented as mean +/- SEM. *p < 0.05, **p < 0.01, ***p < 0.001.

Supplementary Figure 2 | Development of a dominant Type 2 response across tissues during *S. mansoni* infection. Liver, spleen and MLN cells from naïve or infected mice were cultured for 72 h in the presence of 0.5ug anti-CD3. Supernatants were collected and cytokine production (medium alone values subtracted) was assessed by ELISA. Data are pooled from two separate experiments. Significance calculated by two-way ANOVA. Data presented as mean +/-SEM, *p < 0.05, **p < 0.01, ***p < 0.001.

REFERENCES

1. McManus DP, Dunne DW, Sacko M, Utzinger J, Vennervald BJ, Zhou XN, et al. Schistosomiasis. *Nat Rev Dis Primers* (2018) 4:1–19. doi: 10.1038/s41572-018-0013-8
2. Pearce EJ, MacDonald AS. The Immunobiology of Schistosomiasis. *Nat Rev Immunol* (2002) 2:499–511. doi: 10.1038/nri843
3. Houlder EL, Costain AH, Cook PC, MacDonald AS. Schistosomes in the Lung: Immunobiology and Opportunity. *Front Immunol* (2021) 0:1330. doi: 10.3389/fimmu.2021.635513
4. Costain AH, MacDonald AS, Smits HH. Schistosome Egg Migration: Mechanisms, Pathogenesis and Host Immune Responses. *Front Immunol* (2018) 9:3042. doi: 10.3389/fimmu.2018.03042
5. Taylor JJ, Krawczyk CM, Mohrs M, Pearce EJ. Th2 Cell Hyporesponsiveness During Chronic Murine Schistosomiasis is Cell Intrinsic and Linked to GRAIL Expression. *J Clin Invest* (2009) 119:1019–28. doi: 10.1172/JCI36534
6. Ottesen EA, Hiatt RA, Cheever AW, Sotomayor ZR, Neva FA. The Acquisition and Loss of Antigen-Specific Cellular Immune Responsiveness in Acute and Chronic Schistosomiasis in Man. *Clin Exp Immunol* (1978) 33:37–47.
7. Everts B, Smits HH, Hokke CH, Yazdanbakhsh M. Helminths and Dendritic Cells: Sensing and Regulating *via* Pattern Recognition Receptors, Th2 and Treg Responses. *Eur J Immunol* (2010) 40:1525–37. doi: 10.1002/eji.200940109
8. Fallon PG, Richardson EJ, Smith P, Dunne DW. Elevated Type 1, Diminished Type 2 Cytokines and Impaired Antibody Response are Associated With Hepatotoxicity and Mortalities During Schistosoma Mansoni Infection of CD4-Depleted Mice. *Eur J Immunol* (2000) 30:470–80. doi: 10.1002/1521-4141(200002)30:2<470::AID-IMMU470>3.0.CO;2-T
9. Herbert DR, Hölscher C, Mohrs M, Arendse B, Schwegmann A, Radwanska M, et al. Alternative Macrophage Activation is Essential for Survival During Schistosomiasis and Downmodulates T Helper 1 Responses and Immunopathology. *Immunity* (2004) 20:623–35. doi: 10.1016/S1074-7613(04)00107-4
10. Brunet LR, Finkelman FD, Cheever AW, Kopf MA, Pearce EJ. IL-4 Protects Against TNF-Alpha-Mediated Cachexia and Death During Acute Schistosomiasis. *J Immunol* (1997) 159:777–85.
11. Everts B, Perona-Wright G, Smits HH, Hokke CH, Van DerHam AJ, Fitzsimmons CM, et al. Omega-1, a Glycoprotein Secreted by Schistosoma Mansoni Eggs, Drives Th2 Responses. *J Exp Med* (2009) 206:1673–80. doi: 10.1084/jem.20082460
12. Everts B, Hussaarts L, Driessen NN, Meevissen MHJ, Schramm G, van derHam AJ, et al. Schistosome-Derived Omega-1 Drives Th2 Polarization by Suppressing Protein Synthesis Following Internalization by the Mannose Receptor. *J Exp Med* (2012) 209:1753–67. doi: 10.1084/jem.20111381
13. Kaisar MMM, Ritter M, del Fresno C, Jónasdóttir HS, van derHam AJ, Pelgrom LR, et al. Dectin-1/2–Induced Autocrine PGE 2 Signaling Licenses Dendritic Cells to Prime Th2 Responses. *PLoS Biol* (2018) 16:e2005504. doi: 10.1371/journal.pbio.2005504
14. Donnelly S, Stack CM, O'Neill SM, Sayed AA, Williams DL, Dalton JP. Helminth 2-Cys Peroxiredoxin Drives Th2 Responses Through a Mechanism Involving Alternatively Activated Macrophages. *FASEB J* (2008) 22:4022–32. doi: 10.1096/fj.08-106278
15. Carson JP, Gobert GN. Modulation of the Host Immune Response by Schistosome Egg-Secreted Proteins Is a Critical Avenue of Host–Parasite Communication. *Pathogens* (2021) 10:863. doi: 10.3390/pathogens10070863
16. Smith P, Fallon RE, Mangan NE, Walsh CM, Saraiva M, Sayers JR, et al. Schistosoma Mansoni Secretes a Chemokine Binding Protein With Anti-Inflammatory Activity. *J Exp Med* (2005) 202:1319–25. doi: 10.1084/jem.20050955
17. Schramm G, Gronow A, Knobloch J, Wippersteg V, Grevelding CG, Galle J, et al. IPSE/alpha-1: A Major Immunogenic Component Secreted From Schistosoma Mansoni Eggs. *Mol Biochem Parasitol* (2006) 147:9–19. doi: 10.1016/j.molbiopara.2006.01.003
18. Haeberlein SO, Ozir-Fazalalikhan K, Chayé A, AMVeninga M, van derVlugt H, Lucïen EPM, et al. Schistosome Egg Antigens, Including the Glycoprotein IPSE/alpha-1, Trigger the Development of Regulatory B Cells. *PLoS Pathog* (2017) 13:e1006539. doi: 10.1371/journal.ppat.1006539
19. Floudas AC, DFahel C, Khan J, RSaunders A, PAmu S, Sylvie , et al. Composition of the Schistosoma Mansoni Worm Secretome: Identification of Immune Modulatory Cyclophilin a. *PLoS Negl Trop Dis* (2017) 11:e0006012. doi: 10.1371/journal.pntd.0006012
20. Ndlovu H, Nono JK, Abdel Aziz N, Nieuwenhuizen NE, Brombacher F. Interleukin-4 Receptor Alpha Expressing B Cells Are Essential to Down-Modulate Host Granulomatous Inflammation During Schistosomasis. *Front Immunol* (2018) 9:2928. doi: 10.3389/fimmu.2018.02928
21. Grzych JM, Pearce E, Cheever A, Caulada ZA, Caspar P, Heiny S, et al. Egg Deposition is the Major Stimulus for the Production of Th2 Cytokines in Murine Schistosomiasis Mansoni. *J Immunol* (1991) 146:1322–7.
22. Pearce EJ, Caspar P, Grzych J-M, Lewis FA, Sher A. Downregulation of Thl Cytokine Production Accompanies Induction of Th2 Responses by a Parasitic Helminth, Schistosoma Mansoni. *J Exp Med* (1991) 173:159–66. doi: 10.1084/jem.173.1.159
23. de Oliveira Fraga LA, Torrero MN, Tocheva AS, Mitre E, Davies SJ. Induction of Type 2 Responses by Schistosome Worms During Prepatent Infection. *J Infect Dis* (2010) 201:464–72. doi: 10.1086/649841
24. Phythian-Adams AT, Cook PC, Lundie RJ, Jones LH, Smith KA, Barr TA, et al. CD11c Depletion Severely Disrupts Th2 Induction and Development In Vivo. *J Exp Med* (2010) 207:2089–96. doi: 10.1084/jem.20100734
25. Larkin BM, Smith PM, Ponichtera HE, Shainheit MG, Rutitzky LI, Stadecker MJ. Induction and Regulation of Pathogenic Th17 Cell Responses in Schistosomiasis. *Semin Immunopathol* (2012) 34:873–88. doi: 10.1007/s00281-012-0341-9
26. Kalantari P, Bunnell SC, Stadecker MJ. The C-Type Lectin Receptor-Driven, Th17 Cell-Mediated Severe Pathology in Schistosomiasis: Not All Immune Responses to Helminth Parasites Are Th2 Dominated. *Front Immunol* (2019) 10:26. doi: 10.3389/fimmu.2019.00026
27. Ponichtera HE, Shainheit MG, Liu BC, Raychowdhury R, Larkin BM, Russo JM, et al. CD209a Expression on Dendritic Cells is Critical for the Development of Pathogenic Th17 Cell Responses in Murine Schistosomiasis. *J Immunol* (2014) 192:4655–65. doi: 10.4049/jimmunol.1400121
28. Rutitzky L, Smith P, Stadecker M. T-Bet Protects Against Exacerbation of Schistosome Egg-Induced Immunopathology by Regulating Th17-Mediated Inflammation. *Eur J Immunol* (2009) 39:2470–81. doi: 10.1002/eji.200939325
29. Smits HH, Hammad H, van Nimwegen M, Soullie T, Willart MA, Lievers E, et al. Protective Effect of Schistosoma Mansoni Infection on Allergic Airway

Inflammation Depends on the Intensity and Chronicity of Infection. *J Allergy Clin Immunol* (2007) 120:932–40. doi: 10.1016/j.jaci.2007.06.009
30. Walsh CM, Smith P, Fallon PG. Role for CTLA-4 But Not CD25+ T Cells During Schistosoma Mansoni Infection of Mice. *Parasite Immunol* (2007) 29:293–308. doi: 10.1111/j.1365-3024.2007.00947.x
31. Colley DG, Lewis FA, Goodgame RW. Immune Responses During Human Schistosomiasis Mansoni. IV. Induction of Suppressor Cell Activity by Schistosome Antigen Preparations and Concanavalin a. *J Immunol* (1978) 120:1225–32.
32. Hoffmann KF, Cheever AW, Wynn TA. IL-10 and the Dangers of Immune Polarization: Excessive Type 1 and Type 2 Cytokine Responses Induce Distinct Forms of Lethal Immunopathology in Murine Schistosomiasis. *J Immunol* (2000) 164:6406–16. doi: 10.4049/jimmunol.164.12.6406
33. van der Vlugt LEPM, Zinsou JF, Ozir-Fazalalikhan A, Kremsner PG, Yazdanbakhsh M, Adegnika AA, et al. Interleukin 10 (IL-10)-Producing CD1dhi Regulatory B Cells From Schistosoma Haematobium-Infected Individuals Induce IL-10-Positive T Cells and Suppress Effector T-Cell Cytokines. *J Infect Dis* (2014) 210:1207–16. doi: 10.1093/infdis/jiu257
34. van der Vlugt LEPM, Labuda LA, Ozir-Fazalalikhan A, Lievers E, Gloudemans AK, Liu K-Y, et al. Schistosomes Induce Regulatory Features in Human and Mouse CD1dhi B Cells: Inhibition of Allergic Inflammation by IL-10 and Regulatory T Cells. *PLoS One* (2012) 7:e30883. doi: 10.1371/journal.pone.0030883
35. Taylor J, Mohrs M, Pearce E. Regulatory T Cell Responses Develop in Parallel to Th Responses and Control the Magnitude and Phenotype of the Th Effector Population. *J Immunol* (2006) 176:5839–47. doi: 10.4049/jimmunol.176.10.5839
36. Turner JD, Jenkins GR, Hogg KG, Aynsley SA, Paveley RA, Cook PC, et al. CD4+CD25+ Regulatory Cells Contribute to the Regulation of Colonic Th2 Granulomatous Pathology Caused by Schistosome Infection. *PLoS Negl Trop Dis* (2011) 5:e1269. doi: 10.1371/journal.pntd.0001269
37. Hesse M, Piccirillo CA, Belkaid Y, Prufer J, Mentink-Kane M, Leusink M, et al. The Pathogenesis of Schistosomiasis is Controlled by Cooperating IL-10-Producing Innate Effector and Regulatory T Cells. *J Immunol* (2004) 172:3157–66. doi: 10.4049/jimmunol.172.5.3157
38. Kaviratne M, Hesse M, Leusink M, Cheever AW, Davies SJ, McKerrow JH, et al. IL-13 Activates a Mechanism of Tissue Fibrosis That is Completely TGF-β Independent. *J Immunol* (2004) 173:4020–9. doi: 10.4049/jimmunol.173.6.4020
39. Cabeza-Cabrerizo M, Cardoso A, Minutti CM, Pereira da Costa M, Reis e Sousa C. Dendritic Cells Revisited. *Annu Rev Immunol* (2021) 39:131–66. doi: 10.1146/annurev-immunol-061020-053707
40. Hochweller K, Striegler J, Hämmerling GJ, Garbi N. A Novel CD11c.DTR Transgenic Mouse for Depletion of Dendritic Cells Reveals Their Requirement for Homeostatic Proliferation of Natural Killer Cells. *Eur J Immunol* (2008) 38:2776–83. doi: 10.1002/eji.200838659
41. Mohrs M, Shinkai K, Mohrs K, Locksley RM. Analysis of Type 2 Immunity *In Vivo* With a Bicistronic IL-4 Reporter. *Immunity* (2001) 15:303–11. doi: 10.1016/S1074-7613(01)00186-8
42. Tucker MS, Karunaratne LB, Lewis FA, Freitas TC, Liang Y. San. Schistosomiasis. *Curr Protoc Immunol* (2013) 103:62–4. doi: 10.1002/0471142735.im1901s103
43. Vella AT, Pearce EJ. CD4+ Th2 Response Induced by Schistosoma Mansoni Eggs Develops Rapidly, Through an Early, Transient, Th0-Like Stage. *J Immunol* (1992) 148:2283–90.
44. Pearce EJ, Cheever A, Leonard S, Covalesky M, Fernandez-Botran R, Kohler G, et al. Schistosoma Mansoni in IL-4-Deficient Mice. *Int Immunol* (1996) 8:435–44. doi: 10.1093/intimm/8.4.435
45. Schneider CA, Rasband WS, Eliceiri KW. NIH Image to ImageJ: 25 Years of Image Analysis. *Nat Methods* (2012) 9:671–5. doi: 10.1038/nmeth.2089
46. Peña-Llopis S, Brugarolas J. Simultaneous Isolation of High-Quality DNA, RNA, miRNA and Proteins From Tissues for Genomic Applications. *Nat Protoc* (2013) 8:2240–55. doi: 10.1038/nprot.2013.141
47. Langmead B, Salzberg SL. Fast Gapped-Read Alignment With Bowtie 2. *Nat Methods* (2012) 9:357–9. doi: 10.1038/nmeth.1923
48. Roberts A, Pachter L. Streaming Fragment Assignment for Real-Time Analysis of Sequencing Experiments. *Nat Methods* (2013) 10:71–3. doi: 10.1038/nmeth.2251
49. Love MI, Huber W, Anders S. Moderated Estimation of Fold Change and Dispersion for RNA-Seq Data With Deseq2. *Genome Biol* (2014) 15:550. doi: 10.1186/s13059-014-0550-8
50. Durinck S, Spellman PT, Birney E, Huber W. Mapping Identifiers for the Integration of Genomic Datasets With the R/Bioconductor Package biomaRt. *Nat Protoc* (2009) 4:1184–91. doi: 10.1038/nprot.2009.97
51. Yu G, Wang LG, Han Y, He QY. Clusterprofiler: An R Package for Comparing Biological Themes Among Gene Clusters. *OMICS* (2012) 16:284–7. doi: 10.1089/omi.2011.0118
52. Cheever AW, Lenzi JA, Lenzi HL, Andrade ZA. Experimental Models of Schistosoma Mansoni Infection. *Memorias do Instituto Oswaldo Cruz* (2002) 97:917–40. doi: 10.1590/S0074-02762002000700002
53. Abdul-Ghani RA, Hassan AA. Murine Schistosomiasis as a Model for Human Schistosomiasis Mansoni: Similarities and Discrepancies. *Parasitol Res* (2010) 107:1–8. doi: 10.1007/s00436-010-1855-5
54. Boros DL, Pelley RP, Warren KS. Spontaneous Modulation of Granulomatous Hypersensitivity in Schistosomiasis Mansoni. *J Immunol* (1975) 114:1437–41.
55. Weinstock JV, Boros DL. Heterogeneity of the Granulomatous Response in the Liver, Colon, Ileum, and Ileal Peyer's Patches to Schistosome Eggs in Murine Schistosomiasis Mansoni. *J Immunol* (1981) 127:1906–9.
56. Baumgart M, Tompkins F, Leng J, Hesse M. Naturally Occurring CD4 +Foxp3+ Regulatory T Cells are an Essential, IL-10-Independent Part of the Immunoregulatory Network in Schistosoma Mansoni Egg-Induced Inflammation. *J Immunol* (2006) 176:5374–87. doi: 10.4049/jimmunol.176.9.5374
57. Hori S, Nomura T, Sakaguchi S. Control of Regulatory T Cell Development by the Transcription Factor Foxp3. *Science* (2003) 299:981–5. doi: 10.1126/science.1079490
58. Belkaid Y, Rouse BT. Natural Regulatory T Cells in Infectious Disease. *Nat Immunol* (2005) 6:353–60. doi: 10.1038/ni1181
59. Nausch N, Midzi N, Mduluza T, Maizels RM, Mutapi F. Regulatory and Activated T Cells in Human Schistosoma Haematobium Infections. *PLoS One* (2011) 6:16860. doi: 10.1371/journal.pone.0016860
60. Weinstock JV, Boros DL. Organ-Dependent Differences in Composition and Function Observed in Hepatic and Intestinal Granulomas Isolated From Mice With Schistosomiasis Mansoni. *J Immunol* (1983) 130:418–22.
61. Lukacs NW, Boros DL. Identification of Larval Cross-Reactive and Egg-Specific Antigens Involved in Granuloma Formation in Murine Schistosomiasis Mansoni. *Infect Immun* (1991) 59:3237–42. doi: 10.1128/iai.59.9.3237-3242.1991
62. Maizels RM, Smits HH, McSorley HJ. Modulation of Host Immunity by Helminths: The Expanding Repertoire of Parasite Effector Molecules. *Immunity* (2018) 49:801–18. doi: 10.1016/j.immuni.2018.10.016
63. Redpath SA, Werf NvdCervera AM, MacDonald AS, Gray D, Maizels RM. ICOS Controls Foxp3+ Regulatory T-Cell Expansion, Maintenance and IL-10 Production During Helminth Infection. *Eur J Immunol* (2013) 43:705–15. doi: 10.1002/eji.201242794
64. Patton EA, la Flamme AC, Pedras-Vasoncelos JA, Pearce EJ. Central Role for Interleukin-4 in Regulating Nitric Oxide-Mediated Inhibition of T-Cell Proliferation and Gamma Interferon Production in Schistosomiasis. *Infect Immun* (2002) 70:177–84. doi: 10.1128/IAI.70.1.177-184.2002
65. Smith P, Walsh CM, Mangan NE, Fallon RE, Sayers JR, McKenzie ANJ, et al. Schistosoma Mansoni Worms Induce Anergy of T Cells *via* Selective Up-Regulation of Programmed Death Ligand 1 on Macrophages. *J Immunol* (2004) 173:1240–8. doi: 10.4049/jimmunol.173.2.1240
66. Lee HG, Cho MZ, Choi JM. Bystander CD4+ T Cells: Crossroads Between Innate and Adaptive Immunity. *Exp Mol Med* (2020) 52:1255–63. doi: 10.1038/s12276-020-00486-7
67. Atochina O, Daly-Engel T, Piskorska D, McGuire E, Harn DA. A Schistosome-Expressed Immunomodulatory Glycoconjugate Expands Peritoneal Gr1 + Macrophages That Suppress Naive CD4 + T Cell Proliferation *via* an IFN-γ and Nitric Oxide-Dependent Mechanism. *J Immunol* (2001) 167:4293–302. doi: 10.4049/jimmunol.167.8.4293
68. van derKleij D, Latz E, Brouwers JFHM, Kruize YCM, Schmitz M, Kurt-Jones EA, et al. A Novel Host-Parasite Lipid Cross-Talk. Schistosomal Lyso-Phosphatidylserine Activates Toll-Like Receptor 2 and Affects Immune Polarization. *J Biol Chem* (2002) 277:48122–9. doi: 10.1074/jbc.M206941200
69. Trompette A, Gollwitzer ES, Yadava K, Sichelstiel AK, Sprenger N, Ngom-Bru C, et al. Gut Microbiota Metabolism of Dietary Fiber Influences Allergic

Airway Disease and Hematopoiesis. *Nat Med* (2014) 20:159–66. doi: 10.1038/nm.3444
70. Pesce JT, Ramalingam TR, Wilson MS, Mentink-Kane MM, Thompson RW, Cheever AW, et al. Retnla (Relmα/Fizz1) Suppresses Helminth-Induced Th2- Type Immunity. *PLoS Pathog* (2009) 5:1000393. doi: 10.1371/journal.ppat.1000393
71. Li J, Kim S, Lainez N, Coss D, Nair MG. Macrophage-Regulatory T Cell Interactions Promote Type 2 Immune Homeostasis Through Resistin-Like Molecule α. *Front Immunol* (2021) 12:710406. doi: 10.3389/fimmu.2021.710406
72. Skapenko A, Kalden JR, Lipsky PE, Schulze-Koops H. The IL-4 Receptor α-Chain-Binding Cytokines, IL-4 and IL-13, Induce Forkhead Box P3-Expressing CD25 + CD4 + Regulatory T Cells From CD25 – CD4 + Precursors. *J Immunol* (2005) 175:6107–16. doi: 10.4049/jimmunol.175.9.6107
73. Adalid-Peralta L, Fragoso G, Fleury A, Sciutto E. Mechanisms Underlying the Induction of Regulatory T Cells and its Relevance in the Adaptive Immune Response in Parasitic Infections. *Int J Biol Sci* (2011) 7:1412. doi: 10.7150/ijbs.7.1412
74. Mishra S, Srinivasan S, Ma C, Zhang N. CD8+ Regulatory T Cell – a Mystery to be Revealed. *Front Immunol* (2021) 12:708874. doi: 10.3389/fimmu.2021.708874
75. Hussaarts L, van der Vlugt LEPM, Yazdanbakhsh M, Smits HH. Regulatory B-Cell Induction by Helminths: Implications for Allergic Disease. *J Allergy Clin Immunol* (2011) 128:733–9. doi: 10.1016/j.jaci.2011.05.012
76. Oka A, Liu B, Herzog JW, Sartor RB. B Cell Commitment to IL-10 Production: The VertX Il10egfp Mouse. *Methods Mol Biol* (2021) 2270:341. doi: 10.1007/978-1-0716-1237-8_19
77. Chensue SW, Warmington KS, Hershey SD, Terebuh PD, Othman M, Kunkel SL. Evolving T Cell Responses in Murine Schistosomiasis. Th2 Cells Mediate Secondary Granulomatous Hypersensitivity and are Regulated by CD8+ T Cells *In Vivo*. *J Immunol* (1993) 151:1391–400.
78. Jankovic D, Cheever AW, Kullberg MC, Wynn TA, Yap G, Caspar P, et al. CD4+ T Cell–Mediated Granulomatous Pathology in Schistosomiasis is Downregulated by a Bcell–dependent Mechanism Requiring Fc Receptor Signaling. *J Exp Med* (1998) 187:619. doi: 10.1084/jem.187.4.619
79. Ye Z, Huang S, Zhang Y, Mei X, Zheng H, Li M, et al. Galectins, Eosinophiles, and Macrophages may Contribute to Schistosoma Japonicum Egg-Induced Immunopathology in a Mouse Model. *Front Immunol* (2020) 11:146. doi: 10.3389/fimmu.2020.00146
80. Chen X, Xu Z, Wei C, Yang X, Xu L, Zhou S, et al. Follicular Helper T Cells Recruit Eosinophils Into Host Liver by Producing CXCL12 During Schistosoma Japonicum Infection. *J Cell Mol Med* (2020) 24:2566. doi: 10.1111/jcmm.14950
81. Swartz JM, Dyer KD, Cheever AW, Ramalingam T, Pesnicak L, Domachowske JB, et al. Schistosoma Mansoni Infection in Eosinophil Lineage–Ablated Mice. *Blood* (2006) 108:2420–7. doi: 10.1182/blood-2006-04-015933
82. Sher A, Coffman RL, Hieny S, Scott P, Cheever AW. Interleukin 5 is Required for the Blood and Tissue Eosinophilia But Not Granuloma Formation Induced by Infection With Schistosoma Mansoni. *Proc Natl Acad Sci U S A* (1990) 87:61–5. doi: 10.1073/pnas.87.1.61
83. Sabin EA, Kopf MA, Pearce EJ. Schistosoma Mansoni Egg-Induced Early IL-4 Production is Dependent Upon IL-5 and Eosinophils. *J Exp Med* (1996) 184:1871–8. doi: 10.1084/jem.184.5.1871
84. Hsü SYL, Hsü HF, Mitros FA, Helms CM, Solomon RI. Eosinophils as Effector Cells in the Destruction of Schistosoma Mansoni Eggs in Granulomas. *Ann Trop Med Parasitol* (1980) 74:179–83. doi: 10.1080/00034983.1980.11687328
85. Truscott M, Evans DA, Gunn M, Hoffmann KF. Schistosoma Mansoni Hemozoin Modulates Alternative Activation of Macrophages *via* Specific Suppression of Retnla Expression and Secretion. *Infect Immun* (2013) 81:133–42. doi: 10.1128/IAI.00701-12
86. Burke ML, McManus DP, Ramm GA, Duke M, Li Y, Jones MK, et al. Temporal Expression of Chemokines Dictates the Hepatic Inflammatory Infiltrate in a Murine Model of Schistosomiasis. *PLoS Negl Trop Dis* (2010) 4:598. doi: 10.1371/journal.pntd.0000598
87. Burke ML, McManus DP, Ramm GA, Duke M, Li Y, Jones MK, et al. Co-Ordinated Gene Expression in the Liver and Spleen During Schistosoma Japonicum Infection Regulates Cell Migration. *PLoS Negl Trop Dis* (2010) 4: e686. doi: 10.1371/journal.pntd.0000686
88. Namulondo J, Mulindwa J, Nyangiri OA, Egesa M, Noyes H, Matovu E, et al. Gene Expression Changes in Mammalian Hosts During Schistosomiasis: A Review. *AAS Open Res* (2021) 4:54. doi: 10.12688/aasopenres.13312.1
89. Gobert GN, Burke ML, McManus DP, Ellis MK, Chuah C, Ramm GA, et al. Transcriptional Profiling of Chronic Clinical Hepatic Schistosomiasis Japonica Indicates Reduced Metabolism and Immune Responses. *Parasitology* (2015) 142:1453–68. doi: 10.1017/S0031182015000682
90. Dupnik KM, Reust MJ, Vick KM, Yao B, Miyaye D, Lyimo E, et al. Gene Expression Differences in Host Response to Schistosoma Haematobium Infection. *Infect Immun* (2019) 87. doi: 10.1128/IAI.00291-18
91. Groom JR, Luster AD. CXCR3 Ligands: Redundant, Collaborative and Antagonistic Functions. *Immunol Cell Biol* (2011) 89:207–15. doi: 10.1038/icb.2010.158
92. Roy S, Schmeier S, Kaczkowski B, Arner E, Alam T, Ozturk M, et al. Transcriptional Landscape of Mycobacterium Tuberculosis Infection in Macrophages. *Sci Rep* (2018) 8:1–13. doi: 10.1038/s41598-018-24509-6
93. Rani R, Jordan MB, Divanovic S, Herbert DR. IFN-γ-Driven IDO Production From Macrophages Protects IL-4rα-Deficient Mice Against Lethality During Schistosoma Mansoni Infection. *Am J Pathol* (2012) 180:2001–8. doi: 10.1016/j.ajpath.2012.01.013
94. la Flamme AC, Patton EA, Bauman B, Pearce EJ. Il-4 Plays a Crucial Role in Regulating Oxidative Damage in the Liver During Schistosomiasis. *J Immunol* (2001) 166:1903–11. doi: 10.4049/jimmunol.166.3.1903
95. Menzies-Gow A, Ying S, Sabroe I, Stubbs VL, Soler D, Williams TJ, et al. Eotaxin (CCL11) and Eotaxin-2 (CCL24) Induce Recruitment of Eosinophils, Basophils, Neutrophils, and Macrophages as Well as Features of Early- and Late-Phase Allergic Reactions Following Cutaneous Injection in Human Atopic and Nonatopic Volunteers. *J Immunol* (2002) 169:2712–8. doi: 10.4049/jimmunol.169.5.2712
96. Singh KP, Gerard HC, Hudson AP, Boros DL. Dynamics of Collagen, MMP and TIMP Gene Expression During the Granulomatous, Fibrotic Process Induced by Schistosoma Mansoni Eggs. *Ann Trop Med Parasitol* (2004) 98:581–93. doi: 10.1179/000349804225021316
97. Yoshiji H, Kuriyama S, Miyamoto Y, Thorgeirsson UP, Gomez DE, Kawata M, et al. Tissue Inhibitor of Metalloproteinases-1 Promotes Liver Fibrosis Development in a Transgenic Mouse Model. *Hepatology* (2000) 32:1248–54. doi: 10.1053/jhep.2000.20521
98. Athwal VS, Pritchett J, Martin K, Llewellyn J, Scott J, Harvey E, et al. SOX9 Regulated Matrix Proteins are Increased in Patients Serum and Correlate With Severity of Liver Fibrosis. *Sci Rep* (2018) 8:1–10. doi: 10.1038/s41598-018-36037-4
99. Segal-Salto M, Barashi N, Katav A, Edelshtein V, Aharon A, Hashmueli S, George J, et al. A Blocking Monoclonal Antibody to CCL24 Alleviates Liver Fibrosis and Inflammation in Experimental Models of Liver Damage. *JHEP Rep* (2020) 2:100064. doi: 10.1016/j.jhepr.2019.100064
100. Kapungu NN, Li X, Nhachi C, Masimirembwa C, Thelingwani RS. *In Vitro* and *In Vivo* Human Metabolism and Pharmacokinetics of S- and R-Praziquantel. *Pharmacol Res Perspect* (2020) 8:e00618. doi: 10.1002/prp2.618
101. la Flamme AC, Patton EA, Pearce EJ. Role of Gamma Interferon in the Pathogenesis of Severe Schistosomiasis in Interleukin-4-Deficient Mice. *Infect Immun* (2001) 69:7445–52. doi: 10.1128/IAI.69.12.7445-7452.2001
102. Kaplan MH, Whitfield JR, Boros DL, Grusby MJ. Th2 Cells are Required for the Schistosoma Mansoni Egg-Induced Granulomatous Response. *J Immunol* (1998) 160:1850–6.
103. Jankovic D, Kullberg M, Noben-Trauth N, Caspar P, Ward J, Cheever A, et al. Schistosome-Infected IL-4 Receptor Knockout (KO) Mice, in Contrast to IL-4 KO Mice, Fail to Develop Granulomatous Pathology While Maintaining the Same Lymphokine Expression Profile. *J Immunol* (1999) 1:337–42.
104. Paul WE, Zhu J. How are Th2-Type Immune Responses Initiated and Amplified? *Nat Rev Immunol* (2010) 10:225. doi: 10.1038/nri2735
105. Yi S, Zhai J, Niu R, Zhu G, Wang M, Liu J, et al. Eosinophil Recruitment is Dynamically Regulated by Interplay Among Lung Dendritic Cell Subsets After Allergen Challenge. *Nat Commun* (2018) 9:1–14. doi: 10.1038/s41467-018-06316-9
106. Plantinga M, Guilliams M, Vanheerswynghels M, Deswarte K, Branco-Madeira F, Toussaint W, et al. Conventional and Monocyte-Derived CD11b+ Dendritic Cells Initiate and Maintain T Helper 2 Cell-Mediated Immunity to House Dust Mite Allergen. *Immunity* (2013) 38:322–35. doi: 10.1016/j.immuni.2012.10.016

107. Ortiz-Stern A, Kanda A, Mionnet C, Cazareth J, Lazzari A, Fleury S, et al. Langerin+ Dendritic Cells are Responsible for LPS-Induced Reactivation of Allergen-Specific Th2 Responses in Postasthmatic Mice. *Mucosal Immunol* (2010) 4:343–53. doi: 10.1038/mi.2010.73
108. Zhang Y, Wu Y, Qi H, Xiao J, Gong H, Zhang Y, et al. A New Antagonist for CCR4 Attenuates Allergic Lung Inflammation in a Mouse Model of Asthma. *Sci Rep* (2017) 7:1–10. doi: 10.1038/s41598-017-11868-9
109. Jakubzick C, Wen H, Matsukawa A, Keller M, Kunkel SL, Hogaboam CM. Role of CCR4 Ligands, CCL17 and CCL22, During Schistosoma Mansoni Egg-Induced Pulmonary Granuloma Formation in Mice. *Am J Pathol* (2004) 165:1211. doi: 10.1016/S0002-9440(10)63381-0
110. Morais SB, Figueiredo BC, Assis NRG, Alvarenga DM, de Magalhães MTQ, Ferreira RS, et al. Schistosoma Mansoni SmKI-1 Serine Protease Inhibitor Binds to Elastase and Impairs Neutrophil Function and Inflammation. *PLoS Pathog* (2018) 14:1006870. doi: 10.1371/journal.ppat.1006870
111. Chuah C, Jones MK, Burke ML, McManus DP, Owen HC, Gobert GN. Defining a Pro-Inflammatory Neutrophil Phenotype in Response to Schistosome Eggs. *Cell Microbiol* (2014) 16:1666–77. doi: 10.1111/cmi.12316
112. Tittel AP, Heuser C, Ohliger C, Llanto C, Yona S, Hämmerling GJ, et al. Functionally Relevant Neutrophilia in CD11c Diphtheria Toxin Receptor Transgenic Mice. *Nat Methods* (2012) 9:385–90. doi: 10.1038/nmeth.1905
113. Chow A, Brown BD, Merad M. Studying the Mononuclear Phagocyte System in the Molecular Age. *Nat Rev Immunol* (2011) 11:788–98. doi: 10.1038/nri3087

Conflict of Interest: Author RL was employed by company 360biolabs.

The remaining authors declare that the research was conducted in the absence of any commercial or financial relationships that could be construed as a potential conflict of interest.

Publisher's Note: All claims expressed in this article are solely those of the authors and do not necessarily represent those of their affiliated organizations, or those of the publisher, the editors and the reviewers. Any product that may be evaluated in this article, or claim that may be made by its manufacturer, is not guaranteed or endorsed by the publisher.

frontiers | Frontiers in Immunology

ORIGINAL RESEARCH
published: 12 July 2022
doi: 10.3389/fimmu.2022.889645

SmTAL-9, a Member of the *Schistosoma mansoni* Tegument Allergen-Like Family, Is Important for Parasite Survival and a Putative Target for Drug/Vaccine Development

Wilma Patrícia de Oliveira Santos Bernardes[1], *Isabela Thamara Xavier Dutra*[2], *Rosiane Aparecida da Silva-Pereira*[1], *Marina Moraes Mourão*[2] *and Cristina Toscano Fonseca*[1]*

[1] Grupo de Pesquisas em Biologia e Imunologia de Doenças Infecciosas e Parasitárias, Instituto René Rachou, Fundação Oswaldo Cruz, Belo Horizonte, Brazil, [2] Grupo de Pesquisas em Helmintologia e Malacologia Médica, Instituto René Rachou, Fundação Oswaldo Cruz, Belo Horizonte, Brazil

OPEN ACCESS

Edited by:
Fabrizio Bruschi,
University of Pisa, Italy

Reviewed by:
Rashika El Ridi,
Cairo University, Egypt
Martina Sombetzki,
University Hospital Rostock, Germany

***Correspondence:**
Cristina Toscano Fonseca
cristina.toscano@fiocruz.br

Specialty section:
This article was submitted to Parasite Immunology, a section of the journal Frontiers in Immunology

Received: 04 March 2022
Accepted: 02 June 2022
Published: 12 July 2022

Citation:
Bernardes WPOS, Dutra ITX, da Silva-Pereira RA, Mourão MM and Fonseca CT (2022) SmTAL-9, a Member of the Schistosoma mansoni Tegument Allergen-Like Family, Is Important for Parasite Survival and a Putative Target for Drug/Vaccine Development. Front. Immunol. 13:889645. doi: 10.3389/fimmu.2022.889645

The tegument of *Schistosoma mansoni* is involved in essential functions for parasite survival and is known to stimulate immune responses in pre-clinical vaccine trials. Smtal-9, a member of the tegument-allergen-like (TAL) family, is one of the components of the tegument of schistosomula recognized by sera from immunized and protected mice. In this work, we assessed the role of Smtal-9 in parasite survival using the RNAi approach. Also, we cloned and expressed a recombinant form of Smtal-9 and evaluated its ability to induce protection in mice. *Smtal-9* knockdown did not impact parasite survival *in vitro*, but significantly decreased schistosomula size. Additionally, significant reduction in both parasite and egg burdens were observed in mice inoculated with *Smtal-9*-knockdown schistosomula. Immunization using the Smtal-9 as an antigen conferred partial protection against challenge infection. Overall, our results indicate that Smtal-9 is a candidate target for drug and/or vaccine development due to its important role in parasite biology and survival.

Keywords: Smtal-9, immunization, *Schistosoma mansoni*, RNA interference, protection

INTRODUCTION

The schistosome tegument represents one of the interfaces between parasite and host, and is involved in essential functions of parasite biology, such as nutrition, sensory perception, evasion of the immune system and osmoregulation (1). Additionally, it has been demonstrated that the tegument itself, as well as several tegument proteins, such as SmTSP-2, Sm29, Stomatin-like protein-2 and Sm200 are able to induce protective immunity when used in vaccine formulations in pre-clinical trials (2–7).

Among the various parasite tegument proteins, Smtal-1, a member of the tegument-allergen-like (TAL) family, has previously been associated with resistance to infection/reinfection. Smtal-1 has been pointed as the major target of an IgE response that is associated with resistance to reinfection in individuals living in endemic areas for schistosomiasis (8). Additionally, when Smtal-1 was used as antigen in a vaccine formulation, partial resistance against infection was observed in mice (9). Besides the recognition of Smtal-1, IgE antibodies from the sera of individuals living in endemic areas for schistosomiasis also recognize other members from the TAL family, such as Smtal-2 and Smtal-5 (10), but it is not known if this recognition is able to induce some level of resistance to parasite infection.

The *Schistosoma* TAL family includes 13 proteins that are associated with the worm tegument, Smtal-1 to 13 (10–12). These proteins are characterized by the presence of one or two EF-hand motifs in the N-terminal region of the protein, and a dynein light chain (DLC)-1 domain in the C-terminal region (10, 13, 14). These characteristics, together with the demonstration that Smtal–3 can bind the *Schistosoma mansoni* dynein (SmDCL), suggest that proteins from TAL family may be involved in vesicle transport in the parasite tegument (12, 14).

Smtal–9 (Smp_077310.1) is a member of the TAL family which is predicted to be expressed throughout the parasite life cycle, though most abundantly in eggs and adult worms (10). This member of the TAL family was recently biochemically characterized, and the study described its ability to form homodimers and to bind Mn^{2+}, Mg^{2+}, Ca^{2+}, as well as to interact with the calmodulin antagonists CPZ, W7 and TFP, suggesting its involvement in Ca^{2+}–dependent signal transduction (15). In another proteomics study, analyzing the schistosomula tegument preparation (Smteg), a protein spot recognized by sera from mice immunized with Smteg (5) was identified as a putative *S. mansoni* tegumental protein (XP_018655674.1) (unpublished data). According to the online databank WormBase ParaSite, this protein is a product of gene *Smtal–9* (Smp_077310). In this study, we aimed to evaluate the role of Smtal–9 in parasite survival, and to investigate its ability to induce a protective immune response in mice, because of the key role of antibodies against tegument proteins in the protective immunity induced by vaccination (16). Our data indicates that RNAi–mediated *Smtal–9* knockdown in schistosomula negatively impacts on parasite survival within the host, resulting in a reduction in the worm burden, as well as in the number of eggs trapped in the liver and intestine of infected mice. In addition, a transient reduction in *Smtal–9* expression resulted in small–sized parasites *in vitro*. The immune response triggered by a prime–boost immunization protocol using Smtal–9 as antigen, also generated significant levels of protection (19.3 to 28.6%), measured as a reduction in parasite burden. Overall, our data indicate that Smtal–9 is a candidate target for drug and vaccine development.

METHODS

Animals and Parasite Culture

In this study, all procedures involving animals were approved by the Ethics Committee of Animal Use of the Fundação Oswaldo Cruz (FIOCRUZ) under licenses LW26/12 and LW22/16. Female Balb/c and C57BL–6 mice aged 6–8 weeks were used and obtained from the Institute René Rachou (IRR)/FIOCRUZ animal facility. *Schistosoma mansoni* cercariae from the LE strain were obtained from the mollusc facility "Lobato Paraense" of IRR/FIOCRUZ by exposing infected *Biomphalaria glabrata* snails to artificial light for about 2 hours to induce shedding. LE *Schistosoma mansoni*/Belo Horizonte was obtained by Dr. J. Pellegrino in Belo Horizonte, Minas Gerais, Brazil, in 1965 from an infected human patient (17). The line is maintained at the mollusck rearing facility "Lobato Paraense" of IRR/FIOCRUZ by passage through *B. glabrata* and mice or hamsters

RNAi trials were performed using cercariae mechanically transformed into schistosomula according to Milligan and Jolly (17) with modifications. Briefly, cercariae solution was distributed in 50ml conical tubes that were placed on ice for one hour to sediment the cercariae. Then, after centrifugation at 218 xg for 3 minutes at 4°C, the supernatant was removed. The final 7ml solution, enriched with cercariae, was passed through a 22 gauge needle until all tails were removed. After transformation, schistosomula were sedimented in a conic tube, resuspended in Minimal Essential Medium (MEM) and incubated a 37°C for one hour. After that, parasites were placed in Glasgow Minimum Essential Medium (GMEM) (Merck) supplemented with 0.1% lactalbumin (Merck), 5% Schneider's Insect Medium (Merck), 20 mM of HEPES (Merck), 0.1% glucose (Vetec), 0.5% MEM vitamin solution (Gibco, Thermo Fisher Scientific, USA), 2% inactivated fetal bovine serum (Gibco, Thermo Fisher Scientific, USA), 0.2 mM of triiodothyronine (Merck), 1 mM of hydrocortisone (Merck), 0.5 mM of hypoxanthine (Merck), and 1% penicillin/streptomycin (Gibco, Thermo Fisher Scientific, USA) and incubated in a biological oxygen demand (BOD) incubator at 37°C under 5% CO_2 (18).

Smtal–9 ds–RNA Synthesis and Gene Expression Assessment

The sequence of the primers used for double–stranded RNA (dsRNA) synthesis and quantitative real–time PCR (RT–qPCR) were designed using the Primer 3 program (v.0.4.0) (bioinfo.ut.ee/primer3–0.4.0) and purchased from Integrated DNA Technologies Inc. (Coralville, IA). The primers used in the synthesis of the dsRNA carried a T7 promoter sequence added to their 5′–end. The *Smtal–9* mRNA (XM.018790318) containing 354 bp was amplified by PCR using the following primers: forward 5–taatacgactcactatagggAAAACAAGCGC GGGAATTA–3′ and reverse 5–taatacgactcactatagggGCA GAACATGGTGTTTTCCA–3. Total RNA from schistosomula was used as the template for cDNA synthesis and *Smtal–9* amplification. A 360 bp fragment of the *green–fluorescent protein* (*GFP*) gene was used as a nonspecific control for the RNAi and was amplified using the pCRII–GFP plasmid vector (Thermo Fisher Scientific, USA) as a template and the following primers: *gfp*_dsRNA_Forward, 5–taatacgactcactatagggGTGTT CAATGCTTTGCGAGA–3, and *gfp*_dsRNA_Reverse, 5–taatacgactcactatagggCTTTTCGTTGGGATCTTTCG–3'.

The dsRNAs were synthetized using PCR products and T7 RiboMAX™ Express RNAi System Kit (Promega, USA), according to the manufacturer instructions. A Nanodrop Spectrophotometer ND–1000 (Thermo Fisher Scientific, USA) was used to determine the dsRNA concentration. The integrity of the dsRNA was determined by analysis on a 1% agarose gel.

Approximately 12,000 schistosomula were exposed to 200 nM of dsRNA (*smtal–9 or gfp*) in a 6–well plate containing supplemented GMEM medium (3,000 parasites/ml). As an additional control, parasites were incubated in supplemented GMEM only. Cultures were incubated for up to ten days after dsRNA exposure at 37°C, 5% CO_2 and 95% humidity. Approximately 3,000 schistosomula between days four to seven post–dsRNA–exposure were removed from the culture for *Smtal–9* relative gene expression analysis using RT–qPCR. TRIzol Reagent (Thermo Fisher Scientific, USA) was used for the RNA extractions, as recommended by the manufacturer. The extracted RNA was quantified using the Qubit 2.0 Fluorometer (Thermo Fischer Scientific, USA) after removing residual DNA from the extracted RNA with Turbo DNase (2 U/μl) (Thermo Fisher Scientific, USA). The ImProm–II™ Reverse Transcription System (Promega, USA) was used to produce the cDNA for the RT–qPCR. After standardization to determine the appropriate primer concentration, the RT–qPCR experiments were performed using 200 nM of primers that amplify a 126 bp *Smtal–9* fragment (forward 5′–CTCGTTTTTGGACGC TTTTT– 3′ and reverse 5′–CGACGAAGAAATGTTT CTGGA–3′). The *smgapdh* (Smp–056970) gene was used as an endogenous normalization control. A fragment of 53 bp of *smgapdh* was amplified using 900 mM of the following primers (forward 5′–TCGTTGAGTCTACTGGAGTCTTTACG–3′ and reverse 5′–AATATGAGCCTGAGCTTTATCAATGG–3′). The transcript levels of *Smtal–9* were evaluated using the relative $2^{-\Delta\Delta Ct}$ method (19) and calculated as a percentage of difference compared to the nonspecific *gfp*–treated controls and untreated parasites. PCR reactions were performed using a ViiA 7 (Thermo Fisher Scientific, USA) at the Real–Time PCR Facility/RPT09D PDTIS/René Rachou Institute/FIOCRUZ MG.

In Vitro and *In Vivo* RNAi Assay Using Schistosomula

For the RNAi assay, schistosomula were separately treated with either *Smtal–9*– or *gfp*–dsRNA or supplemented medium lacking dsRNA. Schistosomula were examined for phenotypic changes using an inverted fluorescence microscope (Axio Observer, Carl Zeiss), as previously described (19). Parasite viability was evaluated by incubating approximately 100 schistosomula with 5 μg/ml propidium iodide (Sigma–Aldrich), and the stained parasites were observed and counted using a fluorescence microscope with a 544 nm filter (Carl Zeiss). Data from three independent assays using 100 schistosomula er assay were analyzed.

To analyze the role of Smtal–9 in parasite's definitive host, after schistosomula exposure to *Smtal–9*– or *gfp–dsRNA* for 4 days, approximately 270 larvae were subcutaneously inoculated into Balb–c mice. An additional control group was inoculated with untreated schistosomula. Before infection of mice with dsRNA–treated and untreated parasites the *Smtal–9* transcript levels were determined by RT–qPCR to confirm knockdown. Three independent experiments were performed using 10–12 mice in each group per experiment. Fifty days after subcutaneous inoculation, adult worms were recovered by perfusion of the hepatic portal system from mice (20). The liver and gut from mice were weighed and digested with 10% KOH solution for subsequent determination of the egg number per gram of organ. The experimental approach used to investigate the role of Smtal–9 in parasite development and survival is illustrated in the **Supplementary Figure 1**.

In Silico Analysis and Smtal–9 Modelling

The *S. mansoni* Smtal–9 (access number: XP_018655674.1) protein had its molecular weight and isoelectric point predicted using the compute pi/MW tool (https://web.expasy.org/compute_pi/). The protein amino acid sequence was analyzed using SignalP5.0 (https://services.healthtech.dtu.dk/service.php?SignalP–5.0) to predict signal peptides in its sequence. Also, SOSUI Engine version 1.11 (http://harrier.nagahama–i–bio.ac.jp/sosui/sosui_submit.html) and TMHMM (http://www.cbs.dtu.dk/services/TMHMM/) were used to predict transmembrane domains and protein solubility. WolfPSORT (https://wolfpsort.hgc.jp/) was used to predict cellular localization. Post transcriptional changes were predicted using NetNGlyc (http://www.cbs.dtu.dk/services/NetNGlyc/), NetOGlyc (http://www.cbs.dtu.dk/services/NetOGlyc/) and Big–PI prediction (https://mendel.imp.ac.at/gpi/gpi_server.html). The XP_018655674.1 amino acid sequence was compared with the sequences from the WormBase ParaSite databank using the BlastP (BLAST – Basic Local Alignment Search Tool) algorithm (https://parasite.wormbase.org/tools/blast), with the default parameters of this algorithm. Multiple sequence alignments of XP_018655674.1, Smp–077310.1, Smp–077310.2 and Smp–324770.1 were performed using Clustal Omega (http://www.clustal.org/omega/).

T cell epitope prediction was performed using NetMHCII 2.3 (https://services.healthtech.dtu.dk/service.php?NetMHCII–2.3) using default parameters and selecting H2–IaB and H2–IaD to predict epitopes that strongly bind to C57BL–6 and BALB–c MHCII molecules, respectively. B cell linear epitopes were predicted using the BepiPred (https://services.healthtech.dtu.dk/service.php?BepiPred–2.0) with default parameters.

The amino acid sequence of the *S. mansoni* Smtal–9 recombinant protein (**Figure 3**) was submitted to build a three–dimensional homology model by automated comparative modeling using Protein Homology/analogy Recognition Engine V 2.0 (Phyre^2) using Intensive Modelling Mode (21). The resulting structure for the recombinant protein was predicted using seven different templates (d3e2ba1, d1cmia, c6zywM, c7kznP, c5x2eA, c5fx0A and c5x,2dA) with >90% confidence with 90% sequence coverage (173 residues).

Recombinant Antigen Preparation

A synthetic gene containing the coding region sequence for Smtal–9 (access number (XP_018655674.1) was designed using ApE software (www.apesoftware.com), optimized for expression

in bacteria and mammals. The synthetic gene was purchased from IDT Technologies, and contained restriction sites for *BamH*I (GGATCC) at the 5′ end and *Xho*I (CTCGAG) followed by *Age*I (ACCGGT) at the 3′ end. These restriction sites were used to subclone the synthetic gene into the pET28a TEV bacterial expression vector (22) or into the mammalian expression vector pcDNA3.1 V5/His A (Thermo Fisher Scientific, USA). The constructs were inserted into *Escherichia coli* BL21 and DH5α strains. Antibiotic–resistant bacteria clones were selected, and the presence of the construct and the correct orientation of the *Smtal–9* open reading frame were confirmed by Sanger sequencing. The pcDNA 3.1 V5/His A and pcDNA 3.1 V5/His A/*Smtal–9* plasmidial DNA were purified using EndoFree Plasmid Giga Kit (Qiagen), according to manufacturer's instructions. Recombinant Smtal–9 expression in fusion with the 6–histidine–tag was induced by the addition of 1 mM isopropyl–B–D–galactopyranoside to the LB medium. Bacteria were maintained at 37°C for 4 hours at 150 rpm, and then, after a centrifugation step (4800 x g for 10 min) the pellet was resuspended in PBS 0.15 M pH 7.2 containing 1 mM phenylmethylsufonyl fluoride (PMSF) (Sigma Aldrich) and 0.2 mM EDTA (Sigma Aldrich) and lysed by 5 cycles of sonication (5 x 30 seconds using 30% output followed by 1 min on ice). After the last sonication step, the cell lysate was centrifuged at 8000 x g for 10 min, and the pellet resuspended in a buffer containing 20 mM NaH_2PO_4, 0.5 M NaCl, 30 mM imidazole and 0.9% N–Lauroylsarcosine sodium salt (Sigma Aldrich) and used for protein purified using a His Trap HP column (GE Life Science) in an AKTA FPLC equipment (GE Life Science). Elution was performed using a linear gradient from 0 to 100% of 20 mM Na_2HPO_4, 0.5 M NaCl, pH 7.4 with 500 mM of imidazole. Recombinant protein was dialyzed against a 0.15 M PBS solution for 24 hours and quantified using the BCA Protein Assay Kit (Thermo Scientific Pierce, Rockford, IL, USA) before its use in experimental protocols. Protein quality and purity were analyzed using 15% SDS–PAGE, and its recognition by an anti–His (C–term) HRP antibody (Novex, life technology) was assessed by a western blot assay. Briefly, proteins were separated using a 15% SDS–PAGE and transferred to a nitrocellulose membrane at 100 V for one hour. The membrane was blocked over night with 1X TBS containing 0.05% of Tween 20 (TBST) and 5% of powdered skimmed milk. After three washing steps with TBST for 10 minutes each, the membrane was incubated with an anti–His HRP conjugated antibody diluted 1:5000 in TBST plus 3% of powdered skimmed milk for one hour. The membrane was submitted to three additional washing steps, and the recognition of the His–tag in the recombinant protein was detected using ECL™ Prime Western Blotting Detection Reagent (GE Healthcare). The western blot result was acquired using the Amersham Imager 600 equipment (GE).

Prime and Boost Immunization Protocol

A prime–boost immunization protocol was performed using female C57BL–6 mice (12 animals per group) using Smtal–9 as antigen. Five days before the beginning of the immunization protocol, mice were inoculated with 50 µl of cardiotoxin (10 µM) in each quadriceps muscle. At day 0, mice received 100 µg (50 µg/quadriceps muscle) of pcDNA 3.1V5/HIS or pcDNA 3.1V5/HIS/*Smtal9*. Fifteen days after the prime immunization with the DNA vaccine, mice received two doses of the protein vaccine containing 25 µg of rSmtal–9/dose inoculated subcutaneously in a 15–day interval between them. As a control, two groups (pcDNA 3.1V5/HIS + Saline CFA/IFA and pcDNA 3.1V5/HIS/*Smtal9* + Saline CFA/IFA) were inoculated with a saline solution instead of the recombinant protein. Both saline and rSmtal–9 were formulated with complete Freund`s adjuvant at the first boost and incomplete Freund`s adjuvant at the second boost. The immunization regimen and formulations for each experimental group are summarized in **Table 1** and illustrated in **Supplementary Figure 2**. Fifteen days after the last boost, mice were percutaneously infected with approximately 100 *S. mansoni* cercariae (LE strain) and fifty days after challenge infection mice were perfused as previously described (20) for the recovery of worms from the mesenteric veins. The liver and intestine from mice were also obtained, and the number of eggs trapped in these organs was determined as previously described (23). Two independent immunization trials were performed.

Statistical Analysis

The data were analyzed using GraphPad Prism 8.0 (Graph–Pad Software, San Diego, CA, United States). The distribution of the data was analyzed using the Shapiro–Wilk normality test, followed by the Brown–Forsythe or Bartlett`s test to assess the variance homogeneity. When the results from the different groups showed significant differences in variance, the data were analyzed pair by pair using the Student's *t* test or the Mann–Whitney *U* test using the alpha value adjusted according to the number of comparisons made between the groups. When the variances did not differ significantly between groups, one–way ANOVA or the Kruskal–Wallis test, followed by Tukey or Dunn's multiple comparison tests, was used in statistical analysis using a 95% a confidence level. Two–way ANOVA was used to calculate statistically significant differences between groups and over time in the viability assay.

RESULTS

Smtal–9 Expression Is Essential for Parasite Development and Survival *In Vivo*

A RNAi assay was performed to evaluate the role of Smtal–9 in parasite biology. Double–stranded RNA was used to target *Smtal–9* transcripts in schistosomula. The dsRNA used to knockdown *Smtal–9* targets the two protein isoforms of Smtal–9 (Smp–077310.1 and Smp–077310.2) as well as Smp–324770 in RNAi assays (**Supplementary Figure 3A**). The transcript levels were determined in schistosomula at days 4, 5, 6 and 7 post–exposure to dsRNA in comparison to two negative controls: schistosomula exposed to *gfp*–dsRNA and untreated schistosomula. Decreased levels of transcripts were observed in schistosomula exposed to *Smtal–9*–dsRNA at days 4 (80%–76%), 5 (74%–60%), 6 (99%–84%) and 7 (83%–85%) post–exposure

TABLE 1 | Immunization regimen and formulations.

Experimental group	Prime formulation	1st boost formulation	2nd boost formulation
pcDNA 3.1V5/HIS + Saline CFA/IFA	100 µg pcDNA 3.1V5/HIS	Saline + 100 µl of complete Freund`s adjuvant (CFA)	Saline + 100 µl of incomplete Freund`s adjuvant (IFA)
pcDNA 3.1V5/HIS + rSmtal–9 CFA/IFA	100 µg pcDNA 3.1V5/HIS	25 µg of rSmtal–9 + 100µl of complete Freund`s adjuvant (CFA)	25 µg of rSmtal–9 + 100µl of complete Freund`s adjuvant (CFA)
pcDNA 3.1V5/HIS/*Smtal9* + Saline CFA/IFA	100 µg pcDNA 3.1V5/HIS/*Smtal9*	Saline + 100µl of complete Freund`s adjuvant (CFA)	Saline + 100 µl of incomplete Freund`s adjuvant (IFA)
pcDNA 3.1V5/HIS/*Smtal9* + rSmtal9 CFA/IFA	100 µg pcDNA 3.1V5/HIS/*Smtal9*	25 µg of rSmtal–9 + 100µl of complete Freund`s adjuvant (CFA)	25 µg of rSmtal–9 + 100µl of complete Freund`s adjuvant (CFA)

when compared to untreated (**Figure 1A**) and *gfp*–dsRNA treated parasites, respectively (**Figure 1B**), indicating that the RNAi assay succeeded in knocking down *Smtal–9* gene expression. The impact of *Smtal–9* knockdown on schistosomula survival and morphology was evaluated *in vitro* at days 2, 4, 6, 8 and 10 after parasite exposure to specific and nonspecific dsRNA. Parasite treatment with either dsRNA did not impact parasite survival *in vitro*, since no significant differences in parasite viability was observed between dsRNA–exposed and unexposed parasites (**Figure 2A**). Parasite area was also evaluated after exposure to *Smtal–9* specific and nonspecific dsRNA. Four days after treatment with dsRNA, a significant decrease in parasite size was observed in schistosomula treated with *Smtal–9*–dsRNA in comparison to both negative controls (nonspecific *gfp*–dsRNA and untreated parasites) (**Figure 2B**). This difference in parasite size was not observed at days 6 and 8 post–treatment and was only observed between *Smtal–9*–dsRNA–treated and *gfp*–dsRNA–treated parasites on the 10th day (**Figure 2B**). To evaluate the impact of *Smtal–9* expression in parasite survival in the vertebrate host, mice were inoculated with *Smtal–9*–dsRNA–treated schistosomula four days after exposure to dsRNA, when differences in the size–phenotype were observed in *in vitro* cultured parasites. Regardless of the control group, in all assays, there was a significant reduction in parasite burden (56.5 – 71.4%) in mice inoculated with *Smtal–9* knocked–down schistosomula (**Table 2**). Reduced number of eggs trapped in the liver (53.8 – 70%) and in the intestine (64% – 81%) were also observed in mice inoculated with *Smtal–9* knocked–down parasites (**Table 2**).

A Vaccine Formulation Containing Smtal–9 Reduces Parasite Burden in Mice

Since the RNAi functional assay suggested an important role for Smtal–9 in parasite survival within the definitive host, we assessed whether an immune response triggered against this tegument protein would induce protection in mice. *In silico* analysis of the Smtal–9 protein sequence (XP_018655674.1) used to produce the recombinant protein used in this study (**Figures 3A, B**) indicated that Smtal–9 is a soluble cytoplasmic protein with predicted 22kDa and 6.44 isoelectric point. No signal peptide, transmembrane domain nor GPI–anchor site was predicted in this sequence. A BLASTp search of the above sequence against trematode proteins from the parasite WormBase ParaSite databank demonstrated that the sequence used to generate the recombinant proteins and incorporated into the DNA vaccine did not possess the 22 N–terminal amino acids present in the proteins Smp–077310.2 and Smp–324770, nor the 4 N–terminal amino acids from the protein Smp–077310.1 (**Supplementary Figure 3B**). Additionally, our recombinant protein differs from the protein Smp–324770, where a substitution from a phenylalanine to a leucine in position 108 is observed (**Supplementary Figure 3B**).

A linear B cell epitope in the rSmtal–9 sequence was predicted by BepiPred (**Figure 3B**), but according to the predicted secondary structure of the protein obtained by computational modelling using

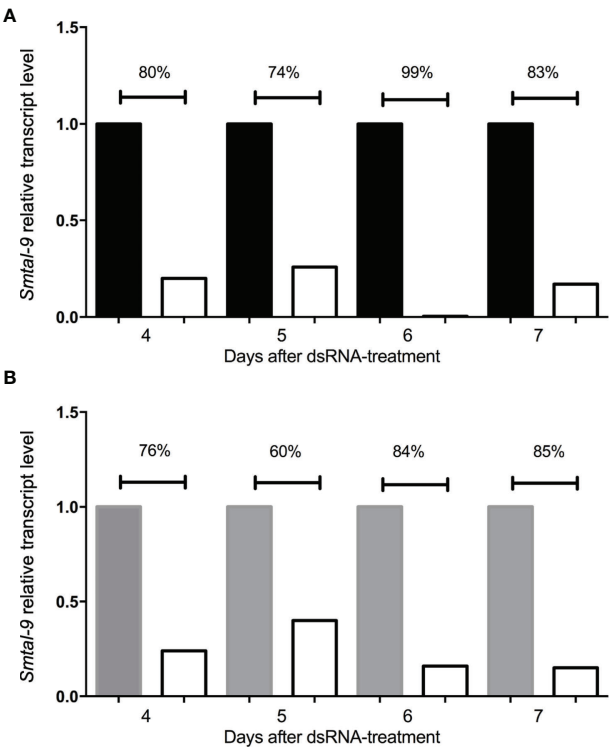

FIGURE 1 | Kinetics of *smtal–9* transcript levels after schistosomula dsRNA exposure for 7 days. Graphical depiction of the relative *smtal–9* transcript levels and their comparison between *smtal–9* dsRNA (white bars in both charts) exposed schistosomula and two different control groups: untreated parasites (black bars in **A**) or parasites treated with *gfp*–specific dsRNA (grey bars in **B**). Transcripts were evaluated between the fourth to the seventh day after dsRNA exposure. Transcript levels of *smtal–9* were evaluated by RT–qPCR. Percentage of reduction of the *smtal–9* transcript levels in *smtal–9*–dsRNA treated parasites was calculated in comparison to the transcript level observed in untreated **(A)** or *gfp*–dsRNA **(B)** treated parasites.

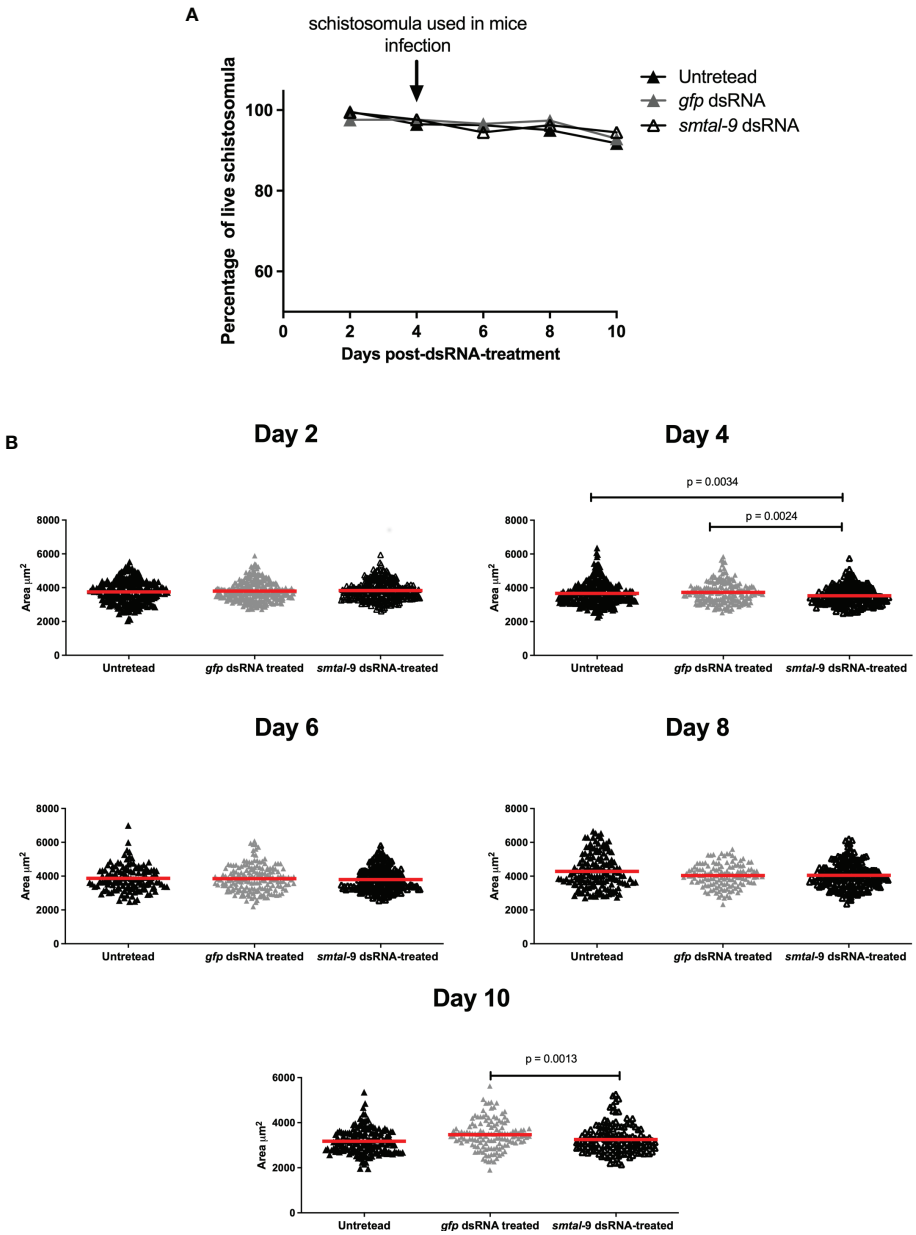

FIGURE 2 | *In vitro* impact of *smtal–9* knockdown on parasite survival and size. Schistosomula were treated with either *smtal–9*–dsRNA (open triangle), *gfp*–dsRNA (grey triangle) or untreated (closed triangle). **(A)** Parasite viability was evaluated every two days after exposure to dsRNA until day 10 post–exposure. The percentage of live parasites was calculated from three independent replicate experiments and differences between groups were determined using one–way ANOVA. **(B)** Parasite size was calculated for parasites recovered from the cultures of each group every two days until the 10th day post–dsRNA–exposure. The size of each parasite is represented in the graphs, with the red line representing the mean parasite area in each group. Significant differences between groups are indicated on the graphs and were determined using the Mann–Whitney *U* test using an adjusted α value.

Phyre2, most of the amino acids in this epitope (60–99) reside within a region that corresponds to an α–helix (**Figure 3C**), which is therefore likely to disrupt the linear B cell epitope. Additionally, NetMHCII predicted four H2–IAd–binding epitopes in rSmtal–9 and no H2–IAb–binding epitopes (**Figure 3B**). Thus, to perform the immunization protocols, C57BL–6 mice were used. The 3D structure of the recombinant protein (**Figure 3D**) demonstrates that the N–terminal part of the recombinant protein is rich in α–helices, while anti–parallel β–sheets can be observed in the C–terminal part of the protein (**Figure 3D**).

The electrophoretic profile of the recombinant protein demonstrates a protein with approximately 25 kDa that can dimerize and migrate at 50 kDa in SDS–PAGE (**Figure 4**). Both the 25 kDa and 50 kDa bands are recognized by the anti–HIS antibody, thus indicating that it represents the recombinant protein that is expressed in fusion with 6X–His–tag (**Figure 4**).

TABLE 2 | Worm burden recovery from mice infected with schistosomula knocked–down *Smtal–9* expression.

	Transcript reduction (%)	Worm burden recoveryMean ± SD	% reduction*&	Egg/gram of liverMean ± SD	% reduction#&	Egg/gram of intestineMean ± SD	% reduction#&
Trial 1							
Untreated		23 ± 16		20119 ± 9920		8956 ± 7722	
Smtal9–dsRNA– treated	48.0%	10 ± 7	56.5% (p = 0.0226)	8437 ± 5774	58.0% (p=0.0026)	2853 ± 2161	68.0% (p=0.0161)
Trial 2							
Untreated		18 ± 11		19797 ± 8823		5815 ± 4790	
Smtal9–dsRNA– treated	86.4%	7 ± 5	61.1% (p = 0.0226)	5959 ± 6017	70.0% (p = 0.0016)	1118 ± 1488	81.0% (p = 0.0041)
Trial 3							
GFP–dsRNA– treated		7 ± 5		6247 ± 4191		1541 ± 1458	
Smtal9–dsRNA– treated	76.0%	2 ± 2	71.4% (p = 0.0178)	2883 ± 1870	53.8% (p = 0.0281)	552 ± 473	64.0% (ns)

*Reduction of in the total number of worms compared to control group.

#Reduction of in the total number of eggs in tissue (liver and intestine) compared to control group.

&Statistically significant differences were determined using the Student's t test or the Mann–Whitney U test.

Furthermore, our results using a prime–boost immunization protocol demonstrates that immunization of mice with Smtal–9 as antigen confers partial protection against infection with a significant reduction in parasite burden in mice (**Table 3**). The highest reduction in parasite burden (25.5% – 34.3%) was observed in mice that received a prime with the DNA vaccine containing the *Smtal–9 gene* and two boosts of a vaccine formulation with the recombinant protein. But even mice that received a prime with the control plasmid lacking the *Smtal*–9 sequence and two boosts with the recombinant protein showed a significant reduction in parasite burden (19.4% – 22.9%) (**Table 3**). Although immunization resulted in a significant decrease in worm burden, this reduction did not result in a significant reduction in the number of eggs trapped in the liver and intestine (**Table 3**).

DISCUSSION

A family of proteins that contains an N–terminal EF Hand motif and a C–terminal dynein light chain domain have been described in worm parasites was reviewed recently (21). In *S. mansoni*, this family of proteins have been denominated as *S. mansoni* tegument–allergen–like (Smtal) due to its location in the parasite tegument and its similarity with allergen (11, 12, 24, 25). The *S. mansoni* TAL family is composed of 13 members (10), and some have been associated with resistance to infection and reinfection (9, 14, 26).

Smtal–9 is a member of the TAL family which forms homodimers and can interact with Ca^{2+}, thus suggesting its role is Ca^{2+}–dependent signaling (15). Its expression is predicted to occur during all the parasite life cycle stages, but most abundantly in adult worms, eggs, and miracidia (10). Smtal–9 has been identified by our group during a proteomic study (unpublished data), in which this protein was recognized by sera from mice immunized with a preparation of the schistosomula tegument called Smteg (7). As immunization with Smteg induces a robust antibody response that transfers protection to a naïve recipient (16), we thus sought to evaluate the role of Smtal–9 in parasite development (*in vitro*) and survival (both *in vitro* and *in vivo*), as well as its ability to induce protection when used in a DNA prime–protein boost vaccination schedule.

Our RNAi assay demonstrated that the use of *Smtal–9*–dsRNA significantly reduced the levels of *Smtal–9* transcript in exposed schistosomula between days 4 to day 7 post–exposure reaching the striking level of reduction of 90%. The knockdown of *Smtal–9* expression resulted in a transient *in vitro* reduction in the schistosomula size in *Smtal–9*–dsRNA exposed parasites at day 4 post–exposure in comparison to both control groups (untreated parasites or *gfp*–dsRNA treated parasites) and at day 10 post–exposure in comparison to *gfp*–dsRNA–treated parasites. It is important to note that the Smtal family is composed of 13 members, and possible redundancy in their function might explain the transient modification observed in *Smtal–9*–dsRNA–treated parasites (27). For instance, besides Smtal–9, the expression of transcripts for *Smtal–1*, *Smtal–2*, *Smtal–8*, *Smtal–10*, *Smtal–12* and *Smtal–13* are all observed in 3 day and 6 day–schistosomula (10).

The exact role of proteins from the Smtal family is not known, but due to its dynein light chain domain, and the demonstration that Smtal–3, a member of the TAL family, can bind the *S. mansoni* dynein (SmDLC), it is speculated that these proteins may be involved in cytoskeletal process (12). Recently, it was demonstrated that Smtal–1 can bind the IQ motif of the voltage–gated calcium channel, called $SmCa_v1B$, thus, suggesting a role for this protein in calcium homeostasis (28). In our *in vitro* assays, the knockdown of *Smtal–9* expression did not impact parasite survival, since no differences in parasite viability was observed between the different groups. In contrast, when confronted with the host immune system, there was a significant reduction in the number of parasites and eggs recovered from mice infected with *Smtal–9*–dsRNA–treated parasites. This outcome demonstrates that Smtal–9 is important for providing the parasite the means to deal with its host environment. To our knowledge, this is the first study to

A **Syntethic gene**

GGATCCATGGACTCTTTCCTGGACGCATTTTTCGCCCTGGACACAGACAACCGTGAAGTTATTTCCC
TGAACGACCTGAGCAGTTACAACAAAAAACACGGCCTGCAGGATTCATTTCCAGAAACCTTCCTGCG
CCGTTTTGACGCCGAAAAGACTGGCGTCATCACCCTGGAGCAGTATTGCAAAGCACTGGGTCTGGT
GCCAAAGCAGGCTCGGGAGCTGCGGAGACGCCGTACCACAGTTCTGCTGGAACAGCTGATTCCTC
GCGATCTGGAGATCATCTATGATGACATGGAACTGGAGATGAAAGTGAAGGTTATGGAACTGTTCATC
AACGACCTGCGGGAGTCTGGTAGAAAGACCAACATCGATATGGAAAAGCTGGACCAGAGTATGCAG
CGCCTGAAAGAGTATCTGGATACACGTTACGGGAAGAGCTGGCACATCATTACTTCCATCAACCAGC
ATCTGGGACGCTTTTCCTATGAACCCAATACACTGTTTCATTTTTGCCTGGGAAGATTCGTTGTTCTG
ATTTGGAAGACACCCTGCTCCGCACTCGAGACCGGT

B **ORF – recombinant SmTal-9**

MDSFLDAFFALD*TDNREVISLNDL*SSYNKKH*GL*LQD*S*FPETFLRRFD*AEKTGVI*TLEQYC*KALGLV*PKQA
*RELRRRRTTVLLEQLIPRDLEIIY**DDMELE***MKVKVMELFIND*LRESGRKTNIDMEK*LDQSMQRLKEYLD
*TRY*GKSWHIITSINQHLGRFSYEPNTLFHFCLGRFVVLIWKTPCSALETGHHHHHH

C

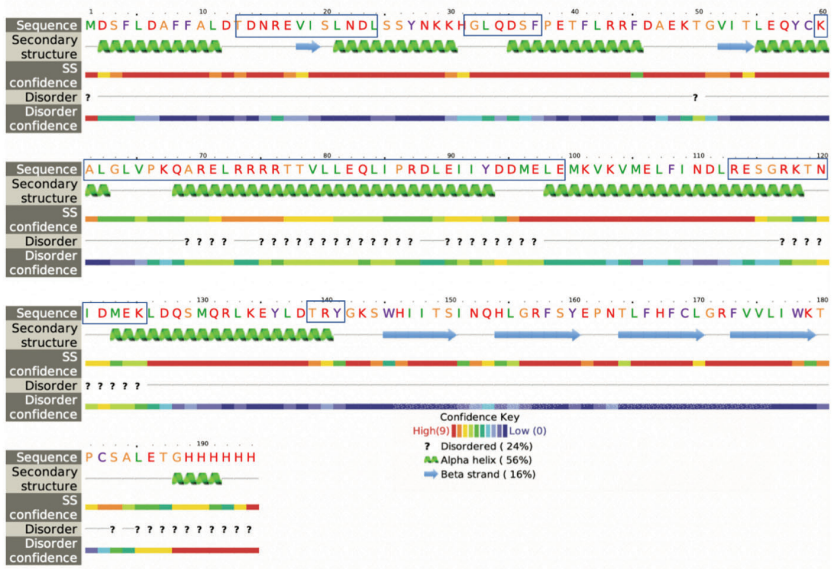

D

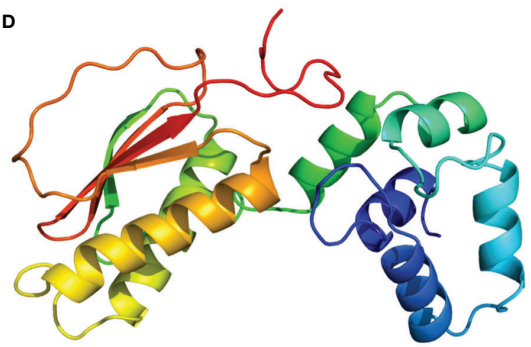

FIGURE 3 | *In silico* analysis of rSmTAL–9. **(A)** Nucleotide sequence of the synthetic gene encoding rSmTAL–9 with the added *BamH*I, and *Xho*I restriction sites in green at the 3' and 5' ends, respectively, and the *Age*I restriction site in blue at the 5' end. The start codon is indicated in red. **(B)** The open reading frame sequence of rSmTAL–9. The linear B cell epitopes predicted by Bepipred is indicated in bold. The amino acids highlighted in purple indicate epitopes that bind the H2–IaD haplotype. The amino acid in red represents a predicted site for O–glycosylation. Boxes highlight the EF–hand motif, while the DLC motif is highlighted in grey, and the His–tag is indicated in orange. **(C)** Secondary structure within rSmTAL–9 amino acid sequence obtained using Phyre in intensive mode. Boxes highlight predicted linear B cell epitopes by Bepipred. **(D)** Three–dimensional model of the rSmTAL–9 obtained using Phyre2 in intensive mode.

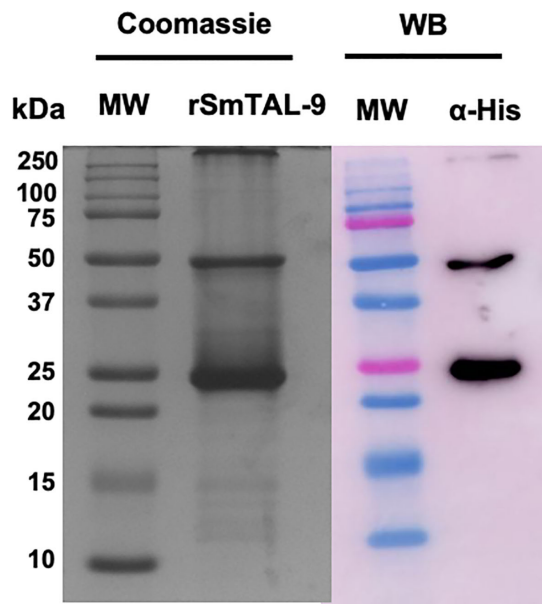

FIGURE 4 | Electrophoretic and western blot analysis of the purified recombinant SmTAL–9. Purified rSmTAL–9 was detected using 15% SDS–PAGE stained with Comassie blue. Precision plus Protein™ Dual color standard from BioRad was used as the molecular weight standard (MW). Recognition of the 6XHis–tag from the recombinant protein was analyzed *via* western blotting using an anti–His (α–His) antibody.

report the role of one member of the Smtal family in parasite survival. The discrepancy between our *in vitro* and *in vivo* assays could be explained by the lack of pressure in the *in vitro* system. This was also previously demonstrated for depleted parasites for other proteins described as essential for parasite development, such as some protein kinases (SmJNK, SmERK, Smp38, and SmFES). For instance, these parasites presented relevant phenotypic alterations after confrontation with the host immune system, ranging from lack of worm maturation, underdeveloped internal structures, and reduced numbers of parasites, among other changes (28–30).

Thus, the impact of the *Smtal–9* expression knockdown on parasite survival *in vivo*, in addition to the fact that the Smtal–9 sequence possesses predicted B and T cell epitopes, suggests this antigen is a potential vaccine candidate. Indeed, the use of this antigen in our prime–boost vaccine schedule, induced a significant reduction in parasite burden in Smtal–9 immunized mice. But this formulation did not impact egg load in the liver or in the intestine. Although our results validate Smtal–9 as a vaccine candidate (proof of concept), better vaccine formulation still need to be developed to improve the protective immunity induced by this antigen. Then, by improving the effect of the vaccine on worm burden is expected to also observe a significant reduction in egg load. In this regard, the use of other adjuvants, optimization of the antigen obtention process and the use of better delivery systems are alternatives to improve vaccine efficacy. Also, a better understanding of the immune mechanisms involved in parasite elimination upon vaccination with Smtal–9 is important to drive the design of a better vaccine.

How the immune response triggered by vaccination acts in parasite elimination is puzzling. Some evidence suggests that antibodies would play an important role in the parasite elimination upon vaccination with Smtal–9: (i) in an immune proteomic assay, Smtal–9 is recognized by sera from mice immunized with a preparation of the schistosomula tegument (Smteg) (data not shown), a vaccine formulation that induces a

TABLE 3 | Protection induced by a prime (DNA vaccination) – boost (recombinant protein) regimen using SmTAL–9 as the antigen.

Immunization – Prime–Boost	Worm burden recovery[&]	Protectionlevel[a]	Egg/gram ofintestine[&]	Percentage reduction[b]	Egg/gram of liver[&]	Percentage reduction[b]
Trial 1						
pcDNA3.1V5/HIS + Saline/CFA/IFA	47 ± 10		8293 ± 3877		13678 ± 4941	
pcDNA3.1V5/HIS + rSmTAL–9/CFA/IFA	38 ± 7 (p = 0.044)*	19.4%*	7324 ± 2952 (p=0.8101)	11.7% ns	13060 ± 3511 (p > 0.999)	4.5% ns
pcDNA3.1V5/HIS/*SmTAL9* + Saline/CFA/IFA	42 ± 9 (p = 0.665)	10.6% ns	8747 ± 4354 (p=0.8101)	0.0% ns	10720 ± 3940 (p = 0.2863)	21.62% ns
pcDNA3.1V5/HIS/*SmTAL9* + rSmTAL–9/CFA/IFA	35 ± 7 (p = 0.0087)*	25.5%*	9611 ± 3636 (p=0.8101)	0.0% ns	13923 ± 3727 (p > 0.999)	0.0% ns
Trial 2						
pcDNA3.1V5/HIS + Saline/CFA/IFA	35 ± 6		9940 ± 3586		27777 ± 8902	
pcDNA3.1V5/HIS + rSmTAL–9/CFA/IFA	27 ± 11 (p =0.022)*	22.9%*	13810 ± 3752 (p=0.0195)*	0.0% ns	24208 ± 6800 (p > 0.999)	12.8% ns
pcDNA3.1V5/HIS/*SmTAL9* + Saline/CFA/IFA	33 ± 6 (p = 0.502)	5.7% ns	11612 ± 4068 (p=0.3633)	0.0% ns	24720 ± 6470 (p > 0.999)	11.0% ns
pcDNA3.1V5/HIS/*SmTAL9* + rSmTAL–9/CFA/IFA	25 ± 5 (p = 0.011)*	28.6%*	12815 ± 8324 (p=0.2998)	0.0% ns	31134 ± 9800 (p > 0.999)	0.0% ns

[a]*Reduction in the total number of worms compared to pcDNA3.1V5/HIS + Saline/CFA/IFA control group.*

[b]*Reduction in the total number of eggs in tissue (liver and intestine) compared to pcDNA3.1V5/HIS + Saline/CFA/IFA control group.*

**Statistically significant differences in comparison to pcDNA3.1V5/HIS + Saline/CFA/IFA control group.*

[&] *Statistically significant differences were determined using Student's t test or the Mann–Whitney U test.*

protective immune response in mice (5), (ii) sera from Smteg–immunized mice can transfer protection to a naïve recipient (16). However, our *in silico* analysis of the protein sequence predicts it has a cytoplasmic location inaccessible to antibodies.

Therefore, what would be the importance of antibodies in the protective immune response since it would seem unlikely to be able to bind its target in live parasites? Data from a recently published proteomic study helps to clarify this question, as Smtal–9 was identified as one of the proteins associated with the *S. mansoni* tegument membrane of the schistosomula (31). This observation suggests that this antigen is exposed to host immune response, and, thus, could be recognized by antibodies produced upon immunization.

The same study also demonstrates that Smtal–9 expression increases during larval maturation, with higher expression levels being observed in 5–day–old parasites (31). Previous observations have demonstrated that schistosomes become refractory to antibody–dependent cellular and complement–mediated damage as they migrate from skin to the lungs (31–33). Thus, we hypothesize that if antibodies play a role in the immune response induced by vaccination with Smtal–9, parasite–killing mechanisms may involve antigen functional blockage rather than an Fc–effector–mediated–killing of the parasite. But this hypothesis, as well as the role of antibody in Smtal–9–induced protective immunity need to be proven by further studies.

Regardless of the mechanism involved in parasite elimination upon vaccination with Smtal–9 antigen, our data demonstrate that Smtal–9 is a promising antigen to be used in a vaccine formulation against schistosomiasis. We also demonstrated, for the first time, that one of the TAL family members, Smtal–9, plays an important role in parasite survival in its definitive host, although its function during parasite development and survival still needs to be determined.

DATA AVAILABILITY STATEMENT

The original contributions presented in the study are included in the article/**Supplementary Material**. Further inquiries can be directed to the corresponding author.

ETHICS STATEMENT

The animal study was reviewed and approved by Ethics Committee of Animal Use of the Fundação Oswaldo Cruz (FIOCRUZ) under licenses LW26/12 and LW22/16.

AUTHOR CONTRIBUTIONS

WB performed the experiments and the data analysis, discussed the data and wrote the manuscript, ID performed the experiments and the data analysis, discussed the data and revised the manuscript, RS–P contributed to the design of the research, performed the experiments, discussed the data and revised the manuscript, MM contributed to the design of the research, provided some reagents, discussed the data and revised the manuscript and CF designed the research, obtained funding, performed the experiments and the data analysis, discussed the data and wrote the manuscript. All authors approved the submitted version.

FUNDING

This study was financed in part by the Coordination for the Improvement of Higher Education Personnel (Coordenação de Aperfeiçoamento de Pessoal de Nível Superior–CAPES) – Finance Code 001, Conselho Nacional de Desenvolvimento Científico e Tecnológico–Brasil (Grant Nos. 407702/2012–1, 303131/2018–7 and 317389/2021–1), Instituto René Rachou – FIOCRUZ–MG, Programa CAPES/Print/FIOCRUZ and Rede De Pesquisa em Imunobiológicos do Estado de Minas Gerais – FAPEMIG (RED00140–16). Fellowships: Pq–CNPq (CF and MM).

ACKNOWLEDGMENTS

We acknowledge the Program for Technological Development in Tools for Health–PDTIS–FIOCRUZ for the use of its Real–Time PCR facility. We thank the Lobato Paraense Mollusk facility at IRR for providing the *S. mansoni* cercariae and the Animal Facilities of the IRR for the provision and maintenance of experimental animals. We thank the IRR's project support service for project management. We thank Sueleny Silva Ferreira Teixeira, Juliano Michel de Araújo and Rafaela Donadoni de Souza for their assistance with the experiments.

SUPPLEMENTARY MATERIAL

The Supplementary Material for this article can be found online at: https://www.frontiersin.org/articles/10.3389/fimmu.2022.889645/full#supplementary-material

REFERENCES

1. Jones MK, Gobert GN, Zhang L, Sunderland P, McManus DP. The Cytoskeleton and Motor Proteins of Human Schistosomes and Their Roles in Surface Maintenance and Host-parasite Interactions. *BioEssays* (2004) 26:752–65. doi: 10.1002/bies.20058
2. Tran MH, Pearson MS, Bethony JM, Smyth DJ, Jones MK, Duke M, et al. Tetraspanins on the Surface of *Schistosoma mansoni* are Protective Antigens Against Schistosomiasis. *Nat Med* (2006) 12:835–40. doi: 10.1038/nm1430
3. Cardoso FC, Macedo GC, Gava E, Kitten GT, Mati VL, de Melo AL, et al. *Schistosoma mansoni* Tegument Protein Sm29 Is Able to Induce a Th1-Type of Immune Response and Protection Against Parasite Infection. *PloS Negl Trop Dis* (2008) 2. doi: 10.1371/journal.pntd.0000308
4. Farias LP, Cardoso FC, Miyasato PA, Montoya BO, Tararam CA, Roffato HK, et al. *Schistosoma mansoni* Stomatin Like Protein-2 Is Located in the Tegument and Induces Partial Protection Against Challenge Infection. *PloS Negl Trop Dis* (2010) 4. doi: 10.1371/journal.pntd.0000597
5. Teixeira De Melo T, Michel De Araujo J, do Valle Durães F, Caliari M, Oliveira SC, Coelho PMZ, et al. Immunization with Newly Transformed *Schistosoma mansoni*

Schistosomula Tegument Elicits Tegument Damage, Reduction in Egg and Parasite Burden. *Parasit Immunol* (2010) 32:749–59. doi: 10.1111/j.1365-3024.2010.01244.x
6. Martins VP, Pinheiro CS, Figueiredo BCP, Assis NRG, Morais SB, Caliari MV, et al. Vaccination With Enzymatically Cleaved GPI-Anchored Proteins From *Schistosoma mansoni* Induces Protection Against Challenge Infection. *Clin Dev Immunol* (2012) 2012:1–11. doi: 10.1155/2012/962538
7. Teixeira de Melo T, Araujo JM, Campos de Sena I, Carvalho Alves C, Araujo N, Toscano Fonseca C. Evaluation of the Protective Immune Response Induced in Mice by Immunization With *Schistosoma mansoni* Schistosomula Tegument (Smteg) in Association With CpG-ODN. *Microbes Infect* (2013) 15:28–36. doi: 10.1016/j.micinf.2012.10.007
8. Dunne DW, Butterworth AE, Fulford AJC, Curtis Kariuki H, Langley JG, Ouma JH, et al. Immunity After Treatment of Human Schistosomiasis: Association Between IgE Antibodies to Adult Worm Antigens and Resistance to Reinfection. *Eu J Immunol* (1992) 22:1483–94. doi: 10.1002/eji.1830220622
9. Pacífico LGG, Fonseca CT, Chiari L, Oliveira SC. Immunization with *Schistosoma mansoni* 22.6kDa Antigen Induces Partial Protection Against Experimental Infection in a Recombinant Protein Form but Not as DNA Vaccine. *Immunobiol* (2006) 211:97–104. doi: 10.1016/j.imbio.2005.06.004
10. Fitzsimmons CM, Jones FM, Stearn A, Chalmers IW, Hoffmann KF, Wawrzyniak J, et al. The *Schistosoma mansoni* Tegumental-Allergen-Like (TAL) Protein Family: Influence of Developmental Expression on Human igE Responses. *PloS Negl Trop Dis* (2012) 6. doi: 10.1371/journal.pntd.0001593
11. Stein L, David J. Cloning of a Developmentally Regulated Tegument Antigen of *Schistosoma mansoni*. *Mol Biochem Parasitol* (1986) 20:253–64. doi: 10.1016/0166-6851(86)90106-44
12. Hoffmann KF, Strand M. Molecular Characterization of a 20.8-kDa *Schistosoma mansoni* Antigen. *J Biol Chem* (1997) 272:14509–15. doi: 10.1074/jbc.272.23.14509
13. Francis P, Bickle Q. Cloning of a 21.7-kDa Vaccine-Dominant Antigen Gene of *Schistosoma mansoni* Reveals an EF Hand-Like Motif. *Mol Biochem Parasitol* (1992) 50:215–24. doi: 10.1016/0166-6851(92)90218-9
14. Mohamed MM, Shalaby KA, LoVerde PT, Karim AM. Characterization of Sm20.8, a Member of a Family of Schistosome Tegumental antigens1Note: Nucleotide Sequence Data Reported in This Paper Is Available in the GenBank^{TM} data base under accession numbers U86673 and U91941.1. *Mol Biochem Parasitol* (1998) 96:15–25. doi: 10.1016/S0166-6851(98)00088-7
15. Carson J, Thomas CM, McGinty A, Takata G, Timson DJ. The Tegumental Allergen-Like Proteins of *Schistosoma mansoni*: A Biochemical Study of Smtal4-TAL13. *Mol Biochem Parasitol* (2018) 221:14–22. doi: 10.1016/j.molbiopara.2018.02.002
16. de Melo TT, de Sena IC, Araujo N, Fonseca CT. Antibodies Are Involved in the Protective Immunity Induced in Mice by *Schistosoma mansoni* Schistosomula Tegument (Smteg) Immunization. *Parasit Immunol* (2014) 36:107–11. doi: 10.1111/pim.12091
17. de Souza CP, Jannotti-Passos LK, de Freitas JR. Degree of Host-Parasite Compatibility Between *Schistosoma mansoni* and Their Intermediate Molluscan Hosts in Brazil. *Mem Inst Oswaldo Cruz* (1995) 90:5–10. doi: 10.1590/S0074-02761995000100003
18. das Graças Amaral Avelar L, Gava SG, Neves RH, Soares Silva MC, Araújo N, Tavares NC, et al. Smp38 MAP Kinase Regulation in *Schistosoma mansoni*: Roles in Survival, Oviposition, and Protection Against Oxidative Stress. *Front Immunol* (2019) 10:21. doi: 10.3389/fimmu.2019.00021
19. Livak KJ, Schmittgen TD. Analysis of Relative Gene Expression Data Using Real-Time Quantitative PCR and the 2–ΔΔCT Method. *Methods* (2001) 25:402–8. doi: 10.1006/meth.2001.1262
20. Pellegrino JSAFA. Perfusion Technic for Recovery of *Schistosoma Mansoni* From Experimentally Infected Guinea Pigs. *Rev Bras Malariol Doenç Trop* (1956) 8:589–97.
21. Kelley LA, Mezulis S, Yates CM, Wass MN, Sternberg MJE. The Phyre2 Web Portal for Protein Modeling, Prediction and Analysis. *Nat Prot* (2015) 10:845–58. doi: 10.1038/nprot.2015.053
22. Carneiro FRG, Silva TCL, Alves AC, Haline-Vaz T, Gozzo FC, Zanchin NIT. Spectroscopic Characterization of the Tumor Antigen NY-REN-21 and Identification of Heterodimer Formation With SCAND1. *Biochem Biophys Res Commun* (2006) 343:260–8. doi: 10.1016/j.bbrc.2006.02.140
23. Bernardes WPDOS, de Araújo JM, Carvalho GB, Alves CC, de Moura Coelho AT, Dutra ITS, et al. Fails to Elicit a Protective Immune Response and Does Not Have an Essential Role in Parasite Survival in the Definitive Host. *J Immunol Res* (2019) 2019:1–16. doi: 10.1155/2019/6793596
24. Santiago ML, Hafalla JCR, Kurtis JD, Aligui GL, Wiest PM, Olveda RM, et al. Identification of the Schistosoma Japonicum 22.6–kDa Antigen as a Major Target of the Human IgE Response: Similarity of IgE–Binding Epitopes to Allergen Peptides. *Int Arch Allergy Immunol* (1998) 117:94–104. doi: 10.1159/000023995
25. Radauer C, Bublin M, Wagner S, Mari A, Breiteneder H. Allergens Are Distributed Into Few Protein Families and Possess a Restricted Number of Biochemical Functions. *Immunol Lett* (2008) 121:847–852.e7. doi: 10.1016/j.jaci.2008.01.025
26. Rezende CMF, Silva MR, Santos ÍGD, Silva GAB, Gomes DA, Goes AM. Immunization With rP22 Induces Protective Immunity Against *Schistosoma mansoni*: Effects on Granuloma Down-Modulation and Cytokine Production. *Immunol Lett* (2011) 141:123–33. doi: 10.1016/j.imlet.2011.09.003
27. Thomas CM, Timson DJ. A Mysterious Family of Calcium-Binding Proteins From Parasitic Worms. *Biochem Soc Trans* (2016) 44:1005–10. doi: 10.1042/BST20150270
28. Thomas CM, Timson DJ. The *Schistosoma mansoni* Tegumental Allergen Protein, Smtal1: Binding to an IQ-Motif From a Voltage-Gated Ion Channel and Effects of Praziquantel. *Cell Calcium* (2020) 86:102161. doi: 10.1016/j.ceca.2020.102161
29. Milligan JN, Jolly ER. Cercarial Transformation and *In Vitro* Cultivation of *Schistosoma mansoni* Schistosomules. *J Vis Exp* (2011) 54. doi: 10.3791/3191
30. de Andrade LF, Mourão M de M, JA G, FS C, LL S, RH N, et al. Regulation of *Schistosoma mansoni* Development and Reproduction by the Mitogen-Activated Protein Kinase Signaling Pathway. *PloS Negl Trop Dis* (2014) 8:e2949. doi: 10.1371/journal.pntd.0002949
31. Sotillo J, Pearson M, Becker L, Mulvenna J, Loukas A. A Quantitative Proteomic Analysis of the Tegumental Proteins From *Schistosoma Mansoni* Schistosomula Reveals Novel Potential Therapeutic Targets. *Int J Parasitol* (2015) 45:505–16. doi: 10.1016/j.ijpara.2015.03.004
32. Dessein A, Samuelson JC, Butterworth AE, Hogan M, Sherry BA, Vadas MA, et al. Immune Evasion by *Schistosoma Mansoni*: Loss of Susceptibility to Antibody or Complement-Dependent Eosinophil Attack by Schistosomula Cultured in Medium Free of Macromolecules. *Parasitol* (1981) 82:357–74. doi: 10.1017/S0031182000066890
33. Tavares NC, Gava SG, Torres GP, de Paiva CÊS, Moreira BP, Lunkes FMN, et al. *Schistosoma mansoni* FES Tyrosine Kinase Involvement in the Mammalian Schistosomiasis Outcome and Miracidia Infection Capability in Biomphalaria glabrata. *Front Microbiol* (2020) 11:963. doi: 10.3389/fmicb.2020.00963

Conflict of Interest: The authors declare that the research was conducted in the absence of any commercial or financial relationships that could be construed as a potential conflict of interest.

Publisher's Note: All claims expressed in this article are solely those of the authors and do not necessarily represent those of their affiliated organizations, or those of the publisher, the editors and the reviewers. Any product that may be evaluated in this article, or claim that may be made by its manufacturer, is not guaranteed or endorsed by the publisher.

frontiers | Frontiers in Immunology

ORIGINAL RESEARCH
published: 14 July 2022
doi: 10.3389/fimmu.2022.941530

Potential Gut Microbiota Features for Non-Invasive Detection of Schistosomiasis

Datao Lin[1,2,3†], Qiuyue Song[1,2,4†], Jiahua Liu[1,2], Fang Chen[5], Yishu Zhang[1,2], Zhongdao Wu[1,2,3], Xi Sun[1,2*] and Xiaoying Wu[2,6*]*

[1] Department of Parasitology, Zhongshan School of Medicine, Sun Yat-sen University, Guangzhou, China, [2] Key Laboratory of Tropical Disease Control, Ministry of Education, Guangzhou, China, [3] Chinese Atomic Energy Agency Center of Excellence on Nuclear Technology Applications for Insect Control, Provincial Engineering Technology Research Center for Diseases-Vectors Control, Guangzhou, China, [4] Department of Clinical Laboratory, Xiangyang No.1 People's Hospital, Hubei University of Medicine, Xiangyang, China, [5] School of Medicine, South China University of Technology, Guangzhou, China, [6] The Third Affiliated Hospital, Sun Yat-sen University, Guangzhou, China

OPEN ACCESS

Edited by:
Thiago Almeida Pereira,
Stanford University, United States

Reviewed by:
Braden C. McFarland,
University of Alabama at Birmingham, United States
Jianhai Yin,
National Institute of Parasitic Diseases (China), China

***Correspondence:**
Datao Lin
lindt5@mail.sysu.edu.cn
Xi Sun
sunxi2@mail.sysu.edu.cn
Xiaoying Wu
wuxy227@mail.sysu.edu.cn

[†]These authors have contributed equally to this work

Specialty section:
This article was submitted to Parasite Immunology, a section of the journal Frontiers in Immunology

Received: 11 May 2022
Accepted: 13 June 2022
Published: 14 July 2022

Citation:
Lin D, Song Q, Liu J, Chen F, Zhang Y, Wu Z, Sun X and Wu X (2022) Potential Gut Microbiota Features for Non-Invasive Detection of Schistosomiasis. Front. Immunol. 13:941530. doi: 10.3389/fimmu.2022.941530

The gut microbiota has been identified as a predictive biomarker for various diseases. However, few studies focused on the diagnostic accuracy of gut microbiota derived-signature for predicting hepatic injuries in schistosomiasis. Here, we characterized the gut microbiomes from 94 human and mouse stool samples using 16S rRNA gene sequencing. The diversity and composition of gut microbiomes in *Schistosoma japonicum* infection-induced disease changed significantly. Gut microbes, such as *Bacteroides*, *Blautia*, *Enterococcus, Alloprevotella*, *Parabacteroides* and *Mucispirillum*, showed a significant correlation with the level of hepatic granuloma, fibrosis, hydroxyproline, ALT or AST in *S. japonicum* infection-induced disease. We identified a range of gut bacterial features to distinguish schistosomiasis from hepatic injuries using the random forest classifier model, LEfSe and STAMP analysis. Significant features *Bacteroides*, *Blautia*, and *Enterococcus* and their combinations have a robust predictive accuracy (AUC: from 0.8182 to 0.9639) for detecting liver injuries induced by *S. japonicum* infection in humans and mice. Our study revealed associations between gut microbiota features and physiopathology and serological shifts of schistosomiasis and provided preliminary evidence for novel gut microbiota-derived features for the non-invasive detection of schistosomiasis.

Keywords: *Schistosoma japonicum*, schistosomiasis, parasites, gut microbiota, non-invasive

INTRODUCTION

Schistosomiasis, one of the most important human parasitic diseases, affects over 240 million people and threatens nearly one-eighth of the world population at risk of infection worldwide (1–3). This zoonotic disease is caused by trematodes of the genus *Schistosoma* including *Schistosoma japonicum* (*S. japonicum*), *Schistosoma mansoni*, *Schistosoma haematobium*, *Schistosoma intercalatum* and

Schistosoma Mekongi (4, 5). In China, *S. japonicum* is the only endemic parasitic flatworm of schistosome. Among the 12 province endemics for schistosomiasis in China, Yunnan, Hubei, Anhui, Jiangxi and Hunan provinces maintained the criteria of transmission control by the end of 2020 (6). There are still 29,517 advanced schistosomiasis cases documented (6), implying that *S. japonicum* infection remains one of the most important public health problems in some endemic areas of China. To achieve the goal of the *National Thirteenth Five Year Plan*, strategies for schistosomiasis control are still required.

The lifecycle of *S. japonicum* includes the several developmental stages of paired adult worms, eggs, ciliated miracidium, mother and daughter sporocyst and cercariae (1, 4). Immature schistosomula migrate downstream to the hepatic portal-mesenteric system. Then, females become mature in the liver and release thousands of eggs. The eggs retained in host tissues can induce hepatic granuloma formation, which ultimately evolves into progressive hepatic fibrosis and portal hypertension in advanced schistosomiasis patients (1, 5, 7). Despite the wide use of praziquantel (PZQ) for the prevention and control of schistosomiasis in endemic regions, hepatic fibrosis remains a serious chronic schistosome-infected disease affecting public health (5, 8). Until now, liver biopsy is the gold standard for the assessment of fibrosis, but the disadvantages such as poor patient compliance, morbidity, mortality and sampling error limited the wide application of liver biopsy (9–11). Therefore, a comprehensive evaluation of the stage of liver fibrosis is still essential. Previous studies have revealed that serum tests (such as aspartate aminotransferase (AST), alanine aminotransferase (ALT) and miR-146a-5p) (9, 12, 13) and liver stiffness measurement (LSM) (11, 14) are some important diagnostic indexes of liver fibrosis. Ultrasonography has been used for the assessment of hepatic fibrosis of advanced schistosomiasis but it showed only a moderate correlation between Ultrasonography and liver biopsy (15, 16). However, the limitations and costs of these invasive indexes and imaging detection restrict their widely used for the detection of liver fibrosis. Thus, research on more non-invasive tools for the prediction of the level of *S. japonicum* infection-induced liver fibrosis is still essential.

Mammals harbor hundreds of gut microbiota that affect host biology and health (17). Recent studies have demonstrated that *Schistosoma* infection can affect the composition and structure of gut microbiota in infected patients (18, 19) and mice (20, 21). Previous research suggested that gut microbiota composition is associated with *S. mansoni* infection burden in rodent models (22). These studies indicated that *Schistosoma* infection is associated with the diversity and composition of gut microbiota in infected mammals. The liver-gut microbiota axis is involved in the physiopathology of liver diseases, implying that gut microbiota may be associated with fibrotic development or progression (23, 24). Evidence suggests that gut microbiota, such as *Veillonellaceae* and *Ruminococcaceae*, are reliably predicted biomarkers for the detection of hepatic fibrosis and damage (25–27). However, the relationship between the gut microbiota and hepatic fibrosis induced by *S. japonicum* remains unclear. Accordingly, whether gut microbiota alterations in *S. japonicum* infection-induced disease can be used as potential non-invasive biomarkers for the detection of the level of hepatic fibrosis is unclear.

In this study, we hypothesized that a strong relationship exists for the development of gut microbiota features derived biomarkers that can be used to predict the hepatic fibrosis and granuloma in *S. japonicum* infection-induced diseases. Here, we comprehensively investigated the relationship among gut microbiomes, serologic detection and the level of hepatic injuries in *S. japonicum*-infected mice, and compared it with the gut microbiota of human individuals. We aimed to develop a panel of gut-microbiota-derived biomarkers for the non-invasive detection of the level of hepatic injuries in schistosomiasis.

Abbreviations: OTU, operational taxonomic unit; PZQ, Praziquantel; AST, aspartate aminotransferase; ALT, alanine aminotransferase; LSM, liver stiffness measurement; 2D SWE, two-dimensional shear wave elastography; PLS-DA, partial least squares discrimination analysis; PCoA, Principal Co-ordinates Analysis; ANOSIM, analysis of similarities; ROC, receiver-operating characteristic; AUC, area under the ROC curves; STAMP, Statistical analysis of metagenomic profiles; LDA, Linear discriminant analysis; LEfSe, Linear discriminant analysis effect size; PCR, Polymerase chain reaction; HBV, Hepatitis C virus; HCV, Hepatitis C virus; CCl4, Tetrachloromethane; IBD, Inflammatory bowel disease; SEA, *Schistosoma* soluble egg antigen; FMT, fecal microbiota transplantation.

MATERIALS AND METHODS

Mice

We purchased 56 male pathogen-free BALB/c mice (6-week-old, 18 ± 2 g) from the Experimental Animal Center of Southern Medical University. The mice were reared in plastic cages with free access to autoclaved sterile water and chow in the Biosafety Level-2 (BSL-2) laboratory of Sun Yat-Sen University. The rearing conditions include controlled temperature and humidity and a 12 h light and 12 h dark cycle. We randomly divided the mice into groups for further experiments.

S. japonicum Cercariae and Infection

The *S. japonicum* cercariae were obtained from infected *Oncomelania hupehensis*, which were purchased from the Chinese Center for Disease Control and Prevention (Shanghai, China). The steps of releasing cercariae from snails were conducted described as in a previous study (28). The mice were infected with 5, 15, 20 or 60 *S. japonicum* cercariae per individual *via* the shaved abdominal skin, and treatment was continued for 7 or 8 weeks. The mice uninfected were served as the control group.

Sample Collection and Detection From Mice

All mice were sacrificed after chloral hydrate asphyxiation and cervical dislocation at 49 or 56 days after infection (dpi) of *S. japonicum*. Luminal content samples were collected from colon intestines at 49 or 56 dpi under sterile conditions and transferred directly into sterile tubes. Left liver lobes and colons were collected and immediately fixed in 4% paraformaldehyde for the histopathological analysis described in the previous study (29). Liver samples were also collected for the detection of hydroxyproline content according to the protocol of the

hydroxyproline assay kit (Nanjing, China). Blood samples were drawn from orbital veins and centrifuged at 1,500 g for 15 min. We then collected the serum samples after clotting for ALT and AST measurements in KingMed Diagnostics (Guangzhou, China). These samples were snap-frozen on dry ice and stored at -80°C until further study.

Histological Staining

The fixed fragments from the liver were sliced into sections for histopathological analysis. These paraffin slices were dewaxed for the Masson's trichrome staining and hematoxylin and eosin (H&E) staining. We captured the images of staining slices using an inverted microscope (Japan). We analyzed the percentage of the granulomatous and fibrotic area using a ZEISS Axio Scan automated slide scanner microscope (Germany). We also obtained a full view of the whole liver tissue. We analyzed the area of the whole tissue and the blue positive region using Image-Pro Plus 6.0 software (Media Cybernetics, USA). We calculated the percentage of the granulomatous and fibrotic areas described in the previous study (29).

Subjects and Sample Collection From Humans

Twenty-six participants (with *S. japonicum* infection or without) of the previous study (30) were more than 30 years old, and they were initially screened for *Schistosoma* spp. eggs in feces using the Kato-Katz method (30, 31), and finally, twenty-six stool samples (15 controls, 11 patients) were colllected (30). To further investigate specific diagnostic biomarkers of schistosomiasis, we analyzed the association between shifts of gut microbiota of humans infected with non-parasitic factors (Such as hepatitis B virus) and the level of liver injuries. To this end, we recruited participants, and all participants from the Third Affiliated Hospital of Sun Yat-sen University were included in the study. All these participants from the Third Affiliated Hospital were >30 years old with non-parasitic factor infection, and the patients display clinical symptoms of liver injuries, and second liver two half-and-half detect provided reliable clinical test results of the participants (**Supplementary Table S1**). The information of participants about age, sex, diagnosis, medication, length of infection, HBsAg, HBsAb, HBeAg, HBeAb, HBcAb was shown in **Supplementary Table S1**. The participants were diagnosed with Hepatitis B virus-induced liver cirrhosis, and a total of twelve fresh fecal samples were collected.

Liver Stiffness Measurement in Humans

Twelve patients with cirrhosis from the Third Affiliated Hospital were included in the present study. All participants were >30 years old with non-parasitic factor infection and the patients displayed clinical symptoms of liver injuries (Clinical information was shown in **Supplementary Table S1**). The participants were subjected to two kind of Liver stiffness measurements: A two-dimensional shear wave elastography (2D SWE) examination and transient elastography which performed using FibroTouch, and the measurements were performed according to the operations manual as described in the previous study (32–35). Twelve fresh fecal samples were collected and stored in Eppendorf tubes at –80°C. All participants gave informed written consent.

DNA Extraction, PCR amplification and Sequencing

Total DNA from fecal samples was isolated using the protocol of the Hipure Stool DNA Kit (Guangzhou, China). After extraction, we detected the DNA quality and quantity examination using NanoDrop 2000 spectrophotometer (USA). The 16S rRNA gene (for V3-V4 regions) from mice gut microbiota was amplified using a bacterial primer set: 338F 5'-ACTCCTACGGGAGGCAGCA-3' and 806R 5'- GGACTACHVGGGTWTCTAAT-3'. We performed the PCR amplification using the Takara PrimeStar DNA polymerase (Dalian, China). The following PCR cycling conditions included: denaturation at 95°C for 5 min, 25 cycles of 95°C for 30 s, 50°C for 30 s, 72°C for 40 s, and final extension at 72°C for 5 min. The PCR products were analyzed using 2% agarose gel electrophoresis. An amplicon library for sequencing was generated from the individual specimens. Finally, all fecal samples were sequenced on an Illumina HiSeq 2500 platform constructed by Biomarker technologies (Beijing, China).

Microbiome Analysis

After the base calling analysis, we transformed the raw data files from the sequencing platform and NCBI (30) into the original sequenced reads and stored them in FASTQ format. QIIME (version 1.8.0) was used to cluster reads into operational taxonomic units (OTUs) and identified at 97% or more similarity (36). To analyze the alpha diversity, we rarified the OTU table using mothur (v. 1.33.3) (37). PERMANOVA and analysis of similarities (ANOSIM) were used to evaluate the beta diversity using mothur. The partial least squares discrimination analysis (PLS-DA), Statistical analysis of metagenomic profiles (STAMP) and principal coordinates analysis (PCoA) graphs (based on Bray Curtis distance) were done in R software (v. 2.15.3). Taxonomic characterization was performed using the linear discriminant analysis (LDA) effect size (LEfSe). Based on the genus or OTUs abundance of gut microbiota of mice, we conducted random forest algorithms with 500 random permutations described in the previous study (38). The relationships among variables were analyzed using Spearman analysis in R. The area under the receiver-operating characteristic (ROC) curves (AUC) was measured using GraphPad Prism (v. 6.0; USA). For range adjustment, all pairwise comparison between two groups was tested using *Wilcoxon*-test.

Overview of the Sequencing Information Gut Bacterial Samples

Finally, a total of 94 bacterial samples obtained from sequencing and NCBI were investigated *via* 16S rRNA gene sequencing. We generated a total of 5,731,918 clean reads from these samples, with an average of 60,977 reads obtained from each sample. After being processed and filtered, over 800 and 504 operational taxonomic units (OTUs) with 97% minimum identity were annotated from human and mouse sequences, respectively.

Statistical Analysis

Data are expressed as the mean ± standard error of the mean (SEM). The differences between groups were analyzed by student's *t*-test using SPSS 19.0 software (USA). $^{*}P < 0.05$, $^{**}P < 0.01$ and $^{***}P < 0.001$ were considered statistically significant.

RESULTS

Distinct Signatures of Gut Microbiomes in *S. japonicum*-Infected Mice With the One-Time Point

The previous study has revealed that *S. japonicum* infection could induce alteration of gut microbiota in mice (29). In this study, *Bacteroidetes* and *Firmicutes* were the dominant phyla in mice (**Figure S1A**). The top 20 genera of gut microbiota in mice were shown (**Figure S1B**). We found significantly different gut bacterial diversities (based on OTU number) and community structures (based on PLS-DA) in *S. japonicum*-infected mice (**Figures 1A, B**, **S1**), regardless of the treatment on mice. In addition, a range of gut bacterial taxa, such as *Bacteroides*, *Blautia* and *Bacteroidaceae*, were considered as biomarkers to distinguish infected and uninfected mice using LEfSe analysis (**Figures 1C**, **S1**).

Distinct Signatures of Gut Microbiomes at the One-Time Point With Different Numbers of *S. japonicum* Infection

Alteration of gut microbiota in mice with varied *S. japonicum* infection is unclear. We found that gut microbiota community structure (based on PCoA) in varied *S. japonicum*-infected mice differed significantly, which was calculated by PERMANOVA analysis based on Bray Curtis distance (**Figures S2A, B**). There was a significant difference in gut bacterial diversities (based on the Simpson index) between infected and uninfected mice (**Figure S2C**). The top 20 genera of gut microbes in mice showed a higher relative of *Bacteroides*, *Alistipes* and *Blautia* in infected mice (**Figure S2D**).

Distinct Signatures of Gut Microbiomes at Different Time Points With Different Numbers of *S. japonicum* Infection

There were significant differences in gut bacterial diversities (based on Shannon index) and community structures (based on PLS-DA; PERMANOVA, P =0.001) between *S. japonicum*-infected and uninfected mice (**Figures 2A, B**). At the genus level, a higher abundance of gut microbes such as *Bacteroides*, *Alloprevotella* and *Blautia* but a lower abundance of gut microbes such as uncultured bacterium f *Muribaculaceae*, *Alistipes* and *Candidatus Saccharimonas* in *S. japonicum*-infected mice were found using Statistical analysis of metagenomic profiles (STAMP) (**Figure 2C**). In addition, thirty bacteria, such as *Bacteroides*, *Alistipes*, *Blautia* and *Desulfovibrio*, were considered as potential predictors for distinguishing *S. japonicum*-infected and uninfected mice based on a machine-learning strategy (**Figure 2D**). Similar results were found using LEfSe analysis (**Figure S3**).

To further investigate specific diagnostic biomarkers of schistosomiasis, we compared the difference in the gut microbiota of mice infected with non-pathogenic factors and pathogenic *S. japonicum*. Previous studies have shown that probiotic *Bacillus subtilis* could affect the composition of gut microbiota and the level of liver disease in mice (29, 39, 40). Here, we showed that gut microbiota diversity and structure of gut microbiota of mice treated with *Bacillus subtilis* (non-pathogenic factor) significantly differed from these of mice

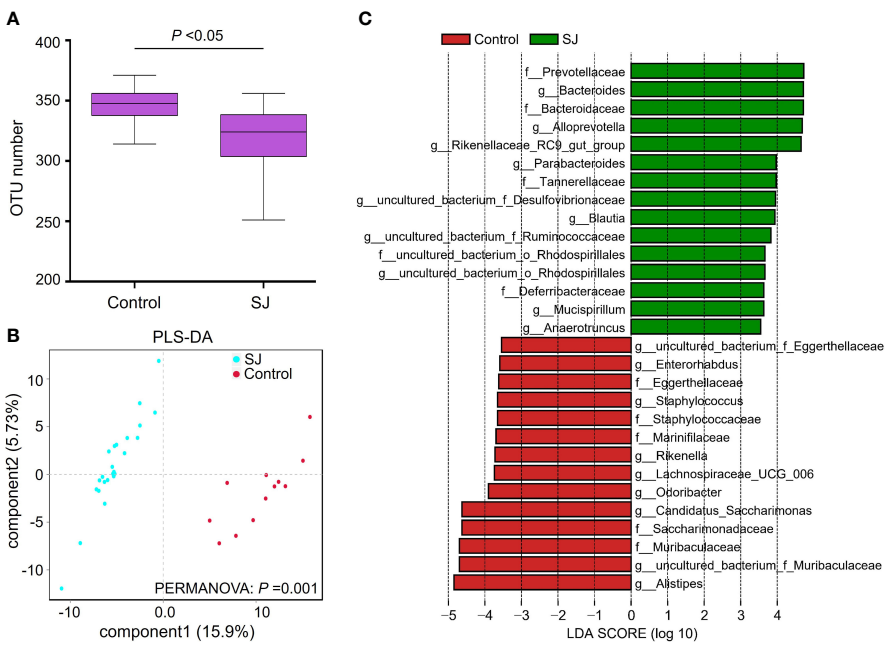

FIGURE 1 | Comparisons of gut microbiota between *S. japonicum*-infected (n = 24) and uninfected (n = 12) mice. **(A)** OTUs analysis. **(B)** PLS-DA analysis. **(C)** Differential gut bacterial taxa were analyzed by LEfSe analysis with LDA score >3.5 between groups. Control: without *S. japonicum* infection mice. SJ: *S. japonicum*-infected mice. *P < 0.05 indicates significant difference.

infected with *S. japonicum* using Shannon index (**Figure S4A**) and PLS-DA analysis (**Figure S4B**), and the diversity of gut microbiota of mice treated with *Bacillus subtilis* is significantly higher than that of *S. japonicum*-infected group. Based on the LEfSe analysis, a range of gut bacterial taxa, such as *Bacteroides*, *Blautia* and *Bacteroidaceae*, could be considered as potential biomarkers to distinguish among control, *S. japonicum*-infected and *Bacillus subtilis*-infected mice (**Figure S4C**). In addition, gut microbes, such as *Bacteroides* and *Blautia*, were considered as potential predictors for distinguishing *S. japonicum*-infected and *Bacillus subtilis*-infected mice based on a machine-learning strategy (**Figure S4D**) and LEfSe analysis (**Figure S4E**).

Relationships Among Granulomatous and Fibrotic Area and Gut Bacterial Variables in Mice

Granuloma showed a significant positive correlation with gut microbes *Bacteroides*, *Alloprevotella*, *Parabacteroides* and *Mucispirillum* but a significant negative correlation with Alistipes, *Lachnospiraceae* NK4A136 group, and Candidatus Saccharimonas (**Figure 3**). Fibrosis showed a significant positive correlation with Hydroxyproline, ALT, AST, *Blautia*, *Enterococcus*, *Lactobacillus*, *Alloprevotella*, *Parabacteroides* and *Rikenellaceae* RC9 gut group but a significant negative relation with uncultured bacterium f *Muribaculaceae*, uncultured bacterium f *Lachnospiraceae* and *Odoribacter*. Hydroxyproline, as well as ALT and AST, also showed a significant correlation with a range of gut microbes.

Distinct Signatures of Gut Microbiomes Between *S. japonicum*-Infected and Uninfected Patients

There were significant differences in gut bacterial community structures (based on PLS-DA; ANOSIM, P =0.025) between *S. japonicum*-infected and uninfected humans (**Figure 4A**). Gut microbes such as *Blautia* and *Pantoea* were considered as biomarkers to distinguish between infected and uninfected humans (**Figures 4B**, **S5**). Importantly, thirty gut bacterial genera, such as *Bacteroides*, *Blautia*, *Bilophila*, *Enterococcus*, *Intestinibacter* and *Desulfovibrio* were considered as a predictor for distinguishing *S. japonicum*-infected and uninfected humans based on a machine-learning strategy (**Figure 4C**). In addition, thirty gut microbes at the family level for distinguishing *S. japonicum*-infected and uninfected humans were shown (**Figure S5C**).

Gut Microbiota Features Reflected the Granulomas or Fibrosis of *S. japonicum* Infection in Hosts

Based on the results from gut microbiomes in mice and humans, three major fibrosis- or granulomas-related taxa, *Bacteroides*, *Blautia*, and *Enterococcus*, were found to be associated with the level of liver injuries induced by *S. japonicum* and could be used for distinguishing *S. japonicum* infection in humans (**Figures 3**, **4**). To assess the utility of these gut microbes for indicating *S. japonicum* infection, the area under the receiver-operating characteristic curve (AUC) was analyzed (**Figure 5**). The ratio of *Bacteroides* could help discriminate between *S. japonicum*-infected patients and normal with an AUC of 0.8385 and it is 0.9639 for the diagnosis of *S. japonicum*-infected and uninfected mice (**Figure 5A**). The values of AUC generated by predictor *Blautia* of gut microbiota in humans and mice were 0.8182and 0.8478, respectively (**Figure 5B**). *Enterococcus* could be used for distinguishing the granulomatous or fibrosis level in *S. japonicum*-infected patients with a rate of 0.8438, but it could be inefficiently used in mice with a lower AUC value (**Figure 5C**). In addition, The values of AUC generated by the combination of gut microbes could be used for the prediction of schistosomiasis, with a high value of AUC (**Tables 1**, **S2, S3**).

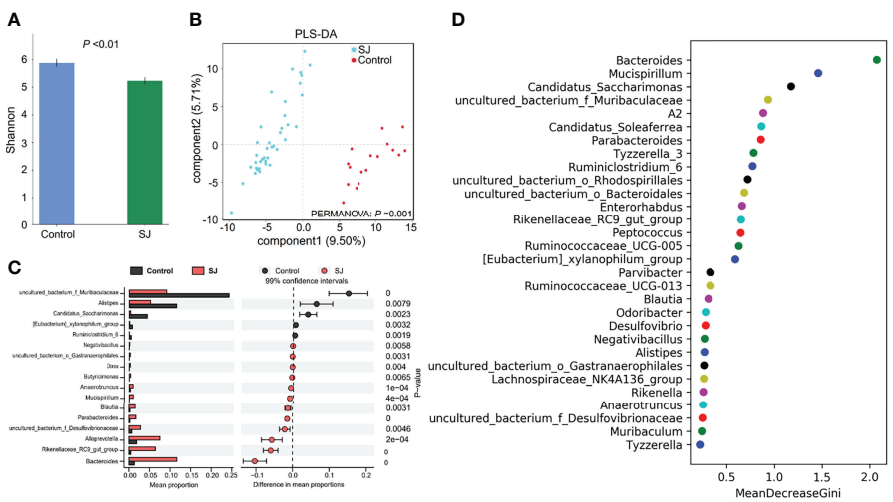

FIGURE 2 | Taxonomic differences of gut microbiota between *S. japonicum*-infected (n=39) and uninfected (n = 17) mice. **(A)** Shannon index. **(B)** PCoA plot. **(C)** The difference of gut microbes in mice at the genus level using STAMP. **(D)** Top 30 of different gut microbes between populations are shown . Control, without *S. japonicum* infection mice. SJ, *S. japonicum*-infected mice.

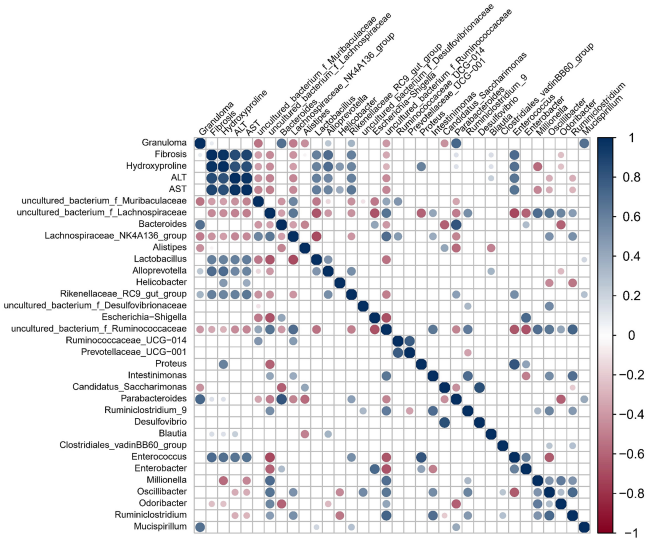

FIGURE 3 | Spearman correlation for variables in *S. japonicum*-infected mice was shown. The circle size indicates the magnitude of the correlation. The circle in color indicates $P < 0.05$, $P < 0.01$ or $P < 0.001$.

However, none of these gut microbiota features was associated with liver injuries induced by the non-parasitic factor (hepatitis B virus, HBV) in humans (**Figure 6**).

DISCUSSION AND CONCLUSIONS

Schistosomiasis is still one of the most prevalent neglected tropical diseases worldwide (1). *S. japonicum* infection could induce a variety of fibrotic diseases and lead to gut microbiota dysbiosis (18, 20, 41). Previous studies have demonstrated that the gut microbiota plays an important role in the progress of hepatic diseases *via* the gut-liver axis (25, 42, 43). These studies suggested that gut microbiota are reliably predicted non-invasive biomarkers for the detection of hepatic fibrosis and damage (25–27). However, few studies explored the relationship between the gut microbiota and the level of hepatic injuries induced by *S. japonicum*. Here, we found significant differences in diversities and composition of gut microbiota of mice infected with *S. japonicum* or without. We revealed that gut microbes such as *Bacteroides*, *Blautia*,

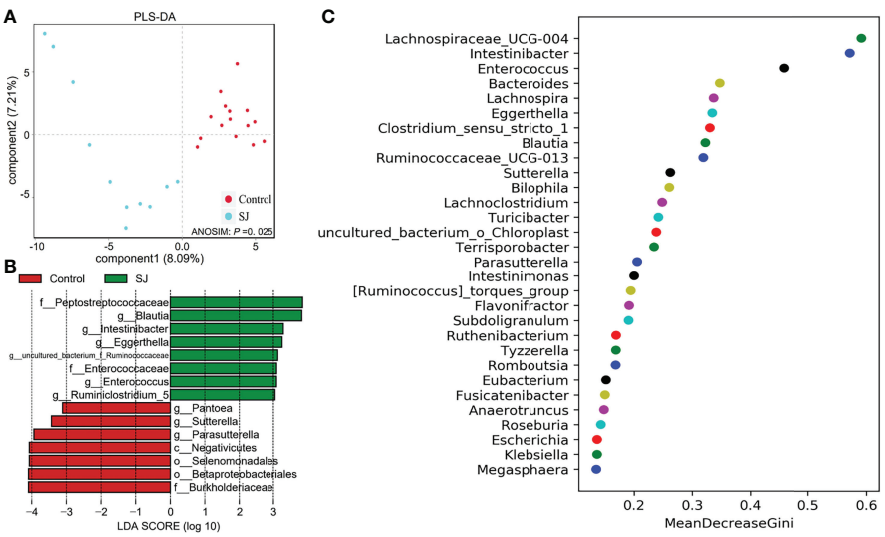

FIGURE 4 | Identification of gut microbial biomarkers in *S. japonicum*-infected (n = 11) and uninfected (n = 15) humans. **(A)** PLS-DA plot. **(B)** Differential gut bacterial taxa analyzed by LEfSe analysis with LDA score >3 between groups. **(C)** Top 30 of different gut microbes between populations are shown. Control, without *S. japonicum* infection humans. SJ, *S. japonicum*-infected humans.

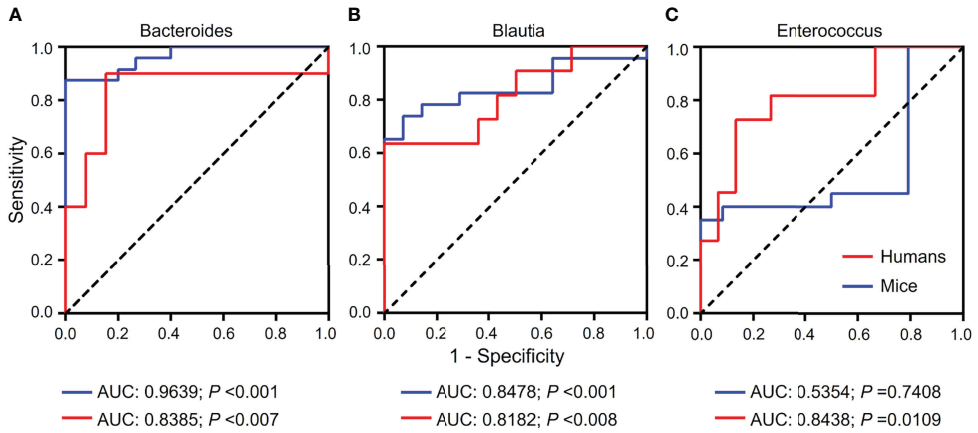

FIGURE 5 | Receiver-operating characteristic (ROC) curves for the diagnosis of granulomas or fibrosis in *S. japonicum*-infected and uninfected hosts. ROC curves using three bacteria including *Bacteroides* **(A)**, *Blautia* **(B)** and *Enterococcus* **(C)** were plotted for the diagnosis. The area under the ROC curves (AUC) was calculated. The rate of identified outliers of *Bacteroides* is 10% and the rate of identified outliers of *Blautia* and *Enterococcus* is 5%.

Enterococcus, and *Mucispirillum* displayed a significant correlation with the level of hepatic granuloma, fibrosis, hydroxyproline, ALT or AST in *S. japonicum* infection-induced disease. Furthermore, novel gut microbiota-derived features *Bacteroides*, *Blautia*, and *Enterococcus* and their combinations could be considered as potential biomarkers for detecting liver injuries induced by *S. japonicum* infection in humans and mice. In total, more non-invasive tools for the prediction of *S. japonicum* infection-induced liver injuries may be beneficial to schistosomiasis control.

Liver injuries and alterations of gut microbiota are associated with the infection of schistosomes and other pathogenic or non-pathogenic factors. These factors, such as *S. japonicum* (20, 29, 44), *S. mansoni* (19, 21, 22), *Clonorchis sinensis* (45), HBV (46, 47), hepatitis C virus (HCV) (48), Tetrachloromethane (CCl4) (49) and alcohol (50), induce the dysbiosis of the gut microbiota of animals and humans and acute or chronic liver injuries such as advanced schistosomiasis, liver cirrhosis and liver cancer. Our study found significant differences in the gut microbiota of mice and humans infected with *S. japonicum*, and *S. japonicum* infection showed a decrease in gut microbial diversity of hosts and an increase in the relative abundance of the genera *Bacteroides*, *Blautia* and *Lactobacillus*. A previous study suggested that the alpha-diversity of intestinal flora in liver fibrosis mice is lower than that in normal mice induced by CCl4 and suggested the decline in *Lactobacillus* in the liver fibrosis mice with NOX4 or RhoA intervention (49). In addition, *Blastocystis* infection induced the decrease of *Bacteroides* in children (51). The abundance of genus *Enterococcus* was significantly downregulated in the intestinal tract of mice with inflammatory bowel disease (IBD) after *Schistosoma* soluble egg antigen (SEA) intervention (44) and was associated with the progression of the HBV related acute-on-chronic liver failure (52). Phyla *Firmicutes* and *Bacteroidetes* represent more than 50% of the total bacterial composition in mice infected with *Schistosoma mansoni* (19), which was similar to our findings, However, there is no significant difference in the relative abundance of genera *Bacteroides*, *Blautia* and *Lactobacillus* after *Schistosoma mansoni* infection. In short, pathogenic factors, as well as non-pathogenic factors, could induce gut microbiota dysbiosis, however, it showed differences in the diversity, abundance or species of gut microbiota of hosts.

It is important to reveal the cause-and-effect relationship between gut microbiota and liver diseases. Previous studies have suggested that gut flora affects cirrhosis (53, 54) and fecal microbiota transplantation (FMT) provides new insights into the interactive mechanism between gut microbiota and liver diseases (54–57). However, the causal association between gut flora and schistosomiasis is unclear, and it deserves further studies.

Although our study has added influence factors such as probiotic supplements (29) that may affect the gut microbiota of mice, there were significant differences in diversities and

TABLE 1 | Receiver-operating characteristic (ROC) curves for the diagnosis of liver injuries using the combination of gut microbes.

Combination[a]	Humans		Mice	
	AUC	Significance[b]	AUC	Significance[b]
Bacteroides+Blautia	0.8308	0.007684	0.965	< 0.0001
Bacteroides+Enterococcus	0.8385	0.006379	0.9446	< 0.0001
Blautia+Enterococcus	0.8701	0.001816	0.8598	0.000623
Bacteroides+Blautia+Enterococcus	0.8308	0.007684	0.9538	< 0.0001

[a]*The rate of identified outliers of the combination of bacteria is 10%.*
[b]*P <0.05 indicates statistically significant.*

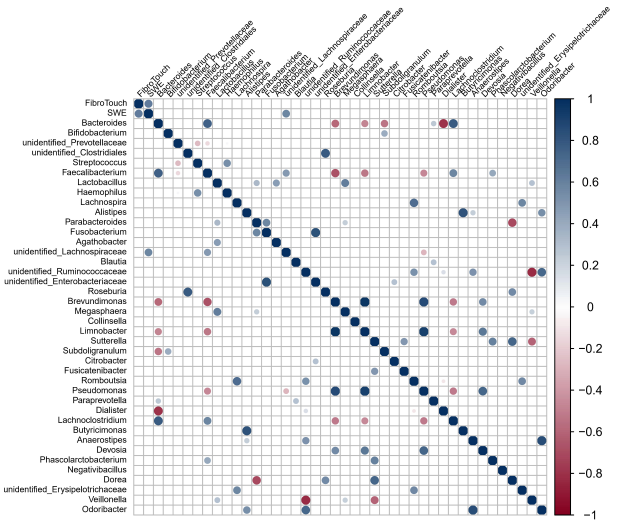

FIGURE 6 | Spearman correlation for variables during fibrosis disease (induced by non-parasitic factors, hepatitis B virus) in humans (n = 12) was shown. Information of participants of study on liver fibrosis induced by non-parasitic factors wes shown in **Table S1**. The methods of FibroTouch and SWE were clinical evaluation strategies in humans. The circle size indicates the magnitude of the correlation. The circle in color indicates $P < 0.05$, $P < 0.01$ or $P < 0.001$.

community structures of gut microbiota between *S. japonicum*-infected and control mice. Our study revealed significant changes in gut bacterial diversity and communities of mice infected with different numbers of *S. japonicum* or in different stages. These results were similar to the previous studies (20, 29, 58). In addition, we obtained and analyzed the gut bacterial data from the previous study (30), and we found significant differences in the compositions of gut microbiota of *S. japonicum* infection-induced patients when compared with the control healthy individuals. Overall, our findings revealed that *S. japonicum* infection could significantly shape the compositions of gut microbiota in both mice and humans.

Previous studies have revealed that gut microbiota played an important role in the liver diseases induced by abiotic factors *via* the gut-liver axis and can be considered as biomarkers to distinguish the level of liver injuries (26, 27, 43). However, whether gut microbiota could be defined as a good biomarker of *S. japonicum* infection-induced liver injuries is controversial. Previous studies have indicated that gut bacterial taxa cannot be used as non-invasive biomarkers for *S. japonicum* infection-induced liver cirrhosis (18), and the researchers suggested that the gut microbiota of *S. japonicum* infection-induced liver cirrhosis patients was similar to that of healthy individuals. But our findings and previous studies (20, 30) revealed that *S. japonicum* infection induced significant changes in the compositions of gut microbiota in both mice and humans. In addition, infection of schistosomes, such as *Schistosoma mansoni* and *Schistosoma haematobium*, is associated with the shifts of gut microbiota in rodent models (21, 59) and humans (19, 41, 60–62). These studies implied that there was a strong relationship between gut microbiota features and schistosome infection-induced diseases in mammals.

Fibrosis-related *Ruminococcaceae* and *Veillonellaceae* species could be used to evaluate their effects on liver damage in mammalian NAFLD models (25). A total of 37 bacterial species, such as *Bacteroides caccae*, *Bacteroides dorei* and *Blautia* sp., were used to construct a random forest classifier model to distinguish mild/moderate NAFLD from advanced fibrosis in humans (26). In our study, a range of gut microbes was identified to distinguish the *S. japonicum* infection in mammals using the random forest classifier model, LEfSe and STAMP analysis. Importantly, we further detected the relationship between these gut bacteria and liver injuries using the Spearman correlation. In total, we found that three gut microbes including *Bacteroides*, *Blautia* and *Enterococcus* and their combinations may define as possible predictors for non-invasive detection of liver injuries of schistosomiasis in mammals (humans and mice) but not for hepatic fibrosis diseases induced by non-parasitic factors in humans, which may highlight the specificity of predicted models.

Enterotypes in the landscape of gut microbial community composition (63) show that *Bacteroides* is one of the important gut microbes to distinct community composition types termed enterotypes (42). *Enterococcus*, a gut pathobiont harboring both humans and mice, is associated with liver disease (64). In addition, *Blautia*, a genus of *Firmicutes* with potential probiotic properties that occurs widely in the feces and intestines of mammals (65), is lessened in chronic liver diseases and hepatocellular carcinoma patients (66). These studies have revealed that *Bacteroides*, *Blautia* and *Enterococcus* were significantly associated with biological aspects of humans and animals. Our findings found these gut microbes with potential predictor properties.

Furthermore, our study identified a range of gut bacterial features (*Bacteroides*, *Blautia* and *Enterococcus*) to distinguish schistosomiasis from hepatic injuries and first showed a significant correlation with the level of hepatic granulomas, fibrosis, hydroxyproline, ALT or AST in *S. japonicum* infection-

induced disease. Previous studies have revealed the association between gut microbiota and schistosomiasis (20, 29, 30), but did not show more details about the relationship between serologic detection and the level of hepatic injuries in schistosomiasis. Our findings provided more evidence for novel gut microbiota-derived features for non-invasive detection of schistosomiasis.

We acknowledged several limitations of this study. First, to distinguish the fibrosis-specific microbiome, we investigated the relationship between gut microbiota and liver fibrosis using 16S rRNA sequencing but not metagenomics as in the previous study (26). This limited our further investigation to the species level of gut microbiota. Second, although we used gut bacterial data from human individuals in the present study (30), our study lacks cross-sectional studies to allow us to further analyze the relationship between the stool microbiota and disease in schistosomiasis from humans. Nevertheless, our findings were sufficient to confirm the differences in gut microbiota changes according to hepatic injuries and revealed a range of gut microbiota features for non-invasive detection of schistosomiasis. However, it needs further study.

In total, we concluded that the gut microbiome profile changed significantly in *S. japonicum* infection-induced disease and provided preliminary evidence of an association between gut microbiota and hepatic injuries in schistosomiasis. We have described several gut microbiota features and combinations as non-invasive biomarkers for diagnosing liver injuries in mammals with *S. japonicum* infection. Further studies are needed.

DATA AVAILABILITY STATEMENT

The data presented in the study are deposited in the GenBank repository, accession number (PRJNA836144). The referenced datasets can be found in GenBank repository (accession numbers PRJNA759360 and PRJNA625383) shown in previous studies.

ETHICS STATEMENT

The experiments on participants were reviewed and approved by the Medical Research Ethics Committee of The Third Affiliated Hospital in Sun Yat-sen University ([2019]02-424-01). The patients/participants provided their written informed consent to participate in this study. The animal experiments were reviewed and approved by the Institutional Animal Care and Use Committee of Sun Yat-sen University (Permit No: 2016-104) and the Medical Research Ethics Committee of Sun Yat-sen University (SYSU-IACUC-2019-B517).

AUTHOR CONTRIBUTIONS

XYW, XS, ZDW and DL conceived and designed the study. DL and QS carried out the experiments and handled the statistical analysis. DL prepared the interpretation of the data and the original draft. DL, JL, FC and YZ critically revised the draft version of the paper. All authors contributed to the article and approved the submitted version.

FUNDING

This work was supported by the National Key R&D Program of China (Nos. 2021YFC2300800, 2021YFC2300801, 2020YFC1200100 and 2016YFC1200500), the Natural Science Foundation of Guangdong Province (Nos. 2019A1515012068, 2020A1515010896 and 2021A1515010976), the National Natural Science Foundation of China (Nos. 82161160343 and 82002168), the Fundamental Research Funds for the Central University (No. 22qntd4813), the 111 Project (No. B12003) and the 6th Nuclear Energy R&D Project (No. 20201192). The funders had no role in study design, data collection and analysis, decision to publish, or preparation of the manuscript.

SUPPLEMENTARY MATERIAL

The Supplementary Material for this article can be found online at: https://www.frontiersin.org/articles/10.3389/fimmu.2022.941530/full#supplementary-material

REFERENCES

1. Colley DG, Bustinduy AL, Secor WE, King CH. Human Schistosomiasis. *Lancet* (2014) 383:2253–64. doi: 10.1016/S0140-6736(13)61949-2
2. Hotez PJ, Brindley PJ, Bethony JM, King CH, Pearce EJ, Jacobson J. Helminth Infections: The Great Neglected Tropical Diseases. *J Clin Invest* (2008) 118:1311–21. doi: 10.1172/JCI34261
3. McManus DP, Dunne DW, Sacko M, Utzinger J, Vennervald BJ, Zhou XN. Schistosomiasis. *Nat Rev Dis Primers* (2018) 4:13. doi: 10.1038/s41572-018-0013-8
4. Lackey EK, Horrall S. Schistosomiasis. Treasure Island (FL): StatPearls Publishing (2021).
5. Verjee MA. Schistosomiasis: Still a Cause of Significant Morbidity and Mortality. *Res Rep Trop Med* (2019) 10:153–63. doi: 10.2147/RRTM.S204345
6. Zhang LJ, Xu ZM, Yang F, Dang H, Li YL, Lu S, et al. [Endemic Status of Schistosomiasis in People's Republic of China in 2020]. *Zhongguo Xue Xi Chong Bing Fang Zhi Za Zhi* (2021) 33:225–33. doi: 10.16250/j.32.1374.2021109
7. Shaker Y, Samy N, Ashour E. Hepatobiliary Schistosomiasis. *J Clin Transl Hepatol* (2014) 2:212–6. doi: 10.14218/JCTH.2014.00018
8. Wu W, Feng A, Huang Y. Research and Control of Advanced Schistosomiasis Japonica in China. *Parasitol Res* (2015) 114:17–27. doi: 10.1007/s00436-014-4225-x
9. Wu YM, Xu N, Hu JY, Xu XF, Wu WX, Gao SX, et al. A Simple Noninvasive Index to Predict Significant Liver Fibrosis in Patients With Advanced Schistosomiasis Japonica. *Parasitol Int* (2013) 62:283–8. doi: 10.1016/j.parint.2013.02.005
10. Wu YM, Xu XF, Wu WL, Wu WX, Gao SX, Zhu WJ. Correlation Between Levels of Liver Fibrosis and Liver Fibrosis Biochemical Parameters of Advanced Schistosomiasis Patients. *Zhongguo Xue Xi Chong Bing Fang Zhi Za Zhi* (2014) 26:65–6. doi: 10.16250/j.32.1374.2014.01.019
11. Liu R, Wen L. Research Progress of Advanced Schistosomiasis. *Chin J Parasitol Parasitic Dis* (2021) 39:429–36. doi: 10.12140/j.issn.1000-7423.2021.04.002

12. Cai P, Mu Y, Olveda RM, Ross AG, Olveda DU, McManus DP. Serum Exosomal Mirnas for Grading Hepatic Fibrosis Due to Schistosomiasis. *Int J Mol Sci* (2020) 21(10):3560. doi: 10.3390/ijms21103560
13. Cai P, Mu Y, Olveda RM, Ross AG, Olveda DU, McManus DP. Circulating Mirnas as Footprints for Liver Fibrosis Grading in Schistosomiasis. *Ebiomedicine* (2018) 37:334–43. doi: 10.1016/j.ebiom.2018.10.048
14. Wu S, Tseng Y, Xu N, Yin X, Xie X, Zhang L, et al. Evaluation of Transient Elastography in Assessing Liver Fibrosis in Patients With Advanced Schistosomiasis Japonica. *Parasitol Int* (2018) 67:302–8. doi: 10.1016/j.parint.2018.01.004
15. Li Y, Chen D, Ross AG, Burke ML, Yu X, Li RS, et al. Severe Hepatosplenic Schistosomiasis: Clinicopathologic Study of 102 Cases Undergoing Splenectomy. *Hum Pathol* (2011) 42:111–9. doi: 10.1016/j.humpath.2010.05.020
16. Luo L. The Value of Four Indexes of Liver Fibrosis Detection Combined With Type-B Ultrasonic Examination in the Diagnosis of Liver Fibrosis of Advanced Schistosomiasis. *J Trop Dis Parasitol* (2012) 10:147–8.
17. Moeller AH, Suzuki TA, Phifer-Rixey M, Nachman MW. Transmission Modes of the Mammalian Gut Microbiota. *Science* (2018) 362:453–7. doi: 10.1126/science.aat7164
18. Gui QF, Jin HL, Zhu F, Lu HF, Zhang Q, Xu J, et al. Gut Microbiota Signatures in Schistosoma Japonicum Infection-Induced Liver Cirrhosis Patients: A Case-Control Study. *Infect Dis Poverty* (2021) 10:43. doi: 10.1186/s40249-021-00821-8
19. Schneeberger P, Coulibaly JT, Panic G, Daubenberger C, Gueuning M, Frey JE, et al. Investigations on the Interplays Between Schistosoma Mansoni, Praziquantel and the Gut Microbiome. *Parasit Vectors* (2018) 11:168. doi: 10.1186/s13071-018-2739-2
20. Hu Y, Chen J, Xu Y, Zhou H, Huang P, Ma Y, et al. Alterations of Gut Microbiome and Metabolite Profiling in Mice Infected by Schistosoma Japonicum. *Front Immunol* (2020) 11:569727. doi: 10.3389/fimmu.2020.569727
21. Jenkins TP, Peachey LE, Ajami NJ, MacDonald AS, Hsieh MH, Brindley PJ, et al. Schistosoma Mansoni Infection Is Associated With Quantitative and Qualitative Modifications of the Mammalian Intestinal Microbiota. *Sci Rep* (2018) 8:12072. doi: 10.1038/s41598-018-30412-x
22. Cortes A, Clare S, Costain A, Almeida A, McCarthy C, Harcourt K, et al. Baseline Gut Microbiota Composition Is Associated With Schistosoma Mansoni Infection Burden in Rodent Models. *Front Immunol* (2020) 11:593838. doi: 10.3389/fimmu.2020.593838
23. Suk KT, Kim DJ. Gut Microbiota: Novel Therapeutic Target for Nonalcoholic Fatty Liver Disease. *Expert Rev Gastroenterol Hepatol* (2019) 13:193–204. doi: 10.1080/17474124.2019.1569513
24. Oikonomou T, Papatheodoridis GV, Samarkos M, Goulis I, Cholongitas E. Clinical Impact of Microbiome in Patients With Decompensated Cirrhosis. *World J Gastroenterol* (2018) 24:3813–20. doi: 10.3748/wjg.v24.i34.3813
25. Lee G, You HJ, Bajaj JS, Joo SK, Yu J, Park S, et al. Distinct Signatures of Gut Microbiome and Metabolites Associated With Significant Fibrosis in non-Obese NAFLD. *Nat Commun* (2020) 11:4982. doi: 10.1038/s41467-020-18754-5
26. Loomba R, Seguritan V, Li W, Long T, Klitgord N, Bhatt A, et al. Gut Microbiome-Based Metagenomic Signature for Non-Invasive Detection of Advanced Fibrosis in Human Nonalcoholic Fatty Liver Disease. *Cell Metab* (2017) 25:1054–62. doi: 10.1016/j.cmet.2017.04.001
27. Bajaj JS, Heuman DM, Hylemon PB, Sanyal AJ, White MB, Monteith P, et al. Altered Profile of Human Gut Microbiome Is Associated With Cirrhosis and its Complications. *J Hepatol* (2014) 60:940–7. doi: 10.1016/j.jhep.2013.12.019
28. Lin D, Zeng X, Sanogo B, He P, Xiang S, Du S, et al. The Potential Risk of Schistosoma Mansoni Transmission by the Invasive Freshwater Snail Biomphalaria Straminea in South China. *PloS Negl Trop Dis* (2020) 14:e8310. doi: 10.1371/journal.pntd.0008310
29. Lin D, Song Q, Zhang Y, Liu J, Chen F, Du S, et al. Bacillus Subtilis Attenuates Hepatic and Intestinal Injuries and Modulates Gut Microbiota and Gene Expression Profiles in Mice Infected With Schistosoma Japonicum. *Front Cell Dev Biol* (2021) 9. doi: 10.3389/fcell.2021.766205
30. Jiang Y, Yuan Z, Shen Y, Rosa BA, Martin J, Cao S, et al. Alteration of the Fecal Microbiota in Chinese Patients With Schistosoma Japonicum Infection. *Parasite* (2021) 28:1. doi: 10.1051/parasite/2020074
31. Katz N, Chaves A, Pellegrino J. A Simple Device for Quantitative Stool Thick-Smear Technique in Schistosomiasis Mansoni. *Rev Inst Med Trop Sao Paulo* (1972) 14:397–400.
32. Zeng J, Zheng J, Jin JY, Mao YJ, Guo HY, Lu MD, et al. Shear Wave Elastography for Liver Fibrosis in Chronic Hepatitis B: Adapting the Cut-Offs to Alanine Aminotransferase Levels Improves Accuracy. *EUR RADIOL* (2019) 29:857–865. doi: 10.1007/s00330-018-5621-x
33. Deng H, Wang CL, Lai J, Yu SL, Xie DY, Gao ZL. Noninvasive Diagnosis of Hepatic Steatosis Using Fat Attenuation Parameter Measured by FibroTouch and a New Algorithm in CHB Patients. *HEPAT MON* (2016) 16:e40263. doi: 10.5812/hepatmon.40263
34. Jin JY, Zheng YB, Zheng J, Liu J, Mao YJ, Chen SG, et al. 2D Shear Wave Elastography Combined With MELD Improved Prognostic Accuracy in Patients With Acute-on-Chronic Hepatitis B Liver Failure. *Eur Radiol* (2018) 28:4465–74. doi: 10.1007/s00330-018-5336-z
35. Zhou M, Yu Z, Zhang J, Hou Y, Zhao Z, Tan Q. The Value of Different Non-Invasive Examination Methods in the Diagnosis of Liver Fibrosis Induced by Chronic Hepatitis B. *China Modern Doctor* (2022) 60:127–30.
36. Caporaso JG, Kuczynski J, Stombaugh J, Bittinger K, Bushman FD, Costello EK, et al. QIIME Allows Analysis of High-Throughput Community Sequencing Data. *Nat Methods* (2010) 7:335–6. doi: 10.1038/nmeth.f.303
37. Grice EA, Kong HH, Conlan S, Deming CB, Davis J, Young AC, et al. Topographical and Temporal Diversity of the Human Skin Microbiome. *Science* (2009) 324:1190–2. doi: 10.1126/science.1171700
38. Li X, Zheng J, Ma X, Zhang B, Zhang J, Wang W, et al. The Oral Microbiome of Pregnant Women Facilitates Gestational Diabetes Discrimination. *J Genet Genomics* (2021) 48:32–9. doi: 10.1016/j.jgg.2020.11.006
39. Rhayat L, Maresca M, Nicoletti C, Perrier J, Brinch KS, Christian S, et al. Effect of Bacillus Subtilis Strains on Intestinal Barrier Function and Inflammatory Response. *Front Immunol* (2019) 10:564. doi: 10.3389/fimmu.2019.00564
40. Lei K, Li YL, Wang Y, Wen J, Wu HZ, Yu DY, et al. Effect of Dietary Supplementation of Bacillus Subtilis B10 on Biochemical and Molecular Parameters in the Serum and Liver of High-Fat Diet-Induced Obese Mice. *J Zhejiang Univ Sci B* (2015) 16:487–95. doi: 10.1631/jzus.B1400342
41. Holzscheiter M, Layland LE, Loffredo-Verde E, Mair K, Vogelmann R, Langer R, et al. Lack of Host Gut Microbiota Alters Immune Responses and Intestinal Granuloma Formation During Schistosomiasis. *Clin Exp Immunol* (2014) 175:246–57. doi: 10.1111/cei.12230
42. Arab JP, Martin-Mateos RM, Shah VH. Gut-Liver Axis, Cirrhosis and Portal Hypertension: The Chicken and the Egg. *Hepatol Int* (2018) 12:24–33. doi: 10.1007/s12072-017-9798-x
43. Acharya C, Bajaj JS. Gut Microbiota and Complications of Liver Disease. *Gastroenterol Clin North Am* (2017) 46:155–69. doi: 10.1016/j.gtc.2016.09.013
44. Zhu T, Xue Q, Liu Y, Xu Y, Xiong C, Lu J, et al. Analysis of Intestinal Microflora and Metabolites From Mice With DSS-Induced IBD Treated With Schistosoma Soluble Egg Antigen. *Front Cell Dev Biol* (2021) 9:777218. doi: 10.3389/fcell.2021.777218
45. Tang Z, Wu Z, Sun H, Zhao L, Shang M, Shi M, et al. The Storage Stability of Bacillus Subtilis Spore Displaying Cysteine Protease of Clonorchis Sinensis and Its Effect on Improving the Gut Microbiota of Mice. *Appl Microbiol Biotechnol* (2021) 105:2513–26. doi: 10.1007/s00253-021-11126-z
46. Guo W, Zhou X, Li X, Zhu Q, Peng J, Zhu B, et al. Depletion of Gut Microbiota Impairs Gut Barrier Function and Antiviral Immune Defense in the Liver. *Front Immunol* (2021) 12:636803. doi: 10.3389/fimmu.2021.636803
47. Wang J, Zhou X, Li X, Guo W, Zhu Q, Zhu B, et al. Fecal Microbiota Transplantation Alters the Outcome of Hepatitis B Virus Infection in Mice. *Front Cell Infect Microbiol* (2022) 12:844132. doi: 10.3389/fcimb.2022.844132
48. Inoue T, Nakayama J, Moriya K, Kawaratani H, Momoda R, Ito K, et al. Gut Dysbiosis Associated With Hepatitis C Virus Infection. *Clin Infect Dis* (2018) 67:869–77. doi: 10.1093/cid/ciy205
49. Wan S, Nie Y, Zhang Y, Huang C, Zhu X. Gut Microbial Dysbiosis Is Associated With Profibrotic Factors in Liver Fibrosis Mice. *Front Cell Infect Microbiol* (2020) 10:18. doi: 10.3389/fcimb.2020.00018
50. Rodriguez-Gonzalez A, Vitali F, Moya M, De Filippo C, Passani MB, Orio L. Effects of Alcohol Binge Drinking and Oleoylethanolamide Pretreatment in the Gut Microbiota. *Front Cell Infect Microbiol* (2021) 11:731910. doi: 10.3389/fcimb.2021.731910

51. Cinek O, Polackova K, Odeh R, Alassaf A, Kramna L, Ibekwe MU, et al. Blastocystis in the Faeces of Children From Six Distant Countries: Prevalence, Quantity, Subtypes and the Relation to the Gut Bacteriome. *Parasit Vectors* (2021) 14:399. doi: 10.1186/s13071-021-04859-3
52. Wang K, Zhang Z, Mo ZS, Yang XH, Lin BL, Peng L, et al. Gut Microbiota as Prognosis Markers for Patients With HBV-Related Acute-on-Chronic Liver Failure. *Gut Microbes* (2021) 13:1–15. doi: 10.1080/19490976.2021.1900996
53. Trebicka J, Bork P, Krag A, Arumugam M. Utilizing the Gut Microbiome in Decompensated Cirrhosis and Acute-on-Chronic Liver Failure. *Nat Rev Gastroenterol Hepatol* (2021) 18:167–80. doi: 10.1038/s41575-020-00376-3
54. Bajaj JS, Fagan A, Gavis EA, Kassam Z, Sikaroodi M, Gillevet PM. Long-Term Outcomes of Fecal Microbiota Transplantation in Patients With Cirrhosis. *GASTROENTEROLOGY* (2019) 156:1921–3. doi: 10.1053/j.gastro.2019.01.033
55. Suk KT, Koh H. New Perspective on Fecal Microbiota Transplantation in Liver Diseases. *J Gastroenterol Hepatol* (2022) 37:24–33. doi: 10.1111/jgh.15729
56. Madsen M, Kimer N, Bendtsen F, Petersen AM. Fecal Microbiota Transplantation in Hepatic Encephalopathy: A Systematic Review. *Scand J Gastroenterol* (2021) 56:560–9. doi: 10.1080/00365521.2021.1899277
57. Bajaj JS, Salzman NH, Acharya C, Sterling RK, White MB, Gavis EA, et al. Fecal Microbial Transplant Capsules are Safe in Hepatic Encephalopathy: A Phase 1, Randomized, Placebo-Controlled Trial. *HEPATOLOGY* (2019) 70:1690–703. doi: 10.1002/hep.30690
58. Song Q, Zhang Y, Zhang B, Liu J, Song L, Sun X, et al. Effects of Different Infection Degrees of Schistosoma Japonicum on Gut Microbiota of Mice (in Chinese). *J Trop Med* (2020) 20:303–8.
59. Zhao Y, Yang S, Li B, Li W, Wang J, Chen Z, et al. Corrigendum: Alterations of the Mice Gut Microbiome *via* Schistosoma Japonicum Ova-Induced Granuloma. *Front Microbiol* (2019) 10:747. doi: 10.3389/fmicb.2019.00747
60. Kay GL, Millard A, Sergeant MJ, Midzi N, Gwisai R, Mduluza T, et al. Differences in the Faecal Microbiome in Schistosoma Haematobium Infected Children vs. Uninfected Children. *PloS Negl Trop Dis* (2015) 9:e3861.
61. Osakunor D, Munk P, Mduluza T, Petersen TN, Brinch C, Ivens A, et al. The Gut Microbiome But Not the Resistome Is Associated With Urogenital Schistosomiasis in Preschool-Aged Children. *Commun Biol* (2020) 3:155. doi: 10.1038/s42003-020-0859-7
62. Ajibola O, Rowan AD, Ogedengbe CO, Mshelia MB, Cabral DJ, Eze AA, et al. Urogenital Schistosomiasis Is Associated With Signatures of Microbiome Dysbiosis in Nigerian Adolescents. *Sci Rep* (2019) 9:829. doi: 10.1038/s41598-018-36709-1
63. Costea PI, Hildebrand F, Arumugam M, Backhed F, Blaser MJ, Bushman FD, et al. Enterotypes in the Landscape of Gut Microbial Community Composition. *Nat Microbiol* (2018) 3:8–16. doi: 10.1038/s41564-017-0072-8
64. Manfredo VS, Hiltensperger M, Kumar V, Zegarra-Ruiz D, Dehner C, Khan N, et al. Translocation of a Gut Pathobiont Drives Autoimmunity in Mice and Humans. *Science* (2018) 359:1156–1161. doi: 10.1126/science.aar7201
65. Liu X, Mao B, Gu J, Wu J, Cui S, Wang G, et al. Blautia-a New Functional Genus With Potential Probiotic Properties? *Gut Microbes* (2021) 13:1–21. doi: 10.1080/19490976.2021.1875796
66. Chen T, Ding R, Chen X, Lu Y, Shi J, Lu Y, et al. Firmicutes and Blautia in Gut Microbiota Lessened in Chronic Liver Diseases and Hepatocellular Carcinoma Patients: A Pilot Study. *Bioengineered* (2021) 12:8233–46. doi: 10.1080/21655979.2021.1982273

Conflict of Interest: The authors declare that the research was conducted in the absence of any commercial or financial relationships that could be construed as a potential conflict of interest.

frontiers | Frontiers in Immunology

TYPE Correction
PUBLISHED 05 August 2022
DOI 10.3389/fimmu.2022.998528

OPEN ACCESS

APPROVED BY
Frontiers Editorial Office,
Frontiers Media SA, Switzerland

*CORRESPONDENCE
Datao Lin
lindt5@mail.sysu.edu.cn
Xi Sun
sunxi2@mail.sysu.edu.cn
Xiaoying Wu
wuxy227@mail.sysu.edu.cn

†These authors have contributed equally to this work

SPECIALTY SECTION
This article was submitted to Parasite Immunology, a section of the journal Frontiers in Immunology

RECEIVED 20 July 2022
ACCEPTED 21 July 2022
PUBLISHED 05 August 2022

CITATION
Lin D, Song Q, Liu J, Chen F, Zhang Y, Wu Z, Sun X and Wu X (2022) Corrigendum: Potential gut microbiota features for non-invasive detection of schistosomiasis.
Front. Immunol. 13:998528.
doi: 10.3389/fimmu.2022.998528

Corrigendum: Potential gut microbiota features for non-invasive detection of schistosomiasis

Datao Lin[1,2,3*†], Qiuyue Song[1,2,4†], Jiahua Liu[1,2], Fang Chen[5], Yishu Zhang[1,2], Zhongdao Wu[1,2,3], Xi Sun[1,2*] and Xiaoying Wu[2,6*]

[1]Department of Parasitology, Zhongshan School of Medicine, Sun Yat-sen University, Guangzhou, China, [2]Key Laboratory of Tropical Disease Control, Ministry of Education, Guangzhou, China, [3]Chinese Atomic Energy Agency Center of Excellence on Nuclear Technology Applications for Insect Control, Provincial Engineering Technology Research Center for Diseases-Vectors Control, Guangzhou, China, [4]Department of Clinical Laboratory, Xiangyang No.1 People's Hospital, Hubei University of Medicine, Xiangyang, China, [5]School of Medicine, South China University of Technology, Guangzhou, China, [6]The Third Affiliated Hospital, Sun Yat-sen University, Guangzhou, China

KEYWORDS

***Schistosoma japonicum*, schistosomiasis, parasites, gut microbiota, non-invasive**

A corrigendum on:

Potential gut microbiota features for non-invasive detection of schistosomiasis

By Lin D, Song Q, Liu J, Chen F, Zhang Y, Wu Z, Sun X and Wu X (2022) *Front. Immunol.* 13:941530. doi: 10.3389/fimmu.2022.941530

In the published article, there was an error in Figure 1 as published. The description of the Y-axis in Figure 1A was incorrectly described. The corrected Figure 1 appears below.

In the published article, there was an error in the **Funding** statement. The grant number was incorrect. The correct **Funding** statement appears below.

"This work was supported by the National Key R&D Program of China (Nos. 2021YFC2300800, 2021YFC2300801, 2020YFC1200100 and 2016YFC1200500), the Natural Science Foundation of Guangdong Province (Nos. 2019A1515012068, 2020A1515010896 and 2021A1515010976), the National Natural Science Foundation of China (Nos. 82161160343 and 82002168), the Fundamental Research Funds for the Central University (No. 22qntd4813), the 111 Project (No. B12003) and the 6th Nuclear Energy R&D Project (No. 20201192). The funders had no role in study design, data collection and analysis, decision to publish, or preparation of the manuscript".

The authors apologize for these errors and state that this does not change the scientific conclusions of the article in any way. The original article has been updated.

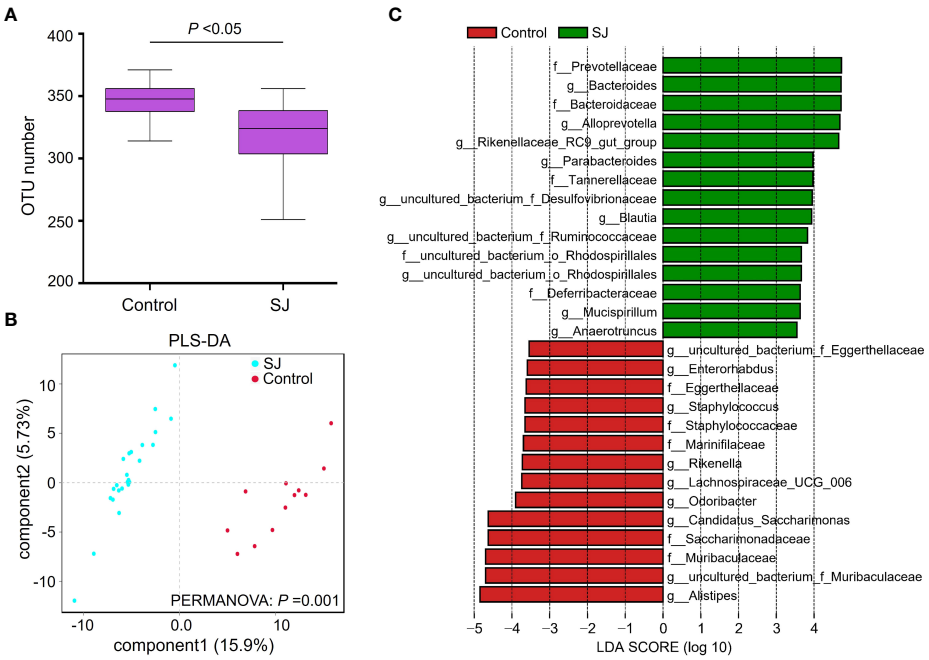

FIGURE 1
Comparisons of gut microbiota between *S. japonicum*-infected (n = 24) and uninfected (n = 12) mice. **(A)** OTUs analysis. **(B)** PLS-DA analysis. **(C)** Differential gut bacterial taxa were analyzed by LEfSe analysis with LDA score >3.5 between groups. Control: without *S. japonicum* infection mice. SJ; *S. japonicum*-infected mice. *P < 0.05 indicates significant difference.

Publisher's note

frontiers | Frontiers in Immunology

TYPE Original Research
PUBLISHED 25 August 2022
DOI 10.3389/fimmu.2022.955034

OPEN ACCESS

EDITED BY
Thiago Almeida Pereira,
Stanford University, United States

REVIEWED BY
Thiago Pereira Silva,
Juiz de Fora Federal University, Brazil
Fausto Edmundo Lima Pereira,
Vila Velha University, Brazil

*CORRESPONDENCE
Marcelo Pelajo-Machado
marcelo.pelajo@fiocruz.br

SPECIALTY SECTION
This article was submitted to Parasite Immunology, a section of the journal Frontiers in Immunology

RECEIVED 27 May 2022
ACCEPTED 08 August 2022
PUBLISHED 25 August 2022

CITATION
Francisco JS, Terra MABL, Klein GCT, Dias de Oliveira BCEP and Pelajo-Machado M (2022) The hepatic extramedullary hematopoiesis during experimental murine *Schistosomiasis mansoni*.
Front. Immunol. 13:955034.
doi: 10.3389/fimmu.2022.955034

The hepatic extramedullary hematopoiesis during experimental murine *Schistosomiasis mansoni*

Juliane Siqueira Francisco[1],
Marcia Andrea Barge Loução Terra[1],
Gabriel Couto Thurler Klein[1],
Barbara Cristina Euzebio Pereira Dias de Oliveira[1]
and Marcelo Pelajo-Machado[1,2]*

[1]Laboratory of Pathology, Instituto Oswaldo Cruz, Fiocruz, Rio de Janeiro, Brazil, [2]Brazilian National Institute of Science and Technology on Neuroimmunomodulation, Oswaldo Cruz Institute, Oswaldo Cruz Foundation, Rio de Janeiro, Brazil

Many years ago, our research group has demonstrated extramedullary hematopoiesis in the peripheral zone of murine hepatic schistosomal granulomas. In the present study, we revisit this phenomenon using new technical and conceptual approaches. Therefore, newborn mice were percutaneously infected by *Schistosoma mansoni* cercariae and euthanized between 35- and 60-days post infection. Liver samples were submitted to histopathology and immunohistochemical analyses. Cells under mitosis and/or expressing Ki67 demonstrated the proliferation of hematopoietic cells both around the parasite's eggs trapped in the liver and around hepatic vessels. After 50 days post infection, proliferating cells at different levels on differentiation were located preferentially in the peripheral zone of the granulomas, around the vessels and inside the sinusoids. The presence of acidic and sulfated glycoconjugates, reticular fibers and the absence of fibronectin characterized the microenvironment for attraction and maintenance of hematopoiesis. Some neutrophils secreted MMP9 from the earliest points of infection, indicating degradation of the extracellular matrix in regions of histolysis and a possible chemoattraction of hematopoietic stem cells to the liver. Fall-3+ cells and Sca-1+ cells indicated that early hematopoietic progenitors could be mobilized to the liver. Groups of vWF+ megakaryocytes suggest chemoattraction of these cells and/or migration, proliferation, and differentiation of very immature progenitors to this organ. The increase of blood vessels and extramedullary hematopoiesis in this environment, where markers of immature hematopoietic and endothelial cells have been identified, points to the possibility of the presence of progenitors for endothelial and hematopoietic cells in the liver during the infection. There is also the possibility of concomitant migration of

10.3389/fimmu.2022.955034

more differentiated hematopoietic progenitors, that proliferate and differentiate in the liver, and the occurrence of angiogenesis caused by inflammation or release of ovular antigens that stimulate the activation and proliferation of endothelial cells. Altogether, these data increase knowledge about a murine model that is of interest for investigating the pathology of the schistosomiasis and also the dynamics of hematopoiesis.

KEYWORDS

schistosomiasis, granuloma, hematopoietic environment, angiogenesis, extramedullary hematopoiesis

Introduction

Schistosomiasis is a parasitic disease commonly related to environment factors and underdevelopment and mainly affects tropical and subtropical areas of the planet (1). It is caused by the helminth of the Trematoda class and genus Schistosoma. The only species that occurs in Brazil is *Schistosoma mansoni*, capable of causing the severe form of the disease with hepatosplenic involvement (2).

The adult worms of *Schistosoma mansoni* inhabit portal and mesenteric veins (3), where they copulate and female initiates oviposition (4). To complete the cycle, eggs need to pass through the intestinal wall and are passed in the feces. However, the blood flow carries part of the eggs and some of them are mainly trapped in liver, spleen and intestines, and stimulate a granulomatous reaction (3).

The deposition of collagenous fibers both in the granuloma and around the vessels of the portal system is responsible for the fibrosis, the main pathological manifestation of schistosomiasis (5, 6). In schistosomal infection, this mechanism may be related to angiogenesis both during the fibrosis formation and after the end of infection, helping to resolve the fibrosis (7, 8).

When mature, hepatic granulomas have three zones: the central, essentially macrophagic; the medial, which is rich in extracellular matrix; and the peripheral, where the arrangement of collagen fibers forms a loose network which harbors extramedullary hematopoiesis (9). This proliferation of hematopoietic cells outside the bone marrow can be observed under physiological and other pathological conditions. In the first case, it is usually related to hematopoietic sites that occur during embryonic development of most vertebrate (10, 11). In the second one, extramedullary hematopoiesis is frequently observed in the spleen and liver of individuals with hematological diseases, such as thalassemia and sickle cell anemia, and infectious diseases, such as some disorders caused by bacteria and murine schistosomiasis mansoni (12–14). Many years ago, some studies, including one from our research group, described the occurrence of extramedullary hematopoiesis in the peripheral zone of hepatic granulomas (15). There, we showed islands of hematopoiesis in the periphery of granulomas, composed by cells of the same myeloid lineage and in different stages of development, together with some mitotic figures, using histopathology and brighfield microscopy techniques (15). Here, we revisit the topic of hepatic extramedullary hematopoiesis in murine schistosomiasis mansoni, using current histology, immunohistology and microscopy tools, and interpreting their findings in light of modern concepts about hematopoiesis and its correlation with angiogenesis.

Materials and methods

Infection

The study was reviewed and approved by the Institutional Ethics Committee for Animal Research of the Oswaldo Cruz Institute (CEUA IOC, license: L-2/13). Five-day-old male Swiss Webster mice were infected by percutaneous exposure to 70 cercariae of the Belo Horizonte strain of *S. mansoni*. Four infected animals were euthanized at 35, 40-, 45-, 50- and 60-days post infection (dpi), along with two control animals. The infection was confirmed by searching schistosoma eggs in the feces of the rodents by Hoffman parasitological technique. The euthanasia was performed by initial administration intraperitoneal injection of Ketamine-Xylazine (120mg/kg and 20mg/kg) and subsequently after finding the loss of the foot reflex, the application was performed injection of 2.5% sodium thiopental (300mg/kg). The experiments were carried out in triplicate.

Paraffin sections and histological stains

Four fragments from different liver lobes with approximately 3mm thick were collected and fixed in Carson's Formalin-Millonig (16) for 48 hours at room temperature, washed and processing

according to standard histological techniques for paraffin embedding. Sections of 5 µm thick (one/block) were obtained from paraffin blocks and stained with hematoxylin-eosin, Gomori's reticulin, Picrosirius (17), Sirius red pH 10,2 (18), and Alcian Blue pH1,0. The slides were analyzed by brightfield microscopy using a Axioscope microscope (Zeiss, Germany) equipped with a Axiocam HRc camera (Zeiss, Germany).

Frozen sections

Another four fragments from different liver lobes with approximately 3mm thick were collected and cryopreserved in OCT compound (Tissue Tek) and kept at -20°C. Sections of 5 µm thick were obtained in a cryostat at -20°C and stored at the same temperature.

Immunofluorescence assay

At least two hours after being obtained, slides from paraffin blocks were deparaffinized, hydrated, washed, and hydrated in PBS. Antigen retrieval was performed in citrate buffer pH 6.0, in Pascal Chamber (Dako, USA) according to the manufacturer's recommendations. In some cases, slides were incubated with blocking solution (2% skim powdered milk, 2.5% bovine serum albumin (Sigma, cat. A2153-100G) and 8% fetal bovine serum (Hyclone, cat. SH30088.03)) in a humid chamber for 30 min at room temperature, washed with PBS and then kept overnight with the following primary antibodies: Von Willebrand Factor (vWF, Cell Marque, cat. 250A -15), CD31 (Abcam, cat. ab28364), Fall 3 (Pharmingen, cat. 01581), VEGF (ThermoFisher, cat. RB-9031-P1), Lyve1 (Abcam, cat. ab17917), Sca-1 (Abcam, cat. ab25031), MMP9 (Abcam, cat. ab38898), Fibronectin (Abcam, cat. ab2413), and Ki67 (Abcam, cat. ab15580).

The slides were further incubated with the 1:750 secondary antibody Alexa Fluor 488 goat anti-rabbit IgG, or Alexa Fluor 594 goat anti-mouse IgG for 1h at 37°C, washed, stained with 1:10,000 Evans Blue, counterstained with 1:5,000 DAPI (ThermoFisher, cat. 03571) and mounted with ProlongGold (ThermoFisher, cat. P36934).

Slides from frozen sections were fixed in acetone at -20°C for 15 min and allowed to dry at room temperature for 15 min. They were washed in PBS and incubated with the blocking solution previously described for 40 min, and then proceeded for the antibodies incubation as described.

The slides prepared for immunofluorescence were analyzed on a LSM 710 confocal microscope (Zeiss, Germany).

Results

Morphological evolution of liver lesions

The oviposition of the adult worm starts around the thirtieth day of infection and continues during all the life of the adult worm. At 35 dpi, it was possible to identify an average of three units of parasite eggs per histological section in the liver. These eggs had a small inflammatory infiltrate located between the hepatocytes and the blood vessel wall and were composed mainly of macrophages and eosinophils (Figure 1A). With the development of the infection, at 40 dpi, there was an increase in the number of cells that made up the inflammatory infiltrate around the egg. These inflammatory cells, in some cases, were located between necrotic hepatocytes (Figure 1B). At 45 days of infection, it was possible to observe some monocytes and eosinophils in the region closest to the egg. Around this area there were some elongated cells among extracellular matrix. At this point, although the granulomas were still immature (Figure 1C).

The first mature granulomas, with central, medial, and peripheral zones, were found at 50 and 60 dpi. At this time, the granulomas that had this conformation showed proliferation of hematopoietic cells in the peripheral zone. The zone of extramedullary hematopoiesis was composed of cells of the myeloid lineage, mainly eosinophils, neutrophils and monocytes, in different stages of maturation (Figures 1D, E).

The largest hepatic vessels, such as central vein, portal vein and portal arteriole, without a parasitic element nearby, also had inflammatory infiltrates around them. From 35 dpi, cells of the myeloid lineage located between the vessel wall and the hepatocytes were observed. At 40 dpi there was an increase in the amount of surrounding inflammatory cells, with the presence of eosinophils, neutrophils, and monocytes (Figure 2A). Cells in mitosis were observed in the periphery of these vessels at 45 days of infection (Figure 2B). The structural organization of the distribution of hematopoietic cells around the vessels is similar to that of the previous points of infection. The main difference is the increase in more immature myeloid cells and in mitosis.

The morphological description of the liver lesions during schistosomal infection pointed to the evolution of the granulomatous structure over the days of infection with definition in three zones, the identification of the peripheral zone of mature granulomas and the periphery of the large vessels as favorable regions for the establishment and maintenance of extramedullary hematopoiesis. The proliferation of hematopoietic cells in these regions has been described from the frequently observed mitoses. Considering the ephemerality of cell division in these cases, it was important to associate other techniques for identifying proliferating cells to improve the topographical and kinetic description of hepatic extramedullary hematopoiesis during schistosomal infection.

Identification of proliferating cells

Ki67 immunostaining was used to confirm the data on cell proliferation, obtained by the analysis of mitotic cells, mainly

10.3389/fimmu.2022.955034

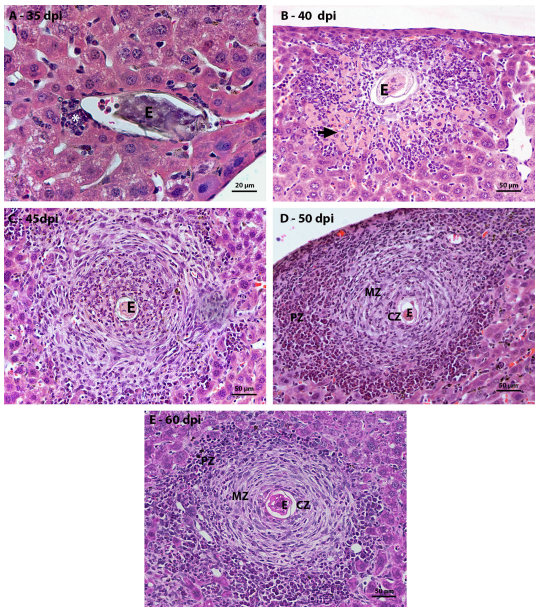

FIGURE 1
Figure 1 Evolution of hepatic granulomatous lesions over the days of infection. HE-stained sections demonstrate: **(A)** a small inflammatory infiltrate (*) composed of eosinophils and macrophages around the egg **(E)** at 35 dpi; **(B)** inflammatory infiltrate (*) greater than that observed at the previous point of infection, located between the necrotic hepatocytes (arrow) around the egg (O); **(C)** Larger granuloma with deposition of fibrous extracellular material, but still disorganized at 45 dpi; (**D**, **E**) Granulomatous lesion found in the acute phase of infection, at 50 and 60 dpi, is organized into three zones – central (CZ), medial (MZ) and peripheral (PZ), with proliferation of hematopoietic cells in the peripheral zone. Bars, A: 20 µm, B – E: 50 µm.

hematopoietic. At 35 dpi, Ki67 positive myeloid cells were found within sinusoids in a region near to a hepatic vessel (Figure 3A). At 40 and 45 dpi, there was an increase in the number of hematopoietic cells expressing Ki67, especially at 45 dpi. These cells were present in the periphery of large vessels, inside granulomas and within sinusoids and belonged mainly to neutrophilic and monocytic lineages (Figures 3B, C; Figures 4A, B). At 50 and 60 dpi, there were cells of monocytic, neutrophilic and eosinophilic lineages positive for Ki67 around large vessels, as well as within sinusoids and granulomas. In the latter case, the location of the cells was restricted to the peripheral zone (Figure 3D; Figures 4C–F).

Thus, it was possible to observe that the location of proliferating hematopoietic cells in the murine schistosomal liver varies according to liver lesions. During the acute phase the proliferating cells are almost restricted to the peripheral zone of the granulomas, around the large vessels and within some sinusoids (Figure 5).

Extracellular matrix elements associated with extramedullary hematopoiesis

In order to characterize the microenvironment favorable to this event, it was important to investigate the stroma of these regions, with special attention to some extracellular matrix elements. Considering the fibrosis present in the disease and the importance of collagen fibers for the organizational structure of the granuloma, picrosirius staining and Gomori's Reticulin histochemistry were performed. In both analyses, it was possible to observe the uniform distribution of fibers throughout the immature granuloma (Figures 6A, C) and the contribution of these structures to the organization of the mature granuloma into three zones. In the peripheral zone of mature granulomas, these reticular or collagen fibers were arranged in a loose-mesh-like that surrounded groups of hematopoietic cells forming small compartments (Figures 6B, D). The analysis of the large vessels that had surrounding hematopoietic cells also showed the presence of these compartments formed by collagen fibers. However, in this case, there was no difference in the perivascular structural organization between 45 and 60 dpi (Figures 7A–D).

Alcian Blue staining pointed to the presence of acidic and sulfated glycoconjugates. They were identified in the full-length immature granulomas (Figure 6E). In the periphery of the large vessels, both in the earliest points (Figure 7E) and in the acute phase of the disease (Figure 7F), staining was absent among the hematopoietic cells. The absence of staining was also identified in the peripheral zone of mature granulomas (Figure 6F). Fibronectin expression showed a morphological pattern similar to the presence of sulfated acid glycoconjugates. The molecule was immuno-identified in the entire extension of the early granulomas (Figure 6G) and absent among the hematopoietic cells that surrounded the great vessels throughout all times of infection (Figures 7G, H) and in the peripheral zone of the mature granulomas (Figure 6H).

The microenvironment favorable to the maintenance of hematopoietic cell proliferation seems then to be dependent on the formation of compartments delimited by collagenous fibers and independent of sulfated acid glycoconjugates and fibronectin.

Extracellular matrix remodeling and possible chemoattraction of hematopoietic cells

Immunostaining identified metalloproteinase 9 (MMP9) in neutrophils present among necrotic hepatocytes at the first points of infection (Figure 8A). In granulomas, cells immunoreactive for this molecule were preferentially located

10.3389/fimmu.2022.955034

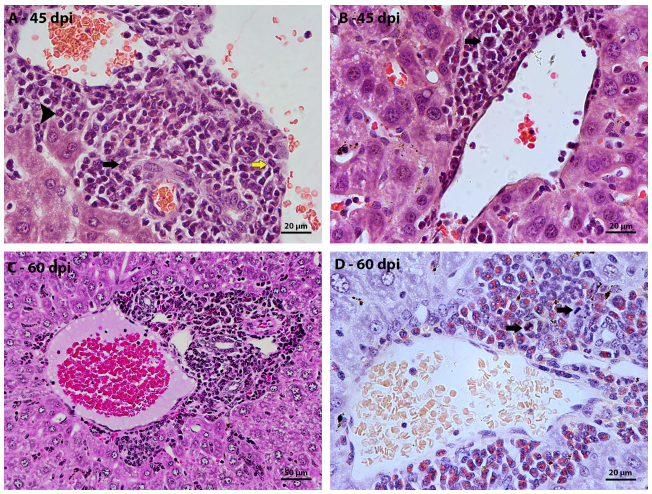

FIGURE 2
Morphological aspect of hepatic perivascular lesions in mice infected with *S. mansoni*. HE-stained sections demonstrate: (**A**) Inflammatory infiltrate composed of myeloid cells, eosinophils (arrowhead), macrophage cells (yellow arrow) and neutrophils (black arrow) in the hepatic portal space of mice at 40 dpi. **(B)** hematopoietic cells of the myeloid lineage, highlighting a cell in mitosis (arrow), in the periphery of a vein at 45 dpi; **(C)** Hepatic portal space with many mature and immature hematopoietic cells at 60 dpi; and **(D)** highlighting cells in mitosis (arrow) in the periphery of vessels in the hepatic portal space at 60 dpi. Bars, **(A, B, D)** 20 µm, **(C)** 50 µm.

in the peripheral zone, forming small groups at the interface with hepatocytes (Figures 8B–D). In the periphery of the vessels with surrounding hematopoietic cells, the neutrophils positive for the molecule did not form clusters but were arranged in a dispersed manner (Figures 9A, B).

The organization of the granuloma structure seems to favor the presence of clusters of cells that express MMP9 and this does not occur in the periphery of the great vessels.

Identification of immature hematopoietic cells in the liver

Considering the possibility of mobilization of immature hematopoietic cells from the bone marrow to the liver, the degree of maturation in which the hematopoietic cells from the periphery of the granulomas and the great vessels presented was investigated. During the labeling of Fall-3, the analysis identified groups of hematopoietic cells close to large vessels and in the periphery of the granulomas with characteristics of immature hematopoietic cells. These cells had loose chromatin, protruding nucleolus, and larger size (Figures 10A–C).

Some isolated cells were found in the periphery of mature granulomas expressing Sca-1, indicating the presence of immature cells in this region. In addition, some blood vessels, including intragranulomatous ones, also expressed the molecule.

Phenotypic characteristics provided by morphological analyzes and the identification of the expression of a molecule present only in more immature hematopoietic cells suggest the migration of immature hematopoietic cells, which establish and proliferate in the schistosomal liver.

Phenotypic analysis of hepatic blood vessels

Immunoreactivity to vWF was present in some rare sinusoids, in portal and central veins when they were associated with the parasite egg, or with surrounding inflammatory infiltrates (Figures 11A, B, D, E) and, in some cases, in wide-lumen blood vessels present in the peripheral zone of mature granulomas (Figure 11E). In addition, vWF is also capable of identifying megakaryocytes. These cells were found between hepatocytes, close to the periphery of the granuloma (Figures 11A, C) or around large vessels with surrounding hematopoietic cells (Figure 11D), at all points of infection analyzed. In some cases, these cells were present in more than one unit per field.

The analysis of immunostaining by CD31 in mature hepatic granulomas showed blood vessels present between the middle and peripheral zones, and others, very characteristic for having a wide lumen, in the peripheral zone (Figures 12B). These vessels were not identified in samples from points of infection with earlier granulomas (Figure 12A). The expression of Lyve-1 in some vessels present in the peripheral zone of mature granulomas suggests the appearance of vessels in this region (Figures 12C, D).

10.3389/fimmu.2022.955034

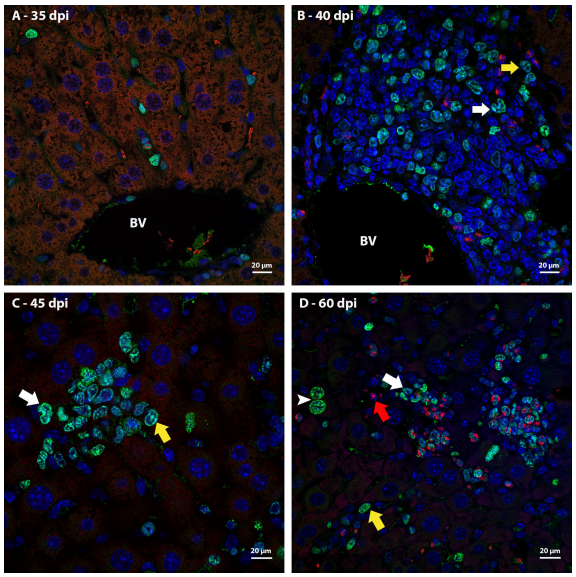

FIGURE 3
Localization of proliferating cells in the periphery of blood vessels in the liver by Ki67 labeling. **(A)** Some Ki67-positive cells are seen into the sinusoids at 35dpi; **(B)** cells of the neutrocytic (white arrow) and monocytic (yellow arrow) lineage that express Ki67 are located among other myeloid cells around a blood vessel at 40 dpi; **(C)** Ki67-positive neutrophils (white arrow) and monocytes (yellow arrow) within a sinusoid at 45 dpi; **(D)** cells of the eosinophilic (red arrow), neutrocytic (white arrow) and monocytic lineages (yellow arrow) in different stages of differentiation that expressing Ki67 are located inside of sinusoid at 60 dpi. At this point of infection also is possible to observe some hepatocytes expressing the molecule which indicates cell proliferation (arrowhead). Bar: 20 µm. Blue: DAPI, Red: Evan's blue, Green: Ki67.

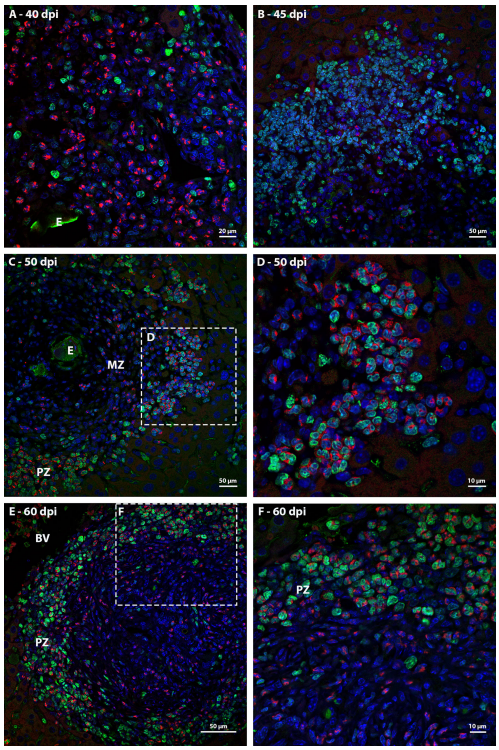

FIGURE 4
Localization of proliferating cells in schistosomal granuloma in the liver by Ki67 labeling. **(A)** Cells of the neutrocytic and monocytic lineage which express Ki67 are arranged among the other inflammatory cells that form the 40-day infection granuloma **(B)** A greater number of hematopoietic cells, mainly of the neutrocytic and monocytic lineage, are stained with Ki67 and are concentrated in the periphery of the granuloma at 45 dpi; **(C, D)** At 50 dpi in addition to cells of the monocytic and neutrocytic lineages, cells of the eosinophilic lineage expressing Ki67 are also observed. These cells are in the peripheral zone of the mature granuloma; **(E, F)** The proliferate Ki67-labeling hematopoietic cells are localized in the peripheral zone of granuloma at 60 dpi, as was observed in the previous point of infection analyzed. Bars, **(A)** 20 µm, **(B, C, E)** 50 µm, **(D, F)** 10 µm. Blue: DAPI, Red: Evan's blue, Green: Ki67.

In the schistosomal liver, there are vessels with activated endothelium that express vWF, in addition to the appearance of new vessels in the middle and peripheral zones of mature granulomas. Some of them are immunoreactive to lymphatic vessel markers.

Discussion

This work confirmed the occurrence of extramedullary hematopoiesis during the schistosomal infection and demonstrated the localization of the proliferating myeloid cells in the liver. We point to some phenotypic characteristics of the hematopoietic cells located in proliferating areas and produced other data, such as the distribution of extracellular matrix compounds, which can help to understand the process of attraction, establishment and maintenance of hepatic extramedullary hematopoiesis. Also, it was identified increase in the quantity of blood vessels, which can be stimulated both directly by the parasite and by mechanisms that have intersection with extramedullary hematopoiesis.

It was identified extramedullary hematopoiesis in the liver of mice infected by *S. mansoni*, as previously observed by Lenzi et al. (15). Using light microscopy, these authors detected myeloid cells in mitosis, mainly in the peripheral zone of granuloma, beginning at the 40th day of infection. Here, we identified myeloid cells in mitosis both in the granuloma and around of large hepatic blood vessels and, to improve the location of the proliferating cells we used immunolabeling for Ki67, which showed proliferating myeloid cells inside the sinusoids since 35 dpi. It can indicate that some inflammatory cells which are attracted to schistosomal liver arrive in this organ in

10.3389/fimmu.2022.955034

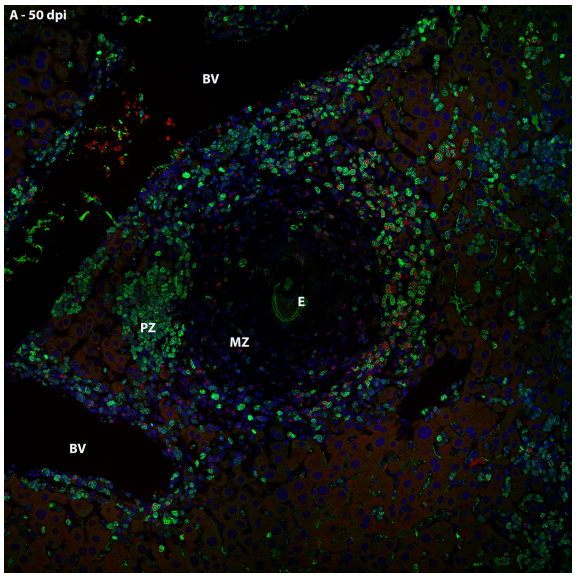

FIGURE 5
General localization of proliferating cells of murine schistosomal liver by Ki67 labeling, during acute phase of the disease. A Hematopoietic cells proliferating in the schistosomal liver of mice are mainly and almost restrictedly located in the periphery of the large vessels, inside some sinusoids and in the peripheral zone of mature granulomas. E, Egg; BV, Blood Vessel; MZ, Medial Zone; PZ, Peripheral Zone. Blue, DAPI; Red, Evan's blue; Green, Ki67.

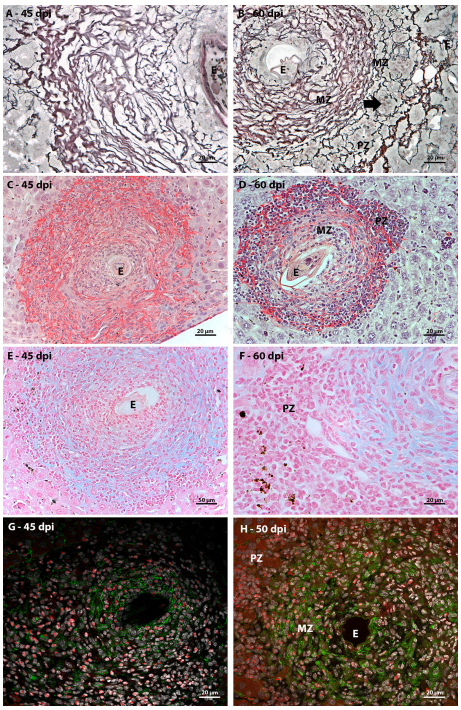

FIGURE 6
Extracellular matrix elements found in hepatic schistosomal granuloma. **(A)** Reticular fibers, highlighted in black by Gomori's reticulin staining, extend throughout the immature granuloma; **(B)** The reticular fibers, evidenced by Gomori's reticulin staining, in the 60 dpi granuloma form a looser mesh-like in the peripheral zone (PZ) of the granuloma, forming compartments (arrow) that house hematopoietic; **(C)** Types I and III collagen fibers are evidenced by Sirius red staining and are present among most of the cells that are part of the granuloma of 45 dpi, with the exception of the closest to the egg **(E)**; **(D)**The collagenous fibers identified by Sirius red staining present in the mature granuloma have the conformation of a network with the looser weft in the peripheral zone (PZ) of the structure. In this region, these thin fibers form small compartments that house isolated hematopoietic cells or in small groups; **(E)** Sulfated acid glycoconjugates can be identified by Alcian Blue staining in the full extent of immature granulomas; **(F)** Alcian blue staining is concentrated in medial zone and is absent in the peripheral zone of mature granulomas; **(G)** In immature granuloma, fibronectin expression occurs more concentrated in the region closest to the egg and more diffused among cells that are distant from the parasitic element; **(H)** Fibronectin expression in mature granuloma can be seen in the medial zone (MD) and is absent in the peripheral zone (PZ). Bars **(C–E)**: 50 µm, **(A, B, F, G, H)** 20 µm. Stains: **(A, B)** Alcian Blue pH 1,0, **(C, D)** Picrosirius, **(E, F)** Gomori's Reticulin. **(G, H)** White: DAPI, Red: Evan's blue, Green: Fibronectin.

proliferation shortly after the start of oviposition, that happens around the 30th day post infection (2). On the other hand, it is possible to suggest that presence of parasite, or the release of soluble eggs antigens (SEA), induces the activation of hepatic resident inflammatory cells, such as Kupffer cells. Although it was previously considered that Kupffer cells are derived from bone marrow HSC, they are actually originated from macrophage progenitors that come from yolk sac and persist in some organs during the adult phase, such as liver. These macrophage progenitors can be responsible for the local proliferation of the Kupffer cells in some cases, like inflammatory events (19, 20).

The proliferating cells which were labelled by Ki67 in granulomas have the distribution pattern related to evolution of each granuloma, that starts in disorganized immature form, the pre-granulomatous exudative stage, and evolute to a mature granuloma, which is in the exudative-productive stage (21). The last is characterized by three well defined zones: central, middle, and peripheral (9). During the exudative-productive stage, the Ki67-positive cells were almost restricted to the peripheral zone of granulomas, while on the immature ones these cells were distributed in a disorganized way around the parasite eggs, as observed by Lenzi et al. (15).

In addition to cellular proliferation in the peripheral zone of granulomas, it was also identified proliferating cells around blood vessels of portal spaces, central veins, and some sinusoids. The myeloid proliferation in these regions resembles the observed in the fetal liver of mice during the embryonic development. Between the 15th and 17th days post coitus occurs a peak in the eosinophilic and neutrophilic lineages production located under the hepatic capsule and around the portal veins,

10.3389/fimmu.2022.955034

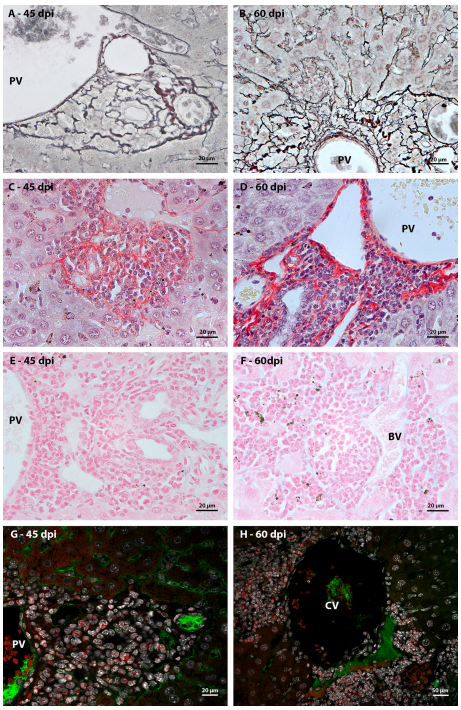

FIGURE 7
Extracellular matrix elements found at the periphery of large hepatic vessels during *Schistosoma mansoni* infection. **(A, B)** the arrangement of reticular fibers, highlighted by Gomori's reticulin, was resembling to the observed in samples stained by picrosirius in both of point of infection; **(C)**, **(D)** At different times of infection, types I and III collagen fibers, identified by picrosirius, are arranged in a similar morphology among the hematopoietic cells that surround the large hepatic vessels. They form compartments like those seen in the periphery of mature granulomas, which harbor groups of hematopoietic cells; **(E)** Absence of Alcian Blue staining, which identifies sulfated acid glycoconjugates, among hematopoietic cells present in the periphery of large hepatic blood vessels (BV), such as portal veins (PV), at earlier points of infection; **(F)** and during the acute phase of the disease; **(G, H)** Anti-fibronectin immunostaining did not identify the expression of the molecule among the hematopoietic cells that surrounded the hepatic blood vessels at the two points of infection (45 and 60 dpi). Bars, **(A–G)** 20 µm, **(H)** 50 µm. Stains: **(A, B)** Alcian Blue pH 1,0, **(C, D)** Picrosirius, **(E, F)** Gomori's Reticulin. **(G, H)** White: DAPI, Red: Evan's blue, Green: Fibronectin.

places where there is mesenchymal stroma (22). In opposite of what is found in mature granulomas, the distribution of proliferating cells around the hepatic blood vessels has the same aspect since the start of the oviposition. This can indicate difference in the modulation of cell proliferation in these two areas.

The extramedullary hematopoiesis described here is different from the observed in hematological disorders and in massive hepatic necrosis, hepatocarcinoma and in adenoma. In these last diseases there is erythroid proliferation among hepatocytes, which provide a endoderm-derived stroma (14, 23) while in murine schistosomiasis it was detected myeloid proliferation in microenvironments with elements of mesenchymal origin.

Hepatic schistosomal granulomas have collagen fibers and it is one of the causes of the hepatic fibrosis in the schistosomiasis (24). In mature granulomas, collagen fibers are present in a great concentration in medial zone and show a loose-mesh-like aspect in peripheral zone. Usually, these compartments were filled with cellular clusters of the same hematopoietic lineages, mainly neutrophilic, monocytic or eosinophilic ones. These data led us to consider the possibility of clonal expansion in these regions.

Although fibronectin is a structural molecule expressed by osteoblasts, pericytes and endothelial cells in bone marrow (25), with many functions in hematopoiesis such as migration, homing (26), retention (27), differentiation, and cell proliferation (28), it was not detected by immunofluorescence both in peripheral zone of the granulomas and among the hematopoietic cells around large vessels. The proliferation of myeloid cells around large vessels with presence of reticular fibers and absence of fibronectin also was observed by Ayres-Silva et al. in mice fetal liver (22). In some cases, such as hematological diseases, the adult liver can support extramedullary hematopoiesis. Some authors suggest that this mechanism happens due to hypoxia and a possible reactivation of hematopoietic stem cell (HSC) niche of the fetal liver (14, 29).

Heparan sulfate is an important glycoconjugate which can participate of regulation of retention and proliferation of HSC, through the link to SDF-1 by endothelial cells and osteoblasts (30). Alvarez-Silva and Borojevic identified heparan sulfate secreted by cells isolated from murine hepatic schistosomal granulomas, which could interact with growth factors *in vitro*, such as G-CSF, and act like a myelopoietic stroma (31). However, our data showed the absence of the sulfated and acid glycoconjugates in regions of hematopoietic proliferation in the schistosomal liver, although it is present in medial zone of granuloma. This led us to suggest that the cells isolated by Alvarez-Silva and Borojevic were from medial zone of granuloma and the extramedullary hematopoiesis which happens in the peripheral zone of granuloma is independent of sulfated and acid glycoconjugates, at least by direct cell-matrix interactions.

MMP9 is a metalloproteinase involved in tissue remodeling through wide-spectrum extracellular matrix degradation, which can occur under pathological or physiological conditions (32). At 35 dpi, MMP9 was expressed by neutrophils inside sinusoids or in areas of necrosis, indicating their participation in the initial histolysis in the liver caused by the arrival of the parasite eggs. Inside the granulomas, at 50 and 60 dpi, the MMP9-positive neutrophils were located along the peripheral zone. In addition to acting in the remodeling of the extracellular matrix, Kawai et al. showed that this molecule can act as chemoattractant of hematopoietic cells Lin^- in liver damage. The mechanism involves an expression enhancement of CXCR4 and its ligand,

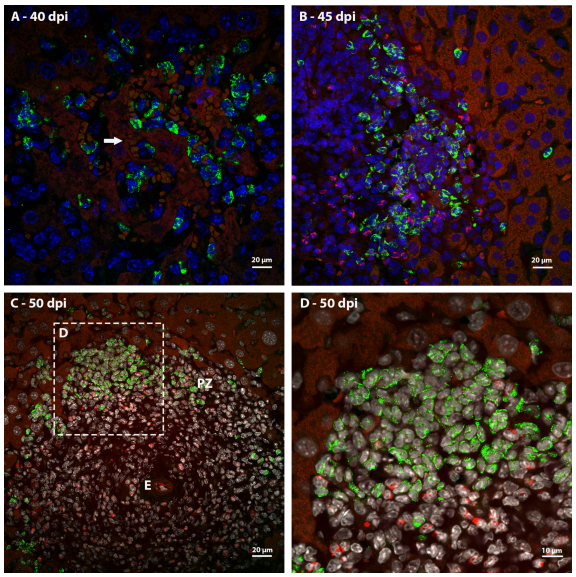

FIGURE 8
Identification of expression of MMP9 in murine liver granulomas by immunofluorescence. **(A)** Neutrophils expressing MMP9 were immunolabeling in an inflammatory infiltrate between necrotic hepatocytes (arrow) at 40 dpi; **(B)** The expression of MMP9 in granulomas found in mice at 45 dpi was concentrated in neutrophils located in de periphery of structure; **(C, D)** Neutrophils at different points of infection express MMP9 preferentially in the peripheral zone of mature granulomas at 50 dpi. Bars, **(A–C)** 20 µm, **(D)** 10 µm. DAPI: blue **(A, B)**, white **(C, D)**, Evan's blue: red, MMP9: green.

SDF-1, which is found in a concentration gradient towards the organ (33). Considering the liver damage caused by schistosomal infection, it is possible that MMP9 also can attract immature hematopoietic cells to cellular proliferation regions, especially in the periphery of granulomas.

In addition to extramedullary hematopoiesis, schistosomal infection may promotes angiogenesis in the liver, as previously reported (7, 8, 34). We confirmed the increase in the number of blood vessels in mature granulomas using the immunolabeling by CD31 molecules. Usually, angiogenesis in schistosomal liver can be associated to hypoxia caused by granulomatous and periportal fibrosis. The generation of vessels caused by hypoxia can be related to expression of HIF, which could stimulate the release of VEGF and promotes the proliferation of endothelial cells (35, 36). Also, it has already been demonstrated that SEA regulates positivity the expression of VEGF (37) and consequently promotes the endothelial proliferation and angiogenesis (38). Furthermore, we identified lymphatic vessels in the peripheral zone of mature granulomas, by immunofluorescence for LYVE-1. This hyaluronan receptor is mainly expressed in lymphatic vessels and can be involved in process of lymphangiogenesis (39, 40).

Although vWF is normally present by endothelial cells, there is a differential expression in different organs (41). Our data showed some blood vessels expressing vWF, mainly large vessels and sinusoids associated to hematopoietic cells. Previous studies have shown that the absence of vWF can lead to endothelial cell proliferation in two ways: 1) vWF participates in formation of Weibel-Palade bodies, which store Angiopoietin-2 (Ang-2). So, in the absence of vWF, Ang-2 links to Tie-2 and act synergically to VEGFR2, promoting angiogenesis; 2) the absence of vWF decrease the expression of αvβ3 and it leads to increase the quantity of membrane VEGFR2, promoting angiogenesis (41–

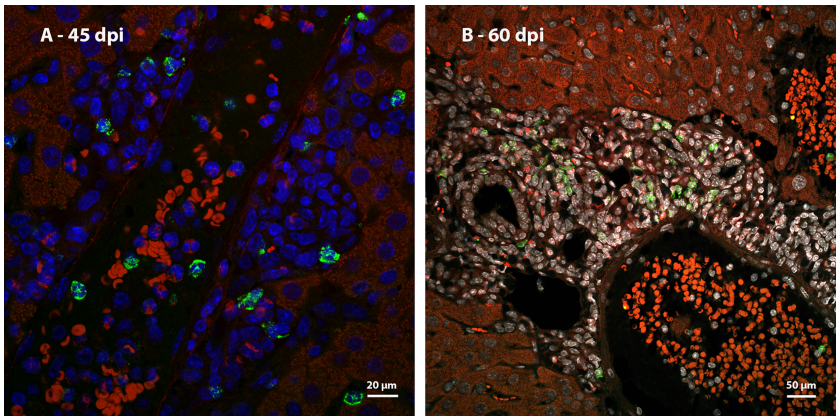

FIGURE 9
Identification of expression of MMP9 in the periphery of large blood vessels in mice infected by *S. mansoni* by immunofluorescence. **(A)** Some neutrophils expressing MMP9 are arranged randomly among others hematopoietic cells in the periphery of a vessel with no apparent parasitic element at 45 dpi and **(B)** 60 dpi. Bars, **(A)** 20 µm, **(B)** 50 µm. DAPI: blue **(A)**, white **(B)**, Evan's blue: red, MMP9: green.

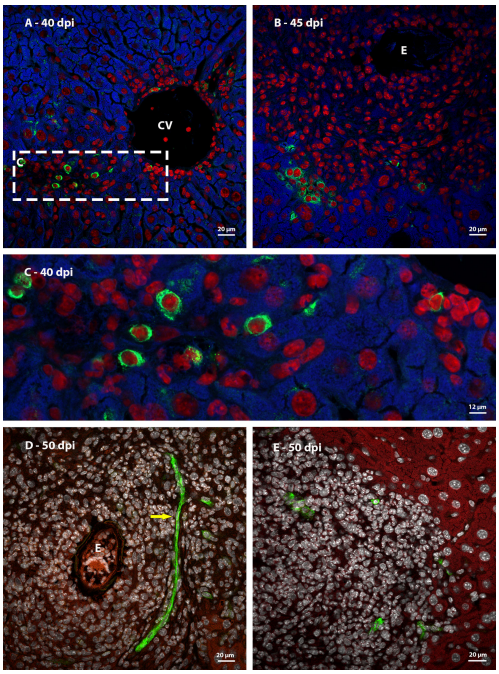

FIGURE 10
Identification of immature hematopoietic cells by immunofluorescence in livers of mice infected by *S. mansoni*. **(A, C)** Fall 3 immunostaining identified cells with characteristics of immature hematopoietic cells (loose chromatin and protruding nucleolus) close to a central vein (CV); **(B)** These cells Fall 3-positives also were found in the periphery of 45 dpi granuloma; **(D, E)** The immunostaining identified the expression of Sca-1 in a blood vessel (arrow) placed on medial zone some cells located in the peripheral zone of 50 dpi granuloma. Bars **(A, B, D, E)** 20 µm, C: 12 µm DAPI: red **(A–C)**, white **(D, E)**, Evan's blue: blue **(A–C)** and red **(D, E)**, Fall 3: green **(A–C)**, Sca-1: green **(D, E)**.

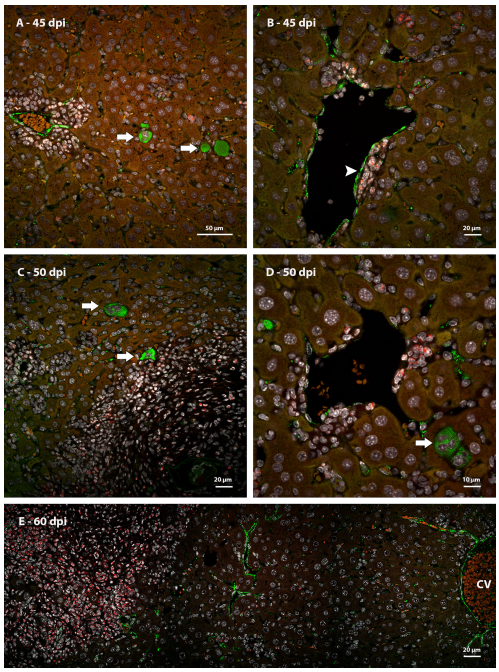

FIGURE 11
Expression of vWF in livers of mice infected by *S. mansoni*, identified by immunofluorescence. **(A)** Detection of more than one megakaryocyte among the hepatocytes in the same area of analysis at 45 dpi; **(B)** Blood vessel vWF-positive with inflammatory cells in the periphery situated between the endothelium and the hepatocytes at 45 dpi; **(C)** **(C)** Megakaryocytes (arrow) are still found in the liver of infected animals during the acute phase of the disease, close to the peripheral zone of the granulomas, but still in contact with hepatocytes, **(D)** and close to a vessel with surrounding hematopoietic cells at 50 dpi; **(E)** central vein (CV), vessels associated with the periphery of the granuloma and some sinusoids express the protein at 60 dpi. Bars, **A**: 50 µm, **(B, C, E)** 20 µm, D: 10 µm. DAPI: white, Evan's blue: red, vWF: green.

43). Based on this data, we suggest that angiogenesis possibly occur manly from some sinusoids which do not express vWF.

In addition to blood vessels, vWF is classically described as a molecule which also identifies cells of the megakaryocytic lineage (44). In addition to the increase of proliferating myeloid cells, the murine schistosomal liver also showed an apparent increase in cells of the megakaryocytic lineage. More than one megakaryocyte was frequently seen together, leading us to consider the possibility of local proliferation. To explain this phenomenon, we suggest two possibilities: 1) Chemoattraction of megakaryocytic progenitors to the schistosomal liver, which find favorable microenvironment to proliferate and differentiate; 2) Attraction of undifferentiated HSC or HSPC, which can differentiate both in other hematopoietic cells and directly in megakaryocytic progenitors or megakaryocytes. The second hypothesis is based on the holocracy theory of hematopoiesis, in which HSC could be capable of differentiate into restrict hematopoietic progenitors, such as Common myeloid progenitor (CMP), Megakaryocyte Erythroid Progenitor (MEP) and Megakaryocyte Progenitor (MkP) (45, 46). Some LT-HSC (Long Term Hematopoietic Stem Cell) which express vWF were stimulated with thrombopoietin and could be capable of maintaining the production of megakaryocytes and platelets for long term (47).

Considering the possibility of the arrival of immature hematopoietic cells to the liver, analyzes were performed to identify Sca-1 expressing cells. This molecule is used as a marker of immature hematopoietic cells and can be present in LT-HSC, ST-HSC (Short Term Hematopoietic Stem Cell) and MMP (Multipotent Progenitor) (48). In this work, we identified hematopoietic cells expressing Sca-1 in mature granulomas, indicating the presence of more immature cells than those previously observed by Lenzi et al. (9), who, by brightfield microscopy, identified promyelocytes and metamyelocytes (15). The expression of Sca-1 was also observed in some blood vessels, which is already described for mice. According to Luna

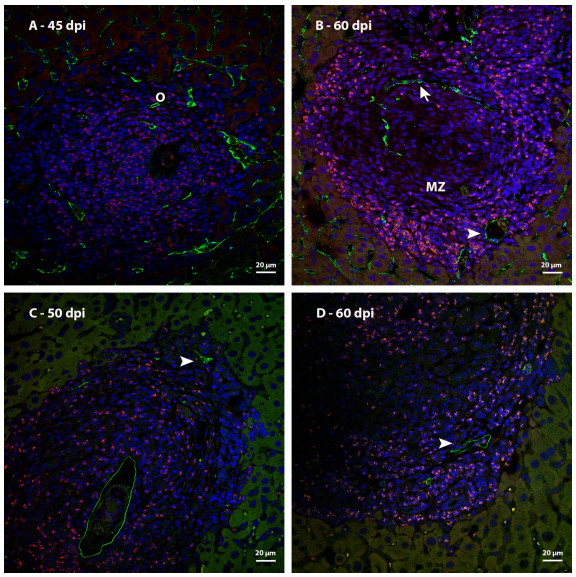

FIGURE 12
Identification of blood vessels in livers of mice infected by S. mansoni, immunostaining by CD31 and Lyve 1. **(A)** Sinusoids that are observed among the other cells that form the granuloma at 45dpi express CD31; **(B)** CD31 immunostaining identified a blood vessel with sinusoidal morphology (arrow) in the medial zone of the granuloma and other vessels with broad lumen (arrowhead) in the peripheral zone of the same granulomas at 60 dpi; **(C)** Identification of lymphatic vessels (arrowhead) located in the periphery of mature granulomas at 50 and **(D)** 60 dpi. Bars, 20 µm. DAPI: blue, Evan's blue: red, CD31: green **(A, B)**, Lyve-1: green **(C, D)**.

et al., (49), the expression of Sca-1 by endothelial cells can support the hypothesis of a common progenitor to hematopoietic and endothelial cells (49).

The schistosomal liver is an environment conducive to the occurrence of angiogenesis and hematopoiesis. The possibility of common progenitors between endothelial and hematopoietic cells is based on the characteristics of the hemogenic endothelium, which occurs during the embryonic life of mammals. Cells derived from this structure are part of the definitive hematopoietic wave, although some of these cells have already been found in adult individuals (50–52). These data, together with the characteristics shared with the hematopoietic fetal liver, lead us to suggest that schistosomiasis is a disease capable of activating a context that contribute to the establishment of a hepatic environment similar to the one found during embryonic development.

The immunolabeling of Fall-3 also was chosen to identify immature hematopoietic cells. In addition to identifying HSC and HSPC, Fall3 is present both in $ly6^a$ and $ly6^b$ cells which suggests that this marker is also capable of identifying more differentiated cells (53). The morphological data generated by the Fall-3 labeling provide us with important information about the phenotypic characterization of cells present in regions of proliferation. It was possible to detect labelled large cells with loose chromatin and protruding nucleolus, that are characteristics commonly found in immature cells. These morphological data reinforce the hypothesis of the arrival of progenitors to the liver that are very immature.

The differences in pattern of distribution of cells and extracellular matrix in zones of schistosomal granuloma can lead us to consider that the structure is analogous to an ecosystem, as suggested by Malta et. Al., 2021 (54). In this context, hematopoietic cells would be occupying a specific niche in the peripheral zone of granuloma, which provide conditions of survival and maintenance of these cells interacting with each other and with cellular matrix elements. The idea of niche in ecological context of granuloma and in production of hematopoietic cells in bone marrow and in the embryological development presents some similarities, as we observed here.

From a physiological perspective, extramedullary hematopoiesis, both perivascular and perigranulomatous, increases the system's ability to produce hematopoietic cells in a context in which the bone marrow is already highly activated and with intense hematopoietic activity. This is possible because, at the same time that the bone marrow is exporting immature cells, either because of the hyperplasia itself, or because of the possible direct mobilization of hematopoietic progenitors, the assembly of hepatic microenvironments favorable to its homing and proliferation is taking place. In addition to a coincidence of events, perhaps this may have some evolutionary importance in the co-evolution of Schistosoma and its mammalian host.

In summary, the present work describes new aspects about hepatic extramedullary hematopoiesis that occurs during murine schistosomal infection. We detailed the characteristics of the perigranulomatous and perivascular niches as microenvironments conducive to the proliferation of hematopoietic cells, in addition to shedding light on the possibility of integrating the processes of hematopoiesis and hepatic angiogenesis triggered by the disease. Also, our data suggests the possibility of direct mobilization of immature hematopoietic cells from bone marrow to both hepatic sites, induced by SEA, which should be a topic of further investigation.

Data availability statement

The raw data supporting the conclusions of this article will be made available by the authors, without undue reservation.

Ethics statement

The animal study was reviewed and approved by Institutional Ethics Committee for Animal Research of the Oswaldo Cruz Institute (CEUA IOC, license: L-2/13).

Author contributions

JF, MT, BD, and MP-M contributed to conception and design of the study. JF, MT, GK, and BD collected samples and executed histology techniques. JF, MT, and MP-M made immunofluorescence analysis. JF and MP-M wrote the manuscript. All authors contributed to manuscript revision, read, and approved the submitted version.

Funding

This work was supported by the Brazilian National Research Council (CNPq INCT-NIM #465489/2014-1 and PQ 313520-2018-6) and the Oswaldo Cruz Institute/Fiocruz (intitutional funding). JF and GK were fellows from the Coordination for the Improvement of Higher Education Personnel (CAPES). The funders had no role in study design, data collection/analysis, decision to publish, or preparation of the manuscript.

Acknowledgments

The authors would like to thank Ester Maria Mota for scientific discussions, Filomena de Fátima Cruz, Iolanda Deolinda de Souza and Monique Lima for the infection of mice with *Schistosoma mansoni* cercariae; João Paulo Rodrigues, Luciana Silva Souza, Luzia Fátima Caputo, Rakel Vieira de Souza and Thalita Paschoal for histotechnology assistance; and also Giulia Caminha and Pedro Paulo de Abreu Manso for support concerning confocal microscopy.

Conflict of interest

The authors declare that the research was conducted in the absence of any commercial or financial relationships that could be construed as a potential conflict of interest.

Publisher's note

References

1. WHO. Global update on implementation of preventive chemotherapy against neglected tropical diseases in 2018. *Weekly Epidemiological Rec No 48* (2021) 96:585–95.

2. dos Santos CO, Coelho P, Lenzi H. *Schistosoma mansoni e esquistossomose uma visaão multidisciplinar*. Rio de Janeiro: Editora Fiocruz (2008) p. 1124 p. R de Janeiro, editor (2008), p. 1124 p.

3. Warren KS. The pathology, pathobiology and pathogenesis of schistosomiasis. *Nature* (1978) 273(5664):609–12. doi: 10.1038/273609a0

4. Pellegrino J, Coelho PM. Schistosoma mansoni: wandering capacity of a worm couple. *J Parasitol* (1978) 64(1):181–2. doi: 10.2307/3279647

5. Lambertucci JR, Lambertucci JR. Revisiting the concept of hepatosplenic schistosomiasis and its challenges using traditional and new tools. *Rev Soc Bras Med Trop* (2014) 47(2):130–6. doi: 10.1590/0037-8682-0186-2013

6. Lambertucci JR. Acute schistosomiasis mansoni: revisited and reconsidered. *Memórias do Instituto Oswaldo Cruz* (2010) 105(4):422–35. doi: 10.1590/S0074-02762010000400012

7. Baptista AP, Andrade ZA. Angiogenesis and schistosomal granuloma formation. *Memórias do Instituto Oswaldo Cruz* (2005) 100(2):183–5. doi: 10.1590/S0074-02762005000200012

8. Andrade ZA, Santana TS. Angiogenesis and schistosomiasis. *Memórias do Instituto Oswaldo Cruz* (2010) 105(4):436–9. doi: 10.1590/S0074-02762010000400013

9. Lenzi HL, Kimmel E, Schechtman H, Pelajo-Machado M, Romanha WS, Pacheco RG, et al. Histoarchitecture of schistosomal granuloma development and involution: Morphogenetic and biomechanical approaches. *Memorias do Instituto Oswaldo Cruz* (1998) 93(Supplement):41–51. doi: 10.1038/273609a0

10. Orkin SH, Zon LI. Hematopoiesis: An evolving paradigm for stem cell biology. *Cell* (2008) 132:631–44. doi: 10.1016/j.cell.2008.01.025

11. Golub R, Cumano A. Embryonic hematopoiesis. *Blood Cells Molecules Dis* (2013) 51(4):226–31. doi: 10.1016/j.bcmd.2013.08.004

12. Kim CH. Homeostatic and pathogenic extramedullary hematopoiesis. *J Blood Med* (2010) 1:13–9. doi: 10.2147/JBM.S7224

13. Yang X, Chen D, Long H, Zhu B. The mechanisms of pathological extramedullary hematopoiesis in diseases. *Cell Mol Life Sci* (2020) 77:2723–38. doi: 10.1007/s00018-020-03450-w

14. Yamamoto K, Miwa Y, Abe-Suzuki S, Abe S, Kirimura S, Onishi I, et al. Extramedullary hematopoiesis: Elucidating the function of the hematopoietic stem cell niche (Review). *Mol Med Rep* (2016) 13:587–91. doi: 10.3892/mmr.2015.4621

15. Lenzi HL, Lenzi JA, Rosman FC, Pelajo-Machado M, Mota EM, Panasco MS, et al. Extramedullary hematopoiesis in murine schistosomiasis mansoni. *Memórias do Instituto Oswaldo Cruz* (1995) 90(2):169–77. doi: 10.1590/S0074-02761995000200008

16. Carson FL, Martin JH, Lynn JA. Formalin fixation for electron microscopy: a re-evaluation. *Am J Clin Pathol* (1973) 59(3):365–73. doi: 10.1093/ajcp/59.3.365

17. Dolber PC, Spach MS. Picrosirius red staining of cardiac muscle following phosphomolybdic acid treatment. *Stain Technol* (1987) 62(1):23–6. doi: 10.3109/10520298709107961

18. Bogomoletz W. Avantages de la coloration par le rouge Sirius de l'amyloide et des éosinophiles. *Arch Anat Cytol Path* (1980) 28(4):252–3.

19. Koyama Y, Brenner DA. Liver inflammation and fibrosis. *J Clin Invest* (2017) 127(1):55. doi: 10.1172/JCI88881

20. Gomez Perdiguero E, Klapproth K, Schulz C, Busch K, Azzoni E, Crozet L, et al. Tissue-resident macrophages originate from yolk sac-derived erythro-myeloid progenitors. *Nature* (2015) 518(7540):547–51. doi: 10.1038/nature13989

21. Amaral KB, Silva TP, Dias FF, Malta KK, Rosa FM, Costa-Neto SF, et al. Histological assessment of granulomas in natural and experimental schistosoma mansoni infections using whole slide imaging. *PLoS One* (2017) 12(9):e0184696. doi: 10.1371/journal.pone.0184696

22. de Paula Ayres-Silva J, Paulo de Abreu Manso P, Rietmann da Cunha Madeira M, Pelajo-Machado M, Leonel Lenzi H. Sequential morphological characteristics of murine fetal liver hematopoietic microenvironment in Swiss Webster mice. *Cell Tissue Res* (2011) 344):455–69. doi: 10.1007/s00441-011-1170-1

23. Gardenghi S, Grady RW, Rivella S. Anemia, ineffective erythropoiesis and hepcidin: interacting factors in abnormal iron metabolism leading to iron overload

in β-thalassemia. *Hematol Oncol Clin North Am* (2010) 24(6):1089. doi: 10.1016/j.hoc.2010.08.003

24. Andrade ZA. Schistosomiasis and liver fibrosis: Review article. *Parasite Immunol* (2009) 31:656–63. doi: 10.1111/j.1365-3024.2009.01157.x

25. Wirth F, Lubosch A, Hamelmann S, Nakchbandi IA. Fibronectin and its receptors in hematopoiesis. *Cells* (2020) 9(12):2717. doi: 10.3390/cells9122717

26. Sagar BMM, Rentala S, Gopal PNV, Sharma S, Mukhopadhyay A. Fibronectin and laminin enhance engraftibility of cultured hematopoietic stem cells. *Biochem Biophys Res Commun* (2006) 350(4):1000–5. doi: 10.1016/j.bbrc.2006.09.140

27. Cancelas JA. Adhesion, migration, and homing of murine hematopoietic stem cells and progenitors. *Methods Mol Biol* (2011) 750:187–96. doi: 10.1007/978-1-61779-145-1_13

28. Khurana S, Schouteden S, Manesia JK, Santamaria-Martínez A, Huelsken J, Lacy-Hulbert A, et al. Outside-in integrin signalling regulates haematopoietic stem cell function *via* periostin-itgav axis. *Nat Commun* (2016) 7:1–14. doi: 10.1038/ncomms13500

29. Johns JL, Christopher MM. Extramedullary hematopoiesis: a new look at the underlying stem cell niche, theories of development, and occurrence in animals. *Veterinary Pathol* (2012) 49(3):508–23. doi: 10.1177/0300985811432344

30. Papy-Garcia D, Albanese P. Heparan sulfate proteoglycans as key regulators of the mesenchymal niche of hematopoietic stem cells. *Glycoconjugate J* (2017) 34 (3):377–91. doi: 10.1007/s10719-017-9773-8

31. Alvarez-Silva M, Borojevic R. GM-CSF and IL-3 activities in schistosomal liver granulomas are controlled by stroma-associated heparan sulfate proteoglycans. *J Leukoc Biol* (1996) 59(3):435–41. doi: 10.1002/jlb.59.3.435

32. Mondal S, Adhikari N, Banerjee S, Amin SA, Jha T. Matrix metalloproteinase-9 (MMP-9) and its inhibitors in cancer: A minireview. *Eur J Medicinal Chem* (2020) 194:112642. doi: 10.1016/j.ejmech.2020.112260

33. Kawai K, Xue F, Takahara T, Kudo H, Yata Y, Zhang W, et al. Matrix metalloproteinase-9 contributes to the mobilization of bone marrow cells in the injured liver. *Cell Transplant* (2012) 21:453–64. doi: 10.3727/096368911X605367

34. Shariati F, Pérez-Arellano JL, Carranza C, López-Abán J, Vicente B, Arefi M, et al. Evaluation of the role of angiogenic factors in the pathogenesis of schistosomiasis. *Exp Parasitol* (2011) 128(1):44–9. doi: 10.1016/j.exppara.2011.01.016

35. Sapieha P, Hamel D, Shao Z, Rivera JC, Zaniolo K, Joyal JS, et al. Proliferative retinopathies: angiogenesis that blinds. *Int J Biochem Cell Biol* (2010) 42(1):5–12. doi: 10.1016/j.biocel.2009.10.006

36. Elpek GÖ. Angiogenesis and liver fibrosis. *World J Hepatol* (2015) 7(3):377. doi: 10.4254/wjh.v7.i3.377

37. Loeffler DA, Lundy SK, Singh KP, Gerard HC, Hudson AP, Boros DL. Soluble egg antigens from *schistosoma mansoni* induce angiogenesis-related processes by up-regulating vascular endothelial growth factor in human endothelial cells. *J Infect Dis* (2002) 185(11):1650–6. doi: 10.1086/340416

38. Freedman DO, Ottesen EA. Eggs of schistosoma mansoni stimulate endothelial cell proliferation. *vitro. J Infect Dis* (1988) 158(3):556–62. doi: 10.1093/infdis/158.3.556

39. Jackson DG. Biology of the lymphatic marker LYVE-1 and applications in research into lymphatic trafficking and lymphangiogenesis. *APMIS* (2004) 112(7–8):526–38. doi: 10.1111/j.1600-0463.2004.apm11207-0811.x

40. Jackson DG, Prevo R, Clasper S, Banerji S. LYVE-1, the lymphatic system and tumor lymphangiogenesis. *Trends Immunol* (2001) 22(6):317–21. doi: 10.1016/s1471-4906(01)01936-6

41. Randi AM, Laffan MA. Von Willebrand factor and angiogenesis: basic and applied issues. *J Thromb Haemost* (2017) 15(1):13–20. doi: 10.1111/jth.13551

42. Yamamoto K, de Waard V, Fearns C, Loskutoff DJ. Tissue distribution and regulation of murine von willebrand factor gene expression *in vivo*. *Blood* (1998) 92 (8):2791–801. doi: 10.1182/blood.V92.8.2791

43. Randi AM, Smith KE, Castaman G. Von willebrand factor regulation of blood vessel formation. *Blood* (2018) 132(2):132. doi: 10.1182/blood-2018-01-769018

44. Augusto P, Silveira A, Deolinda E, Pereira Velloso R, Colombini MP, Carlos De Campos Guerra J, et al. Megakaryocyte. *Learn by Images* (2011) 9(2):247–55. doi: 10.1590/S1679-45082011AI2023

45. Yamamoto R, Morita Y, Ooehara J, Hamanaka S, Onodera M, Rudolph KL, et al. Clonal analysis unveils self-renewing lineage-restricted progenitors generated directly from hematopoietic stem cells. *Cell* (2013) 154(5):1112–26. doi: 10.1016/j.cell.2013.08.007

46. Grinenko T, Eugster A, Thielecke L, Ramasz B, Krüger A, Dietz S, et al. Hematopoietic stem cells can differentiate into restricted myeloid progenitors before cell division in mice. *Nat Commun* (2018) 1):1–10. doi: 10.1038/s41467-018-04188-7

47. Sanjuan-Pla A, Macaulay IC, Jensen CT, Woll PS, Luis TC, Mead A, et al. Platelet-biased stem cells reside at the apex of the haematopoietic stem-cell hierarchy. *Nat (2013)* (7470) 502:232–6. doi: 10.1038/nature12495

48. Cheng H, Zheng Z, Cheng T. New paradigms on hematopoietic stem cell differentiation. *Protein Cell* (2020) 11(1):34–44. doi: 10.1007/s13238-019-0633-0

49. Luna G, Paez J, Cardier JE. Expression of the hematopoietic stem cell antigen sca-1 (LY-6A/E) in liver sinusoidal endothelial cells: possible function of sca-1 in endothelial cells. *Stem Cells Dev* (2004) 13(5):528–35. doi: 10.1089/scd.2004.13.528

50. Eilken HM, Nishikawa SI, Schroeder T. Continuous single-cell imaging of blood generation from haemogenic endothelium. *Nature* (2009) 457(7231):896–900. doi: 10.1038/nature07760

51. Lacaud G, Kouskoff V. Hemangioblast, hemogenic endothelium, and primitive versus definitive hematopoiesis. *Exp Hematol* (2017) 49:19–24. doi: 10.1016/j.exphem.2016.12.009

52. Ginhoux F, Greter M, Leboeuf M, Nandi S, See P, Gokhan S, et al. Fate mapping analysis reveals that adult microglia derive from primitive macrophages. *Science* (2010) 330(6005):841–5. doi: 10.1126/science.1194637

53. Müller-Sieburg CE. Separation of pluripotent stem cells and early b lymphocyte precursors with antibody fall-3. *J Exp Med* (1991) 174(1):161–8. doi: 10.1084/jem.174.1.161

54. Malta KK, Silva TP, Palazzi C, Neves VH, Carmo LAS, Cardoso SJ, et al. Changing our view of the schistosoma granuloma to an ecological standpoint. *Biol Rev* (2021) 96(4):1404–20. doi: 10.1111/brv.12708

frontiers | Frontiers in Immunology

TYPE Original Research
PUBLISHED 31 August 2022
DOI 10.3389/fimmu.2022.955049

OPEN ACCESS

EDITED BY
Thiago Almeida Pereira,
Stanford University, United States

REVIEWED BY
Olfat Ali Hammam,
Theodor Bilharz Research Institute, Egypt
Katia Oliveira,
Universidade Federal de São Paulo, Brazil

*CORRESPONDENCE
Wiliam Castro-Borges
wborges@ufop.edu.br

SPECIALTY SECTION
This article was submitted to Parasite Immunology, a section of the journal Frontiers in Immunology

RECEIVED 28 May 2022
ACCEPTED 11 August 2022
PUBLISHED 31 August 2022

CITATION
Gonçalves-Silva G, Vieira LGMdS, Cosenza-Contreras M, Souza AFP, Costa DC and Castro-Borges W (2022) Profiling the serum proteome during *Schistosoma mansoni* infection in the BALB/c mice: A focus on the altered lipid metabolism as a key modulator of host-parasite interactions. *Front. Immunol.* 13:955049. doi: 10.3389/fimmu.2022.955049

Profiling the serum proteome during *Schistosoma mansoni* infection in the BALB/c mice: A focus on the altered lipid metabolism as a key modulator of host-parasite interactions

Gustavo Gonçalves-Silva[1], Lara Geralda Magela dos Santos Vieira[1], Miguel Cosenza-Contreras[2], Ana Flávia Pinho Souza[1], Daniela Caldeira Costa[3] and Wiliam Castro-Borges[3]*

[1]Programa de Pós-Graduação em Ciências Biológicas, Universidade Federal de Ouro Preto, Ouro Preto, Brazil, [2]Faculty of Biology, University of Freiburg/Institute for Surgical Pathology, University Medical Center, Freiburg, Germany, [3]Departamento de Ciências Biológicas, Instituto de Ciências Exatas e Biológicas Universidade Federal de Ouro Preto, Ouro Preto, Brazil

Schistosomiasis represents a condition in which every aspect of the disease, starting from skin invasion of the cercariae to egg laying by adult worms, incites a tissue response from the vertebrate host. This response, whether acute or chronic, leads to the appearance of reporter molecules of tissue injury in bodily fluids that could be surveyed as markers for disease diagnosis, status and prognosis. In this scenario, the serum proteome associated with a schistosome infection remains poorly explored; particularly by the use of high-throughput mass spectrometric instrumentation. In this study, we aimed to comparatively examine the serum proteome of control versus infected BALB/c mice, spanning the interval between the onset of egg laying and the peak of the acute phase of infection. Compositional analysis of the sera, using one dimensional reversed-phase fractionation of tryptic peptides coupled to mass spectrometry, allowed identification of 453 constituents. Among these, over 30% (143 molecules) were differentially present comparing sera from infected and non-infected mice, as revealed by quantitative label-free shotgun approach. The majority of proteins exhibiting altered levels was categorised as belonging to immune response (acute phase-related proteins) followed by those linked to lipid transport and metabolism. Inspection of the lipid profile from control and infected individuals demonstrated more pronounced and significant alterations in triglycerides, VLDL and HDL fractions ($p<0,001$), attesting for a disturbance in circulating lipid molecules, and suggesting a key role in host-parasite interactions. Our findings provide a global view of the serum proteome in the context of experimental schistosomiasis during the acute phase of infection. It contributes by listing key molecules that could be monitored to inform on the associated inflammatory disease status. We hope it

will shed light into uncovered aspects of the *Schistosoma mansoni* parasitism in the vertebrate host, particularly those related to modulation of the lipid metabolism mediating immune responses.

KEYWORDS

schistosomiasis, serum proteome, lipid metabolism, host-parasite interaction, mass spectrometry

Introduction

Schistosomiasis is a neglected tropical disease affecting millions of people worldwide (1–3). Its clinical manifestations promote in most cases irreversible tissue damage to the host, resulting in a high morbidity disease (4). *Schistosoma mansoni* adult worms dwell for years within the host vasculature, where they interact with circulating host molecules and utilise the nutritional rich constituents of sera to sustain parasitism. Molecular investigations have provided a deep understanding of parasite´s biology (5–7), however much remains to be elucidated on the mechanisms operating in this complex host-parasite interaction. Understanding host responses to schistosomes could reveal biomarkers of active infection and allow for better monitoring on the inflammatory status as a manner to alleviate the long term chronic tissue injuries.

Proteomic investigations aimed at elucidating *S. mansoni*-host interactions have been applied to the liver (8–10) and spleen (11) soluble proteomes in the murine model of the disease. In these occasions, significant changes in protein expression were observed, but how these are triggered is poorly understood. Therefore, analysis of the serum proteome in the context of schistosomiasis could provide the basis to comprehend the metabolic reprogramming operating at target tissues. Recent studies have investigated the serum proteome during *S. japonicum* infection in animal models of the disease and markers of infection have been proposed (12, 13). To our knowledge, we are the first to investigate the serum proteome in the context of *S. mansoni* infection, in the murine model, with a particular focus on proteins related to lipid metabolism.

Here we employed quantitative label-free shotgun proteomic analyses of the serum proteome collected at the 5th and 7th weeks post infection from *S. mansoni* infected BALB/c mice. Compositional analysis of the undepleted sera allowed identification of over 400 constituents, over 30% of which were differentially abundant comparing control and infected individuals. Distinct patterns of protein expression were seen at these two time points, possibly as a response to specific demands related to the onset of egg laying by adult parasites and granuloma formation in the liver. Our findings provide a repertoire of differentially abundant serum constituents in the context of *S. mansoni* infection and uncover key molecules proposed to modulate lipid metabolism during disease establishment.

Materials and methods

Ethics statement

All experiments involving animals were conducted in accordance with the Brazilian Federal Legislation (Arouca's Law number 11,794). The routine methods for maintenance of the *S. mansoni* life cycle and the experimental procedures involving mice were reviewed and approved by the local Ethics Committee on Animal Experimentation 'Comissão de Ética no Uso de Animais' (CEUA), Universidade Federal de Ouro Preto (UFOP), and received the protocol numbers 2017/35 and 2017/34, respectively.

Infection model and experimental design

Twenty-three male and female BALB/c mice aged 35 days were anaesthetised using a combination of ketamine hydrochloride (8 mg/kg) and xylazine (4 mg/kg) administered intraperitoneally. For infected groups, mice were exposed to active penetration by *S. mansoni* cercariae (LE strain) through tail immersion (250 cercariae/animal). The control group was established with 23 non-infected individuals of the same age. After 5th and 7th weeks post-infection, both infected and control mice were weighed and sacrificed using anaesthetic overdose. Spleens were collected and weighed to measure the spleen-to-body weight ratio Supplementary Figure 1. Serum samples were collected and their protein content measured using the BCA protein assay kit (Thermo Scientific, Cramlington, UK). Samples were kept frozen under -20°C and used for the analyses within a maximum of 60 days after collection from animals. The number of samples varied depending on the type of analysis. A total of 40 sera (n = 10 per group) proved suitable (did not display hemolysis

and quantity was not limiting) for analysis of the lipid profile. For proteomic analysis sera from three animals from each group were pooled and this constituted one biological replicate per group. A second biological replicate was prepared by pooling three other sera from each group. Compositional and quantitative proteomic data were obtained from 6 independent LC-MS/MS runs.

In-solution digestion

Briefly, 30 µg protein representing pooled sera from control or 5^{th} and 7^{th} post-infection groups were incubated with RapiGest (Waters, UK), to a final concentration of 1% (w/v) and maintained at 80°C for 10 min. Then, proteins were reduced using dithiothreitol (Sigma Aldrich, St. Louis, MO, USA) to a final concentration of 3,3 mM at 60°C for 10 min. Alkylation was performed at room temperature in the dark, using iodoacetamide (GE Healthcare, Little Chalfont, Buckinghamshire, UK) to a final concentration of 9,4 mM for 30 min. The digestion was performed using sequencing grade trypsin (Promega, Madison, WI, USA) at a ratio of 50:1 (protein/trypsin) during incubation at 37°C for 16 h. To precipitate RapiGest and stop the digestion step, trifluoroacetic acid was added to a final concentration of 0.5% v/v. Afterwards, a centrifugation step was performed for 15 min at 7°C at 20,000 x g (Mikro 200R, Hettich Zentrifugen, Tuttlingen, DEU). The clarified supernatant containing the peptides was then collected and submitted to UHPLC-MS/MS analyses.

Liquid chromatography-mass spectrometry

After the digestion step, approximately 400 ng of peptide samples were injected into the liquid chromatography platform (UHPLC UltiMate R 3000, Dionex, San Jose, USA). Peptides were loaded onto an Acclaim PepMap100 C18 Nano-Trap column (100µm i.d. × 2 cm, 5 µm, 100 Å; Thermo Scientific, Waltham, MA, USA) and washed for 3 min in 3,8% acetonitrile/0.1% Trifluoroacetic acid solution (ACN, HPLC grade, USE), at a flow rate of 5 µL/min. Then, peptides were directed to a reverse phase chromatography using an Acclaim PepMap100 C18 RSLC column (75µm i.d. × 15 cm, 2 µm, 100 Å; Thermo Scientific), in tandem with the trap column on a constant flow rate of 300 nL/min. A multistep gradient was performed, using solvents A (0.1% formic acid, HPLC grade, JTBaker, Mexico) and B (80% ACN, 0.1% formic acid) and applied as follows: a conditioning step with 3,8% of B during 3 min, followed by a ramp from 3,8 to 30% B over 120 min, and subsequently, 30–55% B to 150 min. Then a final ramp with 99% B to 162 min, followed by a reconditioning step with 3,8% B until 180 min. The spectral data was acquired using a Q-Exactive mass spectrometer (Thermo Scientific, Bremen, Germany) operating at full-scan/MS2 mode. The nanospray flex ion source (Thermo Scientific) was set at 3,8 kV on positive mode, with a capillary temperature of 250°C and S-lens levels set to 55. The Data Dependent Acquisition method (DDA) was performed in the top 12 ions with charge states between +2 and +4 from a 1,2 *m/z* window. Survey scans were tuned for a resolution of 70,000 with a mass range between 300 and 2,000 *m/z*, and a AGC target of $1e^6$ ions in up to 120 ms. For MS/MS scans, selected ions were fragmented by Higher Energy Collision Dissociation (HCD) with a stepped Normalized Collisional Energy (NCE) of 28–30. After the dissociation, the fragmentation spectra were acquired using a resolution of 17,500 performing a maximum injection time of 60 ms with a dynamic exclusion time of 40 s and a target value of $5e^5$ (minimum AGC target $6.25e^3$).

Analysis of proteomic data

The spectral data obtained from the UHPLC-MS/MS platform was directed to protein identity search using PEAKS Studio v8,5 (Bioinformatics Solutions Inc.). Searching parameters included: Enzyme: trypsin; maximum of 2 missed cleavage sites; fixed post-translational modifications: cysteine carbamidomethylation (+57,0214 Da) and methionine oxidation (+15,9949 Da) as variable modifications, maximum 3 post-translational modifications per peptide; time window: 4 minutes; mass error tolerance of 10 ppm for precursor ions and 0,1 Da for product ion fragmentation.

The database search was performed with a False Discovery Rate (FDR) of 1%, a protein significance of 13 (p-value ≤0.05) considering only proteins identified with at least one unique peptide. The *Mus musculus* proteome database was downloaded from the UNIPROT website, containing 55,398 protein sequences. Quantitative label-free analysis was performed under fold-change ≥ 2, protein significance of 13 (p-value ≤0,05) using the PEAKSQ significance method, considering proteins identified with at least 1 unique peptide. Cytoscape Software v. 3.9.1 (available at https://cytoscape.org/), underpinned by STRING query tool, was used to construct a protein interaction network for differentially abundant serum constituents and retrieve the top 10 most significant enriched molecular functions they are linked to.

Lipidogram analyses

Lipidogram analyses were performed through measurement of Total Cholesterol, HDL Cholesterol and Triglycerides using colorimetric detection methods (BioClin-Quibasa kits, Belo Horizonte, MG, Brazil) using a Calm SBA2000 equipment (Medsystem). VLDL cholesterol levels were estimated by dividing triglyceride levels by 5, as specified in the literature (14). The atherogenic fraction was calculated by subtracting Total Cholesterol levels from HDL cholesterol. Sera from ten

animals per group (control at 5th and 7th weeks post-infection and respective infected groups) were used for these analyses.

Statistical analysis

Statistical analysis of data obtained from body weights, spleen weights, and lipidogram parameters were evaluated for significant statistical differences (p-value ≤0,05), using the GraphPad Prism v8,0 program (San Diego, California, USA). The Kolmogorov-Smirnov and Shapiro-Wilk tests were applied to evaluate data normality. Then, the t-test or Mann-Whitney test were applied according to parametric or non-parametric distribution. All values were expressed as the mean ± standard deviation. For principal component analysis, the ClustVis (15) platform was used to perform the multivariate analysis.

Results

Assessing disease establishment during experimental schistosomiasis

In this investigation we first seek to evaluate disease progression in the BALB/c model of experimental schistosomiasis aiming to monitor the homogeneity of serum samples for downstream analysis from control and infected individuals. As shown in Supplementary Figure 1A the spleen from infected animals exhibited significant increase in size at 5th and 7th post infection, whilst for non-infected animals it remained unchanged. In addition, the observed splenomegaly throughout the infection period is better monitored by measuring the spleen-to-body ratio (9). As seen in Supplementary Figures 1B, C for both investigated periods, infected animals displayed a marked increase in this ratio compared to control animals, attesting for the successful establishment of murine schistosomiasis. As for the spleen, liver from infected animals were visually enlarged in both periods with increased granuloma formation, particularly at the later time point.

The compositional analysis of undepleted sera in the context of murine schistosomiasis

In order to evaluate the depth of proteome coverage through mass spectrometric analysis of undepleted murine sera, we first combined the spectral data obtained from uninfected and infected animals to interrogate the available *Mus musculus* proteome database. The accumulated 35,555 Peptide-Spectrum Matches resulted in 3450 confidently assigned peptide sequences yielding 453 distinct protein groups (Supplementary Table 1). Inspection of the total accumulated area for the top and least abundant constituents revealed five orders of magnitude difference, attesting for the identification of both high, medium and low abundant serum components (Figure 1A). Approximately 90% of cumulative abundance was accounted for 10 protein identities, the remaining 10% comprising the additional 443 molecules (Figure 1B). The top 10 most abundant proteins were mainly associated with transport, immune function and acute phase response. Serum Albumin

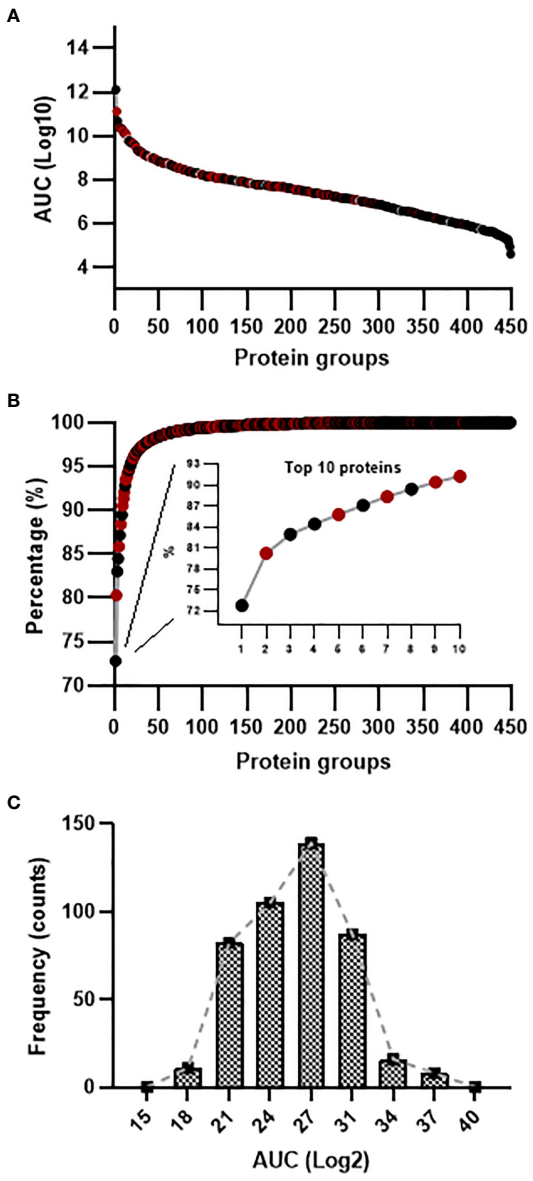

FIGURE 1
Compositional analysis of undepleted serum proteome during *S. mansoni* infection in the BALB/c mice. **(A)** Dynamic range of identified proteins encompassed five orders of magnitude difference between the most and least abundant serum constituent, as judged by Area Under Curve (AUC). **(B)** Cumulative abundance plot revealed 10 molecules contributing to 91% of the total ion signal. **(C)** Frequency histogram for protein abundance in the samples.

was the most abundant component (72.7% of the detected ion signal), followed by Serotransferrin (7.5%) and Pregnancy zone protein (2.9%). Additional seven constituents in the top 10 list (Apolipoprotein A-I, Hemopexin, Immunoglobulin heavy constant mu, Complement C3, Immunoglobulin kappa constant, Alpha-2-HS-glycoprotein and Fibrinogen beta chain) collectively contributed 8,3% to the cumulative ion abundance. The vast majority of identified proteins contributed 8,7% to the total ion signal. This variation in the dynamic range of protein expression was confirmed by analysis of the frequency histogram for protein abundance, which revealed a non-Gaussian distribution ($p<0,0001$), Figure 1C. Next, we performed a comparative label-free quantitative analysis on the mass spectral data to detect differentially abundant serum molecules in the acute phase of murine schistosomiasis.

The host serum proteome is pronouncedly altered during the acute phase of experimental schistosomiasis

The quantitative label-free proteomic analysis revealed 143 shared constituents (31.5% of the total identified proteins) as differentially abundant comparing control and infected individuals. A consolidated list of the top three differentially abundant proteins categorised according to biological process is shown on Table 1 (see Supplementary Table 2 for a list of differentially abundant molecules). A heatmap plot indicated that over ⅔ of the differentially abundant proteins showed positive regulation at the 7th week. The 5th week period represented a transition with a few groups of proteins exhibiting either increased or decreased abundance, whilst for the majority of identities, levels did not differ significantly from control samples (Figure 2A). Only 22 proteins appeared significantly down regulated exclusively at 7 weeks (Figure 2B) and 36 displayed contrasting patterns of abundance at weeks 5 and 7 (Figure 2C). For the remaining differentially abundant proteins (85 molecules) during infection, increased levels relative to controls were observed at these two time points with higher abundance at 7th week; possibly indicating that these molecules accumulated in the serum as the peak of the acute phase had been reached (Figure 2D). Protein lists associated with these distinct patterns of protein expression are provided in Supplementary Table 3.

These proteins were further categorised according to the main biological processes they are related to (Figure 2E). Approximately half (48.21%, 54 molecules) of the differentially abundant molecules were associated with immune response. Among these, immunoglobulin kappa and lambda chains comprised the most prevalent signatures within this group. Immunoglobulin heavy chains belonging to isotypes IgM (mu chain), IgG (gamma chain), IgA (alpha chain) and 5 peptides matching the J chain, which joins two IgM or IgA monomers, confirmed the dominant immunoglobulin profile induced by the parasitic infection. For the majority of Ig entries, positive regulation was seen early at the 5th week and fold changes relative to control were higher at the 7th week. In the Acute Phase Response protein group, the classic C-Reactive Protein, Alpha-1B-glycoprotein and Serum amyloid P-component were the main representatives. In this group, positive regulation was observed at the 5th week (except for Alpha-2-HS-glycoprotein), and increased expression was seen at the 7th week.

Proteins related to lipid metabolism and transport were represented by 13 members. In this category, over 50% were apolipoproteins belonging to subtypes A-II, A-IV, B-100, C-II, C-III, C-IV, and D. Overall, apolipoproteins were up regulated at the peak of acute phase, with most exhibiting down regulation at the 5th week. In this scenario, ApoB100 constitutes an exception, exhibiting a discrete increase (~30%) at the 5th week and reaching approximately 500% increase at the 7th week. In parallel, proteins involved in the control of fat metabolism and immune regulation, such as CD5 antigen-like and adiponectin displayed contrasting patterns of expression in response to the schistosome infection. For lipid transport proteins, whilst corticosteroid-binding globulin displayed down regulation as disease progressed from 5 to 7 weeks, phospholipid transfer protein exhibited an opposite pattern of abundance.

Among the differentially abundant proteins 7 members of the complement system contributed 6,25% to the total of identities (Supplementary Table 2). Equal contribution was provided by metal binding and acute phase response proteins. The former were mostly associated with iron binding and transport represented by ceruloplasmin, serotransferrin and hemopexin, all displaying increased abundance as infection progressed from 5 to 7 weeks. In agreement, decreased levels were seen for alpha and beta haemoglobin subunits. Protein identities related to hemostasis and proteolysis, or its inhibition, contributed <5% each in the total number of differentially abundant serum constituents. Concerning coagulation factors, fibrinogen alpha, beta and gamma chains were consistently up regulated from 5 to 7 weeks post infection. In contrast, coagulation factor XIII B chain and platelet glycoprotein Ib alpha chain exhibited down regulation at these two time points. Alpha-1-antitrypsin, also classified as an acute phase response protein, is a protease inhibitor for which expression levels were high at the 5th week and continued to accumulate, as seen at the 7th week. The same behaviour was shared by kininogen 2, inter-alpha trypsin inhibitor, protein Z-dependent protein inhibitor and the serine protease inhibitor A3N.

Of note, abundance profiles for lipid metabolism and transport proteins at the 5th and 7th weeks were quite divergent (Figure 3), typified by downregulation at 5th week post-infection (except for platelet-activating factor acetylhydrolase), and up regulation at the 7th week for the majority of identities in this group. Three exceptions for this behaviour were adiponectin, corticosteroid-binding globulin and apolipoprotein A-II, which displayed decreased abundance up to the peak of the acute phase

TABLE 1 Consolidated list of the top three differentially abundant proteins categorised according to biological process.

Accession	Description	Coverage (%)	Molecular Mass (Da)	Log_2 5th week/ Control	Log_2 7th week/ Control	Significance
	Lipid Metabolism and Transport Proteins (n=13)					
Q60963	Platelet-activating factor acetylhydrolase	10	49258	1,11	3,36	67,75
P16301	Phosphatidylcholine-sterol acyltransferase	8	49747	0,60	2,76	64,11
Q9QWK4	CD5 antigen-like	42	38863	1,17	2,14	30,03
	Acute Phase Response/Inflammation Proteins (n=7)					
Q00897	Alpha-1-antitrypsin 1-4	45	45998	2,15	5,03	124,24
P12246	Serum amyloid P-component	45	26247	0,82	2,77	91,06
Q60590	Alpha-1-acid glycoprotein 1	28	23895	0,54	2,08	37,12
	Immune Response Proteins (n=54)					
P03976	Ig kappa chain V-II region 17S29.1	27	12390	3,64	7,77	116,64
A0A075B5P4	Ig gamma-1 chain C region secreted form	52	35752	4,27	4,90	119,12
A0A075B664	Immunoglobulin lambda variable 2	14	12165	2,22	4,11	14,21
	Complement System Proteins (n=7)					
D3YXF5	Complement component 7	6	93338	-1,19	3,67	96,63
P06683	Complement component C9	10	62002	2,63	2,51	32,24
P11680	Properdin	14	50327	-0,42	1,92	86,36
	Metal Binding (n=7)					
G3X9T8	Ceruloplasmin	49	121080	0,97	1,64	19,67
Q91X72	Hemopexin	60	51318	1,15	1,50	33,69
Q921I1	Serotransferrin	74	76724	0,20	1,18	28,33
	Hemostasis (n=5)					
E9PV24	Fibrinogen alpha chain	44	87429	0,19	1,60	51,35
Q8K0E8	Fibrinogen beta chain	77	54753	0,17	1,57	41,61
Q8VCM7	Fibrinogen gamma chain	73	49391	0,35	1,27	23,31
	Proteolysis/Inhibition (n=15)					
Q91WP6	Serine protease inhibitor A3N	43	46718	0,68	2,50	54,96
Q61704	Inter-alpha-trypsin inhibitor heavy chain H3	24	99358	0,27	2,06	42,84
Q9JHH6	Carboxypeptidase B2	5	48871	0,06	1,77	45,5
	Proteins related to other processes (n=54)					
Q91XL1	Leucine-rich HEV glycoprotein	24	37431	0,69	3,20	63,36
A0A2R8VHP3	Predicted pseudogene 5478	11	57920	2,49	2,50	26,63
Q9WVF5	Receptor protein-tyrosine kinase	7	72907	1,04	2,05	32,28

Significance set to ≥ 13 meaning p-value ≤ 0,05 (=-Log^{10}(p-value)*10).

in infected animals. In contrast, Apolipoprotein B-100, CD5-antigen like, platelet-activating factor acetylhydrolase, phosphatidylcholine sterol transferase and phospholipid transfer protein exhibited increased abundance throughout the investigated periods. Apolipoproteins C-III, C-IV and D were at reduced levels at week 5 in infected animals but their levels increased relative to non-infected individuals at week 7. In this group, Apolipoprotein C-II displayed the most pronounced fold decrease early at the 5th week, exhibiting a discrete fold increase relative to control animals at the 7th week.

Given the molecular diversity in the serum proteome, 15 unrelated identities, accounting for approximately 14% of those showing altered levels, were grouped as belonging to various biological processes. Among them, known serum markers of cell proliferation (e.g., leucine rich HEV glycoprotein), angiotensin 1-10 and fetuin-B displayed up regulation at the peak of the acute phase. Next, the differentially abundant constituents (apart from immunoglobulins) were interrogated for previously reported protein-protein interactions using Cytoscape software (Figure 4). The retrieved interactome revealed a highly

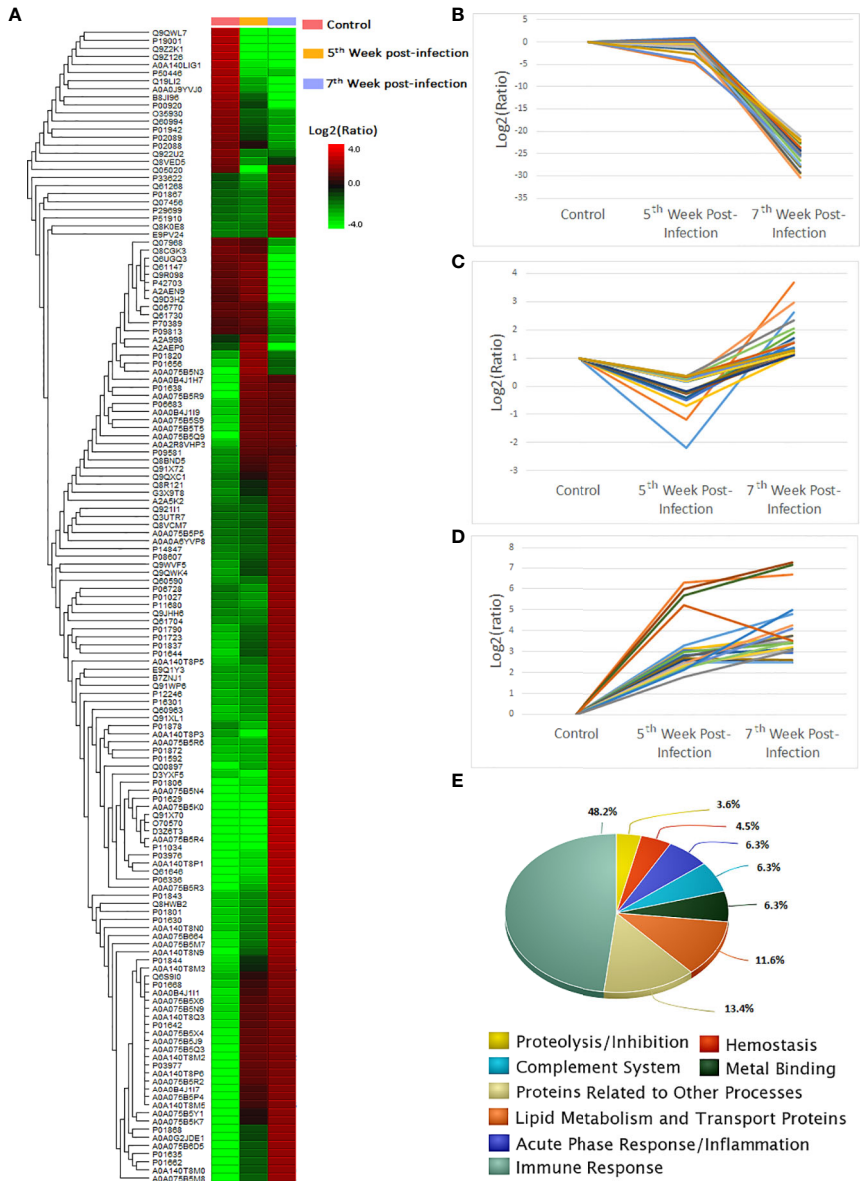

FIGURE 2
Heatmap of differentially abundant serum proteins in the context of *S. mansoni* infection in the murine model. **(A)** A total of 143 molecules with fold changes ≥ 2 were listed. Lipid transport and metabolism related proteins are marked in red. **(B-D)** Distinct expression patterns for differentially abundant serum constituents during *S. mansoni* infection. Molecules displaying downregulation in infected samples **(B)**; downregulation at week 5 post-infection followed by upregulation at week 7 **(C)**; upregulation in both time points **(D)**; list of theses molecule identities is seen on Supplementary Table 3. **(E)** Functional categorisation according to biological processes for differentially abundant serum constituents.

connected protein network not only linking constituents under the same category, but also displaying various possibilities for protein interactions among those from distinct biological processes. A list of top 10 enriched molecular functions associated with the interactome reinforced lipid metabolism and protease inhibition as significantly overrepresented processes. Proteins uniquely found in one of the two time points were listed in Supplementary Table 4. The majority of identities were also represented by immunoglobulin light and heavy chains plus other identities with no clear enrichment to merit their classification according to biological function. As they were not consistently identified in all of the samples, they were not dealt with any further in this study.

In light of the above findings concerning the distinct pattern of serum constituents, we wondered whether the protein profile associated with each condition (non-infected versus infected

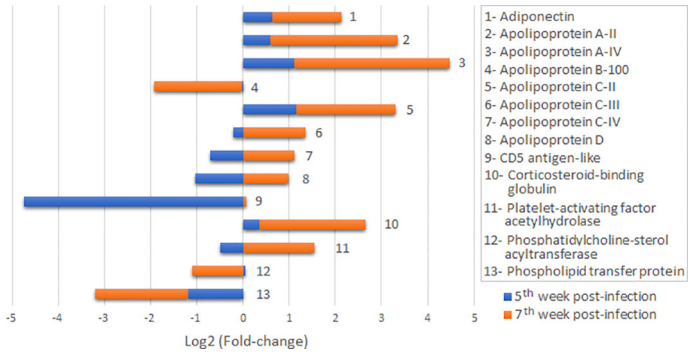

FIGURE 3
Quantitative label-free analysis plot for lipid metabolism and transport proteins at the 5th and 7th weeks post-infection. Protein identities are displayed in alphabetical order. Fold-changes are shown in vertical bars.

animals at the 5th and 7th weeks post infection) would allow segregation of individuals using principal component analysis. As observed in Figure 5, the PCA plot revealed a clear discrimination between groups. In agreement with the quantitative label-free analysis, serum profile from 5 week infected individuals was more closely related to that of control animals. The major fold differences observed for serum constituents at week 7 justifies its position in the PCA plot. This analysis demonstrated that a window of two weeks difference between evaluated samples in the acute phase of murine schistosomiasis promoted distinct profiles in the relative abundance of serum constituents.

Serum lipid profile during acute schistosomiasis

In order to back up the obtained proteomic data and the observed altered levels for proteins related to lipid transport and metabolism, we performed a comparative evaluation of the lipid profile for control and infected individuals at the 5th and 7th weeks post-infection. Lipidogram analyses demonstrated significant alterations in the sera from infected individuals. Decreased levels for Total Cholesterol (Figure 6A) and HDL Cholesterol (Figure 6B) were observed at the 5th week, with marked reduced levels for both VLDL Cholesterol and Triglycerides. At this time point, the non-

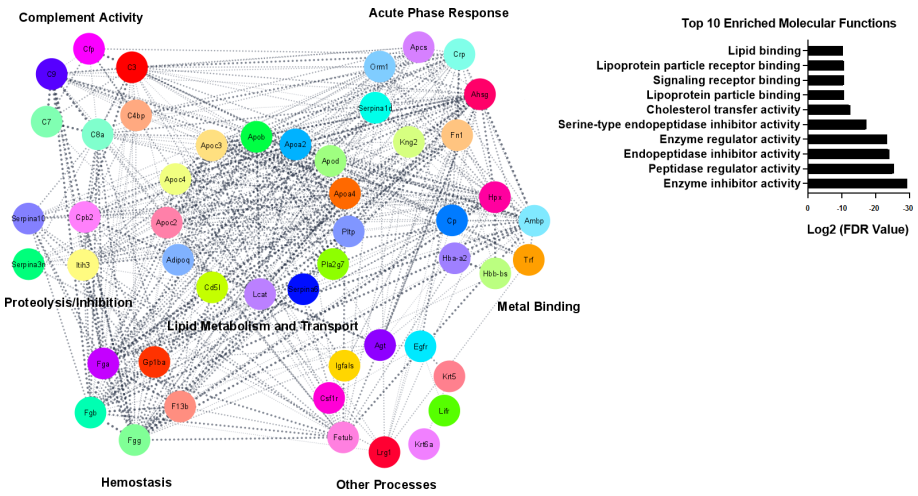

FIGURE 4
Protein interaction network displaying differentially abundant proteins, excluding immunoglobulins. Fifty out of 58 identities composed the interactome. Cytoscape Software v. 3.9.1, underpinned by STRING query tool for interrogation of the *Mus musculus* database, was used to visualise the generated network. Confidence cutoff score was set to > 0.4. Cytoscape also provided the Top 10 enriched molecular functions related to this network. The significant terms and pathways were selected with the threshold of adjusted Log2 FDR < -10. Abbreviations for protein identities are shown in Supplementary Table 2.

10.3389/fimmu.2022.955049

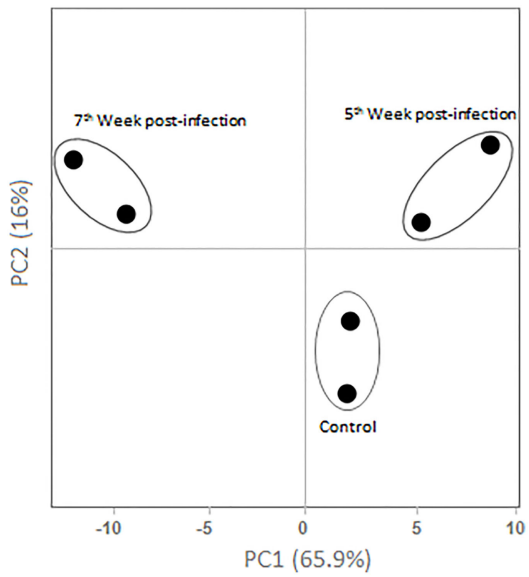

FIGURE 5
Principal Component Analysis. Unit variance scaling was applied, the standard variation with imputation was used to calculate principal components. Axes demonstrates principal component 1 and principal component 2 showing 65.9% and 16% of the total variance, respectively.

HDL Cholesterol, here termed the atherogenic fraction (Figure 6C), remained unchanged. In the late investigated period (7th week post infection), disturbances in circulating lipid molecules were mostly related to VLDL Cholesterol (Figure 6D) and Triglycerides (Figure 6E). At this time point, both Total and HDL Cholesterol levels did not differ significantly. Both evaluated periods exhibited significant changes in the circulating lipid-content of lipoproteins from infected animals, however, with distinct patterns associated with each time point. These results, expressed as mean ± standard deviation, are listed in Supplementary Table 5.

Discussion

In this study, we used mass spectrometry-based label-free quantitative proteomic analyses to comparatively evaluate the serum proteome composition in two distinct phases of murine schistosomiasis. Firstly, at the 5th week post-infection, representing a stage in which parasites have completed their sexual maturation with subsequent pairing and initiation of egg-laying by females. Secondly, at the 7th week post-infection, meaning the peak of the acute phase, characterised by changes from a dominant T_h1 to an egg-induced T_h2 response and extensive granuloma formation, leading to impaired liver function (4). In this investigation, the spleen weight and spleen-to-body weight ratios for control and infected animals were in agreement with previous studies (9–11) allowing to ascertain that schistosomiasis has successfully been established in the murine model.

The obtained compositional analysis reflected the paramount challenge of protein discovery in serum samples. Since no fractionation methods were employed, the number of identified protein groups represented a reasonable achievement for a shotgun approach using non-depleted sera. Although a single molecule (albumin) comprised 73% of the cumulative abundance, the remaining identified proteins highlighted uncovered aspects of the *S. mansoni* parasitism concerning host-parasite interactions. This quantitative label-free proteomic analysis provided a repertoire of differentially abundant serum proteins over the course of *S. mansoni* experimental schistosomiasis up to the peak of its acute phase.

In our previous investigation using shotgun analysis of the soluble liver proteome, we have shown that it undergoes significant alteration in protein expression as schistosomiasis evolves (10). Those findings were also in agreement and complemented earlier findings using the 2D-DIGE approach applied to the murine model of this disease (8, 9). Taking into account that the liver is a secretory organ and its protein products constitute a major source of serum constituents, it was not surprising that relative levels in the serum for liver-derived molecules were significantly altered due to the infection. In the present study, we have identified classical acute-phase response proteins with altered levels early at week 5, but more pronounced alteration at week 7, as shown for C-reactive protein, alpha-1-acid glycoprotein and serum amyloid protein. Their altered levels in the serum of infected animals is possibly a non-specific response to the antigenic burden associated with the parasitism. In agreement, a recent plasma proteome study with patients on acute phase COVID-19 (16) and on infants that had been exposed to Zika Virus (17), demonstrated a similar set of molecules exhibiting altered levels in the plasma associated with both infectious diseases.

Almost one-third of the identified molecules showed altered levels in the serum during experimental schistosomiasis. Complement constituents, acute phase and immune response proteins were responsible for approximately 61% of those differentially abundant, with immunoglobulins representing the largest group in numbers. In this investigation peptides matching IgG have chains contributed with the majority of identities compared to IgA and IgM isotypes. The antigenic stimuli for the induced humoral response are associated with every aspect of the *S. mansoni* life cycle in the vertebrate host, from cercariae penetration (18) to its final establishment in the hepatic portal system (19, 20).

A novel aspect of this host-parasite interaction was revealed by the abundance profile of proteins related to lipid metabolism with implications for immune regulation. CD5 antigen-like is a key regulator of lipid synthesis and inflammatory response mainly secreted by macrophages (21). It circulates in the bloodstream in association with IgM (22).

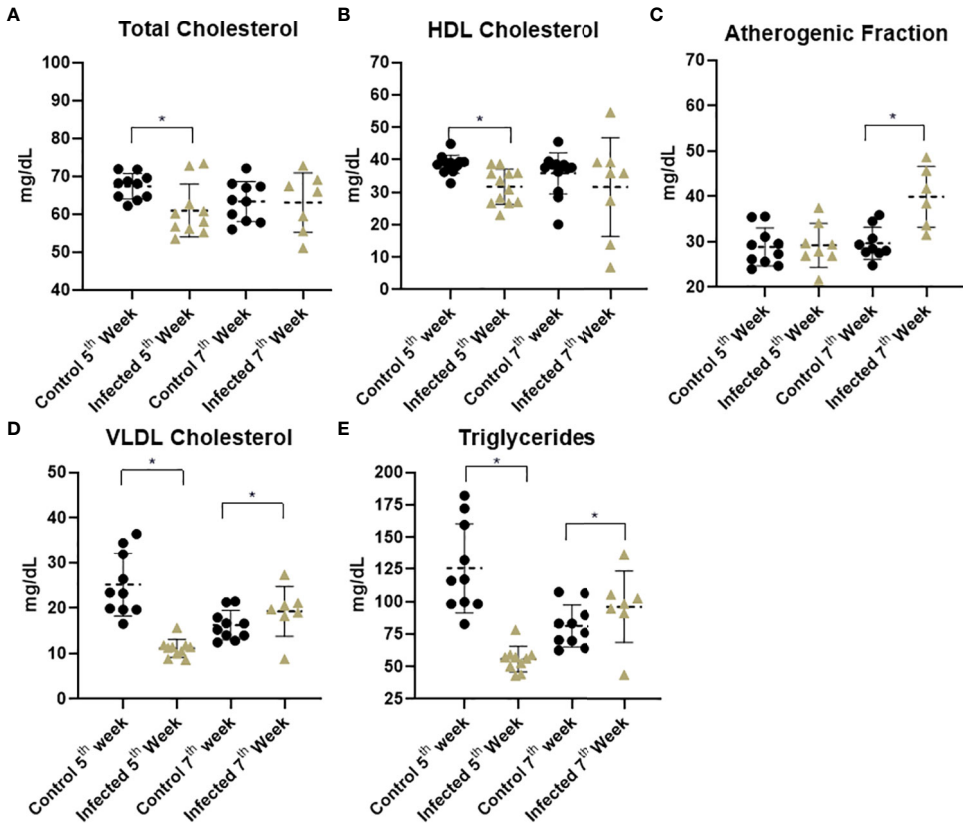

FIGURE 6
Serum lipid profile of experimental groups. Graphics represent the arithmetic means and standard deviations. Asterisks indicate significant differences between the evaluated conditions ($p \leq 0.05$). **(A)** Total cholesterol content of control and infected mice. **(B)** HDL cholesterol demonstrated a decrease at 5th week post infection. **(C)** Infected mice at 7th week displayed a significant increase in the atherogenic fraction. **(D)** VLDL cholesterol levels declined at 5th week post infection and increased at the late time point. **(E)** Triglyceride levels displayed a significant decrease at 5th week post infection followed by an increase at the 7th week.

On adipose tissue, it is internalised by CD36 receptor and binds to fatty acid synthase promoting a decrease in its activity. As a result, lipolysis is stimulated leading to a decrease in lipid droplet content through mobilisation of triglycerides and consequent efflux of fatty acids and glycerol (23, 24). Hepatocytes also incorporate CD5 antigen-like through the same receptor (21, 25). In agreement, the soluble hepatic proteome evaluated during the acute phase of *S. mansoni* infection (10) also demonstrated downregulation of fatty acid synthase in addition to other lipid metabolism-related proteins. In our findings, CD5 antigen-like (Q9QWK4) exhibited increased abundance in both investigated time points. As a classically described immune effector, its expression is positively regulated under inflammatory circumstances (21), justifying its interpretation as a potential biomarker of liver damage (21, 26, 27). To our knowledge, we are the first to report on the differential abundance of CD5 antigen like in the sera of *S. mansoni* infected animals.

In contrast, adiponectin, a classical anti-inflammatory adipose tissue-secreted adipokine which also modulates macrophage function (28) exhibited down regulation in infected animals. Under normal circumstances, it promotes inhibition of inflammatory chemokines and regulates the production of anti-inflammatory cytokines (29). In addition, adiponectin decreases serum levels of triglycerides by enhancing lipoprotein lipase gene expression and activity, leading to decreased levels of circulating triglyceride-rich lipoproteins in the bloodstream (30–32). Moreover, adiponectin augments circulating HDL-C levels by stimulating ApoA-I hepatic synthesis and the ATP-Binding Cassette Transporter A1 pathway (33–35). The decreased abundance in circulating adiponectin observed in our study is in agreement with the inflammatory condition associated with the schistosome infection. The accompanying reduction in HDL cholesterol levels was particularly observed at week 5. At week 7, the sustained low levels of adiponectin are in line

with the increased content of liver derived lipoproteins (mostly composing the atherogenic fraction), a finding reinforced by high levels of apolipoprotein B-100 at the two investigated time points.

Our quantitative data also points to differential lipoprotein remodelling associated with the schistosome infection. Not only lipoproteins were found mainly upregulated, the enzymes phospholipid transfer protein and phosphatidylcholine-sterol acyltransferase, known to participate in the transfer and chemical modification of their lipid contents, increased in abundance as judged by their relative levels at weeks 5 and 7 in infected animals. Of note, various differentially abundant constituents, such as those involved in acute phase response, complement cascade and proteinase inhibitors, have been reported to be ligand-binding partners of lipoproteins, in particular HDL (36, 37). In fact, serum amyloid protein, here found upregulated, is currently considered an exchangeable lipoprotein. It was demonstrated to be associated with VLDL, LDL and HDL leading to enhanced binding of these particles to surface proteoglycans (38). Protocols designed to enrich for lipoproteins in the context of schistosomiasis should provide a better view of their potential ligands and clues to their distinct roles in immune response or sustaining parasitism. Concerning the latter, a recent report has highlighted the lipidomic profile in the *S. mansoni* -infected hamster liver using a combination of mass spectrometric approaches (39). Over 300 lipid markers of infection were appointed in the granulomatous liver, mostly representing phosphatidylcholines, phosphatidylethanolamines, and triglycerides. Our findings provide molecular clues into how lipid metabolism is modulated to attend both host and parasite demands for lipid and lipid-derived molecules. In agreement, the protein-protein interaction network, revealed the potential for complex interactions among molecules related to Lipid Metabolism and Transport group with those belonging to other categories such as acute phase response, complement activity, proteolysis inhibition and hemostasis. Given the predominance of proteins with increased abundance composing this interactome, the various binding possibilities attests for intricate mechanisms of immune response and host metabolism operating in the bloodstream during *S. mansoni* infection.

In this study, quantitative label-free proteomic analysis revealed lipid metabolism related proteins as key modulators

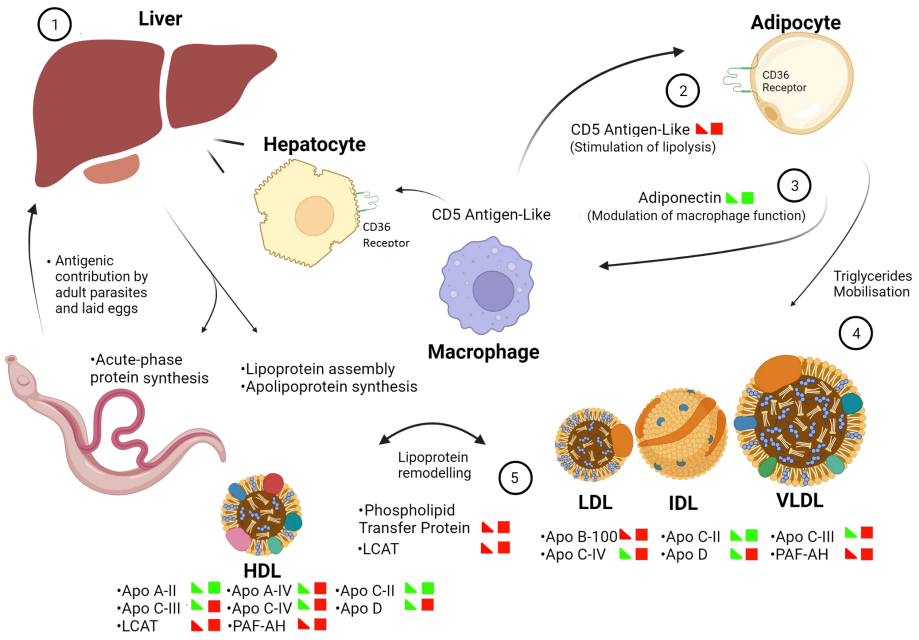

FIGURE 7
Proposed model for lipid metabolism regulation during schistosomiasis and the influence of macrophage and adipose tissue-secreted molecules. Up or down regulation of proteins are represented by half and full squares, meaning the 5th and 7th week post-infection periods, respectively. Colored squares indicate downregulation (green) or upregulation (red). 1) The liver responsible for lipoprotein assembly, apolipoprotein synthesis and overall metabolism receives the antigenic burden associated with adult parasites and laid eggs leading to pronounced changes in protein expression. Macrophages are a hallmark of inflammation during schistosomiasis 2) CD5 antigen-like, mostly secreted by macrophages, can be internalised on hepatocytes and adipocytes through CD36 receptors. 3) Reduced levels of adiponectin secreted by adipocytes contribute to modulate macrophage function and maintenance of the inflammatory status. Adiponectin also influences the serum levels of HDL-C and triglycerides. 4) CD5 antigen-like stimulates lipolysis with consequent triglyceride mobilisation. 5) Altered levels of apolipoproteins and upregulated levels of lipoprotein modifying enzymes (phospholipid transfer protein and LCAT) suggests pronounced lipoprotein remodelling during *S. mansoni* infection. Created with BioRender.com.

of host-parasite interactions during the acute phase of schistosomiasis (Figure 7). The antigenic burden associated with the schistosome infection, in particular during the onset of egg laying, induces an inflammatory condition possibly linked to intense mobilisation of lipids as reflected in the altered lipoprotein profile and proteome of the infected sera. Our study has demonstrated macrophage and adipose tissue-secreted molecules, apolipoproteins/lipoprotein-bound proteins and enzymes differentially abundant, possibly contributing to lipid metabolism modulation. The complex interactions among the differentially abundant serum constituents and target tissues points to intense lipid metabolism regulation during schistosomiasis. It remains to be determined whether the seen alterations in the mouse serum can be translated to human disease to explore novel markers of active infection and inform on the inflammatory status posed by the *S. mansoni* parasitism.

Data availability statement

The mass spectrometry proteomics data have been deposited to the ProteomeXchange Consortium via the PRIDE (40) partner repository with the dataset identifier PXD031974.

Ethics statement

The experimental procedures involving mice were reviewed and approved by the local Ethics Committee on Animal Experimentation 'Comissão de Ética no Uso de Animais' (CEUA), Universidade Federal de Ouro Preto (UFOP), and received the protocol numbers 2017/35 and 2017/34, respectively.

Author contributions

GG-S and WC-B designed, analysed, interpreted data and wrote the manuscript. GG-S and LSV conducted experiments. MC-C and AS conducted instrumental analysis and provided technical expertise. DC contributed to the interpretation of data. All authors reviewed the manuscript. All authors contributed to the article and approved the submitted version.

Funding

This study was financially supported by Fundação de Amparo à Pesquisa do Estado de Minas Gerais (FAPEMIG), grant number: APQ-02745-18, FAPEMIG - Rede Mineira de Imunobiológicos, grant number: 00140-16, Conselho Nacional de Desenvolvimento Científico e Tecnológico (CNPq) grant number: 438798/2018-0 and Universidade Federal de Ouro Preto (UFOP), grant number: 23109.000928/2020-33. GG-S is a recipient of a scholarship from Coordenação de Aperfeiçoamento de Pessoal de Nível Superior - Brasil (CAPES), Finance Code 001. WC-B is a fellow researcher from CNPq (311286/2019-4). The authors also acknowledge the support provided by PROPPI/UFOP and CAPES for fundings provided through the internal call number 18/2022.

Acknowledgments

The authors acknowledge Lobato Paraense Mollusk facility at René Rachou (Fiocruz Minas) for providing the *S. mansoni* cercariae. The BioClin-Quibasa for providing the reagent kits for serum lipids analysis and Laboratório Piloto de Análises Clínicas (Lapac-UFOP). The authors also acknowledge the Laboratório Multiusuário de Proteômica e Biomoléculas (LMU-ProtBio), from Núcleo de Pesquisas em Ciências Biológicas, Universidade Federal de Ouro Preto, MG, Brazil for providing the required equipments and technical expertise.

Conflict of interest

The authors declare that the research was conducted in the absence of any commercial or financial relationships that could be construed as a potential conflict of interest.

Publisher's note

Supplementary material

The Supplementary Material for this article can be found online at: https://www.frontiersin.org/articles/10.3389/fimmu.2022.955049/full#supplementary-material

References

1. Chitsulo L, Engels D, Montresor A, Savioli L. The global status of schistosomiasis and its control. *Acta Trop* (2000) 77(1):41–51. doi: 10.1016/S0001-706X(00)00122-4

2. Engels D, Chitsulo L, Montresor A, Savioli L. The global epidemiological situation of schistosomiasis and new approaches to control and research. *Acta Trop* (2002) 82(2):139–46. doi: 10.1016/S0001-706X(02)00045-1

3. Katz N. *Inquèrito nacional de prevalência da esquistossomose mansoni e geohelmintoses*. Belo Horizonte: CPqRR (2018) p 76.

4. Pearce EJ, MacDonald AS. The immunobiology of schistosomiasis. *Nat Rev Immunol* (2002) 2(7):499–511. doi: 10.1038/nri843

5. Verjovski-Almeida S, DeMarco R, Martins EAL, Guimarães PEM, Ojopi EPB, Paquola ACM, et al. Transcriptome analysis of the acoelomate human parasite schistosoma mansoni. *Nat Genet* (2003) 35(2):148–57. doi: 10.1038/ng1237

6. Berriman M, Haas BJ, LoVerde PT, Wilson RA, Dillon GP, Cerqueira GC, et al. The genome of the blood fluke schistosoma mansoni. *Nature* (2009) 460 (7253):352–8. doi: 10.1038/nature08160

7. Protasio AV, Tsai IJ, Babbage A, Nichol S, Hunt M, Aslett MA, et al. A systematically improved high quality genome and transcriptome of the human blood fluke *Schistosoma mansoni*. *PLoS Negl Trop Dis* (2012) 6(1):e1455. doi: 10.1371/journal.pntd.0001455

8. Manivannan B, Rawson P, Jordan TW, Secor WE, La Flamme AC. Differential patterns of liver proteins in experimental murine hepatosplenic schistosomiasis. *Infect Immun* (2010) 78(2):618–28. doi: 10.1128/IAI.00647-09

9. Manivannan B, Jordan TW, Secor WE, La Flamme AC. Proteomic changes at 8 weeks after infection are associated with chronic liver pathology in experimental schistosomiasis. *J Proteomics* (2012) 75(6):1838–48. doi: 10.1016/j.jprot.2011.12.025

10. Campos JM, Neves LX, de Paiva NCN, de Oliveira E Castro RA, Casé AH, Carneiro CM, et al. Understanding global changes of the liver proteome during murine schistosomiasis using a label-free shotgun approach. *J Proteomics* (2017) 151:193–203. doi: 10.1016/j.jprot.2016.07.013

11. Cosenza-Contreras M, de Oliveira E Castro RA, Mattei B, Campos JM, Gonçalves Silva G, de Paiva NCN, et al. The schistosomiasis SpleenOME: Unveiling the proteomic landscape of splenomegaly using label-free mass spectrometry. *Front Immunol* (2018) 9:3137. doi: 10.3389/fimmu.2018.03137

12. Huang J, Yin X, Zhang L, Yao M, Wei D, Wu Y. Serum proteomic profiling in patients with advanced schistosoma japonicum-induced hepatic fibrosis. *Parasit Vectors* (2021) 14(1):232. doi: 10.1186/s13071-021-04734-1

13. Bi NN, Zhao S, Zhang JF, Cheng Y, Zuo CY, Yang GL, et al. Proteomics investigations of potential protein biomarkers in sera of rabbits infected with schistosoma japonicum. *Front Cell Infect Microbiol* (2021) 11:784279. doi: 10.3389/fcimb.2021.784279

14. Xavier HT, Izar MC, Faria Neto JR, Assad MH, Rocha VZ, Sposito AC, et al. V Diretriz brasileira de dislipidemias e prevenção da aterosclerose. *Arq Bras Cardiol* (2013) 101(4):1–20. doi: 10.5935/abc.2013S010

15. Metsalu T, Vilo J. ClustVis: A web tool for visualizing clustering of multivariate data using principal component analysis and heatmap. *Nucleic Acids Res* (2015) 43(W1):W566–70. doi: 10.1093/nar/gkv468

16. Mohammed Y, Goodlett DR, Cheng MP, Vinh DC, Lee TC, Mcgeer A, et al. Longitudinal plasma proteomics analysis reveals novel candidate biomarkers in acute COVID-19. *J Proteome Res* (2022) 21(4):975–92. doi: 10.1021/acs.jproteome.1c00863

17. Macedo-da-Silva J, Rosa-Fernandes L, Barbosa RH, Angeli CB, Carvalho FR, de Oliveira Vianna RA, et al. Serum proteomics reveals alterations in protease activity, axon guidance, and visual phototransduction pathways in infants with *In utero* exposure to zika virus without congenital zika syndrome. *Front Cell Infect Microbiol [Internet]* (2020) 10:577819. doi: 10.3389/fcimb.2020.577819

18. Curwen RS, Ashton PD, Sundaralingam S, Wilson RA. Identification of novel proteases and immunomodulators in the secretions of schistosome cercariae that facilitate host entry. *Mol Cell Proteomics* (2006) 5(5):835–44. doi: 10.1074/mcp.M500313-MCP200

19. Mathieson W, Wilson RA. A comparative proteomic study of the undeveloped and developed schistosoma *mansoni* egg and its contents: The miracidium, hatch fluid and secretions. *Int J Parasitol* (2010) 40(5):617–28. doi: 10.1016/j.ijpara.2009.10.014

20. DeMarco R, Mathieson W, Manuel SJ, Dillon GP, Curwen RS, Ashton PD, et al. Protein variation in blood-dwelling schistosome worms generated by differential splicing of micro-exon gene transcripts. *Genome Res* (2010) 20 (8):1112–21. doi: 10.1101/gr.100099.109

21. Sanjurjo L, Aran G, Roher N, Valledor AF, Sarrias MR. AIM/CD5L: A key protein in the control of immune homeostasis and inflammatory disease. *J Leukoc Biol* (2015) 98(2):173–84. doi: 10.1189/jlb.3RU0215-074R

22. Kai T, Yamazaki T, Arai S, Miyazaki T. Stabilization and augmentation of circulating AIM in mice by synthesized IgM-fc. *PloS One* (2014) 9(5):e97037. doi: 10.1371/journal.pone.0097037

23. Duncan RE, Ahmadian M, Jaworski K, Sarkadi-Nagy E, Sul HS. Regulation of lipolysis in adipocytes [Internet]. *Annu Rev Nutr* (2007) 27:79–101. doi: 10.1146/annurev.nutr.27.061406.093734

24. Kurokawa J, Arai S, Nakashima K, Nagano H, Nishijima A, Miyata K, et al. Macrophage-derived AIM is endocytosed into adipocytes and decreases lipid droplets *via* inhibition of fatty acid synthase activity. *Cell Metab* (2010) 11 (6):479–92. doi: 10.1016/j.cmet.2010.04.013

25. Maehara N, Arai S, Mori M, Iwamura Y, Kurokawa J, Kai T, et al. Circulating AIM prevents hepatocellular carcinoma through complement activation. *Cell Rep* (2014) 9(1):61–74. doi: 10.1016/j.celrep.2014.08.058

26. Kim WK, Hwang HR, Kim DH, Lee PY, In YJ, Ryu HY, et al. Glycoproteomic analysis of plasma from patients with atopic dermatitis: CD5L and ApoE as potential biomarkers. *Exp Mol Med* (2008) 40(6):677–85. doi: 10.3858/emm.2008.40.6.677

27. Nock S, Johann K, Harder L, Wirth EK, Renko K, Hoefig CS, et al. CD5L constitutes a novel biomarker for integrated hepatic thyroid hormone action. *Thyroid* (2020) 30(6):908–23. doi: 10.1089/thy.2019.0635

28. Yanai H, Yoshida H. Beneficial effects of adiponectin on glucose and lipid metabolism and atherosclerotic progression: Mechanisms and perspectives. *Int J Mol Sci* (2019) 20(5):1190. doi: 10.3390/ijms20051190

29. Fang H, Judd RL. Adiponectin regulation and function. *Compr Physiol* (2018) 8(3):1031–63. doi: 10.1002/cphy.c170046

30. Chan DC, Barrett PH, Ooi EM, Ji J, Chan DT, Watts GF. Very low density lipoprotein metabolism and plasma adiponectin as predictors of high-density lipoprotein apolipoprotein AI kinetics in obese and nonobese men. *J Clin Endocrinol Metab* (2009) 94(3):989–97. doi: 10.1210/jc.2008-1457

31. Qiao L, Zou C, van der Westhuyzen DR, Shao J. Adiponectin reduces plasma triglyceride by increasing VLDL triglyceride catabolism. *Diabetes* (2008) 57 (7):1824–33. doi: 10.2337/db07-0435

32. Kobayashi J, Kusunoki M, Murase Y, Kawashiri M, Higashikata T, Miwa K, et al. Relationship of lipoprotein lipase and hepatic triacylglycerol lipase activity to serum adiponectin levels in Japanese hyperlipidemic men. *Horm Metab Res* (2005) 37(8):505–9. doi: 10.1055/s-2005-870318

33. Oku H, Matsuura F, Koseki M, Sandoval JC, Yuasa-Kawase M, Tsubakio-Yamamoto K, et al. Adiponectin deficiency suppresses ABCA1 expression and ApoA-I synthesis in the liver. *FEBS Lett* (2007) 581(26):5029–33. doi: 10.1016/j.febslet.2007.09.038

34. Matsuura F, Oku H, Koseki M, Sandoval JC, Yuasa-Kawase M, Tsubakio-Yamamoto K, et al. Adiponectin accelerates reverse cholesterol transport by increasing high density lipoprotein assembly in the liver [Internet]. *Biochem Biophys Res Commun* (2007) 358:1091–5. doi: 10.1016/j.bbrc.2007.05.040

35. Van Linthout S, Foryst-Ludwig A, Spillmann F, Peng J, Feng Y, Meloni M, et al. Impact of HDL on adipose tissue metabolism and adiponectin expression. *Atherosclerosis* (2010) 210(2):438–44. doi: 10.1016/j.atherosclerosis.2010.01.001

36. von Zychlinski A, Kleffmann T. Dissecting the proteome of lipoproteins: New biomarkers for cardiovascular diseases? *Trans Proteomics* (2015) 7:30–9. doi: 10.1016/j.trprot.2014.12.001

37. Davidson WS, Shah AS, Sexmith H, Gordon SM. The HDL proteome watch: Compilation of studies leads to new insights on HDL function. *Biochim Biophys Acta Mol Cell Biol Lipids* (2022) 1867(2):159072. doi: 10.1016/j.bbalip.2021.159072

38. Wilson PG, Thompson JC, Shridas P, McNamara PJ, de Beer MC, de Beer FC, et al. Serum amyloid a is an exchangeable apolipoprotein. *Arterioscler Thromb Vasc Biol* (2018) 38(8):1890–900. doi: 10.1161/ATVBAHA.118.310979

39. Wiedemann KR, Peter Ventura A, Gerbig S, Roderfeld M, Quack T, Grevelding CG, et al. Changes in the lipid profile of hamster liver after schistosoma *mansoni* infection, characterized by mass spectrometry imaging and LC–MS/MS analysis. *Anal Bioanal Chem* (2022) 414(12):3653–65. doi: 10.1007/s00216-022-04006-6

40. Vizcaíno JA, Csordas A, Del-Toro N, Dianes JA, Griss J, Lavidas I, et al. 2016 update of the PRIDE database and its related tools. *Nucleic Acids Res* (2016) 44 (22):11033. doi: 10.1093/nar/gkv1145

frontiers | Frontiers in Immunology

TYPE Mini Review
PUBLISHED 02 September 2022
DOI 10.3389/fimmu.2022.955000

OPEN ACCESS

EDITED BY
Thiago Almeida Pereira,
Stanford University, United States

REVIEWED BY
Evaristus Mbanefo,
National Institutes of Health (NIH), United States
Olfat Ali Hammam,
Theodor Bilharz Research Institute, Egypt

*CORRESPONDENCE
Ana C. Madureira
carinamadureira@gmail.com

SPECIALTY SECTION
This article was submitted to Parasite Immunology, a section of the journal Frontiers in Immunology

RECEIVED 27 May 2022
ACCEPTED 16 August 2022
PUBLISHED 02 September 2022

CITATION
Madureira AC (2022) Programmed Cell Death-Ligand-1 expression in Bladder Schistosomal Squamous Cell Carcinoma – *There's room for Immune Checkpoint Blockage? Front. Immunol.* 13:955000. doi: 10.3389/fimmu.2022.955000

Programmed Cell Death-Ligand-1 expression in Bladder Schistosomal Squamous Cell Carcinoma – *There's room for Immune Checkpoint Blockage?*

Ana C. Madureira*

Faculty of Medicine, Eduardo Mondlane University, Maputo, Mozambique

Schistosoma haematobium, the causative agent of urogenital schistosomiasis, is a carcinogen type 1 since 1994. It is strongly associated with bladder squamous-cell carcinoma in endemic regions, where it accounts for 53-69% of bladder-carcinoma cases. This histological subtype is associated with chronic inflammation being more aggressive and resistant to conventional chemo and radiotherapy. Immune-Checkpoint-Blockage (ICB) therapies targeting the Programmed-Cell-Death-Protein-1(PD-1)/Programmed-Cell-Death-Ligand-1(PD-L1) axis showed considerable success in treating advanced bladder urothelial carcinoma. PD-L1 is induced by inflammatory stimuli and expressed in immune and tumor cells. The binding of PD-L1 with PD-1 modulates immune response leading to T-cell exhaustion. PD-L1 presents in several isoforms and its expression is dynamic and can serve as a companion marker for patients' eligibility, allowing the identification of positive tumors that are more likely to respond to ICB therapy. The high PD-L1 expression in bladder-urothelial-carcinoma and squamous-cell carcinoma may affect further ICB-therapy application and outcomes. In general, divergent histologies are ineligible for therapy. These treatments are expensive and prone to auto-immune side effects and resistance. Thus, biomarkers capable of predicting therapy response are needed. Also, the PD-L1 expression assessment still needs refinement. Studies focused on squamous cell differentiation associated with *S. haematobium* remain scarce. Furthermore, in low and middle-income-regions, where schistosomiasis is endemic, SCC biomarkers are needed. This mini-review provides an overview of the current literature regarding PD-L1 expression in bladder-squamous-cell-carcinoma and schistosomiasis. It aims to pinpoint future directions, controversies, challenges, and the importance of PD-L1 as a biomarker for diagnosis, disease aggressiveness, and ICB-therapy prognosis in bladder-schistosomal-squamous-cell carcinoma.

KEYWORDS

***S. haematobium*, PD-L1, Immune-Checkpoint-Blockage therapy, Bladder Squamous Cell Carcinoma, biomarkers**

Introduction

Schistosomiasis is a Neglected Tropical Disease (NTD) that affects over 240 million people worldwide, and 700 million are at risk of infection (1).

The clinical manifestations of the disease's chronic and more severe stages are primarily due to immune reactions against Schistosoma eggs, the principal pathogenic agent, lodged in the tissues leading to granuloma formation (2). Granulomas are comprised of neutrophils, eosinophils, mononuclear cells, lymphocytes, macrophages, multinucleated giant cells, and fibroblasts (3). The granulomatous immune response is essentially coordinated by CD4+ T cells. Nevertheless, CD8+ T cells, B cells, and M2 macrophages also have a role (4, 5). Additionally, the overall egg-induced inflammatory immune response is Th2-biased (6). This polarization can be reverted by Praziquantel-intake as seen by the increase in pro-inflammatory egg-specific cytokine profile, namely Tumor-Necrosis-Factor-alfa (TNF-α), IL-6, Interferon-gamma (INF-γ), IL-12p70 and IL-23, after treatment (7).

The blood fluke *Schistosoma haematobium*, the causative agent of urogenital schistosomiasis, has been considered a carcinogen type 1 since 1994 (8). Moreover, it is strongly associated with bladder-squamous-cell-carcinoma (BSCC) in endemic regions. A Meta-Analysis reported that In Sub-Saharan-Africa it accounts for 53-69% of BC cases (9).

This histological subtype is associated with chronic inflammation being more aggressive and resistant to conventional chemo and radiotherapy (10–15). Immune-Checkpoint-Blockage (ICB) therapies targeting the axis Programmed-Cell-Death-Protein-1(PD-1)/Programmed-Cell-Death-Ligand-1(PD-L1) showed considerable success in treating several carcinomas, including the advanced bladder urothelial carcinoma (aBUC) presenting progressive disease and conventional therapies resistance (16, 17). This axis blockage may lead to complete restoration of the anti-tumor immune response improving disease outcomes (18, 19).

Programmed-Cell-Death-Ligand-1 is induced by inflammatory stimuli and expressed in the immune cells of the hematopoietic line, epithelial cells, and tumor cells, and in the latter, it aids immune evasion. This ligand binds to PD-1 during immune system modulation leading to T cell exhaustion (20). Its expression in the tumor microenvironment can be dynamic and present in several forms: membranar, exosomal, nucleic, and soluble. Such diversity can affect ICB therapy efficacy (21). Furthermore, soluble PD-L1 (sPD-L1) presents several variants, either derived from proteolytic cleavage or *via* matrix metalloproteases (MMPs) and A desintegrin and metalloproteases (ADAM), that are responsible for the shedding of exosomal mPD-L1, or by alternative splicing of PD-L1 pre-mRNA (21). sPD-L1 may also mediate immunosuppression or be responsible for ICB therapy resistance (21, 22).

The expression of mPD-L1 assessed by Immunohistochemistry (IHC) is a companion marker for patients' eligibility for ICB treatment since it allows the identification of tumors that are more likely to be responsive (18, 19, 23). A higher expression is associated with better treatment outcomes. However, it was reported that lower/negative results don't out rule successful ICB therapy (24–26), which may be associated with expression dynamics, tumor heterogeneity, different antibody clones, and staining platforms.

The performance and concordance of the established antibodies and staining platforms have been addressed in BUC and remain elusive (25, 27).

Program-Death-Ligand-1 is known to be overexpressed both in BUC with squamous differentiation and pure SCC (pSCC) and is associated with poorer disease outcomes (28).

This fact can have implications for further immune-therapy application and outcomes since divergent histologies are generally contra-indicated for ICB therapy since, despite mPD-L1 positivity, its overall incidence is low (14). Additionally, studies reported that variant and mixed histologies, including squamous differentiation, might not compromise ICB efficacy (29, 30). ICB treatments are expensive and prone to immune-related adverse events and resistance (31–33). Thus, biomarkers capable of predicting patient response are needed. In low and middle-income-regions, where schistosomiasis is endemic, SCC biomarkers are needed. Expression of sPD-L1 as BC biomarker has been previously approached (34), nevertheless needs further investigation in such settings.

Studies focused on the squamous-cell differentiation-associated or not with *S. haematobium* remain scarce. This mini-review provides an overview of the current literature regarding PD-L1 expression in BSCC and in Schistosomiasis. It aims to pinpoint possible future directions, controversies, and challenges as well as the importance of this ligand as a possible predictor biomarker for diagnosis, disease aggressiveness, and ICB-therapy success in schistosomal bladder-squamous-cell-carcinoma.

Bladder Schistosomal Squamous Cell Carcinoma biomarkers – from *urogenital schistosomiasis to bladder carcinoma*

The exact mechanisms that drive *S. haematobium*-induced bladder carcinoma remain unveiled. The early diagnosis of this condition in a more non-invasive manner is eagerly pursued.

Bernardo et al. (2015) used mass spectrometry and a proteomics approach to evaluate urine biomarkers and study molecular pathways associated with the development of bladder schistosomal – BSCC (BSSCC) (35). They reported a specific profile in patients with BSSCC consisting of higher expression of proteins involved in immunity (complement factor H, complement component 9), negative regulation of endopeptidase activity and inflammation (C-reactive-protein). These proteins are associated with inflammation (mediated by cytokines and chemokines) and signaling pathways related with bladder cancer proliferation (epidermal growth factor (EGF) and fibroblast growth factor (FGF) pathways). Additionally, prolonged inflammation may lead to DNA damage and mutations in the suppressor genes such as TP53 which leads to an overexpression of p53 (36). The study groups presenting only urogenital schistosomiasis (UGS), or BUC revealed a profile associated with microbicide activity such as oxidative stress and immune system related proteins and a profile associated with renal system process, sensory perception and gas and oxygen transport, respectively. The expression of S100 proteins was overlapping in the groups with BSSCC and BC. In patients with UGS, the upregulation of the nuclear factor kappa-light-chain-enhancer of activated B cells (NF-κB), pinpoints the Th2 biased response characteristic from UGS. A recent study, performed in murine models, that addressed the proteome tissue profile in the bladder, after egg-injection, also corroborated that this parasitosis may drive to urothelial hyperplasia and further bladder carcinoma. The study revealed a differentiated expression of several proteins associated with carcinogenic pathways, cellular activity and enhancement of immune inflammatory responses involved in granuloma formation, Th2 responses as well as reduced integrity needed for egg shedding (37). Amongst the proteins associated with malignancy, cell proliferation and cancer poor prognosis was disabled homolog 2 (Dab2) that was reported to be associated with epithelial-mesenchymal transition and tumor aggressiveness in BUC (38). Dab2 has a role in the canonical Tumor-Growth-Factor-beta (TGF-β) signaling in fibroblasts and immune tolerance, especially in regulatory-T-cells (Tregs) - mediated immunosuppression and toll-like receptor (TLR) suppression in antigen presenting cells (APCs) (39, 40). Other proteins associated with inflammation and tissue repair were also upregulated in bladder-egg-injected tissue, namely, complement component 8 (C8a), platelet endothelial cell adhesion molecule (Pecam1) and serine protease inhibitor A3N (Serpina3n) (37).

Several carcinoma biomarkers were investigated in patients with BSCC and BSSCC. Most of them determined by IHC. Badr et al. (2004) evaluated the expression of several tumor markers (p53, bcl2, HER2/neu, MIB-1) related with tumor-suppression, apoptosis inhibition and cell-proliferation. The study population consisted in 15 patients with BSSCC. They concluded that 87% of the cases presented a MIB-1 positive staining, followed by p53 (73%), HER2/neu (27%) and bcl2 (20%) (41). None was significantly associated with disease severity (higher stage and grade). Nevertheless, other authors reported that in patients with *S. haematobium* infection either with BUC or SCC, p53, MIB-1, Bcl-x and Bax were independent prognostic markers (42). Expression of cyclooxygenase (Cox-2), a marker of inflammation and angiogenesis was also associated with disease aggressiveness and poor-prognosis in patients with BSSCC but not in BSCC (43). Later, five biomarkers (Cox-2, p52, Bax, FGF-2, fibrinogen-growth-factor-receptor (FGFR)) were considered the best predictors for oncologic outcomes in a population with SCC where 80.8% presented UGS (44). Furthermore, a study performed in Sudan by Hassan et al. (2013) reported that the expression of Cox2 and Nitric oxide synthase (iNOS) could differentiate schistosomal from non-schistosomal BC, since both markers were highly expressed in patients with BSSCC (45). Nevertheless, these results were not entirely in agreement with another study that showed FGF-2 as the best predictor biomarker for disease outcomes in SCC. Its expression varied significantly according to tumor grade, presence of metastasis and lymphovascular invasion, but not with the presence of UGS (46). Additionally, the overexpression of FGR2 was positively correlated with higher expression of PD-L1 (47).

Were proposed several biomarkers to predict ICB therapy response. NOTCH homolog-4 (NOTCH4) has been correlated with a better response in several carcinomas including BUC (48). A recent study addressed FGFR3 mutations also as possible biomarkers for ICB therapy response. The study included BUC with variant histologies and reported that this marker was not correlated with PD-L1 expression or with pathological response to therapy (49). On the other hand, EFGR expression in bladder tissue has been correlated with squamous differentiation and predicted disease hyper-response after ICB treatment in patients with BUC (50).

Thus, the need of molecular biomarkers to differentiate BUC into molecular subtypes was highlighted given its importance and impact in ICB therapy outcomes. It is known that basal-like sub-types expressing higher levels of the cytokeratin's CK5/6, CK14 and CD44 are associated with worse disease outcome (51). A study by Al-Sharaky et al. (2020) evaluated the expression of CK5, CK14 and CK20 in BUC and after stratification reported that CK5 was significantly associated S. *haematobium* infection in 81.1% of the cases. The sub-group CK5+/CK20- (basal) was only comprised by patients with SCC and schistosomiasis (52). Schistosomiasis was evaluated by microscopic observation of eggs in the bladder tissue which can temper the overall prevalence found (32.2%). More recently, Serag Eldien et al. (2021) reported a significant association between GATA3 lower expression and *S. haematobium* infection while CK5/6 expression was only associated with squamous cell differentiation (53). Patients with pSCC were excluded from the study. Nevertheless, *S. haematobium* infection associated

carcinoma carried poor disease outcome (as short Progression Free Survival).

PD-L1 in infections – *schistosomiasis case*

Infectious pathogens can modulate the host immune system to their benefit. Schistosoma spp are no different since they can polarize naïve-T-cells towards a Th1, Th2, and Treg phenotype depending on the antigen sampled during infection (54).

Studies performed *in vitro* and murine models reported the involvement of PD-L1 and several cells-subsets in Schistosoma infection-associated immune regulation according to the infectious stage of this parasitosis. Smith et al. (2004) demonstrated that *S. mansoni* warms can induce anergy in CD4+ and CD8+ T cells in the initial acute stages of infection *via* selective up-regulation of PD-L1 on the surface of Macrophages (Mϕ) (54). Additionally, the blockage of this ligand restored T-cell activation, thus demonstrating that up-regulated PD-L1 expression in Mϕ induces T-cell hypo-responsiveness granting *S. mansoni* worms the ability to subvert the immune-host response and to reach the egg-laying stage. Besides Macrophages, Dendritic Cells (DCs) were shown to regulate T- cell response either to Schistosome Egg Antigens (SEA) or towards cercaria *via* PD-L1 expression up-regulation. Klaver et al. (2015) showed that DCs stimulation with SEA induced the secretion of Transforming-Growth-Factor-beta (TGF- β) and the surface expression of the co-stimulatory molecules PD-L1 and OX40 ligand (OX40L) (55). PD-L1 and TGF-β induction was stimulated both on the mRNA and protein level. Furthermore, it was observed that the LPS-dependent cytokine induction in DCs was not affected by SEA-heat treatment since the expression of TNF-α, IL-6, and IL-12p70 remained impaired (55).

Later, Winkler et al. (2018) demonstrated that PD-L1 expression, along with PD-L2, IL-10, IL-6, and Macrophage-Inflammatory-Protein-1- alfa (MIP-1-α), was up-regulate on Dermal Dendritic Cells (DDCs) and in immature monocyte-derived DCs (moDCs) after infection by *S. mansoni* cercariae (56). The regulatory ability of extracellular vesicles (EVs), released at the schistosomula stage by *S. mansoni*, was shown to be driven by surface expression of PD-L1 on moDCs. Also, released EVs induced IL-10 and IL-12 overexpression by moDCs (57).

One knows that the induction of IL-10 in B regulatory cells is associated with immunosuppression during helminth infection (58, 59). Xiao et al. (2020) used murine models percutaneously infected with *S. japonicum* cercariae to investigate the B-cells profile and its role in CD4+ T-cells regulation, as well as the regulatory role of PD-L1 during infection (60). They observed that, after *in vitro* stimulation with SEA, B-cells assumed a regulatory phenotype *via* PD-L1 and CD5 up-regulation. Also, B-1a and Marginal-Zone-B-cells (MZB) percentages decreased, while the expression of IL-10, TGF- β, and INF-γ was up-regulated during acute and chronic infection. Additionally, during acute infection, B-cells could affect cytokine responses of CD4+ T-cells generating fewer effector memory cells and higher expression of Bcl-6. At the same time, PD-L1 expression resulted in a recovery of IL-4 production. It was also previously observed in B6 murine models that the expression of PD-L1 and PD-L2 was up-regulated during schistosome infection. Nevertheless, only PD-L2 was significantly reduced in the TLR-2$^{-/-}$ model (61). This result emphasizes the latter's role in the expression of PD-L2, such as the possible different immunological roles of PD-L1 and PD-L2.

A more recent study by Zhang et al. (2021) showed that Myeloid-Derived-Suppressor-Cells (MDSC) in *S. japonicum* infected murine models were able to regulate the T-follicular -helper cells (Tfh-cells) proliferation *via* PD-1/PD-L1 axis (62). The authors reported that SEA and SWA could induce the generation of Tfh-cells in which the PD-1 expression rises along with PD-L1 in MDSC.

The host-immune response towards *S. haematobium* eggs was also addressed in murine models. Bladder-wall egg injection replicated the immune-host response closely related to the human counterpart, including the Th2-biased response, the inflammatory granulomatous environment, fibrosis, egg excretion, and urinary tract morbidity. It was observed in murine models percutaneously infected with cercaria or/and bladder-wall injection an elevation of Th2-cytokines (IL-4, IL-13, and IL-5) at granuloma formation. The systemic profile revealed the same type of response (6). The only bladder cytokine affected by cercaria exposure was leptin (63).

Furthermore, IL-4 and IL-4R were associated with bladder pathogenesis and carcinogenesis in urogenital schistosomiasis (64). The correlation between schistosome antigens and BC was assessed. It was observed that higher antigen densities were correlated with squamous differentiation and with disease aggressiveness (65). Though, the PD-L1 expression wasn't evaluated.

PD-L1 expression in Bladder Squamous Cell Carcinoma – *a brief overview*

A PubMed search with the terms "urothelial carcinoma" AND "PD-L1" retrieved 587 results, while a search using the words "bladder squamous cell carcinoma AND PD-L1" retrieved 41 results. In the latter, only 4 matched the citation. The searches comprised results published between 2006 and 2016, respectively. The difference between results mirrors the lack of studies focused on PD-L1 expression on BC with squamous

differentiation. Nevertheless, the number of publications increased within the last six years. The same string including the term "Schistosomiasis" retrieved one result. Most of the studies evaluated the inter-relationship between clinical-pathological features, the carcinoma subtype, and the expression of PD-L1 assessed by IHC (Table 1). The presence of *S. haematobium* was not evaluated possibly due to the study populations not being from endemic regions or to the retrospective design (Table 1). The only study that included urogenital schistosomiasis was performed in an Egyptian population (69). The PD-L1 expression was evaluated in tumor-micro-arrays (TMA) in a population with pSCC, from which 81.2% had a clinical indication of schistosomiasis. The positivity assessment relied on both immune cells (ICs) and tumour cells (TCs) scores (cut-off of >1%). Only the TCs score showed positivity. A cut-off of 5% was also performed with no positive results. The overall positive PD-L1 expression was 66.9% and the negative PD-L1 expression in the tumor was significantly associated with disease recurrence and cancer-specific mortality after adjusting for pathologic tumor stage, grade, lymph node involvement, and lymphovascular invasion. None of the established companion markers of ICB therapy outcome or staining platforms were used. It wasn't stated how or when Schistosomiasis was diagnosed since the presence of eggs wasn't reported.

Pichler et al. (2017) evaluated the PD-L1 expression as a biomarker for disease outcome in patients with bladder carcinoma (BC) recurrence (66). A high PD-L1 expression in tumor cells (TCs) was associated with worse disease outcomes and was significantly higher in patients with variant histologies (46.2% vs. 20%), though pure or schistosomal-associated squamous-differentiation were not studied. Several molecular characteristics are associated with rare histologies, namely the frequency of biomarkers related to immunotherapy benefits, such as Tumor-Mutational-Burden (TMB), Microsatellite Instability (MSI), PD-L1 gene amplification, and IHC staining of the latter (75). Udager et al. (2018) explored the PD-L1 expression in a cohort of primary pure BSCCs and reported positive staining of 64.7% (68). There were no differences in the clinical-pathological features in this study amongst PD-L1 positive and negative samples. However, the association of PD-L1 expression with basal-like molecular subtypes was established. Also, cyclin-dependent-kinase-inhibitor-2A (CDKN2A) alteration was significantly higher in PD-L1-positive tumors. This was in concordance with Kim et al. (2020) that reported a PD-L1 high positivity strongly correlated with the Basal-Squamous-Like (BASQ) subtype irrespective of antibodies clones used (51).

Necchi et al. (2020) demonstrated that up to 5% and 1% of cases of pSCC and BUC, respectively, featured PD-L1 amplification (76). Remarkably, were no significative differences between these two carcinoma subtypes regarding PD-L1 staining since 2/3 of each study group showed positivity in TCs score and Tumor-Infiltrating-lymphocytes (TILs). Liu et al. (2020) evaluated disease outcomes and progression parameters against PD-L1 expression in non-schistosomal SCC pure and mixed (71). They reported an overall PD-L1 positive staining of 61.2%. The positive PD-L1 TCs score was associated with higher TILs density, independently of tumor histopathologic features and staging. The positivity was also associated with higher Progression-Free-Survival (PFS) and Overall Survival (OS). PD-L1 expression with higher TILs were independent protective factors affecting survival and PFS rate. Gordetsky et al. (2021) stated otherwise since squamous differentiation, in the mix and pure histologies, was associated with worse OS and Cancer-Specific Survival (CSS) and higher PD-L1 expression in TCs was a predictor for worse CSS in pSCC. In the IHC staining the authors used three clinically available antibodies. The positivity score varied accordingly histological subtype being higher in pSCC (73). These conclusions agree with a study performed by Lee et al. (2021). Nevertheless, PD-L1 expression was determined in tumor-infiltrating immune cells (ICs). The overall PD-L1 positivity of 59.4% was closely related to disease aggressiveness and shorter PFS. Furthermore, 53.8% of patients with Mixed BUC presented positive staining though there were no statistically significant differences between histological subtypes (74).

Reis et al. (2019) also assessed the expression of PD-L1 in BC patients with predominant or pure variant histologies using 3 of the antibodies clones available as companion markers for prognosis of ICB (cut-off value of 1 and 5%) and a combined positive score (CPS > 10%) (25). Amongst all of the divergent histologies evaluated, SCCs presented the highest positive score both for TCs and ICs for all the criteria established, though, as seen in Udager et al. (2019), the PD-L1 expression was higher in TCs from the periphery/invasive front of the tumor (68). Nonetheless, the TMB wasn't determine since the basal molecular subtype is enriched with squamous differentiation. Instead, the authors assessed PD-L1 expression in TCs and ICs since these are the accepted host factors associated with ICB therapy's improved outcome. A previous study, also using different established clones for PD-L1 IHC staining, and their established scores, reported that higher-grade tumors showed higher positivity for PD-L1, and SCC demonstrated PD-L1 positivity more frequently than BUC when using one of the clones (67). Nevertheless, the OS, according to histological subtype, wasn't assessed.

A French and Bulgarian cohort study also demonstrated that PD-L1 positive expression was associated with higher tumor grade and stage. A higher CPS in BUC with squamous differentiation (72). Other studies addressed the PD-L1

TABLE 1 Summary of most pertinent publications were PD-L1 expression was addressed by IHC accordingly Squamous differentiation.

Author/ Year/ Country	Study Type	Sample Size	Tumor Subtype N (%)			PD-L1 Positivity or higher positive score N (%)			Conclusions	Limitations
			pSCC	Mixed	UC	pSCC	Mixed	UC		
Pichler et al., 2017 (66) Austria	R	61	9 (14.8)	NA	48 (78.7)	NA	NA	10 (20.8)	Significantly high expression of PD-L1 was seen in the TC score of variant histologies including SCC (46.1%) when compared to pure Urothelial Carcinoma.	Limited number of samples with SCC. Was used a qualitative score for the quantification of PD-L1 (+) immune cells. PD-L1 expression was only reported in the overall mixed subtype.
Davick et al., 2018 (67) USA	R	165	23 (13.9)	NA	130 (78.8)	16 (70)	NA	52 (40)	PD-L1 expression varied according to grade and histological sub-type and was correlated with better OS. SCC showed a higher PD-L1 positivity when compared to UC (cases considered positive with TCs over 1%)	Was used TMA as sampling method for the staining Were only included cystectomy samples and lower stage tumors were under-represented. The scoring method to estimate the % of positive cells was semi-quantitative and can be observer dependent. Also, the number of cases with SCC was limited.
Udager et al., 2018 (68) USA	R	17	17 (100)	NA	NA	11 (64.7)	NA	NA	High PD-L1 expression was associated with basal-like molecular sub-types which may suggest successful ICB.	Small sample size. No comparative analysis was performed using other established staining platforms and scores.
Owyong et al., 2019 (69) Egypt	R	151	151 (100)	NA	NA	101 (66.8)	NA	NA	Most of the cases were previously diagnosed with urogenital Schistosomiasis (80.8%). These patients presented high PD-L1 positivity.	Weren't reported the cases of BSCC with the presence of *S. haematobium* eggs. We're not used established scoring criteria, companion antibodies or platforms for PD-L1 staining.
Reis et al., 2019 (25) USA	R	84	16 (19)	4(4.8)	NA	14 (88)	NA	NA	BCs with squamous differentiation presented higher PD-L1 positivity as well as higher TCs and ICs scores for all the criteria used in the study.	The study did not include pUC, instead compared the PD-L1 expression scores of the variant histologies with previously reported values.
Morsch et al., 2020 (70) Germany	R	108	63 (58.3)	45 (41.7)	NA	52 (82.5)	35 (77.7)	NA	There were no significant differences between the SCC and UC/UCC.	The study didn't include pure UC samples for comparison.
Liu et al., 2020 (71) China	R	67	19 (28.4)	48 (71.6)	NA	13 (68.4)	28 (58.3)	NA	PD-L1 expression and high TILs were associated with poor disease outcomes in patients that underwent radical cystectomy without previous treatment.	Limited sample size. No established companion Abs, platforms or scores were used. Was only considered for PD-L1 positivity the TC score.
Gulinac et al., 2020 (72) France, Hungary	R	105	NA	5 (4.8)	91 (86.7)	2 (40)	NA	27 (30)	There aren't statistically significant differences between PD-L1 expression accordingly histological sub-type. Higher PD-L1 expression was associated with age, gender, and higher tumor grade.	The short representativeness of samples with squamous differentiation comparing to pUC. No established companion Abs, platforms or scores were used.
Goderstsky et al., 2021 (73) USA	R	1478	135 (9.13)	217 (14.7)	1126 (76.2)	133 (86.9)	208 (53.5)	NA	Squamous cell differentiation either in BUCSD and pSCC cases is associated with worse OS and CSS. PD-L1 expression varies accordingly histologic subtype and may predict CSS in SCC patients. The PD-L1 expression didn't varied according to any other demographic or clinical-pathological feature.	The use of TMA for the staining may not grant a representative staining due to tumor heterogeneity. The effect of ICB was not addressed. No comparative analysis was performed with UC.

(Continued)

TABLE 1 Continued

Author/ Year/ Country	Study Type	Sample Size	Tumor Subtype N (%)			PD-L1 Positivity or higher positive score N (%)			Conclusions	Limitations
			pSCC	Mixed	UC	pSCC	Mixed	UC		
Lee et al., 2021 (74) South Korea	R	219	NA	52 (23.7)	167 (76.3)	NA	28 (53.8)	102 (61.1)	No statistically significant differences were found between PD-L1 expression in histological subtypes.	The study didn't include pSCC samples. Was used only one of the established companion Antibodies for the staining.

R, retrospective; NA, Non-Applicable, BUCSC, bladder urothelial carcinoma with squamous differentiation; Abs, antibodies

expression in pSCC, demonstrating that overall, pSCC presented a higher PD-L1 expression when compared with tumors with mixed histology. Still, the difference wasn't statistically significative. It was clear an inter-assay heterogeneity since both ICs and TCs scores varied accordingly to the Antibodies used (70). No comparative analyses were performed regarding pBUC.

Recently, the expression of sPD-L1 as a prognosis marker was examined in the scope of BC and correlated with disease aggressiveness and ICB therapy outcomes (77, 78). Vikerfors et al. (2021) evaluated sPD-L1 expression both in urine and serum of BC patients, from which 9.1% presented squamous-cell features (79). The serum levels weren't significantly different between cases and controls. However, after stratification accordingly, disease aggressiveness, the levels diverged. On the other hand, urinary levels were significantly higher in cases compared to controls. Both were associated with disease aggressiveness, such as metastasis presence. Tosev et al. (2021) reported the same (34). However, the authors didn't study the PD-L1 expression according to the histological subtype.

Discussion – *controversies, challenges, and roads to take*

The high expression of PD-L1 is mainly associated with disease aggressiveness in several carcinomas, including BC with squamous differentiation (Figure 1). This histological subtype was also proposed as a biomarker for ICB-therapy outcomes and disease hyper-progression (50). PD-L1 expression assessment by IHC predicts disease outcomes and ICB therapy success (26). Nevertheless, despite its availability and cost-effectiveness, there

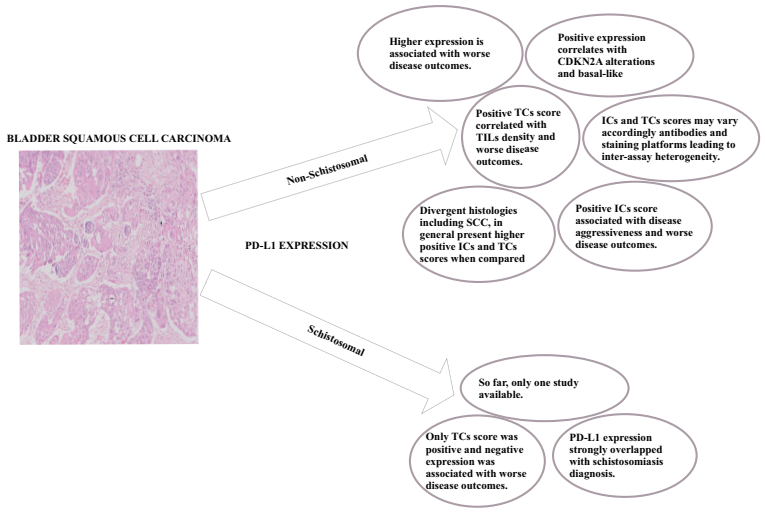

FIGURE 1
Overall key-points regarding PD-L1 expression in Non-Schistosomal and Schistosomal-Squamous-Cell-Carcinoma.

are still pitfalls associated with the inter-assay heterogeneity due to different antibodies and staining platforms as well as different locations where PD-L1 is stained (TCs or ICs) (80). The biopsy can also be a factor for biased results, and challenging staining standardization since the tissue collected can be scarce, leading to misclassification (81). Furthermore, the antibodies available for the staining may not react to all PD-L1 isoforms (25).

The only study that addressed bladder schistosomal SCC didn't use companion antibody clones and presented an unattainable ICs score (69). The authors performed the staining in TMA, which can temper the results given the shortness of tissue sampled. In this regard, further studies are needed since the expression of PD-L1 can be dynamic, as seen in studies that reported divergent expressions or weak correlations between mPD-L1 and sPD-L1 (77, 78). It was shown that mPD-L1 expression correlated with the expression of metalloproteinases in both tissue and serum (77, 82). Krafft et al. (2021) showed a positive correlation between serum MMP-7 and sPD-L1 in patients with BUC, while Pichler et al. (2021) demonstrated an inverse correlation between mPD-L1 and ADAM17 bladder tissue expression (77, 82).

The quantification of sPD-L1 has been associated with disease severity and worse prognosis in several carcinomas (81, 83–85); nevertheless, the studies remain scarce in BC. Urinary sPD-L1 in BC has been associated with disease aggressiveness and treatment outcomes, yet its expression, despite proper, may need further evaluation, namely, to assess the contribution of ICs (34). sPD-L1 can be of great value as a non-invasive form of disease assessment and diagnosis along with other immune mediators, especially in resource-limited settings where *S. haematobium* infection is endemic.

A study by Tetteh-Quarcoo et al. (2019) approached the early correlation between *S. haematobium* infection and carcinogenesis development *via* urinary cytological and wet-mount microscopic analysis. They observed several abnormalities, such as squamous cell metaplasia, inflammatory cells, and hyper-keratinosis, which may lead to a severe form of the disease, such as bladder cancer (86). Later, they showed that Praziquantel intake reduced those abnormalities (87). None of the studies investigated the host-immune response. Nevertheless, other studies reported that several cytokines are associated with *S. haematobium*-induced morbidity, namely TNF-α, IL-10, and IL-6 (88–90). Njaanake et al. (2014) reported a correlation between urinary levels of IL-6 with hematuria, heavy infection, and urinary tract pathology evaluated by ultrasonography (89). Interleukin-6 was associated with BC's poor prognosis. An *in vitro* and *in vivo* study reported a correlation of urinary IL-6 with CD44+ expression in MIBC patients' bladder tissue. Also, CD44+-cells expressed higher levels of PD-L1, which corroborates the role of this pleiotropic cytokine in invasiveness and immune suppression. The abrogation of IL-6 impaired CD44 expression and PD-L1 (91). Korac-Prlica et al. (2020) further referred to the importance of the combinatory immunotherapy approach since carcinogenesis, namely the progression to invasion and squamous differentiation, was impaired by the inhibition of the IL6/STAT3 pathway. Additionally, that fact sensitized BC to anti-PD-L1 immune therapy in an animal model with chemically induced MIBC (92).

In conclusion, the available data shows a correlation between Squamous-Cell differentiation and PD-L1 expression since in carcinomas with such differentiation it is higher. It is known that BUC presents a low PD-L1 (20-30%) expression when compared to other solid tumors (25). The PD-L1 expression reported in BSCC associated with Schistosomiasis was 66.8% which may render it as a plausible target for ICB. Nevertheless, further studies are needed taking into consideration the established criteria for ICB therapy. Furthermore, assess the correlation, role, and utility of cytokines and PD-L1 as disease and prognosis biomarkers, may be pertinent to better understand *S. haematobium*-associated-carcinogenesis, evaluate the benefit of ICB-combinatory-therapy, and overcome resistance and pernicious side-effects.

Author contributions

AM confirms being the sole contributor for this work and has approved it for publication.

Funding

AM is supported by the grant "Enhanced Advanced Biomedical Training in Mozambique" – D43TW010568-013UCSD2017SF – National Institutes of Health (NIH). This publication is of the entire responsibility of the author and does not necessarily reflect the official views of the funding agency.

Acknowledgments

I'm thankful to the Anatomical-Pathology Service from Maputo Central Hospital and to Prof. Doctor Fabiola Fernandes and Dr. Lucília Lovane that kindly provided the Bladder Squamous Cell Carcinoma section image. I am also grateful to the Coordination of the PhD Program in Biosciences and Public Health by the support provided.

Conflict of interest

The author declares that the research was conducted in the absence of any commercial or financial relationships that could be construed as a potential conflict of interest.

Publisher's note

References

1. WHO. *Schistosomiasis*. Geneva - Switzerland: World Health Organization (2022). Available from: https://www.who.int/health-topics/schistosomiasis#tab=tab_1.is.

2. Colley DG, Bustinduy AL, Secor WE, King CH. Human schistosomiasis. *Lancet* (2014) 383(9936):2253–64. doi: 10.1016/S0140-6736(13)61949-2

3. Colley DG, Secor WE. Immunology of human schistosomiasis. *Parasit Immunol* (2014) 36(8):347–57. doi: 10.1111/pim.12087

4. Hams E, Aviello G, Fallon PG. The schistosoma granuloma: friend or foe? *Front Immunol* (2013) 4:89. doi: 10.3389/fimmu.2013.00089

5. Fu CL, Odegaard JI, Hsieh MH. Macrophages are required for host survival in experimental urogenital schistosomiasis. *FASEB J* (2015) 29(1):193–207. doi: 10.1096/fj.14-259572

6. Fu CL, Odegaard JI, Herbert DR, Hsieh MH. A novel mouse model of schistosoma haematobium egg-induced immunopathology. *PloS Pathog* (2012) 8 (3):e1002605. doi: 10.1371/journal.ppat.1002605

7. Bourke CD, Nausch N, Rujeni N, Appleby LJ, Mitchell KM, Midzi N, et al. Integrated analysis of innate, Th1, Th2, Th17, and regulatory cytokines identifies changes in immune polarisation following treatment of human schistosomiasis. *J Infect Dis* (2013) 208(1):159–69. doi: 10.1093/infdis/jis524

8. WHO-IARC. *IARC monographs on the evaluation of carcinogenic risks to humans*. Lyon-France: International Agency for Research on Cancer - WHO (1994).

9. Bowa K, Mulele C, Kachimba J, Manda E, Mapulanga V, Mukosai S. A review of bladder cancer in Sub-Saharan Africa: A different disease, with a distinct presentation, assessment, and treatment. *Ann Afr Med* (2018) 17(3):99–105. doi: 10.4103/aam.aam_48_17

10. Martin JW, Carballido EM, Ahmed A, Farhan B, Dutta R, Smith C, et al. Squamous cell carcinoma of the urinary bladder: Systematic review of clinical characteristics and therapeutic approaches. *Arab J Urol* (2016) 14(3):183–91. doi: 10.1016/j.aju.2016.07.001

11. Kim HS, Seo HK. Immune checkpoint inhibitors for urothelial carcinoma. *Investig Clin Urol* (2018) 59(5):285–96. doi: 10.4111/icu.2018.59.5.285

12. Li G, Hu J, Niu Y. Squamous differentiation in pT1 bladder urothelial carcinoma predicts poor response for intravesical chemotherapy. *Oncotarget* (2018) 9(1):217–23. doi: 10.18632/oncotarget.18563

13. Matulay JT, Woldu SL, Lim A, Narayan VM, Li G, Kamat AM, et al. The impact of squamous histology on survival in patients with muscle-invasive bladder cancer. *Urol Oncol* (2019) 37(6):353.e17–e24. doi: 10.1016/j.urolonc.2019.01.020

14. Dotson A, May A, Davaro F, Raza SJ, Siddiqui S, Hamilton Z. Squamous cell carcinoma of the bladder: poor response to neoadjuvant chemotherapy. *Int J Clin Oncol* (2019) 24(6):706–11. doi: 10.1007/s10147-019-01409-x

15. Fischer-Valuck BW, Michalski JM, Contreras JA, Brenneman R, Christodouleas JP, Abraham CD, et al. A propensity analysis comparing definitive chemo-radiotherapy for muscle-invasive squamous cell carcinoma of the bladder vs. urothelial carcinoma of the bladder using the national cancer database. *Clin Transl Radiat Oncol* (2019) 15:38–41. doi: 10.1016/j.ctro.2018.12.001

16. Ning YM, Suzman D, Maher VE, Zhang L, Tang S, Ricks T, et al. FDA Approval summary: Atezolizumab for the treatment of patients with progressive advanced urothelial carcinoma after platinum-containing chemotherapy. *Oncologist* (2017) 22(6):743–9. doi: 10.1634/theoncologist.2017-0087

17. Suzman DL, Agrawal S, Ning YM, Maher VE, Fernandes LL, Karuri S, et al. FDA Approval summary: Atezolizumab or pembrolizumab for the treatment of patients with advanced urothelial carcinoma ineligible for cisplatin-containing chemotherapy. *Oncologist* (2019) 24(4):563–9. doi: 10.1634/theoncologist.2018-0084

18. Powles T, Eder JP, Fine GD, Braiteh FS, Loriot Y, Cruz C, et al. MPDL3280A (anti-PD-L1) treatment leads to clinical activity in metastatic bladder cancer. *Nature* (2014) 515(7528):558–62. doi: 10.1038/nature13904

19. Powles T, Necchi A, Rosen G, Hariharan S, Apolo AB. Anti-programmed cell death 1/Ligand 1 (PD-1/PD-L1) antibodies for the treatment of urothelial carcinoma: State of the art and future development. *Clin Genitourin Cancer* (2018) 16(2):117–29. doi: 10.1016/j.clgc.2017.11.002

20. Zou W, Wolchok JD, Chen L. PD-L1 (B7-H1) and PD-1 pathway blockade for cancer therapy: Mechanisms, response biomarkers, and combinations. *Sci Transl Med* (2016) 8(328):328rv4. doi: 10.1126/scitranslmed.aad7118

21. Bailly C, Thuru X, Quesnel B. Soluble programmed death ligand-1 (sPD-L1): A pool of circulating proteins implicated in health and diseases. *Cancers* (2021) 13(12):3034. doi: 10.3390/cancers13123034

22. Gong B, Kiyotani K, Sakata S, Nagano S, Kumehara S, Baba S, et al. Secreted PD-L1 variants mediate resistance to PD-L1 blockade therapy in non-small cell lung cancer. *J Exp Med* (2019) 216(4):982–1000. doi: 10.1084/jem.20180870

23. Ionescu DN, Downes MR, Christofides A, Tsao MS. Harmonization of PD-L1 testing in oncology: a Canadian pathology perspective. *Curr Oncol* (2018) 25(3): e209–e16. doi: 10.3747/co.25.4031

24. Bancu A, Cowan R, Chaturvedi A. PD-L1 testing and immunotherapy selection - early laboratory experience and its potential role in head and neck cancer management. *Arch Clin Cases* (2021) 8(1):14–8. doi: 10.22551/2021.30.0801.10179

25. Reis H, Serrette R, Posada J, Lu V, Chen YB, Gopalan A, et al. PD-L1 expression in urothelial carcinoma with predominant or pure variant histology: Concordance among 3 commonly used and commercially available antibodies. *Am J Surg Pathol* (2019) 43(7):920–7. doi: 10.1097/PAS.0000000000001264

26. Aggen DH, Drake CG. Biomarkers for immunotherapy in bladder cancer: a moving target. *J Immunother Cancer* (2017) 5(1):94. doi: 10.1186/s40425-017-0299-1

27. Hodgson A, Slodkowska E, Jungbluth A, Liu SK, Vesprini D, Enepekides D, et al. PD-L1 immunohistochemistry assay concordance in urothelial carcinoma of the bladder and hypopharyngeal squamous cell carcinoma. *Am J Surg Pathol* (2018) 42(8):1059–66. doi: 10.1097/PAS.0000000000001084

28. Zhu L, Sun J, Wang L, Li Z, Wang L, Li Z. Prognostic and clinicopathological significance of PD-L1 in patients with bladder cancer: A meta-analysis. *Front Pharmacol* (2019) 10:962. doi: 10.3389/fphar.2019.00962

29. Miller NJ, Khaki AR, Diamantopoulos LN, Bilen MA, Santos V, Agarwal N, et al. Histological subtypes and response to PD-1/PD-L1 blockade in advanced urothelial cancer: A retrospective study. *J Urol* (2020) 204(1):63–70. doi: 10.1097/JU.0000000000000761

30. Necchi A, Raggi D, Gallina A, Madison R, Colecchia M, Lucianò R, et al. Updated results of PURE-01 with preliminary activity of neoadjuvant pembrolizumab in patients with muscle-invasive bladder carcinoma with variant histologies. *Eur Urol* (2020) 77(4):439–46. doi: 10.1016/j.eururo.2019.10.026

31. Bai J, Gao Z, Li X, Dong L, Han W, Nie J. Regulation of PD-1/PD-L1 pathway and resistance to PD-1/PD-L1 blockade. *Oncotarget* (2017) 8(66):110693–707. doi: 10.18632/oncotarget.22690

32. Ramos-Casals M, Brahmer JR, Callahan MK, Flores-Chávez A, Keegan N, Khamashta MA, et al. Immune-related adverse events of checkpoint inhibitors. *Nat Rev Dis Primers* (2020) 6(1):38. doi: 10.1038/s41572-020-0160-6

33. Christy J, Rafae A, Kandah E, Kunadi A. Early presentation of pembrolizumab-associated pneumonitis. *BMJ Case Rep* (2021) 14(7):e242493. doi: 10.1136/bcr-2021-242493

34. Tosev G, Wahafu W, Reimold P, Damgov I, Schwab C, Aksoy C, et al. Detection of PD-L1 in the urine of patients with urothelial carcinoma of the bladder. *Sci Rep* (2021) 11(1):14244. doi: 10.1038/s41598-021-93754-z

35. Bernardo C, Cunha MC, Santos JH, da Costa JM, Brindley PJ, Lopes C, et al. Insight into the molecular basis of schistosoma haematobium-induced bladder cancer through urine proteomics. *Tumour Biol* (2016) 37(8):11279–87. doi: 10.1007/s13277-016-4997-y

36. Warren W, Biggs PJ, el-Baz M, Ghoneim MA, Stratton MR, Venitt S. Mutations in the p53 gene in schistosomal bladder cancer: a study of 92 tumours from Egyptian patients and a comparison between mutational spectra from schistosomal and non-schistosomal urothelial tumours. *Carcinogenesis* (1995) 16 (5):1181–9. doi: 10.1093/carcin/16.5.1181

37. Osakunor DNM, Ishida K, Lamanna OK, Rossi M, Dwomoh L, Hsieh MH. Host tissue proteomics reveal insights into the molecular basis of schistosoma

haematobium-induced bladder pathology. *PloS Negl Trop Dis* (2022) 16(2): e0010176. doi: 10.1371/journal.pntd.0010176

38. Itami Y, Miyake M, Ohnishi S, Tatsumi Y, Gotoh D, Hori S, et al. Disabled homolog 2 (DAB2) protein in tumor microenvironment correlates with aggressive phenotype in human urothelial carcinoma of the bladder. *Diagn (Basel)* (2020) 10 (1):54. doi: 10.3390/diagnostics10010054

39. Figliuolo da Paz V, Ghishan FK, Kiela PR. Emerging roles of disabled homolog 2 (DAB2) in immune regulation. *Front Immunol* (2020) 11:580302. doi: 10.3389/fimmu.2020.580302

40. Figliuolo da Paz V, Jamwal DR, Gurney M, Midura-Kiela M, Harrison CA, Cox C, et al. Rapid downregulation of DAB2 by toll-like receptor activation contributes to a pro-inflammatory switch in activated dendritic cells. *Front Immunol* (2019) 10:304. doi: 10.3389/fimmu.2019.00304

41. Badr KM, Nolen JD, Derose PB, Cohen C. Muscle invasive schistosomal squamous cell carcinoma of the urinary bladder: frequency and prognostic significance of p53, BCL-2, HER2/neu, and proliferation (MIB-1). *Hum Pathol* (2004) 35(2):184–9. doi: 10.1016/j.humpath.2003.10.006

42. Haitel A, Posch B, El-Baz M, Mokhtar AA, Susani M, Ghoneim MA, et al. Bilharzial related, organ confined, muscle invasive bladder cancer: prognostic value of apoptosis markers, proliferation markers, p53, e-cadherin, epidermal growth factor receptor and c-erbB-2. *J Urol* (2001) 165(5):1481–7. doi: 10.1016/S0022-5347(05)66332-X

43. Youssef R, Kapur P, Kabbani W, Shariat SF, Mosbah A, Abol-Enein H, et al. Bilharzial vs non-bilharzial related bladder cancer: pathological characteristics and value of cyclooxygenase-2 expression. *BJU Int* (2011) 108(1):31–7. doi: 10.1111/j.1464-410X.2010.09854.x

44. Youssef RF, von Rundstedt FC, Kapur P, Mosbah A, Abol-Enein H, Ghoneim M, et al. Utility of biomarkers in the prediction of oncologic outcome after radical cystectomy for squamous cell carcinoma. *J Urol* (2015) 193(2):451–6. doi: 10.1016/j.juro.2014.08.109

45. Hassan HE, Mohamed AA, Bakhiet AO, Ahmed HG. Immunohistochemical expression of COX2 and iNOS in bladder cancer and its association with urinary schistosomiasis among Sudanese patients. *Infect Agent Cancer* (2013) 8(1):9. doi: 10.1186/1750-9378-8-9

46. Youssef RF, Kapur P, Mosbah A, Abol-Enein H, Ghoneim M, Lotan Y. Role of fibroblast growth factor in squamous cell carcinoma of the bladder: prognostic biomarker and potential therapeutic target. *Urol Oncol* (2015) 33(3):111.e1–7. doi: 10.1016/j.urolonc.2014.09.020

47. McNiel EA, Tsichlis PN. Analyses of publicly available genomics resources define FGF-2-expressing bladder carcinomas as EMT-prone, proliferative tumors with low mutation rates and high expression of CTLA-4, PD-1 and PD-L1. *Signal Transduct Target Ther* (2017) 2:e16045. doi: 10.1038/sigtrans.2016.45

48. Long J, Wang D, Yang X, Wang A, Lin Y, Zheng M, et al. Identification of NOTCH4 mutation as a response biomarker for immune checkpoint inhibitor therapy. *BMC Med* (2021) 19(1):154. doi: 10.1186/s12916-021-02031-3

49. Necchi A, Raggi D, Giannatempo P, Marandino L, Fare E, Gallina A, et al. Can patients with muscle-invasive bladder cancer and fibroblast growth factor receptor-3 alterations still be considered for neoadjuvant pembrolizumab? a comprehensive assessment from the updated results of the PURE-01 study. *Eur Urol Oncol* (2021) 4(6):1001–5. doi: 10.1016/j.euo.2020.04.005

50. Miyama Y, Morikawa T, Miyakawa J, Koyama Y, Kawai T, Kume H, et al. Squamous differentiation is a potential biomarker predicting tumor progression in patients treated with pembrolizumab for urothelial carcinoma. *Pathol Res Pract* (2021) 219:153364. doi: 10.1016/j.prp.2021.153364

51. Kim B, Lee C, Kim YA, Moon KC. PD-L1 expression in muscle-invasive urinary bladder urothelial carcinoma according to Basal/Squamous-like phenotype. *Front Oncol* (2020) 10:527385. doi: 10.3389/fonc.2020.527385

52. Al-Sharaky DR, Abdelwahed M, Asaad N, Foda A, Abdou AG. Stratification of urinary bladder carcinoma based on immunohistochemical expression of CK5, CK14 and CK20. *J Immunoassay Immunochem* (2021) 42(3):236–51. doi: 10.1080/15321819.2020.1845726

53. Serag Eldien MM, Abdou AG, Elghrabawy GRA, Alhanafy AM, Mahmoud SF. Stratification of urothelial bladder carcinoma depending on immunohistochemical expression of GATA3 and CK5/6. *J Immunoassay Immunochem* (2021) 42(6):662–78. doi: 10.1080/15321819.2021.1937212

54. Smith P, Walsh CM, Mangan NE, Fallon RE, Sayers JR, McKenzie AN, et al. Schistosoma mansoni worms induce anergy of T cells *via* selective up-regulation of programmed death ligand 1 on macrophages. *J Immunol* (2004) 173(2):1240–8. doi: 10.4049/jimmunol.173.2.1240

55. Klaver EJ, Kuijk LM, Lindhorst TK, Cummings RD, van Die I. Schistosoma mansoni soluble egg antigens induce expression of the negative regulators SOCS1 and SHP1 in human dendritic cells *via* interaction with the mannose receptor. *PloS One* (2015) 10(4):e0124089. doi: 10.1371/journal.pone.0124089

56. Winkel BMF, Dalenberg MR, de Korne CM, Feijt C, Langenberg MCC, Pelgrom L, et al. Early induction of human regulatory dermal antigen presenting cells by skin-penetrating schistosoma mansoni cercariae. *Front Immunol* (2018) 9:2510. doi: 10.3389/fimmu.2018.02510

57. Kuipers ME, Nolte-'t Hoen ENM, van der Ham AJ, Ozir-Fazalalikhan A, Nguyen DL, de Korne CM, et al. DC-SIGN mediated internalisation of glycosylated extracellular vesicles from schistosoma mansoni increases activation of monocyte-derived dendritic cells. *J Extracell Vesicles* (2020) 9(1):1753420. doi: 10.1080/20013078.2020.1753420

58. Pearce EJ, MacDonald AS. The immunobiology of schistosomiasis. *Nat Rev Immunol* (2002) 2(7):499–511. doi: 10.1038/nri843

59. Maizels RM, Yazdanbakhsh M. Immune regulation by helminth parasites: cellular and molecular mechanisms. *Nat Rev Immunol* (2003) 3(9):733–44. doi: 10.1038/nri1183

60. Xiao J, Guan F, Sun L, Zhang Y, Zhang X, Lu S, et al. B cells induced by schistosoma japonicum infection display diverse regulatory phenotypes and modulate CD4(+) T cell response. *Parasit Vectors* (2020) 13(1):147. doi: 10.1186/s13071-020-04015-3

61. Gao Y, Chen L, Hou M, Chen Y, Ji M, Wu H, et al. TLR2 directing PD-L2 expression inhibit T cells response in schistosoma japonicum infection. *PloS One* (2013) 8(12):e82480. doi: 10.1371/journal.pone.0082480

62. Zhang Y, Wu Y, Liu H, Gong W, Hu Y, Shen Y, et al. Granulocytic myeloid-derived suppressor cells inhibit T follicular helper cells during experimental schistosoma japonicum infection. *Parasit Vectors* (2021) 14(1):497. doi: 10.1186/s13071-021-05006-8

63. Loc L, Mbanefo EC, Khludenev G, Lamanna O, Banskota N, Hsieh MH. Schistosoma haematobium cercarial infection alters subsequent systemic immune responses to eggs but has minimal impact on immune responses to egg injection of the bladder. *Parasit Immunol* (2019) 41(1):e12602. doi: 10.1111/pim.12602

64. Mbanefo EC, Fu CL, Ho CP, Le L, Ishida K, Hammam O, et al. Interleukin-4 signaling plays a major role in urogenital schistosomiasis-associated bladder pathogenesis. *Infect Immun* (2020) 88(3):e00669–19. doi: 10.1128/IAI.00669-19

65. Wishahi M, Zakarya A, Hamamm O, Abdel-Rasol M, Badawy H, Elganzoury H, et al. Impact of density of schistosomal antigen expression in urinary bladder tissue on the stratification, cell type, and staging, and prognosis of carcinoma of the bladder in Egyptian patients. *Infect Agent Cancer* (2014) 9:21. doi: 10.1186/1750-9378-9-21

66. Pichler R, Heidegger I, Fritz J, Danzl M, Sprung S, Zelger B, et al. PD-L1 expression in bladder cancer and metastasis and its influence on oncologic outcome after cystectomy. *Oncotarget* (2017) 8(40):66849–64. doi: 10.18632/oncotarget.19913

67. Davick JJ, Frierson HF, Smolkin M, Gru AA. PD-L1 expression in tumor cells and the immunologic milieu of bladder carcinomas: a pathologic review of 165 cases. *Hum Pathol* (2018) 81:184–91. doi: 10.1016/j.humpath.2018.06.028

68. Udager AM, McDaniel AS, Hovelson DH, Fields K, Salami SS, Kaffenberger SD, et al. Frequent PD-L1 protein expression and molecular correlates in urinary bladder squamous cell carcinoma. *Eur Urol* (2018) 74(4):529–31. doi: 10.1016/j.eururo.2018.06.019

69. Owyong M, Lotan Y, Kapur P, Panwar V, McKenzie T, Lee TK, et al. Expression and prognostic utility of PD-L1 in patients with squamous cell carcinoma of the bladder. *Urol Oncol* (2019) 37(7):478–84. doi: 10.1016/j.urolonc.2019.02.017

70. Morsch R, Rose M, Maurer A, Cassataro MA, Braunschweig T, Knüchel R, et al. Therapeutic implications of PD-L1 expression in bladder cancer with squamous differentiation. *BMC Cancer* (2020) 20(1):230. doi: 10.1186/s12885-020-06727-2

71. Liu Z, Meng Y, Cao Y, Chen Y, Fan Y, Li S, et al. Expression and prognostic value of PD-L1 in non-schistosoma-associated urinary bladder squamous cell carcinoma. *Transl Androl Urol* (2020) 9(2):428–36. doi: 10.21037/tau.2020.02.12

72. Gulinac M, Dikov D, Velikova T, Belovezhdov V. Increased PD-L1 expression in high-grade bladder cancer with squamous cell differentiation in Bulgarian and French patients' samples. *Ann Diagn Pathol* (2020) 49:151640. doi: 10.1016/j.anndiagpath.2020.151640

73. Gordetsky JB, Montgomery KW, Giannico GA, Rais-Bahrami S, Thapa P, Boorjian S, et al. The significance of squamous histology on clinical outcomes and PD-L1 expression in bladder cancer. *Int J Surg Pathol* (2021) 30(1):6–14. doi: 10.1177/10668969211027264

74. Lee DH, Jeong JY, Song W. Prognostic value of programmed death ligand-1 expression on tumor-infiltrating immune cells in patients treated with cisplatin-based combination adjuvant chemotherapy following radical cystectomy for muscle-invasive bladder cancer: A retrospective cohort study. *Onco Targets Ther* (2021) 14:845–55. doi: 10.2147/OTT.S291327

75. Yang Y, Jain RK, Glenn ST, Xu B, Singh PK, Wei L, et al. Complete response to anti-PD-L1 antibody in a metastatic bladder cancer associated with novel MSH4 mutation and microsatellite instability. *J Immunother Cancer* (2020) 8(1):e000128. doi: 10.1136/ jitc-2019-000128

76. Necchi A, Madison R, Raggi D, Jacob JM, Bratslavsky G, Shapiro O, et al. Comprehensive assessment of immuno-oncology biomarkers in adenocarcinoma, urothelial carcinoma, and squamous-cell carcinoma of the bladder. *Eur Urol* (2020) 77(4):548–56. doi: 10.1016/j.eururo.2020.01.003

77. Krafft U, Olah C, Reis H, Kesch C, Darr C, Grunwald V, et al. High serum PD-L1 levels are associated with poor survival in urothelial cancer patients treated with chemotherapy and immune checkpoint inhibitor therapy. *Cancers (Basel)* (2021) 13(11):2548. doi: 10.3390/cancers13112548

78. Ando K, Hamada K, Watanabe M, Ohkuma R, Shida M, Onoue R, et al. Plasma levels of soluble PD-L1 correlate with tumor regression in patients with lung and gastric cancer treated with immune checkpoint inhibitors. *Anticancer Res* (2019) 39(9):5195–201. doi: 10.21873/anticanres.13716

79. Vikerfors A, Davidsson S, Frey J, Jerlstrom T, Carlsson J. Soluble PD-L1 in serum and urine in urinary bladder cancer patients. *Cancers (Basel)* (2021) 13 (22):5841. doi: 10.3390/cancers13225841

80. Pichler R, Fritz J, Lackner F, Sprung S, Brunner A, Horninger W, et al. Prognostic value of testing PD-L1 expression after radical cystectomy in high-risk patients. *Clin Genitourin Cancer* (2018) 16(5):e1015–e24. doi: 10.1016/j.clgc.2018.05.015

81. Oh SY, Kim S, Keam B, Kim TM, Kim DW, Heo DS. Soluble PD-L1 is a predictive and prognostic biomarker in advanced cancer patients who receive immune checkpoint blockade treatment. *Sci Rep* (2021) 11(1):19712. doi: 10.1038/s41598-021-99311-y

82. Pichler R, Lindner AK, Schafer G, Tulchiner G, Staudacher N, Mayr M, et al. Expression of ADAM proteases in bladder cancer patients with BCG failure: A pilot study. *J Clin Med* (2021) 10(4):764. doi: 10.3390/jcm10040764

83. Zhang J, Gao J, Li Y, Nie J, Dai L, Hu W, et al. Circulating PD-L1 in NSCLC patients and the correlation between the level of PD-L1 expression and the clinical characteristics. *Thorac Cancer* (2015) 6(4):534–8. doi: 10.1111/1759-7714.12247

84. Zhou J, Mahoney KM, Giobbie-Hurder A, Zhao F, Lee S, Liao X, et al. Soluble PD-L1 as a biomarker in malignant melanoma treated with checkpoint blockade. *Cancer Immunol Res* (2017) 5(6):480–92. doi: 10.1158/2326-6066.CIR-16-0329

85. Huang P, Hu W, Zhu Y, Wu Y, Lin H. The prognostic value of circulating soluble programmed death ligand-1 in cancers: A meta-analysis. *Front Oncol* (2020) 10:626932. doi: 10.3389/fonc.2020.626932

86. Tetteh-Quarcoo PB, Akuetteh BK, Owusu IA, Quayson SE, Attah SK, Armah R, et al. Cytological and wet mount microscopic observations made in urine of schistosoma haematobium-infected children: Hint of the implication in bladder cancer. *Can J Infect Dis Med Microbiol* (2019) 2019:7912186. doi: 10.1155/2019/7912186

87. Tetteh-Quarcoo PB, Ampong A, Dayie N, Ahenkorah J, Udofia EA, Afutu E, et al. Dynamics in morbidity markers and cytological observations made in urine of schistosoma haematobium-infected children: Pre- and post-praziquantel treatment in an endemic setting. *Med Sci (Basel)* (2022) 10(1):14. doi: 10.3390/medsci10010014

88. Wamachi AN, Mayadev JS, Mungai PL, Magak PL, Ouma JH, Magambo JK, et al. Increased ratio of tumor necrosis factor-alpha to interleukin-10 production is associated with schistosoma haematobium-induced urinary-tract morbidity. *J Infect Dis* (2004) 190(11):2020–30. doi: 10.1086/425579

89. Njaanake KH, Simonsen PE, Vennervald BJ, Mukoko DA, Reimert CM, Gachuhi K, et al. Urinary cytokines in schistosoma haematobium-infected schoolchildren from tana delta district of Kenya. *BMC Infect Dis* (2014) 14:501. doi: 10.1186/1471-2334-14-501

90. Bustinduy AL, Sutherland LJ, Chang-Cojulun A, Malhotra I, DuVall AS, Fairley JK, et al. Age-stratified profiles of serum IL-6, IL-10, and TNF-alpha cytokines among Kenyan children with schistosoma haematobium, plasmodium falciparum, and other chronic parasitic Co-infections. *Am J Trop Med Hyg* (2015) 92(5):945–51. doi: 10.4269/ajtmh.14-0444

91. Wu CT, Lin WY, Chen WC, Chen MF. Predictive value of CD44 in muscle-invasive bladder cancer and its relationship with IL-6 signaling. *Ann Surg Oncol* (2018) 25(12):3518–26. doi: 10.1245/s10434-018-6706-0

92. Korac-Prlic J, Degoricija M, Vilovic K, Haupt B, Ivanisevic T, Frankovic L, et al. Targeting Stat3 signaling impairs the progression of bladder cancer in a mouse model. *Cancer Lett* (2020) 490:89–99. doi: 10.1016/j.canlet.2020.06.018

frontiers | Frontiers in Immunology

TYPE Original Research
PUBLISHED 02 September 2022
DOI 10.3389/fimmu.2022.911139

OPEN ACCESS

EDITED BY
Thiago Almeida Pereira,
Stanford University, United States

REVIEWED BY
Nan Hou,
Chinese Academy of Medical Sciences and Peking Union Medical College, China
Rong Liu,
Wuhan University, China
Jianping Cao,
Chinese Center for Disease Control and Prevention (Chinese Center for Tropical Diseases Research), China

*CORRESPONDENCE
Guofeng Cheng
cheng_guofeng@foxmail.com;
chengguofeng@tongji.edu.cn

†These authors have contributed equally to this work

SPECIALTY SECTION
This article was submitted to Parasite Immunology, a section of the journal Frontiers in Immunology

RECEIVED 02 April 2022
ACCEPTED 09 August 2022
PUBLISHED 02 September 2022

CITATION
Giri BR, Li S, Fang C, Qiu L, Yan S, Pakharukova MY and Cheng G (2022) Dynamic miRNA profile of host T cells during early hepatic stages of *Schistosoma japonicum* infection. *Front. Immunol.* 13:911139. doi: 10.3389/fimmu.2022.911139

Dynamic miRNA profile of host T cells during early hepatic stages of *Schistosoma japonicum* infection

Bikash R. Giri[1†], Shun Li[2†], Chuantao Fang[1], Lin Qiu[3], Shi Yan[4], Maria Y. Pakharukova[5,6,7] and Guofeng Cheng[1*]

[1]Shanghai Tenth People's Hospital, Institute for Infectious Diseases and Vaccine Development, Tongji University School of Medicine, Shanghai, China, [2]Key Laboratory of Animal Parasitology of Ministry of Agriculture and Rural Affairs, Shanghai Veterinary Research Institute, Chinese Academy of Agricultural Sciences, Shanghai, China, [3]Shanghai Institute of Nutrition and Health, Chinese Academy of Sciences, Shanghai, China, [4]Institut für Parasitologie, Veterinärmedizinische Universität, Wien, Austria, [5]Institute of Cytology and Genetics, Siberian Branch of Russian Academy of Sciences, Novosibirsk, Russia, [6]Department of Natural Sciences, Novosibirsk State University, Novosibirsk, Russia, [7]Institute of Molecular Biology and Biophysics, Novosibirsk, Russia

Schistosomes undergo complicated migration in final hosts during infection, associated with differential immune responses. It has been shown that $CD4^+$ T cells play critical roles in response to *Schistosoma* infections and accumulated documents have indicated that miRNAs tightly regulate T cell activity. However, miRNA profiles in host T cells associated with *Schistosoma* infection remain poorly characterized. Therefore, we undertook the study and systematically characterized T cell miRNA profiles from the livers and blood of *S. japonicum* infected C57BL/6J mice at 14- and 21-days post-infection. We observed 508 and 504 miRNAs, in which 264 miRNAs were co-detected in T cells isolated from blood and livers, respectively. The comparative analysis of T cell miRNAs from uninfected and infected C57BL/6J mice blood showed that *miR-486b-5p/3p* expression was significantly downregulated and linked to various T cell immune responses and *miR-375-5p* was highly upregulated, associated with Wnt signaling and pluripotency, Delta notch signaling pathways, *etc.* Whereas hepatic T cells showed *miR-466b-3p*, *miR-486b-3p*, *miR-1969*, and *miR-375* were differentially expressed compared to the uninfected control. The different expressions of some miRNAs were further corroborated in isolated T cells from mice and *in vitro* cultured EL-4 cells treated with *S. japonicum* worm antigens by RT-qPCR and similar results were found. In addition, bioinformatics analysis combined with RT-qPCR validation of selected targets associated with the immune system and parasite-caused infectious disease showed a significant increase in the expression of *Ctla4*, *Atg5*, *Hgf*, *Vcl* and *Arpc4* and a decreased expression of *Fermt3*, *Pik3r1*, *Myd88*, *Nfkbie*, *Ppp1r12a*, *Ppp3r1*, *Nfyb*, *Atg12*, *Ube2n*, *Tyrobp*, *Cxcr4* and *Tollip*. Overall, these results unveil the comprehensive repertoire of T cell miRNAs during *S. japonicum* infection, suggesting that the circulatory (blood) and liver systems have distinct miRNAs landscapes that may be important for regulating T cell immune response. Altogether, our findings indicated a dynamic expression pattern of T cell miRNAs during the hepatic stages of *S. japonicum* infection.

10.3389/fimmu.2022.911139

KEYWORDS

Schistosoma japonicum, T cell, infection, immune response, microRNA

Introduction

Schistosoma has a complex life cycle and needs different hosts (intermediate host and definitive host) to complete its life cycle. It has fascinating migratory nature starting from the infection site of the skin epidermis to blood vessels, then through the heart and lungs to the vasculature of the livers (1). During the migratory process, significant morphological changes and worm developments are associated with parasites (2). Ultimately, the parasites can develop into adult worms and then survive within the venous system of the definitive mammalian hosts for many years (3). The circulatory system is accumulated by various immune defenses, including immune cells, phagocytes, complement proteins, and antibodies. The adult schistosomes are shown to adopt several strategies, from coating their outer tegument with antigens from the hosts to secreting excretory-secretory products and extracellular vesicles to modulate the host immune response in its favor (4).

Livers are known as immune-permissive organs with unique anatomy, which contain various immunocompetent cells such as dendritic cells, Kupffer cells (KCs), natural killer (NK) cells, natural killer T cells, regulatory T cells, *etc.* (5, 6). Schistosomes have complicated migration in final hosts. Upon cercaria penetrating the skin epidermis, juvenile schistosomula are transformed and then reaches the dermal blood vessels. Then schistosomula reach the lungs and *S. japonicum* schistosomula found in lungs at day 2 and peaks at 3 days post-infection. Subsequently, S. *japonicum* schistosomula usually migrate into the liver 3 days post-infection and take 8-10 days for them to grow up and develop in the livers. Then, parasites begin to lodge in the portal and mesenteric veins at 11 days post infection. The early phase of *S. japonicum* living in the hepatic portal vein is essential to find a mate and pairing and complete maturation as well as flow to reach the egg laying sites (2, 7). The majority of studies focused on *S. japonicum* eggs induced immune response and liver pathology in final hosts (8), however, early stages of hepatic progression and related host immune response, which is critical for parasite development and maturation, remains poorly characterization. Consequently, it is necessary to determine how *S. japonicum* infection induces host immune response at early hepatic schistosomula stages, which may help to further reveal the relationship between schistosomula modulating host immune response and parasite development.

T helper cells have a crucial role in shaping the immune responses during schistosomiasis (9). During the early phase of infection, cercaria initiates a Th1 immune response, characterized by increased pro-inflammatory cytokines, including TNF-α and IFN-γ, IL-1, and IL-6 (10). When worms develop into adults and lay eggs, however, the Th2 immune response is triggered by their soluble egg antigen (11, 12). The Th2 immune response plays a critical role in the pathogenesis of schistosomiasis (13). Previous studies have suggested that Th17/IL-17 exacerbates egg-induced liver pathology and treatment with anti-IL-17 antibodies remarkably inhibits hepatic granulomatous inflammation (14). Then, Treg cells are recruited in the liver to hepatic granulomas and exert an immunosuppressive role to limit granulomatous inflammation and fibrosis (15, 16). Moreover, recent studies showed that Tfh and Th9 cells potentially promote liver granulomas and fibrogenesis in *S. japonicum* infected murine model of schistosomiasis (17, 18). Overall, these studies suggested that T cell subsets undergo complex crosstalk with antigen-presenting cells that regulate the pathological progression of schistosomiasis (19).

MicroRNAs (miRNAs) are endogenous small non-coding RNAs that regulate various biological processes, including proliferation, development, differentiation, and cell death, *etc.* (20). In the murine liver, some miRNAs such as *miR-146b* and *miR-155* are dysregulated during the mid-phase of schistosome infection, indicating they are potentially involved in the modulation of hepatic inflammation (21, 22). Additionally, some studies have suggested that specific miRNAs can regulate T-cell activation, proliferation, and development by targeting prime transcription factors, signaling molecules, and cytokines (23, 24). For instance, the ablation of mature miRNAs at the early thymocyte developmental stage leads to the developmental arrest and a consequent peripheral mature alpha-beta T and invariant natural killer T (iNKT) cell pool (25–28). Furthermore, the enhanced expressions of *miR-146b* and *miR-155* may induce the recruitment of lymphocytes (B and T lymphocytes) in response to antigens secreted by eggs (29, 30). Besides, the miRNA expression profile of thymic T cells at each developmental stage shows a unique pattern of expression (31). Overall, these studies suggested that miRNAs can regulate T cells differentiation and functions. However, the detailed repertoire of T cell miRNAs has not been explored yet during *Schistosoma* infection particularly for early stage. Understanding of mechanisms of miRNAs mediated T cell immune response during *S. japonicum* infection may help to develop effective strategies against schistosomiasis.

Here, we reported the comprehensive repertoire of T cell miRNA profiles from blood and livers of C57BL/6J mice during *S. japonicum* infection at 14 dpi and 21 dpi using fluorescence-activated cell sorting (FACs) combined with deep sequencing. In comparison to uninfected control, we identified several miRNAs that are differentially and enriched explicitly in T cells of *S. japonicum*-infected mice. The results indicated the dynamic expression profiles of T cell miRNAs in blood and livers, exhibiting unique regulatory signatures during *S. japonicum* infection at early hepatic schistosomula stages (14 dpi and 21 dpi).

Materials and methods

Establishment of schistosomiasis mice model

Male C57BL/6J mice (6–8 weeks old) were procured from Shanghai SLAC Laboratory of Animal Co., Ltd, (Shanghai, China). All animals were housed under standard experimental conditions. All animal experiment protocols were approved by the Animal Management Committee and the Animal Care and Use Committee of the Shanghai Science and Technology Commission of the Shanghai Municipal government for Shanghai Veterinary Research Institute, Chinese Academy of Agriculture Sciences, China (Permit No. SHVRI-SZ-20200720-03). The life cycle of *S. japonicum* (Anhui isolate) was maintained in male mice and the intermediate snail host *Oncomelania hupensis* (Center of National Institute of Parasitic Disease, Chinese Center for Disease Control and Prevention, Shanghai, China). The mice were challenged with 50 ± 2 *S. japonicum* cercariae *via* abdominal skin.

Purification of T cells from peripheral blood and liver

A total of two biological replicates were used for each group (the sample for each biological replicate is pooled from 10 mice, n = 10). At 14- and 21-days post-infection (dpi), blood samples were collected from *S. japonicum* infected mice in anticoagulant blood collection tubes (BD Biosciences, Mountain View, CA, USA). Similarly, blood samples of uninfected mice were collected as a control. The whole blood was diluted with PBS and overlaid on top of the Ficoll (1.084). Then centrifuge at 400 × *g* for 30-40 min at room temperature, during the centrifugation, granulocytes, platelets and red blood cell (RBC) pellet to the bottom of the tube and the peripheral blood mononuclear cells (PBMCs) float over the Ficoll-plasma interface layer. After collection, PBMCs were washed with PBS at 300 × *g* at 4°C twice. Then PBMCs were lysed using RBC lysis buffer (Biolegend, San Diego, USA) and the remaining cells were pelleted and resuspended in 200 µL of wash solution. The fluorochrome-conjugated antibodies against mouse (BV510, Fixable Viability Stain 510, BD Biosciences, Mountain View, USA), CD45, CD45R (B220), CD3e, CD4 and CD8a (eBioscience™, Frankfurt, Germany) with the dilutions as suggested by manufacturer was used to stain immune cells and then cells were sorted using a BD FACsAria II system (BD Biosciences, Mountain View, USA). Firstly, we sorted the live cells by gating BV510 positive cells and then interrogated for surface CD45 expression to sort leukocytes. Later T and B cells were sorted using CD3e and B220 antibodies. Then the CD3e positive population was gated using CD4 and CD8a antibodies to sort T cells. The flow cytometry data were analysed using FlowJo (v10.6.2).

For isolating liver T cells, both infected and uninfected mice were anesthetized, and livers were perfused with RPMI-1640 (Invitrogen, USA) at indicated days of post infection (dpi). The livers were thoroughly washed, minced into small pieces with surgical scissors, and forced through a 70 µm cell strainer (Falcon) using a sterile syringe plunger. The obtained preparation was suspended in 50 mL RPMI-1640 medium and centrifuged for 5 min at 700 × *g* at 4°C. Then, the pellet was resuspended with 30 mL of 40% Percoll (GE Healthcare, Boston, USA), recentrifuged for 20 min at 900 × *g* at 4°C with the off-brake setting twice. The resultant sediments were resuspended in RPMI-1640 and filtered through a 40 µm cell strainer (Falcon). The pellet was resuspended again in 2 mL of RBC lysis buffer (Biolegend, San Diego, USA), incubated for 5 min, then centrifuged for 5 min at 500 × *g* at 4°C. Finally, the pellet obtained was resuspended in 1 mL PBS and the antibodies used in above sections were added with same dilutions and incubated for 30 min at 4°C. After staining, cells were washed with PBS containing 0.04% BSA at 500 × *g* for 5 min at 4°C. The collected cells were resuspended and sorted by flow cytometry as described for T cell purification. The information of antibodies used are listed and provided in Supplementary Table 1.

RNA preparation, sequencing and data analysis

Total RNAs were extracted from sorted peripheral blood T cells and liver T cells (14 dpi, 21 dpi and uninfected control) using a miRNeasy Mini Kit (QIAGEN, Germany). RNA quality was evaluated using an Agilent 2100 Bioanalyzer (Agilent Technologies). Small RNAs in the 18-30 nt fraction were extracted from denaturing 15% polyacrylamide gels and used for library preparation using the TruSeq® Small RNA Library Preparation Kit (Illumina, CA, USA). Twelve resulting small-RNA libraries were subjected to Illumina 50 bp single-end sequencing by Illumina HiSeq™ 2500 sequencing at BGI (The Beijing Genomics Institute). Following sequencing, raw reads were cleaned by removing adapter sequences, reads containing poly-N, low-quality reads, and oligonucleotides with length >32

or <18 nt. The remaining sequences were mapped to the reference genome and another small RNA database, including miRbase, siRNA, piRNA, and snoRNA with Bowtie (32). The covariance models (cm) search was mainly performed for Rfam mapping (33). The software miRDeep2 (34) was used to predict novel miRNA by exploring the secondary structure. The small RNA expression level is calculated by counting absolute numbers of molecules using unique molecular identifiers (35). Differential expression analysis was performed using the DEGseq (36), Q value ≤ 0.05, and the absolute value of Log2Ratio ≥ 1 as the default threshold to judge the significance of expression difference. RNAhybrid (37), miRanda (38) and TargetScan (39) were used to predict the target genes of miRNAs. To annotate gene functions, the target genes were aligned against the Kyoto Encyclopedia of Genes (KEGG) and Gene Ontology (GO) database (40, 41). GO enrichment analysis and KEGG enrichment analysis of target genes were performed using phyper, a function of R. The *P*-value was corrected using the Bonferroni method (42), and a corrected *P*-value ≤ 0.05 was taken as a threshold. GO terms or KEGG terms fulfilling this condition were significantly enriched terms.

Preparation of *S. japonicum* soluble antigen and stimulation of isolated T cells and EL-4 cells

Freshly perfused *S. japonicum* were thoroughly washed in PBS (pH 7.4). PBS solution containing protease and phosphatase inhibitor (Thermo Fisher Scientific Corp., MA, USA) was added and the mixture was homogenized for 30 min on ice and the homogenate was sonicated for 30 min. Then centrifuged at 16,000 x *g* for 30 min and the supernatant was used for *S. japonicum* soluble worm antigen (SWA). Protein concentration was measured by standard Bradford protein assay (Beyotime Biotechnology, China) using bovine serum albumin as standard. T cells were isolated from blood and liver of C57BL/6J mice using CD90.2$^+$ MicroBeads (Miltenyi Biotec, Bergisch Gladbach, Germany) following manufacturers protocol. Isolated cells were cultured RPMI 1640 medium containing 10% fetal bovine serum and 1% penicillin-streptomycin solution, Then, the cells were treated with *S. japonicum* soluble antigen (15 μg/mL) or PBS (control) for 36 h and total RNA was isolated and RT-qPCR was performed to assess the miRNA expression. Similarly, EL-4 cells were treated with *S. japonicum* soluble antigen or PBS (control) and RT-qPCR was carried out to assess selected miRNA expression.

MiRNA and its target gene expression validation by RT-qPCR

A real-time quantitative reverse transcription-polymerase chain reaction (RT-qPCR) was performed to confirm miRNA expressions and the target gene expressions in isolated T cells. Briefly, total RNA was extracted using Trizol (Thermo Fisher Scientific) and reversed transcribed using the miScript II RT Kit (QIAGEN, Hilden, Germany). The miRNA expression was determined using the reverse primer given in the miScript SYBR Green PCR Kit (QIAGEN). For the expressions of target genes, the real-time PCR was performed using the following thermal cycling program: 95°C for 5 min, 40 cycles at 95°C for 10 s, 57°C for 20 s, and 72°C for 36 s. *U6* (a type of small nuclear RNA) and *glyceraldehyde-3-phosphate dehydrogenase* (*GAPDH*) were used as the internal controls. The fold change was calculated using the $2^{-\Delta CT}$ method (43). All the primer sequences are provided in Supplementary Tables 2, 3.

MiRNA target pathway network building

To build a murine miRNA target network, we used the online tool miRTargetLink 2.0 (https://www.ccb.uni-saarland.de/mirtargetlink2) to build the miRNA target network (44). The strongly validated targets with pathways were included to build and visualize the network of several most significantly differentially expressed miRNAs such as *miR-486b-5p*, *miR-375-5p*, *miR-1969*, *miR-486b-3p*, *etc.*

Statistical analyses

The RT-qPCR results were expressed as mean ± SEM from representative triplicate experiments. The comparison among uninfected vs 14 dpi and 21 dpi were analyzed using one-way ANOVA and comparative analysis between two groups were analyzed using Student's T-test. The results at $P \leq 0.05$ were considered statistically significant.

Results

Experimental design and data output

T cells were isolated from murine peripheral blood and liver tissues using flow cytometry (the details of workflow and T cell sorting were shown in Figure 1A and Supplementary Figures 1A, B). The average of live T cells isolated from murine blood were 85.2%, 99.4% and 97.4% at 14 dpi, 21 dpi and uninfected mice, respectively. Similarly, there were 94.4%, 99.6% and 93.95% of average live T cells isolated from livers at 14 dpi, 21 dpi and uninfected mice, respectively (Supplementary Figures 1C, D). In addition, we observed the average of live CD4$^+$ T cells (66.15%, 50.3% and 66.15% for blood; 74.1%, 60.9% and 57.95% for liver) and CD8a$^+$ T cells (25.7%, 22.75% and 26.3% for blood; 10.15%, 20.25% and 15.8% for liver) at 14 dpi, 21 dpi and uninfected mice (Supplementary Figures 1E, F). Then, the isolated T cells

10.3389/fimmu.2022.911139

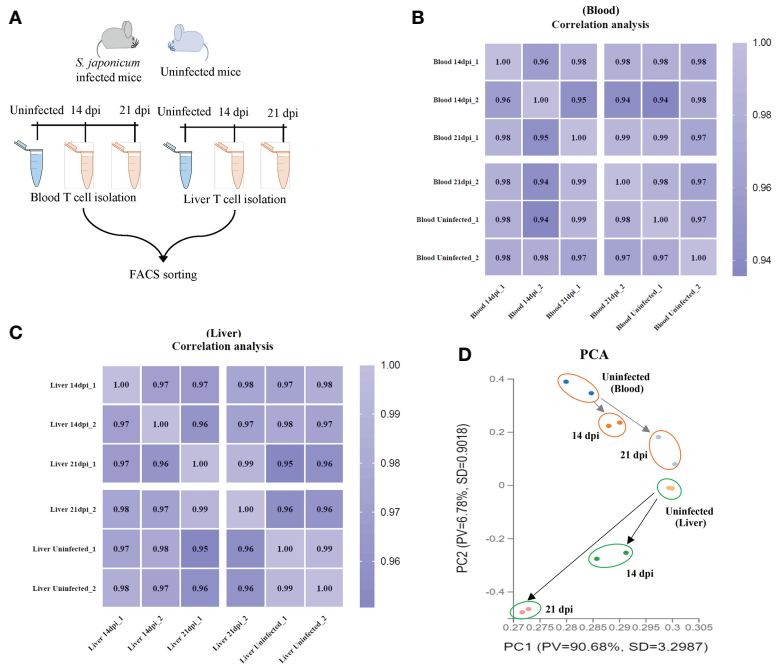

FIGURE 1
T cell isolation and RNA seq analyses. **(A)** Schematic workflow for T cell isolation at different stages of *S. japonicum* infected mice and uninfected mice; **(B, C)** Heatmap of Pearson correlations of T cell miRNA expressions among different samples from blood **(B)** and liver **(C)** at different stages of *S. japonicum* infected mice and uninfected mice. Colors in the heat map indicate the Pearson correlation coefficient among different samples, lighter color indicated higher correlation; **(D)** PCA analyses of T cell samples isolated from blood and liver of *S. japonicum* infected mice at 14 dpi and 21 dpi and uninfected mice.

were subject to RNA isolation for RNA-Seq analyses. Details output data of RNA-seq for each library given in Supplementary Data Sheets 1, 2. The average number of obtained clean reads for T cells isolated from blood were approximately 25.92, 29.51 and 28.12 million and were approximately 33.50, 30.95 and 30.78 million for T cells isolated from liver at 14 dpi, 21 dpi and uninfected mice, respectively (Supplementary Data Sheet 1). The average percentages of the total mapping clean reads were 87.315%, 91.21% and 92.98% for blood T cells at 14 dpi, 21 dpi and uninfected mice and were 86.465%, 85.18% and 89.28% for liver T cells in corresponding groups, respectively (Supplementary Data Sheet 2). The classifications and distributions of small RNAs for each sample given in Supplementary Figures 2A, B. The results showed that most reads are related to intergenic regions followed by unmapped, hairpin, mature, rRNA, tRNA and precursor and others. To determine the cluster of miRNA expression profiles among different samples (blood and liver) for different groups (14 dpi, 21 dpi and uninfected mice), Pearson correlation analysis was performed. The correlation heat map showed that infected and uninfected had distinct clusters based on the miRNA expression profiles (Figures 1B, C). All samples were subjected to principal component analysis (PCA) to assess variations. The results indicated that each T cell sample isolated from different stages (14 dpi, 21 dpi and uninfected control) or organs (blood and liver) is close together, in contrast, a higher dispersion of samples between blood and liver at different stages or organs was observed (Figure 1D).

MiRNA profiles of T cells from blood of *S. japonicum* infected mice

A total of 508 miRNAs was detected in T cells isolated from blood in *S. japonicum* infected at 14 dpi, 21 dpi and uninfected mice, respectively (Figure 2A). Meanwhile, we observed 264 co-detected miRNAs, out of which 50 miRNAs exhibited increased expressions and 81 miRNAs showed decreased expressions compared to the T cells from uninfected control (Supplementary Figures 2C, D). In detail, 60 miRNAs were specifically detected in T cells from uninfected control and 21 dpi, whereas 35 miRNAs were specifically detected from 14 dpi (Figure 2A). The differentially expressed miRNAs between two groups (uninfected vs 14 dpi: 12 decreased and 12 increased; uninfected vs 21 dpi: 15 decreased and 16 increased) showed the co-detected and specific miRNAs (Figure 2B; Supplementary Datasheet 3), among them, we noted 14 co-detected miRNAs (mark in green) and two novel miRNAs (*novel-miR-365-5p* and *novel-miR-243-3p*, mark in blue) at 14 and

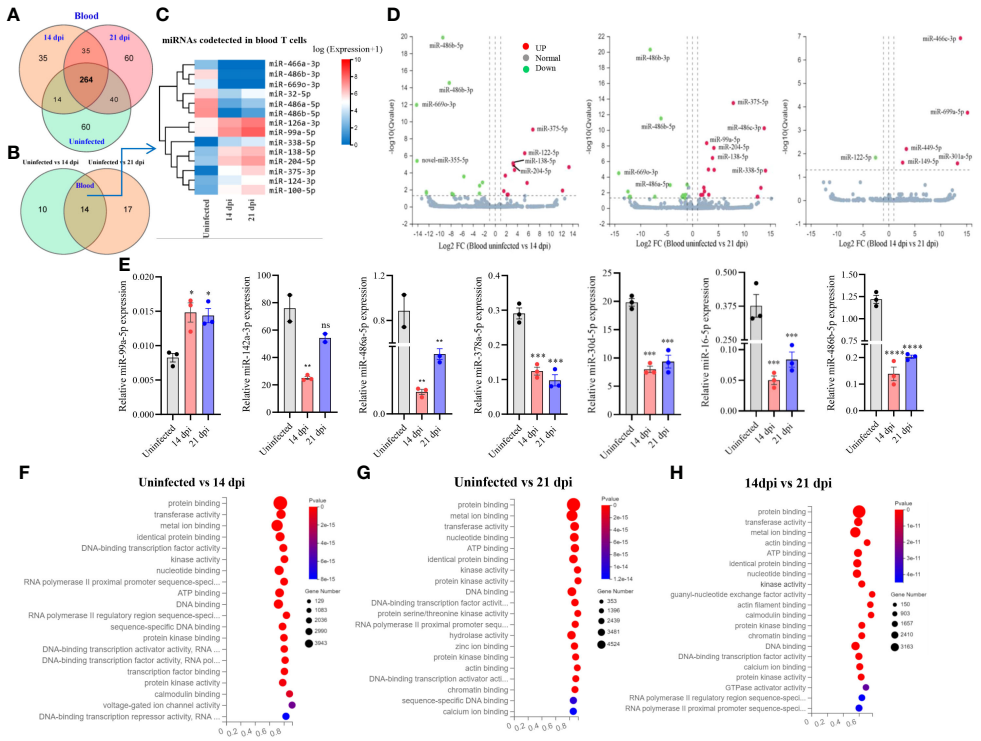

FIGURE 2
Blood T cell miRNA profiles, expression validation and prediction of molecular functions of their targets. **(A)** Venn diagram showing total and co-detected blood T cell miRNAs among uninfected, 14 dpi and 21 dpi groups (the number indicates the common or specific miRNAs identified in different groups); **(B)** Venn diagram showing codetected and specific blood T cell miRNAs between two groups (uninfected vs 14 dpi and uninfected vs 21 dpi); **(C)** Heatmap showing differentially expressed blood T cell miRNAs co-detected between two groups (uninfected vs. 14 dpi and uninfected vs. 21 dpi); **(D)** Volcano plot showing differentially expressed blood T cell miRNAs for different comparative analyses (uninfected control vs 14 dpi; uninfected control vs 21 dpi; 14 dpi vs 21 dpi). Green dot indicates downregulated miRNAs, red dot indicates upregulated miRNAs and grey dot indicates no significantly expressed miRNAs; **(E)** Validation of increased and decreased expressions of miRNAs of blood T cells by RT-qPCR. Data illustrate representative results and show the mean and standard error mean from an experiment carried out in triplicate. Statistical analysis was performed comparing uninfected vs 14 dpi or 21 dpi using one-way ANOVA and * denotes $P \leq 0.05$, ** denotes $P \leq 0.01$, *** denotes $P \leq 0.001$, **** denotes $P \leq 0.0001$ and ns denotes non-significant; **(F–H)** GO enrichment analyses of molecular functions of targets for differently expressed miRNAs (Uninfected vs 14 dpi **(F)**; Uninfected vs 21 dpi **(G)**; 14 dpi vs 21 dpi **(H)** in blood T cells). The results showing 20 most significantly enrichment functions of targets for differentially expressed miRNAs.

21 dpi (Supplementary Figures 3A, B). The heatmap of co-detected miRNAs revealed 14 differentially expressed miRNAs (7 increased and 7 decreased) in blood T cells among 14 and 21 dpi (Figure 2C). Volcano plot analysis indicated that the expressions of *miR-486b-5p/3p* and *miR-669o-3p* were decreased in blood T cells of mice infected with *S. japonicum* (14 dpi and 21 dpi), and in contrast, *miR-375-5p*, *miR-138-5p*, and *miR-204-5p* were upregulated (Figure 2D). We further wanted to know whether there are any specific miRNA expression profiles between 14 dpi and 21 dpi, and the results showed significant downregulation of *miR-122-5p*, whereas upregulation of *miR-669a-5p*, *miR-449a-5p*, *miR-301a-5p*, *miR-149-5p*, and *miR-466c-3p* (Figure 2D). These results indicated that T cell miRNAs altered their expressions at blood of mice during different stages of *S. japonicum* infection.

Subsequently, we validated the expressions of several miRNAs using RT-qPCR and found that the majority of selected miRNAs (75%) showed consistent expressions with RNA-seq results. As shown in Figure 2E, we observed that *miR-99a-5p* expression was significantly increased in T cells of blood from 14 dpi and 21 dpi infected mice compared with uninfected control, whereas *miR-142a-3p*, *miR-486a-5p*, *miR-486b-5p*, *miR-378a-5p*, *miR-16-5p*, and *miR-30d-5p* were decreased. These results were consistent with RNA-Seq data. In addition, analysis of the isolated blood T cells treated with SWA indicated the decreased expressions of *miR-181c-5p, miR-29a-3p, miR-16-5p, miR-30d-5p, miR-142a-3p, miR-151-5p, miR-378a-5p and miR-486b-5p* as compared with that of control (Supplementary Figure 4A). Similar results were also noted in EL-4 T cell treated with SWA (Supplementary Figure 4C). Overall, these results were further corroborated with the differentially expressed miRNAs in blood T cells of *S. japonicum* infected mice. GO analysis of putative targets of the

differentially expressed miRNAs in T cells isolated from blood showed significant enrichment of molecular functions such as protein binding, metal ion binding, nucleotide binding, ATP binding, and DNA binding (Figures 2F–H; Supplementary Datasheet 5). The GO biological processes showed their associations with positive/negative regulation of transcription by RNA polymerase II, multicellular organism development, cell differentiation, *etc.* (Supplementary Figures 3E–G; Supplementary Datasheet 5).

MiRNA profiles of T cells from the livers of *S. japonicum* infected mice

Totally, 504 miRNAs were detected in T cells isolated from the livers in *S. japonicum* infected and uninfected mice, respectively (Figure 3A). Among them, 59 and 85 miRNAs were specifically detected at 21 dpi and uninfected control, respectively, whereas 18 miRNAs were specifically detected at 14 dpi (Figure 3A). We observed 264 co-detected miRNAs, of which 52 and 133 miRNAs were up- and downregulated compared to the uninfected control, respectively (Supplementary Figures 2E, F). Analysis of the differentially expressed miRNAs between two groups (uninfected vs 14 dpi: 3 decreased and 14 increased; uninfected vs 21 dpi: 26 decreased and 26 increased) showed the co-detected and specific miRNAs (Figure 3B; Supplementary Datasheet 3). In addition, seven novel miRNAs (*novel-miR-133-3p*, *novel-miR-120-3p*, *novel-miR-62-5p*, *novel-miR-279-3p*, *novel-miR-389-3p*, *novel-miR-226-3p*, and *novel-miR-44-5p*, mark in blue) were also shown to differentially express in T cell of liver between *S. japonicum* infected mice (14 dpi or 21 dpi and uninfected control (Supplementary Figures 3C, D). The heatmap of miRNAs in liver T cells at 14 dpi and 21 dpi showed four co-detected differentially expressed miRNAs (*miR-10a-5p*, *miR-466b-*

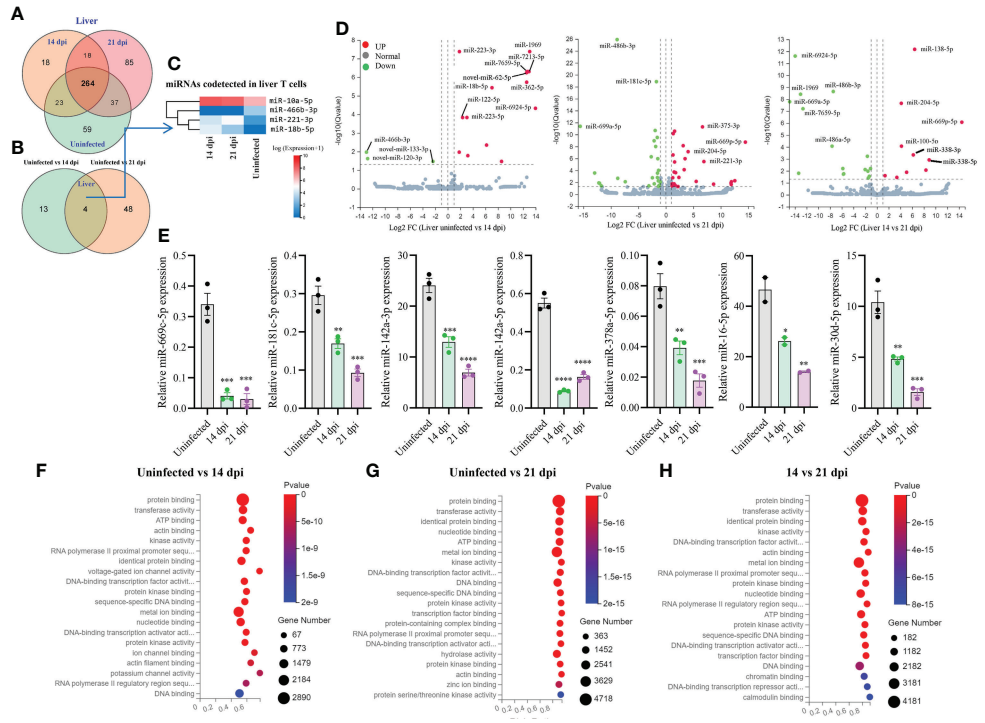

FIGURE 3
Liver T cell miRNAs profiles, validation of expressions, and prediction of molecular functions of their targets. **(A)** Venn diagram showing total and co-detected liver T cell miRNAs among uninfected, 14 dpi and 21 dpi groups (the number indicates the common or specific miRNAs identified in different groups); **(B)** Venn diagram showing co-detected and specific liver T cell miRNAs between two groups (uninfected vs 14 dpi and uninfected vs 21 dpi); **(C)** Heatmap showing the expression of differentially expressed liver T cell miRNAs co-detected between two groups (uninfected vs 14 dpi and uninfected vs 21 dpi); **(D)** Volcano plot showing differentially expressed liver T cell miRNAs for different comparative analyses (uninfected control vs 14 dpi; uninfected control vs 21 dpi; 14 dpi vs 21 dpi). Green dot indicates down regulated miRNAs, red dot indicates upregulated miRNAs and grey dot indicates no significantly expressed miRNAs; **(E)** Validation of selected increased and decreased expressions of liver T cell miRNAs by RT-qPCR. Data illustrate representative results and show the mean and standard error mean from an experiment carried out in triplicate. Statistical analysis was performed comparing uninfected vs 14 dpi or 21 dpi using one-way ANOVA and * denotes $P \leq 0.05$, ** denotes $P \leq 0.01$, *** denotes $P \leq 0.001$, **** denotes $P \leq 0.0001$; **(F–H)** GO enrichment analyses of molecular functions of targets for differently expressed miRNAs (Uninfected vs 14 dpi **(F)**; Uninfected vs 21 dpi **(G)**; 14 dpi vs 21 dpi **(H)** in liver T cells). The results showing 20 most significantly enrichment functions of targets for differentially expressed miRNAs.

3p, *miR-221-3p* and *miR-18b-5p*) (Figure 3C). Volcano plot analysis of differentially expressed miRNAs between uninfected and 14 dpi mice showed the downregulation of *miR-466b-3p*, *novel-miR-120-3p* and *novel-miR-133-3p*, and the upregulation of *miR-223-3/5p*, *miR-1969*, *miR-7213-5p*, *miR-7659-5p*, *novel-miR-62-5p*, *miR-18b-5p*, *miR-362-5p*, *miR-122-5p* and *miR-6924-5p* as well as other 4 miRNAs (Figure 3D). In comparison with uninfected, miRNAs such as *miR-486b-3p*, *miR-181c-5p*, *miR-669a-5p* were downregulated in T cells isolated from 21 dpi murine livers, while *miR-375-3p*, *miR-204-5p*, *miR-669p-5p*, *miR-221-3p* and others exhibited notable upregulation (Figure 3D). In addition, a panel of miRNAs was found to be differentially expressed in liver T cells between 14 dpi and 21 dpi (Figure 3D). The RT-qPCR validations of selected miRNAs indicated *miR-669c-5p*, *miR-181c-5p*, *miR-142a-3p/5p*, *miR-378a-5p*, *miR-16-5p*, and *miR-30d-5p* exhibited significantly decreased expressions in murine liver T cells at 14 dpi and 21 dpi compared to uninfected control (Figure 3E). The RT-qPCR results of these altered expressions of T cell miRNAs were consistent (80%) with RNA-seq results. Furthermore, isolated T cells from liver treated with SWA showed increased expressions of *miR-182-5p, miR-21a-5p* and *miR-222-3p* while decreased expressions of *miR-142a-3p, miR-181c-5p, miR-142a-5p, miR-191-5p* and *miR-467a-5p* were observed (Supplementary Figure 4B). Similar results were also noted in EL-4 T cell treated with SWA (Supplementary Figure 4C). Overall, these results were further corroborated with the differentially expressed miRNAs in liver T cells of *S. japonicum* infected mice. GO enrichment analysis of molecular functions of targets for differentially expressed miRNAs in three groups (uninfected vs 14 dpi; uninfected vs 21 dpi; 14 dpi vs 21 dpi) showed several significant binding functions, including protein binding, metal ion binding, nucleotide binding, ATP binding, DNA binding, *etc.* (Figures 3F–H; Supplementary Datasheet 6). GO analysis of biological processes of targets for differentially expressed miRNAs in these groups showed their significant enrichment with positive/negative regulation of transcription by RNA polymerase II, multicellular organism development, cell differentiation, *etc.* (Supplementary Figures 3H-J; Supplementary Datasheet 6). These results suggest that most targets of these differentially expressed miRNAs were associated with binding potentially involved with posttranscriptional gene regulation.

Comparative analysis of differentially expressed miRNAs between blood and liver T cells

Comparative analysis of T cell miRNAs between blood and liver for 14 dpi, 21 dpi and uninfected control indicated 265, 402 and 351 co-detected miRNAs (Supplementary Figures 3K–M). Whereas differentially expressed miRNAs between liver and blood for 14 dpi, 21 dpi and uninfected control, we found 92 miRNAs and observed one co-detected miRNA (*miR-669a-5p*) (Figure 4A; Supplementary Datasheet 4). We further compared the expression pattern of these differentially expressed miRNAs of T cells between blood and liver at 14 dpi and visualized by heatmaps (Figure 4B). We selected a few miRNAs to validate their expressions between liver and blood of *S. japonicum* infected mice at 14 dpi. The results indicated a higher expression of *miR-223-5p* in T cells isolated from the liver compared to the blood T cell at 14 dpi (Figure 4C). In contrast, a significantly decreased expression was observed in *miR-375-3p*, *miR-138-5p* and *miR-338-3p* in liver T cells at 14 dpi (Figure 4C). In addition, the expression pattern of differentially expressed miRNAs between blood and liver T cells at 21 dpi was shown in Figure 4D. Validation of several selected miRNAs by RT-qPCR showed that the expressions of *miR-669c-5p*, *miR-669d-5p*, *miR-151-3p*, and *novel-miR-389-3p* were significantly increased in blood isolated T cells compared to the liver at 21 dpi (Figure 4E). GO molecular function analysis of enriched terms for targets of differentially expressed miRNAs between blood and livers at 14 dpi and 21 dpi showed these targets were potentially associated with protein binding, metal ion binding, nucleotide binding, ATP binding, DNA binding, *etc.* (Figures 4F, G; Supplementary Datasheet 7). GO analysis of biological processes showed their targets associated with positive and negative regulation of transcription by RNA polymerase II multicellular organism development, cell differentiation and others in case of blood vs liver T cells at 14 dpi and 21 dpi (Figures 4H, I; Supplementary Datasheet 7). These results suggest that there may be specific functional cues that lead to distinct expression patterns observed between blood and liver isolated T cells.

RT-qPCR analysis of selected miRNA targets at different stages of *S. japonicum* infection and bioinformatic analysis of regulatory networks

To assess the regulatory roles of T cell miRNAs, we evaluated the expressions of several selected miRNA targets that are predicted to be associated with the KEGG pathways associated immune system and parasite-caused infectious diseases (Figures 5A–D; Supplementary Datasheet 8). We noted several miRNAs targets potentially associated with parasitic infections and T cell immune response during these stages of infection. RT-qPCR analyses of several selected miRNA targets potentially involved in parasitic infections and T cell immune response (Figure 5E) and their corresponding miRNA expressions (Figure 5F) at blood T cells showed a generally negative correlation, suggesting that the miRNAs could regulate their targets at blood T cells during *S. japonicum* infection. For example, the expressions of targets such as cytotoxic T-lymphocyte-associated protein 4 (*Ctla4*, a target of

10.3389/fimmu.2022.911139

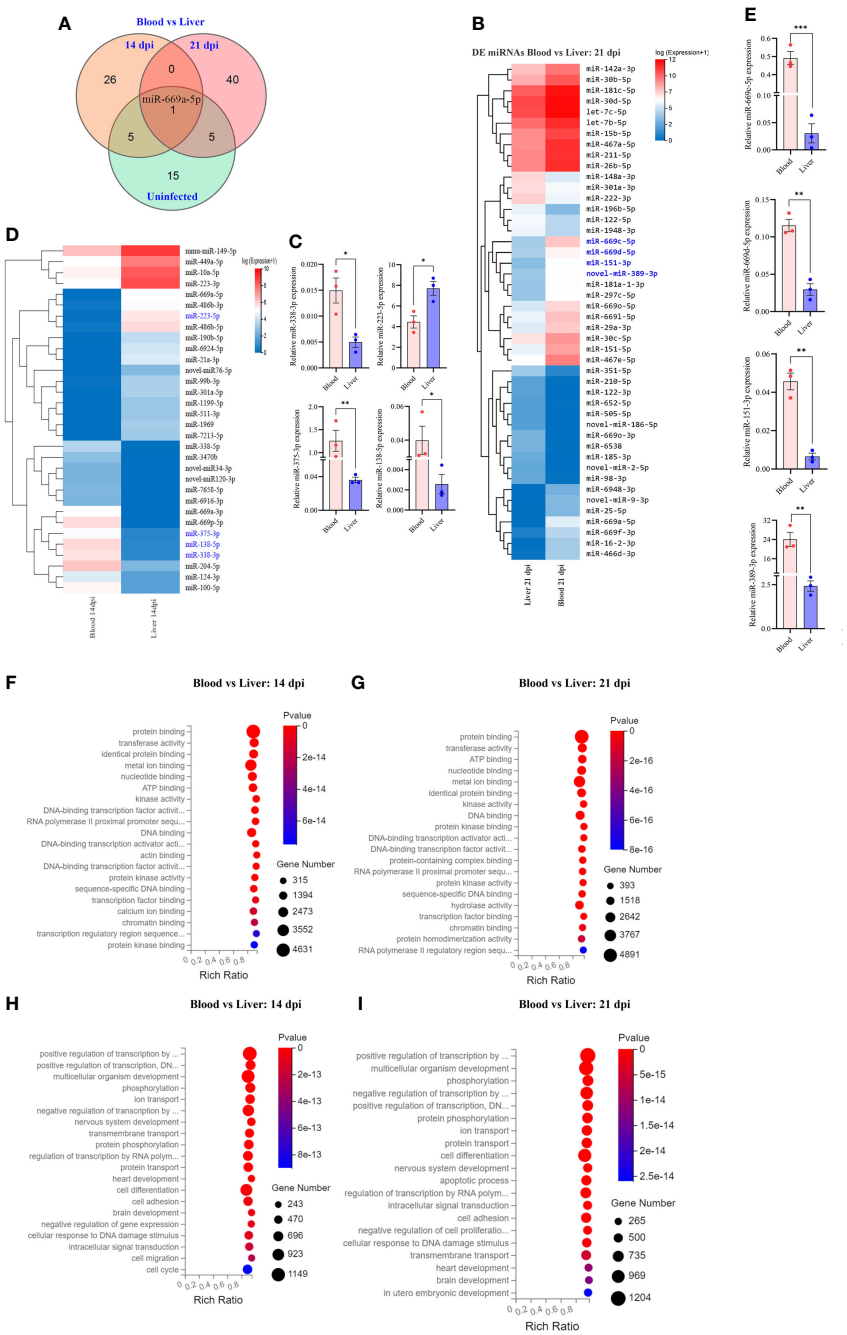

FIGURE 4
Comparative analyses of T cell miRNA expressions between blood and liver at 14 dpi and 21 dpi. **(A)** Comparison of differentially expressed miRNAs between blood and liver showing co-detected and specific miRNAs at 14 dpi, 21 dpi and uninfected control; **(B)** Heatmap showing differentially expressed T cell miRNAs between blood and liver at 14 dpi (miRNAs highlighted in blue color are validated by RT-qPCR); **(C)** RT-qPCR validation of the expressions of selected miRNAs between blood and liver at 14 dpi. Data illustrate representative results and show the mean and standard error mean from an experiment carried out in triplicate. Statistical analysis was performed comparing blood and liver using Student's T-test and * denotes $P \leq 0.05$, ** denotes $P \leq 0.01$. **(D)** Heatmap showing differentially expressed T cell miRNAs between blood vs liver at 21 dpi (miRNAs highlighted in blue color are validated by RT-qPCR); **(E)** Validation of the expressions of selected miRNAs from blood vs liver at 21 dpi by RT-qPCR; For RT-qPCR, data illustrate representative results and show the mean and standard error mean from an experiment carried out in triplicate. Statistical analysis was performed between *S. japonicum* infected mice blood and liver isolated T cells at 14 dpi and 21 dpi using Students T test and ** denotes $P \leq 0.01$, *** denotes $P \leq 0.001$; **(F, G)** GO analysis of molecular functions of targets for differentially expressed T cell miRNAs between blood and liver at 14 dpi **(F)** or at 21 dpi **(G)**; **(H, I)** GO analysis of biological processes of targets for differentially expressed T cell miRNAs between blood and liver at 14 dpi **(H)** or at 21 dpi **(I)**.

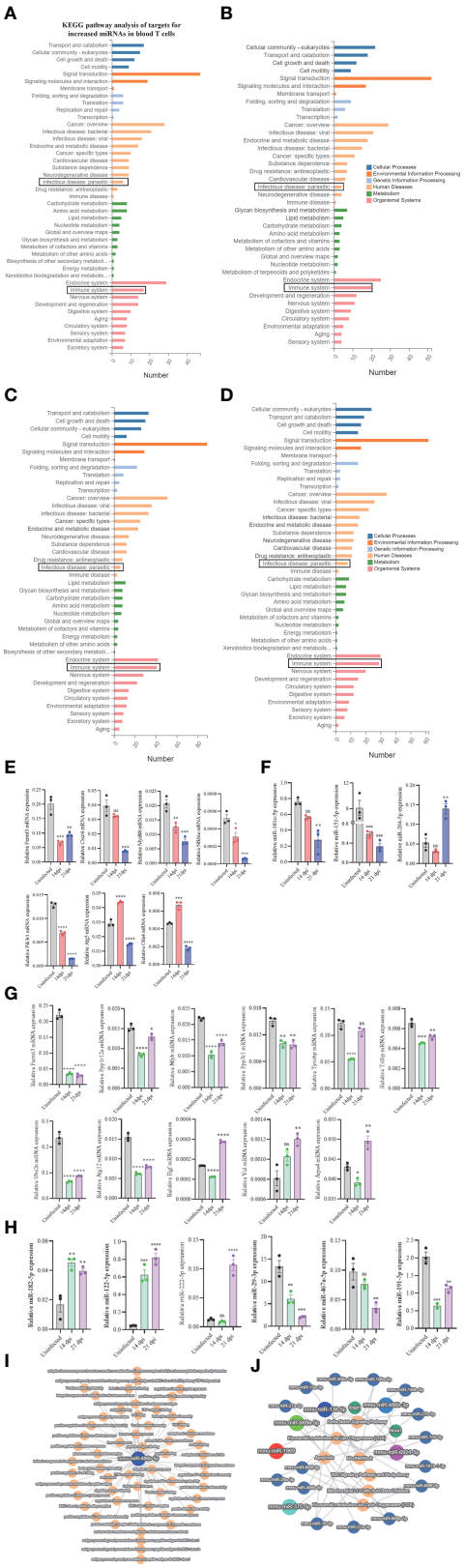

FIGURE 5 (Continued)

FIGURE 5 (Continued)
KEGG analyses of targets for differentially expressed miRNAs and RT-qPCR analysis of the expressions of target genes. **(A–D)** KEGG analysis of up- and downregulated miRNA targets (uninfected vs 14 dpi; uninfected vs 21 dpi) in murine blood **(A, B)** or liver **(C, D)** associated with human disease and organismal systems in blood and liver. Rectangle indicates selected miRNAs targets associated the pathways of infectious (parasitic) disease and immune system; **(E)** RT-qPCR analysis of the expressions of target genes for differently expressed miRNAs in blood T cells. The putative targets associated with parasitic disease and immune system were selected for RT-qPCR analysis. Data illustrate representative results and show the mean and standard error mean from an experiment carried out in triplicate. Statistical analysis was performed comparing uninfected vs 14 dpi or 21 dpi using one-way ANOVA and * denotes $P \leq 0.05$, ** denotes $P \leq 0.01$, *** denotes $P \leq 0.001$, **** denotes $P \leq 0.0001$ and ns denotes non-significant; **(F)** RT-qPCR validation of the expressions of several miRNAs in blood T cells that potentially regulate the corresponding targets as shown in **(E)**. *Pik3r1* and *Nfkbie* are the targets of *miR-204-5p*; *Ctla4* is the target of *miR-151-5p*; *Atg5* is the target of *miR-181c-5p*. Data illustrate representative results and show the mean and standard error mean from an experiment carried out in triplicate. Statistical analysis was performed comparing uninfected vs 14 dpi or 21 dpi using one-way ANOVA and ** denotes $P \leq 0.01$, *** denotes $P \leq 0.001$ and ns denotes non-significant. **(G)** RT-qPCR analysis of the expressions of target genes for differently expressed miRNAs in liver T cells. The putative targets associated with parasitic disease and immune system were selected for RT-qPCR analysis. Data illustrate representative results and show the mean and standard error mean from an experiment carried out in triplicate. Statistical analysis was performed comparing uninfected vs 14 dpi or 21 dpi using one-way ANOVA and * denotes $P \leq 0.05$, ** denotes $P \leq 0.01$, *** denotes $P \leq 0.001$, **** denotes $P \leq 0.0001$ and ns denotes non-significant; **(H)** RT-qPCR validation of the expressions of several miRNAs in liver T cells that potentially regulate the corresponding targets as shown in **(G)**. *Ppp3r1 and Tollip* are the targets of *miR-182-5p*; *Nfyb* and *Ppp1r12a* are the target of *miR-222-3p*; *Arpc4* is the target of *miR-191-5p*; *Fermt3* is the target of *miR-122-5p*; *Vcl* is the target of *miR-467a-5p*; *Hgf* is a target of *miR-29a-3p*. Data illustrate representative results and show the mean and standard error mean from an experiment carried out in triplicate. Statistical analysis was performed comparing uninfected vs 14 dpi or 21 dpi using one-way ANOVA and ** denotes $P \leq 0.01$, *** denotes $P \leq 0.001$ and ns denotes non-significant. **(I)** *miR-486b-5p* decreased in blood T cells as shown in Figure 2E potentially regulates many biological processes by interacting with its corresponding targets; **(J)** Top differentially expressed T cell miRNAs including *miR-486b-5p/3p*, *miR-375-5p*, *miR-1969*, and *miR-6924-5p* are putatively involved in the regulations of Wnt signaling pathway and pluripotency, Delta-Notch signaling pathway, mitochondrial LC-fatty acid beta-oxidation, eicosanoid metabolism *via* cyclo oxygenases (COX) and others by interacting with their targets.

downregulated *miR-151-5p*) and autophagy-related 5 (*Atg5*) (a target of downregulated *miR-181c-5p*) were increased in blood T cells at 14 dpi compared to uninfected control while the expressions of *miR-151-5p* and *miR-181c-5p* were decreased (Figures 5E, F). Similar results were also observed at liver T cells between the expressions of target genes (Figure 5G) and their corresponding miRNAs (Figure 5H). Similarly, the liver isolated T cells target genes such as hepatocyte growth factor (*Hgf*, a target of downregulated *miR-29-3p*), vinculin (*Vcl*, a target of downregulated *miR-467a-5p*) and actin-related protein 2/3 complex, subunit 4 (*Arpc4*, a target of downregulated *miR-191-5p*) shown increased expression at liver T cell of 21 dpi, whereas the *Fermt3* (a target of upregulated *miR-122-5p*), protein phosphatase 1, regulatory subunit 12A (*Ppp1r12a)* and nuclear transcription factor-Y beta (*Nfyb*) (targets of upregulated *miR-222-3p*), toll interacting protein (*Tollip*) and protein phosphatase 3 regulatory subunit B, Beta (*Ppp3r1*) (targets of upregulated *miR-182-5p*) shown decreased expression in liver T cells following *S. japonicum* infection (Figures 5G, H). Additionally, several selected differentially expressed miRNAs at 14 dpi or 21 dpi compared to uninfected control (decreased in blood and liver: *miR-486b-5p/3p*, *miR-6924-5p*; increased in blood and liver: *miR-375-5p* and *miR-1969*) suggested that these miRNAs are related with diverse functions associated with infection. In particular, *miR-486b-5p* shown decreased expression in *S. japonicum* infected mice at 14 dpi and 21 dpi compared to uninfected control (Figure 2E) and is putatively associated with adaptive immune response, peptide binding, T cell-mediated immune response, nuclear outer membrane-endoplasmic reticulum membrane network, antigen binding, protein-containing complex binding, peptide antigen binding, endoplasmic reticulum membrane, and others (Figure 5I). Similarly, differentially expressed miRNAs (downregulated: *miR-486b-3p*, *miR-6924-5p*; upregulated: *miR-1969*, *miR-375-5p*, *miR-669a-5p*, and *miR-138-5p*) were shown to be putatively involved in the regulations of apoptosis, Wnt signaling pathway and pluripotency, eicosanoid metabolism *via* cyclooxygenase (COX), eicosanoid metabolism *via* lipo oxygenase (LOX) and mitochondrial LC-fatty acid beta-oxidation (Figure 5J).

Discussion

T cells are one of most important lymphocytes and the main elements of adaptive immunity. The potential role of miRNAs in regulating T cell proliferation, activation, and differentiation has been well discussed (24, 45). However, the expression profiles of host T cell miRNAs during *Schistosoma* infection are scanty. The liver stages are critical for schistosomula development and schistosome-caused pathology. *Schistosoma* are blood dwelling flatworms. Blood acts as a pipeline for immune system, carry different immune cells from one place to another and respond according to the types of infections. Most of the studies on schistosomes have carried out on the adult worm infection stages to observed mostly eggs induced immune response. However, very few studies have focused on early stages especially on schistosomula and pre-egg laying worms, which are important for worm development and maturation for finally residing. In addition, schistosomula are also considered to be a valuable stage for vaccine development to dump worm parasitism. Therefore, we undertook the study to profile the miRNAs repertoire in peripheral blood and livers to understand T cell miRNA alteration that may be involved in T cell-mediated immune response during the parasitic infection.

Schistosoma infection induces different immune responses. In the early phase of infection, cercaria initiates the Th1 immune response, and the produced eggs induce a shift towards Th2 type immune response (11, 12). The Th2 immune response plays an important role in the pathogenesis of schistosomiasis (46). At 14 and 21 dpi, we observed a significant decrease in the expression of *miR-486b-5p/3p*, *miR-122-5p*, *miR-181c-5p* and *miR-6924-5p etc.* In contrast, a significant increase in the expression of miRNAs such as *miR-375-5p*, *miR-466c-3p*, and *miR-138-5p* in both blood and livers isolated T cells. The functional aspect of some of these miRNAs has been documented previously; however, their specific roles during *S. japonicum* infection remain unknown. Bioinformatic analysis of top differentially expressed miRNAs and their targets suggested their putative roles in infections and immune responses, especially adaptive immune responses (Figures 5I, G). GO analysis of targets of differentially expressed miRNAs suggested that most of the miRNAs may be involved in signal transduction, signal molecule and interactions, infectious disease and others.

We observed the increased expression of *Ctla4* and *Atg5* of growth signal transduction protein kinases in blood (Figure 5E). T cells circulate consistently between blood, lymphoid tissue, and lymph nodes to encounter foreign antigens presented by DCs (47). Ctla4 limits the interactions of $CD4^+$ T-cells with DCs by modulating the threshold for T cell activation and induces T cell motility response in secondary lymphoid organs (48). The other target gene, Atg5, has been shown to be responsible for the activation and differentiation of innate and adaptive immune cells and then promotes the interaction between T cells or B cells and antigen-presenting cells (49). The increased expression of these target genes (*Ctla4* and *Atg5*) during schistosome infection at 14 dpi, especially during blood stages, may potentially involve in T cells mediated immune response. Hgf is a pleiotropic cytokine that influences mitogenesis, motility and differentiation of many different cell types (50). It also maintains the differentiation of hepatic sinusoidal endothelial cells, specializing in lymphocyte recruitment to the liver (51). The increased expression of *Hgf* in liver at 21 dpi may suggested the organ specific immune response during *S. japonicum* infection. Actin-related protein is highly conserved in eukaryotes that nucleate branched actin filaments and generate actin networks (52). It includes five subunits and Arpc2, and 4 forms the core of this complex, and the deficiency in Arpc led to the decrease in the number of peripheral T cell (53). The increased expression of *Arpc4* may suggest to potentially regulate T cells populations during *S. japonicum* infection.

Considering the important roles of miRNAs in T cell development program and function, several groups have documented miRNA profiles in different types of T cells (54–56). We observed a differentially decreased expression of *miR-486b-5p/3p* in T cells isolated from blood and liver. *miR-486a-5p* and *miR-486b-5p* originate from the different pre-miRNAs transcribed from the opposite strand of the same genomic locus; however, they share the same mature sequences (57). Primarily *miR-486-5p* was identified as a tumor-suppressive miRNA in lung cancer (58), and shown decreased expression in breast cancer patients (59). Another study suggested that the inhibition of *miR-486-5p* alleviated LPS-induced cell damage by limiting inflammatory injury, oxidative stress and apoptosis by targeting NRF1 (60). The decreased expression of *miR-486* in the present study may lead to minimal inflammatory response at 14 dpi and 21 dpi of *S. japonicum* infection. *miR-223* is one of the differentially expressed miRNAs identified in our study that has been shown to play a vital role in the immune response, regulating multiple processes from myeloid differentiation to neutrophil, macrophage, and DC function (61). The changes of *miR-223-3p* expression are linked to macrophage apoptosis (62) and play an essential role in maintaining the balance of innate immunity to avoid excess inflammation and tissue damage. Another study indicated that *miR-223* level is negatively associated with lymphocyte apoptosis by targeting FOXO1 during sepsis (63). Further investigation of the roles of these differently expressed miRNAs may gain important insight into how miRNAs involve in immune response during *S. japonicum* infection, then resulting into the development of effective strategies for schistosomiasis control.

Comparative analysis of the identified miRNAs between blood and liver at 14 dpi or 21 dpi, we noted the majority of differently expressed miRNAs was specially associated with *S. japonicum* infection at 14 dpi or 21 dpi (Figure 4A). However, there were a few of differently expressed miRNAs between blood and livers showing to be co-detected between 14 dpi/21 dpi and uninfected controls (Figure 4A). For example, miRNAs such as *miR-10a-5p, miR-149-5p, miR-223-3p, miR-669a-3p* and *miR-669p-5p* showed to be co-detected for different expressions between blood and livers among 14 dpi and uninfected control and *miR-122-5p*, *miR-142a-3p*, *miR-151-5p, miR-211-5p* and *miR-15b-5p* showed to differently express in both 21 dpi and uninfected control. Interestingly, we observed an increased expression of *miR-669a-5p* in T cells isolated from murine blood during *Schistosoma* infection (14 dpi vs 21 dpi) while a decreased expression of this miRNA in T cells isolated from liver was observed. The results suggested that *miR-669a-5p* may have different roles in different organs during *Schistosoma* infection. *miR-122* levels have been suggested to be a diagnostic marker for liver disease. The decreased expression of *miR-122* in T cells isolated from blood and liver of *S. japonicum*-infected mice may potentially be associated with increased adaptive immune response and decreased innate immunity since the increased level of *miR-122* was shown to link with hepatocyte innate immunity (64). Comparative analysis of T cell miRNA profiles between blood and liver shows dynamic expression patterns. Among them, we noted *miR-669a-5p* was shown to be the common differentially expressed between blood and livers. Unfortunately, the role of *miR-669a* in immune response remain unknown although a study suggested its role in the

prevention of skeletal muscle differentiation and in postnatal cardiac progenitors (65). Consequently, it is worth to investigate whether *miR-669a-5p* regulates T cell response during the early stage of *S. japonicum* infection.

In conclusion, our study presents a comprehensive dataset of differentially expressed T cell miRNAs from blood and liver of *S. japonicum* infected mice at differently early hepatic schistosomula stages. Several panels of differentially expressed miRNAs, such as *miR-486a-5p/3p*, *miR-486b-5p/3p*, *miR-375-3p*, *miR-466a-5p/3p*, *miR-466b-5p/3p*, *miR-223-3p*, *miR-181c-5p*, *etc.*, were identified to be putatively associated with T cell immune response showing dynamic expressions during *S. japonicum* infection. Further studies unpinning the potential role of these miRNAs are expected to provide the translational value for understanding and application of miRNAs mediated T cell immune response during *Schistosoma* infection.

Data availability statement

The data presented in the study are deposited in China National GeneBank DataBase, accession number CNP0003350.

Ethics statement

The animal study was reviewed and approved by The Animal Management Committee and the Animal Care and Use Committee of the Shanghai Science and Technology Commission of the Shanghai Municipal government for Shanghai Veterinary Research Institute, Chinese Academy of Agriculture Sciences, China.

Author contributions

Conceptualization, BG and GC; investigation, SL, BG, and LQ; writing original draft, BG; Supervision, GC; review and editing, BG, GC, CF, SY, and MP. All authors contributed to the article and approved the submitted version.

Funding

This study was supported, in whole or in part, by the Key Program for International S&T Cooperation Projects of China (2021YFE0191600 to GC), the State Key Laboratory of Veterinary Etiological Biology (SKLVEB2020KFKT018 to GC), the Research Fund for International Young Scientists from NNSF (31950410564 to BG) and the National Natural Science Foundation of China (31472187 and 31672550 to GC). The funders had no role in study design, data collection, analysis, decision to publish, or manuscript preparation.

Conflict of interest

The authors declare that the research was conducted in the absence of any commercial or financial relationships that could be construed as a potential conflict of interest.

Publisher's note

Supplementary material

The Supplementary Material for this article can be found online at: https://www.frontiersin.org/articles/10.3389/fimmu.2022.911139/full#supplementary-material

SUPPLEMENTARY FIGURE 1
Flow cytometry sorting of T cells and cell viability analysis. **(A, B)** Representative flow cytometry sorting of T cells isolated from blood **(A)** and liver **(B)** of *S. japonicum* infected mice and uninfected control; **(C, D)** Flow cytometry analysis of percentage of live T cells isolated from the blood **(C)** and liver **(D)** of *S. japonicum* infected mice and uninfected control; **(E, F)** Flow cytometry analysis of percentage of $CD4^+$ and $CD8a^+$ cells isolated from the blood **(E)** and liver **(F)** of *S. japonicum* infected mice and uninfected control. Representative results presented as the average from two biological replicates.

SUPPLEMENTARY FIGURE 2
Classifications of distributions of small RNAs identified by RNA seq and heatmap showing differently expressed miRNAs. **(A)** Classifications of distributions of small RNAs identified from T cells isolated from murine blood for each library; **(B)** Classifications of distributions of small RNAs identified from T cells isolated from murine livers for each library; **(C)** Heatmap showing increased expressions of miRNAs in blood T cells; **(D)** Heatmap showing decreased expressions of miRNAs in blood T cells; **(E)** Heatmap showing increased expressions of miRNAs in liver T cells; **(F)** Heatmap showing decreased expressions of miRNAs in liver T cells; **(G)**. Heatmap of miRNAs expression showing increased miRNAs such as *miR-10a-5p* in uninfected liver vs uninfected blood T cells. Red color showed higher expression and blue color showed lower expression.

SUPPLEMENTARY FIGURE 3
Differentially expressed miRNAs from blood/liver T cells between *S. japonicum* infected mice and uninfected control and predictions of the biological processes of their targets. **(A)** Heatmap showing differentially expressed miRNAs from blood T cells between uninfected control and *S. japonicum* infected mice at 14 dpi**; (B)** Heatmap showing differentially expressed miRNAs from blood T cells between uninfected control and *S. japonicum* infected mice at 21 dpi; **(C)** Heatmap showing differentially expressed miRNAs from liver T cells between uninfected control and *S. japonicum* infected mice at 14 dpi; **(D)** Heatmap showing differentially expressed miRNAs from liver T cells between uninfected control and *S. japonicum* infected mice at 21 dpi. **(E)** GO analyses of biological processes of the targets for differentially expressed miRNAs (uninfected vs 14 dpi) from blood T cells; **(F)** GO analyses of biological processes of the targets

for differentially expressed miRNAs (uninfected vs 21 dpi) from blood T cells; **(G)** GO analyses of biological processes of the targets for differentially expressed miRNAs (14 dpi vs 21 dpi) from blood T cells; **(H)** GO analyses of biological processes of the targets for differentially expressed miRNAs (uninfected vs 14 dpi) from liver T cells; **(I)** GO analyses of biological processes of the targets for differentially expressed miRNAs (uninfected vs 21 dpi) from liver T cells; **(J)** GO analyses of biological processes of the targets for differentially expressed miRNAs (14 dpi vs 21 dpi) from blood T cells; **(K-M)** Comparative analysis of differently expressed T cell miRNAs for each biological replicate between blood and liver at 14 dpi **(K)**, 21 dpi **(L)** and uninfected **(M)**.

SUPPLEMENTARY FIGURE 4
RT-qPCR analysis of selected miRNA expressions in isolated T cells and *in vitro* cultured EL-4 cells treated with *S. japonicum* worm antigens (SWA). **(A)** RT-qPCR analysis of the expressions of selected miRNAs in blood T cells isolated from mice treated with or without SWA; **(B)** RT-qPCR analysis of the expressions of selected miRNAs in liver T cells isolated from T cells treated with or without SWA; **(C)** RT-qPCR analysis of the expressions of selected miRNAs in EL-4 cells treated with or without SWA. Data illustrate representative results and show the mean and standard error mean from an experiment carried out in triplicate. Statistical analysis was performed on T cells from blood and liver and EL-4 cells between SWA treatment and controls using Student's T-test and * denotes $P \leq 0.05$, ** denotes $P \leq 0.01$, *** denotes $P \leq 0.001$. **** denotes $P \leq 0.0001$.

SUPPLEMENTARY DATA SHEET 1
T cells raw reads filtration.

SUPPLEMENTARY DATA SHEET 2
T cells clean reads mapping.

SUPPLEMENTARY DATA SHEET 3
The list of differentially expressed T cell miRNAs in blood or liver among uninfected control, 14 dpi and 21 dpi.

SUPPLEMENTARY DATA SHEET 4
The list of differently expressed T cell miRNAs between blood and livers in uninfected control, 14 dpi and 21 dpi.

SUPPLEMENTARY DATA SHEET 5
The list of GO enrichment analysis of target mRNAs of differentially expressed miRNAs in blood.

SUPPLEMENTARY DATA SHEET 6
The list of GO enrichment analysis of target mRNAs of differentially expressed miRNAs in liver.

SUPPLEMENTARY DATA SHEET 7
The list of GO enrichment analysis of target mRNAs for differentially expressed miRNAs between blood and liver.

SUPPLEMENTARY DATA SHEET 8
The list of KEGG pathway analysis target genes for increased/decreased miRNAs in blood/liver T cells.

SUPPLEMENTARY TABLE 1
Details of antibodies used for isolating T cells from liver and blood of mice.

SUPPLEMENTARY TABLE 2
List of RT-qPCR primers used to validate T cell miRNA expressions.

SUPPLEMENTARY TABLE 3
List of primers used for analyzing the expressions of miRNA targets by RT-qPCR.

References

1. Miller P, Wilson RA. Migration of the schistosomula of *Schistosoma mansoni* from the lungs to the hepatic portal system. *Parasitology* (1980) 80:267–88. doi: 10.1017/S0031182000000743

2. Nation CS, Da'dara AA, Marchant JK, Skelly PJ. Schistosome migration in the definitive host. *PloS Negl Trop Dis* (2020) 14:e0007951–e0007951. doi: 10.1371/journal.pntd.0007951

3. Kusel JR, Al-Adhami BH, Doenhoff MJ. The schistosome in the mammalian host: Understanding the mechanisms of adaptation. *Parasitology* (2007) 134:1477–526. doi: 10.1017/S0031182007002971

4. Hambrook JR, Hanington PC. Immune evasion strategies of schistosomes. *Front Immunol* (2021) 11. doi: 10.3389/fimmu.2020.624178

5. Thomson AW, Knolle PA. Antigen-presenting cell function in the tolerogenic liver environment. *Nat Rev Immunol* (2010) 10:753–66. doi: 10.1038/nri2858

6. Crispe IN. Immune tolerance in liver disease. *Hepatology* (2014) 60:2109–17. doi: 10.1002/hep.27254

7. He YX. Biology of schistosoma japonicum. from cercaria penetrating into host skin to producing egg. *Chin Med J (Engl)* (1993) 106:576–83.

8. Colley DG, Secor WE. Immunology of human schistosomiasis. *Parasit Immunol* (2014) 36:347–57. doi: 10.1111/pim.12087

9. Mathew RC, Boros DL. Anti-L3T4 antibody treatment suppresses hepatic granuloma formation and abrogates antigen-induced interleukin-2 production in *Schistosoma mansoni* infection. *Infect Immun* (1986) 54:820–6. doi: 10.1128/iai.54.3.820-826.1986

10. de Jesus AR, Silva A, Santana LB, Magalhães A, De Jesus AA, De Almeida RP, et al. Clinical and immunologic evaluation of 31 patients with acute schistosomiasis mansoni. *J Infect Dis* (2002) 185:98–105. doi: 10.1086/324668

11. Fallon PG, Smith P, Dunne DW. Type 1 and type 2 cytokine-producing mouse CD4+ and CD8+ T cells in acute *Schistosoma mansoni* infection. *Eur J Immunol* (1998) 28:1408–16. doi: 10.1002/(SICI)1521-4141(199804)28:04<1408::AID-IMMU1408>3.0.CO;2-H

12. Fairfax K, Nascimento M, Huang SC, Everts B, Pearce EJ. Th2 responses in schistosomiasis. *Semin Immunopathol* (2012) 34:863–71. doi: 10.1007/s00281-012-0354-4

13. Allen JE, Sutherland TE. Host protective roles of type 2 immunity: Parasite killing and tissue repair, flip sides of the same coin. *Semin Immunol* (2014) 26:329–40. doi: 10.1016/j.smim.2014.06.003

14. Rutitzky LI, Da Rosa JRL, Stadecker MJ. Severe CD4 T cell-mediated immunopathology in murine schistosomiasis is dependent on IL-12p40 and correlates with high levels of IL-17. *J Immunol* (2005) 175:3920–6. doi: 10.4049/jimmunol.175.6.3920

15. Hesse M, Piccirillo CA, Belkaid Y, Prufer J, Mentink-Kane M, Leusink M, et al. The pathogenesis of schistosomiasis is controlled by cooperating IL-10-Producing innate effector and regulatory T cells. *J Immunol* (2004) 172:3157–66. doi: 10.4049/jimmunol.172.5.3157

16. Taylor JJ, Mohrs M, Pearce EJ. Regulatory T cell responses develop in parallel to Th responses and control the magnitude and phenotype of the Th effector populatio. *J Immunol* (2006) 176:5839–47. doi: 10.4049/jimmunol.176.10.5839

17. Chen X, Yang X, Li Y, Zhu J, Zhou S, Xu Z, et al. Follicular helper T cells promote liver pathology in mice during *Schistosoma japonicum* infection. *PloS Pathog* (2014) 10:e1004097. doi: 10.1371/journal.ppat.1004097

18. Wang Y, Lin C, Cao Y, Duan Z, Guan Z, Xu J, et al. Up-regulation of interleukin-21 contributes to liver pathology of schistosomiasis by driving GC immune responses and activating HSCs in mice. *Sci Rep* (2017) 7:1–11. doi: 10.1038/s41598-017-16783-7

19. Zheng B, Zhang J, Chen H, Nie H, Miller H, Gong Q, et al. T Lymphocyte-mediated liver immunopathology of schistosomiasis. *Front Immunol* (2020) 11. doi: 10.3389/fimmu.2020.00061

20. Bartel DP. MicroRNAs: Genomics, biogenesis, mechanism, and function. *Cell* (2004) 116:281–97. doi: 10.1016/S0092-8674(04)00045-5

21. Cai P, Piao X, Liu S, Hou N, Wang H, Chen Q. MicroRNA-gene expression network in murine liver during *Schistosoma japonicum* infection. *PloS One* (2013) 8:e67037. doi: 10.1371/journal.pone.0067037

22. Morishita A, Oura K, Tadokoro T, Fujita K, Tani J, Masaki T. MicroRNA interference in hepatic host-pathogen interactions. *Int J Mol Sci* (2021) 22:3554. doi: 10.3390/ijms22073554

23. Podshivalova K, Salomon DR. MicroRNA regulation of T-lymphocyte immunity: Modulation of molecular networks responsible for T-cell activation, differentiation, and development. *Critic Rev Immunol* (2013) 33:435–76. doi: 10.1615/CritRevImmunol.2013006858

24. Giri BR, Mahato RI, Cheng G. Roles of microRNAs in T cell immunity: Implications forStrategy development against infectious diseases. *Med Res Rev* (2019) 39:706–32. doi: 10.1002/med.21539

25. Cobb BS, Nesterova TB, Thompson E, Hertweck A, O'connor E, Godwin J, et al. T Cell lineage choice and differentiation in the absence of the RNase III enzyme dicer. *J Exp Med* (2005) 201:1367–73. doi: 10.1084/jem.20050572

26. Muljo SA, Ansel KM, Kanellopoulou C, Livingston DM, Rao A, Rajewsky K. Aberrant T cell differentiation in the absence of dicer. *J Exp Med* (2005) 202:261–9. doi: 10.1084/jem.20050678

27. Chong MM, Zhang G, Cheloufi S, Neubert TA, Hannon GJ, Littman DR. Canonical and alternate functions of the microrna biogenesis machinery. *Gene Dev* (2010) 24:1951–60. doi: 10.1101/gad.1953310

28. Seo K-H, Zhou L, Meng D, Xu J, Dong Z, Mi Q-S. Loss of microRNAs in thymus perturbs invariant NKT cell development and function. *Cell Mol Immunol* (2010) 7:447–53. doi: 10.1038/cmi.2010.49

29. Cho S, Lee H-M, Yu I, Choi YS, Huang H-Y, Hashemifar SS, et al. Differential cell-intrinsic regulations of germinal center b and T cells by miR-146a and miR-146b. *Nat Commun* (2018) 9:1–13. doi: 10.1038/s41467-018-05196-3

30. Chen L, Gao D, Shao Z, Zheng Q, Yu Q. miR-155 indicates the fate of CD4+ T cells. *Immunol Lett* (2020) 224:40–9. doi: 10.1016/j.imlet.2020.05.003

31. Kirigin FF, Lindstedt K, Sellars M, Ciofani M, Low SL, Jones L, et al. Dynamic microRNA gene transcription and processing during T cell development. *J Immunol* (2012) 188:3257–67. doi: 10.4049/jimmunol.1103175

32. Langmead B, Trapnell C, Pop M, Salzberg SL. Ultrafast and memory-efficient alignment of short DNA sequences to the human genome. *Genome Biol* (2009) 10:R25. doi: 10.1186/gb-2009-10-3-r25

33. Nawrocki EP, Eddy SR. Infernal 1.1: 100-fold faster RNA homology searches. *Bioinformatics* (2013) 29:2933–5. doi: 10.1093/bioinformatics/btt509

34. Friedländer MR, Chen W, Adamidi C, Maaskola J, Einspanier R, Knespel S, et al. Discovering microRNAs from deep sequencing data using miRDeep. *Nat Biotechnol* (2008) 26:407–15. doi: 10.1038/nbt1394

35. Kivioja T, Vähärautio A, Karlsson K, Bonke M, Enge M, Linnarsson S, et al. Counting absolute numbers of molecules using unique molecular identifiers. *Nat Methods* (2011) 9:72–4. doi: 10.1038/nmeth.1778

36. Wang L, Feng Z, Wang X, Wang X, Zhang X. DEGseq: an r package for identifying differentially expressed genes from RNA-seq data. *Bioinformatics* (2010) 26:136–8. doi: 10.1093/bioinformatics/btp612

37. Krüger J, Rehmsmeier M. RNAhybrid: microRNA target prediction easy, fast and flexible. *Nucleic Acids Res* (2006) 34:W451–4. doi: 10.1093/nar/gkl243

38. Enright AJ, John B, Gaul U, Tuschl T, Sander C, Marks DS. MicroRNA targets in *Drosophila*. *Genome Biol* (2003) 5:R1. doi: 10.1186/gb-2003-5-1-r1

39. Agarwal V, Bell GW, Nam JW, Bartel DP. Predicting effective microRNA target sites in mammalian mRNAs. *Elife* (2015) 4:e05005. doi: 10.7554/eLife.05005

40. Ashburner M, Ball CA, Blake JA, Botstein D, Butler H, Cherry JM, et al. Gene ontology: Tool for the unification of biology. the gene ontology consortium. *Nat Genet* (2000) 25:25–9. doi: 10.1038/75556

41. Kanehisa M, Goto S. KEGG: Kyoto encyclopedia of genes and genomes. *Nucleic Acids Res* (2000) 28:27–30. doi: 10.1093/nar/28.1.27

42. Abdi H. The bonferonni and Šidák corrections for multiple comparisons. *Encyclopedia measurement Stat* (2007) 3:103–107.

43. Schmittgen TD, Livak KJ. Analyzing real-time PCR data by the comparative CT method. *Nat Protoc* (2008) 3:1101–8. doi: 10.1038/nprot.2008.73

44. Kern F, Aparicio-Puerta E, Li Y, Fehlmann T, Kehl T, Wagner V, et al. miRTargetLink 2.0–interactive miRNA target gene and target pathway networks. *Nucleic Acids Res* (2021) 49:W409–16. doi: 10.1093/nar/gkab297

45. Jeker LT, Bluestone JA. Micro RNA regulation of T-cell differentiation and function. *Immunol Rev* (2013) 253:65–81. doi: 10.1111/imr.12061

46. Meningher T, Barsheshet Y, Ofir-Birin Y, Gold D, Brant B, Dekel E, et al. Schistosomal extracellular vesicle-enclosed mirRNAs modulate host T helper cell differentiation. *EMBO Rep* (2020) 21:e47882. doi: 10.15252/embr.201947882

47. Brunner-Weinzierl MC, Rudd CE. CTLA-4 and PD-1 control of T-cell motility and migration: Implications for tumor immunotherapy. *Front Immunol* (2018) 9:2737–7. doi: 10.3389/fimmu.2018.02737

48. Schneider H, Downey J, Smith A, Zinselmeyer BH, Rush C, Brewer JM, et al. Reversal of the TCR stop signal by CTLA-4. *Science* (2006) 313:1972–5. doi: 10.1126/science.1131078

49. Ye X, Zhou X-J, Zhang H. Exploring the role of autophagy-related gene 5 (ATG5) yields important insights into autophagy in Autoimmune/Autoinflammatory diseases. *Front Immunol* (2018) 9. doi: 10.3389/fimmu.2018.02334

50. Adams DH, Harvath L, Bottaro DP, Interrante R, Catalano G, Tanaka Y, et al. Hepatocyte growth factor and macrophage inflammatory protein 1 beta: Structurally distinct cytokines that induce rapid cytoskeletal changes and subset-preferential migration in T cells. *Proc Natl Acad Sci U.S.A.* (1994) 91:7144–8. doi: 10.1073/pnas.91.15.7144

51. Zhang YW, Vande Woude GF. HGF/SF-met signaling in the control of branching morphogenesis and invasion. *J Cell Biochem* (2003) 88:408–17. doi: 10.1002/jcb.10358

52. Mullins RD, Heuser JA, Pollard TD. The interaction of Arp2/3 complex with actin: Nucleation, high affinity pointed end capping, and formation of branching networks of filaments. *Proc Natl Acad Sci U.S.A.* (1998) 95:6181–6. doi: 10.1073/pnas.95.11.6181

53. Zhang Y, Shen H, Liu H, Feng H, Liu Y, Zhu X, et al. Arp2/3 complex controls T cell homeostasis by maintaining surface TCR levels *Via* regulating TCR+ endosome trafficking. *Sci Rep* (2017) 7:8952. doi: 10.1038/s41598-017-08357-4

54. Landgraf P, Rusu M, Sheridan R, Sewer A, Iovino N, Aravin A, et al. A mammalian microRNA expression atlas based on small RNA library sequencing. *Cell* (2007) 129:1401–14. doi: 10.1016/j.cell.2007.04.040

55. Kuchen S, Resch W, Yamane A, Kuo N, Li Z, Chakraborty T, et al. Regulation of microRNA expression and abundance during lymphopoiesis. *Immunity* (2010) 32:828–39. doi: 10.1016/j.immuni.2010.05.009

56. Rossi RL, Rossetti G, Wenandy L, Curti S, Ripamonti A, Bonnal RJ, et al. Distinct microRNA signatures in human lymphocyte subsets and enforcement of the naive state in CD4+ T cells by the microRNA miR-125b. *Nat Immunol* (2011) 12:796–803. doi: 10.1038/ni.2057

57. Dori M, Cavalli D, Lesche M, Massalini S, Alieh LHA, De Toledo BC, et al. MicroRNA profiling of mouse cortical progenitors and neurons reveals mir-486-5p as a regulator of neurogenesis. *Development* (2020) 147:dev190520. doi: 10.1242/dev.190520

58. Pang W, Tian X, Bai F, Han R, Wang J, Shen H, et al. Pim-1 kinase is a target of miR-486-5p and eukaryotic translation initiation factor 4E, and plays a critical role in lung cancer. *Mol Cancer* (2014) 13:240–0. doi: 10.1186/1476-4598-13-240

59. Rask L, Balslev E, Søkilde R, Høgdall E, Flyger H, Eriksen J, et al. Differential expression of miR-139, miR-486 and miR-21 in breast cancer patients sub-classified according to lymph node status. *Cell Oncol (Dordr)* (2014) 37:215–27. doi: 10.1007/s13402-014-0176-6

60. Chang Q, Ji M, Li C, Geng R. Downregulation of miR−486−5p alleviates LPS −Induced inflammatory injury, oxidative stress and apoptosis in chondrogenic cell ATDC5 by targeting NRF1. *Mol Med Rep* (2020) 22:2123–31. doi: 10.3892/mmr.2020.11289

61. Yuan S, Wu Q, Wang Z, Che Y, Zheng S, Chen Y, et al. miR-223: An immune regulator in infectious disorders. *Front Immunol* (2021) 12. doi: 10.3389/fimmu.2021.781815

62. Xi X, Zhang C, Han W, Zhao H, Zhang H, Jiao J. MicroRNA-223 is upregulated in active tuberculosis patients and inhibits apoptosis of macrophages by targeting FOXO3. *Genet Test Mol Biomarkers* (2015) 19(12):650–6. doi: 10.1089/gtmb.2015.0090

63. Liu D, Wang Z, Wang H, Ren F, Li Y, Zou S, et al. The protective role of mir-223 in sepsis-induced mortality. *Sci Rep* (2020) 10:17691. doi: 10.1038/s41598-020-74965-2

64. Xu H, Xu SJ, Xie SJ, Zhang Y, Yang JH, Zhang WQ, et al. MicroRNA-122 supports robust innate immunity in hepatocytes by targeting the RTKs/STAT3 signaling pathway. *Elife* (2019) 8:e41159. doi: 10.7554/eLife.41159

65. Crippa S, Cassano M, Messina G, Galli D, Galvez BG, Curk T, et al. miR669a and miR669q prevent skeletal muscle differentiation in postnatal cardiac progenitors. *J Cell Biol* (2011) 193:1197–212. doi: 10.1083/jcb.201011099

frontiers | Frontiers in Immunology

TYPE Original Research
PUBLISHED 05 September 2022
DOI 10.3389/fimmu.2022.956871

OPEN ACCESS

EDITED BY
Thiago Almeida Pereira,
Stanford University, United States

REVIEWED BY
Jacob A Tennessen,
Harvard University, United States
Amina Ibrahim,
Theodor Bilharz Research Institute, Egypt

*CORRESPONDENCE
Benjamin Gourbal
benjamin.gourbal@univ-perp.fr

†These authors have contributed equally to this work and share first authorship

SPECIALTY SECTION
This article was submitted to Parasite Immunology, a section of the journal Frontiers in Immunology

RECEIVED 30 May 2022
ACCEPTED 08 August 2022
PUBLISHED 05 September 2022

CITATION
Pichon R, Pinaud S, Vignal E, Chaparro C, Pratlong M, Portet A, Duval D, Galinier R and Gourbal B (2022) Single cell RNA sequencing reveals hemocyte heterogeneity in *Biomphalaria glabrata*: Plasticity over diversity.
Front. Immunol. 13:956871.
doi: 10.3389/fimmu.2022.956871

Single cell RNA sequencing reveals hemocyte heterogeneity in *Biomphalaria glabrata*: Plasticity over diversity

Rémi Pichon[1†], Silvain Pinaud[2†], Emmanuel Vignal[3], Cristian Chaparro[1], Marine Pratlong[4], Anaïs Portet[5], David Duval[1], Richard Galinier[1] and Benjamin Gourbal[1*]

[1]IHPE, Univ Montpellier, CNRS, IFREMER, Univ Perpignan Via Domitia, Perpignan, France, [2]Cambridge Institute, Li Ka Shing Center, Cancer Research UK, Cambridge, United Kingdom, [3]IHPE, Univ Montpellier, CNRS, IFREMER, Univ Perpignan Via Domitia, Montpellier, France, [4]Plateforme MGX - Montpellier GenomiX, Institut de Génomique Fonctionnelle, Montpellier, France, [5]Molecular Immunity Unit, Department of Medicine, Medical Research Council (MRC) Laboratory of Molecular Biology, University of Cambridge, Cambridge, United Kingdom

The freshwater snail *Biomphalaria glabrata* is an intermediate host of *Schistosoma mansoni*, the agent of human intestinal schistosomiasis. However, much is to be discovered about its innate immune system that appears as a complex black box, in which the immune cells (called hemocytes) play a major role in both cellular and humoral response towards pathogens. Until now, hemocyte classification has been based exclusively on cell morphology and ultrastructural description and depending on the authors considered from 2 to 5 hemocyte populations have been described. In this study, we proposed to evaluate the hemocyte heterogeneity at the transcriptomic level. To accomplish this objective, we used single cell RNA sequencing (scRNAseq) technology coupled to a droplet-based system to separate hemocytes and analyze their transcriptome at a unique cell level in naive *Biomphalaria glabrata* snails. We were able to demonstrate the presence of 7 hemocyte transcriptomic populations defined by the expression of specific marker genes. As a result, scRNAseq approach showed a high heterogeneity within hemocytes, but provides a detailed description of the different hemocyte transcriptomic populations in *B. glabrata* supported by distinct cellular functions and lineage trajectory. As a main result, scRNAseq revealed the 3 main population as a super-group of hemocyte diversity but, on the contrary, a great hemocytes plasticity with a probable capacity of hemocytes to engage to different activation pathways. This work opens a new field of research to understand the role of hemocytes particularly in response to pathogens, and towards *S. mansoni* parasites.

KEYWORDS

single cell RNA seq, *B. glabrata*, hemocytes, innate immune system, *S. mansoni*

10.3389/fimmu.2022.956871

Introduction

In invertebrates, innate immune response is mainly carried out by the hemocytes, appearing as a complex family of cells specialized in immunity (1). These cells carry both the so-called cellular response of the innate immune system, through encapsulation and phagocytosis of pathogens. But also, part of the humoral response by secreting in the hemolymph many cytolytic/cytotoxic compounds like antimicrobial factors, oxygen/nitrogen reactive species (ROS/NOS), proteases or toxins (2–4).

Despite the important role played by hemocytes in the invertebrates' immune response, these cells are still very poorly characterized. Different types of invertebrate hemocytes have been described in the literature (5), mainly according to their differential abilities to respond to pathogens, from phagocytosis, cell to cell adhesion or degranulation of humoral factors (1), but also based on their morphological features (shape, size, intracytoplasmic granules, vacuoles). However, hemocyte morphology studied alone is not sufficient to define a clear functional classification of hemocytes. Indeed, a direct relationship between hemocyte morphology and their specific immunological functions against pathogens is quite impossible to establish. However, the development of new technology of sequencing at the single cell level [single cell transcriptomics (scRNAseq) (6)] is now available to access the invertebrate hemocyte functional diversity.

Single-cell transcriptomics approaches have been firstly, and successfully developed in vertebrate models to describe the high specialization of innate immune cells and study their heterogeneities (7–9). Then, this technology was successfully transferred to various other non-vertebrate models, especially for infectious diseases such as plasmodium sp., the agent responsible for malaria disease Thousands of cells across the different parasite differentiation stages were sequenced to produce the very first parasite developmental cell atlas (10, 11). Such a tool allows the definition of new-targeted therapeutic strategies and the understanding of the mechanisms of transmission to its hosts. The study of metazoan parasite species, such as *Schistosoma mansoni*, the agent responsible for human intestinal Schistosomiasis has also benefits from this technology. The scRNA seq approaches on stem cell populations from juvenile *Schistosoma* allowed to precisely define 9 transcriptomic populations of somatic cells, and the characterization of conserved gene sets involved in the regulation of germline cells (12). This technology has proven to be a major asset also in the description of hemocyte populations in invertebrate hosts, improving the definition of the heterogeneity of immune cell populations in insects such as Drosophila, mosquitoes and silkworm (13, 14) or crustacean shrimp (15–19). ScRNA seq has allowed redefining, for the silkworms, the complexity of hemocyte populations in this model and the impact of a baculovirus infection (*Bombyx mori nucleopolyhedrovirus*) on some hemocyte populations (20). In addition, for mosquitoes, hemocyte complexity following infection by *Plasmodium* has been characterized, with the definition of 6 transcriptomic clusters in comparison to the 3 populations historically described based on morphological traits (21). These scRNAseq approaches have been shown to be very efficient in all these invertebrate host/parasite models and demonstrate the feasibility of this technique to decipher the complexity of hemocyte cell populations as well as to understand the immunological mechanisms activated in hemocytes in response to pathogens.

In the present study we paid a particular attention to a schistosomiasis vector snail, the gastropod *Biomphalaria glabrata*. Schistosomiasis remains today the second human parasitic disease after Malaria, in terms of morbidity and mortality in endemic areas (22), mainly South-America and sub-Saharan Africa. Schistosomiasis disease is caused by a flatworm of the genus *Schistosoma* which uses the gastropod *Biomphalaria* as an obligatory intermediate host to complete its life cycle. Thus, the comprehension of the immunological interactions between *B. glabrata* and *S. mansoni* would help in developing new strategies to fight or control this disease. Many studies to date have focused on these molecular interactions (23), and research has rapidly identified the key role played by hemocytes in recognition and/or killing of the parasite (3). However, despite their potential importance, knowledge on *Biomphalaria* hemocytes remains very sparse and a clear description of morphological populations or subpopulations, their proportion, and their functions are still a matter of debate (24).

Among those studies on the description of hemocyte populations in *Biomphalaria*, the morphological description of the cells by optical microscopy coupled with lectin surface labeling highlighted at least four hemocyte populations (25). Currently, some works describe two populations, hyalinocytes and granulocytes (26, 27) using a combination of light and electron transmission microscopy as well as flow cytometry approaches. Other results using optical and electron microscopy (24), describe five morphologically distinct populations of hemocytes: hyalinocytes (that can be split into three subpopulations of hyalinocytes I, II and III), granulocytes and blast-like cells. However, despite these morphological characteristics, it is still complex to define their specific biological functions. It has been demonstrated that some morphologically similar cells display different biological functions or that distinct hemocyte populations display similar functions. For example, *Biomphalaria glabrata* hyalinocytes and granulocytes are known to be involved directly in the cellular response through non-self-recognition, phagocytosis and encapsulation (25). In this context, a recent study (28) has attempted to describe the function of specific hemocyte populations using a serial dilution method to isolate granulocytes and hyalinocytes and described more accurately

the specific functions associated with these cells using a massive transcriptomic sequencing approach. Finally, it has been demonstrated for blast-like cells, often considered as prohemocytes (undifferentiated cells) (24), that differential gene expression patterns could be observed, indeed some subpopulations of blast-like cells produce for example a complement like factor, named BgTEP1 (29, 30), acting as an opsonin molecule involved in the immune response against *S. mansoni* parasite, demonstrating an unexpected level of cellular complexity yet indistinguishable morphologically.

This is why, herein we used a droplet-based system of single cell RNA sequencing (31) to describe without *a priori* and for the first time, the level of heterogeneity and diversity of hemocyte populations in the freshwater snail *B. glabrata.* We discovered a slight diversity of transcriptomic populations defined by sets of marker genes specific to each of the populations combined with cell lineage relationship between different hemocyte subpopulations. These transcriptomic populations are still rather complex to correlate with the published morphological populations from microscopy, flow cytometry and label-free proteomic analyses, mostly because of the shallowness of the *Biomphalaria glabrata* genome/transcriptome/proteome annotation. In addition to bringing new clues of rather hemocyte plasticity than diversity in *Biomphalaria glabrata*, we proposed and discussed herein that complementary approaches must be used to eventually define hemocyte populations and start to face hemocyte biology where it matters most.

Materials and methods

Biological sample experiments

We used a *Biomphalaria glabrata* strain originated from Recife locality in Brazil (BgBRE2), recovered in 1975 and maintained since then under constant laboratory conditions. Snails were maintained at 26°C in glass aquaria and fed with green leaf lettuce *ad libitum*.

Hemocytes preparation for morphological characterization

10 snails (size: 8-10 mm) were retained to collect hemocytes by puncturing the hemolymph (30µL per snail) according to a widely used protocol previously established using the defence reflex of hemolymph released from the cephalo-pedal sinus when the snail shrinks in its shell (32). Hemolymph was transferred on a polystyrene slide (Caplugs evergreen) and stood in a humid chamber for 30 min for hemocytes to adhere to the slide. Then, hemocytes were stained with a panoptic May-Grünwald Giemsa (MGG) type staining method by MCDh (RAL Diagnostics) following the manufacturer recommendations. Briefly, hemocyte slides were sunk during 6 min in MCDh1 solution, 1min in a first bath of MCDh2, 2 min in a second bath of MCDh2, 1min in MCDh3, then 10 seconds in MCDh4. Slides were dried and mounted with Dako® fluorescent mounting medium (Agilent, S3023) and finally the hemocyte populations and their proportions were counted under light microscopy using a 100X objective (Supplementary Table 1).

Hemocytes preparation for droplet scRNA sequencing

Pooled hemolymph (500µl) from 50 snails was recovered into 2ml tubes and mixed with 1.5ml of modified anticoagulant solution (98mM NaOH, 186mM NaCl, 1.7mM EDTA, 1.7mM citric acid) (13). Sample was passed through a 30µm pre-separation filter (Miltenyi Biotec) to eliminate cell aggregates and obtain a suspension of unique cells. Then hemocytes were counted using a Malassez chamber and cell viability was measured with trypan blue exclusion technique. Samples were then spin-down (2700g, 5min, 4°C) to pellet the hemocytes and re-suspended in 50µl of anticoagulant solution [30% of BGE medium (33)] and 70% anticoagulant modified solution). To obtain a concentration of 1000 cells per microliter. Samples were then processed by MGX platform (IGH Montpellier, France) for scRNA droplet isolation (Chromium, 10X genomics) and RNA sequencing.

Single-cell RNA sequencing and data processing

Single cell processing procedure is defined by the MGX platform (Montpellier GenomiX). Single cell suspension was obtained by a Chromium Single-Cell Controller (10X Genomics). Library preparation was performed with Single Cell 3' Reagent kits V3.1 (10X Genomics) using 10x Next GEM Technology barcode and validated by DNA quantification with Fragment Analyzer (kit High Sensitivity NGS) and qPCR (ROCHE LightCycler 480). Libraries were sequenced with an illumina NovaSeq 6000 (Illumina) and SBS (Sequence By Synthesis) techniques using NovaSeq Reagent kits (100 cycles). Output results and matrix generation were processed with 10X Genomics Cell ranger v3.1.0 software (http://10xgenomics.com).

All available mitochondrial gene sequences were recovered from the NCBI database (34, 35) and gene names corresponding to these sequences (Supplementary Table 2) were retrieved using blastn (36) on the *Biomphalaria glabrata* genome annotation version 1.6 available on Vector Base website (https://vectorbase.org/vectorbase/app/record/dataset/TMPTX_bglaBB02, 15/10/2021) (37).

Cell clustering and genes expression

Filtered matrix sorted by Cell Ranger (10X Genomics Cell Ranger 3.1.0) was used and analyzed on R (Version 4.1.0 (2021–05–18)) using Seurat package [Version 4.0.4 (38)]. Hemocytes with more than 50 unique expressed genes were kept and genes expressed in 3 or more cells were retained for the generation of the gene-cell data matrix and downstream analysis. Low quality cells were filtered out excluding cells with less than 750 or more than 3100 unique expressed genes and cells with a proportion of mitochondrial transcript higher than 5% were excluded from the analysis. Log-normalized method given by the Seurat package was used to normalize the data. Thereafter, 2.000 highly variable genes were obtained using FindVariableFeatures function, these genes were scaled and used to perform Principal Component Analysis (PCA). JackStrawPlot and ElbowPlot functions were used to determine the top principal component (15:25) that is most representative of the data set for each reduction. The dataset clustering was conducted by the FindClusters function according to identified PCs. Visualization in two dimensions of the clustering was made through the use of non-linear dimensional reduction, UMAP (Uniform Manifold Approximation and Projection for dimension reduction) and tSNE (t-distributed Stochastic Neighbor Embedding) projection. We used Seurat (FindAllMarkers option using wilcoxon rank sum test for each cluster) to determine differentially expressed genes and gene markers (Supplementary Table 2) for each cluster (Log2FC>0.25 and min.pct > 0.25) and created a heatmap to represent the top n marker genes defining each cluster. Cluster-specific marker genes were determined by selecting shared characteristics as being differentially overexpressed with Log2FC > 1, expressed by a majority of cells (>80%) within the cluster and a minority of cells (<10%) in other clusters. All these marker genes were used to perform a GO enrichment analysis (fisher exact test, P-value > 0.01) using Blast2GO omicsbox (39) on *Biomphalaria glabrata* reference genome V1.6.

Cell trajectory analysis

The cell lineage analysis was performed with bioinformatic tools Monocle3 (40) and slingshot (41) on the data processed by the Seurat package mentioned above after conversion to SingleCellExperiment object. Some transcriptomic clusters considered as being the most distant and different with respect to the marker genes that define them were removed from the analysis to perform this cell lineage. To identify temporally expressed genes we used a general additive model (GAM) based on bioinformatic workshop (42). R script used for all the bioinformatic analysis done with Seurat and Monocle3 packages were available on Zenodo (accession #: 10.5281/zenodo.6951346).

Flow cytometry, cells sorting and Label-Free proteomic sequencing

Pooled hemolymph of 300 BgBRE snails was used for cytometry cell sorting. Briefly, hemolymph was extracted from the snails as previously described and immediately used for flow cytometry and cell sorting, 25 µL of hemolymph was recovered from each snail for a total of 3.5 ml. Cell sorting was performed, using a FACS Canto from BD Biosciences (RIO Imaging Platform, Montpellier, France), according to the FSC and SSC parameters to discriminate each hemocyte population according to their size and granularity. With the help of FACSDIVA software, four gates were defined based on different SSC and FSC parameters (low SSC/FSC to high SSC/FSC). Hits detected in these gates were sorted, recovered on microscopic slides and observed under a light microscope to confirm the enrichment of different morphological hemocyte populations associated with the different settings of cell sorting gates. Finally, sorted hemocyte samples were recovered for label-free proteomic analysis. Recovered hemocytes were lysed in hypotonic buffer, protein extracts were quantified (2D-Quant kit protein quantification) and 200 µg of proteins were solubilized in laemmli buffer 4x (Biorad, hercules Califonia, USA), boiled at 95-100°C for 5 min, frozen at -80°C and send for label free sequencing to EDyP service facilities (INSERM, CEA, Grenoble, France). Protein preparation and mass spectrometry-based proteomic analyses were conducted as described in (43, 44). Protocol repeated, hereafter, from Pinaud et al., 2019. Briefly, extracted proteins were stacked in the top of an SDS-PAGE gel (NuPAGE 4 to 12%; Invitrogen) before in-gel digestion was performed using trypsin (sequencing grade; Promega). Resulting peptides were analyzed in duplicate by online nanoscale liquid chromatography tandem mass spectrometry (nanoLC-MS/MS) (UltiMate 3000 and LTQ-Orbitrap Velos Pro; Thermo Scientific) using a 120-min gradient. Peptides and proteins were identified using Mascot software (Matrix Science) and confronted against either, Uniprot database and translated genome of *Biomphalaria glabrata* snail (available at vector base: https://vectorbase.org/vectorbase/app). Qualitative differences between samples were considered as potential markers of sorted hemocyte populations and used to infer scRNAseq clusters to a potential morphological population of hemocytes.

Results

Morphological description of *Biomphalaria glabrata* hemocytes

There is no real consensus on the morphological characterisation of hemocyte diversity for *Biomphalaria glabrata*.

To clarify this purpose, we decided to establish an "hemocytogram" of circulating *B. glabrata* hemocytes after plating. Three distinct hemocyte populations were identified: hyalinocytes, blast-like cells and granulocytes (Figures 1A–D). The hyalinocytes are large cells (size around 35 µm) with a large nucleus, characterized by different chromatin states (with a dense purple heterochromatin and a pale purple euchromatin) (Figure 1A). In their cytoplasm can be observed large unstained vacuoles. These cells are characterized by a great capacity of adherence to plastic slides and by their capacity to produce large and long pseudopodia (Figure 1A). They represented the main quantity of circulating hemocytes in *Biomphalaria glabrata*, 66.7% +/- 9% (Figure 1E). The blast-like cells (Figure 1D), represented 21% +/- 6% of circulating hemocytes (Figure 1E), they were small cells (around 8µm), displaying a high nucleocytoplasmic ratio with very low adhesion capacities. These cells appear with a rounded shape even after plating on plastic slides (Figure 1D). Nuclei appeared very dense upon MCDh staining with a dark purple color (Figure 1D) indicating potentially a low level of gene transcription, these cells being often considered as pro-hemocytes. Finally, the third type of hemocytes were the granulocytes (Figures 1B, C) that represented 12.3% +/- 3% of circulating hemocytes (Figure 1E), and were not able to adhere efficiently to plastic slides. Very few cells were able to form small filopodia and were mainly characterized by a spherical shape (Figure 1C). Granulocytes have a dense dark purple nucleus and always show neutrophilic (deep purple) to basophilic (dark blue) granules in their cytoplasm. However, among the population of granulocytes, we were able to distinguish some morphological differences. Some granulocytes were able to adhere efficiently to the slide and form long pseudopodia that could make them difficult to distinguish from hyalinocytes (Figure 1B), except that these cells possessed intracytoplasmic granulations, which make them belonging to granulocytes. The proportion of these different cell populations in hemolymph remain in agreement with the data available in the literature (24) although the sizing of these cells on plastic slides appeared very hazardous due to their variable adhesion capacities, the plasticity of their morpho-anatomic parameters, and their important size and shape variability. Thus, we were not able to define clearly, (i) the exact number of hemocyte populations and (ii) the delimitation between hemocyte subtypes. Facing such limitations, we proposed to use a scRNA-seq approach to decipher the hemocyte populations and their potential role or function using their transcriptional activity and gene expression patterns rather than their morphological parameters.

Identification of 7 distinct clusters in *B. glabrata* hemocytes by scRNA-seq

To examine hemocyte heterogeneity by scRNA-seq, isolated hemocytes from a pool of 50 naive snails were subjected to droplet scRNAseq. Approximately 3000 cells were captured using the 10X Genomics Chromium microfluidic technique and submitted to RNA sequencing. After an initial process by CellRanger (10x Genomics Cell Ranger 3.1.0), the sequencing data were aligned to the *B. glabrata* reference genome (90.1% reads mapped to the genome). We obtain 2624 estimated cells with a median gene per cell corresponding to 1885 genes among the 19 820 total genes detected and a sequencing saturation at 66%. To retain high quality single cell RNA-seq data, we removed low-quality cells with gene number less than 750 and mitochondrial genes less than 5%. Seurat R package (Version 4.0.4) was used for data processing. Following such quality control, 2193 high-quality cells were used for further analysis. For each cell, an average number of 2470 genes expressed were obtained and 7 transcriptomic clusters were identified (Figure 1F). Regarding read coverage by clusters, cells in clusters 0, 2, 4 and 5 have a higher number of reads compared to cells in clusters 3, 1 and 6 (Supplementary Figure 1). These last 3 clusters may represent cells with low transcriptional activity or small cells like blast-like cells.

Most of the hemocytes gathered within a main cluster (cluster 0) which represented 73.8% of the total cells. The other clusters (cluster 1 to 6) represented from 7.7% (cluster 1) to 1.9% of the cells respectively (Figure 1F). We were able to define transcriptomic profiles and specific marker genes for each cluster (Figures 1G, H). Cluster 0 does not have genes that are completely specific to it and appears to share several defined marker genes with the clusters 4 and 5 (Figure 1H). Some marker genes of the Cluster 2 are also overlapping with cells of cluster 3, but the latter possess a very specific list of marker genes.

Gene expression signatures and candidate markers for each hemocyte cluster

Annotation and understanding of *Biomphalaria glabrata* genome/transcriptome/proteome are still very sparse. Amongst the 31 985 defined genes for about 44 406 transcripts, less than the half possess at least a protein domain information, making every enrichment or functional analysis conditioned by annotation bias. Also, it exists a redundancy in *B. glabrata* gene annotation, meaning that same gene annotation or transcripts can have different gene name/position and different transcripts. Knowing such limits but in order to create a transcriptomic identity card for the different clusters, we were interested in the function of the marker genes detected with Seurat (Supplementary Table 2). When possible (sufficient number of genes), we performed a Gene Ontology enrichment analyses with the blast2GO tool (Supplementary Table 3), taking into account only the marker genes present in at least 80% of the hemocytes from the cluster considered.

Analysis of the enriched functions (Supplementary Table 3) showed that hemocytes from Cluster 0 expressed genes mostly

10.3389/fimmu.2022.956871

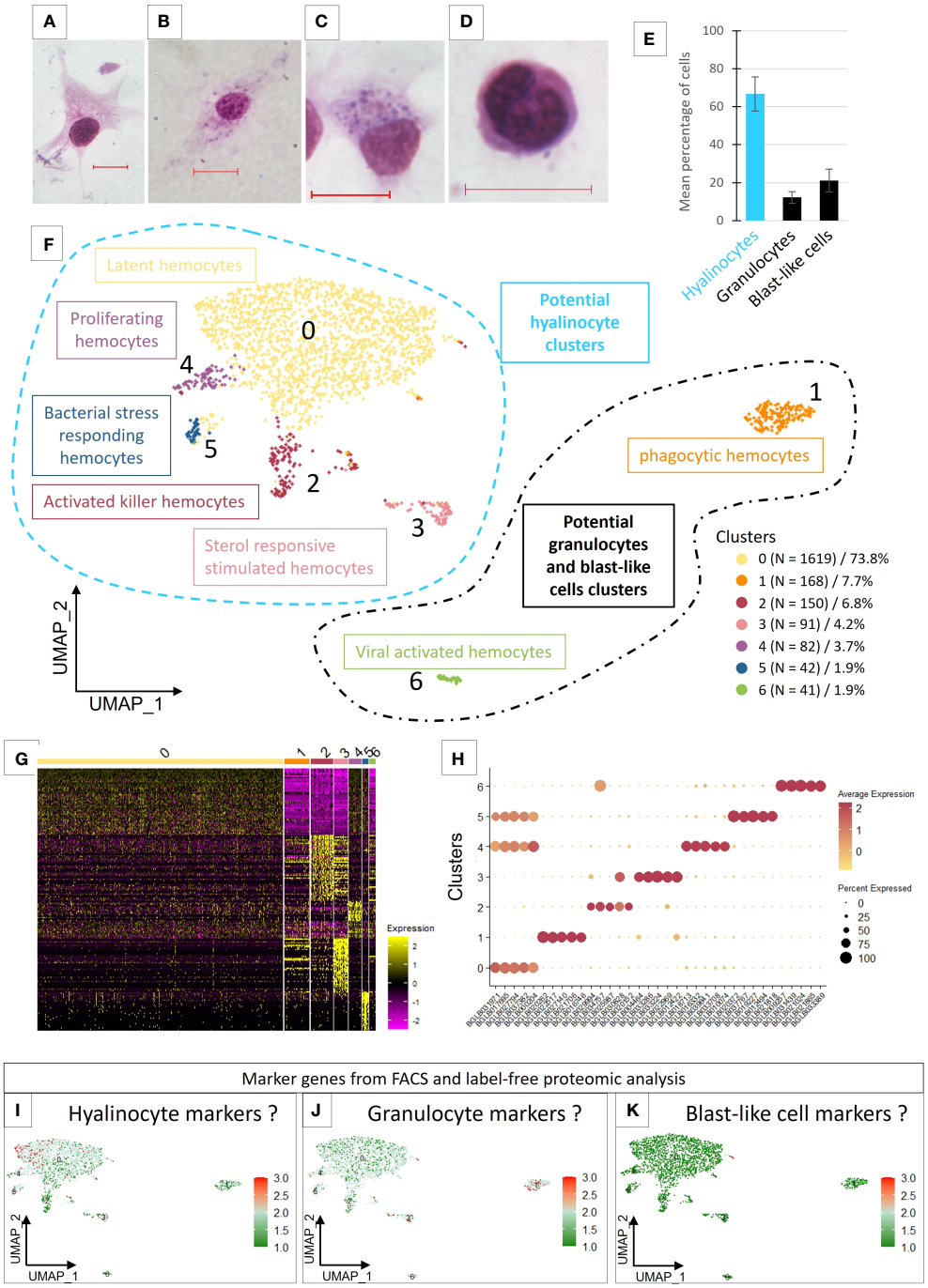

FIGURE 1
(A–D) Light microscopy observation of MCDh-stained hemocytes. Red bars 10µm. **(A)** hyalinocyte; **(B, C)** granulocytes; **(D)** blast-like cell. **(E)** Average number of hemocytes (1844 cells total) from 10 naive individuals according to three morphological types. **(F)** Uniform Manifold Approximation and Projection for Dimension Reduction (UMAP) plot of the 7 hemocyte clusters identified in *B glabrata* by scRNA-seq and their respective count of the cell number present in each transcriptomic cluster. **(G)** Heatmap representing the differential expression of the top 50 marker genes defined for each of the 7 transcriptomic clusters. **(H)** Dotplot representing the average expression of the 5 genes defined as markers for each cluster according to the percentage of cells expressing these genes per cluster. **(I–K)** represent the average expression levels of the genes defined as markers by the flow cytometry approach coupled with label free proteomics. Dotplot and UMAP representation of marker genes average expression of hyalinocyte **(I)**, Granulocyte **(J)** and blast-like cells **(K)**.

related to metabolism, energy production and protein synthesis but also functions involved in actin and cytoskeleton reorganization. These cells probably have an important translational activity but no specific specialization. We have in this cluster active cells, with generalist functions of cell maintenance but also cells able to express marker genes already described in the literature. Indeed, we found however several Pattern Recognition Receptors (PRRs) that can recognize different types of pathogens, and some of which have a very important role in immunity against *S. mansoni* parasite and especially in the recognition of this parasite, such as FREPs (45), MAM and LDL-receptor class A domain-containing 1-like (46) or genes containing von Willebrand factor EGF and pentraxin domain-containing 1 (47) that have been described in other models and which could have a role in suppressing or modulating the immunity (Supplementary Table 2). We proposed that cluster 0, named latent hemocytes (Figure 1F), is composed of circulating hemocytes that are waiting for activation in the case of a potential encounter and infection with a pathogen or the activation of alarmins. Moreover, some of the marker genes in this cluster are also expressed in clusters 4 and 5, which might suggest a strong cell filiation between these three clusters.

The five marker genes selected to characterize cluster 4 (Supplementary Table 2), were all genes involved in functions related to DNA replication and cell proliferation. Enrichment analyses confirm these functions (Supplementary Table 3). The cells in this cluster represent only 3.7% of the total number of cells (Figure 1E) considered in the analysis and may correspond to proliferating cells. Indeed, proliferation of circulating hemocytes has been yet demonstrated in naive *B. glabrata* snails with a proportion of 1.8% of hemocytes in proliferation (47), but no references has mentioned a specific hemocyte population capable of proliferating. These cells, considered as proliferating hemocytes (Figure 1F), thus appear to derive from cluster 0 and to be proliferating in response to an unknown stimulation or for maintaining a basal hemocyte turn-over.

Cluster 5 is defined by a few but specific marker genes with strong differential expression (log2FC) for the selected genes compared to all remaining cells (Supplementary Table 2). Most of these genes are not annotated. Some could have functions related to lipid metabolism (ganglioside GM2 activator) or being involved in response to pathogens (antimicrobial peptides, holotricin-3-like, PRRs),. This cluster could correspond to bacterial stress responding hemocytes (Figure 1F).

Concerning cluster 3, the enriched functions (Supplementary Table 3) are mainly related to the cellular component of gene ontology. The enriched functions of this cluster tend to show active cells able to set up vacuolization and degradation processes by the lysosome. Thus, many cathepsins (L1-like, Z, B), G-type lectins, cystatin-B (48) are involved in these functions. At least 7 genes encoding proteases, cathepsins (B, Z and D) and cathepsin like (L1) are represented as marker genes in this cluster and one cathepsin Z (BGLB004464) is specific to this cluster (Supplementary Table 2). Some of these molecules are known in the *B. glabrata*/*S. mansoni* model to have a possible role in the interaction with the parasite (49). We also find in this cluster functions involved in sterol and cholesterol metabolism, shown to have a role in modulating some immune pathways (50). This reinforces the idea that this cluster is a cluster of activated cells probably responding to a circulating factor and using sterols to respond, that is why we named this cluster sterol responsive stimulated hemocytes (Figure 1F).

In cluster 2, cells express some genes involved in immunity such as several cathepsins (L1-like, B, D, Z) as we can find in cluster 3 but with lower differential expression (Supplementary Table 2). This cluster is mainly marked by C-type lectin, peptidoglycan-recognition SC2-like or an apolipophorins-like isoform X1 which is initially known for lipid transport but which may also have a role in the immune response and especially in encapsulation (23, 51). Other genes are strongly involved in different signaling pathways (MAPK, ERBB2, etc.) or in the regulation of cell necrosis and vacuole formation (Supplementary Table 3). The cells that make up this cluster could therefore be activated killer hemocytes (Figure 1F), either dying or degrading possible phagocytosed pathogens.

Cluster 1 represents 7.7% of the total cells (Figure 1E) in the analysis and is marked mainly by functions involved in the activation of the immune response and different pathways related to cell phagocytosis capabilities as well as functions involved in vacuolization and cytoskeleton rearrangement processes (Supplementary Table 3). Among the genes selected as potential marker genes for this cluster (Supplementary Table 2), we also find immune genes such as a fibrinogen-related protein J1 precursor and a cathepsin B-like. Thus, this cluster could be composed of activated cells possessing phagocytosis capabilities and as described with a smaller RNA content would be strongly considered as a blast-like cell cluster.

Cluster 6 expressed genes involved in cell differentiation and migration functions (ERBB2 signaling pathway) as well as genes having immune-related annotations like cathepsin and apolipophorins, an immune receptor role like toll-like receptor or macrophage mannose receptor or even functions annotated to be involved in response to virus (Supplementary Table 3). This cluster is also marked by a high ribosomal activity marked by rRNA metabolic process and ribosome biogenesis functions and therefore probably a high translational activity. They are therefore cells with membrane and vesicular activity accompanied by modifications of the cytoskeleton, which could correspond once again to active phagocytic cells, may be in response to virus infection. We named this cluster viral activated hemocytes (Figure 1F).

10.3389/fimmu.2022.956871

Label free proteomic from FFC/SSC-sorted hemocyte populations

Preliminary analyses of cell sorting by flow cytometry were coupled with label free proteomic analysis to attempt to associate morphology and final gene products with the objective to find specific markers of hemocyte populations. We can notice that the distribution of hemocytes according to the size and granulometry forms a continuum and does not allow to discriminate with accuracy one or more cell types or populations based on such cytometry characteristics (Supplementary Figure 2). Compared to a cell description on a microscopy slide where the hemocytes have specific adhesion capacities for each population, the hemocytes sorted by cytometry no longer have these characteristics. The cells are in suspension and therefore probably keep a round shape which prevents a simple discrimination by size and granulometry. However, the classical three morphological populations (hyalinocyte, granulocyte and blast-like cells) were attempted to be enriched by sorting in each of the gates (P1 to P4) (Supplementary Figure 2). Each of these gates corresponds to a specific FFC/SSC ratio gradient. The P4 fraction corresponds to cells defined as small to medium size with medium granularity. This fraction may allow an enrichment in hyalinocytes. The P3 fraction corresponds to cells of medium size and medium granulometry, which may allow the enrichment of blast-like cells but also some hyalinocytes. The P2 fraction corresponds to cells of small size and high granulometry, which did not give any enrichment of cells and was mostly composed of cell debris. This fraction was therefore not retained for the proteomic analyses. Finally, the P1 fraction corresponds to large size cells with high granulometry, which corresponds to a sample potentially enriched in granulocytes. The label-free proteomic analyses produce, for each of these sorted cell populations, the protein enrichment (Supplementary Table 4). The average expression of the genes encoding these proteins are used in the scRNA seq analysis to produce an expression mapping among the 7 clusters already described.

Unfortunately, the protein enrichment and the gene analysis from the identified proteins is not sufficient to obtain specific markers that fit with scRNAseq clustering. Indeed, all clusters seem to express all genes determined from the label free analysis. However, slight differences in the expression of these genes in some clusters are highlighted. First, we can see that few genes are specific to the fraction corresponding to an enrichment in blast-like cells. These genes are found to be carried by cells belonging to cluster 1 even though these cells seem to be closer to cluster 0 in the UMAP representation (Figure 1K). Genes representing the hyalinocyte-enriched fraction would be expressed by cells from clusters 0, 3 and 4 (Figure 1I) whereas clusters 1, 3 and 6 would represent cells expressing genes attributed to the granulocyte-enriched fraction (Figure 1J).

Overall results lead us to consider that cluster 0 may contain all the known cell types, since we have in this cluster the expression of all the genes that are supposed to define our enriched fractions in the three different hemocyte morphological populations. Only markers expressed specifically by clusters 1 and 6 seem belonging to the fraction enriched in granulocytes. These two clusters are also very particular because they are very different in this analysis from all other clusters and express their own marker genes. The lineage analyses do not allow us to establish a link between these clusters and the other clusters, which prevents us from studying in more detail the links that may exist between all the other clusters and cluster 0. This is why we decided to subset out cluster 1 and 6 for further analyses.

Cell lineage

The cell lineage analysis on all the 7 transcriptomic clusters was inconclusive. The most differentiated clusters in the analysis (clusters 1 and 6) prevent from defining relationships between cells in the other clusters. For this reason, we removed clusters 1 and 6 and re-run the cell lineage clustering analyses (Figure 2A). We identified 2 particular cell lineages (Figure 2B), both probably originating from cluster 0 chosen by default as the starting point of the pseudo-time trajectory construction. The first lineage path connects clusters 0, 4 and 3 and the second lineage connects clusters 0 and 2 (Figure 2B). Cluster 5 is not linked by the pseudotime analysis to the other clusters because it shares too many similarities in terms of expressed marker genes with cluster 0 (Figure 2C) and the probable lack of a sufficient number of cells for this cluster prevents a correct trajectory analysis. From the calculated pseudotime, we have estimated the top 100 most variable genes along this lineage (Figure 2D). We can immediately notice that most of the genes that define the lineages towards cluster 2 and 3 are genes known to be involved in various immune responses such as an integrin, toll-like receptor, several cathepsins, or an antimicrobial peptide hydramacin. These gene sets reinforce the hypothesis that clusters 4 and 3 may represent two steps of hemocyte activation following a yet unknown signalling with the cluster 4 as an intermediate state and the cluster 3 as a terminal state of activation. Furthermore, for each of these clusters we are able to assign specific genes with a possible link to immune responses. A set of these genes alone can define each of the differentiated clusters in our analysis as cluster 2 (Figure 2G), cluster 3 (Figure 2H) and cluster 5 (Figure 2I).

Use of the literature to define different transcriptomic clusters

The preliminary flow cytometry and microscopy approaches do not allow us to accurately connect morphotypes with scRNAseq transcriptomic clusters. We therefore relied on the

10.3389/fimmu.2022.956871

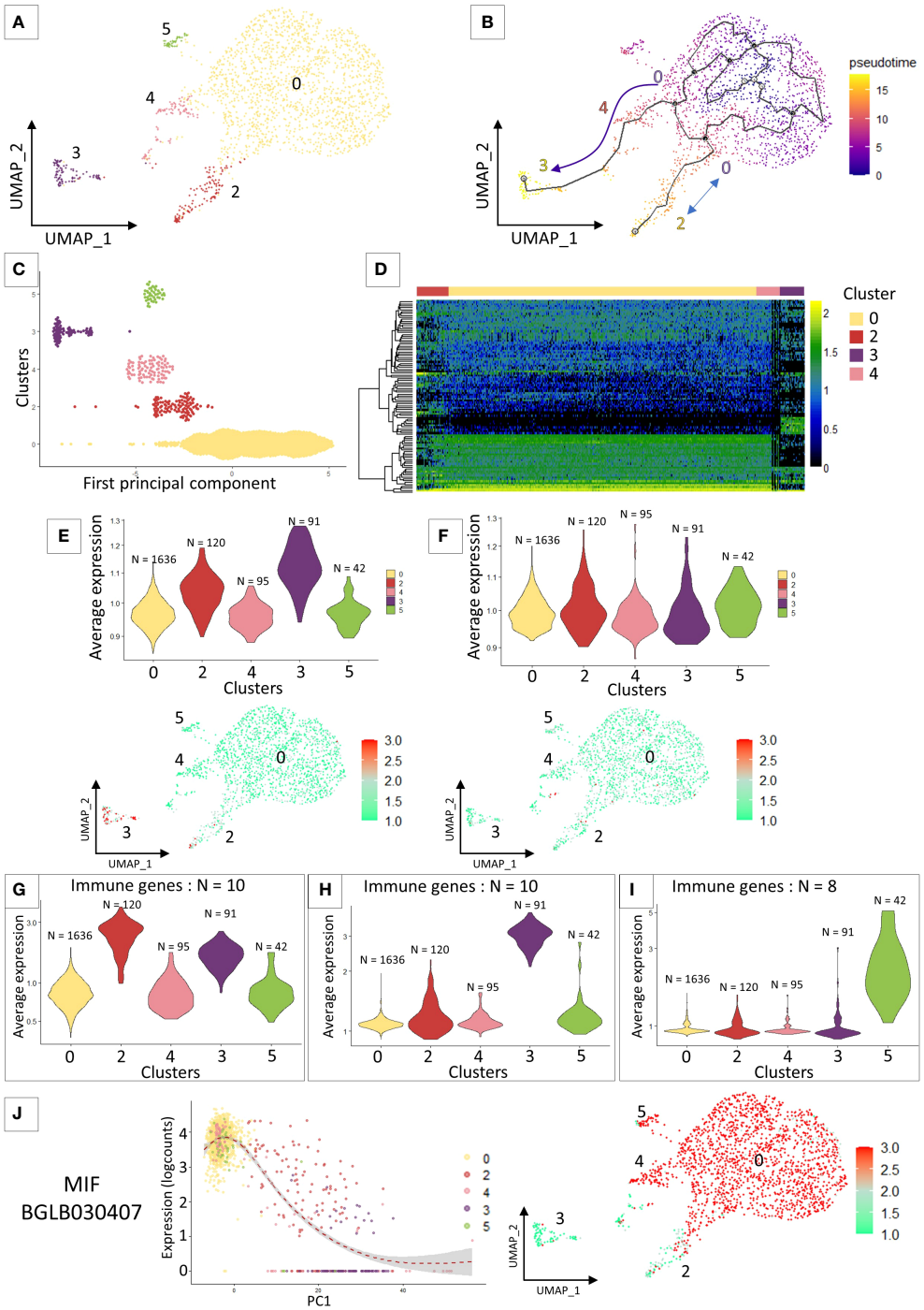

FIGURE 2
(A) UMAP representation of cluster 5 identified after removing clusters 1 and 6 from the previous analysis and performing reclustering. **(B)** Pseudo time analysis on the UMAP representation. Arrows represent the direction of the possible differentiation process between the different transcriptomic clusters. **(C)** Dotplot of the cluster cells ordered along the pseudo time. **(D)** heatmap representing the expression of the 100 most variable genes that characterized the pseudo-time analysis across the 4 clusters. **(E)** and **(F)** VlnPlot and UMAP representation of the average expression of marker genes from the literature. **(E)** represents granulocyte marker genes and **(F)** represents hyalinocyte marker genes. **(G, H)** and **(I)** Average expression of an immune gene set belonging to different "activated" clusters such as cluster 2 **(G)**, cluster 3 **(H)** and cluster 5 **(I)**. **(J)** Expression of the MIF gene along the pseudo-time (left graph) and the representation of its expression by the different cells of the analysis on the UMAP representation (right graph).

literature to find marker genes for our different hemocyte populations. As the latter is currently very limited, we focused on the recent work of Li and collaborators (28) that analyse in *Biomphalaria* the transcriptomic expression of hyalinocytes and granulocytes. We selected immune genes that authors were able to extract from their analysis and that were more strongly expressed either by hyalinocytes or granulocytes. We retrieved those immune gene orthologs, indistinguishable from the two mollusk strains (BS-90 and M-line strains) studied, from each of the two morphological hemocyte populations. We then averaged the expression of all genes, by cell type, that we are able to detect in our scRNAseq analysis to determine which transcriptomic cluster would be very likely to express these immune gene pools (Figures 2E, F). The immune marker genes defined for hyalinocytes using this approach, do not fit a particular cluster for this cell morphotype. All the immune genes taken in this analysis are expressed in all the clusters (Figure 2F) and especially are not differentially expressed between the clusters (Figure 2F). On the other hand, and as expected from previous analyses, the immune genes expressed by granulocytes in the literature are found to be more expressed in a part of the cells of cluster 2 and in the majority of the cells of cluster 3 (Figure 2E). These genes defined as granulocyte-specific were also found to be slightly over-expressed in cluster 1. Furthermore, if we look at some specific genes, found in a few rare articles defining a gene for a probable hemocyte population in *Biomphalaria*, such as granulin (BgGRN: BGLB011796), suspected to be expressed by some granulocyte subtypes (28, 52, 53), we notice that this gene seems to evolve along the pseudotime to be expressed by clusters 2 and 3. A gene that might be associated with granulin would be a toll-like receptor (54) that is found in our analyses to be expressed also by cells of cluster 2 (Supplementary Figure 3). All of these evidences could lead us to believe that a specialization of hemocytes takes place from cluster 0 to clusters 4 and 3 or to cluster 2. The latter could then be associated with possible granulocytic activated cells. We also find the expression of a gene belonging to the Macrophage Migration Inhibitory Factor family (MIF: BGLB030407), this protein has been shown to be overexpressed in some granulocyte-like hemocytes (55) and could serve as regulating hemocyte, proliferation activation and encapsulation response. The gene coding for this protein in our analysis is not found in cluster 3 and expressed in all the other clusters and in particular with a gradient of expression between cells in cluster 2 (Figure 2J). We can speculate that this gene expression pattern could then be an activation sign of certain hemocytes and of differentiation towards granulocyte cells.

Discussion

Our current knowledge about *Biomphalaria glabrata* hemocytes is still very sparse. The different populations of hemocytes have been only described so far by transmission electron microscopy (TEM) and flow cytochemistry approaches, or by optical microscopy and cell morphology description (24, 26, 27). Very few studies also address the question of the cell lineage of these hemocytes and the characterization of the hematopoiesis, by the amoebocyte producing organ (APO) (56, 57). To date, the scientific community agrees on the presence of at least 3 morphological populations defined only by their behaviour toward plating: hyalinocytes, granulocytes and blast-like cells. However, it seems to be a greater complexity and plasticity within these three large populations, and this diversity is very dependent on the tools used to characterize them (microscopy, flow cytometry, scRNA-seq).

Moreover, even the name given for each population was inconsistent in the literature, this increases the complexity of description of these populations [i.e., large adherent cells were called sometimes hyalinocytes or granulocytes depending on the paper considered (24, 26)]. For us, when hemocytes are allowed to adhere to a plastic slide, it is immediately obvious that the non-granulocytes adhere much better to the support by forming long pseudopodia and are considered as hyalinocytes (Figure 1A). However, it can also be seen that there are cells that are morphologically very close to hyalinocytes with intracytoplasmic granulations, that could be considered as adherent granulocytes or granular hyalinocytes (Figure 1B). Thus, the characterization of hemocytes by microscopy is very dependent on the technique employed (TEM, light microscopy, staining regent used,) or the support used for plating (polystyrene, plastic or glass slides). Moreover, distinguishing those hemocyte populations was particularly complicated in flow cytometry when all hemocytes are in suspension, they all display a spherical shape resulting in a continuum of size and granularity. Nevertheless, we have counted these different populations in naive snails and found that the majority of hemocytes were hyalinocyte-like cells, then blast-like cells and finally granulocytes (Figure 1E). These data are fairly consistent with the proportions determined by (24).

The scRNA-seq technology brings *de-novo* and without *a-priori* gene enrichment and heterogeneity information from a complex cell suspension. It brings information as well about potential role and function of each hemocyte transcriptional population but can also determine a possible lineage relationship between all these cells. For this purpose, we decided to study circulating hemocytes of naive *B. glabrata* snail, considered as not having undergone any experimental infection. We identified 2 large groups (Figure 1F) based on their transcriptomic identity, where a large and complex population of probable hyalinocyte (cluster 0, 2, 3, 4 and 5) is well separated from 2 distant populations (clusters 1 and 6) of differentiated hemocytes which could then be associated with probable blast-like cells, because of the few transcripts found in these two clusters (Supplementary Figure 1) or with granulocytes (Figure 1F).

Moreover, the population distribution from microscopic observations fit the overall distribution of those 3 clusters (Figure 1E) (Figure 1F). All combined reveal a greater heterogeneity among circulating *B. glabrata* hemocytes compared to what have been defined by microscopy approaches alone (Figure 1E) but most likely potentially supported by a plasticity of hemocyte population (potentially from hyalinocyte activation pathway) rather than lineage-separated circulating cells. This high plasticity of hemocytes could also be accentuated by the large number of snails used to collect the hemocytes, which could add some inter-individual variation in the data analysis. This diversity in the origin of the hemocytes would then show the activation capacity of certain hemocyte types according to the specific physiological status of each individual, this could also explain the small number of cells observed for certain activated clusters such as cluster 3, which may originate from solely few individuals within the snails pool. The understanding of this plasticity rather than diversity of *B. glabrata* hemocytes will now deserve further investigation.

For each of these clusters, we provided a cell identity map by identifying their particular gene markers (Supplementary Table 3) to which we selected at least 5 marker genes defined as highly specific to each transcriptomic cluster (Supplementary Table 1). These marker genes helped us to define specific functions expressed by each of these hemocyte transcriptomic populations. However, the lack of deep annotation and literature for specific hemocyte markers prevent us from defining with precision a link between transcriptomic profile and morphological identity. At first glance, we hypothesised that hemocyte heterogeneity may be supported by plasticity in activation from few populations rather than large diversity of functionalized populations.

In an attempt to connect morphological features and scRNAseq clusters, we used FACS approaches of cell sorting based on basic morphological features such as size and granularity (FSC and SSC) of the hemocytes before analysing them with a global label-free proteomic approach. Nonetheless, as previously shown (47), *B. glabrata* hemocytes formed a continuum of size and granularity that does not allow us to accurately sort any particular hemocyte population. However, by defining specific gates on the FACS it was possible to recover fractions enriched by the three populations commonly accepted in our model (Supplementary Figure 2). From these sorted cell fractions, we performed a protein extraction, which was subjected to label-free LC-MS analyses. But unfortunately, the genes coding for the identified proteins did not allow us to link the hemocyte morphotypes to the different transcriptomic clusters. Indeed, we do not find by any particular differential expression of the marker genes defined for the hyalinocyte and blast-like cell fractions. However, a certain pattern seems to emerge for the genes belonging to the granulocyte-enriched fraction, which seem to be slightly overexpressed in the cells of clusters 1 and 6. These data seem to be corroborated by different genes identified from the literature that were assigned to granulocyte clusters. Indeed, we find genes such as granulin, some toll-like receptors more strongly expressed in these clusters 1 and 6 or cell differentiation factors such as MIF gene (Figure 2J) which is practically no longer expressed in clusters 1 and 6 and these hemocytes follow a particular expression pattern along the pseudotime when we use the cluster 0 as starting point. Clusters 1 to 6 would therefore represent differentiating or differentiated cells. These hemocyte clusters are composed of rather active cells even if in these clusters the RNA count is low (Supplementary Figure 1). The marker gene set detected is however very specific to these clusters and strongly linked to various immune responses.

However, we decided to remove clusters 1 and 6 from the analyses because the genes expressed in these two clusters are very different from the other clusters. It was then impossible to obtain a cell lineage between these two clusters and the rest of the clusters grouped around cluster 0. Either the cells that compose clusters 1 and 6 are from different progenitors or they are from different cell lines that we were not able to capture by this drop-seq approach. To solve this problem one possibility would be to increase the number of hemocytes captured in order to detect the rare hemocytes in our study model that could link all the transcriptomic clusters in the analysis. With this increase in the number of hemocytes captured, it would also be important to increase the depth and sensitivity of sequencing in order to be able to detect more genes in all cells like the use of well-based scRNAseq methods including smartseq2-3 (58, 59). For example in this analysis, we were not able to detect certain genes known to be expressed in hemocytes such as biomphalysin or BgTEP (30, 60). BgTEP were known to be expressed by a subpopulation of blast-like cells (29), thus using BgTEP as a marker gene would be particularly relevant, if we were able to detect it in scRNAseq approach.

Cluster 0 regroups the majority of the cells in our analysis and preferentially expresses a multitude of PRRs and genes involved in energy production. The cells of this cluster may be probably be considered as latent, sentinel cells, harboring a large diversity of receptors waiting to be activated by a contact with a stimulus (pathogen, circulating alarmins, etc). The cells in this cluster also express all the marker genes of the three hemocyte morphotypes defined on the basis of data from proteomics or the literature. It would therefore seem that this cluster is possibly composed of several different hemocyte morphotypes or only hyalinocytes cells due to the large number of genes expressed which would suggest large cells, waiting for a biotic or abiotic signal to engage in a specific differentiation pathway. One possible scenario would be that some of these cells, from cluster 0, would enter into division (which could represent cluster 4) and then produce active cells (represented here by the cells of cluster 3 linked in the pseudo-time to cells of cluster 4). This differentiation from cluster 0 to cluster 4 and cluster 3, may also be supported by the analysis of the MIF gene

(Figure 2J) which could be considered as a differentiation factor towards granulocytes because of the decreasing of its expression along the pseudotime (Figure 2J) in the clusters identified in differentiation. This hypothesis of a progressive hemocyte differentiation may also be supported by recent studies conducted on crayfish (61) showing that in crustaceans a greater plasticity of hemocytes is also find and that the majority of hemocytes in this model are derived from a single common lineage. These hemocytes therefore tend to differentiate into functionally different populations where granulocyte-like hemocytes would be the terminal stage of differentiation. Based on our results, can we propose that a similar process of cell activation occurs in *B. glabrata* snails or more largely in invertebrates? This question will deserve further investigations.

One way to confirm this hypothesis would be to experimentally expose snails, and therefore hemocytes, to various pathogens and see if new populations would be able to emerge from this cluster 0. However, it is interesting to note that we find in cluster 6 and cluster 5, some sets of marker genes involved in responses to pathogens such as bacteria (cluster 5) or virus (cluster 6). These clusters could represent hemocytes that can be involved in the control of microbiota communities. Indeed, it is yet hypothesized that the immune system is necessary for the control and maintenance of the microbial communities associated with the holobionts in *B. glabrata* snails. This is particularly true for bacteria (62, 63) and potentially for virus control (64) in which clusters 5 and 6 may potentially be involved.

All the results in this study still prevent us from assigning each transcriptomic cluster to a particular hemocyte morphotype with certainty. However, this scRNAseq analysis provides the basis for further descriptions of the function of each hemocyte type. The marker genes defined in this analysis allow us to draw an identity map of each of the transcriptomic clusters, and will be a terrific tool that can be used in a near future for the morphological validation of each of these cell groups. For example, a gene coding for a transmembrane protein (transmembrane 97-like) is highly expressed in cluster 1 and could be of great interest to determine if this cluster corresponds to one or more morphological cell types. But how can we physically separate our hemocytes? How to define more precisely the cells of cluster 0? The next challenges concerning the description of these hemocytes will consist in developing and combining more cutting-edge technology approaches of physical separation of hemocytes. We have summarized in Figure 3 an exhaustive list of all the techniques and analysis that will need to be performed on these hemocytes to reveal their possible functions in the organism and the morphology associated with each of these functions.

These approaches can be split in two strategies, using hemocytes and complex tissues as a bulk or using single isolated cells. More in-drop isolated scRNAseq sequencing would bring new information about response to infection or injury in hemocytes. More sequencing would bring more accurate marker genes that could be used for targeted approaches such as *in-situ* hybridisation, siRNA or CRISPR-Cas9. Unfortunately, those approaches could still not be relevant to obtain membrane markers that could be used for FACS purposes. Indeed, surface markers often have low levels of RNA abundance and can be under the method sensitivity threshold. For this purpose, we propose to enrich hemocyte membrane proteins for MS-MS analysis to identify proteins

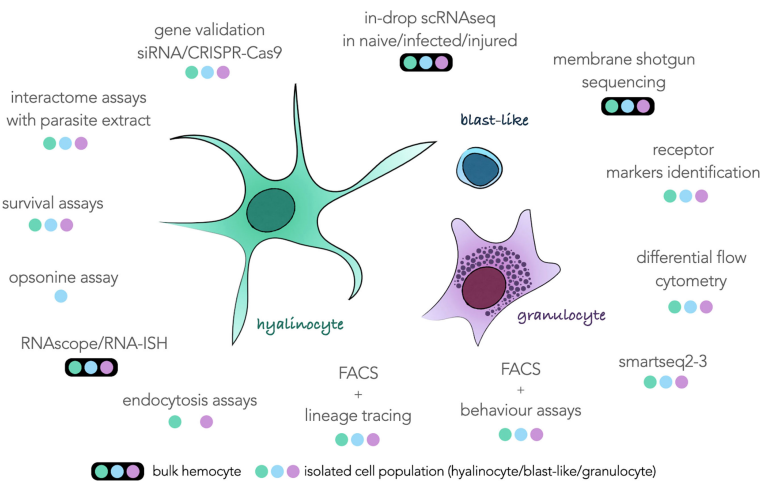

FIGURE 3
Schematic representation of the three hemocyte populations commonly described surrounded by all the techniques feasible on this type of cell and taking into account either bulk hemocytes (colored dots circled in black) or hemocytes taken individually (colored dots) according to their morphological characteristics. The three colored dots refer to the colors of each hemocyte population in the center of the figure.

harbored on hemocyte surfaces. Those proteins can then be used as targets for antibody-based isolation (FACS, MACS) or immunohistochemistry. As soon as several sub-populations of hemocyte can be isolated in flow cytometry gates, a novel era may start for the *Biomphalaria glabrata* community working on immunity. Obviously, it would pave the way for basic flow-cytometry immunology where cell populations are monitored following an immune stress, alarmin injection or parasite infection. The improvement of FACS techniques, coupled with approaches of more sensitive scRNAseq technologies such as smart-seq methods would increase the quality of transcriptome obtained for each population and be useful to characterize each of the morphological populations and their behaviour to certain pathogens or parasites. Moreover, those sorted sub-populations could then be used for *in-vitro* endocytosis or opsonin assays where we may observe the ability of the different hemocytes to interact, induce phagocytosis or actively endocyte differentially treated beads, parasites or pathogens.

Finally, determining the links between the different morphological populations and their functions is an essential step in understanding snail immune mechanisms, particularly in the context of immune response and innate immune memory acquisition towards the parasite *S. mansoni* responsible for intestinal schistosomiasis in humans. Much evidence leads to hemocyte while suggesting a support for innate immune memory. Here, we bring new evidence proving the plasticity over the diversity of hemocytes population in *Biomphalaria glabrata* and we bring new guidelines to transform hemocyte immunology research in invertebrates.

Data availability statement

The datasets presented in this study can be found in online repositories. The data presented in the study are deposited in the Sequence Read Archive (SRA) repository, accession number PRJNA844512.

Author contributions

Investigation and experimental procedures: RP, MP, AP, RG and BG. Bioinformatic analysis: RP, SP, CC. Writing—Original Draft Preparation: RP, SP and BG. Writing—Review & Editing: RP, SP, EV, DD, RG, and BG. Project. Administration: RG and BG. Funding Acquisition: DD and BG. All authors contributed to the article and approved the submitted version.

Funding

This study is set within the framework of the "Laboratoires d'Excellences (LABEX)" TULIP (ANR-10-LABX-41). DD and BG were supported by the ANR AEROSNAIL (ANR-19-CE11-0016-01) from the French National Research Agency (ANR). BG was supported by the BQR from the University of Perpignan. All authors contributed to the article and approved the submitted version.

Acknowledgments

Thanks to cytometry facilities of the MRI platform (Montpellier ressource imagerie) as well as the EDyP service platform for their help in the development and implementation of cell sorting and label-free proteomics. Thanks to the technical staff of the IHPE laboratory, Jean-Francois Allienne for his expertise in molecular biology, Anne Rognon and Damien Pouzol for the maintenance of mollusc strains and their expertise on animal experimentation.

Conflict of interest

The authors declare that the research was conducted in the absence of any commercial or financial relationships that could be construed as a potential conflict of interest.

Publisher's note

Supplementary material

The Supplementary Material for this article can be found online at: https://www.frontiersin.org/articles/10.3389/fimmu.2022.956871/full#supplementary-material

SUPPLEMENTARY FIGURE 1
UMAP **(A)** and vlnplot **(B)** of RNA count by cell among the different transcriptomic clusters.

SUPPLEMENTARY FIGURE 2
Graph representing the distribution of occurrence by flow cytometry as a function of SSC and FSC measurement. The four colored windows noted from P1 to P4, correspond to the selection criteria of the occurrences to carry out the cellular sorting. The results of the microscopic observations of each of these fractions are noted on the right of the graph.

SUPPLEMENTARY FIGURE 3
(A) Expression of the granulin (BGLB011796) and **(B)** toll-like receptor (BGLB008602) gene along the pseudo-time and the representation of its expression by the different cells of the analysis on the UMAP representation.

References

1. Melillo D, Marino R, Italiani P, Boraschi D. Innate immune memory in invertebrate metazoans: a critical appraisal. *Front Immunol* (2018) 9:1915. doi: 10.3389/fimmu.2018.01915

2. Iwanaga S, Lee BL. Recent advances in the innate immunity of invertebrate animals. *BMB Rep* (2005) 38(2):128–50. doi: 10.5483/BMBRep.2005.38.2.128

3. Coustau C, Gourbal B, Duval D, Yoshino TP, Adema CM, Mitta G. Advances in gastropod immunity from the study of the interaction between the snail biomphalaria glabrata and its parasites: A review of research progress over the last decade. *Fish shellfish Immunol* (2015) 46(1):5–16. doi: 10.1016/j.fsi.2015.01.036

4. Tetreau G, Pinaud S, Portet A, Galinier R, Gourbal B, Duval D. Specific pathogen recognition by multiple innate immune sensors in an invertebrate. *Front Immunol* (2017) 8:1249. doi: 10.3389/fimmu.2017.01249

5. Buchmann K. Evolution of innate immunity: clues from invertebrates *via* fish to mammals. *Front Immunol* (2014) 5:459. doi: 10.3389/fimmu.2014.00459

6. Shalek AK, Satija R, Adiconis X, Gertner RS, Gaublomme JT, Raychowdhury R, et al. Single-cell transcriptomics reveals bimodality in expression and splicing in immune cells. *Nat* (2013) 498(7453):236–40. doi: 10.1038/nature12172

7. Proserpio V, Mahata B. Single-cell technologies to study the immune system. *Immunology* (2016) 147(2)::133–40. doi: 10.1111/imm.12553

8. Stubbington MJ, Rozenblatt-Rosen O, Regev A, Teichmann SA. Single-cell transcriptomics to explore the immune system in health and disease. *Science* (. 2017) 358(6359):58–63. doi: 10.1126/science.aan6828

9. Papalexi E, Satija R. Single-cell RNA sequencing to explore immune cell heterogeneity. *Nat Rev Immunol* (2018) 18(1):35–45. doi: 10.1038/nri.2017.76

10. Reid AJ, Talman AM, Bennett HM, Gomes AR, Sanders MJ, Illingworth CJ, et al. Single-cell RNA-seq reveals hidden transcriptional variation in malaria parasites. *elife* (2018) 7:e33105. doi: 10.7554/eLife.33105

11. Howick VM, Russell AJ, Andrews T, Heaton H, Reid AJ, Natarajan K, et al. The malaria cell atlas: Single parasite transcriptomes across the complete plasmodium life cycle. *Science* (2019) 365(6455):eaaw2619. doi: 10.1126/science.aaw2619

12. Diaz Soria CL, Lee J, Chong T, Coghlan A, Tracey A, Young MD, et al. Single-cell atlas of the first intra-mammalian developmental stage of the human parasite schistosoma mansoni. *Nat Commun* (2020) 11(1):1–16. doi: 10.1038/s41467-020-20092-5

13. Severo MS, Landry JJ, Lindquist RL, Goosmann C, Brinkmann V, Collier P, et al. Unbiased classification of mosquito blood cells by single-cell genomics and high-content imaging. *Proc Natl Acad Sci* (2018) 115(32):E7568–77. doi: 10.1073/pnas.1803062115

14. Kwon H, Mohammed M, Franzén O, Ankarklev J, Smith RC. Single-cell analysis of mosquito hemocytes identifies signatures of immune cell subtypes and cell differentiation. *Elife* (2021) 10:e66192. doi: 10.7554/eLife.66192.sa2

15. Cattenoz PB, Sakr R, Pavlidaki A, Delaporte C, Riba A, Molina N, et al. Temporal specificity and heterogeneity of drosophila immune cells. *EMBO J* (2020) 39(12):e104486. doi: 10.15252/embj.2020104486

16. Cho B, Yoon SH, Lee D, Koranteng F, Tattikota SG, Cha N, et al. Single-cell transcriptome maps of myeloid blood cell lineages in drosophila. *Nat Commun* (2020) 11(1):1–18. doi: 10.1038/s41467-020-18135-y

17. Tattikota SG, Cho B, Liu Y, Hu Y, Barrera V, Steinbaugh MJ, et al. A single-cell survey of drosophila blood. *Elife* (2020) 9:e54818. doi: 10.7554/eLife.54818

18. Koiwai K, Koyama T, Tsuda S, Toyoda A, Kikuchi K, Suzuki H, et al. Single-cell RNA-seq analysis reveals *penaeid* shrimp hemocyte subpopulations and cell differentiation process. *Elife* (2021) 10:e66954. doi: 10.7554/eLife.66954.sa2

19. Feng M, Swevers L, Sun J. Hemocyte clusters defined by scRNA-seq in *Bombyx mori*: In silico analysis of predicted marker genes and implications for potential functional roles. *Front Immunol* (2022) 13:852702–852702. doi: 10.3389/fimmu.2022.852702

20. Feng M, Xia J, Fei S, Peng R, Wang X, Zhou Y, et al. Identification of silkworm hemocyte subsets and analysis of their response to baculovirus infection based on single-cell RNA sequencing. *Front Immunol* (2021) 12:1521. doi: 10.3389/fimmu.2021.645359

21. Raddi G, Barletta ABF, Efremova M, Ramirez JL, Cantera R, Teichmann SA, et al. Mosquito cellular immunity at single-cell resolution. *Science* (2020) 369 (6507):1128–32. doi: 10.1126/science.abc0322

22. Verjee MA. Schistosomiasis: still a cause of significant morbidity and mortality. *Res Rep Trop Med* (2019) 10:153–63. doi: 10.2147/RRTM.S204345

23. Castillo MG, Humphries JE, Mourão MM, Marquez J, Gonzalez A, Montelongo CE. *Biomphalaria glabrata* immunity: Post-genome advances. *Dev Comp Immunol* (2020) 104:103557. doi: 10.1016/j.dci.2019.103557

24. Cavalcanti MGS, Mendonça AMB, Duarte GR, Barbosa C, De Castro C, Alves LC, et al. Morphological characterization of hemocytes from biomphalaria glabrata and biomphalaria straminea. *Micron* (2012) 43(2–3):285–91. doi: 10.1016/j.micron.2011.09.002

25. Matricon-Gondran M, Letocart M. Internal defenses of the snail *Biomphalaria glabrata*: I. characterization of hemocytes and fixed phagocytes. *J Invertebrate Pathol* (1999) 74(3):224–34. doi: 10.1006/jipa.1999.4876

26. Prokhorova EE, Serebryakova MK, Tokmakova AS, Ataev GL. Hemocytes of mollusc *Biomphalaria glabrata* (Gastropoda, pulmonata). *Invertebrate Survival J* (2018) 15(1):346–351.

27. Tokmakova AS, Serebryakova MK, Prokhorova EE, Ataev GL. Study of the proliferative activity of hemolymph cells in pulmonate molluscs. *Invertebrate Survival J* (2020) 17:63–74.

28. Li H, Gharamah AA, Hambrook JR, Wu X, Hanington PC. Single-cell RNA-seq profiling of individual biomphalaria glabrata immune cells with a focus on immunologically relevant transcripts. *Immunogenetics* (2021) 74:77–89. doi: 10.1007/s00251-021-01236-3

29. Portet A, Galinier R, Pinaud S, Portela J, Nowacki F, Gourbal B, et al. BgTEP: an antiprotease involved in innate immune sensing in biomphalaria glabrata. *Front Immunol* (2018) 9:1206. doi: 10.3389/fimmu.2018.01206

30. Duval D, Pichon R, Lassalle D, Laffitte M, Gourbal B, Galinier R. A new assessment of thioester-containing proteins diversity of the freshwater snail *Biomphalaria glabrata*. *Genes* (2020) 11(1):69. doi: 10.3390/genes11010069

31. Zheng GX, Terry JM, Belgrader P, Ryvkin P, Bent ZW, Wilson R, et al. Massively parallel digital transcriptional profiling of single cells. *Nat Commun* (2017) 8(1):1–12. doi: 10.1038/ncomms14049

32. Mitta G, Galinier R, Tisseyre P, Allienne JF, Girerd-Chambaz Y, Guillou F, et al. Gene discovery and expression analysis of immune-relevant genes from biomphalaria glabrata hemocytes. *Dev Comp Immunol* (2005) 29(5):393–407. doi: 10.1016/j.dci.2004.10.002

33. Hansen EL. A cell line from embryos of Biomphalaria glabrata (Pulmonata): Establishment and characteristics. In: *Invertebrate Tissue culture: Research applications* Ed K Maramorosch (1976) 75–97. doi: 10.1016/B978-0-12-470270-7.50011-2

34. Wheeler DL, Barrett T, Benson DA, Bryant SH, Canese K, Chetvernin V, et al. Database resources of the national center for biotechnology information. *Nucleic Acids Res* (2007) 36(suppl_1):D13–21. doi: 10.1093/nar/gkm1000

35. Zhang SM, Bu L, Laidemitt MR, Lu L, Mutuku MW, Mkoji GM, et al. Complete mitochondrial and rDNA complex sequences of important vector species of biomphalaria, obligatory hosts of the human-infecting blood fluke, schistosoma mansoni. *Sci Rep* (2018) 8(1):1–10. doi: 10.1038/s41598-018-25463-z

36. Altschul SF, Gish W, Miller W, Myers EW, Lipman DJ. Basic local alignment search tool. *J Mol Biol* (1990) 215(3):403–10. doi: 10.1016/S0022-2836(05)80360-2

37. Giraldo-Calderón GI, Emrich SJ, MacCallum RM, Maslen G, Dialynas E, Topalis P, et al. VectorBase: an updated bioinformatics resource for invertebrate vectors and other organisms related with human diseases. *Nucleic Acids Res* (2015) 43(D1):D707–13. doi: 10.1093/nar/gku1117

38. Hao Y, Hao S, Andersen-Nissen E, Mauck WMIII, Zheng S, Butler A, et al. Integrated analysis of multimodal single-cell data. *Cell* (2021) 184(13):3573–3587. doi: 10.1016/j.cell.2021.04.048

39. Götz S, García-Gómez JM, Terol J, Williams TD, Nagaraj SH, Nueda MJ, et al. High-throughput functional annotation and data mining with the Blast2GO suite. *Nucleic Acids Res* (2008) 36(10):3420–35.Z. doi: 10.1093/nar/gkn176

40. Cao J, Spielmann M, Qiu X, Huang X, Ibrahim DM, Hill AJ, et al. The single-cell transcriptional landscape of mammalian organogenesis. *Nature* (2019) 566(7745):496–502. doi: 10.1038/s41586-019-0969-x

41. Street K, Risso D, Fletcher RB, Das D, Ngai J, Yosef N, et al. Slingshot: cell lineage and pseudotime inference for single-cell transcriptomics. *BMC Genomics* (2018) 19(1):1–16. doi: 10.1186/s12864-018-4772-0

42. Lyu R, Qiao P, Kiselev V, Andrews T, Westoby J, Büttner M, et al. *Analysis of single cell RNA-seq data"* (2019). Available at: https://scrnaseq-course.cog.sanger.ac.uk/website/index.htmlhttps://biocellgen-public.svi.edu.au/mig_2019_scrnaseq-workshop/index.html.

43. Milbradt J, Kraut A, Hutterer C, Sonntag E, Schmeiser C, Ferro M, et al. Proteomic analysis of the multimeric nuclear egress complex of human cytomegalovirus. *Mol Cell Proteomics* (2014) 13(8):2132–46. doi: 10.1074/mcp.M113.035782

44. Pinaud S, Portet A, Allienne JF, Belmudes L, Saint-Beat C, Arancibia N, et al. Molecular characterisation of immunological memory following homologous or

heterologous challenges in the schistosomiasis vector snail, biomphalaria glabrata. *Dev Comp Immunol* (2019) 92:238–52. doi: 10.1016/j.dci.2018.12.001

45. Lu L, Loker ES, Adema CM, Zhang SM, Bu L. Genomic and transcriptional analysis of genes containing fibrinogen and IgSF domains in the schistosome vector *Biomphalaria glabrata*, with emphasis on the differential responses of snails susceptible or resistant to schistosoma mansoni. *PloS Negl Trop Dis* (2020) 14 (10):e0008780. doi: 10.1371/journal.pntd.0008780

46. Lu L, Bu L, Zhang SM, Buddenborg SK, Loker ES. An overview of transcriptional responses of schistosome-susceptible (M line) or-resistant (BS-90) *Biomphalaria glabrata* exposed or not to *Schistosoma mansoni* infection. *Front Immunol* (2021) 12. doi: 10.3389/fimmu.2021.805882

47. Portet A, Pinaud S, Chaparro C, Galinier R, Dheilly NM, Portela J, et al. Sympatric versus allopatric evolutionary contexts shape differential immune response in *Biomphalaria*/*Schistosoma* interaction. *PloS pathogens* (2019) 15(3): e1007647. doi: 10.1371/journal.ppat.1007647

48. Vergote D, Bouchut A, Sautiere PE, Roger E, Galinier R, Rognon A, et al. Characterisation of proteins differentially present in the plasma of biomphalaria glabrata susceptible or resistant to *Echinostoma caproni*. *Int J Parasitol* (2005) 35 (2):215–24. doi: 10.1016/j.ijpara.2004.11.006

49. Myers J, Ittiprasert W, Raghavan N, Miller A, Knight M. Differences in cysteine protease activity in *Schistosoma mansoni*-resistant and-susceptible biomphalaria glabrata and characterization of the hepatopancreas cathepsin b full-length cDNA. *J Parasitol* (2008) 94(3):659–68. doi: 10.1645/GE-1410R.1

50. Foo CX, Bartlett S, Ronacher K. Oxysterols in the immune response to bacterial and viral infections. *Cells* (2022) 11(2):201. doi: 10.3390/cells11020201

51. Whitten MM, Tew IF, Lee BL, Ratcliffe NA. A novel role for an insect apolipoprotein (apolipophorin III) in β-1, 3-glucan pattern recognition and cellular encapsulation reactions. *J Immunol* (2004) 172(4):2177–85. doi: 10.4049/jimmunol.172.4.2177

52. Pila EA, Gordy MA, Phillips VK, Kabore AL, Rudko SP, Hanington PC. Endogenous growth factor stimulation of hemocyte proliferation induces resistance to schistosoma mansoni challenge in the snail host. *Proc Natl Acad Sci* (2016) 113 (19):5305–10. doi: 10.1073/pnas.1521239113

53. Hambrook JR, Gharamah AA, Pila EA, Hussein S, Hanington PC. *Biomphalaria glabrata* granulin increases resistance to *Schistosoma mansoni* infection in several *Biomphalaria* species and induces the production of reactive oxygen species by haemocytes. *Genes* (2019) 11(1):38. doi: 10.3390/genes11010038

54. Pila EA, Tarrabain M, Kabore AL, Hanington PC. A novel toll-like receptor (TLR) influences compatibility between the gastropod *Biomphalaria glabrata*, and the digenean trematode schistosoma mansoni. *PloS Pathog* (2016) 12(3):e1005513. doi: 10.1371/journal.ppat.1005513

55. Baeza Garcia A, Pierce RJ, Gourbal B, Werkmeister E, Colinet D, Reichhart JM, et al. Involvement of the cytokine MIF in the snail host immune response to the parasite schistosoma mansoni. *PloS Pathog* (2010) 6(9):e1001115. doi: 10.1371/journal.ppat.1001115

56. Sullivan JT, Pikios SS, Alonzo AQ. Mitotic responses to extracts of miracidia and cercariae of schistosoma mansoni in the amebocyte-producing organ of the snail intermediate host *Biomphalaria glabrata*. *J Parasitol* (2004) 90(1):92–6. doi: 10.1645/GE-3266

57. Barbosa L, Silva LM, Coelho PMZ, Santos SR, Fortes-Dias CL. Primary culture of the region of the amebocyte-producing organ of the snail biomphalaria glabrata, the intermediate host of *Schistosoma mansoni*. *Memórias do Instituto Oswaldo Cruz* (2006) 101(6):639–43. doi: 10.1590/S0074-02762006000600010

58. Hagemann-Jensen M, Ziegenhain C, Chen P, Ramsköld D, Hendriks GJ, Larsson AJ, et al. Single-cell RNA counting at allele and isoform resolution using smart-seq3. *Nat Biotechnol* (2020) 38(6):708–14. doi: 10.1038/s41587-020-0497-0

59. Picelli S, Björklund ÅK, Faridani OR, Sagasser S, Winberg G, Sandberg R. Smart-seq2 for sensitive full-length transcriptome profiling in single cells. *Nat Methods* (2013) 10(11):1096–8. doi: 10.1038/nmeth.2639

60. Galinier R, Portela J, Moné Y, Allienne JF, Henri H, Delbecq S, et al. Biomphalysin, a new β pore-forming toxin involved in *Biomphalaria glabrata* immune defense against schistosoma mansoni. *PloS Pathog* (2013) 9(3):e1003216. doi: 10.1371/journal.ppat.1003216

61. Li F, Zheng Z, Li H, Fu R, Xu L, Yang F. Crayfish hemocytes develop along the granular cell lineage. *Sci Rep* (2021) 11(1):1–16. doi: 10.1038/s41598-021-92473-9

62. Huot C, Clerissi C, Gourbal B, Galinier R, Duval D, Toulza E. Schistosomiasis vector snails and their microbiota display a phylosymbiosis pattern. *Front Microbiol* (2020) 10:3092. doi: 10.3389/fmicb.2019.03092

63. Portet A, Toulza E, Lokmer A, Huot C, Duval D, Galinier R, et al. Experimental infection of the Biomphalaria glabrata vector snail by Schistosoma mansoni parasites drives snail microbiota dysbiosis. *Microorganisms* (2021) 9 (5):1084.

64. Galinier R, Tetreau G, Portet A, Pinaud S, Duval D, Gourbal B. First characterization of viruses from freshwater snails of the genus biomphalaria, the intermediate host of the parasite *Schistosoma mansoni*. *Acta Tropica* (2017) 167:196–203. doi: 10.1016/j.actatropica.2016.12.021

frontiers | Frontiers in Immunology

TYPE Original Research
PUBLISHED 03 October 2022
DOI 10.3389/fimmu.2022.929552

OPEN ACCESS

EDITED BY
Thiago Almeida Pereira,
Stanford University, United States

REVIEWED BY
Fausto Edmundo Lima Pereira,
Vila Velha University, Brazil
Henrique Borges da Silva,
Mayo Clinic Arizona, United States

*CORRESPONDENCE
Lúcia H. Faccioli
faccioli@fcfrp.usp.br

†PRESENT ADDRESS
Camila O. S. Souza,
Laboratory of Parasitic Diseases,
National Institute of Allergy and
Infectious Diseases, National Institute
of Health, Bethesda, Maryland,
United States.

SPECIALTY SECTION
This article was submitted to
Parasite Immunology,
a section of the journal
Frontiers in Immunology

RECEIVED 27 April 2022
ACCEPTED 12 September 2022
PUBLISHED 03 October 2022

CITATION
Souza COS, Elias-Oliveira J,
Pastore MR, Fontanari C, Rodrigues VF,
Rodriguez V, Gardinassi LG and
Faccioli LH (2022) CD18 controls the
development and activation of
monocyte-to-macrophage axis during
chronic schistosomiasis.
Front. Immunol. 13:929552.
doi: 10.3389/fimmu.2022.929552

CD18 controls the development and activation of monocyte-to-macrophage axis during chronic schistosomiasis

Camila O. S. Souza[1,2†], Jefferson Elias-Oliveira[1,2], Marcella R. Pastore[1,3], Caroline Fontanari[1], Vanessa F. Rodrigues[4], Vanderlei Rodriguez[4], Luiz G. Gardinassi[5] and Lúcia H. Faccioli[1*]

[1]Departamento de Análises Clínicas, Toxicológicas e Bromatológicas, Faculdade de Ciências Farmacêuticas de Ribeirão Preto, Universidade de São Paulo, Ribeirão Preto, Brazil, [2]Programa de Pós-Graduação em Imunologia Básica e Aplicada, Faculdade de Medicina de Ribeirão Preto, Universidade de São Paulo, Ribeirão Preto, Brazil, [3]Programa de Pós-Graduação em Biociências e Biotecnologia Aplicadas à Farmácia, Faculdade de Ciências Farmacêuticas de Ribeirão Preto, Ribeirão Preto, Brazil, [4]Departamento de Bioquímica e Imunologia, Faculdade de Medicina de Ribeirão Preto, Universidade de São Paulo, Ribeirão Preto, Brazil, [5]Departamento de Biociências e Tecnologia, Instituto de Patologia Tropical e Saúde Pública, Universidade Federal de Goiás, Goiânia, Brazil

Schistosomiasis is a neglected tropical disease caused by worms of the genus *Schistosoma* spp. The progression of disease results in intense tissue fibrosis and high mortality rate. After egg deposition by adult worms, the inflammatory response is characterized by the robust activation of type 2 immunity. Monocytes and macrophages play critical roles during schistosomiasis. Inflammatory Ly6C^{high} monocytes are recruited from the blood to the inflammatory foci and differentiate into alternatively activated macrophages (AAMs), which promote tissue repair. The common chain of β_2-integrins (CD18) regulates monocytopoiesis and mediates resistance to experimental schistosomiasis. There is still limited knowledge about mechanisms controlled by CD18 that impact monocyte development and effector cells such as macrophages during schistosomiasis. Here, we show that *CD18^{low}* mice chronically infected with *S. mansoni* display monocyte progenitors with reduced proliferative capacity, resulting in the accumulation of the progenitor cell denominated proliferating-monocyte (pMo). Consequently, inflammatory Ly6C^{high} and patrolling Ly6C^{low} monocytes are reduced in the bone marrow and blood. Mechanistically, low CD18 expression decreases *Irf8* gene expression in pMo progenitor cells, whose encoded transcription factor regulates CSFR1 (CD115) expression on the cell surface. Furthermore, low CD18 expression affects the accumulation of inflammatory Ly6C^{high} CD11b^{+} monocytes in the liver while the adoptive transference of these cells to infected-*CD18^{low}* mice reduced the inflammatory infiltrate and fibrosis in the liver. Importantly, expression of *Il4*, *Chil3l3* and *Arg1* was downregulated, CD206^{+}PD-L2^{+} AAMs were reduced and there were lower levels of IL-10 in the liver of *CD18^{low}* mice chronically infected with *S. mansoni*. Overall, these

findings suggest that CD18 controls the IRF8-CD115 axis on pMo progenitor cells, affecting their proliferation and maturation of monocytes. At the same time, CD18 is crucial for the appropriate polarization and function of AAMs and tissue repair during chronic schistosomiasis.

KEYWORDS

β2 integrin, monocytes, proliferation, alternatively activated macrophages, schistosomiasis

Introduction

The common chain of β_2 integrins (CD18) is constitutively expressed by diverse leukocytes and is involved in host-pathogen interactions, adhesion and trans-endothelial migration of leukocytes, phagocytosis and killing of pathogens, and monocytopoiesis during schistosomiasis (1–3). Mice that express low levels of CD18 (*CD18^{low}*) exhibit reduced accumulation of inflammatory Ly6C^{high} and patrolling Ly6C^{low} monocytes in the bone marrow (BM) and blood during infection with *S. mansoni*, which correlates with increased egg counts on feces and higher mortality (3). The accumulation of *S. mansoni*-eggs into tissue induces high levels of IL-4, IL-13, IL-5, and IL-10 that trigger Th2 granuloma formation, a hallmark of chronic schistosomiasis (4). Granulomas are structures composed by non-immune and immune cells which are recruited to limit the tissue damage caused by eggs (5). In general, the cellular infiltrate in liver from *S. mansoni*-infected mice is characterized by increased numbers of monocytes, neutrophils, eosinophils and macrophages around the parasites eggs (6). Low CD18 expression does not affect the accumulation of neutrophils or monocyte-derived macrophages (MDM) and monocyte-derived dendritic cells (MDC) in the liver, however, it reduces specific monocyte subsets during infection with *S. mansoni* (3). Therefore, we hypothesized that CD18 is required by progenitor cells as well as by mature monocytes to resist immunopathology caused by *S. mansoni* infection.

Leukocyte adhesion deficiency type 1 (LAD1) is caused by mutations on *ITGB2* (CD18) gene in humans, which are affected by recurrent bacterial and fungal infections (7). Patients with chronic granulomatous disease (CGD) express reduced levels of CD18, which are associated with impaired innate immune cell recruitment and uncontrolled inflammatory responses (8). Previous studies show that CD18 knockout (*CD18$^{-/-}$*) or CD18 hypomorphic (CD18^{HYP}) mice exhibit increased numbers of Sca-1$^+$ c-Kit$^+$ cells (LSK pools) and increased neutrophils in the bone marrow (9, 10), suggesting that CD18 regulates the proliferation of hematopoietic stem and progenitor cells (HSPCs) that form hematopoietic niches (11, 12). During *S. mansoni* infection, lower CD18 expression does not affect neutrophil hematopoiesis in the bone marrow (3). CD18 controls the proliferation of granulocytes/macrophages progenitors (GMP) (9), suggesting a role for proliferative precursors during monocytopoiesis (13, 14). In adult life, the development of monocytes is initiated from the common bone marrow-derived precursor called the 'monocyte-macrophages DC progenitor' (MDP), followed by sequential steps of 'common monocyte progenitor' (cMoP) that give rise to the proliferating-monocyte (pMo) progenitor, which matures into monocytes (14).

After *S. mansoni* infection, most macrophages at inflammatory sites are derived from blood monocytes (6, 15–17). Both tissue resident macrophages and MDMs become alternatively activated macrophages (AAMs) *via* IL-4Rα signaling by IL-4 and IL-13 (15, 18). In general, the alternative phenotype is characterized by expression of high levels of arginase-1 (*Arg1)*, chitinase-like 3 (*Chi3l3)*, resistin-like alpha (*Relma)* and mannose receptor C-type 1 *(Mrc1)* (19). However, only monocyte-derived AAMs upregulates the expression of retinaldehyde dehydrogenase 2 (*Raldh2)* and programmed cell death ligand 2 (*Pdcd1lg2*) (20–22). Furthermore, AAMs produce IL-10 and TGF-β (23), cytokines that promote healing and tissue repair during schistosomiasis (24, 25). On the other hand, the integrin formed by pairing of CD11b – CD18 (αM/β2), MAC-1, forms a complex with IL-13Rα1 on the surface of macrophages (26) and dampens the alternative activation during the chronic inflammation (27).

To investigate the molecular role of CD18 on monocyte progenitor cells and alternative activation of macrophages during schistosomiasis, we used a mice model that expresses low levels of CD18 (*CD18^{low})*, thus resembling humans with moderate ITGB2 deficiency (28). We found that CD18 affects the expression of the proliferation marker, Ki-67 and regulates the proliferation of monocyte progenitors during infection by *S. mansoni*. Gene expression of *Irf8* was reduced in pMo cells of infected-*CD18^{low}* mice, and consequently affected CD115 expression in the cell surface, resulting in failure of monocyte maturation in the BM and blood. The frequency of inflammatory Ly6C^{high} CD11b$^+$ monocytes was reduced in the liver of infected *CD18^{low}* mice and the adoptive transference of

these cells ameliorated the inflammatory infiltrate and tissue fibrosis, independently of the parasite burden. Of importance, CD18 regulates the expression of genes involved in alternative activation, such as *Il4*, *Chil3l3* and *Arg1* and impact $CD206^{+}$ $PD\text{-}L2^{+}$ AAMs, which was associated with lower levels of IL-10 in the liver. These data fill important gaps about the molecular mechanisms driven by CD18 during monocytopoiesis and alternative activation of macrophages in response to infection by *S. mansoni*.

Materials and methods

Animals

Male 8-week-old (22-26g) C57BL/6 (wild-type, WT) and homozygous $CD18^{low}$ mice on the C57BL/6 background were obtained from the animal facilities of the Faculdade de Ciências Farmacêuticas de Ribeirão Preto, Universidade de São Paulo (FCFRP – USP). $CD18^{low}$ ($B6.129S\text{-}Itgb2^{tm1bay}$) mice were purchased at The Jackson Laboratory. The $CX_3CR1^{gfp/gfp}$ mice on the C57BL/6 background was donate by Dr. João Santana Silva from Faculdade de Medicina de Ribeirão Preto, Universidade de São Paulo (FMRP – USP). To obtain $CX_3CR1^{gfp/+}$ mice, $CX_3CR1^{gfp/gfp}$ animals were backcrossed for ten generations with C57BL/6 mice. All experiments using animals were approved by the Comissão de Ética no Uso de Animais da Faculdade de Ciências Farmacêuticas de Ribeirão Preto (Protocol Number 14.1.607.53.9 and 19.1.46.60.4) and carried out in accordance to the ethical principles for animal research adopted by the Sociedade Brasileira de Ciência em Animais de Laboratório.

Parasite maintenance and experimental infection

Schistosoma mansoni LE strain was maintained by routine passage through *Biomphalaria glabrata* snails and BALB/c mice (20-25g) from the animal facilities of the Faculdade de Medicina de Ribeirão Preto - Universidade de São Paulo (FMRP – USP). Recovery of cercariae was described previously (3). For infection, mice were subcutaneously inoculated with 80 cercariae/animal with a sterile syringe and 22 G x 1" needle (BD Biosciences, Franklin Lakes, New Jersey, USA). At 7 weeks post infection (wpi) the animals were euthanized for posterior analyses.

Quantification of worm's burden and fecal eggs

Parasite burdens were recovered by portal perfusion with 20 mL/animal of perfusion buffer [58 mM $Na_3C_6H_5O_7$ and 145 mM NaCl (Sigma Aldrich, St. Louis, Missouri, USA)] at 37°C. The worms were washed and counted using a dissecting microscope. The fecal eggs were recovered in stool sample/animal by Kato-Katz technique, as previously described (29).

Histopathological analysis

Animals from each experimental group were euthanized at 7 wpi. The liver was excised, fixed with 10% formalin for 24h, and embedded in paraffin. The tissue sections (5µm) were stained with H&E and Picrosirius red coloration for evaluate inflammatory infiltrated and fibrosis, respectively. Images were captured with a digital video camera (Leica® Microsystems, Heebrugg, Switzerland) adapted to DMR microscope (Leica®, Microsystems GmbH, Wetzlar, Germany). The images were processed using the Leica QWin software (Leica Microsystems Image Solution®, Cambridge, UK). The inflammatory infiltrated and fibrosis were quantified with Image J (V1.51) software.

Anti-CD18 treatment *in vivo*

Naïve C57BL/6 mice were treated with anti-CD18 (clone: GAME-46) *via* intravenous route (2mg/kg of body weight) over 3 days. Controls were treated with saline buffer. Schematic representation of the treatment with anti-CD18 is shown in Figure 3E.

Flow cytometry of bone marrow, blood, and liver cells

The BM was flushed out from two femurs and tibias using RPMI with help of 26 G x ½" needle. Peripheral blood was drawn from the retro-orbital plexus. The red blood cells in BM flush and blood were lysed, and remaining cells were washed in PBS containing 5% FBS, centrifuged and resuspended in RPMI 1640 containing 5% FBS. Cell suspensions were used in further analysis. Liver cells suspension were obtained after tissue digestion at 37°C for 45 min in 4 mL/liver of digestion buffer [HBSS, 0.05% collagenase II (Sigma Aldrich, St. Louis, Missouri, USA) and 1 mg/mL DNase (Sigma Aldrich, St. Louis, Missouri, USA)]. The enzymatic digestion was stopped by adding 100 µL of FBS and the tissue fragments passed through a cell strainer 100 µM pore size (Corning Inc. New York, USA). The resulting suspension was centrifuged at 1,300 rpm, 10 min, 4°C. The cellular pellet was resuspended in 40% of isotonic Percoll and centrifuged at room temperature for 30 min at 1.500 g. Next, red blood cells were lysed, and remaining cells were washed in PBS, centrifuged, and resuspended in RPMI 1640 containing 5% FBS. Suspensions of 2×10^6 cells were used in further analysis. For viability, cells were counted in trypan blue or used the Fixable

Viability Stain (FVS) (1:100) (BD Horizon™). The following antibodies were used: CD3 (1:100; clone: 17A2); CD19 (1:100; clone: 1D3); Ly6G (1:100; clone: 1A8); NK1.1 (1:100; clone: PK136); Ter-119/Erythroid (1:100; clone: TER-119) CD45R/B220 (1:100; clone: RA3-6B2); CD117/c-Kit (1:100; clone: 2B8); CD135 (1:100; clone: A2F10); CD115 (1:200; clone: CSF-1R); Ly6C (1:100; clone: AL-21 or HK1.4); CD11a (1:100; clone: 2D7); CD11b (1:100; clone: M1/70); CD11c (1:100; clone: HL3); Ki-67 (1:200; clone B56) CD45 (1:100; clone: 30-F11), CX_3CR1 (1:200; clone: SA011F11), F4/80 (1:100; clone: BM8), CD206 (1:100; clone: C068C2) and CD273 / PD-L2 (1:100; clone: TY25). All antibodies used in flow cytometry were purchased from Biolegend (San Diego, CA, EUA) or BD Biosciences (Franklin Lakes, New Jersey, USA). Data acquisition was performed using a BD LSRFortessa™ flow cytometer and FACSDiva software (BD Biosciences, Franklin Lakes, New Jersey, USA). 100,000 events were acquired for samples from bone marrow, blood and liver. Data were plotted and analyzed using FlowJo software v. 10.8.0 (Tree Star, Inc, Ashland, OR, USA)

Cell sorting from BM

Bone marrows (two femurs and tibias) from three chronically infected WT or *CD18^{low}* mice were flushed out using RPMI with 26 G x ½" needle. Pooled cell suspensions were stained with Fixable Viability Stain (FVS) (1:1000) (BD Horizon™); following the antibodies: CD3 (1:100; clone: 17A2), CD19 (1:100; clone: 1D3), NK1.1 (1:100; clone: PK136) Ly6G (1:100; clone A18), CD117 / c-Kit (1:200; clone: 2B8), CD115 (1:200; clone: CSF-1R), Ly6C (1:200; clone: AL-21) and CD11b (1:200; clone M1/70) washed and after isolated using a BD FACSMelody™ Cell Sorter. Two populations were separated, proliferating-monocyte progenitor (pMo) (FVS^- Lin^- $CD117^+$ $CD115^+$ $Ly6C^+$ $CD11b^-$) and inflammatory $Ly6C^{high}$ monocytes (FVS^- Lin^- $CD117^+$ $CD115^+$ $Ly6C^{high}$ $CD11b^+$). Suspensions of 1 x 10^5 proliferating-monocyte progenitor (pMo) and 1 x 10^6 inflammatory $Ly6C^{high}$ monocytes were used in further analysis.

Cell sorting of inflammatory $Ly6C^{high}CD11b^+$ and patrolling $Ly6C^{low}CD11b^+$monocytes from the BM of $CX_3CR1^{gpf/+}$ animals and adoptive transference

Bone marrows (two femurs and tibias) of three non-infected *$CX_3CR1^{gfp/+}$* mice were flushed out using RPMI and 26 G x ½" needle. Pooled cell suspensions were stained with antibodies: Ly6G (1:200; clone 1A8), Ly6C (1:200; clone AL-21) and CD11b (1:200; clone M1/70) washed and isolated using a BD FACSMelody™ Cell Sorter. Suspensions of 2 x 10^5 inflammatory $Ly6C^{high}$ ($Ly6G^-$ $Ly6C^{high}$ $CD11b^+$ CX_3CR1^{low}) and 1 x 10^5 patrolling $Ly6C^{low}$ ($Ly6G^-$ $Ly6C^{low}$ $CD11b^+$ CX_3CR1^{low}) monocytes were transferred by intravenous route to infected-*CD18^{low}* mice in different days shown in the experimental design shown in Figure 4A.

Quantitative real-time polymerase chain reaction

For BM lysates and isolated pMo and inflammatory $Ly6C^{high}$ monocytes, the total RNA was extracted using the RNA*later*® (Sigma-Aldrich) and PureLink™ RNA Mini Kit (Invitrogen™) according to the manufacturer instructions. For liver homogenates, the total RNA was extracted using the TRIzol® and the SV Total RNA Isolation System Kit (Promega®) according to the manufacturer instruction. Complementary DNA was synthesized with the High Capacity cDNA Reverse Transcription Kit (Applied Biosystems). SYBR Green Mix–based real-time quantitative PCR assays were performed using the StepOnePlus Real-Time PCR System (Applied Biosystems). The mean cycle threshold (Ct) values of triplicate measurements were used to calculate the expression of the target genes, which were normalized to the housekeeping gene *Gapdh* to liver and BM cells, and analyzed with the $2^{-\Delta\Delta Ct}$ method. All primers (Supplementary Table 1) were designed using the Primer Express software package v2.0 (Applied Biosystems), based on the nucleotide reference sequences available at GenBank database.

Statistical analyses

The data were normally distributed. Significant differences between experimental groups were evaluated using one-way ANOVA and Tukey's multiple comparison test or Student's t-test. Error bars represent mean ± SD. Analyses were performed using GraphPad Prism software v8.2.1 (GraphPad Software Inc., San Diego, CA, USA). Statistical significance was set at $p < 0.05$.

Results

CD18 affects Ki-67 expression and maturation of monocyte progenitors during schistosomiasis

To assess the biological function of CD18 in regulating the bone marrow-derived precursors of monocytes during chronic schistosomiasis, WT and *CD18^{low}* mice were infected subcutaneously with 80 cercariae and after 7 wpi, the monocytopoiesis was characterized in the BM with flow cytometry (Figure S1A). Compared to controls, *CD18^{low}* mice exhibited increased percentage of MPD (Figure 1A), but absolute

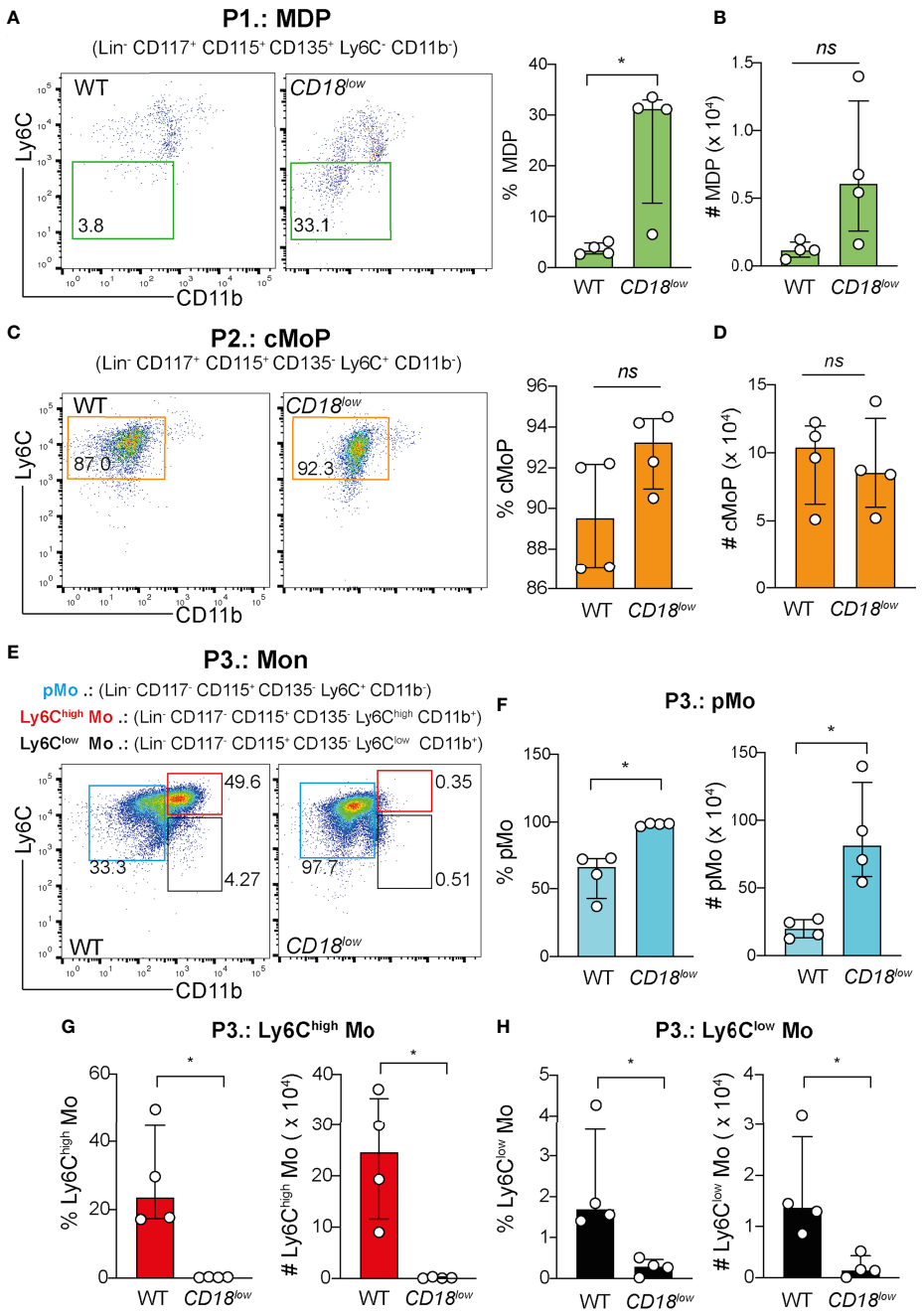

FIGURE 1
CD18 is required for monocyte progenitors in BM during chronic schistosomiasis. BM of *S. mansoni*-infected C57BL/6 and *CD18*^{low} mice were analyzed by flow cytometry. **(A)** Representative dot plots and graph displaying the percentage of MDP progenitor cells (Lin$^-$ CD117$^-$ CD115$^+$ CD135$^+$ Ly6C$^-$ CD11b$^-$). **(B)** Scatter plot with bar show the absolute numbers of MPD progenitor cells. **(C)** Representative dot plots and graph displaying the percentage of cMoP progenitor cells (Lin$^-$ CD117$^+$ CD115$^+$ CD135$^+$ Ly6C$^+$ CD11b$^-$). **(D)** Scatter plot with bar show the absolute number of cMoP progenitor cells. **(E)** Representative dot plots displaying the pMo progenitor cells (Lin$^-$ CD117$^-$ CD115$^+$ CD135$^-$ Ly6C$^+$ CD11b$^-$), inflammatory Ly6C^{high} monocytes (Lin$^-$ CD117$^-$ CD115$^+$ CD135$^-$ Ly6C^{high} CD11b$^+$) and patrolling Ly6C^{low} monocytes (Lin$^-$ CD117$^-$ CD115$^+$ CD135$^-$ Ly6C^{low} CD11b$^+$). **(F)** Scatter plot with bar show the percentage and absolute numbers of pMo progenitor cells. **(G)** Scatter plot with bar show the percentage and absolute numbers of inflammatory Ly6C^{high} monocytes. **(H)** Scatter plot with bar show the percentage and absolute numbers of patrolling Ly6C^{low} monocytes. Median with interquartile range are shown for one representative experiment (n= 4 WT and *CD18*^{low} infected mice at 7 weeks) out of three independent experiments. Data were analyzed with Mann-Whitney test (*p < 0.05, ns p > 0.05, compared to WT in each time-point). The symbol (#) indicates the absolute numbers of each progenitor population.

numbers of cells were similar (Figure 1B). There were no significant differences in cMoP progenitors between experimental groups (Figures 1C, D). The final steps of monocyte maturation can be characterized by different levels of Ly6C and CD11b expression: Ly6C^{+} CD11b^{-} (pMo), Ly6C^{high} CD11b^{+} (inflammatory monocytes) and Ly6C^{low}CD11b^{+} (patrolling monocytes) (Figure 1E). Strikingly, we observed that both percentage and absolute numbers of pMo increased in the BM of infected *CD18^{low}* mice (Figures 1E, F). In accordance, the percentage and absolute number of inflammatory Ly6C^{high} (Figures 1E, G) and patrolling Ly6C^{low} (Figures 1E, H) monocytes were significantly diminished in the BM of *CD18^{low}* animals. We also analyzed the frequency of blood monocytes using a flow cytometric gating hierarchy including the CX_3CR1 marker (Figure S1B). Corroborating previous findings (3), the percentage and absolute numbers of inflammatory Ly6C^{high} and patrolling Ly6C^{low} monocytes were reduced in *CD18^{low}* mice (Figure S1B).

Furthermore, CD18 deficiency has been associated with the proliferation of myeloid cells (9, 12), suggesting that CD18 affects the proliferation of monocyte progenitors and development during chronic schistosomiasis. To test this hypothesis, we quantified the expression of the proliferation marker, Ki-67, in progenitors and mature monocytes. Compared with WT mice, Ki-67 expression was significantly reduced in MPD (Figures 2A, B), cMoP (Figures 2A, C) and pMo (Figures 2A, D) progenitors in the BM of *CD18^{low}* mice at 7 wpi. There were no significant differences in Ki-67 expression in inflammatory Ly6C^{high} (Figures 2A, E) and patrolling Ly6C^{low} (Figures 2A, F) monocytes. Collectively, these data suggest that low CD18 expression impacts the proliferation of monocyte precursors, a process that is required for the differentiation into mature monocytes (14). Therefore, a potential development arrest may drive the accumulation of these cells, reducing mature monocytes in the BM and blood during chronic *S. mansoni* infection.

CD18 regulates IRF8-dependent CD115 expression in pMo progenitors during chronic schistosomiasis

The transcription factors IRF8 (30, 31) and KLF4 (32, 33) control the development of Ly6C^{high} monocytes, while NR4A1 (34) is necessary for the maturation of Ly6C^{low} monocytes. Because we observed the accumulation of pMo progenitors and reduced Ki-67 expression in the cells from *CD18^{low}* mice, we next investigated if CD18 affects the gene expression of transcription factors controlling the maturation of monocytes. Using FACS-sorting, we isolated the pMo (Ly6C^{+}CD11b^{-}) and inflammatory Ly6C^{high} monocytes from the BM of naïve and chronically infected WT and *CD18^{low}* mice. Compared to WT mice, *Irf8* expression was significantly reduced in the pMo cells from *CD18^{low}* animals (Figure 3A). There were no significant differences in *Klf4* and *Nr4a1* expression in pMo cells between the mouse strains (Figure 3B). Inflammatory Ly6C^{high} monocytes from both experimental groups displayed similar expression of *Irf8, Klf4* and *Nr4a1*. IRF8 signaling enhances the expression of colony stimulating factor 1 receptor (CSF1R; also know as CD115), which is necessary for the development and maintenance of monocytes (35) and tissue macrophages (36). Therefore, CD18 may provide critical signals to maintain a functional CSF1-CSF1R axis in these cells during schistosomiasis. To test this hypothesis, we quantified the cell surface expression of CD115 in pMo and inflammatory Ly6C^{high} monocytes. As expected, the expression of CD115 was significantly reduced in the surface of pMo (Figure 3C) and Ly6C^{high} monocytes (Figure 3D) from *CD18^{low}* mice at 7 wpi. To validate these findings and establish the impact of CD18 over CD115 expression, we treated naïve WT mice with anti-CD18 and analyzed CD115 expression in pMo and inflammatory Ly6C^{high} monocytes from the BM, according to the experimental design in Figure 3E. Compared to control mice, CD115 expression was reduced in the surface of pMo from anti-CD18 treated mice (Figure 3F), while CD18 blockage did not change the CD115 expression in inflammatory Ly6C^{high} monocytes in the BM (Figure 3G). Taken together, these results suggest that CD18 affects the IRF8-CD115 axis, which may modulate the proliferation of monocyte precursors and impact the generation of mature monocytes during chronic *S. mansoni* infection.

CD18 regulates αM-CD11b subunit expression in hepatic Ly6C^{high} monocytes during schistosomiasis

Because CD18 partners with different α-subunits to compose distinct integrins such as $\alpha_L\beta_2$ (CD11a/CD18 or LFA-1), $\alpha_M\beta_2$ (CD11b/CD18 or Mac-1 or CR3), $\alpha_X\beta_2$ (CD11c/CD18 or p150/95 or CR4) and $\alpha_D\beta_2$ (CD11d/CD18) (1) and monocytes play a critical roles in regulating tissue damage (37), we investigated the gene expression of α-subunits in the liver from *S. mansoni*-infected WT mice at 7wpi. We found increased *Itgam* expression compared to *Itgal* (Figure S2A). Additionally, we performed a flow cytometry analysis to evaluate the cell surface expression of α-subunits on CD45^{+} cells in the liver. The analysis revealed an increased frequency of CD11b^{+} cells compared to CD11a^{+} cells in the liver of *S. mansoni*-infected mice at 7 wpi (Figures S2B, C). Accordingly, our previous work showed that, lower CD18 expression reduces the percentages of Ly6C^{inter} and patrolling Ly6C^{low} monocytes in the liver during chronic schistosomiasis (3). Therefore, we applied the flow cytometric gating hierarchy shown in Figure S2B to evaluate the α-subunits in hepatic inflammatory Ly6C^{high} and patrolling Ly6C^{low} monocytes.

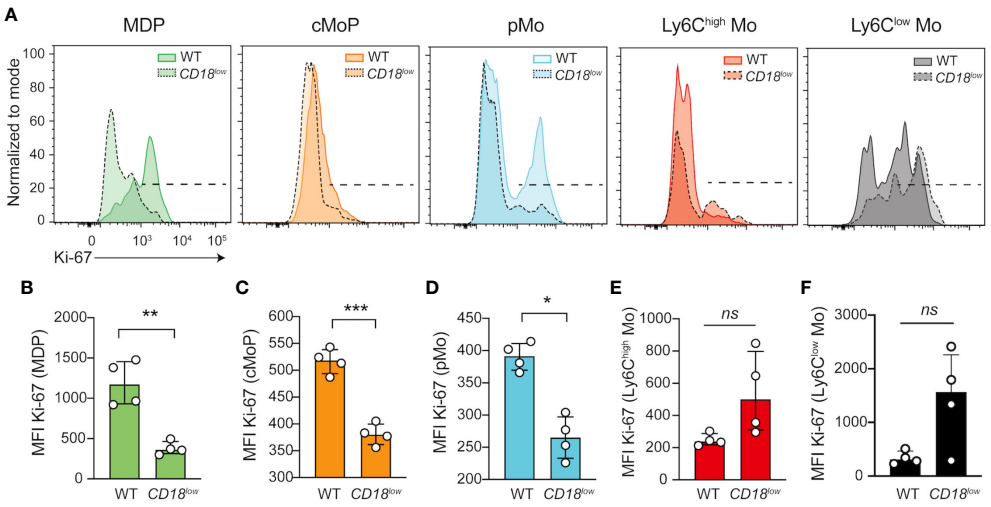

FIGURE 2
CD18 controls the expression of Ki-67 in monocyte progenitors in BM during chronic schistosomiasis. BM of *S. mansoni*-infected C57BL/6 and *CD18*^{low} mice were analyzed by flow cytometry. **(A)** Representative histogram graph showed the median florescent intensity (MFI) of Ki-67 in MPD (Lin$^-$ CD117$^-$ CD115$^+$ CD135$^+$ Ly6C$^-$ CD11b$^-$), cMoP (Lin$^-$ CD117$^+$ CD115$^+$ CD135$^+$ Ly6C$^+$ CD11b$^-$) and pMo (Lin$^-$ CD117$^-$ CD115$^+$ CD135$^-$ Ly6C$^+$ CD11b$^-$) progenitor cells and in distinct monocytes subsets, Ly6C^{high} (Lin$^-$ CD117$^-$ CD115$^+$ CD135$^-$ Ly6C^{high} CD11b$^+$) and Ly6C^{low} (Lin$^-$ CD117$^-$ CD115$^+$ CD135$^-$ Ly6C^{low} CD11b$^+$). **(B)** Scatter plot with bar show MFI of Ki-67 in MPD progenitor cells. **(C)** Scatter plot with bar show Ki-67 MFI in cMoP progenitor cells. **(D)** Scatter plot with bar show MFI of Ki-67 in pMo progenitor cells. **(E)** Scatter plot with bar show MFI of Ki-67 in inflammatory Ly6C^{high} monocytes. **(F)** Scatter plot with bar show MFI of Ki-67 in patrolling Ly6C^{low} monocytes. Median with interquartile range are shown for one representative experiment (n= 4 WT and *CD18*^{low} infected mice at 7 weeks) out of three independent experiments. Data were analyzed with Mann-Whitney test (* $p < 0.05$, ** $p < 0.01$, *** $p < 0.001$, ns $p > 0.05$, compared to WT in each time-point).

Compared to WT mice, CD11b and CD11c expression was reduced in inflammatory Ly6C^{high} monocytes in the livers of infected-*CD18*^{low} mice, while α-subunits were not altered in patrolling Ly6C^{low} monocytes compared to both animals (Figures S2D, E). Furthermore, we observed that the percentage of Ly6C^{high} CD11b$^+$ monocytes was significantly diminished in the liver of *CD18*^{low} mice (Figure S2F). Of note, there were no significant differences in the percentage of CD11a$^+$ or CD11c$^+$ inflammatory Ly6C^{high} monocytes (Figure S2F) or any of patrolling Ly6C^{low} monocytes (Figure S2G).

Adoptive transference of inflammatory Ly6C^{high} monocytes ameliorate the liver damage in infected-*CD18*^{low} mice during chronic schistosomiasis

To validate that CD18 is required by monocytes to protect from pathology, we isolated inflammatory Ly6C^{high}CD11b$^+$ or patrolling Ly6C^{low}CD11b$^+$ monocytes from a naïve CX$_3$CR1-GFP reporter mice by FACS sorting, and transferred to infected *CD18*^{low} mice, according to the experimental design in Figure 4A. Low CD18 expression results in increased worm burdens and release of eggs compared to WT mice (Figures 4B, C). The adoptive transference of inflammatory Ly6C^{high}CD11b$^+$ or Ly6C^{low}CD11b$^+$ monocytes to infected-*CD18*^{low} mice did not impact these parameters at 7 wpi (Figures 4B, C). Inflammatory Ly6C^{high} monocytes reduce Ly6C expression and accumulate in the hepatic granulomas around the *S. mansoni* eggs (6, 15, 16), but low CD18 expression does not affect granuloma areas in responses to *S. mansoni* eggs (3). Thus, we performed histological analyses of livers from both groups of mice infected at 7 weeks by staining with hematoxylin & eosin (H&E) and picrosirius red to evaluate the inflammatory infiltrated and fibrosis, respectively. The numbers of granulomas were similar between WT and *CD18*^{low} mice receiving Ly6C^{high}CD11b$^+$ or Ly6C^{low}CD11b$^+$ monocytes and controls (Figure 4D). Compared to WT, *CD18*^{low} mice displayed increased inflammatory infiltrate in the liver (Figure 4E) and the adoptive transference of WT inflammatory Ly6C^{high} CD11b$^+$ monocytes to infected-*CD18*^{low} reduced the inflammatory infiltrate in the liver, which became comparable to WT mice (Figure 4E). There were no significant differences in mice receiving WT patrolling Ly6C^{low}CD11b$^+$ monocytes (Figure 4E). Consistently, we observed increased collagen deposition in livers of *CD18*^{low} compared to WT mice (Figure 4F), while *CD18*^{low} mice that received WT inflammatory Ly6C^{high} monocytes exhibited diminished hepatic fibrosis (Figure 4F). Adoptive transference of WT patrolling Ly6C^{low} CD11b$^+$ monocytes had no effects to control the fibrosis in liver (Figure 4F). Overall, these data show that CD18 is critical for the generation of inflammatory Ly6C^{high} monocytes, which are required to control the inflammation and fibrosis in liver during chronic schistosomiasis.

10.3389/fimmu.2022.929552

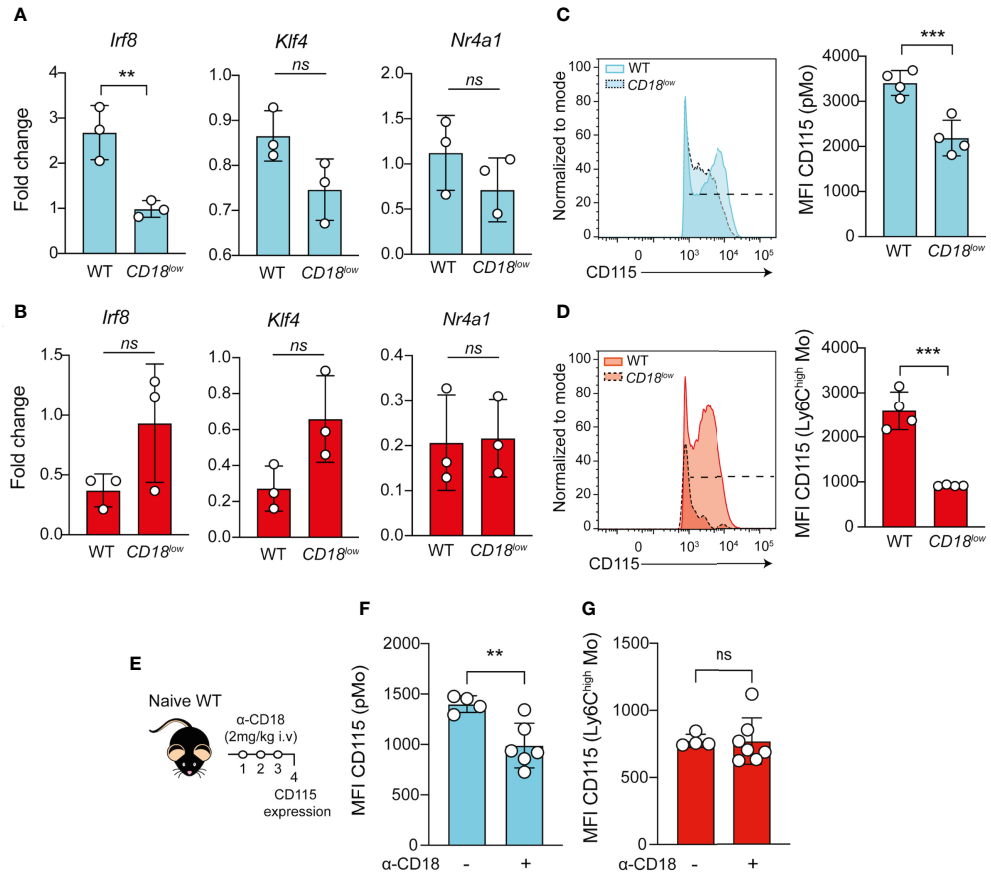

FIGURE 3
Low CD18 expression impacts the expression of IRF8 and CD115 in proliferating-monocyte isolated from BM of *S. mansoni*-infected mice. Proliferating-monocytes (pMo) progenitor cells and inflammatory Ly6C^{high} monocytes were isolated by FACS-sorting from the BM of uninfected and *S. mansoni*-infected C57BL/6 and *CD18^{low}* mice. **(A)** Scatter plot with bar show the *Irf8*, *Klf4* and *Nr4a1* expression in the proliferating-monocytes progenitor cells at 7 wpi. **(B)** Scatter plot with bar show the *Irf8*, *Klf4* and *Nr4a1* expression in the inflammatory Ly6C^{high} monocytes at 7 wpi. Data represent one independent experiment using a pool of three animals (N=9 WT and *CD18^{low}* infected mice at 7 weeks. Results are expressed as mean ± SD. Statistically significant differences were evaluated with unpaired t test (** $p < 0.01$ compared to WT in each time-point). BM of *S. mansoni*-infected C57BL/6 and *CD18^{low}* mice were analyzed by flow cytometry. **(C)** Representative histogram and scatter plot with bar show the CD115 MFI on pMo (Lin$^-$ CD117$^-$ CD115$^+$ CD135$^-$ Ly6C$^+$ CD11b$^-$) progenitor cells **(D)** Representative histogram and scatter plot with bar show the CD115 MFI on inflammatory Ly6C^{high} (Lin$^-$ CD117$^-$ CD115$^+$ CD135$^-$ Ly6C^{high} CD11b$^+$) monocytes. Data represent one representative experiment (n= 4 WT and *CD18^{low}* infected mice at 7 weeks) out of three independent experiments. Statistically significant differences were evaluated with unpaired t test (*** $p < 0.001$, ns $p > 0.05$, compared to WT in each time-point). **(E)** Schematic representation of the treatment with anti-CD18 (intravenous 2mg/Kg) in naïve WT mice. **(F)** Scatter plot with bar show the CD115 MFI on pMo progenitor cells. **(G)** Scatter plot with bar show the CD115 MFI on inflammatory Ly6C^{high} monocytes. Data represent one independent experiment (n= 4 non treated WT mice and n=7 WT anti-CD18 treated mice per group). Statistically significant differences were evaluated with unpaired t test (** $p < 0.01$, ns $p > 0.05$, compared to nontreated WT mice).

The alternative activation of macrophages requires CD18 during chronic schistosomiasis

Ly6C^{high} monocytes give rise to AAM in liver granulomas, which are key players of tissue damage repair and granuloma formation during schistosomiasis (6, 15). To understand whether CD18 is required for the polarization and function of AAM, we evaluated the expression of genes characterizing the alternative activation of macrophages in the liver from WT and *CD18^{low}* mice at 7 wpi. Compared to WT mice, the expression of *Il4* (Figure 5A), *Chi3l3* (Figure 5B) and *Arg1* (Figure 5C) was reduced in *CD18^{low}* animals. Next, we evaluated the accumulation of AAM in the liver using the flow cytometric gating hierarchy shown in Figure S3. There were no significant differences in PD-L2 and CD206 expression on AAMs between WT and *CD18^{low}* mice (Figures 5D–F). However, both percentage and absolute numbers of PD-L2$^+$CD206$^+$ AAMs decreased in the liver of

10.3389/fimmu.2022.929552

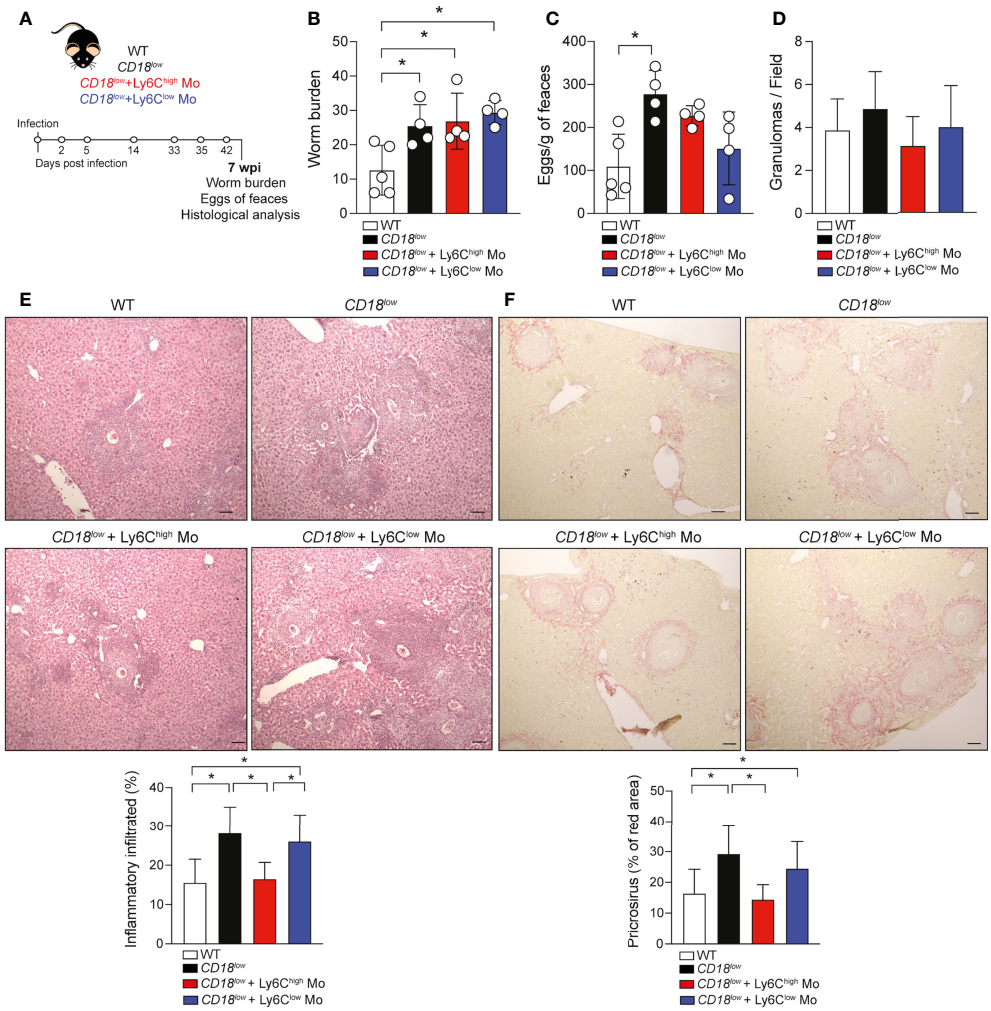

FIGURE 4
Adoptive transference of inflammatory Ly6C^{high} monocytes promotes the tissue repair in infected-*CD18^{low}* mice during chronic schistosomiasis. WT and *CD18^{low}* mice were subcutaneous infected with 80 cercariae of *S. mansoni*. **(A)** Schematic representation of the adoptive transference of inflammatory Ly6C^{high} CD11b^{+} and patrolling Ly6C^{low} CD11b^{+} monocytes previously isolated from uninfected *CX$_3$CR1$^{gpf/wt}$* reporter mice by FACS-sorting. **(B)** Scatter plots with bar show the parasite worm burden determined by perfusion of the hepatic portal system from WT and *CD18^{low}* mice treated or not with inflammatory Ly6C^{high}CD11b^{+} and patrolling Ly6C^{low} CD11b^{+}monocytes at 7 wpi. **(C)** Scatter plots with bar show the eggs/g of feces from WT and *CD18^{low}* mice treated or not with inflammatory Ly6C^{high} CD11b^{+} and patrolling Ly6C^{low} CD11b^{+}at 7 wpi. **(D)** Bar plots show the numbers of granuloma by field from WT and *CD18^{low}* mice receiving inflammatory Ly6C^{high} CD11b^{+} or patrolling Ly6C^{low} CD11b^{+} and controls at 7 wpi. **(E)** Photomicrographs of liver lesion stained with H&E coloration and bar plots show the percentage of the inflammatory infiltrated from WT and *CD18^{low}* mice receiving inflammatory Ly6C^{high} CD11b^{+} or patrolling Ly6C^{low} CD11b^{+} and controls at 7 wpi. **(F)** Photomicrographs of liver lesion stained with picrosirius red staining and bar plots show the percentage of fibrosis (red area) from WT and *CD18^{low}* mice receiving inflammatory Ly6C^{high}CD11b^{+} or patrolling Ly6C^{low}CD11b^{+} and controls at 7 wpi. All photomicrography was analyzed using a light microscope, scale bar: 50µM (n= 4 WT or *CD18^{low}* control mice and n=4 *CD18^{low}* adoptive transferred mice per group). Data are expressed as mean ± SD. Statistically significant differences were evaluated with ANOVA followed by Bonferroni's multiple comparisons test (*p < 0.05).

CD18^{low} mice compared to WT animals at 7 weeks (Figures 5D, G, H). IL-4Ra signaling in AAM induces IL-10 production which is necessary for the maintenance of granulomas around the eggs (38). We observed that *S. mansoni*-infected *CD18^{low}* mice displayed reduced abundance of IL-10 in the liver (Figure 5I), thus the reduced AAM population may reflect into lower IL-10 levels. Taken together, these data suggest that CD18 affects the phenotype and function of AAM during chronic schistosomiasis.

Discussion

Our study showed that low levels of CD18 affect pMo progenitor cells, which accumulate in the BM, while reducing mature monocytes, immune cells that play critical roles during schistosomiasis (39). The data also suggest that CD18, and potentially the integrin Mac-1, regulates the gene expression of *Irf8*, which in turn is required for CD115 expression. Without

10.3389/fimmu.2022.929552

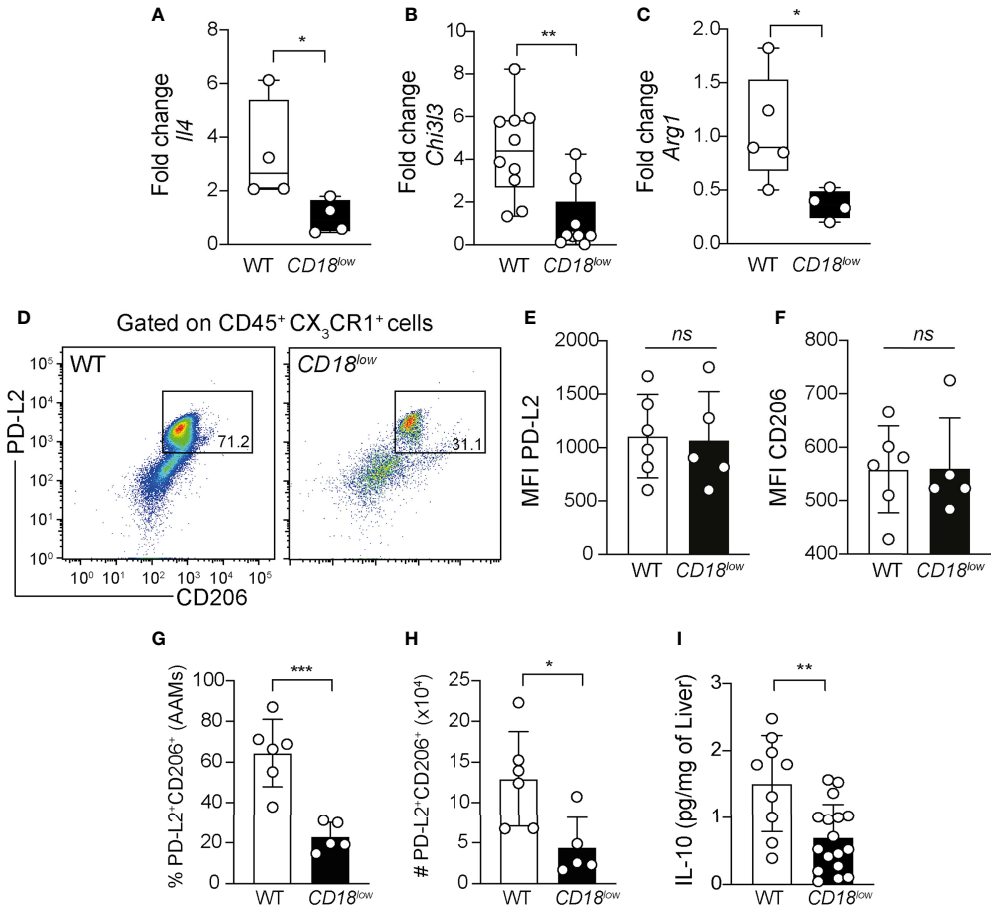

FIGURE 5
Low CD18 expression impacts alternative activation of macrophages in livers of *S. mansoni*-infected mice. WT and *CD18*^{low} mice were subcutaneous infected with 80 cercariae of *S. mansoni* and the livers were collected at 7 wpi. Graphs display the qRT-PCR analysis of *Il4* **(A)** *Chil3l3* **(B)** and *Arg1* **(C)** expression in the liver. Data were analyzed from one representative experiment **(A, C)** or pool **(B)** out of two independent experiments. Statistically significant differences were evaluated with Mann-Whitney test (*p< 0.05, **p<0,01 compared to WT in each-time point). **(D)** Representative dot plots display the flow cytometric data of CD45$^+$CX$_3$CR1$^+$PL-D2$^+$CD206$^+$ alternatively activated macrophages (AAMs). **(E, F)** Scatter plot with bar show the median fluorescent intensity (MFI) of PD-L2. **(F)** and CD206 **(F)** in AAMs. **(G, H)** Scatter plot with bar show the percentage **(G)** and absolute numbers **(H)** of these cells in the liver. Median with interquartile range is shown for one representative experiment (n= 6 WT and n=5 *CD18*^{low} infected mice at 7 weeks) out of three independent experiments. Data were analyzed with Mann-Whitney test (* p < 0.05, *** p < 0.001, ns p > 0.05, compared to WT mice in each time-point). **(I)** Scatter plot with bar show the levels of IL-10 by ELISA in the liver. Data are from a pool of three independent experiments and were analyzed with Mann-Whitney test (**p < 0.01 compared to WT mice). The symbol (#) indicates the absolute numbers of AAMs.

optimal CD115 signaling, pMo may fail to mature into inflammatory Ly6Chigh monocytes, which are required to protect from immunopathology and death (3). Previous studies suggest that CD18 influences the formation of hematopoietic niches (11, 12) by triggering the proliferation and differentiation of HSPCs, which lead to myeloid (3, 9, 40, 41) and lymphoid cells hematopoiesis (42). It is important to note that proteomic analysis of monocytes and their progenitors showed that ITGB2 is involved in the discrimination between the developmental stages (14). Additionally, naïve CD18$^{-/-}$ mice display accumulation of granulocyte-macrophages progenitor (GMP) cells in the BM, which is associated with a higher GATA2 expression and activation of IgE – FcεRI axis leading the GMP expansion and granulocyte and monocyte production (9). Curiously, arteriosclerotic progression has been associated with HSPC expansion in the BM and their recruitment to injured arteries *via* CD18 expression (40). In line with this metabolic disorder, *S. mansoni*-infected male Apolipoprotein E deficient (*ApoE*$^{-/-}$) mice on high-fat diet (HFD) modulates oxygen consumption on bone marrow myeloid progenitors, culminating in Ki-67 expression and expansion of GMP (43). Here, we found that low levels of CD18 reduced Ki-67 expression in monocyte precursors, which suggests lower proliferation and maturation of these cells during *S. mansoni*

infection, but further studies are necessary to confirm the precise biochemical pathways by which CD18 controls monocytopoiesis during schistosomiasis.

Impaired development of monocytes has been correlated with defective mTOR signaling, which results in the activation of STAT5 and downregulation of IRF8-dependent CD115-expression in myeloid progenitor cells in the BM (30). IRF8-deficient mice display reduced frequency and numbers of mature monocytes in BM and blood, while the IRF8-transduced cells increase *Itgam, Csfr1* and *Cd14* expression (32). Furthermore, IRF8 signaling modulates the effector functions of macrophages and dendritic cells by increasing the cell surface expression of other integrin families such as β8 and β7 (44). We observed a significant reduction of IRF8 gene expression in pMo of *S. mansoni*-infected *CD18^{low}* mice, which also displayed reduced CD115 expression in their surface. Of interest, CD115 expression was also reduced in inflammatory Ly6C^{high} monocytes. By blocking CD18 *in vivo* in naïve WT animals, we confirmed that CD18 is required for CD115 expression in pMo, but not inflammatory Ly6C^{high} monocytes, emphasizing their importance for monocyte development and maturation even in absence of infection. However, limitations of our study include whether Mac-1 mediates the intracellular cascades regulating IRF8 at the transcriptional level and whether reduced levels of IRF8 indeed cause lower CD115 expression and signaling in pMo during schistosomiais.

Once they infiltrate into inflammatory tissue, monocytes and macrophages mediate effector responses to *S. mansoni* eggs and contribute to granuloma formation together with other immune and non-immune cells (39). In the tissue, Mac-1 integrin (CD11b/CD18) is required for effective macrophage responses and tissue remodeling (45). The sensibilization with soluble eggs antigen (SEA) of *S. mansoni* induces high expression of Mac-1 that correlates with reduction of liver fibrosis (46). Overall, our data demonstrate that low CD18 expression affects the maturation of inflammatory Ly6C^{high}CD11b^{+} monocytes, while adoptive transference of these cells, but not patrolling monocytes, ameliorated the inflammatory infiltrate and fibrosis in liver from *S. mansoni*- infected *CD18^{low}* mice. Ideally, adoptive transfer of pMo progenitors from WT mice would better reveal their contribution in this context, while, adoptive transfer of inflammatory monocytes and/or pMo progenitors from *CD18^{low}* mice donors shell confirm the requirement of CD18 by inflammatory monocytes for the polarization of AAM. In support of our findings, cellular therapy of monocytes (CD14^{+} CD11b^{+}) contributes to tissue remodeling, reduces the production of TGF-β and upregulates *Fizz1* (M2 marker) expression in the liver during experimental schistosomiasis (37).

During *S. mansoni* infection, IL-4Rα signaling is dispensable to blood monocyte influx and their conversion to MDM (16). However, IL-4 and IL-13 trigger the extracellular matrix remodeling and promote the alternative activation of macrophages (6, 15, 39, 47), while the alternative activation is inhibited by the direct interaction of Mac-1 integrin with IL-13Rα1 on the cellular surface (26). In contrast our data suggest that Mac-1 is needed for the alternative activation of macrophages during *S. mansoni* infection. We observed a decreased expression of genes related to AAM, reduced frequency and numbers of PD-L2^{+}CD206^{+} AAMs, and decreased levels of IL-10 in the liver from *S. mansoni*-infected *CD18^{low}* mice. AAM limit liver and intestinal fibrosis caused by deposition of eggs, becoming essential to host protection against pathology caused by *S. mansoni* infection (48). Interestingly, IL-10$^{-/-}$ mice infected with *S. mansoni* display higher pathology and less well-defined granulomas (49) while patients with severe schistosomiasis produce lower levels of IL-10 than those without fibrosis (50).

The data suggest a model in which CD18, and possibly Mac-1 integrin, induce the proliferation of monocyte progenitors as well as the IRF8 - CD115 axis. This could be required for the maturation of monocytes in the bone marrow. Furthermore, the data suggest that CD18 is needed for the phenotype and function of AAM, which would impact not only schistosomiasis, but also other helminthic, infectious and inflammatory diseases.

Data availability statement

The original contributions presented in the study are included in the article/Supplementary Material. Further inquiries can be directed to the corresponding author.

Ethics statement

The animal study was reviewed and approved by The Comissão de Ética no Uso de Animais da Faculdade de Ciências Farmacêuticas de Ribeirão Preto (Protocol Number 14.1.607.53.9 and 19.1.46.60.4) and carried out in accordance to the ethical principles for animal research adopted by the Sociedade Brasileira de Ciência em Animais de Laboratório.

Author contributions

CS and LF conceived the study. CS, JE-O, MP, CF, VR and LG performed experiments. CS conduced data analysis and wrote the original draft. CS and LG reviewed and edited the paper. CS, LG and LF inputted intellectual concepts. VR maintained parasites and provided infection model. LF provide resources and coordinated the study. All authors read and approved the final manuscript.

Funding

This work was supported by São Paulo Research Foundation (Fundação de Amparo à Pesquisa do Estado de São Paulo

(FAPESP), Grant n. #2014/07125-6 to LHF; and scholarship #2018/22667-0 to COSS); the Conselho Nacional de Desenvolvimento Científico e Tecnológico (CNPq) Grant n. #302514/2015-5, #408093/2018-8 and #303259/2020-5), and Coordenação de Aperfeiçoamento de Pessoal de Nível Superior (CAPES) – Final Code 001. LGG and LHF are research fellows from the CNPq.

Acknowledgments

We are thankful to Fabiana Rosseto de Moraes and Denize Ferraz for help us with the acquisition of flow cytometry data and FACS-cell sorting, respectively. Elaine Medeiros Floriano for the help with histology staining. Izaira Tincani Brandão and Viviani Nardini Takahashi for the help with technical assistance. Ronaldo Araujo, Fabio Junior Marsola and Reinaldo Fernando Bastista for animal maintenance and all and Dr. Faccioli's laboratory members for their scientific discussion and insightful comments. We also thank Lizandra Guidi Magalhões, Ph.D. for helping with *S. mansoni* life cycle during COVID-19 pandemic.

Conflict of interest

The authors declare that the research was conducted in the absence of any commercial or financial relationships that could be construed as a potential conflict of interest.

Publisher's note

Supplementary material

The Supplementary Material for this article can be found online at: https://www.frontiersin.org/articles/10.3389/fimmu.2022.929552/full#supplementary-material

References

1. Schittenhelm L, Hilkens CM, Morrison VL. β2 integrins as regulators of dendritic cell, monocyte, and macrophage function. *Front Immunol* (2017) 8:1866. doi: 10.3389/fimmu.2017.01866

2. Fagerholm SC, Guenther C, Llort Asens M, Savinko T, Uotila LM. Beta2-integrins and interacting proteins in leukocyte trafficking, immune suppression, and immunodeficiency disease. *Front Immunol* (2019) 10:254. doi: 10.3389/fimmu.2019.00254

3. Souza COS, Espíndola MS, Fontanari C, Prado MKB, Frantz FG, Rodrigues V, et al. CD18 regulates monocyte hematopoiesis and promotes resistance to experimental schistosomiasis. *Front Immunol* (2018) 9:1970. doi: 10.3389/fimmu.2018.01970

4. Pearce EJ, MacDonald AS. The immunobiology of schistosomiasis. *Nat Rev Immunol* (2002) 2:499–511. doi: 10.1038/nri843

5. Schwartz C, Fallon PG. Schistosoma "Eggs-iting" the host: Granuloma formation and egg excretion. *Front Immunol* (2018) 9:2492. doi: 10.3389/fimmu.2018.02492

6. Nascimento M, Huang SC, Smith A, Everts B, Lam W, Bassity E, et al. Ly6Chi monocyte recruitment is responsible for Th2 associated host-protective macrophage accumulation in liver inflammation due to Schistosomiasis. *PloS Pathog* (2014) 10:e1004282. doi: 10.1371/journal.ppat.1004282

7. Etzioni A, Frydman M, Pollack S, Avidor I, Phillips ML, Paulson JC, et al. Brief report: recurrent severe infections caused by a novel leukocyte adhesion deficiency. *N Engl J Med* (1992) 327:1789–92. doi: 10.1056/NEJM199212173272505

8. Hartl D, Lehmann N, Hoffmann F, Jansson A, Hector A, Notheis G, et al. Dysregulation of innate immune receptors on neutrophils in chronic granulomatous disease. *J Allergy Clin Immunol* (2008) 121:375–382.e9. doi: 10.1016/j.jaci.2007.10.037

9. Zhang L-J, Yan C, Schouteden S, Ma X-J, Zhao D, Peters T, et al. The impact of integrin β2 on Granulocyte/Macrophage progenitor proliferation. *Stem Cells Dayt Ohio* (2019) 37:430–40. doi: 10.1002/stem.2961

10. Leon-Rico D, Aldea M, Sanchez R, Segovia JC, Weiss LA, Hidalgo A, et al. Brief report: reduced expression of CD18 leads to the *in vivo* expansion of hematopoietic stem cells in mouse bone marrow. *Stem Cells Dayt Ohio* (2014) 32:2794–8. doi: 10.1002/stem.1762

11. Mei Y, Han X, Liu Y, Yang J, Sumagin R, Ji P. Diaphanous-related formin mDia2 regulates beta2 integrins to control hematopoietic stem and progenitor cell engraftment. *Nat Commun* (2020) 11:3172. doi: 10.1038/s41467-020-16911-4

12. Tsuji T, Waga I, Tezuka K, Kamada M, Yatsunami K, Kodama H. Integrin beta2 (CD18)-mediated cell proliferation of HEL cells on a hematopoietic-supportive bone marrow stromal cell line, HESS-5 cells. *Blood* (1998) 91:1263–71. doi: 10.1182/blood.V91.4.1263

13. van Furth R, Hirsch JG, Fedorko ME. Morphology and peroxidase cytochemistry of mouse promonocytes, monocytes, and macrophages. *J Exp Med* (1970) 132:794–812. doi: 10.1084/jem.132.4.794

14. Hettinger J, Richards DM, Hansson J, Barra MM, Joschko A-C, Krijgsveld J, et al. Origin of monocytes and macrophages in a committed progenitor. *Nat Immunol* (2013) 14:821–30. doi: 10.1038/ni.2638

15. Girgis NM, Gundra UM, Ward LN, Cabrera M, Frevert U, Loke P. Ly6C (high) monocytes become alternatively activated macrophages in schistosome granulomas with help from CD4+ cells. *PloS Pathog* (2014) 10:e1004080. doi: 10.1371/journal.ppat.1004080

16. Rolot M, Dougall A M, Javaux J, Lallemand F, Machiels B, Martinive P, et al. Recruitment of hepatic macrophages from monocytes is independent of IL-4Rα but is associated with ablation of resident macrophages in schistosomiasis. *Eur J Immunol* (2019) 49:1067–81. doi: 10.1002/eji.201847796

17. Rückerl D, Cook PC. Macrophages assemble! but do they need IL-4R during schistosomiasis? *Eur J Immunol* (2019) 49:996–1000. doi: 10.1002/eji.201948158

18. Jenkins SJ, Ruckerl D, Cook PC, Jones LH, Finkelman FD, van Rooijen N, et al. Local macrophage proliferation, rather than recruitment from the blood, is a signature of TH2 inflammation. *Science* (2011) 332:1284–8. doi: 10.1126/science.1204351

19. Gordon S, Martinez FO. Alternative activation of macrophages: mechanism and functions. *Immunity* (2010) 32:593–604. doi: 10.1016/j.immuni.2010.05.007

20. Broadhurst MJ, Leung JM, Lim KC, Girgis NM, Gundra UM, Fallon PG, et al. Upregulation of retinal dehydrogenase 2 in alternatively activated macrophages during retinoid-dependent type-2 immunity to helminth infection in mice. *PloS Pathog* (2012) 8:e1002883. doi: 10.1371/journal.ppat.1002883

21. Gundra UM, Girgis NM, Ruckerl D, Jenkins S, Ward LN, Kurtz ZD, et al. Alternatively activated macrophages derived from monocytes and tissue macrophages are phenotypically and functionally distinct. *Blood* (2014) 123:e110–22. doi: 10.1182/blood-2013-08-520619

22. Gundra UM, Girgis NM, Gonzalez MA, San Tang M, van der Zande HJP, Lin J-D, et al. Vitamin a mediates conversion of monocyte-derived macrophages into tissue-resident macrophages during alternative activation. *Nat Immunol* (2017) 18:642–53. doi: 10.1038/ni.3734

23. Barron L, Wynn TA. Macrophage activation governs schistosomiasis-induced inflammation and fibrosis. *Eur J Immunol* (2011) 41:2509–14. doi: 10.1002/eji.201141869

24. Herbert DR, Orekov T, Roloson A, Ilies M, Perkins C, O'Brien W, et al. Arginase I suppresses IL-12/IL-23p40-driven intestinal inflammation during acute schistosomiasis. *J Immunol Baltim Md 1950* (2010) 184:6438–46. doi: 10.4049/jimmunol.0902009

25. Dewals BG, Marillier RG, Hoving JC, Leeto M, Schwegmann A, Brombacher F. IL-4Rα-Independent expression of mannose receptor and Ym1 by macrophages depends on their IL-10 responsiveness. *PloS Negl Trop Dis* (2010) 4:e689. doi: 10.1371/journal.pntd.0000689

26. Cao C, Zhao J, Doughty EK, Migliorini M, Strickland DK, Kann MG, et al. Mac-1 regulates IL-13 activity in macrophages by directly interacting with IL-13Rα1. *J Biol Chem* (2015) 290:21642–51. doi: 10.1074/jbc.M115.645796

27. Yakubenko VP, Bhattacharjee A, Pluskota E, Cathcart MK. αMβ2 integrin activation prevents alternative activation of human and murine macrophages and impedes foam cell formation. *Circ Res* (2011) 108:544–54. doi: 10.1161/CIRCRESAHA.110.231803

28. Wilson RW, Ballantyne CM, Smith CW, Montgomery C, Bradley A, O'Brien WE, et al. Gene targeting yields a CD18-mutant mouse for study of inflammation. *J Immunol* (1993) 151:1571–8.

29. Tarafder MR, Carabin H, Joseph L, Balolong E, Olveda R, McGarvey ST. Estimating the sensitivity and specificity of kato-Katz stool examination technique for detection of hookworms, ascaris lumbricoides and trichuris trichiura infections in humans in the absence of a "gold standard". *Int J Parasitol* (2010) 40:399–404. doi: 10.1016/j.ijpara.2009.09.003

30. Zhao Y, Shen X, Na N, Chu Z, Su H, Chao S, et al. mTOR masters monocyte development in bone marrow by decreasing the inhibition of STAT5 on IRF8. *Blood* (2018) 131:1587–99. doi: 10.1182/blood-2017-04-777128

31. Tamura T, Kurotaki D, Koizumi S. Regulation of myelopoiesis by the transcription factor IRF8. *Int J Hematol* (2015) 101:342–51. doi: 10.1007/s12185-015-1761-9

32. Kurotaki D, Osato N, Nishiyama A, Yamamoto M, Ban T, Sato H, et al. Essential role of the IRF8-KLF4 transcription factor cascade in murine monocyte differentiation. *Blood* (2013) 121:1839–49. doi: 10.1182/blood-2012-06-437863

33. Alder JK, Georgantas RW, Hildreth RL, Kaplan IM, Morisot S, Yu X, et al. Kruppel-like factor 4 is essential for inflammatory monocyte differentiation *In vivo*. *J Immunol Baltim Md 1950* (2008) 180:5645–52. doi: 10.4049/jimmunol.180.8.5645

34. Hanna RN, Carlin LM, Hubbeling HG, Nackiewicz D, Green AM, Punt JA, et al. The transcription factor NR4A1 (Nur77) controls bone marrow differentiation and the survival of Ly6C – monocytes. *Nat Immunol* (2011) 12:778–85. doi: 10.1038/ni.2063

35. Stanley ER, Chitu V. CSF-1 receptor signaling in myeloid cells. *Cold Spring Harb Perspect Biol* (2014) 6 (6):a021857. doi: 10.1101/cshperspect.a021857

36. Rojo R, Raper A, Ozdemir DD, Lefevre L, Grabert K, Wollscheid-Lengeling E, et al. Deletion of a Csf1r enhancer selectively impacts CSF1R expression and development of tissue macrophage populations. *Nat Commun* (2019) 10:3215. doi: 10.1038/s41467-019-11053-8

37. de Souza VCA, Moura DMN, de Castro MCAB, Bozza PT, de Almeida Paiva L, Fernandes CJB, et al. Adoptive transfer of bone marrow-derived monocytes ameliorates schistosoma mansoni -induced liver fibrosis in mice. *Sci Rep* (2019) 9:6434. doi: 10.1038/s41598-019-42703-y

38. Faz-López B, Morales-Montor J, Terrazas LI. Role of macrophages in the repair process during the tissue migrating and resident helminth infections. *BioMed Res Int* (2016) 2016:e8634603. doi: 10.1155/2016/8634603

39. Souza COS, Gardinassi LG, Rodrigues V, Faccioli LH. Monocyte and macrophage-mediated pathology and protective immunity during schistosomiasis. *Front Microbiol* (2020) 11:1973. doi: 10.3389/fmicb.2020.01973

40. Wang X, Gao M, Schouteden S, Roebroek A, Eggermont K, van Veldhoven PP, et al. Hematopoietic stem/progenitor cells directly contribute to arteriosclerotic progression *via* integrin β2. *Stem Cells Dayt Ohio* (2015) 33:1230–40. doi: 10.1002/stem.1939

41. Gomez JC, Doerschuk CM. The role of CD18 in the production and release of neutrophils from the bone marrow. *Lab Invest* (2010) 90:599–610. doi: 10.1038/labinvest.2010.4

42. McIntyre CL, Monin L, Rop JC, Otto TD, Goodyear CS, Hayday AC, et al. β2 integrins differentially regulate γδ T cell subset thymic development and peripheral maintenance. *Proc Natl Acad Sci* (2020) 117:22367–77. doi: 10.1073/pnas.1921930117

43. Cortes-Selva D, Gibbs L, Maschek JA, Nascimento M, Ry TV, Cox JE, et al. Metabolic reprogramming of the myeloid lineage by schistosoma mansoni infection persists independently of antigen exposure. *PloS Pathog* (2021) 17:e1009198. doi: 10.1371/journal.ppat.1009198

44. Yoshida Y, Yoshimi R, Yoshii H, Kim D, Dey A, Xiong H, et al. The transcription factor IRF8 activates integrin-mediated TGF-β signaling and promotes neuroinflammation. *Immunity* (2014) 40:187–98. doi: 10.1016/j.immuni.2013.11.022

45. Trottein F, Nutten S, Papin JP, Leportier C, Poulain-Godefroy O, Capron A, et al. Role of adhesion molecules of the selectin-carbohydrate families in antibody-dependent cell-mediated cytoxicity to schistosome targets. *J Immunol* (1997) 159:804–11.

46. El-Ahwany EG, Hanallah SB, Zada S, El Ghorab NM, Badir B, Badawy A, et al. Immunolocalization of macrophage adhesion molecule-1 and macrophage inflammatory protein-1 in schistosomal soluble egg antigen-induced granulomatous hyporesponsiveness. *Int J Parasitol* (2000) 30:837–42. doi: 10.1016/S0020-7519(00)00068-0

47. Rolot M, Dewals BG. Macrophage activation and functions during helminth infection: Recent advances from the laboratory mouse. *J Immunol Res* (2018) 2018:e2790627. doi: 10.1155/2018/2790627

48. Herbert DR, Hölscher C, Mohrs M, Arendse B, Schwegmann A, Radwanska M, et al. Alternative macrophage activation is essential for survival during schistosomiasis and downmodulates T helper 1 responses and immunopathology. *Immunity* (2004) 20:623–35. doi: 10.1016/s1074-7613(04)00107-4

49. Sadler CH, Rutitzky LI, Stadecker MJ, Wilson RA. IL-10 is crucial for the transition from acute to chronic disease state during infection of mice with schistosoma mansoni. *Eur J Immunol* (2003) 33:880–8. doi: 10.1002/eji.200323501

50. Mutengo MM, Mduluza T, Kelly P, Mwansa JCL, Kwenda G, Musonda P, et al. Low IL-6, IL-10, and TNF-α and high IL-13 cytokine levels are associated with severe hepatic fibrosis in schistosoma mansoni chronically exposed individuals. *J Parasitol Res* (2018) 2018:9754060. doi: 10.1155/2018/9754060

frontiers | Frontiers in Immunology

TYPE Original Research
PUBLISHED 10 October 2022
DOI 10.3389/fimmu.2022.954282

OPEN ACCESS

EDITED BY
Thiago Almeida Pereira,
Stanford University, United States

REVIEWED BY
Sandra Grossi Gava,
René Rachou Institute,
Oswaldo Cruz Foundation
(FIOCRUZ), Brazil
Melanie Hannebelle,
Stanford University, United States
Naiara Clemente Tavares,
Laboratório de Imunologia Celular e
Molecular, Instituto René Rachou,
Fundação Oswaldo Cruz
(FIOCRUZ), Brazil

*CORRESPONDENCE
Tianfang Wang
twang@usc.edu.au

SPECIALTY SECTION
This article was submitted to
Parasite Immunology,
a section of the journal
Frontiers in Immunology

RECEIVED 27 May 2022
ACCEPTED 27 September 2022
PUBLISHED 10 October 2022

CITATION
Fogarty CE, Phan P, Duke MG,
McManus DP, Wyeth RC, Cummins SF
and Wang T (2022) Identification of
Schistosoma mansoni miracidia
attractant candidates in infected
Biomphalaria glabrata using
behaviour-guided
comparative proteomics.
Front. Immunol. 13:954282.
doi: 10.3389/fimmu.2022.954282

Identification of *Schistosoma mansoni* miracidia attractant candidates in infected *Biomphalaria glabrata* using behaviour-guided comparative proteomics

Conor E. Fogarty[1,2], Phong Phan[1,2], Mary G. Duke[3], Donald P. McManus[3], Russell C. Wyeth[4], Scott F. Cummins[1,2] and Tianfang Wang[1,2]*

[1]Centre for Bioinnovation, University of the Sunshine Coast, Maroochydore, QL, Australia, [2]School of Science, Technology and Engineering, University of the Sunshine Coast, Maroochydore, QL, Australia, [3]Infection and Inflammation Program, Queensland Institute of Medical Research (QIMR) Berghofer Medical Research Institute, Brisbane, QL, Australia, [4]Department of Biology, St. Francis Xavier University, Antigonish, NS, Canada

Schistosomiasis, caused by infection with *Schistosoma* digenetic trematodes, is one of the deadliest neglected tropical diseases in the world. The *Schistosoma* lifecycle involves the miracidial infection of an intermediate freshwater snail host, such as *Biomphalaria glabrata*. Dispersing snail host-derived *Schistosoma* miracidia attractants has been considered a method of minimising intermediate host infections and, by extension, human schistosomiasis. The attractiveness of *B. glabrata* to miracidia is known to be reduced following infection; however, the relationship between duration of infection and attractiveness is unclear. Excretory-secretory proteins (ESPs) most abundant in attractive snail conditioned water (SCW) are key candidates to function as miracidia attractants. This study analysed SCW from *B. glabrata* that were naïve (uninfected) and at different time-points post-miracidia exposure (PME; 16h, 1-week, 2-weeks and 3-weeks PME) to identify candidate ESPs mediating *Schistosoma mansoni* miracidia behaviour change, including aggregation and chemoklinokinesis behaviour (random motion, including slowdown and increased turning rate and magnitude). Miracidia behaviour change was only observed post-addition of naïve and 3W-PME SCW, with other treatments inducing significantly weaker behaviour changes. Therefore, ESPs were considered attractant candidates if they were shared between naïve and 3W-PME SCW (or exclusive to the former), contained a predicted N-terminal signal peptide and displayed low identity (<50%) to known proteins outside of the *Biomphalaria* genus. Using these criteria, a total of 6 ESP attractant candidates were identified, including acetylcholine binding protein-like proteins and uncharacterised proteins. Tissue-specific RNA-seq analysis of the genes

encoding these 6 ESPs indicated relatively high gene expression within various *B. glabrata* tissues, including the foot, mantle and kidney. Acetylcholine binding protein-like proteins were highly promising due to their high abundance in naïve and 3W-PME SCW, high specificity to *B. glabrata* and high expression in the ovotestis, from which attractants have been previously identified. In summary, this study used proteomics, guided by behavioural assays, to identify miracidia attractant candidates that should be further investigated as potential biocontrols to disrupt miracidia infection and minimise schistosomiasis.

KEYWORDS

Biomphalaria glabrata, *Schistosoma mansoni*, attractant candidates, behavioural analysis, proteomic comparison

Introduction

Schistosomiasis is one of the most socioeconomically consequential neglected tropical diseases in the developing world and is caused by digenetic trematodes of the genus *Schistosoma*. The most common causes of human schistosomiasis are infection with *Schistosoma mansoni*, *Schistosoma haematobium* and *Schistosoma japonicum*, which together comprise over 95% of global human schistosomiasis cases (1). Over 200 million people are estimated to be infected with schistosomes, with endemicity ubiquitous in several Middle Eastern, South American and sub-Saharan African nations (2). Most infections are asymptomatic; however, a substantial minority of those infected suffer serious effects, resulting in an estimated over 200,000 deaths per year due to schistosomiasis (3).

Currently, the most common schistosomiasis management method is mass drug administration with praziquantel, a chemotherapeutic drug boasting high efficacy against all *Schistosoma* spp., few side effects and wide spread use for decades (4, 5). However, praziquantel mass drug administration does not prevent re-infections and the drug is less effective against immature schistosomes (6–8). Therefore, other methods of minimising the spread of schistosomiasis are under investigation. Vaccine development and non-pharmacological methods, such as improving sanitation, education and infrastructure, have been thoroughly investigated (9). However, another promising direction in schistosomiasis control is in preventing schistosomes from infecting their respective hosts through targeted chemosensory biocontrols. Due to the high species-specificity and sensitivity of chemosensory responses, the usage of attractants is an enticing, low-risk, targeted method. Chemosensory interference with aquatic species behaviour has recently been demonstrated on several pests, including cane toad (*Rhinella marina*) larvae (10) and European carp (*Cyprinus carpio*) (11), indicating the efficacy of this approach in aquatic settings.

The *Schistosoma* lifecycle involves the infection of an intermediate molluscan host and a definitive mammalian host. Miracidia (which hatch from eggs released into freshwater from definitive hosts) and cercariae (which escape from infected snails) are non-feeding stages which infect molluscan and mammalian hosts, respectively. *Schistosoma* cercariae can infect various mammalian species, including ruminants, humans and mice (12, 13). In contrast, miracidia can only infect snail hosts of a specific genus, such as *Biomphalaria* in the case of *S. mansoni* miracidia. The most widely studied miracidia-host interaction is that between *S. mansoni* miracidia and *Biomphalaria glabrata*, both of which have complete genome databases (14–16). It has been observed that proximity to *B. glabrata* snail-conditioned water (SCW) induces miracidia behaviour change, including chemoklinokinesis (random movement in proximity to a chemical, including slowdown and turning) and aggregation (increased quantity of miracidia presence around the SCW). Chemoklinokinesis has been observed in miracidia of many digenetic trematodes (17, 18). Miracidia of some *S. mansoni* strains display high host specificity, such as Egyptian strain *S. mansoni* for sympatric *Biomphalaria alexandrina* over allopatric *B. glabrata*, indicating preference for sympatric hosts (19). This suggests that miracidia receptors have evolved to identify *Biomphalaria*-specific ligands released into the water. Recent SCW analyses demonstrated that snail-derived peptides and excretory-secretory proteins (ESPs) were the primary stimulants for miracidia behaviour change, while small molecules were less likely to be attractants (20). One such attractant peptide is P12 (—R-*DITSGLDPEVADD*-KR—), which is highly expressed in the central nervous system, foot, heart and kidney and produced identical changes in miracidia behaviour to naïve

Abbreviations: AChBP, Acetylcholine-binding protein; ESP, excretory–secretory protein; FDR, false discovery rate; FOV, field of view; GO, gene ontology; LC-MS/MS, liquid chromatography with tandem mass spectrometry; PBS, phosphate-buffered saline; PME, post-miracidia infection; QIMR, Queensland Institute of Medical Research; SCW, snail-conditioned water.

(uninfected) *B. glabrata* SCW (20). However, aside from P12, few attraction chemicals have been identified (21). Comparative analyses of the chemical composition of attractive and non-attractive SCW may enable the identification of *S. mansoni* miracidia attractants in the former.

In addition to displaying a strong preference for *Biomphalaria*, *S. mansoni* miracidia also display a stronger preference for SCW from naïve *B. glabrata* than SCW from infected *B. glabrata*. When placed in a T-maze, *S. mansoni* miracidia show a significant preference for naïve SCW, but not infected SCW, over an empty chamber (22). This may be due to infected *B. glabrata* releasing fewer attractant ESPs or *S. mansoni* sporocysts (the asexually reproductive stages which miracidia transform into post-infection) releasing deterrent chemicals. Regardless of the mechanism, *S. mansoni* miracidia have an evolutionary justification to avoid infected molluscan hosts; excessive infection of a molluscan host leads to poorer cercarial output. For example, it has been observed that *Galba truncatula* release fewer cercariae when infected with five *Fasciola hepatica* miracidia than when infected with one miracidium (23). Therefore, because infected snails are known to be less attractive to miracidia, comparing SCW from naïve and infected snails may inform the identification of attractant chemicals in the former.

There are some indications that miracidia attraction to snail hosts varies with the duration of host infection. A recent study observed that SCW from *B. glabrata* 3 weeks post-miracidia exposure (PME) induced miracidia aggregation (24). This suggested that attractants may still be present post-infection. Testing SCW from *B. glabrata* at different time-points PME would reveal the relationship between infection duration and attractiveness. If miracidia behaviour change varies substantially between SCW from different time-points PME, a comparative proteomic analysis of ESPs from *B. glabrata* SCW at different time-points post-infection could facilitate the discovery of novel miracidia attractant candidates.

In this study, we aimed to compare SCW collected from *B. glabrata* at different time-points post-exposure to *S. mansoni* miracidia to identify attractant candidates. Firstly, behavioural bioassays were conducted on *S. mansoni* miracidia following the addition of *B. glabrata* SCW from 16h-PME, 1-week PME (1W-PME) and 2W-PME, with 3W-PME and naïve SCW derived from an earlier study (24). Secondly, the ESPs were subjected to semi-quantitative proteomic analysis using LC-MS/MS to identify attractant candidates. Finally, the attractant candidates were analysed using the *B. glabrata* transcriptome to observe their relative expression in different tissue. The findings of this study elucidated the effect of host infection duration on *S. mansoni* miracidia attractiveness and identified several attractant candidates.

Materials and Methods

Biomphalaria glabrata and Swiss mice maintenance conditions and ethics guidelines

The conduct and procedures involving animal experimentation were approved by the Animal Ethics Committee of the QIMR Berghofer Medical Research Institute, Brisbane (project number P3705). This study was performed in accordance with the recommendations in the Guide for the Care and Use of Laboratory Animals of the National Institutes of Health. The Swiss mice used in this study were subject to Biosecurity Quarantine Control and hence held in a quarantine containment area within a Specific Pathogen Free Animal Facility. The *S. mansoni* were maintained with an Australian Department of Agriculture, Fisheries and Forestry Biosecurity permit. The *B. glabrata* snails (NMRI strain) were maintained in an aerated tank of calcium carbonate conditioned-water (pH-neutral) at 27°C in a 12h alternating cycle of light and darkness. Their diet consisted of algae tablets and lettuce which was washed thoroughly with reverse osmosis water to prevent the introduction of dirt or other undesirable particles.

Snail-conditioned water collection and semi-purification

Samples of SCW were collected from *B. glabrata* that were naïve and 16h-PME, 1W-PME, 2W-PME and 3W-PME. These time-points were chosen, and each SCW treatment was extracted from a different batch, because frequent SCW collection increases snail stress and accelerates death. No further SCW treatments were collected after 3W-PME due to the high rate of cercarial release after this time-point causing high stress and low SCW protein quantities. The *B. glabrata* snails (60 for each treatment) were washed four times with freshly prepared calcium carbonate-conditioned Milli-Q water to remove any contaminants from the tank and separated into three 50 mL beakers, each containing 20 snails. Snails were incubated in 20 mL of pH-neutral spring water at room temperature for 2 h. Snails were removed and returned to the aquarium, 20 mL of methanol was added to the water samples and mixed thoroughly. The mixture was filtered through a 0.45 µm Durapore PVDF filter (Bedford, MA, USA) to remove contaminants. Filtered samples were immediately frozen on dry ice until lyophilisation using a Savant SpeedVac Concentrator (Thermo Scientific, MA, USA).

Schistosoma mansoni miracidia isolation and behavioural bioassay

Swiss mice infected with *S. mansoni* were euthanised with CO_2 gas and their livers were finely sliced and placed in room-temperature phosphate-buffered saline (PBS) to collect the eggs of *S. mansoni*. Two sliced livers were shaken to a smooth consistency in 50 mL PBS. The mixture was centrifuged at 2,000×g for 10 s at 20˚C, the supernatant was removed and pellet re-suspended in 50 mL of room temperature PBS. This step was repeated three times until the supernatant was transparent. The eggs were divided between three 50 mL tubes in pH-neutral water covered by alfoil under a light for 2h at room temperature to maximise the quantity of miracidia attained. A total of 2h were allowed for hatching because the infected livers were stored at 4°C the night before being sliced and the eggs were not purified with any further steps (such as using collagenase or filters) (25). The top 4 mL of the water was collected every 30 min for 2 h and the number of miracidia were counted under a microscope. The miracidia were concentrated through centrifuging the water at 4,000×g for 15 min at 20°C and the supernatant was removed. The miracidia were resuspended in 10 mL of Milli-Q water, vortexed and 30 miracidia per 100 µL were counted. This method of SCW behavioural bioassay has been described in detail elsewhere (20).

Briefly, miracidia water aliquots in 100 µL volumes were placed on a hydrophilic glass slide (StarFrost® superclean, hydrophilic slides, ground edges 90°, white, ProSciTech Pty Ltd) to ensure the miracidia were consistently clear and monitored using an Olympus-CKX41 microscope (Olympus) equipped with an Olympus DPI Digital Microscope Camera DP22 (15 frames per second at 2.8-megapixel image quality). Miracidia baseline behaviours were recorded for one minute, followed by addition of 2 µL of SCW, after which a further minute of behaviours was recorded. This process was conducted with nine replicates of *B. glabrata* SCW at 16h-PME, 1W-PME and 2W-PME resuspended in 100 µL of Milli-Q water.

Data for the positive control (naïve SCW), negative control (Milli-Q water) and 3W-PME SCW were obtained in nine replicates from videos recorded in an earlier study (24). There were some minor methodological differences in that study, such as the use of 200 µL aliquots on petri dishes instead of 100 µL aliquots on glass slides, concentrating miracidia at 5,000×g instead of 4,000×g and using 25 snails instead of 20 for behavioural bioassay SCW collection. Behaviour bioassays using Milli-Q and naïve SCW were conducted again using the updated parameters and the new data was compared to the data from the earlier study to observe if the changes in parameters affected miracidia behaviour change. It was calculated that there were no significant differences in any behaviour metrics when comparing different Milli-Q water data and slightly greater decreases in velocity (34% instead of 22%, $P = 0.0134$) and increases in duration of presence (120% instead of 104%, $P = 0.0448$) when comparing naïve SCW data (Table S1). Therefore, we concluded that the changes in parameters did not affect behaviour changes enough to alter the conclusions of this paper and hence the naïve SCW, Milli-Q and 3W-PME SCW data were compared to the new PME SCW data.

The videos were analysed using a method described previously (20). Briefly, miracidia were identified when they were within the field of view (FOV). Videos were split into pre-addition and post-addition segments and imported into FIJI software (26). Miracidia contrast was improved using a rolling mean background subtraction method (27). Employing the TrackMate plugin (28), miracidia locations along an x-y axis were tracked in each frame and assembled into complete tracks for each miracidium present in the FOV. Changes were manually performed to prevent miracidia track overlap and eliminate tracks created by remaining liver particles that were unlikely to affect behaviour. The MTrackJ plugin (29) was used to calculate several measures of movement: average velocity (mm/s), angular standard deviation (degrees; measures the standard deviation in the change in angles between consecutive points, therefore reflecting the magnitude and frequency of turns), duration of presence (seconds) and miracidia tracks per min. Behaviour changes of interest included aggregation, signified by an increased quantity of miracidia per min, and chemoklinokinesis, indicated by decreased average velocity and increased duration of presence (both indicating slowdown) and increased angular standard deviation (SD; indicating magnitude and frequency of angle change) between pre-addition and post-addition videos.

For statistical analysis, we used an align-and-rank transform (ART) implemented in the ARTool R package to conduct a nonparametric two-way ANOVA with SCW treatments as a between-subjects factor and pre/post-addition as a within-subjects factor (30). This method avoids the requirement for a normally distributed response variable and accommodates the repeated measures nature of our pre-addition versus post-addition comparisons. This was followed by *post-hoc* contrasts of the changes between pre and post SCW addition for all SCW treatments against Milli-Q water, in addition to the changes between pre and post SCW addition for all PME SCW treatments against naïve SCW (31). A change of $P < 0.05$ was considered significant. Statistical analysis and figure preparation were both performed using R version 4.1.3 with R Studio (32), and the following packages: readxl version 1.4.0 (33), tidyverse version 1.3.1 (34), magrittr version 2.0.3 (35), forcats version 0.5.1 (36), lme4 version 1.1-29 (37), AICcmodavg version 2.3-1 (38), car version 3.1-0 (39), multcomp version 1.4-19 (40), ggplot2 version 3.3.6 (41), plotrix version 3.8-2 (42), ARTool version 0.11.1 (30) and UpSetR version 1.4.0 (43). On the generated box-plot, points beyond 1.5x the interquartile range either below the lower quartile or above the upper quartile are indicated as outliers.

In-solution trypsin digestion for SCW and sample preparation for LC-MS/MS

While previous studies have identified attractant proteins, such as P12, without in-solution trypsin digestions prior to analysis, preparation typically produced increased result sensitivity (20). Protein concentrations in all *B. glabrata* SCW triplicates, naïve and all time-points PME, were quantified using the BCA (Bicinchoninic Acid) method (44). A total of 25 µg of protein in 100 µL of 6M urea was used from each sample. Aliquots of 1.5 µL of 200 mM dithiothreitol were added to each sample, which were then incubated at 37°C for 1 h. Aliquots of 6 µL of 200 mM iodoacetamide were added to each sample and incubated in the dark at room temperature for 1 h. Volumes of 6 µL of 200 mM dithiothreitol were added to each sample and incubated at room temperature for 45 min. The urea was diluted with 775 µL of Milli-Q water, vortexed, and 20 µL of 100 µg/mL trypsin was added to each sample. The samples were digested at 37°C for 16h. A 15 µL aliquot of 10% formic acid was added to decrease the pH below 3. A Sep-Pak Plus C18 cartridge (Waters) was prepared for each SCW replicate to concentrate the samples. The protocol used was that prescribed for the product (Sep-Pak C18 Plus Short Cartridge, 360 mg Sorbent per Cartridge, 55-105 µm). An 8 mL aliquot of 0.5% acetic acid in 70% acetonitrile, 29.5% Milli-Q water was run through the column and the solution was frozen at -80°C before lyophilisation. Each lyophilised sample was resuspended in 50 µL of 0.1% formic acid and frozen at -20°C until LC-MS/MS analysis.

uHPLC tandem QTOF MS/MS analyses

SCW treatments were analysed by LC-MS/MS attached to an ExionLC liquid chromatography system (AB SCIEX, Concord, Canada) and a QTOF X500R mass spectrometer (AB SCIEX, Concord, Canada) equipped with an electrospray ion source. A 15 µL aliquot of each *B. glabrata* SCW sample was injected into a 100 mm × 1.7 µm Aeris PEPTIDE XB-C18 100 uHPLC column (Phenomenex, Sydney, Australia) equipped with a SecurityGuard column for mass spectrometry analysis. Linear gradients of 5-35% solvent B over a 10-min period at a flow rate of 400 µL/min, followed by a gradient from 35-80% solvent B over 2 min and 80-95% solvent B in 1 min were used for peptide elution. Solvent B remained at 95% for 1 min to wash the column after which it was decreased to 5% for equilibration prior to the injection of the subsequent sample. Solvent A consisted of 0.1% formic acid in Milli-Q water while solvent B contained 0.1% formic acid in 100% acetonitrile. The ion spray voltage was set to 5500 V, the declustering potential was set to 100 V, the curtain gas flow was set at 30, ion source gas 1 was set at 40, the ion source gas 2 was set at 50 and spray temperature was set at 450°C. The mass spectrometer acquired the mass spectral data in an Information Dependant Acquisition mode. Full scan TOFMS data was acquired over the mass range 350-1400 and for product ion ms/ms 50-1800. Ions observed in the TOF-MS scan exceeding a threshold of 100 cps and a charge state of +2 to +5 were set to trigger the acquisition of product ion. The data were acquired and processed using SCIEX OS software (AB SCIEX, Concord, Canada).

Protein identification

LC-MS/MS data were imported to PEAKS studio (Bioinformatics Solutions Inc., Waterloo, ON, Canada, version 7.0) with the assistance of MSConvert module of ProteoWizard (3.0.1) (45). For the current study, the proteomic data were analysed with the BglaB1.6 database to compare ESPs from different *B. glabrata* SCW treatments (https://vectorbase.org/vectorbase/app/record/dataset/TMPTX_bglaBB02) (15). MS/MS spectra of ESPs were also analysed with reference to the *S. mansoni* database (https://parasite.wormbase.org/Schistosoma_mansoni_prjea36577/Info/Index). *De novo* sequencing of peptides, database searches and characterising specific PTMs (post-translational modifications) were used to analyse the raw data; false discovery rate (FDR) was set to ≤ 1%, and [-10×log(*P*)] was calculated accordingly where *P* was the probability that an observed match was a random event. The PEAKS used the following parameters: (i) precursor ion mass tolerance, 20 ppm; (ii) fragment ion mass tolerance, 0.1 Da (the error tolerance); (iii) tryptic enzyme specificity with two missed cleavages allowed; (iv) monoisotopic precursor mass and fragment ion mass; (v) a fixed modification of cysteine carbamidomethylation; and (vi) variable modifications including lysine acetylation, deamidation on asparagine and glutamine, oxidation of methionine and conversion of glutamic acid and glutamine to pyroglutamate. ESPs were considered to be present at a specific time-point with confidence only when they were present in at least two of the three replicates. This ensures that ESPs are not removed from consideration due to absence from one replicate. The mass spectrometry proteomics data have been deposited to the ProteomeXchange Consortium *via* the PRIDE partner repository with the dataset identifier PXD031989 (46).

Semi-quantitative protein analysis

Semi-quantitative analysis of ESPs of all *B. glabrata* SCW triplicates, naïve and PME, was carried out using the label-free quantification module PEAKS Q of PEAKS Studio v7.0, based on the relative intensities of featured peptides detected in replicates. The concentrations of extracted ESPs in different replicate samples were measured using BCA method on a NanoDrop 2000c spectrophotometer (Thermo Scientific, Waltham, USA) for the purpose of normalisation. Biological triplicates of each time-point

were used in tandem repeats for LC-MS/MS procedure as described above, and the relative concentrations of ESPs were compared and presented as the final results. The mass shift between different runs was set to 20 ppm, and 0.3 min was used for evaluating the retention time shift tolerance. Featured peptides with FDR threshold 1%, including PTMs mentioned above, were included in the quantitative analysis. The result of peptides was first filtrated based on: (i) ratio *versus* quality-score and a fold change of 8 was used; (ii) ratio *versus* average-area (MS signal intensity) set to a fold change of 8; (iii) charge of featured peptides set to between 2 and 5; (iv) fold change of peptide ≥1; and (v) featured peptide detected in more than one sample of the triplicate. Furthermore, protein results were filtered with FDR ≤ 1%, the number of unique peptides ≥1 and fold change ≥1.5. Proteins which did not meet these criteria could not be semi-quantitatively analysed. The abundance of proteins was normalised and compared, and proteins were clustered using one minus Pearson correlation.

Prediction of secreted proteins, gene ontology and KEGG pathway analysis

Identified ESPs were subjected to BLASTp using non-redundant protein sequences of NCBI. Protein N-terminal signal peptide sequences were predicted using SignalP 5.0 (47) with the transmembrane domains predicted by TMHMM (48). For SignalP predictions, positive identifications were made when both neural network and hidden Markov model algorithms gave coincident estimations. Herein, a protein was designated as secreted only when it met the criterium of SignalP for containing an N-terminal signal peptide and did not have a transmembrane domain predicted by TMHMM. BLAST results were combined and imported to BLAST2GO (49) (version 5.1), to perform gene ontology (GO) and KEGG pathway analyses. Fisher's exact test was carried out to evaluate the enrichment of GO terms in SCW ESPs with reference to entire proteome of *B. glabrata* (50). The SCW ESPs were also referenced with respect to the *S. mansoni* proteome. The significant GO terms with $P < 0.01$ were considered as over-represented, and FDRs were calculated from *P*-values using the Benjamini-Hochberg procedure (51).

Identification and analysis of *Schistosoma* miracidia attractant candidates

ESPs shared between SCW samples that induced miracidia behaviour change (naïve and 3W-PME), including aggregation and chemoklinokinesis, were initially identified as miracidia attractant candidates. Therefore, ESPs shared between 3W-PME SCW and naïve SCW analysed following an in-gel digestion, reported previously by Fogarty et al. (24), were also considered. Another essential criterion for consideration as an attractant candidate was high specificity to the *Biomphalaria* genus (identity percentage cut-off of below 50% in species outside the *Biomphalaria* genus according to BLASTp using non-redundant protein sequences of NCBI). Further proteomic analyses were performed to assign cellular function, including using Pfam (52), Panther (53) and InterProScan (54). Phylogenetic analyses used protein sequence alignments generated using MEGA X software (version 10.1.8) (34) with parameters set as follows: algorithm, ClustalW; gap opening penalty, 10; gap extension penalty, 0.2. Visualisation of alignments was carried out on TeXworks software (55) and edited in Adobe Illustrator. The evolutionary history was inferred using the Maximum Likelihood method based on the Jones-Taylor-Thornton matrix-based model. The tree with the highest log likelihood was shown (56). Initial tree for the heuristic search was obtained automatically by applying Neighor-Joining and BioNJ algorithms to a matrix of pairwise distances estimated using a Jones-Taylor-Thornton model, and then selecting the topology with superior log likelihood. The tree is drawn to scale, with branch lengths measured in the number of substitutions per site. All positions containing gaps and missing data were eliminated.

Predicted structure homology modelling was performed using the SWISS-MODEL workspace (57). In brief, a template search with BLAST and HHblits was performed using the primary amino acid sequence against the SWISS-MODEL template library. An initial HHblits profile was built (58), then models were built based on the target-template alignment using ProMod3 (59). The global and per-residue model quality was assessed using the QMEAN scoring function (60). Furthermore, *B. glabrata* proteins were considered more likely to be attractant candidates if they contained features of a secreted precursor protein (N-terminal signal peptide, no transmembrane domains). *B. glabrata* tissue gene expression data was retrieved from a previous study (15). Gene expression levels of these transcriptomes were calculated by mapping raw sequence data against the *B. glabrata* reference genome (structural version annotation BglaB1.6) derived from Vectorbase (https://vectorbase.org/vectorbase/app/record/dataset/TMPTX_bglaBB02) using CLC Genomic Workbench with default parameters (61). A heatmap was constructed using log base 2 of TPM (transcript per million) of protein precursors following the previously described guideline (62).

Results

Schistosoma mansoni miracidia behaviour bioassays

Schistosoma mansoni miracidia were exposed to SCW derived from *B. glabrata* at different time-points post-

miracidia exposure (16h-PME, 1W-PME and 2W-PME). Data for the control and from the SCW of *B. glabrata* that were naïve and 3W-PME were derived from an earlier paper (24). For each treatment, we tested for miracidia behaviour change, consisting of aggregation (increased quantity of miracidia tracks) and chemoklinokinesis (random movement, signified by decreased average velocity and increased duration of presence and angular SD), in the FOV between pre- and post-addition (Table S2). Compared to the negative control (Milli-Q water) (Figure 1A; Video S1), naïve SCW induced both chemoklinokinesis and aggregation, with expected changes in all behavioural measures (Figure 1B): a significant 21.96% decrease in mean velocity ($P < 0.0001$), a significant 154.38% increase in the mean miracidia tracks per min ($P < 0.0001$), a significant 82.64% increase in mean angular SD ($P < 0.0001$) and a significant 104.16% increase in mean duration of presence ($P < 0.0001$) (Table 1). These changes indicate aggregation accompanied by random motion (i.e. evidence of attraction) (Video S2). In contrast, 16h-PME, 1W-PME and 2W-PME SCW only induced minor or insignificant chemoklinokinesis and no significant aggregation (Table 1). 16h-PME SCW exposure significantly increased mean angular SD by 28.55% ($P = 0.0275$) and significantly decreased mean velocity by 14.30% ($P = 0.0358$) (Figure 1C; Video S3). 1W-PME SCW induced the weakest behaviour change, causing no significant differences in any behaviour metrics relative to the control (Figure 1D; Video S4). 2W-PME SCW exposure only induced a significant increase in mean angular SD by 27.57% ($P = 0.0480$) (Figure 1E; Video S5). These behaviour changes were significantly less extreme than those induced by naïve SCW, including the decrease in velocity induced by 16h-PME SCW ($P = 0.0045$) and increase in angular SD induced by both 16h-PME and 2W-PME SCW ($P \leq 0.0001$).

The addition of 3W-PME SCW produced the greatest increase in aggregation and chemoklinokinesis among miracidia-exposed *B. glabrata* SCW treatments (Figure 1F). These behaviour changes included a significant 20.33% decrease in mean velocity ($P < 0.0001$), a significant 105.45% increase in the mean miracidia tracks per min ($P < 0.0001$) a significant 69.37% increase in the mean angular SD ($P < 0.0001$) and a significant 32.01% increase in mean duration of presence ($P = 0.0355$) (Figures 1G–J; Video S6). There were no significant differences in the changes in velocity and angular SD between the naïve and 3W-PME SCW; however, naïve SCW induced significantly greater increases in aggregation ($P = 0.0129$) and duration of presence ($P = 0.0004$) than 3W-PME SCW (Table 1). This suggests that 3W-PME SCW does not induce identical behaviour change to naïve SCW; however, it nonetheless induced considerably stronger behaviour changes than the earlier time-points PME. Thus, it appeared that *B. glabrata* exposed to *S. mansoni* miracidia had a time-limited reduction in attractiveness to other miracidia. Therefore, attractants were likely most abundant in naïve and 3W-PME SCW. No SCW treatments induced a significant decrease in the quantity or duration of miracidia presence in the FOV, suggesting that there was no significant deterrent behaviour induced by exposure to any treatment.

Biomphalaria glabrata SCW ESP comparative proteomics

Triplicates of SCW collected from *B. glabrata*, naïve and at different time-points PME, were analysed by proteomics (Table S3). *B. glabrata* ESPs were considered present with confidence when present in at least two of three replicates (Table S4). Using this cut-off, a respective total of 50, 51, 36, 57 and 83 confidence *B. glabrata* ESPs were detected in the naïve, 16h-PME, 1W-PME, 2W-PME and 3W-PME SCW treatments (Figure 2A). The number of confidence *B. glabrata* ESPs exclusive to naïve, 16h-PME, 1W-PME, 2W-PME and 3W-PME SCW were 9, 19, 11, 15 and 45, respectively (Table 2). The greatest overlap in proteins (9 ESPs) occurred between naïve and 3W-PME SCW, while 4 ESPs (M4 family metallopeptidase, uncharacterized protein LOC106074992, mammalian ependymin-related protein 1-like and A disintegrin and metalloproteinase with thrombospondin motifs 1) were shared between all SCW treatments.

A semi-quantitative analysis was performed to determine the relative abundance of ESPs within different SCW treatments (Table S5). Proteins abundant in at least two replicates of naïve SCW included cathepsin B, haemoglobin type 1 and 2, calmodulin-like protein 5 and acetylcholine-binding protein-like (AChBP-like) protein (Figure 2B). Abundant ESPs in 3W-PME SCW included haemoglobins type 1 and 2, biomphalysin 2, AChBP-like proteins and several uncharacterised proteins. Some ESPs were highly abundant in both 3W-PME and naïve SCW and relatively low in abundance in all other SCW treatments, including haemoglobin and AChBP-like proteins. Gene ontology analysis was conducted on *B. glabrata* SCW ESPs to investigate differences between SCW treatments (Figure S1). The only function exclusively enriched in both naïve and 3W-PME SCW was obsolete pathogenesis (GO:0009405). This describes the process of one organism inflicting harm on another, and its enrichment was entirely due to the exclusivity of biomphalysin to these SCW treatments.

The SCW ESPs were also referenced against the *S. mansoni* protein database. A total of 10 ESPs were identified with confidence across all SCW treatments, 7 of which were from 16h-PME SCW (Table S4). However, these ESPs were predominantly ubiquitous, including tubulin alpha-1A chain, polyubiquitin-B, polyubiquitin-C and calmodulin, and thus are unlikely to function as semiochemicals (attractant or deterrent) due to their lack of species specificity.

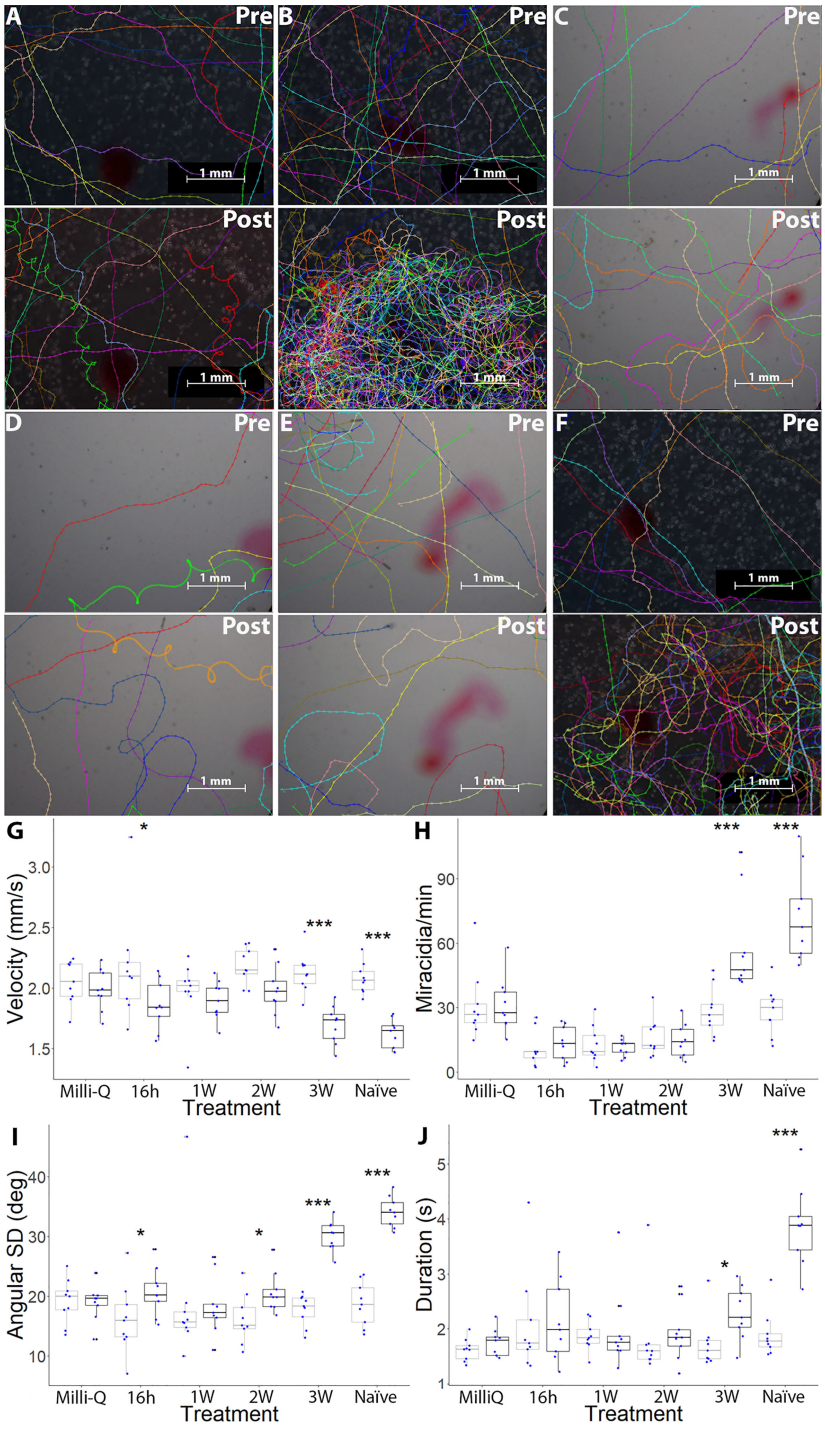

FIGURE 1
Changes in *S. mansoni* miracidia behaviour from 1 min pre-addition and post-addition of pH-neutral Milli-Q water, 16h-PME, 1W-PME, 2W-PME, 3W-PME and naïve SCW. A representation of miracidia tracks, generated in TrackMate and manually corrected, pre-addition and post-addition of 2 µL of **(A)** Milli-Q water, **(B)** naïve SCW, **(C)** 16h-PME SCW, **(D)** 1W-PME SCW, **(E)** 2W-PME SCW and **(F)** 3W-PME SCW (24). See Video S1-S6 for representative videos. Scale bars are in the bottom right-hand corner of every representative image. Boxplot indicates median, 25th and 75th percentiles, minima and maxima. **(G)** Mean velocity (mm/s); **(H)** average track per min; **(I)** angular SD (degrees) and **(J)** average duration of presence (s). Blue dots indicate the data attained from nine individual replicates of data from each treatment. Points beyond 1.5× the interquartile range either below the lower quartile or above the upper quartile are indicated as outliers. A two-way ANOVA test was used to calculate *P*-values for the mixed-effects interaction of pre-addition and post-addition SCW treatments against Milli-Q water: $*P < 0.05$, $**P < 0.01$, $***P < 0.001$. Colour: Grey: Pre-addition; Black: Post-addition.

TABLE 1 Two-way ART ANOVA interaction effects, testing changes in each of the behaviour measurements pre vs post-addition of SCW.

Metric	Interaction F	df	P-value	Contrasts (pre-post)	Milli-Q	16h	1W	2W	3W	Naïve
Mean velocity (mm/s)	9.04	5,48	**<0.0001**	vs Milli-Q	–	**0.0358**	0.7458	0.0833	**<0.0001**	**<0.0001**
				vs Naïve	**<0.0001**	**0.0045**	**<0.0001**	**0.0015**	0.5492	–
Tracks per min	27.59	5,48	**<0.0001**	vs Milli-Q	–	0.9541	0.2731	0.3074	**<0.0001**	**<0.0001**
				vs Naïve	**<0.0001**	**<0.0001**	**<0.0001**	**<0.0001**	**0.0129**	–
Angular SD (degrees)	13.39	5,48	**<0.0001**	vs Milli-Q	–	**0.0275**	0.3493	**0.0480**	**<0.0001**	**<0.0001**
				vs Naïve	**<0.0001**	**<0.0001**	**<0.0001**	**<0.0001**	0.3138	–
Average duration of presence (s)	11.35	5,48	**<0.0001**	vs Milli-Q	–	0.4327	0.6003	0.5412	**0.0355**	**<0.0001**
				vs Naïve	**<0.0001**	**<0.0001**	**<0.0001**	**<0.0001**	**0.0004**	–

Measurements: mean velocity (mm/s), average number of tracks per min, angular SD (degrees) and average duration of presence (s). If the interaction effect was significant, pairwise contrasts testing determined whether the difference in behaviour change pre vs post addition was significant between both Milli-Q and each SCW treatment or between naïve SCW and each of the other SCW treatments (SCW collected 16h, 1W, 2W and 3W post-miracidia exposure). Significant data (p-value < 0.05) is in bold.

Identification and analysis of *Biomphalaria glabrata* miracidia attractant candidates

Snail-conditioned water derived from naïve and 3W-PME *B. glabrata* both induced significant aggregation and chemoklinokinetic behaviour in *S. mansoni* miracidia. Therefore, ESPs were considered more likely to be attractant candidates if shared between naïve and 3W-PME *B. glabrata* SCW, or specific to the latter. To provide a more robust comparative dataset, 3W-PME SCW ESPs shared with naïve SCW from both this study and an in-gel digestion from an earlier study (24) were considered. Of the 161 proteins identified with confidence in this paper, 79 were shared with naïve SCW in the earlier paper. Of these, only 9, 1, 13 and 5 ESPs were shared with ESPs specific to 16h-PME, 1W-PME, 2W-PME and 3W-PME SCW, respectively, supporting that differences in ESPs are primarily a result of infection instead of the method of analysis. A total of 18 non-redundant proteins met this criterion for consideration as attractant candidates, including biomphalysin 2 and 20, two AChBP-like proteins, mucin-5AC-like protein, calmodulin-like protein 5 isoform X1, haemoglobin types 1 and 2, thioester-containing protein 1 and 6 uncharacterised proteins (Table 3; Table S6).

Due to the specificity in snail host genus preference of *S. mansoni* miracidia, ESPs were considered more likely to function as attractants if they were lacking similar homologues outside the *Biomphalaria* genus (Table 3). Additionally, ESPs predicted to lack an N-terminal signal peptide or contain a transmembrane domain were excluded, as they were considered unlikely to be excretory-secretory (File S1). A total of 6 ESPs ultimately met all our criteria and therefore represented

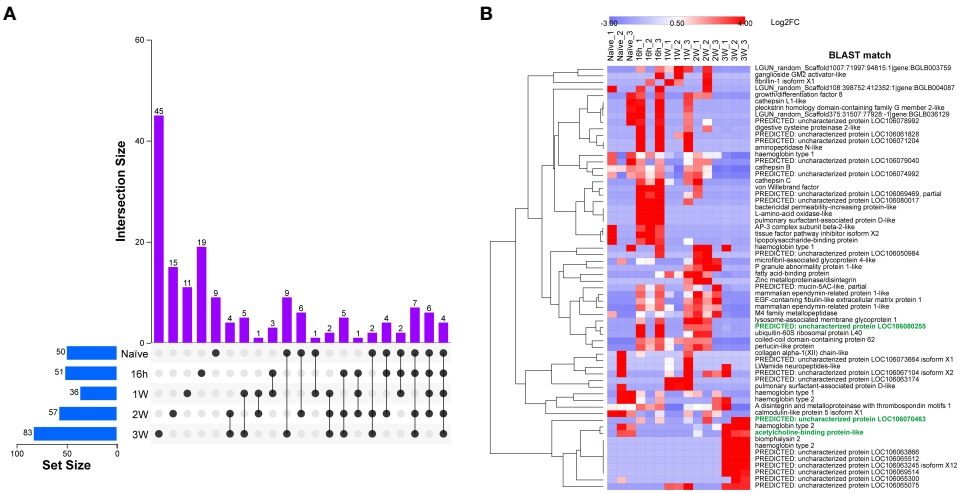

FIGURE 2
Identification and quantification of ESPs present with confidence from naïve, 16h-PME, 1W-PME, 2W-PME and 3W-PME *B glabrata* SCW. **(A)** An UpSet plot displaying confidence ESP distribution across SCW treatments; **(B)** Heatmap displaying the relative abundance of ESPs identified from SCW triplicates using a label-free semi-quantitative proteomic method. Attractant candidates are denoted with green font.

TABLE 2 Non-redundant ESPs, identified with confidence, exclusive to *B. glabrata* SCW from snails that were naïve and at 16h-, 1W-, 2W- and 3W-PME to *S. mansoni* miracidia.

Time-point post-miracidia exposure	Accession No.	Description	−10lgP	Coverage (%)[a]	No. of peptides	No. unique[b]	BLASTp e-value
16h	BGLB004262-PB	ganglioside GM2 activator-like	23.68	4	1	1	6.22E-152
	BGLB008634-PB	AP-3 complex subunit beta-2-like	18.86	1	1	1	0
	BGLB009288-PB	multiple EGF and TSP domain-containing protein	15.95	2	1	1	0
	BGLB012280-PB	tissue factor pathway inhibitor isoform X2	44.84	32	3	3	2.04E-45
	BGLB016060-PA	bactericidal permeability-increasing protein-like	117.2	23	11	9	0
	BGLB017086-PA	Hypothetical predicted protein	22.59	6	2	2	0
	BGLB021854-PA	CD109 antigen	29.06	2	2	2	0
	BGLB026410-PA	chorion peroxidase-like	42.64	5	2	2	0
	BGLB030199-PA	L-amino acid oxidase-like	19.3	5	1	1	3.56E-122
	BGLB033580-PA	serpin family protein	62.78	12	5	5	0
	BGLB035660-PA	Bsmp protein	38.61	7	2	2	0
	BGLB036153-PA	uncharacterized protein LOC106069469, partial	44.72	11	3	3	2.96E-105
	BGLB037955-PA	golgin subfamily a member 4	17.59	0	1	1	0
	BGLB040188-PA	lipopolysaccharide-binding protein	120.97	31	11	9	5.39E-164
1W	BGLB008299-PB	actin-5C	49.62	5	2	2	0
	BGLB011796-PB	progranulin-like isoform X1	55.8	2	1	1	0
	BGLB011796-PC	fibrillin-1 isoform X1	55.8	2	1	1	0
	BGLB021817-PA	polyubiquitin-B isoform X2	16.08	6	1	1	1.76E-104
	BGLB035643-PA	uncharacterized protein LOC106055144	30.4	8	1	1	7.28E-80
2W	BGLB000141-PA	microfibril-associated glycoprotein 4-like	37.26	7	3	3	0
	BGLB016967-PA	calmodulin-like protein 5 isoform X3	41.59	10	1	1	9.67E-82
	BGLB019617-PA	uncharacterized protein LOC106050984	48.27	11	1	1	1.64E-54
	BGLB031523-PB	uncharacterized protein LOC106067104 isoform X3	69.5	12	2	2	4.40E-137
	BGLB034051-PA	uncharacterized protein LOC106054319	21.21	6	1	1	2.59E-116
	BGLB040281-PA	Zinc metalloproteinase/disintegrin	36.23	3	1	1	0
3W	BGLB000016-PA	biomphalysin 8	24.5	2	1	1	0
	BGLB000033-PA	biomphalysin 2	131.13	17	10	8	0
	BGLB005531-PC	kazrin-like isoform X1	19.44	1	1	1	0
	BGLB014188-PB	serine/threonine-protein phosphatase 6 regulatory ankyrin repeat subunit B-like	17.05	1	1	1	0
	BGLB026487-PA	HEAT repeat domain-containing protein	67.97	6	2	2	0
	BGLB026513-PB	uncharacterized protein LOC106063245 isoform X1	26.91	5	1	1	4.01E-92
	BGLB027975-PA	uncharacterized protein LOC106065300	105.39	22	6	6	1.86E-112
	BGLB028940-PA	uncharacterized protein LOC106063866	105.39	23	6	6	9.07E-129
	BGLB029397-PA	uncharacterized protein LOC106074740	74.38	36	3	3	2.03E-71
	BGLB030954-PA	golgin subfamily B member 1	17.93	3	1	1	0
	BGLB031282-PA	von Willebrand factor d and egf domain-containing protein	16.74	0	1	1	0
	BGLB032561-PA	uncharacterized protein LOC106069515	31.78	10	1	1	3.39E-85
	BGLB035882-PA	uncharacterized protein LOC106054306 (ovipostatin-like)	41.87	7	1	1	8.73E-136
	BGLB036679-PA	uncharacterized protein LOC106077041	17.24	6	1	1	1.91E-72
	BGLB037163-PA	uncharacterized protein LOC106079133	97.22	54	7	7	2.59E-80
	BGLB038355-PA	uncharacterized protein LOC106069514	74.68	16	3	3	3.78E-100
Naïve	BGLB000202-PA	biomphalysin 20	59.12	6	2	2	0
	BGLB001498-PB	calmodulin isoform X2	37.29	12	2	1	5.91E-119
	BGLB005344-PB	beta-glucuronidase isoform X1	32.35	2	1	1	0

(Continued)

TABLE 2 Continued

Time-point post-miracidia exposure	Accession No.	Description	−10lgP	Coverage (%)[a]	No. of peptides	No. unique[b]	BLASTp e-value
	BGLB020170-PA	thioester-containing protein 1	23.22	7	1	1	3.05E-100
	BGLB024127-PA	calmodulin, striated muscle	16.37	6	1	1	9.23E-99
	BGLB030391-PA	probable serine carboxypeptidase CPVL	34.18	3	1	1	0
	BGLB034203-PA	zinc finger ZZ-type and EF-hand domain-containing protein 1-like	15.79	0	1	1	0
	BGLB035135-PA	endothelin-converting enzyme 2-like isoform X3	31.14	2	1	1	0

[a]The whole protein sequence coverage from the peptides identified with LC-MS/MS.
[b]The number of identified peptides unique to the protein.
Details of coverage, peptide match number and BLAST confidence (e-value) are shown.

promising miracidia attractant candidates, including two AChBP-like proteins and uncharacterised proteins LOC106070463, LOC106080255, LOC106056935 and LOC106067104 isoform X1 (File S2). Of these, only AChBP-like proteins were exclusive to naïve and 3W-PME SCW. Uncharacterised proteins LOC106056935 and LOC106067104 isoform X1 were also shared with 2W-PME SCW and uncharacterised proteins LOC106070463 and LOC106080255 were present in all SCW treatments except for 1W-PME (Table 3). The relative abundance of attractant candidates across the SCW treatment triplicates was also considered. An AChBP-like protein was of highest abundance in at least two replicates of both naïve and 3W-PME SCW, yet absent from all other SCW treatment replicates (see Figure 2B). In contrast, uncharacterised protein LOC106070463 had low abundance in naïve SCW, while uncharacterised protein LOC106080255 had low abundance in both naïve and 3W-PME SCW. Relative abundance could not be calculated for uncharacterised protein LOC106056935 or LOC106067104 isoform X1 because these proteins did not meet the criteria for semi-quantitative comparison.

The AChBP-like proteins and uncharacterised proteins LOC106067104 isoform X1 and LOC106070463 showed some similarity to other known proteins; therefore, they were explored in more depth by comparative sequence analysis. Phylogenetic analysis of the AChBP-like proteins (BGLB020983 and BGLB025228) identified in the *B. glabrata* SCW revealed some similarity with known AChBP-like proteins, yet only high confidence similarity with two *Bulinus truncatus* AChBP-like proteins (KAH9489187 and KAH9514736) (Figure 3A). Another *B. glabrata* AChBP-like protein (XP 013093195), not identified in any SCW treatment, displayed closer identity with other gastropod molluscs than with the *B. glabrata* AChBP-like proteins identified in the SCW. Comparative protein sequence analysis of the two *B. glabrata* AChBP-like proteins with the two *B. truncatus* AChBP-like proteins showed most conservation within multiple cysteine residues, as well as specific proline (P), tryptophan (W) and valine (V) residues (Figure 3B). Additionally, according to both Pfam and Panther analyses, both AChBP-like proteins were predicted to contain a ligand-gated ion channel, suggesting potential for receptor interaction (Table S6).

Homology was also relatively high between uncharacterised proteins LOC106067104 isoform X1 and LOC106070463 (Figure 4A). Despite sharing only 42% overall amino acid identity, several highly conserved regions were identified between the two uncharacterised proteins, including IALSTF/LLEDPLVQED/DRKVSA/AGLY, in addition to two predicted dibasic cleavage sites. Furthermore, they had predicted structural similarity based on predicted protein structure models (Figure 4B), in which both exhibited most similar sequence identity (23-28% identity) to a Junction 23, DHR14-DHR18 protein (PDB # 6w2v.2). Four additional sequences with similarity were present in *B. glabrata*, which together show phylogenetic clustering and with only minor identity with two proteins derived from evolutionary distant species (*Elysia marginata* and *Plakobranchus ocellatus*). Uncharacterised protein LOC106070463 displayed similar homology with other *B. glabrata* uncharacterised proteins, including LOC106070462 (49%), LOC106067104 isoform X2 (42%), LOC106067104 isoform X3 (39%) and LOC106067108 (49%). Homology was lower with *Plakobranchus ocellatus* PoB_002393000 (33%) and *Elysia marginata* ElyMa_006483900 (27%), indicating highest conservation within *B. glabrata*.

We also investigated the expression of attractant candidate transcripts across different *B. glabrata* tissues using a previous study (15) (Table S7). This demonstrated that uncharacterised protein LOC106067104 isoform X1 was most highly upregulated in the salivary gland. Both uncharacterised proteins LOC106080255 and LOC106070463 were relatively highly expressed in the mantle, kidney and heart, with the former also highly expressed in the foot (Figure 5). Uncharacterised protein LOC106056935 was also highly expressed in the kidney and heart, in addition to the genitalia and, to a lesser degree, salivary gland. Of the two AChBP-like proteins, one was most highly expressed in the digestive gland and ovotestis and the other was highly expressed in most tissue.

TABLE 3 Attractant candidate ESPs identified as shared between *B. glabrata* 3W-PME and naïve SCW, or unique to the latter.

Attractant candidate	SCW treatment	Accession no.	Description	−10lgP	Coverage (%)[a]	No. peptides	No. unique[b]	BLASTp e-value	Signal peptide	Trans-membrane domain	Identity (%)	Pfam
Y	Naïve, 16h, 2W, 3W	BGLB017354-PA	Uncharacterized protein LOC106070463	95.44	25	5	5	2.62E-162	Y	0	32.69	–
Y	Naïve, 3W	BGLB020983-PA/ BGLB020983-PB	Acetylcholine-binding protein-like	37.27	7	1	1	1.3E-164	Y	0	35.71	Ligand-gated ion channel
Y	Naïve, 2W, 3W	BGLB021783-PA	Uncharacterized protein LOC106056935	65.41	6	4	4	0	Y	0	–	–
Y	Naïve, 3W	BGLB025228-PA/ BGLB025228-PB	Acetylcholine-binding protein-like	98.17	17	4	4	2.94E-166	Y	0	41.71	Ligand-gated ion channel
Y	Naïve, 16h, 2W, 3W	BGLB029661-PA	Uncharacterized protein LOC106080255	62.86	8	2	2	0	Y	0	38.87	H-type lectin domain
Y	Naïve, 2W, 3W	BGLB031523-PA	Uncharacterized protein LOC106067104 isoform X1	145.85	36	7	7	8.00E-149	Y	0	29.60	–
N	Naïve, 3W	BGLB000033-PB	Biomphalysin 2	131.13	17	10	8	0	Y	0	51.99	Aerolysin
N	Naïve	BGLB000202-PA	Biomphalysin 20	59.12	6	2	2	0	N	0	31.65	Aerolysin
N	Naïve	BGLB010468-PB	Haemoglobin type 2	55.78	25	4	1	1.48E-82	N	0	62.39	Globin
N	Naïve, 3W	BGLB011149-PB	Haemoglobin type 2	38.55	7	2	1	0	N	0	56.68	Globin
N	Naïve, 16h, 2W, 3W	BGLB013891-PB	PREDICTED: mucin-5AC-like, partial	17.13	2	1	1	1.29E-119	N	0	–	–
N	Naïve, 3W	BGLB018373-PA	Haemoglobin type 2	107.9	53	9	6	4.34E-82	N	0	63.30	Globin
N	Naïve, 16h, 2W, 3W	BGLB019194-PA	Haemoglobin type 1	80.57	4	3	3	4.34E-82	Y	TMhelix(7-29), outside (30-783)	67.59	Globin
N	Naïve	BGLB020170-PA	Thioester-containing protein 1	23.22	7	1	1	3.05E-100	N	0	74.31	TED_ complement
N	Naïve, 16h, 1W, 2W, 3W	BGLB027972-PA	Uncharacterized protein LOC106074992	35.43	5	1	1	5.26E-149	N	0	29.48	–
N	Naïve, 3W	BGLB030063-PA	Haemoglobin type 1	68.35	12	2	2	1.81E-138	N	0	69.57	Globin
N	Naïve, 2W, 3W	BGLB033943-PA	Calmodulin-like protein 5 isoform X1	64.1	16	2	2	1.00E-75	Y	0	56.73	EF-hand_5
N	Naïve, 3W	BGLB035882-PA	Uncharacterized protein LOC106054306/Ovipostatin-like	41.87	7	1	1	8.73E-136	Y	0	62.07	–

[a]The whole protein sequence coverage from the peptides identified with LC-MS/MS.
[b]The number of identified peptides unique to the protein.
Details include SCW treatment of presence, accession no., description, coverage, peptide match number, BLAST confidence (e-value), predicted signal peptide and transmembrane domain presence, highest identity of proteins outside of *Biomphalaria* and Pfam analysis data. ESPs were designated as attractant candidates if they were predicted to contain a signal peptide and lack a transmembrane domain and have a maximum identity of below 50% outside of *Biomphalaria*.

10.3389/fimmu.2022.954282

10.3389/fimmu.2022.954282

Discussion

The aim of this study was to comparatively analyse *B. glabrata* SCW at different time-points post-exposure to *S. mansoni* miracidia to identify attractant candidates. This was achieved through comparing the effects of SCW from naïve and 16h-PME, 1W-PME, 2W-PME and 3W-PME *B. glabrata* on miracidia behaviour. Following this, SCW ESPs were analysed using proteomics to identify proteins shared between 3W-PME and naïve SCW, or exclusive to the latter. Attractant candidates were identified based off specificity to *Biomphalaria* and features consistent with being secreted. This facilitated the identification of 6 attractant candidate ESPs with confidence.

Schistosoma mansoni miracidia behaviour bioassay

Schistosoma mansoni miracidia behaviour change around *B. glabrata* SCW involves aggregation and chemoklinokinesis (random motion, most commonly increased turning and slowdown) (18, 63, 64). These patterns were observed to varying degrees among the SCW treatments in our study. 3W-PME SCW produced the most similar increases in aggregation and chemoklinokinesis to those induced by naïve SCW. There were no significant differences in changes in miracidia turning or slowdown between 3W-PME and naïve SCW. However, naïve SCW induced significantly greater increases in the quantity and duration of miracidia presence in the FOV. These observations imply that 3W-PME and naïve SCW contain the greatest quantities of attractant ESPs. 16h-PME and 2W-PME SCW both slightly increased turning; however, these increases were significantly smaller than those induced by naïve SCW. This suggests that these SCW treatments likely contained smaller quantities of attractant ESPs. 1W-PME SCW did not produce significant changes in any behavioural metrics, indicating it contained the lowest quantity of SCW attractant(s). The behaviour changes induced by 16h-PME, 1W-PME and 2W-PME SCW can be most accurately characterised as failing to induce behaviour changes associated with attraction, because none of these treatments induced significant aggregation, instead of inducing deterrent behaviour. This is because they induced behaviour changes that were not significantly different to the control, rather than decreasing the quantity or duration of miracidia presence in the FOV. Experiments in search of deterrents should consider exposing miracidia to sporocyst-conditioned water.

It is unknown why SCW from shorter durations PME induced weaker, if any, aggregation and chemoklinokinesis. Because heavily infected *B. glabrata* have drastically shortened lifespans, and thus are sub-optimal hosts, miracidia attraction to 3W-PME SCW was unexpected. It may be speculated that intramolluscan cercariae, germ balls and daughter sporocyst generations do not inhibit the production of miracidia attractants as effectively as mother sporocysts. From these behavioural bioassay results, it may be suspected that the decrease in attractant chemical abundance post-miracidia exposure is only a temporary phenomenon and that infected *B. glabrata* may regain their attractiveness to *S. mansoni* miracidia throughout infection. Future studies should observe SCW from snails after 3W-PME, following the release of potentially hundreds of cercariae, to see if reinfection of snails is more common than was previously believed.

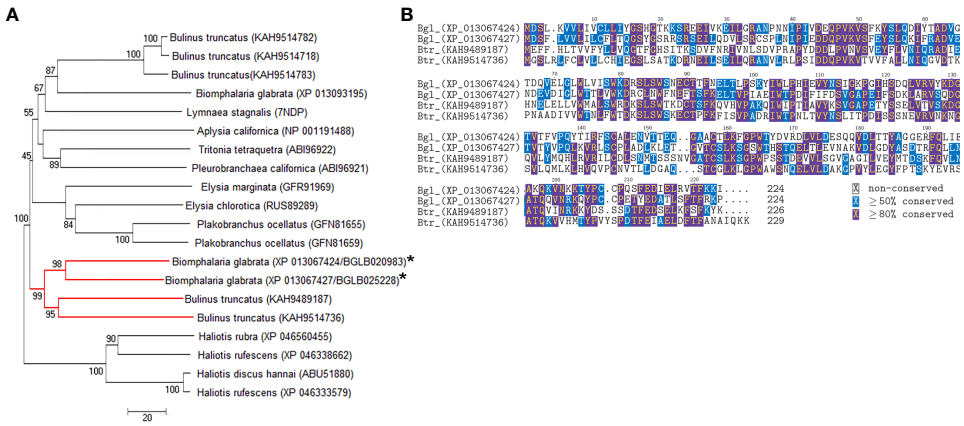

FIGURE 3
Comparative analysis of AChBP-like proteins in molluscs. **(A)** Phylogenetic analysis with *B glabrata* proteins identified in SCW denoted with asterisk and the red branch demonstrating the clade of interest. **(B)** Protein multiple sequence alignment. Bgl, *B glabrata*; Btr, *B truncatus*.

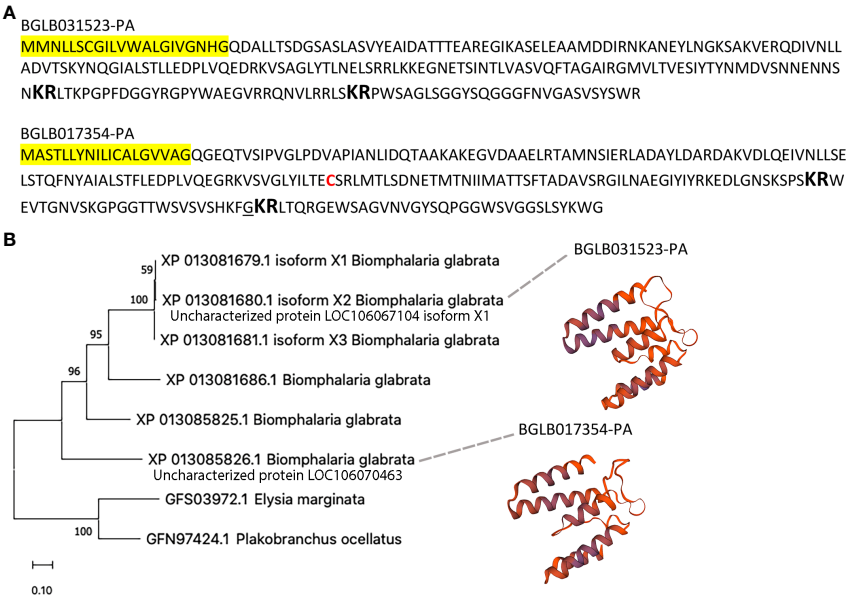

FIGURE 4
Characterisation of *S. mansoni* attractant candidates uncharacterised proteins LOC106067104 isoform X1 and LOC106070463. **(A)** Annotation of protein sequences, including signal peptide (yellow highlight), dibasic cleavage sites (large bold), cysteine residue (red font) and amidation (underline). **(B)** Phylogenetic analysis and protein models.

Attractant candidate identification and analysis

Naïve and 3W-PME *B. glabrata* SCW induced similar behaviour change in *S. mansoni* miracidia. Therefore, ESPs were considered more likely to be attractant candidates if they were specific to naïve SCW or shared with 3W-PME SCW. For consideration as attractant candidates, ESPs were also required to be specific to *Biomphalaria* because ubiquitous proteins are less likely to function as attractants given the parasite's requirement for species-specificity. This was previously demonstrated by the discovery of the *B. glabrata* attractant peptide, P12, where the protein precursor lacked any known homologues outside of the species (20). Additionally, attractant candidates were required to contain a predicted signal peptide, and lack a transmembrane domain, to confirm that they are excretory-secretory. A total of 6 ESPs met these criteria, including two AChBP-like proteins and uncharacterised proteins LOC106070463, LOC106080255, LOC106056935 and LOC106067104 isoform X1.

Of the attractant candidates identified, AChBP-like proteins appeared of most interest due to their exclusivity and abundance within several replicates of both naïve and 3W-PME SCW. Additionally, they were predicted to contain ligand-gated ion channel domains, suggesting potential to interact with miracidia receptors, including GPCRs and other ligand-gated channels (65). Immunolocalization should be conducted with these proteins to investigate potential miracidia receptor binding capacity. Furthermore, the relatively high expression of one of these proteins in the *B. glabrata* ovotestis may also be noteworthy because *S. mansoni* infections cause chemical castration in infected *Biomphalaria*, a phenomenon which has been well-characterised (66). Ovotestis are among the organs most affected by infection, as evidenced by the significantly decreased concentrations of sex hormones, such as estradiol and testosterone, post-exposure to *S. mansoni* miracidia (67). However, by 4 weeks PME, the concentrations of these hormones in the ovotestis were not significantly different compared to snails prior to infection. Thus, the decreased attractiveness of infected SCW, followed by increased attraction at 3W-PME, appears to loosely correlate with the concentration of these endogenous sex hormones. However, data regarding the role of sex hormones in miracidia attraction is conflicted. A behaviour analysis of miracidia showed that sexual maturity did not significantly impact miracidia preference of SCW or *B. glabrata* over a control (22). Nevertheless, proteins associated with reproduction have been implicated in inducing behaviour change in miracidia. An example is the *B. glabrata* buccalin peptide (21), a miracidia attractant known to play a role in reproduction in snails (and other molluscs) (68, 69). This suggests that sex-related chemicals may be a contributing factor to miracidia attraction; however, the snails likely release several other attractants unrelated to reproduction.

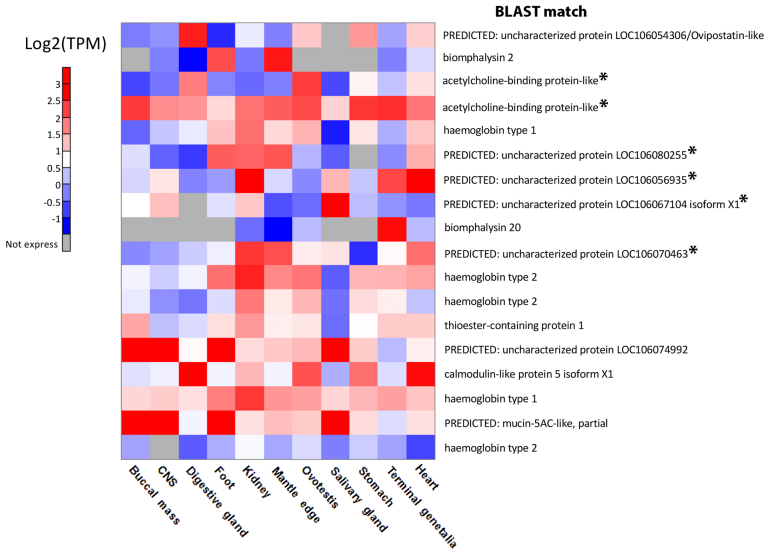

FIGURE 5
A heatmap displaying the $\log_2$ gene expression levels of attractant candidates in *B glabrata* tissues. Colour: Red: High expression; Blue: Low expression; Grey: No expression. Attractant candidates have been denoted with an asterisk.

Several additional proteins met our criteria as present in naïve and 3W-PME SCW, but seemed less likely as candidates once further analysis was completed. Uncharacterised proteins LOC106080255 and LOC106070463 were present with confidence in all SCW treatments except for 1W-PME SCW. Furthermore, although present, both proteins were low in abundance in naïve SCW. The encoding genes of both proteins were highly expressed in the foot, kidney and heart, with the encoding gene of LOC106080255 also highly expressed in the mantle. The foot and mantle are common entry points for miracidia and therefore are of interest when identifying attractants. Uncharacterised protein LOC106056935 was only absent from 16h-PME and 1W-PME SCW and its relative abundance could not be calculated. Similar to the aforementioned attractant candidates, its encoding gene was highly expressed in the kidney and heart. Uncharacterised protein LOC106070463 displayed strong homology with uncharacterised protein LOC106067104 isoform X1, which was also present with confidence in naïve, 2W-PME and 3W-PME SCW. However, the abundance of uncharacterised protein LOC106067104 isoform X1 could not be calculated and it was only highly expressed in the salivary gland. Therefore, none of these additional proteins were as promising as attractant candidates as the AChBP-like proteins.

The capacity of 3W-PME and naïve SCW to induce behaviour changes associated with attraction in *S. mansoni* miracidia may be partially explained by the presence of the P12 peptide (20). P12 has several precursor proteins, one of which (uncharacterized protein LOC106065300) was shared exclusively between these two SCW treatments. However, the precursor protein was more consistently abundant in 3W-PME SCW, with high abundance in two replicates of 3W-PME SCW and in only one of naïve SCW. Furthermore, another P12 precursor protein, the uncharacterized protein LOC106063866, was exclusive to 3W-PME SCW and highly abundant in all of its triplicates. The relatively low abundance or absence of these precursors from naïve SCW, despite producing greater behaviour change, may be explained by the presence of other attractant proteins or peptides. AChBP-like proteins are promising as attractant candidates due to their abundance in at least two replicates of both naïve and 3W-PME SCW. Other peptides from the P12 precursor proteins have all previously been discovered and tested; hence, no new attractant candidates could be identified from these precursor proteins (20). Therefore, the presence of other attractants, such as the AChBP-like proteins, are necessary to explain the greater behaviour change induced by naïve SCW despite its lower abundance of P12 precursors.

Analysis of other SCW ESPs

Outside of the attractant candidates, another protein of interest identified in naïve and 3W-PME SCW was ovipostatin-like protein, an uncharacterised protein highly expressed in the *B. glabrata* ovotestis. While its relative abundance could not be calculated and it was not sufficiently specific to *Biomphalaria* to constitute a species-specific

attractant candidate, its exclusivity to naïve and 3W-PME SCW and predicted signal peptide made it of interest. Ovipostatins are a family of proteins originally characterised in *Lymnaea* snails as accessory gland proteins exclusively produced in the prostate (70, 71). It has been identified as highly upregulated during sexual activity, notably 24 hours post-ejaculation (72). Its presence in 3W-PME SCW is consistent with a transcriptomic analysis of *Biomphalaria pfeifferi* post-exposure to miracidia, where ovipostatin 2 was downregulated within one day post-exposure and several days thereafter; however, ovipostatin 5 was upregulated when the snail began to shed *S. mansoni* cercariae. This suggests that later generation sporocysts, germ balls and cercariae do not inhibit the production of ovipostatins as effectively as earlier generation sporocysts. *B. glabrata* ovipostatins, therefore, warrant further investigation to observe their potential effect on miracidia behaviour.

Conclusions and future directions

This study performed proteomic characterisation on SCW from *B. glabrata*, naïve and at 16h-PME, 1W-PME, 2W-PME and 3W-PME and compared their effect on *S. mansoni* miracidia behaviour. The results indicate that 3W-PME SCW and naïve SCW induce comparable behaviour change, including aggregation and chemoklinokinesis, in miracidia. 16h-PME and 2W-PME SCW caused minor increases in miracidia slowdown and turning, while 1W-PME SCW did not produce any significant changes in behaviour. A total of 6 excretory-secretory attractant candidates were identified as specific to *Biomphalaria* and specific to naïve *B. glabrata* SCW or shared with 3W-PME SCW. This included two AChBP-like proteins and 4 uncharacterised proteins. These attractant candidates should be tested on *S. mansoni* miracidia to observe if they induce behaviour change, as this may disrupt infections and mitigate schistosomiasis.

Data availability statement

The datasets presented in this study can be found in online repositories. The names of the repository/repositories and accession number(s) can be found below: ProteomeXchange Consortium *via* the PRIDE partner repository with the dataset identifier PXD031989.

Ethics statement

The conduct and procedures involving animal experimentation were approved by the Animal Ethics Committee of the QIMR Berghofer Medical Research Institute, Brisbane (Project number P3705). This study was performed in accordance with the recommendations in the Guide for the Care and Use of Laboratory Animals of the National Institutes of Health. The Swiss mice used in this study were subject to Biosecurity Quarantine Control and hence held in a quarantine containment area within a Specific Pathogen Free Animal Facility. *S. mansoni* were maintained with an Australian Department Agriculture, Fisheries and Forestry Biosecurity permit.

Author contributions

CF conceived the study. SC and TW participated in the study design. DM provided the access to snail and parasite materials. CF carried out the experiments and analyzed the data under the supervision of TW and RW. PP performed the transcriptomic comparison. MD maintained the *S. mansoni* miracidia and *B. glabrata* snails and collected samples. CF drafted the manuscript. SC, TW, CF and PP generated the figures. SC, DM, RW and TW provided critical inputs to help draft the manuscript. All authors contributed to the article and approved the submitted version.

Funding

This study was supported by Australian Research Council Discovery Project (ARC DP180103694). The funders were not involved in the design, data collection and analysis, preparation or publication of the manuscript.

Acknowledgements

B. glabrata snails were provided by the NIAID Schistosomiasis Resource Center of the Biomedical Research Institute (Rockville, MD) through NIH-NIAID Contract HHSN272201700014I for distribution through BEI Resources. We wish to acknowledge QCIF for its support in this research. The authors thank the University of the Sunshine Coast for providing CF a Research Training Program Scholarship and the QIMR Berghofer Medical Research Institute for maintaining the *B. glabrata* snails and *S. mansoni*.

Conflict of interest

The authors declare that the research was conducted in the absence of any commercial or financial relationships that could be construed as a potential conflict of interest.

Publisher's note

Supplementary material

The Supplementary Material for this article can be found online at: https://www.frontiersin.org/articles/10.3389/fimmu.2022.954282/full#supplementary-material

SUPPLEMENTARY FIGURE 1
Gene ontology enrichment analysis of ESPs in SCW of *B. glabrata*, naïve and at 16h-PME, 1W-PME, 2W-PME and 3W-PME. The GO terms enriched in **(A)**: naïve SCW; **(B)**: 16h-PME SCW; **(C)**: 1W-PME SCW; **(D)**: 2W-PME SCW and **(E)**: 3W-PME SCW. The *B. glabrata* genome-derived proteome was used as the reference set in the analysis and P-value was set to below 0.05. Colour: Yellow: Biological Process; Pink: Molecular Function; Purple: Cellular Component.

FILE S1
SignalP schematic of attractant candidates.

FILE S2
Annotation of attractant candidates derived from *B. glabrata* SCW, including signal peptide (yellow highlight), dibasic cleavage sites (large bold), cysteine residue (red font) and amidation (underline).

SUPPLEMENTARY TABLE 1
Behavioural bioassay guided data, including tracks data, from *S. mansoni* miracidia one min pre-addition and post- addition of Milli-Q water and naïve from an earlier study (24) and using the parameters employed for 16h-, 1W- and 2W-PME SCW. A Two-way ART ANOVA interaction effects analysis, testing changes in each of the behaviour measurements pre vs post-addition of SCW. Measurements: mean velocity (mm/s), average duration of presence (s), angular SD (degrees) and average number of tracks per min. If the interaction effect was bolded, pairwise contrasts testing whether the change in behaviour pre vs post addition was different was conducted between Milli-Q and naïve SCW data attained using bioassays with different parameters.

SUPPLEMENTARY TABLE 2
Behavioural bioassay guided data, including tracks data, from *S. mansoni* miracidia one min pre-addition and post- addition of Milli-Q water and naïve, 16h-PME, 1W-PME, 2W-PME and 3W-PME *B. glabrata* SCW.

SUPPLEMENTARY TABLE 3
A list of all proteins and corresponding peptides identified in all replicates of 16h-PME, 1W-PME, 2W-PME, 3W-PME and naïve *B. glabrata* SCW with reference to the *B. glabrata* and *S. mansoni* proteomes.

SUPPLEMENTARY TABLE 4
A list of all proteins identified in at least two replicates of 16h-PME, 1W-PME, 2W-PME, 3W-PME and naïve *B. glabrata* SCW with reference to the *B. glabrata* and *S. mansoni* proteomes.

SUPPLEMENTARY TABLE 5
Semi-quantitative description of proteins in naïve, 16h-PME, 1W-PME, 2W-PME and 3W-PME *B. glabrata* SCW, including supporting peptides and $\log_2$ (Fold change).

SUPPLEMENTARY TABLE 6
A complete description of ESPs identified as shared between 3W-PME and naïve SCW or specific to the latter. This includes attractant candidate status, SCW treatment presence, gene ontology, Pfam and Panther analysis, TMHMM and SignalP results and unique peptides.

SUPPLEMENTARY TABLE 7
Gene expression levels derived from the *B. glabrata* reference genome (structural version annotation BglaB1.6) derived from Vectorbase (https://vectorbase.org/vectorbase/app/record/dataset/TMPTX_bglaBB02) using CLC Genomic Workbench with default parameters.

SUPPLEMENTARY VIDEO 1
A representative video of *S. mansoni* miracidia one min pre-addition and post- addition of Milli-Q water (Speed ×2, MP4 5.51 Mb). A scale bar is in the bottom right-hand corner of the video.

SUPPLEMENTARY VIDEO 2
A representative video of *S. mansoni* miracidia one min pre-addition and post- addition of naïve *B. glabrata* SCW (Speed ×2, MP4 5.52 Mb). A scale bar is in the bottom right-hand corner of the video.

SUPPLEMENTARY VIDEO 3
A representative video of *S. mansoni* miracidia one min pre-addition and post- addition of 16h-PME *B. glabrata* SCW (Speed ×2, MP4 3.55 Mb). A scale bar is in the bottom right-hand corner of the video.

SUPPLEMENTARY VIDEO 4
A representative video of *S. mansoni* miracidia one min pre-addition and post- addition of 1W-PME *B. glabrata* SCW (Speed ×2, MP4 3.57 Mb). A scale bar is in the bottom right-hand corner of the video.

SUPPLEMENTARY VIDEO 5
A representative video of *S. mansoni* miracidia one min pre-addition and post- addition of 2W-PME *B. glabrata* SCW (Speed ×2, MP4 3.14 Mb). A scale bar is in the bottom right-hand corner of the video.

SUPPLEMENTARY VIDEO 6
A representative video of *S. mansoni* miracidia one min pre-addition and post- addition of 3W-PME *B. glabrata* SCW (Speed ×2, MP4 5.30 Mb). A scale bar is in the bottom right-hand corner of the video.

References

1. Guo W, Zheng LY, Wu RM, Fan XL. Design, synthesis, and cercaricidal activity of novel high-efficient, low-toxic self-spreading peg-n-salicylanilide derivatives against cercariae larvae of schistosome *japonicum* floating on the water surface. *Chem Biol Drug Des* (2015) 85(5):527–33. doi: 10.1111/cbdd.12439

2. Steinmann P, Keiser J, Bos R, Tanner M, Utzinger J. Schistosomiasis and water resources development: systematic review, meta-analysis, and estimates of people at risk. *Lancet Infect diseases* (2006) 6(7):411–25. doi: 10.1016/S1473-3099(06)70521-7

3. Verjee MA. Schistosomiasis: Still a cause of significant morbidity and mortality. *Res Rep Trop Med* (2019) 10:153–63. doi: 10.2147/RRTM.S204345

4. Ferraro F, Corvo I, Bergalli L, Ilarraz A, Cabrera M, Gil J, et al. Novel and selective inactivators of triosephosphate isomerase with anti-trematode activity. *Sci Rep* (2020) 10(1):2587. doi: 10.1038/s41598-020-59460-y

5. Spangenberg T. Alternatives to praziquantel for the prevention and control of schistosomiasis. *ACS Infect Dis* (2020) 7:939–42. doi: 10.1021/acsinfecdis.0c00542

6. Becker JM, Ganatra AA, Kandie F, Mühlbauer L, Ahlheim J, Brack W, et al. Pesticide pollution in freshwater paves the way for schistosomiasis transmission. *Sci Rep* (2020) 10(1):3650. doi: 10.1038/s41598-020-60654-7

7. Tan WP, Hwang T, Park JW, Elterman L. *Schistosoma haematobium*: A delayed cause of hematuria. *Urol* (2017) 107:e7–8. doi: 10.1016/j.urology.2017.06.021

8. Rollinson D, Knopp S, Levitz S, Stothard JR, Tchuem Tchuenté LA, Garba A, et al. Time to set the agenda for schistosomiasis elimination. *Acta Trop* (2013) 128 (2):423–40. doi: 10.1016/j.actatropica.2012.04.013

9. Merrifield M, Hotez PJ, Beaumier CM, Gillespie P, Strych U, Hayward T, et al. Advancing a vaccine to prevent human schistosomiasis. *Vaccine* (2016) 34 (26):2988–91. doi: 10.1016/j.vaccine.2016.03.079

10. McCann S, Crossland M, Greenlees M, Shine R. Invader control: factors influencing the attraction of cane toad (*Rhinella marina*) larvae to adult parotoid exudate. *Biol Invasions* (2019) 10:1895–904. doi: 10.1007/s10530-019-01969-z

11. Lim H, Sorensen P. Making and using female sex pheromone implants which attract mature male common carp. (2010).

12. He YX, Salafsky B, Ramaswamy K. Host–parasite relationships of schistosoma japonicum in mammalian hosts. *Trends Parasitol* (2001) 17(7):320–4. doi: 10.1016/S1471-4922(01)01904-3

13. Martins AV. Non-human vertebrate hosts of schistosoma haematobium and schistosoma mansoni. *Bull World Health Organ* (1958) 18(5-6):931–44.

14. Berriman M, Haas BJ, LoVerde PT, Wilson RA, Dillon GP, Cerqueira GC, et al. The genome of the blood fluke schistosoma mansoni. *Nature* (2009) 460 (7253):352–8. doi: 10.1038/nature08160

15. Adema CM, Hillier LW, Jones CS, Loker ES, Knight M, Minx P, et al. Whole genome analysis of a schistosomiasis-transmitting freshwater snail. *Nat Commun* (2017) 8:15451. doi: 10.1038/ncomms15451

16. Eveland LK, Haseeb MA. Laboratory rearing of biomphalaria glabrata snails and maintenance of larval schistosomes in vivo and in vitro. In: Toledo R, Fried B, editors. *Biomphalaria snails and larval trematodes*. New York, NY: Springer New York (2011). p. 33–55.

17. Haas W, Haberl B, Kalbe M, Kömer M. Snail-host-finding by miracidia and cercariae: chemical hst cues. *Parasitol Today* (1995) 11(12):468–72. doi: 10.1016/0169-4758(95)80066-2

18. Saladin KS. Behavioral parasitology and perspectives on miracidial host-finding. *Z für Parasitenkunde* (1979) 60(3):197–210. doi: 10.1007/BF00929167

19. Hassan AHM, Haberl B, Hertel J, Haas W. Miracidia of an Egyptian strain of *Schistosoma mansoni* differentiate between sympatric snail species. *J Parasitol* (2003) 89(6):1248–50. doi: 10.1645/GE-85R

20. Wang T, Wyeth RC, Liang D, Bose U, Ni G, McManus DP, et al. A biomphalaria glabrata peptide that stimulates significant behaviour modifications in aquatic free-living *Schistosoma mansoni* miracidia. *PloS Negl Trop Dis* (2019) 13 (1):e0006948. doi: 10.1371/journal.pntd.0006948

21. Phan P, Liang D, Zhao M, Wyeth RC, Fogarty C, Duke MG, et al. Analysis of rhodopsin G protein-coupled receptor orthologs reveals semiochemical peptides for parasite (Schistosoma mansoni) and host (Biomphalaria glabrata) interplay. *Sci Rep* (2022) 12(1):8243. doi: 10.1038/s41598-022-11996-x

22. Magalhães LA, Zanotti-Magalhães EM, de Carvalho JF. Observations on the miraxonal attraction exercised by sexually immature or adult biomphalaria glabrata infected or not by schistosoma mansoni. *Rev saude publica* (1997) 31 (2):121–4. doi: 10.1590/S0034-89101997000200003

23. Vignoles P, Aimeur F, Titi A, Rondelaud D, Mekroud A, Dreyfuss G. Total cercarial output in two populations of galba truncatula experimentally infected with fasciola hepatica. *J Helminthol* (2010) 84(1):77–80. doi: 10.1017/S0022149X09990253

24. Fogarty CE, Zhao M, McManus DP, Duke MG, Cummins SF, Wang T. Comparative study of excretory-secretory proteins released by schistosoma mansoni-resistant, susceptible and naive biomphalaria glabrata. *Parasit Vectors* (2019) 12(1):452. doi: 10.1186/s13071-019-3708-0

25. Dalton JP, Day SR, Drew AC, Brindley PJ. A method for the isolation of schistosome eggs and miracidia free of contaminating host tissues. *Parasitology* (1997) 115(Pt 1):29–32. doi: 10.1017/S0031182097001091

26. Schindelin J, Arganda-Carreras I, Frise E, Kaynig V, Longair M, Pietzsch T, et al. Fiji: an open-source platform for biological-image analysis. *Nat Methods* (2012) 9(7):676–82. doi: 10.1038/nmeth.2019

27. Wyeth RC, Braubach OR, Fine A, Croll RP. Videograms: A method for repeatable unbiased quantitative behavioral analysis without scoring or tracking. In: Kalueff AV, Cachat JM, editors. *Neuromethods* (Totowa, NJ: Humana Pres) (2011). p. 15–33.

28. Tinevez JY, Perry N, Schindelin J, Hoopes GM, Reynolds GD, Laplantine E, et al. TrackMate: An open and extensible platform for single-particle tracking. *Methods* (2017) 115:80–90. doi: 10.1016/j.ymeth.2016.09.016

29. Meijering E, Dzyubachyk O, Smal I. Methods for cell and particle tracking. *Methods enzymol* (2012) 504:183–200. doi: 10.1016/B978-0-12-391857-4.00009-4

30. Kay MEL, Higgins J, Wobbrock J. *ARTool: Aligned rank transform for nonparametric factorial ANOVAs* (2021). Available at: https://github.com/mjskay/ARTool.

31. Elkin L, Kay M, Higgins J, Wobbrock J. An aligned rank transform procedure for multifactor contrast tests. *The 34th Annual ACM Symposium on User Interface Software and Technology*. New York, NY, USA: Association for Computing Machinery (2021), 754–68. doi: 10.1145/3472749.3474784

32. Team R. RStudio: Integrated development environment for r. (2021).

33. Wickham H, Bryan J. Readxl: Read excel files. (2019).

34. Wickham H, Averick M, Bryan J, Chang W, D'Agostino L. Welcome to the {tidyverse}. *J Open Source Software* (2019) 4(43):1686. doi: 10.21105/joss.01686

35. Bache SM, Wickham H. Magrittr: A forward-pipe operator for r. (2020).

36. Wickham H. Forcats: Tools for working with categorical variables (Factors). (2021).

37. Bates D, Machler M, Bolker B, Walker S. Fitting linear mixed-effects models using {lme4}. *Journal of Statistical Software* (2015) 67:1–48. doi: 10.18637/jss.v067.i01

38. Mazerolle MJ. AICcmodavg: Model selection and multimodel inference based on (Q)AIC(c). (2020).

39. Fox J, Weisberg S. An {R} companion to applied regression. In: *Sage* Thousand Oaks, CA: SAGE (2019).

40. Hothorn T, Bretz F, Westfall P. Simultaneous inference in general parametric models. *Biometrical J* (2008) 50(3):346–63. doi: 10.1002/bimj.200810425

41. Wickham H. *ggplot2: Elegant graphics for data analysis*. Verlag New York: Springer (2016).

42. Lemon J. Plotrix: a package in the red light district of r. *R-News* (2006) 6 (4):8–12.

43. Conway JR, Lex A, Gehlenborg N. UpSetR: an r package for the visualization of intersecting sets and their properties. *Bioinf (Oxford England)* (2017) 33 (18):2938–40. doi: 10.1093/bioinformatics/btx364

44. He F. BCA (Bicinchoninic acid) protein assay. *Bio-protocol* (2011) 1(5):e44. doi: 10.21769/BioProtoc.44

45. Chambers MC, MacLean B, Burke R, Amodei D, Ruderman DL, Neumann S, et al. A cross-platform toolkit for mass spectrometry and proteomics. *Nat Biotechnol* (2012) 30(10):918–20. doi: 10.1038/nbt.2377

46. Perez-Riverol Y, Bai J, Bandla C, García-Seisdedos D, Hewapathirana S, Kamatchinathan S, et al. The PRIDE database resources in 2022: a hub for mass spectrometry-based proteomics evidences. *Nucleic Acids Res* (2022) 50(D1):D543–D52. doi: 10.1093/nar/gkab1038

47. Petersen TN, Brunak S, Von Heijne G, Nielsen H. SignalP 4.0: Discriminating signal peptides from transmembrane regions. *Nat Methods* (2011) 8(10):785–6. doi: 10.1038/nmeth.1701

48. Krogh A, Larsson B, von Heijne G, Sonnhammer EL. Predicting transmembrane protein topology with a hidden Markov model: application to complete genomes. *J Mol Biol* (2001) 305(3):567–80. doi: 10.1006/jmbi.2000.4315

49. Conesa A, Gotz S, Garcia-Gomez JM, Terol J, Talon M, Robles M. Blast2GO: a universal tool for annotation, visualization and analysis in functional genomics research. *Bioinf (Oxford England)* (2005) 21(18):3674–6. doi: 10.1093/bioinformatics/bti610

50. Ackermann M, Strimmer K. A general modular framework for gene set enrichment analysis. *BMC Bioinf* (2009) 10:47. doi: 10.1186/1471-2105-10-47

51. Benjamini Y, Hochberg Y. Controlling the false discovery rate: a practical and powerful approach to multiple testing. *J R Stat Soc Ser B (Methodological)* (1995) 57:289–300. doi: 10.1111/j.2517-6161.1995.tb02031.x

52. Finn RD, Coggill P, Eberhardt RY, Eddy SR, Mistry J, Mitchell AL, et al. The pfam protein families database: towards a more sustainable future. *Nucleic Acids Res* (2016) 44(D1):D279–85. doi: 10.1093/nar/gkv1344

53. Mi H, Ebert D, Muruganujan A, Mills C, Albou LP, Mushayamaha T, et al. PANTHER version 16: a revised family classification, tree-based classification tool, enhancer regions and extensive API. *Nucleic Acids Res* (2021) 49(D1):D394–d403. doi: 10.1093/nar/gkaa1106

54. Blum M, Chang H-Y, Chuguransky S, Grego T, Kandasaamy S, Mitchell A, et al. The InterPro protein families and domains database: 20 years on. *Nucleic Acids Res* (2020) 49(D1):D344–D54. doi: 10.1093/nar/gkaa977

55. Beitz E. TEXshade: shading and labeling of multiple sequence alignments using LATEX2 epsilon. *Bioinf (Oxford England)* (2000) 16(2):135–9. doi: 10.1093/bioinformatics/16.2.135

56. Jones DT, Taylor WR, Thornton JM. The rapid generation of mutation data matrices from protein sequences. *Comput Appl Biosci CABIOS* (1992) 8(3):275–82. doi: 10.1093/bioinformatics/8.3.275

57. Waterhouse A, Bertoni M, Bienert S, Studer G, Tauriello G, Gumienny R, et al. SWISS-MODEL: homology modelling of protein structures and complexes. *Nucleic Acids Res* (2018) 46(W1):W296–w303. doi: 10.1093/nar/gky427

58. Steinegger M, Meier M, Mirdita M, Vöhringer H, Haunsberger SJ, Söding J. HH-suite3 for fast remote homology detection and deep protein annotation. *BMC Bioinf* (2019) 20(1):473. doi: 10.1186/s12859-019-3019-7

59. Studer G, Tauriello G, Bienert S, Biasini M, Johner N, Schwede T. ProMod3-a versatile homology modelling toolbox. *PloS Comput Biol* (2021) 17(1):e1008667. doi: 10.1371/journal.pcbi.1008667

60. Studer G, Rempfer C, Waterhouse AM, Gumienny R, Haas J, Schwede T. QMEANDisCo-distance constraints applied on model quality estimation. *Bioinf (Oxford England)* (2020) 36(6):1765–71. doi: 10.1093/bioinformatics/btz828

61. Mortazavi A, Williams BA, McCue K, Schaeffer L, Wold B. Mapping and quantifying mammalian transcriptomes by RNA-seq. *Nat Methods* (2008) 5 (7):621–8. doi: 10.1038/nmeth.1226

62. Ryan MC, Stucky M, Wakefield C, Melott JM, Akbani R, Weinstein JN, et al. Interactive clustered heat map builder: An easy web-based tool for creating sophisticated clustered heat maps. *F1000Res* (2019) 8:1750. ISCB Comm J-1750. doi: 10.12688/f1000research.20590.2

63. Samuelson JC, Quinn JJ, Caulfield JP. Hatching, chemokinesis, and transformation of miracidia of schistosoma mansoni. *J Parasitol* (1984) 70 (3):321–31. doi: 10.2307/3281558

64. Roberts TM, Ward S, Chernin E. Behavioral responses of schistosoma mansoni miracidia in concentration gradients of snail-conditioned water. *J Parasitol* (1979) 65(1):41–9. doi: 10.2307/3280200

65. Li S, Wong AH, Liu F. Ligand-gated ion channel interacting proteins and their role in neuroprotection. *Front Cell Neurosci* (2014) 8:125. doi: 10.3389/fncel.2014.00125

66. Faro MJ, Perazzini M, Corrêa Ldos R, Mello-Silva CC, Pinheiro J, Mota EM, et al. Biological, biochemical and histopathological features related to parasitic castration of biomphalaria glabrata infected by schistosoma mansoni. *Exp Parasitol* (2013) 134(2):228–34. doi: 10.1016/j.exppara.2013.03.020

67. Habib MR, Ghoname SI, Ali RE, El-Karim RMG, Youssef AA, Croll RP, et al. Biochemical and apoptotic changes in the nervous and ovotestis tissues of biomphalaria alexandrina following infection with schistosoma mansoni. *Exp Parasitol* (2020) 213:107887. doi: 10.1016/j.exppara.2020.107887

68. In VV, Ntalamagka N, O'Connor W, Wang T, Powell D, Cummins SF, et al. Reproductive neuropeptides that stimulate spawning in the Sydney rock oyster (Saccostrea glomerata). *Peptides* (2016) 82:109–19. doi: 10.1016/j.peptides.2016.06.007

69. Stewart MJ, Wang T, Koene JM, Storey KB, Cummins SF. A "Love" dart allohormone identified in the mucous glands of hermaphroditic land snails. *J Biol Chem* (2016) 291(15):7938–50. doi: 10.1074/jbc.M115.704395

70. Swart EM, Starkloff NC, Ypenburg S, Ellers J, van Straalen NM, Koene JM. The effect of mating on female reproduction across hermaphroditic freshwater snails. *Invertebrate Biology* (2020) 139(1). doi: 10.1111/ivb.12275

71. Koene JM, Sloot W, Montagne-Wajer K, Cummins SF, Degnan BM, Smith JS, et al. Male Accessory gland protein reduces egg laying in a simultaneous hermaphrodite. *PloS One* (2010) 5(4):e10117. doi: 10.1371/journal.pone.0010117

72. Swart EM, Davison A, Ellers J, Filangieri RR, Jackson DJ, Mariën J, et al. Temporal expression profile of an accessory-gland protein that is transferred *via* the seminal fluid of the simultaneous hermaphrodite lymnaea stagnalis. *J Molluscan Stud* (2019) 85(2):177–83. doi: 10.1093/mollus/eyz005

Frontiers in Immunology

Explores novel approaches and diagnoses to treat immune disorders. The official journal of the International Union of Immunological Societies (IUIS) and the most cited in its field, leading the way for research across basic, translational and clinical immunology.

Discover the latest Research Topics

See more →

Frontiers

Avenue du Tribunal-Fédéral 34
1005 Lausanne, Switzerland
frontiersin.org

Contact us

+41 (0)21 510 17 00
frontiersin.org/about/contact